

12.3 SEISMICITY AND SEISMIC HAZARDS

The assessment of seismic hazards at Yucca Mountain focuses on characterizing the potential vibratory ground motion and fault displacement that will be associated with future earthquake activity in the vicinity of the site. The evaluation of these hazards serves as a basis to define inputs for the preclosure seismic design of a potential geologic repository (YMP 1997b). The evaluation also provides information that can be used in evaluating the impact of different tectonic scenarios on the ability of the repository to contain and isolate waste during the postclosure period.

Seismic hazards at Yucca Mountain are assessed probabilistically (YMP 1997a). The assessment is founded on the evaluation of a large database that incorporates information on all known seismic sources in the Yucca Mountain region, including their maximum earthquakes, source geometry, and earthquake recurrence. Much of this information is based on the detailed history of past earthquakes on nearby Quaternary faults. The historical earthquake record and information on the attenuation of ground motion are also important components of this database. The seismic hazard assessment considers tectonic models that have been proposed for the Yucca Mountain area (see Section 4.3) and information from analog sites in the Basin and Range Province to characterize the patterns and amounts of fault displacement. The probabilistic assessment explicitly incorporates uncertainties in the characterization of seismic sources, fault displacement, and ground motion. The resulting hazard calculations thus represent a sound basis for seismic design and performance assessment by reflecting the interpretations that are supported by data along with the associated uncertainties in those interpretations.

This section presents the data and interpretations that support the hazard assessment, followed by a description of the hazard assessment and the results. The section begins by describing the approach used to compile the historical earthquake record for the Yucca Mountain region. A description of the seismicity within 300 km of the site, including its distribution and characteristics, follows (Section 12.3.3). Next, information on prehistoric earthquakes is presented, including a description of all known and suspected Quaternary faults in the Yucca Mountain region. (It should be noted that the information presented in this section, particularly the characterization of seismic sources, does not necessarily represent the interpretations of the experts involved in the probabilistic seismic hazard analysis [PSHA] project [Section 12.3.10].) The experts' seismic source characterizations are summarized in Section 12.3.10.2. Empirical and numerical modeling results of ground motion in the Yucca Mountain region are then discussed. The integration of these data and interpretations into a PSHA of vibratory ground motions and fault displacement and a deterministic ground motion evaluation are described. Finally, the methodology to develop seismic design parameters for vibratory ground motions based on the assessed hazard is briefly presented. At this time, the design parameters are being developed, and thus no results are yet available.

When referring to earthquake magnitudes, the following scales are cited and abbreviated as follows: M_L indicates Richter local; M_w indicates moment; M_s indicates surface wave; m_b indicates body wave; M_c or M_d indicates coda duration; M_I indicates intensity-based; and M indicates unspecified.

12.3.1 Data Sources

The principal sources of data used in the evaluation of seismic hazards at Yucca Mountain comprise two types: (1) data collected outside the Yucca Mountain Site Characterization Project (YMP) and (2) data collected under the approved quality assurance programs of the U.S. Geological Survey (USGS) and the Civilian Radioactive Waste Management System Management and Operating Contractor.

12.3.2 Earthquake Record

Seismic hazard evaluations rely on a description of the temporal and spatial distribution of earthquakes (both prehistoric and historical), their magnitudes, and how they relate to the seismotectonic processes of the region. Seismically active regions around the world are characterized by the occurrence of many small-magnitude (M less than 5) earthquakes that typically occur much more frequently than the rare, but potentially more hazardous, larger magnitude events. These larger earthquakes produce potentially damaging strong ground shaking and often result in geomorphic expression at the Earth's surface either through primary and secondary surface faulting or other local deformation. Variations of a power law distribution of earthquake magnitudes form the basis for estimating earthquake recurrence from the historical record of earthquake activity within a given region. The process may also involve relating the historical seismicity to the Quaternary history of surface faulting and possibly to geodetic estimates of the regional strain budget to define and characterize seismic sources. The temporal and spatial occurrence of earthquakes for a given region is evaluated from two sources: the historical (instrumental and reported effects) and prehistoric (paleoseismic) earthquake records.

12.3.2.1 Prehistoric Earthquake Record

The identification and documentation of earthquakes occurring prior to historical times is possible by studying the geologic record of past events. Larger events that rupture to the surface often leave geological evidence in the form of offset strata and characteristic earthquake-related deposits. Geologic fault studies at Yucca Mountain reveal that the recurrence times of large-magnitude earthquakes are on the order of tens of thousands of years (Whitney 1996, Chapters 4.1 to 4.13, Chapter 5), much longer than the 130-yr. historical earthquake record of the Yucca Mountain region. Thus, the prehistoric earthquake history of the Yucca Mountain site spans at least the past several hundred thousand years and is particularly important for probabilistic seismic hazard assessments because it extends the record for larger magnitude events.

Geologic studies of faulted deposits are the basis for identifying the occurrence of large-magnitude, surface-rupturing earthquakes and evaluating their size, age, and occurrence rate. Aerial photographs were examined to locate and map evidence of Quaternary surface faulting, such as fault scarps or small slope changes produced by faulting of geologically young colluvial and alluvial deposits or geomorphic surfaces. Typically these deposits and surfaces are Quaternary in age, which spans approximately the past 2 m.y. At the most promising locations, trenches were excavated across the fault scarps, and the late to middle Quaternary soils and stratigraphy were mapped specifically to document the size and age of surface-faulting displacement events. The ages of critical deposits were determined where possible, using

appropriate geochronologic techniques, to assess the timing of past earthquakes. Fault slip rates were estimated from the age of offset geological deposits and the amount of fault displacement. The prehistoric earthquake record has been constructed from the results of these paleoseismic and geochronologic studies and is discussed in Section 12.3.7.

12.3.2.2 Historical Earthquake Record

Information on historical seismicity in the Yucca Mountain region is obtained by:

- Compiling and assessing the historical earthquake record for the southern Great Basin and adjacent regions
- Monitoring contemporary seismicity at Yucca Mountain and in the surrounding region with both local and regional seismographic networks.

The early part of the historical record includes earthquakes known primarily through noninstrumental means. Compilation and assessment of reports of earthquake damage, effects, and felt ground motion form the primary basis for documenting the occurrence and size of many historic events. The historical earthquake record also includes events that were instrumentally recorded by limited distributions of seismographs (particularly prior to 1978).

Beginning in 1978, seismic monitoring in the Yucca Mountain region improved with the installation of a network of high-dynamic-range seismic stations that were capable of recording very small magnitude earthquakes. Instrumentally recorded events have formed the basis of the earthquake record since that time. Instrumental recording in the Yucca Mountain region is discussed in more detail in Section 12.3.3.1.

For both seismic monitoring and the compilation of past activity, attempts were made to identify seismic events that were not earthquakes, such as chemical explosions associated with mining activities in the region and underground nuclear explosions at the Nevada Test Site. Aftershocks of the Nevada Test Site blasts and earthquakes induced by reservoir impounding (e.g., Lake Mead) were also identified.

12.3.3 Historical Seismicity of the Yucca Mountain Region

The region of interest for assessing probabilistic seismic hazards at Yucca Mountain is a function of earthquake magnitude and the rate of earthquake occurrence. Because earthquake ground motions attenuate with distance, the farther an earthquake occurs from Yucca Mountain, the larger it must be to contribute significantly to the hazard at the site. At a distance of 100 km (62 mi.) from Yucca Mountain, earthquakes must reach a size on the order of M_w 8 to produce median peak horizontal ground accelerations of 0.1 g (98 cm/s^2) at the site (Pezzopane 1996, Figure 11.3). Similarly, if distant earthquakes are infrequent, ground motions from closer events of similar or lesser size will be more significant to the probabilistic hazard at the site. Thus, as distance from Yucca Mountain increases, seismic hazard studies focus on the longer and more active faults.

Although the focus of the hazard studies is the area within 100 km (62 mi.) of Yucca Mountain, the historical seismicity within 300 km (186 mi.) of Yucca Mountain is considered and described

in the following sections. (This radius was selected to be consistent with U.S. Nuclear Regulatory Commission guidelines.) This examination allows the seismicity of the Yucca Mountain vicinity to be evaluated within a broader regional context and provides an appropriate basis for the characterization of “background” earthquakes as part of the probabilistic seismic hazard analyses.

The discussion of historical seismicity in the Yucca Mountain region begins with a history of seismographic monitoring. The distribution and type of operating seismographs determines the completeness of the instrumentally documented record. Next, significant earthquakes and earthquake sequences are discussed. Information on these events is derived from instrumental recordings and from field investigations of fault surface ruptures. The section finishes with a description of areas of general seismicity in the Yucca Mountain region.

12.3.3.1 History of Seismographic Network Monitoring

Seismic monitoring of the southern Great Basin began in the early 1900s with isolated stations installed and operated by the University of California, Berkeley, and the University of Nevada, Reno. In the late 1950s and early 1960s, a global network called the Worldwide Standardized Seismograph Network came into existence, thereby providing the capability to record earthquakes larger than about M_L 4 in the southern Great Basin. Later, networks of stations were installed to monitor and study specific areas such as the Nevada Test Site and portions of the western United States. Milestones in monitoring are presented in Table 12.3-1. Networks that are relevant to assessing seismicity of the southern Great Basin are listed in Table 12.3-2.

Seismic Monitoring before 1979—In the early 1900s, the first seismographs were in operation in California (Figure 12.3-1a). One of the earliest seismographs was a drum recorder that began operation in 1911 at the University of Nevada, Reno. This instrument was used to refine the location and magnitude for the largest historical earthquake within 100 km (62 mi.) of Yucca Mountain, the 1916 M_L 6.1 Death Valley, California, earthquake (Gross and Jaumé 1995, p. 37). The development and installation of seismographs accelerated from 1932 on, and standardization of earthquake magnitude scales and an improvement in earthquake location techniques soon followed. The detection capability for earthquakes in the western Basin and Range Province in the early and mid-1900s improved with increasing numbers of seismograph stations in California (Figure 12.3-1b). A seismograph station established at Tinemaha, California, in 1929 by the California Institute of Technology was the first seismic monitoring equipment installed in the southern Great Basin (Figure 12.3-1).

From 1936 to 1940, seismographs were installed in the Lake Mead area near Las Vegas due to a number of felt earthquakes following the filling of Lake Mead (Anderson, L.W. and O’Connell 1993, pp. 63 to 66). In 1973, Rogers and Lee (1976) deployed a microearthquake network in the Lake Mead area and recorded approximately 1,300 small-magnitude earthquakes during the short deployment.

Underground nuclear testing began in 1951, and in 1961 the National Oceanic and Atmospheric Administration (formerly the U.S. Coast and Geodetic Survey) began monitoring seismicity around the Nevada Test Site (King et al. 1971, p. 1) (Figure 12.3-1). By the late 1960s, several regional stations were operating in Nevada, augmented by stations in southern Utah and eastern

California. A network of 18 telemetered stations was installed in 1968 in the eastern and southern Nevada Test Site. In the 1970s, Sandia and Lawrence Livermore National Laboratories upgraded and expanded the regional network coverage with the installation of several stations to support the nuclear testing program.

The Yucca Mountain Analog Network, 1978 to 1992—In 1978 and 1979, the USGS established a 47-station seismograph network out to a distance of 160 km (99 mi.) from Yucca Mountain in support of YMP efforts (Figure 12.3-2a). In 1981, six seismograph stations at Yucca Mountain were added to the network. The network was based on the analog technology of the 1970s and was the primary source of earthquake data in the southern Great Basin from 1979 through October 1995. Stations were initially configured with vertical-component 1-Hz sensors; horizontal components were added at a few sites in late 1984. The network was operated at a high gain or sensitivity in an attempt to record any microseismicity (M less than 2) associated with potentially active faults near Yucca Mountain. Magnitudes were usually estimated with coda duration (time of the earthquake signal) and coda decay methods for larger events, and these methods were then calibrated to M_L . By the late 1980s, some stations with horizontal components were operated at a low gain to preserve on-scale records and to calibrate coda-amplitude magnitudes with standard magnitude scales (Rogers et al. 1987, pp. 11 to 14).

In September 1992, maintenance and operation of the analog network were transferred to the University of Nevada, Reno, Seismological Laboratory. All seismic data from the analog and digital stations operating in the southern Great Basin are now telemetered along a microwave network to the University of Nevada, Reno. Radio links telemeter the signals from the remote seismograph sites to the regional microwave network. At the University of Nevada, Reno, earthquakes are located and M_d is calculated for all events, and M_L is calculated for many events greater than M_d 2.

Three-Component Digital Network near Yucca Mountain, 1995 to Present—A high-dynamic-range, three-component, digitally telemetered network in operation since 1995 is currently the primary seismic network at the Yucca Mountain site. The digital network spans a radius of 50 km (31 mi.) out from Yucca Mountain (Figure 12.3-2b), in contrast to the 160-km-radius (99-mi.-radius) area covered by the analog network. Since 1998, 26 stations, including one in Alcove 5 of the Exploratory Studies Facility (ESF), have been in operation. The digital network has enabled a decrease in the magnitude detection threshold in the Yucca Mountain block from about M_L 0.5 to about M_L -1.0 during times of low cultural noise. The regional detection threshold is approximately M_L 1.0, a decrease of 0.5 to 1.0 magnitude units from the earlier analog network capabilities. Earthquake location accuracy has improved because of the recording of horizontal component S-wave arrivals.

Strong-Motion Network near Yucca Mountain—In addition to the high-dynamic-range seismograph network, 10 strong-motion accelerometers also monitor Yucca Mountain. These stations are designed to record larger ground motions from nearby moderate to large earthquakes. Such events would exceed the ability of the high-dynamic-range stations to record on-scale data. Nine of the strong-motion instruments are located at the surface and one is sited in Alcove 5 of the ESF. In combination with the high-dynamic-range seismograph network, the strong motion stations allow on-scale recording of earthquakes at the site with magnitudes ranging from less than 0 to greater than 6.5.

Other Regional Seismic Networks—Other regional seismic networks on the edges of the southern Great Basin contribute data in the Yucca Mountain region (Table 12.3-2). To the north, the University of Nevada, Reno, operates a statewide regional network, which monitors seismicity in northern and central Nevada and areas along the state border with California, such as Mammoth Lakes. The University of Utah operates a number of stations in southern Utah, and the California Institute of Technology operates stations in the southern Owens Valley and Ridgecrest, California, areas. Northern Arizona University operates a small network of five analog telemetered stations around Flagstaff, Arizona.

12.3.3.2 Historical Seismicity Catalog for Yucca Mountain

As part of the probabilistic seismic hazard analyses project, a catalog of historical and instrumental earthquakes was compiled for the region within 300 km (186 mi.) of the potential repository site at Yucca Mountain (Wong and Stepp 1998, Appendix G). This region includes all of the relevant and potentially relevant seismic sources (Pezzopane, Bufe et al. 1996; McKague et al. 1996). The resulting combined catalog contains 271,223 earthquakes of approximately M_L 1 and greater from 1868 to 1996. All known magnitudes are listed in the catalog. Figure 12.3-3 shows events greater than M_w 3.5 in the catalog. The earthquake catalog for Yucca Mountain was compiled from several sources, including the catalogs of Meremonte and Rogers (1987), the Decade of North American Geology, the University of Nevada, Reno, the University of California, Berkeley, the California Institute of Technology, and the USGS for eastern California and the Great Basin (Table 12.3-3) (Wong and Stepp 1998, Appendix G).

Catalog completeness has improved significantly with time, but the catalog is still considered to be complete only for historical events of M_w 5.5 and larger within the 100-km (62-mi.) radius around Yucca Mountain (Rogers et al. 1991, p. 166). Estimated periods for which the Yucca Mountain catalog is complete for the southern Great Basin as a function of magnitude interval are provided in Table 12.3-4.

The accuracy of information in the historical catalog is affected by several variables (e.g., accuracy of historical accounts, detection capability, instrumental precision), especially the variability in seismic network coverage over time. The spatial distribution of seismicity in the 300-km (186-mi.) catalog is a function of the density of seismographic network coverage in a particular region over time and is somewhat an artifact of the more thoroughly represented aftershock sequences of the modern period. For example, a significant portion of the catalog is derived from a recent series of moderate-sized earthquakes, aftershock sequences, and volcanic swarm activity in the Mammoth Lakes, California, area. This modern sequence began in 1978 and has continued to the present. Although these events figure prominently in terms of the number of earthquakes in the catalog, they represent an insignificant portion of the total moment release along the western Basin and Range Province in the past two decades. When compared to the large-magnitude (greater than M_w 6.5) historical earthquakes of the Central Nevada Seismic Belt (Wallace, R.E. 1984, p. 5764), the total deformation or strain release represented by this sequence is minor. For example, the Cedar Mountain earthquake of 1932 occurred prior to complete instrumental coverage; therefore, only the larger aftershocks (relatively few) were recorded despite its large energy release.

Earthquake Magnitude Scale—Since the Yucca Mountain catalog was compiled from several source catalogs, each using a variety of different magnitude scales that also changed with time, a uniform magnitude scale was required to compute the earthquake recurrence for the region. In addition, it was necessary to assign magnitudes to historical earthquakes that occurred prior to calibrated seismographic instrumentation. Such magnitude estimates are usually based on the felt area or the maximum Modified Mercalli intensity. This is particularly problematic in the Basin and Range Province, where settlement and population growth have been erratic and sparse due to the boom and bust nature of mining operations and the rugged environment. For each earthquake in the catalog, M_w was estimated from the best available magnitude. When available, published relationships between seismic moment (M_0) and M_w and M_L were used. A detailed description can be found in Wong and Stepp (1998, Appendix G).

Identification of Nevada Test Site Explosions and Induced Seismicity—Nevada Test Site explosions and their induced earthquake aftershocks and reservoir-induced seismicity events at Lake Mead were identified in the earthquake catalog. Nuclear explosions were identified and flagged in the catalog. Nevada Test Site aftershocks were identified and flagged using a space-time window. The Lake Mead area-induced seismicity (Anderson, L.W. and O'Connell 1993; Rogers and Lee 1976) was identified but not removed from the catalog. It is unlikely that earthquakes in the Lake Mead area will contribute significantly to ground motion hazard at the Yucca Mountain site.

12.3.3.3 Significant Earthquakes and Earthquake Sequences

The historical and instrumental earthquake record within 300 km (186 mi.) of Yucca Mountain (Figure 12.3-3) includes the reported earthquakes of the southern Basin and Range Province and portions of the southern Sierra Nevada and Mojave Desert in California. The catalog contains all reported felt and instrumentally located earthquakes since 1868, including a few events of greater than M_w 5 that are located slightly outside of the 300-km-radius (186-mi.-radius) region, as discussed below. These are included because they are associated with surface ruptures that form important historical analogs for assessing fault displacement hazards at the potential repository site (Pezzopane and Dawson 1996).

Several events of greater than M_w 5.5 are located within 100 km (62 mi.) of Yucca Mountain. The earliest entry is the 1916 M_L 6.1 (M_s 5.9) Death Valley event (Gross, S. and Jaumé 1995) (Figures 12.3-3 and 12.3-4). Of earthquakes greater than M_w 5.5 in the 100-km (62 mi.) compilation, only five events occurred outside of the areas of underground nuclear explosions and can be unequivocally designated as tectonic in origin. All of these greater than M_w 5.5 tectonic earthquakes, except the 1992 Little Skull Mountain event, are near the Death Valley-Furnace Creek fault zone (Figure 4.2-2), and all occurred prior to 1966 (Figure 12.3-4). Many earthquakes of M_w 4 and greater within 100 km (62 mi.) also occur near the Furnace Creek fault system, the most active tectonic feature in this region.

Significant historical earthquakes and earthquake sequences in the 300-km (186-mi.) Yucca Mountain region are described below and illustrated on Figures 12.3-3 and 12.3-5. Significant events are listed in Table 12.3-5.

1872 Owens Valley, California, Earthquake—Possibly the largest historical earthquake in the Basin and Range Province, M_w 7.8, occurred in 1872 along the Owens Valley fault zone in eastern California. Based on reported effects of shaking, numerous aftershocks over M_L 6 followed the earthquake. Because no instrumental record of the sequence exists, the magnitude was estimated from felt area and surface-rupture dimensions. Much of the central Owens Valley has had limited seismicity since the 1872 sequence.

Beanland and Clark (1994) conducted one of the most recent and detailed investigations of the 1872 earthquake rupture. The 1872 earthquake produced a 100 ± 10 -km-long (62 ± 6 -mi.-long) zone of surface faulting along the entire length of Owens Valley, from southern Owens Lake to north of Big Pine, California. Vittori et al. (1993, p. 159) describe additional faulting and deformation related to the 1872 event within and south of Owens Lake. Other reported geologic effects included fissures and cracking as far north as Bishop, California (Stover and Coffman 1993, p. 105); liquefaction, especially in the area of Owens Lake; and rockfalls and landslides in Yosemite Valley and as far away as the White Mountains (Beaty and dePolo 1989, p. 222).

1916 Death Valley Earthquake—The 1916 M_L 6.1 Death Valley earthquake is the largest to occur within 100 km (62 mi.) of Yucca Mountain. Townley and Allen (1939, p. 192) describe it as the strongest earthquake of the year based on its seismograms. However, due to its remote location, no damage was reported and it was only felt at maximum Modified Mercalli IV at Rhyolite. S. Gross and Jaumé (1995, p. 38) relocated the earthquake by comparing waveforms recorded during the 1992 Little Skull Mountain earthquake with a heliocorder recording of the 1916 event from the Reno seismograph station. The revised location suggests that the 1916 earthquake occurred near the Death Valley fault zone. They suggested a revised magnitude of M_s 5.9 based on amplitude of the signal on the 1916 heliocorder record.

The 1932 Cedar Mountain Earthquake—The 1932 M_L 7.2 Cedar Mountain earthquake (and also the 1954 M_w 7.1 Fairview Peak and M_w 6.8 Dixie Valley events) occurred within the Central Nevada Seismic Belt northwest of Yucca Mountain (Wallace 1984, p. 5764) (Figure 12.3-3). Teleseismic waveform modeling shows that the 1932 Cedar Mountain earthquake consisted of at least two subevents of M_w 6.8 and M_w 6.6 (Doser 1988, p. 15,007). Amplitude measurements from seismograms recorded at the California Institute of Technology (Pasadena, California) indicate a M_L 7.2 for the earthquake (Slemmons et al. 1965, pp. 524, 541).

The Cedar Mountain earthquake produced widely distributed surface faulting. Gianella and Callaghan (1934, p. 377) recognized a zone of rupture approximately 38 mi. (61 km) in length by 4 to 9 mi. (6 to 14 km) in width. Additional ruptures were observed by dePolo et al. (1994, pp. 50 to 51) at the southern end of the faulted area, which increased the rupture length to as much as 80 km (50 mi.) and the width to as much as 17 km (11 mi.). Individual rupture zones are typically several hundreds of meters in length, and the longest extend for up to 16 km (10 mi.). Surface ruptures such as left-stepping en echelon fissures and fractures, mole tracks, and swell and depression morphology collectively indicate lateral slip. Right-lateral displacements range from 0.5 to 1.5 m (1.6 to 4.9 ft), and the maximum single-trace right-lateral displacement was 2.0 ± 0.5 m (6.6 ± 1.6 ft) (dePolo et al. 1994, pp. 50 to 51). Many of the ruptures associated with the Cedar Mountain event occurred along identifiable preexisting scarps. Geologic effects induced by the event included liquefaction, changes in spring and well flows, cracking in alluvium in the epicentral area, and landslides in the adjacent ranges. An analysis of the rupture

pattern and tabulation of the geological effects can be found in Pezzopane and Dawson (1996, pp. 9-21 to 9-51, 9-64, 9-65).

1934 Excelsior Mountains Earthquake—The 1934 M_L 6.3 (M_w 6.1) Excelsior Mountains, Nevada, earthquake took place in the Mono Lake-Excelsior Mountains region of the west-central Walker Lane in Nevada and eastern California, a source of continuing seismicity (Figure 12.3-3). The region is characterized by scattered, persistent microseismicity and northeast-striking, left-lateral and left-oblique-slip faults (dePolo et al. 1993, pp. 274, 279 to 280).

The Excelsior Mountains event occurred on a northeast-striking fault and produced left-oblique fault ruptures (Callaghan and Gianella 1935, p. 167; dePolo et al. 1993, p. 287). The poorly constrained focal mechanism and depth of this event show a predominantly normal fault source with a moderate dipping fault plane ($40^\circ \pm 8^\circ$) with a subordinate left-oblique-slip component (Doser 1988, p. 15,014). Left-lateral slip is consistent with the sense of displacement on faults north of the Excelsior Mountains.

The 1934 Excelsior Mountains earthquake produced a 1.5- to 1.7-km-long (0.9 to 1.1-mi.-long) scarp along a preexisting bedrock fault in the Excelsior Mountains. The north side of the fault is downdropped relative to the south side, and forms an uphill-facing scarp. The ruptures follow an older fault trace across the ridges on the south side of the Excelsior Mountains, but along part of its length, the 1934 earthquake may have ruptured previously unfaulted rock. Open en echelon fissures with scarp heights ranging from 15.3 to 46 cm (6 to 18 in.) indicate possible left-lateral movement along the fault. Reported geologic effects included numerous rockfalls, fissures that formed in alluvium, and changes in spring flows in nearby marshes.

1947 Manix, California, Earthquake—The M_w 6.5 Manix earthquake produced faulting along a 4-km (2.5-mi.) section of the Manix fault zone (Buwalda and Richter 1948, p. 1367) (Figure 12.3-3). The left-lateral displacements of up to 5 cm (2 in.) on a northeast-striking fault contrast with the many northwest-striking, right-lateral faults elsewhere in the Mojave Desert. Other reported geologic effects included cracking along the banks of the Mojave River and a report of liquefaction near the Mojave River (Richter 1947, p. 179; Stover and Coffman 1993, p. 138).

1954 Fairview Peak Earthquake—The M_w 7.1 Fairview Peak and the M_w 6.8 Dixie Valley earthquakes occurred in December 1954 within a period of 6 min. The southern portion of the aftershock zone of the Fairview Peak event lies at the edge of the 300-km (186-mi.) region, and minor seismicity continues to occur there (Figure 12.3-3). The Fairview Peak earthquake probably initiated at the northern end of the 1932 Cedar Mountain rupture zone. The focal mechanism determined by Doser (1986, p. 12,574) has a nodal plane that aligns with the overall strike of the surface rupture and dips $60^\circ \pm 5^\circ E$; the slip vector is predominantly right-lateral strike-slip.

The Fairview Peak earthquake ruptured several faults along a discontinuous 64-km-long (40-mi.-long) zone (Caskey et al. 1996, Figure 1, Table 1). The longest of the individual faults is the Fairview fault, which is approximately 32 km (20 mi.) long. The sense of displacement is normal-right-oblique, with a maximum vertical displacement of 3.8 m (12.5 ft) and maximum right-lateral displacement of 2.9 m (9.5 ft) along the Fairview fault, resulting in a net surface

1985, Figure 8, p. 582) (Figure 12.3-3). The zone of surface faulting stretches for 16 km (10 mi.), from near McGee Creek on the Hilton Creek fault across the caldera margin and into the caldera. Normal displacements on ruptures in the Long Valley caldera form a graben with west- and east-facing scarps. Vertical displacements on faults within the caldera are generally less than 5 cm (2 in.), and many of the surface ruptures are only ground-surface cracks. Vertical to eastside-down displacements of 20 cm (8 in.) occurred on the Hilton Creek fault but may have been enhanced by slumping. Many ruptures occurred on surface fault traces, although it is controversial whether or not the surface faulting was a direct manifestation of seismogenic faulting at depth. Slip on the Hilton Creek fault may have been triggered by other earthquakes in the sequence, or these features may represent only surficial ground failure rather than faulting. Reported geologic effects included widespread rockfalls and landslides, lurch cracks, and liquefaction in the Mammoth Lakes region.

1981 Mammoth Lakes Earthquake Sequence—A 1981 swarm of earthquakes culminated with a M_w 5.6 (M_s 5.8) event that produced small surface displacements along faults that had ruptured during the 1980 Mammoth Lakes earthquake sequence (Figure 12.3-3). Extensional cracks were observed at three places and the maximum vertical displacement was 10 to 20 mm (0.4 to 0.8 in.). Reported geologic effects included liquefaction, rockfalls, and changes in geyser and spring behavior in the Mammoth Lakes region.

1986 Chalfant Valley Earthquake Sequence—The Chalfant Valley sequence occurred near the White Mountains beneath the Volcanic Tablelands, 15 km (9 mi.) east of the Long Valley caldera (Smith, K.D. and Priestley 1988; dePolo and Ramelli 1987) (Figure 12.3-3). The sequence is associated with three distinct faulting events (M_w 6.3, M_w 5.8, and M_w 5.5) and their aftershocks (including one with M_w 5.5) that occurred over a period of 11 days. All three of these earthquakes had predominantly strike-slip motion. The mainshock (M_w 6.3) occurred in the hanging wall block of the White Mountains fault zone and was the largest earthquake in the Central Nevada Seismic Belt since the 1954 Fairview Peak-Dixie Valley earthquakes.

The primary characteristic of the sequence is the conjugate fault geometry with left-lateral slip for the initial M_w 5.8 event, followed 24 hours later by right-lateral slip during the mainshock (Savage and Gross 1995, p. 629). Mainshock rupture extended for 12 to 15 km (7 to 9 mi.) on a northwest-striking, southwest-dipping (55°) fault plane. Surface fracturing in the Volcanic Tablelands area was confined to the hanging wall of the mainshock fault plane. A peak horizontal acceleration of about 0.46 g was recorded at a sediment site on an alluvial fan about 12 km (7 mi.) northeast of the mainshock epicenter.

The Chalfant sequence produced surface ruptures along the White Mountains fault zone and within the Tablelands fault system west of the White Mountains. Surface ruptures along the White Mountains fault zone extended for 12 ± 2 km (7 ± 1 mi.), whereas cracks and open fissures in loose sand along preexisting faults in the Tablelands fault system were widely scattered, discontinuous, and occurred in a broad zone as much as 26 km (16 mi.) in length. Surface ruptures along the White Mountains fault zone have right-lateral displacements with a maximum single-trace displacement of 5 cm (2 in.). The total right-lateral displacement across the zone in the same area is about 11 cm (4 in.). Although extensive fracturing occurred at the surface along mapped Holocene faults in the Volcanic Tablelands area, it is uncertain whether any of this is primary rupture. Lienkaemper et al. (1987, p. 297) concluded that faulting along

displacement of 4.6 m (15.1 ft). Both the Phillips Wash and Fairview faults have displacements that are eastside down, whereas the West Gate, Gold King, and Louderback faults exhibit westside down displacements. Normal-right-oblique slip occurs along portions of the Louderback Mountains and West Gate faults, whereas the Gold King fault shows dominantly normal slip and the Phillips Wash fault exhibits normal-left-oblique slip. The average surface displacement over the entire zone is estimated to be 1.0 m (3.3 ft). The normal-oblique-slip observed for this event may represent a transition zone between right-lateral displacements in the south (e.g., 1872 Owens Valley and 1932 Cedar Mountain earthquakes) and the normal faulting in the north (e.g., 1954 Dixie Valley event). The slip vector of the Fairview Peak event differs from the mostly normal slip recorded in earlier Quaternary deposits.

1954 Dixie Valley Earthquake—The 1954 M_w 6.8 Dixie Valley earthquake ruptured the northern portion of the 100-km-long (62-mi.-long) zone of surface faulting produced by the Fairview Peak-Dixie Valley earthquake sequence (Figure 12.3-3). Surface faulting from the Dixie Valley earthquake formed a 46-km-long (29-mi.-long) zone, which at the southern end lies parallel to the surface faulting from the Fairview Peak earthquake along the opposite side of the valley. Displacements related to the Dixie Valley earthquake are normal, down to the east, with a maximum vertical displacement of 2.8 m (9.2 ft) and an average surface displacement of 92 cm (36 in.). Caskey et al. (1996, p. 775) determined that the fault dips at relatively low angles of 25° to 35° E near the surface, but the nodal plane of the focal mechanism of Doser (1986, p. 12,583) indicates that the fault dips $60^\circ \pm 20^\circ$ E at seismogenic depths. Reported geologic effects included spring flow changes, water fountains, liquefaction, landslides, rockfalls, mudflows, and fractures in alluvium (Caskey et al. 1996, pp. 772 to 773; Slemmons 1957, p. 353).

1975 Galway Lake, California, Earthquake—The M_w 5.2 Galway Lake earthquake (Figure 12.3-3) produced surface faulting along a 6.8-km-long (4.2-mi.-long) section of the Galway Lake fault zone (Hill, R.L. and Beeby 1977, pp. 1379 to 1382). Surface ruptures are expressed primarily as left-stepping en echelon fractures, shattered ground, and mole tracks. The surface-rupture zones range in width from 1 to 100 m (3 to 330 ft). Displacements were mostly right-lateral, generally between 0.2 and 0.5 cm (0.08 and 0.20 in.) with a maximum single-trace displacement of 1.5 cm (0.6 in.). Rare vertical separations between 0.5 and 1 cm (0.2 and 0.4 in.) lack a consistent sense of displacement. Reported geologic effects included downslope mass movement of rocks in the epicentral area.

1979 Homestead Valley, California, Earthquake—The M_w 5.5 Homestead Valley earthquake (Figure 12.3-3) produced a 3.25-km-long (2.01-mi.-long) zone of surface ruptures, discontinuous left-stepping en echelon cracks, and mole tracks (Hill, R.L. et al. 1980, pp. 62 to 65, 67). Displacements were mostly right-lateral, with a subordinate dip-slip displacement, and down to the east. A maximum right-lateral single-trace displacement of 7.5 cm (3.0 in.) was observed along the northern half of the primary rupture zone, and a maximum vertical displacement of 4 cm (1.6 in.) was observed in the southern part of the rupture zone. Other reported effects included rockfalls and slumping along stream channels.

1980 Mammoth Lakes Earthquake Sequence—The 1980 sequence of four earthquakes of M_L greater than 6 produced surface faulting along small faults in the Long Valley caldera and along the Hilton Creek fault, a Sierra Nevada frontal fault system (Clark et al. 1982; Hill, D.P., et al.

the White Mountains zone was associated with the mainshock, whereas dePolo and Ramelli (1987, p. 295) concluded that surface faulting was probably sympathetic slip. Reported effects included small landslides and numerous small rockfalls that occurred within the epicentral area.

1992 Landers, California, Earthquake—The June 28, 1992, M_w 7.3 Landers earthquake produced 85 km (53 mi.) of surface ruptures distributed over five major faults and several minor faults (Sieh et al. 1993, pp. 171 to 173) (Figure 12.3-3). Rupture occurred over portions of five principal faults (Johnson Valley, Landers, Homestead Valley, Emerson, and Camp Rock) connected by a series of right-steps. Displacements are mostly right-lateral, with a maximum displacement of 6.1 m (20 ft). The maximum vertical slip was 1.0 m (3.3 ft) or more, and left-lateral displacements of up to 50 cm (20 in.) occurred mostly along east-trending faults. Geologic effects included widespread rockfalls and ground fissuring.

Dreger (1994, p. 713) modeled the mainshock rupture at long periods and interpreted the source to consist of two subevents of seismic moments 2×10^{26} and 6×10^{26} dyne-cm. Rupture directivity effects were one of the more important aspects of the Landers event and most likely contributed to the triggering of seismicity, including the Little Skull Mountain earthquake to the north (Bodin and Gomberg 1994, p. 835).

1993 Eureka Valley, California, Earthquake Sequence—The 1993 M_w 6.1 Eureka Valley earthquake produced extensive cracking and minor surface ruptures on faults of the Eureka Valley (Figure 12.3-3). Satellite interferometry data analyzed by Peltzer and Rosen (1995, p. 1335) showed a maximum displacement of 3 cm (1.2 in.) in the southeast part of the epicentral region. Surface ruptures along west-dipping faults were mostly discontinuous cracks that extended 4 to 5 km (2 to 3 mi.), with vertical displacement of up to 2 cm (0.8 in.) over about 100 m (330 ft).

The Eureka Valley earthquake occurred on a northeast-striking ($N10^\circ E$), west-dipping ($43^\circ \pm 5^\circ W$) normal fault. The Eureka Valley mainshock hypocenter was constrained to an 11.8-km (7.3-mi.) depth, nearly identical to the Little Skull Mountain earthquake. The aftershock zone for the Eureka Valley earthquake extended approximately 20 km (12 mi.), whereas the Little Skull Mountain aftershock zone extended only about 10 km (6 mi.), suggesting either a low stress drop for the mainshock or initiation of activity on faults near the source area.

1999 Hector Mine, California, Earthquake—On October 16, a M_w 7.1 earthquake struck the Mojave Desert about 20 km (12 mi.) northeast of the 1992 Landers event. Both events occurred within the Eastern California Shear Zone. Very little damage occurred due to the remote location of the earthquake. The event was the result of right-lateral strike-slip faulting along the Bullion fault and the newly named Lavic Lake fault (Jones 2000). Surface faulting extended for a total distance of 45 km (28 mi.) with average and maximum displacements of nearly 3 and 5.2 m (10 and 17 ft), respectively (Jones 2000).

12.3.3.4 Areas of Significant Seismicity

In this section, specific areas of significant seismicity within the 300-km (186-mi.) Yucca Mountain region are discussed.

Coso Volcanic Field and Ridgecrest, California, Area—The Ridgecrest, California, area and the Coso volcanic field north of Ridgecrest have been the locations of a series of M_L 4.9 and greater earthquakes and extended aftershock sequences beginning in 1994 and ongoing small-magnitude seismicity in the Coso volcanic field. Earthquake sequences in the Ridgecrest area occurred in 1938, 1961, and 1982 (Roquemore et al. 1996, p. 106). The 1982 sequence produced cracking along the Little Lake fault zone, which lies east of the Airport Lake fault zone.

A M_d 5.3 earthquake on August 17, 1995, produced a less than 1-km-long (0.6-mi.-long) zone of discontinuous surface cracking along a fault trace that ruptured again in a M_d 5.4 event on September 20, 1995 (Figure 12.3-5). The September 20, 1995, earthquake produced surface faulting along 2.5 km (1.5 mi.) of the Airport Lake fault zone, expressed mostly as left-stepping en echelon fractures and scarps with a maximum vertical displacement of 1 cm (0.4 in.) and a maximum right-lateral displacement of 0.8 cm (0.3 in.) (Hauksson et al. 1995, p. 58).

Garlock Fault, Southern Sierra Nevada, Southeastern California—The trace of the Garlock fault in southeastern California is outlined by concentrated zones of seismicity and microseismicity (Figure 12.3-5). It includes the northeastern extent of mainshock rupture and aftershock activity of the 1952 M_w 7.5 Kern County, California, earthquake, which was the result of rupture on the White Wolf fault (Ellsworth 1990, p. 163) (Figure 12.3-3). The Kern County earthquake, however, triggered slip on sections of the Garlock fault, and nearby moderate- to large-magnitude events are sometimes associated with increased levels of seismicity on creeping segments of the fault.

Mammoth Lakes-Chalfant Valley-Bishop, California—The Mammoth Lakes, California, volcanic area, within and adjacent to the Long Valley caldera, has been the location of a series (1940 to present) of moderate-sized (M_L 5 to 6) earthquakes, aftershock sequences, and volcanic-related earthquake swarms (Hill, D.P., et al. 1985, p. 575, Figure 4) (Section 12.3.3.3) (Figure 12.3-3). Several middle Pleistocene and more recent eruptions (approximately 750 ka) of the Long Valley caldera since the late Pleistocene shaped the physiography of the Mammoth Lakes-Chalfant Valley-Bishop, California, area (Bailey and Koeppen 1977). Foreshock-mainshock-aftershock sequences (mainshocks of M_L greater than 6) in the caldera and volcanic earthquake swarms in and adjacent to the caldera have numbered in the tens of thousands from 1980 to the present (Hill, D.P. et al. 1990, pp. 328, 330 to 333).

A recent series of moderate-sized earthquakes began in October 1978 and culminated with four M_L greater than 6 earthquakes during a 48-hour period from May 25 to May 27, 1980 (Section 12.3.3.3). The activity continued with the 1984 M_w 5.8 Round Valley and 1986 M_w 6.3 Chalfant earthquakes (Priestley et al. 1988, p. 216; Smith, K.D. and Priestley 1988, p. 172) (Section 12.3.3.3). Swarm-like earthquake activity and occasional tremor activity around the caldera were accompanied by inflation of a resurgent dome (Savage and Clark 1982, pp. 531 to 533; Cockerham and Pitt 1984, p. 503).

An earthquake swarm under Mammoth Mountain near the town of Mammoth Lakes in 1989 included a number of deep, low-frequency earthquakes. These and other earthquakes in the Mammoth Lakes area may have been associated with magma movement (Julian and Sipken 1985, pp. 11, 168; Pitt and Hill 1994, p. 1682). The recent series of moderate-sized earthquakes

show strike-slip motion, but dominantly normal offsets occur on Holocene faults that bound the Sierra Nevada and White Mountains.

Mojave Desert—The Mojave Desert, approximately 150 to 200 km (93 to 124 mi.) south of Yucca Mountain, contains several zones of persistent seismicity (Figure 12.3-5). The 1992 M_w 7.3 Landers earthquake was the largest surface-faulting event observed in the region (Section 12.3.3.3). The Landers earthquake occurred in the southern Mojave Desert, where broad zones of right-lateral and minor normal faults splay northward from the San Andreas, distributing 8 to 10 mm/yr. (0.3 to 0.4 in./yr.) of right-lateral motion along the Eastern California shear zone (Savage et al. 1990, p. 2115). In comparison to the Basin and Range Province, seismicity in the Mojave Desert region is shallower, with more surface-faulting events and predominantly strike-slip motion. Other notable events previously described include the 1947 Manix, 1975 Galway Lake, and 1979 Homestead Valley earthquakes (Section 12.3.3.3 and Figure 12.3-3).

Mono Lake-Excelsior Mountains Area—Faults in the Excelsior-Mono domain (Stewart 1988) could be analogous to the structural domain of the northeast-striking Rock Valley, Wahmonie, Cane Springs, and Mine Mountain fault systems in the south-central Nevada Test Site area. These domains disrupt the north-northwest-striking grain of the Walker Lane. Faults near Excelsior Mountains and in the Nevada Test Site region are zones of persistent seismicity (Figure 12.3-5) and may represent structural transition zones fundamental to the processes of strain accommodation within the Walker Lane belt.

Nevada-Utah-Arizona Borders Area—The 1966 M_L 5.5 to 6.1 Clover Mountains earthquake occurred near the Nevada-Utah-Arizona borders and was marked by an extended aftershock sequence (Boucher et al. 1967; Beck, P. 1970) (Figure 12.3-3). T.C. Wallace et al. (1983, p. 594) determined a nearly pure strike-slip mechanism for the mainshock from regional records, consistent with the short-period mechanism of Boucher et al. (1967, p. 205). No surface rupture was reported. The local structural grain is characterized by east-west-striking faults, which are not consistent with the right-lateral strike-slip mechanism for the mainshock.

The 1902 M_L 6.0 Pine Valley and 1992 M_L 5.9 St. George earthquakes occurred east of the Clover Mountain sequence in Utah (Figure 12.3-3). This area is of generally low seismicity and the moderate- and larger-sized earthquakes are associated with the Colorado Plateau-Basin and Range transition zone.

Northern Amargosa Valley-Sarcobatus Flat—Seismicity in the Northern Amargosa Valley is distributed in the vicinity of Beatty and the Bullfrog Hills (Figure 12.3-4), some of which may be related to mining. In Sarcobatus Flat, earthquakes have occurred in four clusters since the beginning of instrumental monitoring (Rogers et al. 1987, p. 43). These clusters, which lie 10 to 20 km (6 to 12 mi.) apart, trend north along the length of the valley. Focal mechanisms for the three southern clusters suggest right-lateral slip along northeast-trending structures. These mechanisms are anomalous with respect to general trends observed in the southern Great Basin (Figure 12.3-6) and represent local variability in the tectonic stress field. The fourth cluster, in the northern part of the valley, shows normal faulting on a northeast-trending fault (Rogers et al. 1987, p. 47).

Northern Death Valley Area—Seismicity associated with the Furnace Creek fault zone in Northern Death Valley is distributed over a much larger area than the mapped surface traces of the faults (Figure 12.3-5). Earthquakes extend northeast from the northern end of the Furnace Creek fault through the Gold Mountain-Mount Dunfee region. The largest recent event in this area was an M_L 4 earthquake at Gold Mountain. The focal mechanism for this event shows left-lateral slip. In 1983, a northeast-trending cluster of events occurred near Gold Mountain. A composite focal mechanism for these earthquakes suggests left-oblique normal faulting on a northeast-striking plane (Rogers et al. 1987, p. 44).

Northern Nevada Test Site—The northern region of the Nevada Test Site includes the Timber Mountain caldera, Pahute Mesa, Rainier Mesa, and Yucca Flat. These areas experienced considerable earthquake activity associated with nuclear testing, in contrast to seismicity that is tectonic in origin in the southern part of the Nevada Test Site (Figure 12.3-4). Discriminating naturally occurring earthquake activity from events associated with underground nuclear explosions is problematic (Section 12.3.6.1). The relative number of artificial and induced earthquakes in the testing areas (Vortman 1991, Appendix T) suggests that the natural seismicity of the region is close to the background activity of the southern Basin and Range Province. In 1979 and 1983, several swarms of microearthquakes occurred in the region, apparently unrelated to the underground nuclear explosions. Two sequences occurred during the period of active testing in the vicinity of Dome Mountain and Thirsty Canyon (Rogers et al. 1981; Rogers et al. 1987, p. 40). Focal mechanisms indicate mainly right-lateral strike-slip faulting on north-trending structures and normal faulting on northeast-trending structures.

Pahranagat Shear Zone Area—The Pahranagat shear zone, located between the 1966 Clover Mountains sequence area and the northern Nevada Test Site (Figure 12.3-5), has been a constant source of M 3 to 4 earthquakes over the recent period of seismic monitoring. This level of seismicity appears to be characteristic of active northeast-striking faults or structural zones within the Basin and Range Province. High-angle, strike-slip focal mechanisms are consistently reported in this region. The Clover Mountains, St. George, and Pine Valley earthquakes and the Pahranagat shear zone activity constitute most of the events located within the eastern half of the Southern Nevada Seismic Belt of the southern Great Basin (Rogers et al. 1991, p. 154).

12.3.4 General Features of the Instrumental Seismicity in the Southern Great Basin

The more recent instrumentally recorded seismicity in the southern Great Basin is generally expressed as clusters of earthquakes distributed in an east-west belt between latitudes 36° and 38°N , referred to here as the Southern Nevada Seismic Belt (Figure 12.3-5). The earthquake clusters are diffusely distributed around mapped faults, covering areas larger than the surface projections of the rupture. Most events are not readily associated with the surface traces of known faults. These clusters may align with local structural grain, and composite and single event focal mechanisms (see below) suggest that the P- and T-axes planes correlate with regional stress directions inferred from other data.

The comparison of the energy release maps for the pre-1978 and post-1978 periods show that, averaged over decades, the seismically active zones appear to be releasing moment at about the same rates. Rogers et al. (1991, p. 165) show that the historical rate of occurrence of the largest earthquakes (M_w greater than 7) in the Central Nevada Seismic Belt west and northwest of Yucca

Mountain is larger by an order of magnitude than that indicated by geologic evidence. R.E. Wallace (1987, p. 868) noted evidence in the western Basin and Range Province of active periods lasting hundreds to thousands of years followed by quiescent periods of 10 to 30 k.y. For a larger region but shorter time scale, Bufe and Topozada (1981, p. 111) described a period of relative quiescence encompassing both California and western Nevada and extending from 1960 to 1980. The current active period for M less than 6 also encompasses the same large region, as characterized by Bufe (1992, p. 373).

12.3.4.1 Seismogenic Depths

Earthquakes in the southern Great Basin occur predominantly between depths of 2 and 15 km (1 and 9 mi.), as illustrated on Figure 12.3-7. The histogram is dominated by the 1992 Little Skull Mountain sequence, which now constitutes 20 to 30 percent of the seismicity catalog for the southern Great Basin in the Nevada Test Site area. The Little Skull Mountain sequence occurred mainly between depths of 5 and 12 km (3 and 7 mi.), and the distribution peaks near the lower portion of the seismogenic zone. The sequence was well recorded and depth constraints were very good. Rogers et al. (1987, pp. 55 to 56) showed that the seismicity in the southern Great Basin is distributed between about 2 and 15 km (1 and 9 mi.). In contrast, the 1993 Rock Valley sequence occurred at depths less than 3 km (2 mi.), as determined using near-source (less than one focal depth) three-component digital recorders in the immediate epicentral area (Shields et al. 1995, p. F426).

Rogers et al. (1987, p. 61) showed that most of the seismic energy released in the southern Great Basin occurs at depths less than 12 km (7 mi.), but this study represents a very short period of time (1982 to 1983) with minimal moment release. Several larger magnitude earthquakes have been reported to nucleate deeper than 15 km (9 mi.), although these events occurred early in the instrumental record; therefore, the focal depths may not be well constrained (Doser and Smith 1989, pp. 1394, 1397). Nucleation depths ranging from 10 to 20 km (6 to 12 mi.) have been determined from waveform modeling for several major mainshock earthquakes in the Basin and Range Province, including the 1954 Dixie Valley earthquake; the 1959 Hebgen Lake, Montana, earthquake; and the 1983 Borah Peak, Idaho, earthquake. All three of these earthquakes are associated with surface faulting on range-bounding normal faults (Doser and Smith 1989, p. 1388). Critical to the estimation of maximum moment from a particular structure is whether rupture can propagate to these depths, which would not necessarily correspond to hypocentral depth.

Earthquakes in the southern Great Basin also tend to distribute in vertical tubular-shaped clusters rather than along planar fault zones. Rogers et al. (1987, p. 77) interpreted this distribution of hypocenters to be activity at the intersections of faults. These vertically distributed localized clusters of seismicity occur between depths of 10 and 15 km (6 and 9 mi.).

12.3.4.2 Focal Mechanisms

Focal mechanisms of earthquakes of M_L greater than 3.5 within the southern Great Basin from 1987 to 1997 are shown on Figure 12.3-6. These mechanisms, plus others and hypocentral alignments, indicate that right-lateral slip on northerly-trending faults is today the predominant mode of stress release near the site. However, faulting on east-northeast (left-lateral) and

northeast (normal) faults has been observed, as well as oblique slip on structures of intermediate orientation with the appropriate dip angles (Figure 12.3-6). Geologic evidence of fault movement at Yucca Mountain reflects multiple tectonic episodes of faulting over millions of years and under the influence of different stress regimes (Sections 4.3.3.1 and 4.6.3), and, thus, is not always consistent with these contemporary observations. The principal extensional (minimum compression) stress axes inferred from earthquake mechanisms trend northwest and plunge approximately horizontal (Figure 12.3-8). The principal compressional (maximum compression) stress axes from earthquake mechanisms are concentrated along a belt (girdle) that sweeps from vertical (normal faulting) to northeast and horizontal (strike-slip faulting) (Figure 12.3-8). Thus, regional stress orientations indicate north-south and east-west orientations for high-angle fault planes, with right-lateral slip on the north-striking and left-lateral slip on the east-west striking surfaces. Normal and oblique slips are indicated on fault surfaces with orientations intermediate to these directions. The style of faulting determined from the focal mechanisms is not a function of depth.

Harmsen and Rogers (1986) analyzed the stress field from a set of regional earthquake focal mechanisms. The presence of both strike-slip and dip-slip mechanisms in particular localities was interpreted to indicate an axially symmetric stress field, in which the intermediate and maximum compressive stresses are nearly equal (Harmsen and Rogers 1986, p. 1560). They suggested that because no large earthquakes were present in the data set, movement along a variety of fault plane orientations was accommodated by an ample number of small preferably oriented faults. Rogers et al. (1987, pp. 60 to 70), Rogers et al. (1991), and Bellier and Zoback (1995) also discuss and analyze the modern stress field in regions of Nevada near Yucca Mountain.

12.3.5 Seismicity in the Vicinity of Yucca Mountain

The southern portion of the Nevada Test Site, southeast of Yucca Mountain, is one of the more seismically active regions in the southern Great Basin (Figure 12.3-4). Most of the seismicity in this region, including the 1992 M_L 5.6 Little Skull Mountain earthquake, is concentrated around the Rock Valley, Mine Mountain, and Cane Springs fault zones, and around the southern boundary of the Timber Mountain caldera (Figure 12.3-9). Some of the activity near the eastern Nevada Test Site boundary, particularly the 1971 Massachusetts Mountain earthquake and 1973 Ranger Mountain swarms (Figure 12.3-4), may have been triggered following the initiation of testing in the Yucca Flat area, but considerable numbers of small to moderate earthquakes are related to natural tectonic strain release (Gomberg 1991a, Figure 10; 1991b).

A wide, northeast-trending zone of seismicity centers on the Rock Valley fault zone. This area includes the 1971 M_L 4.6 Massachusetts Mountain earthquake, the 1973 Ranger Mountain sequence, the 1992 M_L 5.6 Little Skull Mountain earthquake, the 1993 Rock Valley sequence, and other earthquake clusters (Harmsen 1993, 1994a, 1994b; Meremonte et al. 1995; Shields et al. 1995) (Figure 12.3-4). Seismicity in the Rock Valley zone extends along the Mine Mountain system and to the south, subparallel to the South Specter Range fault (R.E. Anderson, Bucknam et al. 1995).

Earthquakes within the immediate vicinity (20 km [12 mi.]) of Yucca Mountain are shown on Figure 12.3-9. In this area, as elsewhere in the Great Basin, little correlation exists between the

distribution of epicenters and Quaternary faults. The earthquakes have focal depths ranging from near-surface to 5 to 12 km (3 to 7 mi.). Focal mechanisms of earthquakes near Yucca Mountain are strike-slip to normal oblique-slip along moderately to steeply dipping fault planes (Figure 12.3-9). The nodal planes are consistent with right-lateral faulting on north- to north-northwest-striking planes or normal left oblique-slip on northeast- to east-striking faults, and are similar to regional focal mechanisms (Rogers et al. 1987, p. 91).

Two M 3.5 earthquakes in 1948, which were initially reported as being at Yucca Mountain, were reevaluated by von Seggern and Brune (1994, pp. 16 to 20). The initial locations of these two events were constrained by first motion data at California seismic stations. The waveforms and S minus P times at the regional stations operating in 1948 were more consistent with a source near the Rock Valley fault zone rather than at Yucca Mountain. By a comparison of waveforms from Little Skull Mountain aftershocks and heliocorder records from the California Institute of Technology station for a well-located 1948 Rock Valley area event, they concluded that the two 1948 events most likely occurred in the Rock Valley area and not at Yucca Mountain. The 1948 events were most likely part of one localized earthquake sequence in the Rock Valley area. S. Gross and Jaumé (1995, pp. 77 to 78) also analyzed a number of small events that were in the historical catalog and reported to be in the Yucca Mountain block from 1978 to 1992 by reviewing the archived waveform data. They noted that some of the events were incorrectly identified as earthquakes and included a list of them in their report.

Brune et al. (1992, p. 164) and Gomberg (1991a, pp. 16411 to 16412, 1991b, pp. 16397 to 16398) showed that the Yucca Mountain zone of quiescence is a real feature of the seismicity and not an artifact of network design or detection capability. An experiment in high-resolution monitoring of seismicity at the potential site by Brune et al. (1992) also confirmed the existence of the quiescent zone. Modeling of the strain field in southern Nevada by Gomberg (1991b, pp. 16396 to 16397) suggests that this area is not accumulating significant strain, and that Yucca Mountain is an isolated block within the structural framework of the southern Great Basin. Other than the 1992 Little Skull Mountain event, the largest earthquake near Yucca Mountain after the inception of the Southern Great Basin Seismic Network in 1978 was an M_L 2.1 event, which occurred on November 18, 1988, and was located 12 km north-northwest of the potential repository at a depth of 11 km (Harmsen and Bufe 1992).

Paleoseismic events on a number of faults at Yucca Mountain (Section 12.3.7) have very long return times, and strain may accumulate for a long time between large surface-rupture earthquakes on the faults. Little or no microseismicity may occur on the faults during this long strain buildup. Many faults in the Great Basin with paleoseismic evidence for prehistoric surface-rupture earthquakes have little or no associated historical seismicity.

12.3.5.1 The 1992 Little Skull Mountain Sequence

The largest and most significant earthquake recorded by the Southern Great Basin Seismic Network since its establishment in 1978 was the June 29, 1992, M_L 5.6 Little Skull Mountain earthquake (Lum and Honda 1992; Harmsen 1994b; Walter 1993; Meremonte et al. 1995) (Figures 12.3-4 and 12.3-9). This event produced a horizontal ground acceleration of 0.21 g at Lathrop Wells about 11 km (7 mi.) from the epicenter. The earthquake caused minor damage to the Yucca Mountain Field Operations Center in Jackass Flat, which was located on the surface

projection of the buried fault. The event was felt throughout the region. The earthquake appears to have been triggered by the 1992 Landers event that occurred approximately 20 hours earlier (Section 12.3.6.2).

The Little Skull Mountain earthquake initiated at a depth of 11.7 km (7.3 mi.), and the rupture was confined between depths of 5 and 12 km (3 and 7 mi.). Fault rupture propagated unilaterally from southwest to northeast for about 6 km (4 mi.), and the epicenter of the mainshock plots was near the southwestern end of the aftershock zone. There was no evidence of primary or secondary surface rupture. Rockfalls along the south-facing cliffs of Little Skull Mountain were observed shortly after the earthquake. The distribution of rockfalls was found to be consistent with the ground shaking predicted from the source model and provided a means of calibrating the distribution of ground shaking in the epicentral region (Brune, J.N. and Smith 1996, p. A193). The earthquake occurred on a northeast-striking fault plane dipping steeply to the southeast (Harmsen 1994b, p. 1485; Meremonte et al. 1995, p. 1039) and involved normal slip with a small left-slip component. Table 12.3-6 is a compilation of short-period and waveform-based focal mechanisms and reported seismic moments for the Little Skull Mountain earthquake.

Three aftershocks of M_L greater than 4 occurred, not on the mainshock fault plane but on adjacent off-fault structures accommodating the stress change from mainshock rupture. These events also triggered stations of the Blume and Associates strong motion network in Las Vegas. The first M_L 4 aftershock occurred in the coda of the mainshock and the location could only be constrained to be east of the mainshock epicenter. Focal mechanisms for two of the four M_L 4+ events show northeast-trending, southeast-dipping fault plane solutions.

The Little Skull Mountain earthquake could not be correlated with any mapped faults, although the aftershocks coincide with the projections of the Wahmonie, Cane Springs, and Mine Mountain fault systems into the Rock Valley fault zone. Dip angles determined for the mainshock fault plane from the short-period focal mechanisms vary from 65° , consistent with the early aftershock activity, to 56° (Harmsen 1994b, p. 1485). The dip of structures in the Little Skull Mountain area has implications for the orientation of faults at depth in the Yucca Mountain site area.

The Little Skull Mountain earthquake occurred in an area of persistent recent seismicity, present throughout the recording period of the Southern Great Basin Seismic Network (Figure 12.3-9). This area may be a zone of stress concentration, accommodating strain from fault systems throughout the south-central Nevada Test Site area. The Rock Valley fault zone is the primary Quaternary fault system in this group and has the most associated seismicity. The Little Skull Mountain mainshock locates directly along the crest of Little Skull Mountain, or at hypocentral depth at the base of the seismogenic zone potentially near an intersection with the Rock Valley fault system.

The sequence was recorded on a number of portable digital seismographs deployed in the epicentral area by the USGS (Meremonte et al. 1993) and the University of Nevada, Reno (Sheehan et al. 1994). These data were used to develop high-quality locations for the special aftershock studies and contributed to ground motion modeling in the probabilistic seismic hazard analyses project (Wong and Stepp 1998) (Section 12.3.10).

12.3.5.2 Earthquakes in the Rock Valley Area

Following the Little Skull Mountain earthquake, earthquake activity in the southern Rock Valley fault zone increased (Smith, K.D. et al. 1996, p. A193; Shields et al. 1995, p. F426). Only two M 3+ earthquakes were included in the Southern Great Basin Seismic Network earthquake catalog from 1979 until the Little Skull Mountain sequence. Since the Little Skull Mountain earthquake, three M 3.5+ earthquakes and the sequence of very shallow, small-magnitude (M_d less than or equal to 3.8) earthquakes occurred in southern Rock Valley in mid-1993. This activity is diminishing, suggesting that the Little Skull Mountain event may have in part triggered the increased Rock Valley activity (Smith, K.D. et al. 1996, p. A193).

The shallow sequence of earthquakes in 1993 was recorded on a near-source portable digital instrument. This station recorded more than 500 earthquakes, of which only 140 triggered the regional seismic network and could be located. S minus P times for the events averaged about 0.5 s at this station, and relocations of the earthquakes place them at a depth of only about 2 km (1 mi.). The largest event of the sequence (M_d 3.8) also occurred at a 2-km (1-mi.) depth. Stress drops were on the order of 10 bars (1 MPa) for all of the larger events. A cluster of earthquake activity also occurred southeast of the Rock Valley fault zone in the Spotted Range in late 1993. This cluster of seismicity was the most active in the region east of the Nevada Test Site since the 1973 Ranger Mountain sequence, but was confined to a small volume and included only one earthquake greater than M 3.

12.3.5.3 1995 to 1999 Microearthquakes at Yucca Mountain

From May 1995 through March 1999, 28 microearthquakes have occurred generally within 10 km (6 mi.) of the Yucca Mountain block (Table 12.3-7). These earthquakes triggered at least three stations of the three-component digital network, and three of them were large enough to trigger the older, less sensitive analog net. The events ranged from M about -1 to 1 in size. These microearthquakes occurred throughout the Yucca Mountain block, and all had focal depths between 5 and 10 km (3 and 6 mi.). Short-period focal mechanisms were determined for four of the earthquakes. Although not enough information from the focal mechanism data was available to unequivocally correlate the earthquakes with specific mapped faults, the solutions are consistent with normal to normal-oblique-slip on faults with orientations similar to several Quaternary faults mapped at the surface. Although small earthquakes (M less than 1) were occurring at the rate of about one per month from 1995 to 1996, as of March 1997, none had been observed directly within the Yucca Mountain block since August 12, 1996 (Table 12.3-7), suggesting that the restricted time period of the sequence is not strictly a function of the installation and detection threshold of the digital network at the site.

12.3.5.4 The 1999 Frenchman Flat Earthquake Sequence

The January 27, 1999, M_w 4.7 Frenchman Flat earthquake was the largest event within the Nevada Test Site since the M_L 5.6 Little Skull Mountain earthquake in 1992. Both events are located near the Rock Valley fault zone, but the distribution of aftershocks and focal mechanisms indicate that the Rock Valley fault system was not involved in either event (Smith, K. 2000). The Little Skull Mountain earthquake occurred near the western end of Rock Valley; the Frenchman Flat event took place at its eastern end where the Rock Valley fault zone appears to

terminate into the basin at Frenchmen Flat. The Frenchman Flat mainshock was preceded by an extended foreshock sequence that included a M_L 4.2 earthquake. Portable instrumentation installed in the aftershock zone shortly after the mainshock recorded the early aftershock period; aftershock locations constrained with portable instrument phase data are shown in Figure 12.3-10. The mainshock appears to have resulted from normal slip on a northeast-striking fault (Smith, K. 2000).

12.3.5.5 The 1999 Scotty's Junction Earthquake Sequence

The M_L 5.7 Scotty's Junction earthquake occurred on August 1, 1999, about 11 km (7 mi.) north of Scotty's Junction, Nevada. The earthquake involved primarily normal faulting on a moderately dipping, north-northeast-striking fault plane (Smith, K. 2000). The aftershock distribution (Figure 12.3-11) shows a slight alignment with the Sarcobatus Flat fault (Section 12.3.7.8) bordering the volcanic tuffs to the east of the mainshock. Mainshock depth is estimated to be at about 7 km (4 mi.), although permanent station coverage in the epicentral area is poor. The mainshock was preceded by a foreshock sequence that included 13 events with M_L greater than 2 beginning on July 31, 1999. Two aftershocks of M_L 4.8 and 4.9 occurred within the first two days after the mainshock (Smith, K. 2000).

12.3.6 Induced and Triggered Seismicity

Identification of induced events is necessary to properly evaluate the distribution, characteristics, and recurrence of natural tectonic seismicity for the probabilistic seismic hazard analyses. Seismological analyses by the USGS and University of Nevada, Reno routinely attempt to distinguish between the natural tectonic seismicity of the region and seismicity induced by human activities, including underground nuclear explosions, their collapses and aftershocks, Ochemical explosions associated with testing and mining activity, and seismicity associated with the filling and subsequent level changes of Lake Mead.

At least one event, the 1992 Little Skull Mountain earthquake, appears to have been triggered by seismic waves from a large distant earthquake. This type of earthquake triggering has implications for the failure condition of faults in the area. Chemical blasting may have triggered seismicity in the Bullfrog Hills west of the Bare Mountain fault and in various mining sites around the region. The Nevada Test Site is the site of nuclear testing, and the level of seismic activity may reflect tectonic release following the underground nuclear explosions. The area around Lake Mead has experienced high levels of microseismicity related to the filling of the reservoir behind Hoover Dam.

12.3.6.1 Earthquakes Triggered by Underground Nuclear Explosions

Large underground nuclear explosions (approximately 1 Mt) have been known to trigger release of natural tectonic strain (Wallace, T.C. et al. 1983, 1985). Future testing could induce displacements on faults in the Yucca Mountain site vicinity, but little coseismic release and related effects have been observed beyond about 15 km (9 mi.) from even the largest nuclear blasts (1 Mt). The underground nuclear explosion testing area closest to Yucca Mountain is the Buckboard area, approximately 25 km (16 mi.) to the northeast. Future underground nuclear

explosions would probably not be close enough to trigger seismicity on local faults at Yucca Mountain.

Vortman (1991) proposed that small-magnitude earthquakes are mainly induced by dynamic stresses associated with seismic energy generated during the explosion or seem to be due to the altered static stress field resulting from the explosion. That is, some events are triggered by the arrival of the underground nuclear explosion phase; others appear to be responding to changes in an altered stress field caused by the explosion. An underground nuclear explosion may cause a stress change of several bars, a fraction of the lithostatic stress in the hypocentral region. Some of the southern Great Basin may be in a state of critical stress in which a small perturbation in the load on a fault, such as underground nuclear explosion-induced stress changes, could cause the release of accumulated tectonic strain.

Portable instruments recorded about 2,500 earthquakes greater than M 2.0 from December 1968 through December 1970 and several other nuclear explosions following the Benham shot. R.M. Hamilton et al. (1971) reported that 94 percent of the events with well-constrained focal mechanisms were shallower than 5 km (3 mi.), but some events were as deep as 8 km (5 mi.). Focal mechanisms show normal slip on north- to northeast-striking fault planes, implying a down-to-the-west-northwest sense of motion for these earthquakes. Extensive aftershock sequences followed several underground nuclear explosions in the Pahute Mesa area from 1968 through 1970 (Hamilton, R.M. et al. 1971). These sequences were not confined to the shot locations, but were distributed along several mapped faults as far as 15 km (9 mi.) from the shot points. Aftershocks of underground nuclear explosions also occurred in the Yucca Flat and Rainier Mesa areas on the eastern Nevada Test Site, although they are not as numerous as the triggered earthquakes in the Pahute Mesa area. An increase in seismicity occurred in the 1970s following the initiation of underground testing in the southeastern Nevada Test Site south and east of Yucca Flat.

12.3.6.2 Lake Mead Area

Since 1936, Lake Mead, the reservoir impounded by Hoover Dam, has been the site of induced seismicity (Rogers and Lee 1976; Anderson, L.W. and O'Connell 1993). Microseismicity continues to the present day in the Colorado River area east of Las Vegas. A summary from L.W. Anderson and O'Connell (1993) follows.

The first felt earthquakes in the Lake Mead area occurred in 1936, 1 yr. after the filling of Lake Mead. No instrumentation was located at Lake Mead and no record of microseismicity in the area existed prior to 1936. Based on records of Lake Mead earthquakes at California Institute of Technology stations, magnitudes have been revised from those based on felt reports. Only one M_L 5 event occurred, although several M_L 4.9 events occurred. A special study (Rogers and Lee 1976) in 1973 using portable instruments resulted in the location of about 1,000 small earthquakes in the Lake Mead zone of seismicity. The largest events recorded were M_L 3. Hypocentral depth estimates were better constrained than in previous studies. Depths ranged from near the surface to 13 km (8 mi.), with most of the activity between depths of 2.5 and 9.5 km (1.6 and 5.9 mi.) and with a peak at about 5 km (3 mi.). Focal mechanisms from Rogers and Lee (1976, p. 1675) show a range of faulting styles, with a preference for strike-slip motion and northwest extension consistent with the regional stress field. A recalculation of the

recurrence relations by L.W. Anderson and O'Connell (1993, p. 70) using the Rogers and Lee (1976) magnitude estimates shows a b-value of 1.29 for the Lake Mead seismicity as compared to a b-value of 0.9 estimated from a regional (200 km [124 mi.]) declustered catalog. A swarm of five M greater than 3 earthquakes (main event M 3.7) in the Eldorado Mountains area near Henderson, Nevada, was also followed by the deployment of portable seismographs by the USGS. Focal mechanisms determined from that study also showed a range of normal, oblique, and strike-slip solutions consistent with the known regional extension direction.

12.3.6.3 Other Triggered Earthquakes

The triggering of aftershocks by underground nuclear explosions at the Nevada Test Site and the continued occurrence of induced seismicity near Lake Mead suggest that a number of faults in the southern Great Basin may be near failure. Evidence strongly suggests that the Little Skull Mountain earthquake was triggered by the Landers earthquake 225 km (140 mi.) to the south less than 24 hr. earlier. An increase in microearthquake activity in the vicinity of Yucca Mountain was observed beginning in the coda of the Landers event (Bodin and Gomberg 1994). The activity accelerated over the next 23 hr., culminating in the Little Skull Mountain mainshock, perhaps indicating that the Little Skull Mountain region was near failure and that the Landers earthquake hastened the time of rupture.

The Landers earthquake also apparently triggered smaller earthquakes in the western United States as far away as the Yellowstone caldera (Hill, D.P. et al. 1993). Following the Landers mainshock, Johnston et al. (1995) observed a transient strain change associated with an increase in seismicity at the Long Valley caldera. The occurrence of the Landers earthquake produced an unprecedented increase in seismicity in the Eastern California shear zone (Roquemore and Simila 1994) and in the Sierra Nevada-Great Basin boundary zone, prompting several studies of the possible triggering mechanisms. The specific mechanism involved remains uncertain, but the dynamic strain associated with the propagation of long-period surface waves from the Landers earthquake may have initiated a failure process involving fluids or sympathetic slip or creep (Hill, D.P. et al. 1993; Bodin and Gomberg 1994). Bodin and Gomberg (1994) proposed that dynamic stresses resulting from surface waves from the Landers earthquake initiated the Little Skull Mountain sequence, and Gomberg and Bodin (1994) have proposed a model in which static strain was propagated through interconnecting fault systems, ultimately triggering failure of the fault at Little Skull Mountain.

Perturbations in the timing of earthquakes as a result of tectonic or nontectonic triggers have no impact on probabilistic hazard estimates, which assume earthquakes behave in a Poissonian manner, but they may affect the timing of earthquakes where near-failure conditions exist. The earthquakes probably would occur at some later time, as evidence suggests that some faults in the southern Great Basin may be at a critical stress state, but the amount of time in which the failure process is accelerated is uncertain.

12.3.7 Prehistoric Earthquakes at Yucca Mountain

Prehistoric earthquake studies have been conducted to determine the magnitude and frequency of surface rupture on active faults in the Yucca Mountain area. These studies provided some of the information necessary for the seismic source characterization component of the probabilistic

seismic hazard analyses project for Yucca Mountain (Section 12.3.10). The seismic source models developed for the evaluation are fully described in Wong and Stepp (1998), whereas this section summarizes the prehistoric earthquake information considered in developing these models.

12.3.7.1 Prehistoric Earthquake Data

Investigations were conducted to identify faults in the Yucca Mountain area that have evidence of Quaternary displacements (Reheis 1991, 1992; Reheis and Noller 1991; Dohrenwend et al. 1991; Dohrenwend et al. 1992; Anderson, R.E., Bucknam et al. 1995; Anderson, R.E., Crone et al. 1995; Piety 1996). These studies were reconnaissance in nature, consisting of a combination of literature research, aerial photographic interpretation, and field traverses to evaluate offset geomorphic surfaces and fault scarps. These studies identified 105 faults with known or suspected Quaternary activity within a 100-km (60-mi.) radius of the potential repository site at Yucca Mountain (Figure 12.3-12). Summaries of each fault included in the probabilistic seismic hazard analyses (Wong and Stepp 1998) or considered relevant by Pezzopane (1996) are presented in Section 12.3.7.8.

Studies, including detailed field mapping, have also been conducted of faults at and near Yucca Mountain with known or suspected Quaternary activity (Faulds et al. 1994; Simonds et al. 1995; Whitney and Taylor 1996). This work identified the location and surface characteristics of the mapped faults and identified locations where Quaternary displacement is evident. Specific physiographic and structural evidence for Quaternary displacements was identified and mapped. Bedrock faults that lack evidence for Quaternary displacements also were mapped (Scott and Bonk 1984; Scott 1992).

Displaced or deformed alluvial and colluvial deposits record late Quaternary faulting along nine local faults in the Yucca Mountain area (Figure 12.3-13). These faults include, from west to east, the Northern Crater Flat, Southern Crater Flat, Windy Wash, Fatigue Wash, Solitario Canyon, Iron Ridge, Stagecoach Road, Bow Ridge, and Paintbrush Canyon faults. Estimates of several paleoseismic parameters for local site faults, including information on fault lengths, probable rupture lengths, and geometric relations between faults, are primarily based on the map compilation of Simonds et al. (1995).

The Quaternary faults at Yucca Mountain share common characteristics (see Section 4.6). They bound east-dipping fault blocks and displace bedrock down to the west; displacement is dominantly dip-slip, with varying amounts of left-oblique slip. Sections of some of the faults, particularly those on the west side of Yucca Mountain, are associated with piedmont fault scarps developed in basin-fill alluvium. Displacement generally increases to the south along each north-trending fault. Fault lengths (with evidence of Quaternary movement) range from less than 2 km to about 28 km (2 to about 17 mi.). The faults are closely spaced, with interfault distances on the order of 0.5 to 2 km (0.3 to 1.2 mi.) measured perpendicular to strike.

The faults at Yucca Mountain display anastomosing geometries in plan view (Figure 12.3-13). Numerous bifurcations and splays are indicated by the merging and branching of individual fault strands. These patterns indicate that many of the faults or fault splays are structurally interconnected along strike. The overall pattern suggests that the faults on the east and west

sides of Yucca Mountain represent two major subparallel interconnected fault systems. How these systems are kinematically related to one another is not obvious from the mapping or from geophysical data. However, a number of factors suggest that distributed faulting events (i.e., simultaneous rupture on more than one individual fault), have occurred on both the east and west sides of Yucca Mountain. Fault characteristics that support distributed faulting include the following:

- Close spacing between faults
- Interconnectedness of many faults
- Timing of paleoseismic events (summarized in Section 12.3.7.3 and Pezzopane, Whitney, and Dawson [1996])
- Patterns of principal and distributed faulting observed from historical earthquake ruptures in the Great Basin (Pezzopane and Dawson 1996).

Prehistoric earthquakes are interpreted on the basis of displacement of Quaternary deposits and timing of surface ruptures at specific locations. A total of 52 exploratory trenches and natural exposures have been excavated, cleaned, and logged in the past 20 years as part of seismotectonic investigations in the Yucca Mountain site area (Swadley et al. 1984; Whitney and Taylor 1996). Forty of these trenches and exposures are located across nine local Quaternary faults described above. In the central repository block, the remaining 12 trenches are situated across bedrock faults, which lack direct evidence for Quaternary activity. Twenty-eight trenches display clear evidence for displacement of Quaternary deposits across the fault traces. The other trenches lack evidence of Quaternary displacement, either because the trench did not intersect a fault in surficial deposits or because undisturbed deposits were found to overlie a bedrock fault. Trenches that expose unfaulted Quaternary deposits above bedrock faults also provide constraints on the maximum possible length of prehistoric surface ruptures during the Quaternary age.

An additional 11 trenches were excavated across the nearby Bare Mountain and Rock Valley faults, located within a 20-km (12-mi.) radius of the site. All of these trenches exposed displaced Quaternary deposits.

The number of sites at which trenches were excavated on an individual fault varies from two to eight. Trenches were placed where geomorphic characteristics suggested that maximum or most recent displacement could be studied. Because trenches were not located along the entire extent of rupture of an individual fault, trench data provide minimum rupture length information for the faulting scenarios discussed below and in Section 12.3.7.3.

Paleoseismic data important to seismic hazard assessment that were collected or interpreted from trench sites include fault geometry, the character and ages of faulted and unfaulted Quaternary surficial deposits and soils, the number and ages of individual surface displacement events, displacement amounts, earthquake recurrence, and fault slip rates (Allen 1986; Schwartz, D.P. 1988; dePolo and Slemmons 1990; Reiter 1990; Coppersmith 1991). Paleoseismic data, summarized in Tables 12.3-8 and 12.3-9, are based on the detailed descriptions of individual trench investigations reported by Whitney and Taylor (1996).

Data were collected at each trench or exposure using a prescribed set of basic logging procedures (Whitney and Taylor 1996, pp. 4.0-8 to 4.0-12). Trench walls were cleaned to allow identification and mapping of faults, deformation features, and the stratigraphic and soil relations of surficial deposits. Structures, stratigraphic contacts, and soil-horizon boundaries were identified and flagged, and the relative position of flagged features were measured and plotted on trench logs using one of three methods: (1) manual gridding and plotting, (2) theodolite measurement, and (3) close-range photogrammetry (Hatheway and Leighton 1979; Fairer et al. 1989; Coe et al. 1991). Deformation features, stratigraphic units, and soils were measured and described and, where possible, stratigraphic units and soils related to faulting events were sampled for geochronologic dating. An example log is shown on Figure 12.3-14. Logs of excavations and field data were integrated to derive paleoseismic interpretations of the stratigraphic position of faulted units, the amount of displacement per event, recurrence of faulting events, and slip rates.

The term "event" refers to a specific coseismic surface rupture or deformation occurrence. It may include either displacement or only fracturing with no displacement. Table 12.3-8 is a listing of the "events" recognized from paleoseismic studies at Yucca Mountain. Commonly, an event is associated with a distinct stratigraphic horizon, or event horizon, that represents the land surface at the time of the earthquake. Some events at different sites may not be separate prehistoric earthquakes, but instead may be associated with a single earthquake with rupture distributed on adjacent faults. Attempts to temporally and spatially correlate events between sites along different Yucca Mountain faults are referred to as rupture scenarios. Identification of rupture scenarios is discussed in more detail in Section 12.3.7.3 and Pezzopane, Whitney, and Dawson (1996).

Several criteria were used to identify individual fault displacement events in trench wall exposures:

- Abrupt offset or backtilting of marker horizons, contacts, or units across the fault
- Recognition of buried deposits or features, such as scarp-derived colluvial wedges or debris-filled fault fissures, which commonly are associated with surface ruptures (Nelson, A. 1992)
- Upward termination of fractures, fissures, or shears at the base of a stratigraphic horizon.

Commonly, uncertainties are associated with the identification of some rupture events at a given site due to ambiguities and complexities in structural and stratigraphic relationships. Thus, a qualitative rating of the confidence in identification of events was developed (Table 12.3-8b). In some trenches, paleoseismic reconstructions primarily depend on interpretations of fault-related colluvial deposition in the hanging wall adjacent to the fault, not on offset Quaternary deposits. The result may be an overestimation of the number of events. Direct measurement of offset of Quaternary units is available from only six trenches and natural exposures, because most trenches were located where faults separate bedrock from colluvium. Not all events are represented in the stratigraphic record because of a number of factors, including poor stratigraphic definition, pedogenesis, deformation during subsequent events, and erosion or

nondeposition of units. The completeness of event recognition varies from site to site, but generally decreases as the age of deposits increases.

A range of geologic interpretations may be made from deposits and structures observed in exploratory trenches at Yucca Mountain. The interpretations may include the following: (1) independent fault rupture; (2) distributed faulting; (3) triggered slip; (4) aseismic strain, such as fault creep and folding; (5) mass movements, possibly induced by earthquakes, volcanic eruptions, or climatic events; (6) fissures and compaction related to deposition, groundwater fluctuations, or pore water volume changes, also possibly induced by local earthquakes, volcanic eruptions, or climate changes; (7) mechanical piping associated with groundwater fluctuations, possibly induced by local earthquakes, volcanic eruptions, or climate changes; (8) bioturbation from plant roots and animal and insect burrows; (9) expansive effects associated with pedogenic carbonate accumulation and crystallization, especially in the fault zone, within the footwall, or near the bedrock-alluvium contact; (10) effects associated with shrink/swell behavior of expansive clays during periods of hydration and dehydration; (11) channeling and hillslope erosion along old bedrock faults; and (12) deposition due to climate change. Within the context of the recognized geologic, hydrologic, and seismotectonic setting of Yucca Mountain, all of these mechanisms could produce or enhance some of the fault-related features exposed at Yucca Mountain. Some mechanisms (1 and 2) occur during only moderate- to large-magnitude local earthquakes, whereas others (3, 5, 6, and 7) could be associated with almost any size local or regional earthquake. A number of mechanisms (5 through 12) are nontectonic processes that likely have operated at Yucca Mountain at different times and to differing degrees. Distinguishing which of these processes is responsible for a specific feature or deposit is difficult because similar-looking features (e.g., cracks and fissures) may originate from different processes. Thus, care must be taken to consider these sources of uncertainty when interpreting the paleoseismic history for Yucca Mountain.

Accounting for the various geologic processes, evidence exists for recurrent middle to late Quaternary fault displacement activity on the block-bounding Quaternary faults in the Yucca Mountain site area (Tables 12.3-8 and 12.3-9). At least two, and as many as eight, individual displacement events are evident. These events are associated with discrete displacements related to either individual or scenario earthquakes (see Section 12.3.7.4). The events due to fracturing and fissuring with no detectable offset are nearly as common as displacement events. The fracturing events, if tectonic in origin, record relatively frequent, small- to moderate-magnitude earthquakes that do not produce measurable rupture at the surface. Alternatively, they are a record of distributed faulting and fracturing produced by rarer, larger-magnitude, surface-rupture earthquakes on one of several nearby faults, or large distant earthquakes.

12.3.7.2 Fault Slip Rates

Fault slip rate is the time-averaged rate of displacement on a fault in millimeters per year. Slip rate is an important paleoseismic parameter; it is a standardized measure of activity on the fault, which can be directly used for comparing the activity of many different faults. Fault slip rates are calculated by dividing the amount of cumulative net slip by the age of a specific faulted deposit or horizon. Fault slip rates were computed at each trench site from measurements of the observed net displacement of one or more dated units. Minimum, maximum, and preferred slip

rates were calculated at each site. These rates vary over a large range of values. The range of slip rates reflects uncertainties in both age control and displacement measurements.

In practice, attention must be directed at the relative time spans included in slip-rate calculations (McCalpin 1995). Meaningful slip rates should span at least several seismic cycles, as indicated by multiple displacement events. This is particularly important for long recurrence, low slip-rate faults such as those observed at Yucca Mountain. Fortunately, deposits as old as middle to late Quaternary are exposed at most trench sites (Section 12.3.7.3). These deposits provide sufficiently long paleoseismic records to yield valid average fault slip rates. At Yucca Mountain, slip rates are averaged values derived from the oldest faulted units with adequate age control, which typically are displaced by two, and commonly three or more, events.

The spatial distribution of fault slip-rate measurements for local faults at Yucca Mountain is determined by the distribution of trench sites with suitable paleoseismic data (Figure 12.3-13). One to four slip-rate determinations were computed for nine of the Quaternary faults at Yucca Mountain, as well as the nearby Bare Mountain and Rock Valley faults. The level of study of known and suspected Quaternary faults at distances greater than about 25 km from Yucca Mountain is lower, except for the large, high slip-rate Death Valley and Furnace Creek faults (Figure 12.3-12). Trench-derived paleoseismic data, most suitable for slip-rate calculations, are not available for most regional faults. Instead, estimates, with large uncertainties, are derived from the observed offset of geomorphic surfaces using generalized ages based on soil development (Whitney and Taylor 1996, p. 4.0-12). The morphology and distribution of alluvial fan surfaces adjacent to the range front have been used to calculate Quaternary slip rates on the Bare Mountain fault (Ferrill et al. 1996, 1997), but results from these analyses are controversial (Anderson, L.W. et al. 1997; Ferrill et al. 1997).

Estimates of slip rates for faults at Yucca Mountain vary from 0.001 to 0.07 mm/yr. (4×10^{-5} to 3×10^{-3} in./yr.). (See Table 12.3-9, Section 12.3.7.8, and Whitney and Taylor [1996] for more detailed discussions.) Preferred slip rates are on the order of 0.002 to 0.003 mm/yr. (8×10^{-5} to 1×10^{-4} in./yr.) and 0.05 mm/yr. (2×10^{-3} in./yr.). For comparison, slip rates for regional faults in the southern Basin and Range Province range over several orders of magnitude, from 0.00001 mm/yr. to as high as 6 to 13 mm/yr. (0.24 to 0.51 in./yr.) for the very active Furnace Creek fault (Klinger and Piety 1996, p. 56) (Section 12.3.7.8).

Even given the uncertainties in slip-rate estimation, the slip rates at Yucca Mountain are low to very low. For example, faults with slip rates of 0.01 mm/yr. (4×10^{-4} in./yr.) or less are associated with extremely low rates of activity in a classification of active faulting developed by Slemmons and dePolo (1986). The slip rates observed at Yucca Mountain fall within the moderately low to low activity fault classification in a regional scheme developed by dePolo (1994a, p. 49) that uses slip rates to categorize the activity of normal faults in the Basin and Range Province. The slip rates on faults at Yucca Mountain are equal to or less than the lowest values in a regional compilation of slip rates developed by McCalpin (1995) from fault studies in the entire Basin and Range Province. Only slip rates from the Pitaycachi fault in the southern Basin and Range Province are in the same general range of values as the Yucca Mountain faults. It should be noted that paleoseismic investigations capable of providing slip rates are rarely conducted on faults with these low rates of activity.

The spatial distribution of slip rates among faults at Yucca Mountain is shown on Figure 12.3-15. Slip rates are generally lowest at northern sites, intermediate at central sites, and highest at the southernmost sites. This southern increase in the level of Quaternary tectonism resembles other late Cenozoic tectonic patterns at Yucca Mountain. For example, the cumulative offset of bedrock units generally increases to the south along faults at Yucca Mountain (Scott 1990). Similarly, in the Yucca Mountain area the total amount of extension across all of the faults increases to the south (Fridrich et al. 1996). Also, the amount of paleomagnetic rotation of volcanic rocks increases southward (Rosenbaum et al. 1991; Hudson et al. 1994).

The Stagecoach Road and southern Windy Wash faults (Figure 12.3-12) provide a comparison between long- and short-term slip rates (Whitney, Menges et al. 1996). Long-term rates are from offsets of two volcanic units dated at 8.5 to 3.7 Ma. These units are vertically displaced approximately 100 m (328 ft) vertically across the southern ends of the faults, yielding long-term slip rates of 0.012 to 0.027 mm/yr. (5×10^{-4} to 1×10^{-3} in./yr.) over Plio-Quaternary time. The rates are generally similar, within the same order of magnitude, for preferred late Quaternary slip rates of 0.01 to 0.05 mm/yr. (4×10^{-4} to 2×10^{-3} in./yr.) computed from the paleoseismic trench data.

Volcanic units of differing ages display similar amounts of offset, suggesting a 2- to 4-m.y. hiatus in significant Pliocene activity on both faults. Fox and Carr (1989) suggest a similar hiatus in the Crater Flat basin, with basin extension and faulting resuming with the 3.7-Ma episode of volcanism. This hypothesis is also supported by the analysis of Fridrich et al. (1996).

12.3.7.3 Timing of Surface-Displacement Events and Possible Distributive Rupture Scenarios

Estimates of timing of surface-rupture events form the basis for developing earthquake recurrence models, computing fault slip rates, and correlating displacements along faults in distributive faulting scenarios. The timing of individual events at a given site is constrained by ages of faulted and unfaulted deposits and soils either exposed in trenches excavated across the fault or located adjacent to the surface trace of the fault.

The ages of faulting events are best constrained at trench sites where successfully dated stratigraphic or soil units can be directly tied to displacement events. In some cases, the dated units are features, including scarp-derived colluvial wedges on the hanging wall and fissure fills or carbonate laminae in fault zones, that can be directly associated with a faulting event. In the cases of colluvial wedges and fissure fills, they may postdate the event by a few hours or years. More typically, age control is provided by faulted or unfaulted deposits or soils that stratigraphically overlie or underlie the event horizon. This condition provides only upper and lower temporal bounds on the rupture event. Without a direct physical line to the event, the amount of time between deposition of the dated units and the event itself is unknown. In some cases, this intervening amount of time can be approximated by observing the degree of soil development on the deposits. Pedogenesis suggests a period of surface stability during which deposition and erosion are minimal (Birkeland 1984).

Ages of regional fault displacement events have been estimated from one or more geomorphic characteristics, including the surface expression of the fault, fault scarp morphology, and

relationship of the fault to adjoining Quaternary surfaces and deposits, with age assignments based on surface morphology or soil development.

Ages of faulted and unfaulted units and soils are based on geochronologic studies. An ongoing integrated program, initiated in 1992, provides specific geochronologic control for paleoseismic investigations at Yucca Mountain (Paces et al. 1994, 1995; Whitney and Taylor 1996). This program employs two basic absolute dating techniques: thermoluminescence analysis of fine-grained, polymineralic sediment, and U-Th disequilibrium series (U-series) analyses of pedogenic carbonate-silica laminae and clast rinds, matrix soil carbonate, and rhizoliths (carbonate-replaced root casts). These techniques have undergone extensive testing, development, and refinement during the course of the studies.

Additional geochronologic constraint is provided by correlation of trench deposits and soils with a composite Quaternary chronosequence of surficial deposits in Yucca Mountain (Section 4.4.3) (Whitney, Taylor, and Wesling 1996; Taylor 1986; Peterson 1988; Hoover, D.L. 1989; Wesling et al. 1992; Lundstrom et al. 1993; Peterson et al. 1995). Age assignments for map units in this regional chronosequence are based on a number of geochronologic techniques, including ^{14}C dating of charcoal, ^{14}C and cation ratio dating of rock varnish on geomorphic surfaces, thermoluminescence dating, and U-series and U-trend dating of soil carbonate. Some age-dating techniques that were used earlier in the project, such as U-trend dating of soil carbonate, have since been found to be unreliable (e.g., Latham 1995). Data from these techniques have not been used in the geologic site characterizations. Compilations of all Quaternary age determinations completed in the Yucca Mountain area as part of both trench-specific and regional stratigraphic studies are in Whitney, Taylor, and Wesling (1996, Tables 3.4-2 and 4.1.4-1).

The distribution and quality of geochronologic control of displacement-event ages varies widely on faults studied in the Yucca Mountain area. Samples for dating have been collected from mapped lithologic units and soils at almost all trench sites that contain evidence for paleoseismic events. Thus, at least one, and commonly two or more, data sites are on all of the trenched Quaternary faults in the Yucca Mountain vicinity (Figure 12.3-13). The number of samples collected varies widely among sites; typically at least 3 and locally as many as 12 dates were determined at a single locality.

Individual age determinations vary widely in quality and resolution. This variation primarily reflects intrinsic problems in the suitability of the materials available in the trenches for sampling and analysis. Commonly, only loose sand and silt could be collected for thermoluminescence and porous, impure secondary carbonate affected U-series dates. The quality of dates obtained generally has improved with time due to continual refinement of sampling and laboratory procedures. In particular, the reliability and precision of U-series ages has improved since 1994 with use of mass spectrometry analysis of small, precisely located samples and collection of more reliable materials, such as secondary silica rinds on clasts.

Geochronologic studies have revealed that deposits and soils exposed in trenches vary in age from late Holocene (1 to 2 ka) to early Pleistocene (1 Ma). For example, trenches have exposed deposits that are as old as 400 k.y. on the Windy Wash and Fatigue Wash faults, up to 750 k.y. (Bishop ash in natural exposures) on the Paintbrush Canyon fault, and over 900 k.y. (U-series-dated soil) on the Solitario Canyon fault. The mapped Quaternary stratigraphy provides a long

record of paleoseismic activity for characterization of the long recurrence, low slip-rate faults at Yucca Mountain. The resolution and completeness of the paleoseismic record of faulting events decreases with increasing age. In particular, in deposits older than 500 k.y., fewer events are recognizable and the geologic context of those identified is more poorly understood. This situation is due to incompleteness of older stratigraphic records, deformational overprinting by younger events, and commonly poorer resolution in age control for older deposits. The inventory is most complete and the age data are of highest quality for displacement events that occurred within the past 150 k.y. Thus, this time interval is emphasized in developing recurrence models and rupture scenarios.

Table 12.3-8, updated from Pezzopane, Whitney, and Dawson (1996), provides maximum and minimum age estimates for each event interpreted at trench sites where direct age control is available (see also Whitney and Taylor 1996). Indirect evidence for event timing accounts for the wide time range given for most of the events. Additional uncertainty in event ages is due to error in the bounding age estimates themselves. Preferred dates or ranges of ages (Table 12.3-8) are based on available geologic constraints in addition to the bounding dates of trench units. A midpoint or midrange of the bounding dates was chosen to represent the preferred age of the event if no additional constraints could be made.

Nine rupture scenarios were developed for the main Quaternary faults at Yucca Mountain (Table 12.3-10). The scenarios accommodate distributed displacements on more than one fault during a single prehistoric earthquake (Figure 12.3-16 and Table 12.3-9). Methods for identifying scenarios and the characteristics of each scenario are described by Pezzopane, Whitney, and Dawson (1996). The scenarios are based on correlations of event timing data within the past 150 k.y. between individual trench sites on each of the faults. The scenario correlations are developed from simple probability distribution plots with three basic shapes (boxcar, triangle, and trapezoid), which represent the minimum, maximum, and preferred timing constraints for a given event at each site, using the timing data in Table 12.3-8. The event timing distributions are superposed upon one another and a simple average is calculated from the number and sum of the overlapping distributions. Peaks in the cumulative probability density function occur at times when more than one event's distribution function overlaps with another event's timing. At times when two or more events overlap, the cumulative average is higher than when no events overlap. Thus, the shape and overall range of the cumulative distribution characterizes the resultant event correlations and their timing distributions for the different recurrences presented here. Scenarios identified in this manner are then tested for reasonableness using other geologic constraints, such as correlations of deposits and soils offset by the event at the trench sites involved in the scenario, the spatial association of these sites, and the structural and geophysical relationships of faults in the scenario. Preferred ages for all of the nine rupture scenarios thus identified are listed in Table 12.3-10. The correlations are rated also as high, moderate, or low on the basis of both geochronologic and geologic constraints.

12.3.7.4 Per-Event Displacements

Per-event displacements are an important paleoseismic parameter for estimating the maximum magnitude of prehistoric earthquakes (see Section 12.3.7.7). The most precise per-event displacements were estimated directly from trench log data. Up to eight measurements of per-event displacement are available for faults at and adjacent to the Yucca Mountain area

(Table 12.3-8). Fewer data on per-event displacements are available for regional faults, and the estimates generally are less precise. They are based primarily on the projected measurement of geomorphic surfaces across topographic scarps or the surface trace of the faults (Section 12.3.7.8).

Per-event displacement data are obtained from trench logging in the following manner. Where possible, displacements associated with each faulting event are determined directly by measuring the apparent offset of marker horizons across the fault, and then subtracting the amount of offset related to any younger events identified higher in the stratigraphic section. This procedure cannot be used if different deposits are present on opposite sides of the fault. For example, at some sites, late Quaternary deposits on the hanging-wall block are faulted against much older deposits or bedrock on the footwall block. Several methods are used in this situation. In some cases, rupture amounts are derived from the thickness of fault-related colluvial wedges, which may result in minimum estimates that are 50 to 80 percent of the actual surface displacement (e.g., Swan et al. 1980, p. 1441). An alternative method involves measuring vertical separation between a displaced event horizon in the hanging-wall block and the stratigraphically highest faulted unit on the footwall block. Displacements per event are then derived by subtracting from this measurement the offsets related to events stratigraphically higher in the hanging-wall block. A similar technique uses the stratigraphic thickness of deposits between successive event horizons on the hanging-wall block as a maximum estimate for the displacement associated with the stratigraphically lower event. Measurement uncertainties, inherent in all of these methods, are included in the range of displacements reported. The resolution of per-event displacement measurements generally decreases with increasing age due to the propagation of measurement error for successively older displacements in an event sequence.

Dip-slip values for single-event displacements are adjusted to derive net-slip estimates wherever possible. The amount of normal-oblique slip is calculated for any site that contains possible slip indicators. Examples of slip indicators include Quaternary slickensides on bedrock shears or, less reliably, fault striations on carbonate coatings. At some sites, units in the hanging wall are deformed near the main fault zone either by backtilting towards the fault surface or by development of antithetic grabens. The effects of this secondary deformation are removed by projection of displaced horizons into the fault zone from undeformed sections of the hanging wall and footwall prior to measuring displacements on the main fault. All measurement uncertainties are incorporated in derivations of net single-event displacements. Slip indicators clearly associated with Quaternary displacements were rarely observed. Consequently, studies in Whitney and Taylor (1996) often report dip-slip estimates of single displacements that do not consider modest components of lateral slip. The few slip indicators observed increased displacement amounts by factors of 1.1 to 1.7.

Table 12.3-8 includes maximum, minimum, and preferred estimates of displacements for each event. Table 12.3-9 summarizes this information for each fault. Most of the uncertainty in the estimates results from measurement uncertainties noted above. Preferred values are based on additional geologic constraints and/or the judgment of the investigator. Preferred per-event displacements vary from near 0 to 824 cm (0 to 324 in.). Fracture events with no detectable offsets are also identified in the table. Disregarding events that occurred more than 500 ka, 12 events have preferred displacements equal to or greater than 50 cm (20 in.) or maximum displacements equal to or greater than 100 cm (39 in.). These displacement events form the basis

for one of the inter-event recurrence models (model 1) described in Section 12.3.7.6. Displacements per event are larger (150 to 824 cm [59 to 324 in.]) for the Rock Valley and Bare Mountain faults. Available estimates of single-event displacements for regional faults are in the general range of those for site faults, with the exception of displacements of 240 to 470 cm (94 to 185 in.) on the Death Valley-Furnace Creek fault system.

Single-event displacements are also tabulated for each of the nine scenarios of distributive faulting at Yucca Mountain described in the previous section. Paleoseismic displacements are compiled and plotted as a function of position along the faults, providing a crude slip distribution for each scenario earthquake (see Pezzopane, Whitney, and Dawson 1996). A method is used to project along-trace fault lengths and paleoseismic study sites onto a north-south plane using a join line at 36°50"N. Displacements associated with each rupture scenario are plotted at the projected position onto this line.

Generally, several scenarios exhibit asymmetrically shaped slip distributions, with displacements increasing to the south. At least one scenario (scenario U) displays a more symmetric triangular-shaped distribution, whereas scenarios V and S appear to be relatively flat.

12.3.7.5 Rupture Length Constraints

Coseismic surface-rupture length is an important parameter used to define the maximum magnitudes of prehistoric earthquakes. Estimated rupture lengths for prehistoric earthquakes are restricted by surficial mapping data, the locations of trenches, and displacement-event timing data. As noted previously, trench sites generally are located for purposes other than defining paleorupture length. The length of a rupture is determined by the lateral extent a given event can be identified along one or more faults. In some cases, this identification is accomplished via event correlations between sites using similarities in ages and other supportive geologic criteria (see Section 12.3.7.3). Surface-rupture lengths may be equivalent to the total fault length or may be restricted to a specific portion, or segment, of the fault, as discussed below.

Lengths of individual site faults and regional faults in the Yucca Mountain area have been measured along their curvilinear traces (Tables 12.3-8 and 12.3-11, Section 12.3.7.8) (Pezzopane 1996, Table 11-1; Piety 1996). Maximum, minimum, and preferred lengths are given in Table 12.3-8 for the site faults. These variations in length reflect the manner in which specific disconnected sections of mapped fault traces could be linked together. Individual site fault lengths vary from 1 to 35 km (0.6 to 22 mi.). Fault lengths in the region surrounding the site range from several kilometers to more than 300 km (186 mi.) for the Death Valley-Furnace Creek-Fish Lake fault system. Except for very long, likely segmented faults, the total measured length of a fault represents its maximum rupture potential. This assumption is considered reasonable, especially for short faults at Yucca Mountain with mapped lengths of 5 to 30 km (3 to 19 mi.) based on the relationships identified by D.L. Wells and Coppersmith (1994) and Pezzopane and Dawson (1996).

Fault lengths determined from their mapped surface traces do not always correspond to the length of coseismic surface rupture. Coseismic surface rupture may be segmented, that is, confined to a particular section of the fault because of geometric irregularities, physical characteristics of the fault zone, or by the magnitude of the associated earthquake (Aki 1979,

1984; Schwartz, D.P. and Coppersmith 1984, 1986; Schwartz, D.P. 1988). Segmentation of fault rupture can be proposed only when analysis of timing constraints on displacement events from multiple sites along a fault or system of faults is used. Even then, resolution of chronologic methods is not sufficient to preclude multiple closely timed events. Rupture segmentation is considered likely on most of the long regional faults, although adequate timing data for faulting events generally are not available to precisely define segment boundaries and lengths.

The presence of rupture segmentation on local Yucca Mountain faults is not well established. However, based on geometric complexities, possible fault segments are identified on at least three local site faults: the Paintbrush Canyon, Solitario Canyon, and Windy Wash faults (Table 12.3-8). The distribution and resolution of events data are not sufficient to uniquely constrain any rupture segmentation on these three faults. Most of the geometric segments are short (5 to 10 km [3 to 6 mi.]) and are, therefore, considered unlikely to rupture independently; however, the displacement-timing data suggest that the entire lengths of the faults may not have ruptured in all displacement events. To account for possible rupture segmentation on site faults, minimum rupture lengths are determined for each scenario rupture based on the distribution of sites that contain a given event.

Maximum and minimum lengths are estimated for the nine rupture scenarios proposed for distributed faulting on local site faults (Section 12.3.7.3, Table 12.3-10, Figure 12.3-16). The fault trace lengths and locations of paleoseismic study sites associated with each scenario are projected into a common plane using the projection technique developed for scenario displacements. This method provides a way to obtain composite rupture lengths for scenario events that span more than a single fault at Yucca Mountain. This projection method has inherent distortion that may overestimate rupture length by 1 to 2 km (0.6 to 1.2 mi.).

Minimum rupture lengths are derived from the northernmost and southernmost trenches that contain the same displacement event associated with a particular scenario. In instances where no trench data are available to constrain the surface-rupture extent, the endpoints of ruptures along nearby faults with trench data are used. In most cases, this results in a partial rupture length relative to the entire length of the projected fault system. Note that on some faults, estimates of minimum rupture length are based on paleoseismic evidence that indicates that an event at a site did not occur. This results in a rupture length that is shorter than would be obtained using the trench-to-trench length method. Maximum rupture lengths are estimated by using the longest fault or combination of faults based on the preferred fault length measurements (Table 12.3-8). Maximum scenario rupture lengths are derived by assuming that an entire fault ruptured if any study site had evidence for the scenario event. As with the minimum rupture length estimates, the maximum scenario rupture length using the entire fault length can be superseded when paleoseismic data preclude the occurrence of a particular scenario event. Thus, in a few cases, the maximum rupture length is shorter than the length of any individual fault involved in the scenario rupture.

12.3.7.6 Recurrence Intervals

Recurrence interval is defined in this section as the time interval between successive surface-rupture earthquakes. It is an important temporal measure of fault behavior in seismic hazard analysis. Recurrence intervals are calculated for individual faults at all relevant sites using

paleoseismic data of the number and timing of coseismic surface-rupture events. Individual recurrence intervals are estimated when there is adequate age control to isolate the timing between specific pairs of events. Recurrence interval errors are smaller when dated units are colluvial wedges or fissures that can be directly tied to faulting events. Unfortunately, this condition is rare in the study trenches. More commonly, deposition occurred at an unknown time prior to or following an event. Thus, the ages for events bracketed by the poorly dated deposits are uncertain. In these cases, an average recurrence interval is calculated by dividing the time bracketed with the age estimates by the number of potential events. Uncertainties in both the dating of units (reported as $\pm 2\sigma$) and the number of possible events are incorporated into the reported ranges of recurrence intervals. Late Quaternary recurrence intervals typically are shorter than those of older (greater than 100 to 200 ka) events because small displacement events are better preserved in younger deposits and these deposits are more likely to have better age control.

At least one, and commonly two or more, recurrence interval estimates are made along individual faults at Yucca Mountain (Whitney and Taylor 1996). Average recurrence intervals of individual faults range from 5 to 270 k.y.; preferred average recurrence intervals for all events range from 5 to 200 k.y. (Table 12.3-9). The long recurrence intervals are likely due to relatively small numbers of observed displacements in middle Pleistocene deposits. The range in preferred recurrence intervals between specific events is similar, although they are less than or equal to 50 k.y. for a few faults (e.g., Stagecoach Road and Rock Valley faults) and as great as 100 to 200 k.y. (with large errors associated with poor age control). Average recurrence intervals of 10 to 30 k.y. estimated for the Stagecoach Road and Rock Valley faults are poorly resolved because of poor date constraints on some events.

Estimates of recurrence intervals for regional faults are, in general, based on limited paleoseismic data. Recurrence intervals vary from up to 100 k.y. to as little as 0.5 to 1.5 k.y. for the Death Valley and Furnace Creek faults (see Section 12.3.7.8 for discussion of these sources).

Because the Quaternary faults in the Yucca Mountain site area have independent rupture histories, the potential repository site has experienced local earthquakes, on average, more frequently than the average recurrence interval of any given fault. Three recurrence models, presented in Pezzopane, Whitney, and Dawson (1996), describe composite prehistoric earthquake events on multiple Quaternary faults in the site area.

Recurrence model 1 is based on surface-rupture displacement data. Each large displacement (greater than or equal to 50 cm [20 in.]) event, on each fault, is considered to be an independent seismic event. Events older than 500 ka, or those with poorly constrained ages, are omitted. As described in Section 12.3.7.4, 12 events have preferred displacements equal to or greater than 50 cm (20 in.) or maximum displacements equal to or greater than 100 cm (39 in.). Eight of these 12 large-displacement events occurred between 15 and 150 ka. The remaining four events occurred between 200 and 500 ka based on U-series-dated soils. If the 12 events occurred within 485 k.y. (500 ka to 15 ka is 485 k.y.) and are separated by 11 equal intervals of time, the average recurrence interval is 44 k.y. (Table 12.3-12). Considering that eight events occurred within 135 k.y. (150 ka to 15 ka is 135 k.y.) and are separated by seven equal time intervals, the average recurrence interval is 19 k.y. for the younger events. However, the 12 events are combined from

several sites. Some of the large-displacement events may be repeated as a result of uncertainties between sites, thus model 1 probably is not reliable.

Recurrence model 2 treats the data in Table 12.3-8 as though each interpreted paleoseismic event, including events characterized by fracturing and small offsets (0 to 15 cm [0 to 6 in.]), on each fault is an independent earthquake. Thirty-nine events are identified within the past 500 k.y. This estimate includes all events recognized at all sites, even events at different sites along the same fault. It also disregards the fact that numerous paleoseismic events recognized along different faults appear correlative in time. Model 2 average recurrence intervals are approximately 13 k.y. (Table 12.3-12). This model is considered unlikely because, given the numerous, closely spaced, and anastomosing (in map view) faults at Yucca Mountain, it is more likely that multiple fault events occur in the region.

Multiple fault events form the basis for recurrence model 3. This model attempts to correlate events using stratigraphic and geochronological constraints from the trench studies and develops the nine rupture scenarios described previously (Section 12.3.7.3) (Pezzopane, Whitney, and Dawson 1996). Nine events within 150 k.y. yield an average recurrence interval of 17 ± 5 k.y. (Table 12.3-12).

12.3.7.7 Magnitude Distribution

Estimates of paleoearthquake magnitudes are derived from empirical relations using paleoseismic surface-rupture lengths and displacements for faults with known or suspected Quaternary activity. Magnitudes are also estimated for regional faults. These estimates use empirical magnitude-rupture relations developed for maximum single-event displacement and/or surface-rupture lengths for all fault slip types (Wells, D.L. and Coppersmith 1994). The D.L. Wells and Coppersmith (1994) relationships were chosen because they closely fit the magnitudes and displacements of 24 historical surface-rupture earthquakes in extensional regimes, consistent with the Basin and Range Province (Pezzopane and Dawson 1996).

Maximum earthquake magnitude was estimated for all known or suspected Quaternary faults in the Yucca Mountain region (Table 12.3-11) (Pezzopane 1996). The maximum earthquake is the estimated size of the largest earthquake that can occur on a fault in the present tectonic regime given the physical constraints of the fault, such as length and dip. Maximum earthquake magnitudes are estimated using moment magnitude and surface-rupture length empirical relationships (Wells, D.L. and Coppersmith 1994). Fault length is used because it is more reliably and consistently measured for all faults in the region, regardless of whether any paleoseismic data are available to estimate displacement. The analysis uses maximum fault length (the entire mapped or inferred length) and the conservative assumption that the entire length ruptures during a single earthquake (i.e., no segmentation). Using the length of individual fault segments to measure earthquake magnitude reduces the estimated maximum magnitude. Maximum magnitudes computed in this analysis range from M_w 5.1 to 7.9 for faults within a 100-km radius of the potential repository site (Table 12.3-11). These results will be superseded by maximum magnitude distributions constructed as part of the probabilistic seismic hazard analyses (Section 12.3.10).

More detailed estimates of prehistoric earthquake magnitudes are available for site faults using paleoseismic information (Pezzopane, Whitney, and Dawson 1996). Specifically, paleomagnitudes are computed for events from all three recurrence models (described in Section 12.3.7.6) using the relationship between maximum surface displacement and moment magnitude (Wells, D.L. and Coppersmith 1994). Preferred paleoseismic displacements (Table 12.3-8) are used for the following reasons:

- Only the largest displacement events are selected (model 1).
- For each fault the maximum preferred value from all trenches was selected for each event and investigators reported preferred displacement values that tended towards maximum values.
- Trenches are sited where fault scarps display maximum apparent offset.

The 12 large-displacement events in recurrence model 1 yield a range of magnitude estimates ranging from M_w 6.4 to 6.9. Prehistoric earthquake magnitudes calculated for recurrence model 2 vary from M_w 5.6 to 6.9. The range in values is large because all events at all sites are included. Magnitudes calculated from displacements assigned to the nine rupture scenarios of recurrence model 3 range from M_w 6.2 to 6.9 (Table 12.3-10). This range of values is similar to that derived from the large single-fault events of model 1.

For recurrence model 3, the largest preferred displacement value measured on an individual fault or at a single site (Table 12.3-8) is used to calculate moment magnitude for each distributed rupture scenario. Displacements in each scenario are not summed because smaller displacements on related faults are considered to be distributed secondary ruptures. This assumption may not be appropriate for scenario U because both eastside and westside faults may have moved simultaneously. If these are individual structures that penetrate to seismogenic depths, the displacements and rupture areas should be summed to estimate the magnitude. If, however, the westside and eastside faults merge at shallow depth and displacement along the eastside fault is secondary, the magnitude should be estimated by summing the displacements across the westside faults. Summing displacements on the westside faults for scenario U provides an estimated total displacement of 2 m (7 ft), which corresponds to an M_w 6.9.

Magnitudes are also estimated using minimum and maximum rupture lengths of each rupture scenario in recurrence model 3 and using the relationship between surface-rupture length and magnitude (Wells, D.L. and Coppersmith 1994). For each scenario, rupture lengths are measured from the composite fault lengths and distribution of trench sites containing evidence for the event using the projection method described in Section 12.3.7.5 (Table 12.3-8). Magnitudes based on minimum and maximum scenario rupture lengths range from about M_w 6.2 to 6.7 (Table 12.3-10). The scenario rupture lengths depend on how individual faults and fault segments are combined into rupture zones, which is subject to differences of interpretation. Maximum scenario rupture lengths are estimated on the conservative assumption that the entire fault length ruptures during the event.

Figure 12.3-17 compares magnitudes derived from scenario rupture lengths with those derived from displacement data. If magnitudes derived from scenario rupture lengths were the same as

magnitudes derived from displacement data, the points would plot along the diagonal line. However, in almost all scenarios, the maximum rupture lengths are more consistent with those derived from displacement data than the minimum rupture length-based estimates.

Preferred scenario magnitudes listed in Table 12.3-10 are derived by considering the single displacement data and scenario rupture length data independently, then assessing which values (rupture lengths or displacements) are most reasonable given the geological constraints. Preferred scenario magnitudes range from M_w 6.2 to 6.9.

12.3.7.8 Descriptions of Known and Suspected Quaternary Faults in the Yucca Mountain Region

One of the primary objectives of the YMP is to identify faults with known or suspected Quaternary activity that may have a potential impact on the design and performance of a high-level radioactive waste facility. Included in the region of interest, generally within a 100-km (62-mi.) radius of the potential repository site, are diverse fault types, including long, continuous, high slip-rate, oblique-slip, and strike-slip faults of the Eastern California Shear Zone to the west of Yucca Mountain; potentially long, mostly discontinuous, moderately active normal- and oblique-slip faults of the Walker Lane belt, located northwest and south-southeast of Yucca Mountain; and the intermediate length, moderately segmented, and moderately active range-bounding normal faults typical of that part of the Basin and Range Province that lies east and northeast of Yucca Mountain.

Several investigations of regional scope were conducted to identify and characterize faults by Reheis (1991, 1992); Reheis and Noller (1991); Dohrenwend et al. (1991, 1992); Piety (1996); Anderson, R.E., Bucknam et al. (1995); and Anderson, R.E., Crone et al. (1995). Numerous studies of local faults have also been conducted at and near Yucca Mountain, including detailed mapping of trench exposures at selected localities. Results of these local fault studies are described briefly here and in more detail in Whitney and Taylor (1996). Faults and fault systems near the potential repository site that have been trenched and are described in detail include Bare Mountain, Bow Ridge, Crater Flat, Fatigue Wash, Ghost Dance, Iron Ridge, Paintbrush Canyon, Rock Valley, Solitario Canyon, Stagecoach Road, and Windy Wash faults (Table 12.3-8). Descriptions of faults within and adjacent to the immediate site area (generally within 10 km) are based on results of recent large-scale along-fault mapping, exploratory trench studies, geochronological studies, and a compilation of detailed fault data presented by Simonds et al. (1995).

During the course of fault investigations in the Yucca Mountain region, approximately 100 individual faults have been considered as possible sources of seismicity and potentially significant levels of ground motion (Pezzopane 1996) (Section 12.3.8). A total of 67 faults or combinations of faults are considered by Pezzopane (1996) to be relevant or potentially relevant sources of seismicity, depending on whether evidence of Quaternary movement is demonstrable or only suspected (Table 12.3-11). Two or more closely spaced faults aligned end to end are combined in some cases because an event incorporating the combined rupture length would result in a large-magnitude event and associated ground motions would be substantially larger than if rupture occurred on only one of the faults (Table 12.3-11) (Pezzopane 1996).

The descriptions presented here are summaries and focus on the evidence for Quaternary activity. Note that delineations of known and suspected Quaternary faults are strongly dependent on information contained in published literature. In particular, significant limitations are associated with combining short, individual fault traces (or related geomorphic features) into a single seismotectonic source with a given length and rupture age. Where uncertainties exist, the maximum mapped lengths are given in the fault descriptions. The Quaternary histories of many regional faults are poorly known because the faults are poorly exposed. Even in instances where faults are well exposed or trenched, a complete sequence of Quaternary deposits with which to accurately date the history of Quaternary fault movements is rarely preserved.

In this section, the faults are described in alphabetical order. Approximate age ranges of various time intervals included in the Quaternary period are Holocene (less than 10 ka), late Pleistocene (10 to 128 ka), middle Pleistocene (128 to 760 ka), and early Pleistocene (760 ka to 1.6 Ma). The late Tertiary period extends from 1.6 to 5.0 Ma. In instances where specific age limits within the Quaternary have not been determined (or reported), surficial deposits or fault movements are stated only as being Quaternary in age. Fault distances refer to the distances between the closest point on the surface trace of a given fault to both the preclosure controlled area boundary and the center of the potential repository site at Yucca Mountain. Fault length refers to the maximum length of a given fault or fault zone as reported or shown on maps in published references (e.g., Piety 1996). Unless otherwise indicated, the following descriptions for regional faults, including temporal and behavioral data, are from Piety (1996) and the field reconnaissance work is from R.E. Anderson, Bucknam et al. (1995) and R.E. Anderson, Crone et al. (1995). Piety's (1996) report is an excellent synthesis of most of the data available for characterizing regional faults, and it contains an extensive list of published references.

The known or suspected Quaternary faults and their seismic source parameters are listed in Table 12.3-11 in order of increasing minimum distance from Yucca Mountain and are shown on Figures 12.3-12 and 12.3-13.

Also included are several local faults that exhibit no evidence for Quaternary activity (e.g., Ghost Dance fault), but are of potential regulatory interest.

Amargosa River Fault Zone—This 15-km-long (9-mi.-long) fault zone is a diffuse band of scarps extending northwest across the central part of Ash Meadows, about 38 km (24 mi.) southwest of Yucca Mountain. Scarps have small vertical offsets (1 to 3 m [3 to 10 ft]) and unknown amounts of horizontal offset. The evidence for Quaternary activity is strike-slip offset along a single fault. Movement along the fault probably occurred during the late Pleistocene (Keefer and Pezzopane 1996, p. 3-4). The age of the most recent event is more than 10 k.y. (Keefer and Pezzopane 1996, p. 3-4).

Amargosa River-Pahrump Faults—If the Amargosa River-Pahrump fault systems (see description of Pahrump fault below), which have a combined length of about 130 km (81 mi.), are structurally related and act seismically as a single feature, the estimated values for the maximum moment magnitude and peak acceleration will be greater than the estimated values for either one figured separately (Table 12.3-11).

Area Three Fault—This fault is located in the east-central part of Yucca Flat, about 44 km (27 mi.) east-northeast of the potential repository site. Total fault length may be as much as 12 km (7 mi.), depending upon whether individually mapped shorter fault segments are connected. Structural and stratigraphic relations indicate Quaternary activity; the latest movement may be as recent as Holocene (Fernald et al. 1968; Swadley and Hoover 1990). Displacements of surficial deposits were triggered during underground nuclear explosions.

Ash Meadows Fault—This fault consists of discontinuous lineaments and subdued scarps that extend north-south for at least 30 to 40 km (19 to 25 mi.), and possibly as much as 60 km (37 mi.). It is located along the eastern side of the Amargosa Desert through Ash Meadows. At its northern end, the fault, which exhibits normal dip-slip movement, is about 34 km (21 mi.) southeast of the potential repository site. At one locality, the larger of two multiple-event scarps has 3.4 m (11.2 ft) of surface offset on middle or early Pleistocene deposits and 1.8 m (5.9 ft) of surface offset on late Pleistocene alluvium (Keefer and Pezzopane 1996, p. 3-5). Typically, scarp offsets attributed to the most recent event range from 0.7 to 1.5 m (2.3 to 4.9 ft) and are commonly less than 1 m (3 ft). The age of this event is considered late Pleistocene, based on scarp morphology and the estimated age of the youngest offset geomorphic surface. These measurements provide a maximum slip rate of 0.1 mm/yr.; a lower slip rate of less than 0.01 mm/yr. is estimated for smaller scarps along most of the fault length. The recurrence interval for surface-rupture events is probably in the range of several tens of thousands of years (Keefer and Pezzopane 1996, p. 3-5).

Bare Mountain Fault—This fault is generally north-striking, east-dipping (60° to 80°), with normal-oblique slip (dextral). It forms the structural boundary between Bare Mountain to the west and Crater Flat basin on the east (Reheis 1988; Monsen et al. 1992). The fault is approximately 20 km (12 mi.) long and lies about 14 km (9 mi.) west of the potential repository site. Direct evidence for the total amount of bedrock offset along the Bare Mountain fault is not available because it is located within surficial deposits for most of its length. In several places, fault scarps are developed in middle Pleistocene alluvial fans (Anderson, L.W. and Klinger 1996, p. 21). One to two surface-rupture events are interpreted at three trench sites excavated along the fault. Estimates of average preferred single displacements range from 80 to 150 cm (32 to 59 in.). Available data indicate that the most recent surface-rupture event is more than 14 ka and as old as 100 ka. The recurrence of moderate to large surface-rupture events is on the order of tens of thousands to 200 k.y. or more. The late Quaternary slip rate interpreted from trenching data is on the order of 0.08 to 0.01 mm/yr. (3×10^{-3} to 4×10^{-4} in./yr.) (Anderson, L.W. and Klinger 1996, p. 65). Ferrill et al. (1996) infer a higher slip rate of 0.06 mm/yr. (2×10^{-3} in./yr.) along the southern end of the fault, based on more indirect and controversial methods of using variations in the morphology and distribution of alluvial fan surfaces adjacent to the range front (Ferrill et al. 1997).

Belted Range Fault—This normal fault generally trends north with a maximum length of 54 km (34 mi.). It is located about 55 km (34 mi.) north of Yucca Mountain. Total down-to-the-west displacement exceeds 610 m (2,001 ft). Quaternary displacement is expressed by a relatively continuous, 22-km-long (14-mi.-long) zone of well-defined alluvial scarps (Keefer and Pezzopane 1996, p. 3-5). Total scarp offsets range from 0.6 m (2.0 ft) in the youngest faulted alluvium to 11.3 m (37.1 ft) in older alluvium. Scarps with less than 1 m (3.3 ft) of surface offset probably result from a single faulting event, whereas those with larger offsets show evidence of

multiple displacements. The most recent movement along the Belted Range fault is probably early Holocene to latest Pleistocene, based on scarp morphology and the surface characteristics of the youngest offset alluvial fans (Keefer and Pezzopane 1996, p. 3-5). Poorly constrained late Pleistocene slip-rate estimates vary from 0.01 to 0.1 mm/yr. (4×10^{-4} to 4×10^{-3} in./yr.). Timing data are too poorly resolved to determine recurrence intervals.

Black Cone Fault—This north- to northwest-striking fault located northeast of Black Cone in the central part of Crater Flat lies about 8.5 km (5.3 mi.) west of the potential repository site. This 7-km-long (4-mi.-long), down-to-the-east normal fault offsets Quaternary deposits of middle to late Pleistocene age and locally produces subtle scarps with as much as 0.5 m (1.6 ft) of topographic relief (Keefer and Pezzopane 1996, p. 3-6). No trenches have been excavated to provide temporal or behavioral data.

Boomerang Point Fault—This 5-km-long (3-mi.-long) north- to northeast-striking dip-slip fault is located along the western side of Boomerang Point in the western part of the potential repository site (Scott and Bonk 1984). The fault dip averages about 75° west. Down-to-the-west displacement in mid-Tertiary volcanic rocks is about 30 m (98 ft). No evidence exists for displacement of Quaternary surficial deposits along the southern end of the fault.

Bow Ridge Fault—This fault is a prominent north to northeast-striking, west-dipping, normal-oblique (sinistral) slip fault. It is up to 10 km (6 mi.) long and lies in the eastern part of the potential repository site. The fault is buried beneath alluvium and colluvium for most of its extent along the western margin of Midway Valley. The best topographic expression of the fault occurs where a 760-m-long (2,493-ft-long) section follows the base of the west side of Exile Hill, although the fault is buried by colluvium (Menges and Whitney 1996a, p. 4.2-16). Tertiary volcanics are displaced at least 125 m (410 ft) down to the west at this locality. The fault dips 65° W to 85° W. Trenches and the Exploratory Studies Facility (ESF) expose a complex fault zone in highly fractured Tertiary volcanic bedrock and colluvial deposits that have been subjected to multiple Quaternary faulting events. At least two and possibly three surface-rupture events are evident in late to middle Pleistocene colluvial deposits at Trench 14D (Menges and Whitney 1996b, p. 4.4-24). A minimum age of 30 to 130 k.y. is established for the most recent surface-rupture event. Displacements range from 15 to 80 cm (6 to 32 in.) for the most recent faulting events and from 20 to 165 cm (8 to 65 in.) for all events. Average recurrence intervals vary from 70 to 215 k.y. (preferred range, 100 to 140 k.y.). Average slip rates are 0.002 to 0.007 mm/yr. (8×10^{-5} to 3×10^{-4} in./yr.), with a preferred value of 0.003 mm/yr. (1×10^{-4} in./yr.) (Menges and Whitney 1996b, p. 4.4-26).

Bullfrog Hills Fault Zone—This fault zone includes several north- to northwest-striking faults in the Bullfrog Hills area, about 38 km (24 mi.) northwest of the potential repository site. The longest fault is 7 km (4 mi.); others are about 4 km (3 mi.) long. Displacements have been observed to be down to the southwest. Parts of all faults have been mapped either as concealed by Quaternary deposits or as faulted contacts between Tertiary bedrock and Quaternary alluvium.

Buried Hills Faults—These faults include several north-striking discontinuous faults in a zone that extends for a total distance of about 26 km (16 mi.). The faults, located 53 km (33 mi.) east of Yucca Mountain, show both down-to-the-east and down-to-the-west displacements. Based

largely on air photo interpretation, the faults are shown primarily as weakly to moderately expressed lineaments and scarps on surfaces of Quaternary and Tertiary deposits (Reheis 1992). In a few places, faults are also portrayed as juxtaposing Quaternary alluvium against bedrock (Keefer and Pezzopane 1996, p. 3-7).

Cane Spring Fault—This fault is a northeast-striking, left-lateral fault that is part of the Spotted Range-Mine Mountain structural zone. This zone also includes the Mine Mountain, Rock Valley, and Wahmonie faults. The fault lies about 29 km (18 mi.) east of the potential repository site and may be as much as 27 km (17 mi.) in length, depending on how many individual faults are included. Tertiary volcanic rocks are displaced largely by left-lateral strike-slip displacement with a smaller component of normal dip-slip motion. Total amount of displacement along the fault has not been determined. In general, the fault is shown to be concealed by Quaternary alluvium, except for sections shown as fault contacts between Tertiary bedrock and younger Tertiary or early Quaternary surficial deposits (Reheis, M.C. and Noller, J.S. 1991, p. 1.3). Although recent studies do not indicate Quaternary activity, the fault is situated in proximity to faults of known Quaternary activity (e.g., Rock Valley, Mine Mountain) and historical seismicity has occurred in the vicinity of the fault.

Carpetbag Fault System—This fault system, located about 43 km (27 mi.) northeast of Yucca Mountain, consists of several subparallel, north-striking, steeply east-dipping, normal-oblique fault strands in a zone about 30 km (19 mi.) long. The fault system is largely concealed at the surface; its total length is derived from geophysical studies and other subsurface imaging techniques. Vertical displacement of Tertiary volcanic rocks is 600 m (1,969 ft). The amount of right-lateral slip could be even greater, to account for as much as 1,500 m (4,921 ft) of horizontal extension. Several episodes of Quaternary fracturing (and perhaps minor faulting) were interpreted from U-series dating of secondary CaCO₃ in fracture-fill deposits (Shroba et al. 1988a, p. 231, 1988b, p. 30). The approximate timing of fractures was 30, 45, 65, 100, 125 to 130, and 230 ka. No surface rupture appears to have occurred during the last 130 k.y. and possibly the last 230 k.y. The slip rate along this fault system between about 30 ka and 125 to 130 ka or earlier has been nearly zero. The average recurrence interval for fracture events is inferred to be about 25 k.y. during the last 125 to 130 k.y. A 1.5-m-high (5-ft-high) scarp was formed along part of the fault system as a result of an underground nuclear explosion at Yucca Flat (Carr 1974, Figure F; Shroba et al. 1988a, p. 231).

Carrara (Highway 95) fault—This 23- to 34-km-long (14- to 21-mi.-long) feature has been described by Slemmons (1997b, p. 1) as a potential active fault and potential earthquake source. The closest distance of the Carrara fault to the repository is 17 km. Slemmons (1997a) cites evidence for late Quaternary activity along the Carrara fault that includes a potential late Quaternary uplifted block based on drill hole data, outcrops and geophysical information; a 25-m-high (82-ft-high) scarp located above the Bare Mountain alluvial fans; deformation of a Pleistocene clay layer; a negative geodetic anomaly between Beatty and Las Vegas at the Carrara fault; and seismic reflection, aeromagnetic and isostatic gravity data that indicate faulting. In addition, Stamatakos et al. (1997a) report alignment of surficial features such as possible fault scarps and push-up ridges along the proposed Carrara fault and suggest that they indicate an active, first-order fault.

Slemmons (1997b, p. 2) describes the "Carrara feature" as linear with nearly continuous surface expression that strikes N50°-55°W from the Betty fluvial scarp to near the Lathrop Cone and then strikes about N75°-90°W at the south end of Yucca Mountain. Near Yucca Mountain the feature is mainly expressed on gravity and aeromagnetic maps. Blakely et al. (2000, p. 14) describe a short but prominent magnetic anomaly along Highway 95 that coincides with the proposed Carrara fault. Stamatakos et al. (1997a, p. F453) report that detailed gravity and ground magnetic surveys indicate that both dextral strike-slip and down-to-the-southwest motion have occurred along the fault. They suggest that preliminary estimates of slip along the fault, based on offset magnetic anomalies, include a minimum of 300 m vertical and 3 km horizontal displacement. Aerial reconnaissance shows a 10- to 15-km-long elongate uplifted block that appears to be partly controlled by fault scarps that influences Late Pleistocene stream channels (Slemmons, 1997b, p. 2). Slemmons (1997b, p. 2) reports discussions with Jim Yount (USGS) who reports tectonic and fluvial scarps along an uplifted horst-like block with an upper surface of late Quaternary age (ca 125 ka). Slemmons (1997b, p. 2) states that in the absence of additional field studies, his observations, based largely on aerial reconnaissance, of geomorphic features suggest that the Carrara fault is active but definitive evidence is still needed. Connor et al. (2000, pp. 423 to 424) suggest that some volcanic centers and vent alignments may be fault controlled. They consider the intersection of faults in the vicinity of the Carrara fault to coincide with the location of the Carrara Fault Basalt.

Checkpoint Pass Fault—This fault lies 44 km (27 mi.) east-southeast of Yucca Mountain. It strikes northeast to east for a distance of 8 km (5 mi.). Displacements are predominantly left-lateral strike-slip, but some segments show dip-slip, down-to-the-west movement. In places, the fault juxtaposes Quaternary alluvium against bedrock (Keefer and Pezzopane 1996, p. 3-8). It is also shown as being concealed by alluvial deposits of Quaternary and Tertiary age along a large part of its length (Keefer and Pezzopane 1996, p. 3-8).

Cockeyed Ridge-Papoose Lake Fault—Two northwest-striking normal faults, in a segmented zone about 21 km (13 mi.) long, make up the Cockeyed Ridge-Papoose Lake fault. The faults are located 53 km (33 mi.) east-northeast of the site area. Most of this fault is shown to displace Quaternary deposits in the form of weakly expressed lineaments or scarps (Keefer and Pezzopane 1996, p. 3-9).

Crater Flat Fault System—This fault system, located about 6 km (4 mi.) west of the potential repository site, consists of two fault zones. Abrupt changes in orientation, differences in geomorphic expression, and contrasts in paleoseismic history revealed in exploratory trenches (Coe 1996; Taylor 1996) suggest that the two fault zones are separate structures; it is unlikely that they are different segments of a single fault zone. The amount of down-to-the-west displacement of bedrock across the fault system is unknown.

The approximately 11-km-long (7-mi.-long) Northern Crater Flat fault comprises two subparallel, northeast-striking strands that are 300 to 600 m (984 to 1,969 ft) apart. Up to five events have been interpreted from evidence of faulted middle to early Pleistocene alluvium (Coe 1996). The most recent event may be Holocene in age (Coe 1996, p. 4.11-8). Individual displacements are up to 50 cm (20 in.); however, the two most recent events are small, less than 5 cm (2 in.). Local graben formation and backtilting reduce the cumulative net tectonic displacement to a maximum of 100 cm (39 in.). A slip rate of 0.002 to 0.003 mm/yr. (8×10^{-5} to

1×10^{-4} in./yr.) is estimated for the Northern Crater Flat fault. This rate may be refined pending results of additional dating. Preliminary recurrence intervals are in the range of 120 to 160 k.y. (Coe 1996, p. 4.11-12).

The Southern Crater Flat fault is characterized by a northeast-striking basalt-alluvium contact, fractured carbonate-cemented alluvium, subtle scarps in alluvium, and a linear stream channel (Simonds et al. 1995; Menges and Whitney 1996a). The nearly vertical fault is about 8 km (5 mi.) long. Two trenches excavated across the fault provide evidence for three Quaternary events. Preliminary age estimates for the events are 2 to 8, 8 to 60, and greater than 250 k.y. (Taylor 1996). Individual displacements vary between 5 and 32 cm (2 and 13 in.), with preferred estimates of 18 to 20 cm (7 to 8 in.). A slip rate of 0.002 mm/yr. (8×10^{-5} in./yr.) is estimated for the last 250 k.y. Taylor (1996) estimates recurrence intervals of 5 to 60 k.y. for the Southern Crater Flat fault.

Crossgrain Valley Fault Zone—This northeast-trending, 9-km-long (6-mi.-long) fault zone lies 48 km (30 mi.) southeast of Yucca Mountain. Motion is left-lateral strike-slip with a down-to-the-northwest normal dip-slip component. The fault zone displaces surfaces on both Quaternary and Tertiary deposits. Several sections are shown as moderately to strongly expressed lineaments or scarps in surfaces on Quaternary deposits (Reheis 1992, p. 1.3; Dohrenwend et al. 1991). In other places, faults within the zone are shown as forming the contact between alluvium and bedrock or as being concealed beneath the alluvium.

Death Valley Fault—This north-northwest-striking, down-to-the-west predominantly normal fault bounds the eastern side of Death Valley along the western side of the Black Mountains. At its nearest point, the fault is about 55 km (34 mi.) southwest of the potential repository site. It has a total length of 100 km (62 mi.), which includes the southernmost section, referred to as the southern Death Valley fault. Late Pleistocene and Holocene fault scarps are prominent along the fault. Recent studies indicate that three and possibly four surface-rupture events have occurred along the central portion of the fault in the last 2 to 4 k.y. (Klinger and Piety 1996, p. 56). Based on scarp morphology and offset of a 0.2- to 2.0-ka surface, the age of the most recent event may be nearly historic. Scarps are west-facing, with heights ranging from 5 to 9.4 m (16 to 31 ft). Maximum vertical displacement of late Pleistocene surfaces is 15 m (49 ft). Scarps, interpreted to be the result of several large-magnitude earthquakes, provide evidence for an average of 2.4 m (7.9 ft) of surface offset per event. Based on per-event displacements, deformational style, geomorphic expression, and other structural evidence, Klinger and Piety (1996, p. 56) estimate paleorupture lengths of at least 45 km (28 mi.) to as large as 60 km (37 mi.).

Estimates of fault slip rates range from 0.15 mm/yr. (6×10^{-3} in./yr.) to as much as 11.5 mm/yr. (0.45 in./yr.) during the Holocene, depending on which segment of the fault is measured. A late Holocene slip rate of 3 to 5 mm/yr. (0.12 to 0.20 in./yr.) is estimated for one segment of the Death Valley fault at a locality where an alluvial fan surface with an estimated age of about 2 to 4 k.y. has been displaced vertically 10.5 m (34.4 ft) (Klinger and Piety 1996, p. 56). These rates are considerably larger than those estimated for the late Tertiary to middle Pleistocene time interval, suggesting either a significant increase in fault activity or a deficiency in evidence for long-term activity. Based on evidence for three or more late Holocene (less than 2 ka), surface-

rupture events on the Death Valley fault, the average recurrence interval is less than 650 yr. The average Holocene recurrence interval ranges from 0.5 to 1.3 k.y. (Klinger and Piety 1996, p. 56).

Death Valley-Furnace Creek Fault System—This combined fault system (which includes the southern Death Valley fault) extends along the eastern side of Death Valley as a nearly continuous series of normal and right-lateral faults for about 205 km (127 mi.). The fault's closest distance to the potential repository site is 50 km (31 mi.). If considered a single structural feature, the estimated values for maximum moment magnitude and peak acceleration are greater than the values estimated for each separate fault system (Table 12.3-11) (Pezzopane 1996).

Death Valley-Furnace Creek-Fish Lake Valley Fault System—This fault system includes the active Fish Lake Valley fault to the north. The right-lateral, oblique-slip Fish Lake Valley fault provides an additional 83 km (52 mi.) to the Death Valley-Furnace Creek fault system (Keefer and Pezzopane 1996, p. 3-11). This combined fault system, at almost 300 km (186 mi.) long, is the longest and most active fault system in the Yucca Mountain region. At its closest approach, the system lies 50 km (31 mi.) west of Yucca Mountain.

Drill Hole Wash Fault—This fault extends northwest along Drill Hole and Teacup washes on the northeastern side of the repository block. It is concealed by surficial deposits, except for a short distance where it crosses a spur of bedrock near the confluence of the two drainages. Drillhole data from Drill Hole Wash and from the ESF excavation indicate the presence of two interconnected faults that offset the Tertiary volcanic rocks (Keefer and Pezzopane 1996, p. 3-11). The mapped length of the fault is about 4 km (2 mi.). The principal displacement is normal oblique-slip with a right-lateral sense of offset. Middle Pleistocene to early Holocene surficial sediments cover most of the fault without evidence of disruption.

Dune Wash Fault—This south- and southeast-striking fault is mapped along the eastern side of the potential repository site for a distance of 3 km (2 mi.). It is mapped in exposures of bedrock as a west-dipping normal fault with down-to-the-west displacement. Toward the northern end of the fault, Tertiary volcanic rocks are displaced 50 to 100 m (164 to 328 ft) (Keefer and Pezzopane 1996, p. 3-11). No evidence of Quaternary movement has been found in surficial deposits that bury the fault toward the south.

East Busted Butte Fault—This down-to-the-east normal fault bounds the eastern side of Busted Butte and may extend along Fran Ridge, suggesting a maximum length of 11 km (7 mi.) and a distance of roughly 3 km (2 mi.) to the potential repository site. Small, arcuate scarps offset middle to late Quaternary deposits, but the details of Quaternary activity are not known (Wong and Stepp 1998, p. AAR-19). This fault was not considered in the analysis by Pezzopane (1996).

East Lathrop Cone Fault—This short (less than or equal to 9 km [6 mi.]), northeast-striking fault lies on the eastern side of Lathrop Wells basalt cone, about 11 km (7 mi.) south of Yucca Mountain. This down-to-the-west fault may be part of the Paintbrush Canyon-Stagecoach Road fault system. A small scarp (less than 0.5 m [1.6 ft] high) offsets late Quaternary alluvium (Wong and Stepp 1998, p. AAR-15), but little else is known about this fault's Quaternary activity. This fault was not considered in the analysis by Pezzopane (1996).

East Nopah Fault—This northwest-striking fault is located about 85 km (53 mi.) from the potential repository site. The minimum mapped length of the fault is about 17 km (11 mi.) (Hoffard, J.L. 1991, p. 28). The fault may extend farther but no detailed mapping has been conducted to the north or south. To the north, strong vegetation lineaments occur along the western side of Stewart Valley; however, evidence does not support actual displacement through Chicago Pass between Pahrump and Stewart valleys. Hoffard (1991, p. 30) suggests that the fault terminates at the north through a series of north-striking, left-stepping, normal faults. Individual faults within the East Nopah fault are 1.8 to 3.0 km (1.1 to 1.9 mi.) long. The fault is complex; the southern 9 km (6 mi.) consists of an echelon faults. Because of the nearly linear surface trace of the overall fault, even through topography, Hoffard (1991, p. 33) suggests that it may be nearly vertical. Evidence for right-lateral displacement along the East Nopah fault includes the straight and narrow fault trace, scarps facing both east and west, juxtaposition of fan deposits of different ages, lack of substantial topographic expression, apparent right-lateral displacement of drainages, and left-stepping en echelon faults. Scarps along the fault formed in early Pleistocene (more than 800 ka) and late Tertiary surfaces are up to 8 m (26 ft) high (Hoffard, J.L. 1991, p. 40). The highest scarps occur where older alluvial fan remnants are juxtaposed against younger fan deposits. Neither vertical nor horizontal estimates of displacement have been calculated, although it appears that the lateral component exceeds the vertical slip. The most recent surface-rupture event is estimated to be middle to late Pleistocene, based on faulted fan surfaces older than 10 k.y. and younger than 300 to 500 k.y. At a single locality, an early Holocene to latest Pleistocene surface may be faulted. No evidence for faulting of early to late Holocene surfaces is reported. At a single location, a vertical slip rate of 0.006 to 0.06 mm/yr. was calculated for the fault using a 3-m-high (10-ft-high) scarp formed in a middle to late Pleistocene surface (50 to 500 ka) (Hoffard, J.L. 1991, p. 48). No recurrence interval information is available. This fault was not considered in the analysis by Pezzopane (1996).

East Pintwater Range Fault—This north-striking fault is located along the eastern side of the Pintwater Range, about 81 km (50 mi.) east of the potential repository site. It consists of a 58-km-long (36-mi.-long) zone of discontinuous normal faults with down-to-the-east displacements. Scarps are mapped at one location in depositional or erosional surfaces of possibly early to middle Pleistocene age (Keefer and Pezzopane 1996, p. 3-12). In general, other faults within the zone are visible as weakly to moderately expressed lineaments and scarps in surfaces on Quaternary deposits (Reheis 1992).

Eleana Range Fault—This 13-km-long (8-mi.-long) northeast-striking normal fault is located about 37 km (23 mi.) northeast of the potential repository site. Displacement is down to the east. Over much of its length, this fault is considered to form the contact between Quaternary alluvium and Paleozoic and Proterozoic bedrock. Scarps are mapped in alluvial surfaces at several localities. The youngest surfaces in which scarps are mapped are late Pleistocene, but most are early Pleistocene (more than 740 k.y.) and Pliocene in age.

Emigrant Fault—This 13-km-long (8-mi.-long), north-striking fault is located about 73 km (45 mi.) from the potential repository site. Displacement along the fault has been depicted as down to the west but no style of faulting has been reported. Prominent lineaments or scarps have been mapped in Quaternary deposits. No information about the amount of displacement, slip rate, or recurrence is available. This fault was not considered in the analysis by Pezzopane (1996).

Emigrant Valley North Fault—This fault includes numerous short, subparallel normal faults within Emigrant Valley. It is located 60 km (37 mi.) northeast of the potential repository site. The faults are in a 28-km-long (17-mi.-long) northeast-trending zone. Displacements are predominantly down to the northwest with possible minor strike-slip movement. Aerial photograph interpretations indicate fault scarps in late Quaternary alluvial fan deposits and possibly in pluvial lake deposits (Reheis 1991, p 2).

Emigrant Valley South Fault—This 20-km-long (12-mi.-long) fault is located about 66 km (41 mi.) from the potential repository site. It is probably more appropriate to refer to the Emigrant Valley South fault as a fault zone because its estimated width is reported to be between 4 and 9 km (2 and 6 mi.). The zone is defined by short, subparallel, north-northeast-striking fault traces and lineaments east of and between Papoose Lake and Groom Lake. The style of faulting within the zone is equivocal; scarps show both east- and west-side-down motion. A single fault may show evidence for strike-slip displacement. The age of displacements is poorly constrained; evidence for Quaternary activity includes weakly to moderately expressed lineaments and scarps on surfaces of unknown age developed in Quaternary deposits and faults in Quaternary deposits (Reheis 1992, p. 4). No further information about amount of displacement, slip rate, or recurrence interval is available.

Fatigue Wash Fault—This 16-km-long (10-mi.-long) fault is north-northeast-striking, with down-to-the-west, normal-oblique (sinistral) slip. It is located about 3.5 km (2.2 mi.) west of the potential repository site. Average dip of the fault is 73°W. Displacement of Miocene volcanic bedrock is 75 m (246 ft) (Menges and Whitney 1996a, p. 4.2-11). The majority of Quaternary slip appears to have taken place along the central and southern portions of the fault (Coe, Oswald et al. 1996). Two trenches were excavated across the fault. The trenches and seven topographic profiles provide evidence for three to six paleoearthquakes (five preferred) since the early to middle Pleistocene (Coe, Oswald et al. 1996, p. 4.8-18). Four of the five preferred events occurred since 730 ka; the two most recent events probably occurred between 8 and 100 ka. The age of the most recent event, which resulted in up to 40 cm (16 in.) of vertical offset of the youngest soil, is constrained to between 8 and 70 k.y. (20 to 60 k.y. preferred). The penultimate event, with a displacement of about 25 cm (10 in.), is constrained to between 15 and 100 k.y. in age (60 to 70 k.y. preferred). Earlier events include one between 100 and 450 ka with a displacement of 25 to 125 cm (10 to 49 in.), another event between 450 and 730 ka (displacement about 54 cm [21 in.]), and an old event that occurred prior to 730 ka. Estimates of the average recurrence interval range from 120 to 250 k.y. The Quaternary slip rate, estimated from 2.0 ± 0.2 m (6.6 ± 0.7 ft) of cumulative vertical offset of middle Pleistocene deposits mapped in the trench, is 0.001 to 0.015 mm/yr. ($4 \times 10^{-5} \pm 6 \times 10^{-4}$ in./yr.). A slip rate derived from scarp data to the north is 0.009 ± 0.006 mm/yr. ($4 \times 10^{-4} \pm 2 \times 10^{-4}$ in./yr.). The preferred slip rate for the entire fault ranges from 0.003 to 0.015 mm/yr. (1×10^{-4} to 6×10^{-4} in./yr.).

Furnace Creek Fault Zone—This significant component of the Death Valley-Furnace Creek-Fish Lake Valley fault system is a northwest-striking, right-lateral strike-slip fault. It is nearly coincident with the axis of northern Death Valley for a distance of about 145 km. (90 mi.). The point of the fault closest to the Yucca Mountain site is 50 km (31 mi.) away. Total lateral displacement on the fault is on the order of tens of kilometers. Evidence for multiple late Pleistocene to Holocene surface-rupture events is common along the fault. Displacements are as young as 0.2 to 2 k.y. and several are less than 10 k.y. Recent studies (Klinger and Piety 1996,

p. 56) document at least three late Holocene surface-rupture events. The average lateral displacement for the most recent event is about 4.7 m (15.4 ft). Average individual displacements for other events are 2.5 to 3.5 m (8.2 to 11.5 ft). The age of the most recent event is not well constrained. A short-term slip rate of 6 to 13 mm/yr. (0.24 to 0.51 in./yr.) is estimated based on a 248- to 330-m (814- to 1,083-ft) offset of a 25- to 40-ka alluvial fan. A long-term slip rate of 8 to 10 mm/yr. (0.31 to 0.39 in./yr.) is based on a 6- to 8-km (4- to 5-mi.) right-lateral offset of an alluvial fan deposit that overlies a tephra bed correlated with the 760-ka Bishop ash. The late Quaternary recurrence interval for surface-rupture events along the Furnace Creek fault zone is about 600 to 800 yr. The maximum surface rupture length is estimated to be about 105 km (65 mi.) (Klinger and Piety 1996, p. 56).

Ghost Dance-Abandoned Wash Fault—The Abandoned Wash fault is a down-to-the-west normal fault that displaces Tertiary bedrock. The fault trends southwest from the southern end of the Ghost Dance fault for about 2 km (1.2 mi.). The Ghost Dance and Abandoned Wash faults, located less than 1 km (0.6 mi.) from the Yucca Mountain site, have a combined length of about 5 km (3 mi.) and, if active, could rupture as a single feature. However, evidence does not support Quaternary offsets on either fault (Taylor et al. 1996, p. 4.5-34; Menges and Whitney 1996a, p. 4.2-15).

Ghost Dance Fault Zone—This fault zone is located in the central part of the potential repository site. The total length of the fault is uncertain; however, Taylor et al. (1996) report a length of about 6 to 8 km (4 to 5 mi.). The fault is mapped for approximately 3 km (2 mi.) as a zone of numerous splays that not only parallels the main north-trending trace of the zone, but locally branches away from the main trace. Spengler et al. (1993) interpret the fault zone as complex, varying in width from a few meters to as much as 213 m (699 ft), with individual faults commonly spaced 15 to 46 m (49 to 151 ft) apart. The estimated width of the zone varies from 2 to 150 m (7 to 492 ft). Cumulative down-to-the-west bedrock displacement ranges from up to 5 m (16 ft) at its northern end to 12 to 15 m (39 to 49 ft) in the central portion (Taylor et al. 1996, p. 4.5-8). No latest Pleistocene or Holocene offset or fracturing has been documented in numerous trenches excavated across the fault. A single fractured bedrock exposure, in Trench 4a, has associated secondary carbonate and opaline silica laminae that provide U-series age estimates of 22 to 265 ka. An unfractured deposit overlies the fractured bedrock and provides U-series ages of 45 to 50 ka. Thus, the fracturing event may range from about 45 to more than 265 ka (Taylor et al. 1996, p. 4.5-25). The Ghost Dance fault bifurcates; one branch connects with the Abandoned Wash fault to the southwest (Day et al. 1996), and the other branch trends southeast, but does not appear to connect with the Dune Wash fault (Keefer and Pezzopane 1996, p. 3-14).

Grapevine Fault—This 20-km-long (12-mi.-long), northwest-striking fault is located approximately 58 km (36 mi.) west of Yucca Mountain. It is a normal fault with down-to-the-southwest displacement. Vertical displacement of Tertiary rocks may be up to several thousand meters. Although activity was highest during late Pliocene and early Pleistocene time, recurrent movement as recent as Holocene time is documented.

Grapevine Mountains Fault—Two principal normal faults and subsidiary faults mark the Grapevine Mountains fault along the northwestern end of the Grapevine Mountains, about 67 km (42 mi.) northwest of Yucca Mountain. The faults with down-to-the-west displacement trend

northeast for a distance of 31 km (19 mi.). The principal faults juxtapose Quaternary alluvium against bedrock. Portions of one normal fault form scarps in early to middle and possibly late Pleistocene surfaces.

Hunter Mountain-Panamint Valley Faults—These combined faults extend for 185 km (11.5 mi.). The Hunter Mountain fault may be seismogenically linked to the Panamint Valley fault. Both faults exhibit evidence for Holocene activity. The length of the combined faults is sufficient to make them relevant seismic sources.

Indian Springs Valley Fault Zone—This fault zone, bounding the western side of Indian Springs Valley, consists of subparallel faults in a 28-km-long (17-mi.-long), north-to-northwest-trending zone. The fault zone is 67 km (42 mi.) east of Yucca Mountain. Down-to-the-east displacement along the fault zone is variously expressed as fault contacts between Quaternary alluvium and bedrock or as weakly to moderately expressed lineaments and scarps in surfaces on Quaternary and Tertiary deposits.

Iron Ridge Fault—This up to 21-km-long (13-mi.-long) fault extends southeast from about 2 km (1.2 mi.) south of the potential repository site. The fault may serve as the southeastern splay of the Solitario Canyon fault. It may also connect with the Stagecoach Road fault; however, there is no direct evidence that the faults are structurally or temporally connected. In addition, paleoseismic evidence indicates that the Iron Ridge fault is significantly less active than the Stagecoach Road fault (Ramelli et al. 1996). The fault forms a bedrock-alluvial contact for half its total length where prominent scarps between bedrock and colluvium are visible locally (Keefer and Pezzopane 1996, p. 3-16). Displacement is primarily normal dip-slip with down-to-the-west motion. The average dip of the fault is about 70°W. At one locality, evidence for multiple late Quaternary faulting events is documented (Keefer and Pezzopane 1996, p. 3-16). Paleoseismic evidence from a single trench suggests one to possibly four events including a probable Holocene event with displacements up to 10 cm (4 in.). Several poorly resolved middle Quaternary events associated with individual displacements of 170 to 200 cm (67 to 79 in.) are also reported (Ramelli et al. 1996). Age constraints are insufficient to estimate recurrence intervals or slip rates. Soil stratigraphic relationships suggest no correlation of events with either the Solitario Canyon or Stagecoach Road faults.

Kawich Range Fault Zone—This fault zone comprises numerous subparallel northeast- to northwest-striking normal faults with down-to-the-west displacements. The zone, located along the western side of the Kawich Range, is about 57 km (35 mi.) north of the potential repository site. Over its 84-km (52-mi.) length, the zone contains faults that are mostly in bedrock or form the bedrock-alluvium contact. Recent work suggests that latest Pleistocene scarps in alluvium are up to 2.6 m (8.5 ft). The scarps are discontinuous and span 3.6 to 7.4 km (2.2 to 4.6 mi.) of the fault zone (Keefer and Pezzopane 1996, p. 3-16). Evidence for recurrent late Quaternary movement is equivocal.

Kawich Valley Fault Zone—This fault zone comprises a cluster of faults near the middle of the northern end of Kawich Valley and scattered faults along the western side of the valley. Generally, the faults strike north for a distance of about 43 km (27 mi.). This zone is located 61 km (38 mi.) north of the Yucca Mountain site. The fault is expressed primarily as weakly

developed lineaments and east-facing scarps in Quaternary deposits and erosion surfaces (Keefer and Pezzopane 1996, p. 3-16).

Keane Wonder Fault Zone—This fault zone consists of a 25-km-long (16-mi.-long) anastomosing group of northwest-striking fault strands and topographic lineaments mapped along the southwestern flank of the Funeral Mountains in Death Valley (Keefer and Pezzopane 1996, p. 3-17). The fault zone lies 43 km (27 mi.) southwest of Yucca Mountain. Style of faulting is primarily normal, with down-to-the-southwest displacement. No evidence of late Quaternary faulting and only equivocal evidence of isolated middle Pleistocene or older faulting is reported. However, clear evidence for recurrent late Quaternary faulting is reported along a 2-km-long (1.2-mi.-long) fault splay near the southern end of the fault zone (Keefer and Pezzopane 1996, p. 3-17). The youngest faulted fan surface at this locality is offset 1.8 m (5.9 ft); older fan deposits have been offset as much as 8 to 10 m (26 to 33 ft). The most recent event is estimated to have occurred 4 to 8 ka; earlier events are estimated between 70 to 730 ka.

Mercury Ridge Faults—The Mercury Ridge faults are two northeast-striking faults that bound Mercury Ridge. They are located about 48 km (30 mi.) east-southeast of the potential repository site. The maximum length of the longest fault is 10 km (6 mi.). Both normal dip-slip and strike-slip motions have been documented. Both faults have been mapped as either forming the bedrock-alluvium contact or as concealed by Quaternary and Tertiary alluvium (Keefer and Pezzopane 1996, p. 3-17).

Midway Valley Fault—This fault is concealed within Midway Valley, about 3 km (2 mi.) east of the potential repository site. It is shown in structure sections (Scott and Bonk 1984) and in gravity and magnetic surveys (Ponce 1993). These geophysical surveys suggest down-to-the-west displacements of Tertiary bedrock by up to 40 to 60 m (131 to 197 ft). Neither method has detected displacement of overlying early and middle Quaternary deposits in surface mapping or trenches in Midway Valley (Keefer and Whitney 1996, p. 4.3-7). The geophysical profiles define a structure at least 1 km (0.6 mi.) and possibly as much as 5 km (3 mi.) long.

Mine Mountain Fault Zone—This fault zone is a major feature of the Spotted Range-Mine Mountain structural zone. It extends along the southern flank of Mine Mountain as two northeast-striking subparallel faults separated by as much as 200 m (656 ft). Depending upon how various sections are connected, the length of the zone may be up to 27 km (17 mi.). The closest distance between its projected trace and the potential repository site is about 19 km. The fault dip is unknown. The Tiva Canyon Tuff has a left-lateral offset of 1.2 km (0.8 mi.) at Mine Mountain. It is reported that the fault zone was active sometime during the period from 7 to 10 Ma (Keefer and Pezzopane 1996, p. 3-18). Fault activity may have continued into the Pleistocene epoch at a lower rate, but clear evidence of Pleistocene faulting has been found at only one locality at the northeastern corner of Shoshone Mountain. The absolute age of this displacement is unknown; however, soil and caliche development in the deposit suggests that the faulting is older than about 50 k.y.

Oak Springs Butte Faults—These faults consist of a series of north-striking normal faults located along the eastern side of the Belted Range. They form a zone 21 km (13 mi.) long located 57 km (35 mi.) northeast of Yucca Mountain. These faults are also referred to as the Oak Springs Butte faults by Piety (1996, p. 257) and Keefer and Pezzopane (1996, p. 3-18) Both

down-to-the-east and down-to-the-west displacements are documented. The youngest observed fault in the zone is evident as a scarp in late Pleistocene depositional or erosional surfaces (Dohrenwend et al. 1992). Short portions of other faults in the zone form weakly to moderately expressed lineaments or scarps in Tertiary deposits or fault contacts between Quaternary alluvium and bedrock (Keefer and Pezzopane 1996, p. 3-18).

Oasis Valley Fault Zone—This fault zone forms a 20-km-long (12-mi.-long) cluster of north-striking normal faults in Oasis Valley, along 24 km (15 mi.) northwest of Yucca Mountain. Dip-slip motion is both down to the east and down to the west. No compelling evidence for late Quaternary movement has been found along this fault zone (Keefer and Pezzopane 1996, p. 3-19). However, a 2.5-km-long (1.6-mi.-long) section of a prominent strand forms a distinct air photo lineament that may reflect minor early Pleistocene displacement.

Pagany Wash Fault—This fault is one of the northwest-striking right-lateral strike-slip faults mapped across the northeastern part of the site area about 2.5 km (1.6 mi.) from the potential repository site. It occurs in Tertiary volcanic rocks throughout much of its 4-km (2.5-mi.) length; a few short portions are exposed as small scarps in bedrock. A 1-km (0.6-mi.) portion is buried by middle Pleistocene deposits toward the northwestern end of the wash (Keefer and Pezzopane 1996, p. 3-19). The fault terminates against the Solitario Canyon fault to the northwest and the north-striking Bow Ridge fault to the southeast. A trench excavated across Pagany Wash exposes a tightly cemented shear zone in bedrock that underlies undisplaced bedrock regolith and colluvial units, suggesting a lack of late Quaternary activity (Keefer and Pezzopane 1996, p. 3-19).

Pahrump Fault Zone—This fault zone is a northwest-striking, high-angle, west-dipping, right-lateral, oblique fault zone. It lies 70 km (44 mi.) southeast of the potential repository site and extends for about 70 km (44 mi.) along the eastern side of Stewart Valley and into central Pahrump Valley. Compelling evidence for late Quaternary deformation is present along only about an 18.5-km-long (11.5-mi.-long) section. Right-lateral displacement of Paleozoic rocks is estimated to be greater than 16 to 19 km (10 to 12 mi.) (Keefer and Pezzopane 1996, p. 3-19), with a minimum vertical displacement of about 300 m (984 ft) (Stewart 1988, p. 694). The amount of Quaternary slip, assumed to be primarily right-lateral, is unknown. Age of the most recent activity is Quaternary, evidenced by a few scarps of limited length and small offsets of surficial deposits (Keefer and Pezzopane 1996, p. 3-20). Scarps range from 0.7 to 2.0 m (2.3 to 6.6 ft) in height. Though poorly constrained, these scarps may be early to middle Holocene in age (Keefer and Pezzopane 1996, p. 3-20). Based on the geomorphic expression of 15-m-high (49-ft-high) scarps in early Pleistocene or Tertiary sediments, the Quaternary slip rate on the Pahrump fault zone is low.

Pahute Mesa Faults—A number of faults have been mapped on Pahute Mesa north of Yucca Mountain. Lengths range from 0.5 to 4 km (0.3 to 2.5 mi.), with the longest series of overlapping fault traces in a zone measuring about 9 km (6 mi.) in length. The nearest of the faults is 48 km (30 mi.) from the potential repository site. The faults have diverse east to northwest trends and generally have dip-slip movement, although some evidence suggests a right-lateral strike-slip component. Based on air photo interpretations, weak to prominent lineaments or scarps have been delineated on surfaces of both Quaternary and Tertiary deposits (Reheis 1992).

Paintbrush Canyon Fault—This fault is located 4 km (2.5 mi.) east of the potential repository site. It continues from about 10 km (6 mi.) north of Yucca Wash to as far south as the northern end of the Stagecoach Road fault, for an overall length of about 26 km (16 mi.) (Menges and Whitney 1996b). Estimates of the amount of Tertiary bedrock displacement range from 250 to 500 m (820 to 1,640 ft) down to the west (Menges and Whitney 1996a, p. 4.2-19). Average dip on the fault is about 70°W. Measurements on slickenside indicate that net displacement is normal dip-slip to left-oblique (Menges and Whitney 1996a, p. 4.2-20). Paleoseismic studies, including exploratory trenching and exposure logging, reveal multiple Quaternary surface-rupture events along the Paintbrush Canyon fault. The most recent event may be as young as early Holocene to latest Pleistocene. Fault relationships, exposed on the western side of Busted Butte in eolian sand deposits, record the last 600 to 700 k.y. of Pleistocene depositional and faulting history (Menges and Whitney 1996b, p. 4.4-10). Three to seven faulting events are identified. Deposits associated with the oldest event are located above a sand unit with interbedded silicic ash that is correlated to the Bishop ash. Three to four events occurred after formation of a soil dated at about 400 ka. The youngest event occurred within a time period of 7 to 20 ka (Menges and Whitney 1996b, p. 4.4-11). Three to four faulting events are recorded in Quaternary deposits exposed in Trench MWV-T4 excavated at the southeastern edge of Midway Valley (Menges and Whitney 1996b, p. 4.4-14). The most recent event displaces a unit dated at 40 ka. This faulted unit is overlain by an unfaulted unit dated at about 6 ka (Menges and Whitney 1996b, p. 4.4-15). Trench A1, excavated at the northwestern base of Alice Ridge, provides better timing constraints for the most recent event at 7 to 20 ka. Evidence supports at least four events at this site (Menges and Whitney 1996b, p. 4.4-15). The amount of late Quaternary cumulative slip estimated from the Midway Valley trench is 1 to 3.6 m (3.3 to 11.8 ft). Total Quaternary displacement from the Busted Butte exposures is 2.3 to 10.8 m (7.5 to 35 ft). Total cumulative displacements are 1.45 to 1.7 m (4.75 to 5.6 ft) at Alice Ridge. Single displacements vary widely both within and among sites, with preferred dip-slip ranges of 0 to 2.6 m for Busted Butte, 0.2 to 1.4 m (0.7 to 4.6 ft) for Midway Valley, and 0.05 to 0.4 m (0.2 to 1.3 ft) for Alice Ridge. Combined age and displacement data indicate average recurrence intervals of 20 to 50 k.y. and a slip rate of 0.001 to 0.03 (preferred 0.002 to 0.015) mm/yr. for the Midway Valley trench locality. Preferred recurrence intervals of 50 to 120 k.y. and a slip rate of 0.001 to 0.01 (preferred 0.007) mm/yr. are estimated for the Busted Butte locality. Preferred recurrence intervals of 80 to 100 k.y. and slip rates of 0.001 to 0.004 (preferred 0.002) mm/yr. (4×10^{-5} to 2×10^{-4} in./yr. [preferred 8×10^{-5} in./yr.]) are estimated for the Alice Ridge site (Menges and Whitney 1996b, p. 4.4-21). The average recurrence interval for the entire Paintbrush Canyon fault is 20 to 270 k.y. (20 to 120 k.y. preferred) with a slip rate of 0.001 to 0.03 mm/yr. (4×10^{-5} to 1×10^{-3} in./yr.) (0.002 to 0.015 mm/yr. [8×10^{-5} to 6×10^{-4} in./yr.] preferred).

Paintbrush Canyon-Stagecoach Road Faults—The combined length of these two faults is about 33 km (21 mi.). The minimum distance to the potential repository site is 4 km (2.5 mi.). Each fault displays a history of recurrent Quaternary activity. If the faults behave seismically as a single feature, the potential rupture could cause moment magnitudes and peak accelerations that are larger than the ruptures that might occur on either individual fault (Table 12.3-11) (Pezzopane 1996).

Panamint Valley Fault—This 100-km-long (62-mi.-long) fault bounds the eastern side of the north-trending Panamint Range. The fault is about 95 km (59 mi.) south-southwest of Yucca

Mountain. The sense of displacement is predominantly normal dip-slip, with evidence for significant right-lateral motion along some sections of the zone. The fault displays abundant evidence for late Quaternary or Holocene activity, with scarps from up to 61 m (200 ft) high formed during multiple faulting events (Keefer and Pezzopane 1996, p. 3-21). Dip-slip displacements associated with the most recent event at the southern end of the fault are 0.4 to 1.2 m (1.3 to 3.9 ft) along the range-front fault (Zhang et al. 1990, p. 4859). Right-lateral displacement of topographic ridges at various locations are 24 ± 4 m (79 ± 13 ft), 27 ± 4 m (89 ± 13 ft), and 37 ± 4 m (121 ± 13 ft) (Zhang et al. 1990, pp. 4862 to 4863). The maximum age estimate for the ridges is 17 ± 4 k.y. (Zhang et al. 1990, p. 4866). Scarps from older events show right-lateral displacements of 6 to 7 m (20 to 23 ft) for possibly two events and 11 ± 2 m (36 ± 7 ft) for three to four events (Zhang et al. 1990, pp. 4861 to 4862). Based on a maximum right-lateral displacement of 37 ± 4 m (121 ± 13 ft) of a ridge dated at 17 ± 4 ka, a minimum Holocene-latest Pleistocene lateral slip rate of 2.4 ± 0.8 mm/yr. (0.09 ± 0.03 in./yr.) is estimated (Zhang et al. 1990, pp. 4865 to 4866). The average recurrence interval ranges from 0.7 to 2.5 k.y. (Smith, R.S.U. 1979, p. 415).

Plutonium Valley-North Halfpint Range Fault Zone—This fault zone is located along the western side of the Halfpint Range at its junction with Plutonium Valley and Yucca Flat. Various strands of this north- to northwest-trending fault zone can be traced for a total distance of about 26 km (16 mi.). The zone is located 46 km (29 mi.) east-northeast of the potential repository site. Faults within the zone primarily have normal dip-slip motion, with both down-to-the-east and down-to-the-west orientations. Short sections of this fault zone are expressed as weak lineaments and scarps on surfaces in Quaternary and Tertiary deposits (Keefer and Pezzopane 1996, p. 3-22). Other sections either form a fault contact between bedrock and Quaternary alluvium or are concealed by the alluvium (Keefer and Pezzopane 1996, p. 3-22).

Rock Valley Fault Zone—The 30-km-long (19-mi.-long) Rock Valley fault zone comprises three principal sets of faults within Rock Valley, including long, east-northeast-striking left-lateral faults; short, northeast-striking connecting faults of varying displacement styles; and minor, northwest-striking normal and strike-slip faults. Within the first set of faults, three strands are prominent and have been studied the most. The fault zone, located about 27 km (17 mi.) southeast of Yucca Mountain, has been episodically active since late Oligocene time. Total left-lateral displacement across the three subparallel strands is less than 4 km (2.5 mi.) (Keefer and Pezzopane 1996, p. 3-22). Quaternary activity has been distributed across the three principal fault strands within Rock Valley. The southernmost strand extends for a distance of about 14 km (9 mi.) and has continuous scarps up to 2.5 km (1.6 mi.) long (Coe, Yount, and O'Leary 1996). The northernmost strand extends for an inferred distance of about 18.5 km (11.5 mi.). The eastern portion of the fault has no expression in Pleistocene-aged deposits. Farther to the west, scarps are present in fan remnants (Coe, Yount, and O'Leary 1996). The third strand occurs between these two faults. It is referred to as the "medial strand" and has a continuous mapped length of 9.5 km (5.9 mi.) and may extend as much as 7.5 km (4.7 mi.) farther to the west. Quaternary scarps are preserved principally in the prominent central and northern part of the Rock Valley fault zone with scarp heights up to 2.5 m (8.2 ft).

Two exploratory trenches (RV1 and RV2) were excavated in 1978 and logged in 1984 across the medial strand (Yount et al. 1987). Eight additional trenches were excavated in 1995, with four

excavated on the northern strand (site RV3) and four excavated on the southern strand (sites RV4 and RV5). The trenches along the medial strand provided evidence of multiple Quaternary events; however, unreliable dates were obtained from those excavations. The most recent event had a vertical displacement of between 10 and 30 cm (4 and 12 in.) (Coe, Yount, and O'Leary 1996). Although not directly measured, a left-lateral component of displacement using a 22° rake yields a possible 0.85 m (2.8 ft) of net displacement (Yount et al. 1987). Up to four events are observed from exposures along the northern fault strand (Coe, Yount, and O'Leary 1996). The most recent event occurred between 4 and 17 ka; dates for the prior three events are pending. About 14.2 m (46.6 ft) of lateral and 2.3 m (7.5 ft) of vertical cumulative net-slip are associated with these four events based on total offset of a channel thalweg (Coe, Yount, and O'Leary 1996). Three events were interpreted from the trenches along the southern fault strand. The most recent event occurred at about 2 to 3 ka based on evidence from Trench RV4 (Coe, Yount, and O'Leary 1996). This event does not correspond with the most recent event along the northern strand, suggesting that these faults have behaved independently, at least recently. Slip rates have been calculated for the individual strands and for the entire fault zone. The northern strand has a slip rate of less than 0.05 mm/yr. (2×10^{-3} in./yr.); the southern strand has a poorly constrained slip rate of less than 0.002 mm/yr. (8×10^{-5} in./yr.); and the medial strand has a poorly constrained slip rate of 0.02 mm/yr. (8×10^{-4} in./yr.) based on the most recent event (Coe, Yount, and O'Leary 1996). A slip rate range of 0.002 to 0.05 mm/yr. (8×10^{-5} to 2×10^{-3} in./yr.) is estimated for the entire fault zone (Coe, Yount, and O'Leary 1996, p. 4.13-26). An average recurrence interval for the entire fault zone ranges from 5 to more than 10 k.y. (Coe, Yount, and O'Leary 1996, p. 4.13-27). Repeated, clustered, small-magnitude (M_L 4.0) earthquakes within and in the vicinity of Rock Valley indicate that faults within the zone remain seismically active (Section 12.3.5.2). An M 3.5 strike-slip earthquake that occurred along the zone on September 7, 1995, had a hypocentral depth of 4 km (2.5 mi.) (Shields et al. 1995).

Rocket Wash-Beatty Wash Fault—This fault strikes generally north for a distance of approximately 17 km (11 mi.). It is located about 19 km (12 mi.) northwest of the potential repository site. The zone consists of a series of north-trending fault strands. Miocene volcanic rocks have been displaced 10 to 30 m (33 to 98 ft) both down to the east and down to the west. Geomorphic and geologic relationships indicate that most or all displacement on this fault zone occurred in the late Miocene.

Sarcobatus Flat Fault Zone—This fault zone is located along the western margin of Pahute Mesa and northeast of Sarcobatus Flat, about 52 km (32 mi.) northwest of the potential repository site. The 51-km-long (32-mi.-long), north- to northwest-trending zone contains a series of relatively short faults (maximum length 12 km [7.5 mi.]). Tertiary rocks are generally displaced down to the west. A single, 100-m-long (328-ft-long) scarp with about 0.6 m (2.0 ft) of relief occurs in alluvium; however, evidence does not suggest a fault scarp. Several short, inconspicuous lineaments in Quaternary deposits are recognizable on aerial photographs, but no lineaments examined in the field show surface offsets (Keefer and Pezzopane 1996, p. 3-23).

Sever Wash Fault—This 4-km-long (2-mi.-long) northwest-striking, right-lateral strike-slip fault occurs about 3 km (2 mi.) north of the potential repository site (Scott and Bonk 1984). The near-vertical main trace of the fault is exposed in Tertiary volcanic rocks on the southern flank of Sever Wash. Evidence for right-lateral strike-slip movement includes slickensides and Reidel

shears (Day et al. 1996). Portions of the fault are concealed by unfaulted Holocene alluvium along the floor of the wash (Keefer and Pezzopane 1996, p. 3-23).

Solitario Canyon Fault—The main trace of this north-striking fault extends southward from Yucca Wash for about 18 km (11 mi.). It is located about 1 km (0.6 mi.) from the western boundary of the potential repository site. At about 2 km (1.2 mi.) south of the potential repository site, the Solitario Canyon fault appears to splay. The southeastern splay of the fault is referred to as the Iron Ridge fault (Ramelli et al. 1996). The structural and tectonic relationships between the two faults are not well understood. Bedrock displacement varies from 61 m (200 ft) down to the east at the northern end to more than 500 m (1,640 ft) down to the west at the southern end (Keefer and Pezzopane 1996, p. 3-24). Average dip of the fault plane is 73°W. Slickensides indicate that the fault has primarily normal slip with minor left-lateral slip. A continuous 14-km-long (9-mi.-long) Quaternary tectonic and erosional scarp is present at the bedrock-surficial deposit contact. Eleven trenches and one natural exposure have been documented. Evidence from five exploratory trenches suggests four late Quaternary surface-rupture events (Ramelli et al. 1996, Table 4.7-3). The evidence provides an estimated cumulative dip-slip of 2.1 m (6.9 ft) (Ramelli et al. 1996). Individual displacement amounts vary from fracturing to 1.3 m (4.3 ft). An equivocal most recent event occurred between 14 and 40 ka (15 to 30 ka preferred) (Ramelli et al. 1996, p. 4.7-3). All four observed events probably occurred within the last 250 k.y. The average late Quaternary recurrence interval is within the range of 35 to 100 k.y., with preferred values of 50 to 70 k.y. (Ramelli et al. 1996, p. 4.7-48). Preliminary average slip rates range from 0.01 to 0.02 mm/yr. (4×10^{-4} to 8×10^{-4} in./yr.); the preferred rate is 0.01 mm/yr. (4×10^{-4} in./yr.) (Ramelli et al. 1996, p. 4.7-49). A faulted basaltic ash is present in four trenches along the fault. The ages of faulting events associated with the ash are estimated between 60 and 100 k.y. (preferred age of 75 ± 10 k.y.) (Ramelli et al. 1996, p. 4.7-48). The ash date is based on preliminary U-series ages and tentative geochemical correlations of the ash with likely source eruptions at the Lathrop Wells cone, which yield $^{40}\text{Ar}/^{39}\text{Ar}$ ages of 77.3 ± 6.0 and 76.6 ± 4.9 k.y. for associated flows (Heizler et al. 1999, p. 767).

South Ridge Faults—These faults consist of two principal faults, one of which is nearly 19 km (12 mi.) long. The faults strike east to northeast and have variable dip-slip to strike-slip displacement. They are located 50 km (31 mi.) east-southeast of Yucca Mountain. One fault is mapped as the contact between bedrock and Quaternary alluvium. Sections of the other fault are either prominently to weakly expressed lineaments and scarps on surfaces in Tertiary deposits or are concealed by Quaternary and Tertiary alluvium (Keefer and Pezzopane 1996, p. 3-24).

Spotted Range Faults—These faults are located primarily along the western side of Spotted Range, approximately 59 km (37 mi.) east-southeast of the potential repository site. Several north- to northeast-striking normal faults with down-to-the-west displacements are combined for a length of more than 30 km (19 mi.). Individual faults juxtapose Quaternary alluvium against bedrock or occur as scarps on Quaternary and Tertiary surfaces (Keefer and Pezzopane 1996, p. 3-24).

Stagecoach Road Fault—This north- to northeast-striking normal to left-oblique fault is mapped along the southeastern corner of Yucca Mountain. It is located about 10 km (6 mi.) south of the potential repository site (Scott 1992). It is mapped in middle Pleistocene alluvium for approximately 4 to 5 km (2 to 3 mi.) south of Stagecoach Road, where it is concealed by

Holocene surficial deposits. The fault has variously been connected northward with the Iron Ridge fault or northeastward with the Paintbrush Canyon fault (Keefer and Pezzopane 1996, p. 3-25). Estimated bedrock displacement is 400 to 600 m (1,312 to 1,968 ft) down to the west (Keefer and Pezzopane 1996, p. 3-25). Average dip of the fault is 73°W. Trenches expose evidence for two to four late Quaternary faulting events between about 5 to 118 ka (Menges and Whitney 1996b, p. 4.4-30). The most recent event is estimated to be early Holocene to latest Pleistocene (5 to 17 ka) (Menges and Whitney 1996b, p. 4.4-32; Menges et al. 1998). Individual displacement estimates vary from 0.14 to 0.99 m (0.46 to 3.25 ft). Age relationships provide an average recurrence interval estimate of 5 to 50 k.y., with a preferred range of 10 to 30 k.y. (Menges and Whitney 1996b, p. 4.4-33). Slip rates range from 0.006 to 0.07 mm/yr. (2×10^{-4} to 3×10^{-3} in./yr.), with a preferred value of 0.03 to 0.05 mm/yr. (1×10^{-3} to 2×10^{-3} in./yr.) (Menges and Whitney 1996b; p. 4.4-33). Menges and Whitney (1996b, p. 4.4-33) report that these are the shortest recurrence intervals and highest slip rates estimated for any Quaternary faults in the Yucca Mountain area.

Sundance Fault—Spengler et al. (1994) described this fault as a series of near-vertical, northwest-striking faults that intersect the Ghost Dance fault in the northern part of the repository block. Detailed mapping indicates that the total length of the fault is 1 km (0.6 mi.), and that it cannot be traced across the Ghost Dance fault (Keefer and Pezzopane 1996, p. 3-25). Cumulative down-to-the-northeast displacement of Tiva Canyon Tuff bedrock is up to 11 m (36 ft) in surface exposures. The fault, developed entirely in bedrock, shows no evidence for Quaternary activity.

Tolicha Pass Fault Zone—This fault comprises several north- to northwest-striking faults located about 42 km (26 mi.) northwest of Yucca Mountain. The combined length of the faults is approximately 22 km (14 mi.). Displacements are mapped as down to the southwest, but at some localities movement is apparently down to the northeast. At a single location, right-lateral, oblique-slip is reported (Keefer and Pezzopane 1996, p. 3-25). Moderately to prominently expressed lineaments and scarps are mapped in Quaternary surfaces from photo interpretation (Reheis 1992). R.E. Anderson, Bucknam et al. (1995) found no unequivocal evidence for Quaternary faulting in the field or evidence supportive of a through-going fault in this area.

Towne Pass Fault—This 38-km-long (24-mi.-long), down-to-the-west normal fault is located about 76 km (47 mi.) from the potential repository site. The fault extends from Panamint Valley to Emigrant Wash in Death Valley. Several investigators have identified evidence for Quaternary and, in some locations, Holocene activity. No detailed paleoseismic investigations are reported by Piety (1996). The amount of displacement is reported only as a long-term rate ranging from at least 153 m (502 ft) in deposits of unknown age to a long-term amount of at least 2,380 m (7,808 ft) that accounts for most of the elevation of the Panamint Range south of Towne Pass. Also, most of the displacement on the fault is older than an overlying, unfaulted late Pliocene basalt. No additional information about slip rate and recurrence interval along the Towne Pass fault is available.

Wahmonie Fault—This northeast-striking fault is within the 30- to 60-km-wide (19- to 37-mi.-wide) Spotted Range-Mine Mountain structural zone. The zone comprises small-displacement, left-lateral faults. The length of the Wahmonie fault is approximately 15 km (9 mi.), and its closest distance to the potential repository site is 22 km (14 mi.). Based on the

presence of scarps and lineaments in 270- to 740-ka deposits and burial of the fault by Holocene deposits, the most recent event is probably Pleistocene (Keefer and Pezzopane 1996, p. 3-26). At the southwestern end of the fault, displacement is down to the northwest; at the northeast end, it is down to the southeast. The total displacement along the fault is unknown.

West Pintwater Range Fault—This west-dipping normal fault trends north along the western flank of the Pintwater Range. The fault, located about 76 km (47 mi.) east of Yucca Mountain, is discontinuous over a length of about 82 km (50 mi.). Down-to-the-west displacements are expressed as prominent lineaments and scarps primarily in early to middle and/or late Pleistocene and Tertiary deposits. At its northern end, the fault is mapped as the contact between bedrock and Holocene to Pliocene alluvium and colluvium (Keefer and Pezzopane 1996, p. 3-26).

West Specter Range Fault—This fault bounds the western flank of a south-trending arm of the Specter Range, about 33 km (21 mi.) southeast of Yucca Mountain. The fault strikes north for a distance of about 9 km (6 mi.). Displacement is predominantly normal dip-slip, down to the west, and possibly has a minor lateral component. Approximately 40 percent of the fault has scarps in Quaternary materials and about 35 percent has tonal or vegetational lineaments or drainage alignments that may be associated with surface rupture. The remaining 25 percent is concealed by unfaulted Quaternary deposits (Keefer and Pezzopane 1996, p. 3-26). The most recent surface-rupture event is interpreted to be latest Pleistocene or Holocene along the northern section of the fault. The total surface offset, represented by scarps in alluvium, ranges from 0.3 to 0.5 m (1.0 to 1.6 ft) on the youngest faulted alluvium (about 15 ka) to as much as 1.4 m (4.6 ft) on older faulted alluvium (more than 128 ka). A poorly constrained recurrence interval of 113 k.y. and a slip rate of less than 0.004 mm/yr. (2×10^{-4} in./yr.) for the period of time between 15 and 128 ka (Keefer and Pezzopane 1996, p. 3-27) are estimated for this fault.

West Spring Mountains Fault—This 60-km-long (37-mi.-long), north- to northwest-striking, west-dipping, predominantly normal-slip fault bounds the southwestern side of the northern Spring Mountains. The fault is about 53 km (33 mi.) southeast of the potential repository site. The main fault has predominantly normal-slip, but scarps along the southern extension have a left-stepping pattern that suggests a possible right-lateral component of slip. The fault forms scarps in Pleistocene surfaces. The most recent surface-rupture event occurred during latest Pleistocene or early Holocene time. It resulted in 1.8 to 2.0 m (5.9 to 6.6 ft) of surface offset along the central section of the fault (Keefer and Pezzopane 1996, p. 3-27). The longest scarps are located along the 11-km-long (7-mi.-long) central section of the fault, suggesting that either larger or more frequent displacement events occur on the central section than elsewhere along the fault. Scarps up to 13.4 m (44.0 ft) (9.4 m [30.8 ft] of surface offset) formed in middle Pleistocene alluvial fans along the central section may record an average recurrence interval of more than 28 k.y. and a long-term slip rate of less than 0.07 mm/yr. (3×10^{-3} in./yr.) (Keefer and Pezzopane 1996, p. 3-27).

Windy Wash Fault—This fault, located on the eastern side of Windy Wash and about 4.5 km (2.8 mi.) west of the potential repository site, is north- to northeast-striking, west-dipping, with normal-oblique motion. The fault is mapped for about 22 km (14 mi.) as a discontinuous structure from the southern rim of the Claim Canyon caldera to the southeastern edge of Crater Flat (Keefer and Pezzopane 1996, p. 3-27). The amount of down-to-the-west Tertiary bedrock

displacement is reported to be less than 500 m (1,640 ft) (Keefer and Pezzopane 1996, p. 3-27). The average dip of the fault is 77°W to vertical. Slickenside orientations vary and indicate mostly dip-slip motion, with small components of right- and left-lateral slip. Evidence for Quaternary displacement along the northern and southern parts of the fault is limited to fault scarps in alluvium and fractures in the hanging walls of fault-line scarps. Trenches excavated across scarps in alluvium along the central portion of the fault contain evidence for three to eight events since about 400 ka (Whitney, Simonds et al. 1996, pp. 4.9-23 to 4.9-30). The most recent event displaces a late Holocene vesicular silty sand deposit, by less than 0.1 m (0.3 ft), that underlies the modern desert pavement (Whitney, Simonds et al. 1996). Individual vertical displacements for the other events range from 0.08 to about 1.0 m (0.3 to about 3.3 ft) (Whitney, Simonds et al. 1996, pp. 4.9-24 to 4.9-30). An average recurrence interval ranges from 40 to 57 k.y. (40 to 45 k.y. preferred), and average slip rates range from 0.009 to 0.01 mm/yr. (3.5×10^{-4} to 4×10^{-4} in./yr.) (Whitney, Simonds et al. 1996, p. 4.9-31). A long-term slip rate of 0.27 mm/yr. (0.01 in./yr.), calculated from 101 m (331 ft) of net offset of a 3.7-Ma (K-Ar) basalt flow (Whitney, Simonds et al. 1996, pp. 4.9-33 to 4.9-34), is significantly higher than the short-term rate.

Yucca Fault—This north-striking, east-dipping fault is about 32 km (20 mi.) long. The fault is located within Yucca Flat, about 40 km (25 mi.) northeast of the potential repository site. The fault dips at 75° to 80°E near the surface, but appears to flatten to 55° to 65°E at depth. Tertiary volcanic rocks are displaced vertically 200 m (656 ft) down to the east. An apparent right-lateral component of motion may equal or exceed this amount. Evidence for Quaternary activity includes scarps in Quaternary deposits (scarp heights up to 15.3 m [50.2 ft]) and faulted Quaternary deposits (Keefer and Pezzopane 1996, p. 3-28). Deposits from 160 to 800 ka are displaced along much of the fault. The youngest surface-rupture event may be late Pleistocene. In places, the fault is concealed by small deposits of Holocene alluvium.

Yucca Lake Fault—This northwest-striking fault exhibits normal motion with down-to-the-northeast displacement. Total length of the fault is about 17 km (11 mi.). The fault lies about 36 km (22 mi.) northeast of the potential repository site. Cornwall (1972) reports that the fault displaces Quaternary alluvium along a 13-km (8-mi.) section. No additional paleoseismic information is available for the fault.

12.3.8 Relevant Earthquake Sources

Pezzopane (1996) evaluated the relevance of faults in the Yucca Mountain region to the seismic hazard assessment for the potential repository site. This evaluation was subsequently updated in the deterministic seismic hazard analysis (Section 12.3.11). The objectives were to provide a preliminary evaluation of whether known and suspected Quaternary faults within the region are subject to displacement and to evaluate whether maximum earthquakes on these faults could produce an 84th percentile peak horizontal acceleration on rock at the potential repository site that equals or exceeds 10 percent of gravity ($0.1 g$) (98 cm/s^2) (McConnell et al. 1992). Faults with known Quaternary activity meeting this criterion were defined as “relevant” earthquake sources. “Potentially relevant” earthquake sources are similarly defined, with the only difference being that Quaternary displacement is suspected, but not documented. Results of this study were made available to the expert panel evaluating seismic sources for their consideration in

characterizing inputs to the probabilistic seismic hazard analyses (Section 12.3.10). The remainder of this section is from Pezzopane (1996), unless otherwise referenced.

One hundred and three known or suspected individual faults and six fault combinations (assumed compound rupture on two or more faults) were identified for consideration as potential independent earthquake sources within the region (within 285 km [177 mi.] of the Yucca Mountain site) (Table 12.3-11). This evaluation was based on compilations of regional and local faults by Piety (1996) and Simonds et al. (1995). The evidence for Quaternary displacement, together with estimates of maximum fault length, were tabulated for each fault. Empirical relations were used with maximum fault lengths to calculate maximum earthquakes (Section 12.3.7.8). Ground motions were calculated using the maximum magnitudes and minimum fault-to-site distances with the average of five attenuation relations. The evaluation did not consider time-dependent data, such as fault slip rates or earthquake recurrence rates. It thus provides an evaluation of the potential level of peak acceleration an estimated maximum earthquake on each fault would produce at the site independent of time. The evaluations resulted in the identification of 67 faults or fault combinations that are classified as either relevant or potentially relevant earthquake sources.

Brief descriptions of the faults classified as relevant or potentially relevant are given in Section 12.3.7.8. The descriptions, which incorporate much of the information from Piety (1996) and Simonds et al. (1995), as well as the results of recent paleoseismic studies of faults within and near the potential repository site (Whitney and Taylor 1996), summarize the documented evidence for Quaternary fault activity, such as slip-rate data, and supplement the data presented in this section.

Thirty-two Quaternary faults or fault combinations were identified as relevant seismic sources. Five more faults, which have only suspected Quaternary activity, were considered relevant because the faults may be structurally related to historical seismicity or other Quaternary faults or both, resulting in a total of 37 relevant fault sources, all within 100 km (62 mi.) of Yucca Mountain (Figure 12.3-18). Thirty potentially relevant faults were also identified (Figure 12.3-18). Some of the suspected Quaternary faults at Yucca Mountain are only a few kilometers long and are structurally bounded by longer, more prominent Quaternary faults. On the basis of their limited potential rupture dimensions, these local faults are unlikely to be individual seismogenic sources; yet some of the short, intrablock faults are relevant to fault displacement hazard assessments because they could slip during nearby earthquakes on the bounding Quaternary faults. All but 6 of the 67 relevant and potentially relevant faults and fault combinations are located within 60 km of Yucca Mountain. More than half of the 37 relevant faults and most of the 30 potentially relevant sources have only limited paleoseismic data with which to assess Quaternary activity, slip rates, and recurrence intervals for use in probabilistic hazard assessments.

12.3.9 Estimation of Vibratory Ground Motion

The vibratory ground motions adopted for the seismic design of the potential repository should incorporate the effects of the seismic sources, propagation path, and local site geology specific to the Yucca Mountain region and site to the extent possible. Ideally, recorded ground motions from earthquakes in the Yucca Mountain region or Basin and Range Province would be used to

develop attenuation relations for application at Yucca Mountain, but such data are small in amount and are not sufficient to adequately constrain any empirical models. The few data recorded in the Yucca Mountain region and Basin and Range Province and the geophysical and seismological properties derived for the region do nevertheless provide valuable information for estimating ground motions at the potential repository site.

Ground motions could be estimated from the empirical attenuation relations used for sites in the western United States, but these are based primarily on strong motion records from reverse and strike-slip earthquakes in California. The style-of-faulting factors incorporated in some recent attenuation relations distinguish between reverse- and strike-slip mechanisms. Normal faulting events are usually grouped with strike-slip events because the few normal faulting recordings have not shown ground motions larger than predicted for strike-slip events. Thus, characterizing ground motions at Yucca Mountain using attenuation relations involves resolving whether (and to what extent) existing attenuation models for the western United States are applicable to the Basin and Range Province, in general, and to Yucca Mountain, in particular. The seismological questions asked must include whether differences in the factors that influence ground motions in the Yucca Mountain region and in the western United States would lead to significant differences in ground motion estimates for the two regions. These factors include seismic source properties, regional crustal properties, and shallow geologic site properties at the repository. Generally, comparisons must be made between Yucca Mountain factors and average factors inherent in the strong motion database for the western United States.

Four ground motion studies that address these issues have been completed recently. The first study, conducted by the USGS, was an empirical analysis of worldwide ground motion data from extensional regimes (Spudich et al. 1996). Expansion beyond the Basin and Range Province was necessary to build up a large enough database to yield statistically significant results. The second study comprised numerical modeling of selected scenario earthquakes near Yucca Mountain in which ground motions were estimated using seismological models of the source, path, and site effects (Schneider et al. 1996). The numerical modeling allowed the region-specific crustal structure and site-specific rock properties to be incorporated in the ground motion estimates. The third study, conducted by the University of Nevada, Reno, used weak motion recordings to characterize the near-surface attenuation at Yucca Mountain (Su et al. 1996). The fourth study is a ground motion characterization performed as part of the probabilistic seismic hazard analyses project (Section 12.3.10) and is the most comprehensive of the four (Wong and Stepp 1998). It incorporated results from the other three studies and resulted in ground motion attenuation relations specific to Yucca Mountain. The results of these four studies are described in the following sections.

12.3.9.1 Key Seismologic Parameters

Several key seismologic parameters are integral to the four ground motion studies discussed subsequently, particularly the various modeling studies. Insofar as they form the input to the various models, the parameters, and often their uncertainties, must be accurately quantified. The following discussion presents the current understanding of several of these parameters. The values assigned to the parameters used in each study are included in their primary references.

Path Q and Geometrical Spreading—The attenuation properties for the southern Great Basin (including Yucca Mountain) vary widely, depending upon the data set and the analysis method. Several studies have observed the ground motion attenuation rate with distance, which includes the combined effects of geometrical spreading and the damping parameter “Q.” In a study of Modified Mercalli intensities for the 1952 Kern County earthquake, Evernden (1975, p. 1297) concluded that the ground motion decay rate toward the southern Great Basin was slightly lower than in southern California. On the other hand, Chavez and Priestley (1985, p. 1596) found slightly greater attenuation in the southern Great Basin than in southern California from an evaluation of the M_L scale. And in the most recent study, Herrmann (Schneider et al. 1996, p. 5-3) showed comparable rates of decay in normalized geometrical spreading curves from the southern Great Basin and New Madrid.

Considering Q alone, and taking $Q(f) = Q_0 f^\eta$ where Q_0 and η are model parameters and f is frequency, various investigators have found significant differences in Q_0 and η (Schneider et al. 1996, p. 5-3). Computed values of Q_0 at 1 Hz vary between about 140 and over 750, with η values ranging from 0.04 to 1.05.

Influences of the following factors contribute to these differences:

- Assumptions about geometrical spreading and scattering
- Other source, path, and site effects
- Widely varying frequency bands, source-receiver distances, and regions of coverage
- Scattering versus anelastic Q
- Vertical versus horizontal component records
- Earthquake versus explosion sources.

Although the apparent differences in Q can be quite large, it is likely that a significant portion of these differences have origins in one or more of these factors.

For ground motion estimation at Yucca Mountain, uncertainty in Q has a relatively small impact on ground motion variability due to the dominance of close-in sources, as suggested by the seismic hazards analysis of the ESF (Wong et al. 1996). However, the uncertainty is a factor at very high frequencies, for very low Q values, and for long travel paths (e.g., 50 to 100 km [31 to 62 mi.]).

Two-Dimensional Crustal Structure—Many underground nuclear explosions have been recorded at Yucca Mountain and in the surrounding region. Some of these data have been analyzed by Walck and Phillips (1990). The data constitute 1,829 recordings from 109 events; of the recordings, 429 are from Yucca Mountain, including 128 downhole recordings.

Based on these data, Walck and Phillips (1990) developed two-dimensional velocity profiles from Pahute Mesa to Yucca Mountain and from Yucca Flat to Yucca Mountain. The two-dimensional structure is more prominent from Yucca Flat to Yucca Mountain than from Pahute Mesa to Yucca Mountain. For very shallow sources, such as underground nuclear explosions, this structure can have a significant effect on the ground motion. However, the effect on ground motions from earthquake sources at typical seismogenic depths (5 to 15 km [3 to 9 mi.]) compared to the near-surface explosion sources has not been evaluated.

Site Kappa—Recordings of regional earthquakes at Yucca Mountain have been used by Su et al. (1996) to evaluate the near-surface attenuation (or spectral decay) parameter kappa at 12 sites. Their data set comprises broadband digital recordings of 20 aftershocks of the 1992 Little Skull Mountain earthquake. These aftershocks occurred southeast of Yucca Mountain at distances of about 15 to 30 km (9 to 19 mi.), focal depths of 9 to 12 km (6 to 7 mi.), and magnitude range M_L 2.6 to 4.5. The recording sites are located generally east and southeast of Yucca Mountain within about 40 km. (25 mi.) Thus, the results represent an estimate of kappa only for paths between Yucca Mountain and sites about 30 km (19 mi.) to the southeast.

The computational approach involves simultaneous least-squares fitting of kappa, seismic moment, and corner frequency to the S-wave spectra (Anderson, J.G. and Humphrey 1991). (The corner frequency is the frequency where the high- and low-frequency trends intersect on an earthquake source spectrum.) The equation forms assume that the source spectrum corresponds to a Brune pulse with the displacement spectrum falling off proportional to ω^{-2} (where ω is circular frequency), and that geometric spreading is $1/R$ (where R is distance). All other differences between the source and site spectra, including all path and site effects, are mapped into kappa.

The values of site kappa vary between a minimum of 0.005 s at a station on Paleozoic rock and a maximum of 0.03 s for a station on soil over Tertiary rock. Kappa measured at a tuff site on the Yucca Mountain crest is 0.023 s, and on the flank on tuff it is 0.014 s. The median kappa for all sites is 0.015 s, with a median standard deviation of the computed kappas of about 0.003 s. The average kappa of the two tuff sites is 0.018 s. These values are lower than those for typical California soft rock (0.03 to 0.04 s). Therefore, at low levels of shaking, damping from the tuff is less than that for California soft rock conditions, leading to larger high-frequency ground motion on the tuff as compared to that on California soft rock, assuming that all other parameters are the same.

Although these results pertain to conditions in the Yucca Mountain region, the values obtained are limited by the data set available for interpretation. The data are deficient in large-magnitude earthquakes (M_w 6.5 and larger); the smaller magnitudes limit the strains that develop in the media, and consequently limit any potential nonlinear site effects. The data are also limited in the range of source-to-site recording distances and geometries. Variations in properties due to deeper structure, which would be sampled by earthquakes at longer distances, and due to any azimuthal differences in structure cannot be evaluated.

Local Seismic Velocity Structure—Of the many geotechnical and geophysical studies completed at the potential repository site, only very recent studies have reliably measured in situ velocities (Majer et al. 1996a). Most geophysical surveys were not conducted to measure near-surface values, and the results are not reliable within the uppermost several hundred meters. Furthermore, the few geotechnical investigations yielding dynamic properties are not consistent with in situ velocity measures (Majer et al. 1996b). Only the Vertical Seismic Profile logging performed by Majer et al. (1996a) and Balch and Erdemir (1996) provides a reliable measure of the velocity profiles at six borings at Yucca Mountain. The results of these investigations are specifically applicable only at low strain. At strains of engineering interest, the shape of the strain-dependence must be assumed.

Vertical Seismic Profile surveys have been performed in six boreholes (Figure 12.3-19) (G-2, G-4, NRG-6, SD-12, and WT-2 by Majer et al. [1996b]; UZ#16 by Balch and Erdemir [1996]). These boreholes all lie near or outside the current boundary of the potential repository. The borings have not directly sampled the repository block or the materials around the entire perimeter of the block. Therefore, conclusions made about repository conditions are inferences only.

Testing in boreholes G-4 and SD-12 used a hammer source, which adequately samples shallow strata. Testing in the remaining boreholes and other testing in SD-12 used a vibroseis source. The deepest depth sampled was about 2,200 ft (671 m) in borehole G-2. The Vertical Seismic Profile field measurements were processed to obtain P- and S-wave interval velocities (Majer et al. 1996b). The S-wave velocities from all borehole tests are shown on Figure 12.3-20.

Interval velocities were used to infer a representative velocity profile to a depth of about 1,000 ft (305 m) (Table 12.3-13). The S-wave profile is shown on Figure 12.3-21, together with the thermal-mechanical layer velocities. The extreme upperbound and lowerbound limits on the velocities reflect the wide spread in the interpreted interval velocities.

Below these depths, the velocity structure can be inferred to depths of about 3 km (2 mi.) from refraction survey data (Mooney and Schapper 1995), assuming a constant Poisson's ratio of 0.25. Below 3 km (2 mi.), the only available information on the velocity structure is found in the profiles used in regional earthquake locations (Harmsen 1993, Appendix F). This deeper structure is shown on Figure 12.3-22.

Earthquake Stress Drop—An evaluation of stress drops for earthquakes in extensional regimes was performed in support of the ground motion characterization effort in the probabilistic seismic hazard analyses project (Wong and Stepp 1998, p. 5-11). (Stress drop is the difference in stress across the fault before and after an earthquake.) Stress drop affects high-frequency ground motions so that a value greater than the typical value for western U.S. earthquakes will increase high frequency motions above what is given by western U.S. empirical attenuation relations.

For the YMP, a data set composed of earthquake records from extensional tectonic regimes, including both normal and strike-slip mechanisms, was compiled by Spudich et al. (1997) (further discussed in Section 12.3.9.2). These data were supplemented with data from the 1995 Dinar, Turkey, earthquake, which were not available to Spudich et al. (1997). The final data set comprised 210 horizontal components from 140 sites in 24 earthquakes, a magnitude range of M_w 5.1 to 6.9, and distances from 0 to 102 km (63 mi.). The Fourier spectra of these data were fit to a Brune-type spectrum with ω^{-2} spectral roll-off. A two-step inversion process was adopted to decouple the inversions for kappa and for stress drop. Stress drops computed for each earthquake were weighted to yield a median value for each mechanism.

The median stress drop for normal faulting earthquakes was about 45 bars (4.5 MPa), and the value for strike-slip earthquakes (in extensional regimes) was about 55 bars (5.5 MPa). In comparison, stress drops for western U.S. earthquakes are about 70 to 100 bars (7 to 10 MPa) (e.g., Atkinson 1995, p. 1341). These differences in stress drop contribute to lower high-frequency motions in extensional regimes compared to transpressional regimes, such as coastal

California. The differences in normal faulting stress drop compared with the western U.S. values account for about a 15 percent reduction of normal faulting ground motion relative to western U.S. motion. Within extensional regimes, the stress-drop differences between mechanisms result in ground motions in normal faulting earthquakes, which are about 85 percent of the ground motions from strike-slip events.

12.3.9.2 Strong Motion Attenuation in Extensional Regimes

Spudich et al. (1996) conducted an empirical study of strong ground motions recorded in extensional regimes to assess whether the attenuation was different from standard attenuation models for shallow crustal earthquakes in other tectonic regions, particularly California. They also developed a new set of attenuation relations based solely on these extensional regime data.

The earthquakes used in their study were all located in extensional tectonic regimes. Because the number of events in the entire Basin and Range Province is limited, the database includes ground motion recorded world wide. Earthquakes with normal dip-, oblique-, and strike-slip mechanisms were evaluated together. A total of 373 recordings (253 horizontal and 120 vertical recordings) is included in the final database. These represent earthquakes between M_w 5.1 and 6.9 and distances up to about 100 km (62 mi.).

Extensional Data and Western U.S. Empirical Attenuation Relations—Several representative attenuation relations based on western U.S. data were compared to the extensional data by Spudich et al. (1996): Boore et al. (1994), Idriss (1991), Sadigh et al. (1993), Campbell (1989, 1990), Campbell and Bozorgnia (1994), and Sabetta and Pugliese (1996). These relations generally represent the state of the art in ground motion attenuation studies at the time of the Spudich et al. (1996) study.

The mean residual, or bias, was computed for each attenuation relation and indicates whether that model systematically underpredicts or overpredicts the extensional strong motion data. In general, the computed residuals indicate that the standard western U.S. attenuation relations overpredict ground motions from extensional regimes by about 15 to 35 percent on average (Spudich et al. 1996). At Yucca Mountain, near-fault ground motion is important because of the hazard contributions from local faults (Wong and Stepp 1998, p. 7-22). Therefore, the bias was computed for a subset of the extensional data that included only sites at distances less than 20 km (12 mi.) (Spudich et al. 1996). For this short distance range, the overprediction is somewhat greater than for the full data set, although the standard deviations of the residuals are also larger.

The standard errors of the western U.S. models were compared to the standard errors computed from the extensional regime database for all distances and for distances less than 20 km (12 mi.) (Spudich et al. 1996). For all distances, the computed standard errors are consistent with the range of standard errors from the attenuation models. For distances less than 20 km (12 mi.), the computed standard errors are toward the lower end of the range of the attenuation model standard errors, but the uncertainty in the estimated standard error is much larger. The standard errors in the western U.S. attenuation models appear to be comparable and thus applicable to extensional regimes.

Spudich et al. (1996) also evaluated the distance and magnitude scaling inherent in the western U.S. relations against the extensional data. They found that the distance attenuation represented by the extensional data set is weaker than in the western U.S. attenuation models. No systematic difference was found in the magnitude scaling of events in the extensional database as compared to the western U.S. models.

Extensional Regime Attenuation Relation—Spudich et al. (1996) developed a new attenuation relation to estimate ground motions in extensional regimes. The model is based on a functional form developed by Boore et al. (1994):

$$\log Y = b_1 + b_2(M-6) + b_3(M-6)^2 + b_4R + b_5\log R + b_6\Gamma \quad (\text{Eq. 12.3-1})$$

in which Y is the ground motion parameter, M is moment magnitude, $R = (r_b^2 + h^2)^{1/2}$ (r_b is horizontal distance and h is depth from Boore et al. [1997]), and Γ is 0 for rock sites and 1 for soil sites.

The extensional regime data set is rather sparse in terms of the magnitudes represented, and has little data from rock sites at distances less than 10 km (6 mi.). Consequently, in the regression analysis several model parameters were fixed to values determined by Boore et al. (1994). The fixed parameters include the magnitude scaling terms (b_2 and b_3) and the depth term (h). All other parameters were estimated, and the resulting coefficients are listed in Table 3 of Spudich et al. (1997).

Comparisons of median predictions from this model with those from several western U.S. attenuation models illustrate their differences. Figure 12.3-23 compares median acceleration response spectra for a rock site on the footwall of a dipping fault (57.5°) at a rupture distance of 10 km (6 mi.) for M_w 5, 6, and 7 events. Figure 12.3-24 makes the same comparisons for a rock site on the hanging wall. In general, at short to moderate periods the Spudich et al. (1997) model predictions are less than, or lie at the lower limit of, the western U.S. values. At long periods, the Spudich et al. (1997) model is similar to the western U.S. models. Notably, however, the Spudich et al. (1997) model has a much larger standard deviation at long periods than is usual for the western U.S. relations.

A third comparison is made for a rock site 25 km (16 mi.) from a M_w 6.5 strike-slip event (Figure 12.3-25). At this larger distance, the Spudich et al. (1997) model prediction is about 30 to 40 percent lower than the average of the western U.S. values.

12.3.9.3 Little Skull Mountain Earthquake Ground Motions

The June 29, 1992, M_L 5.6 Little Skull Mountain earthquake is the largest recorded earthquake within 20 km (12 mi.) of Yucca Mountain. Moreover, it is the only earthquake in the Yucca Mountain region (excluding aftershocks) for which significant recordings of strong motion are available.

Focal mechanisms and seismic moments have been derived by several investigators. In general, the mainshock mechanism and moment are very well constrained, with a dip of 56° and rake angle indicating a normal mechanism (Table 12.3-14). Based on aftershock locations, the

rupture plane extended about 4 km (2 mi.) along strike and 6 km (4 mi.) down dip with the hypocenter at the lower southwestern corner of the rectangle. The mainshock seismic moment was computed at about 3.7×10^{24} dyne-cm.

The stress drops of the mainshock and two large aftershocks were estimated from a point source inversion of the Fourier amplitude spectra (Schneider et al. 1996, pp. 6-6 to 6-11). The stress-drop estimates are listed in Table 12.3-15 and are consistent with those of other Basin and Range Province earthquake sequences (Section 12.3.9.1).

The earthquake strong ground motion recordings provided a valuable opportunity for comparison with existing empirical attenuation relations. An analysis of residuals with respect to five attenuation relationships was performed by Abrahamson and Becker (1996, Chapter 10). In general, the residuals indicate that for larger distances, the empirical relations tend to overpredict the observed ground motions for the Little Skull Mountain earthquake. The average level of all residuals tends to decrease with period. The underprediction of ground motion at high frequencies can be attributed to lower kappa at the site compared with typical western U.S. values.

As part of the Scenario Earthquake Modeling Project, the ground motions from the Little Skull Mountain earthquake also were modeled by six groups as part of a model evaluation and validation process. Detailed results of this study are provided by Schneider et al. (1996) and are summarized in the following section.

12.3.9.4 Scenario Earthquake Modeling Project

Due to the lack of near-fault strong motion data from earthquakes in the Yucca Mountain region and the Basin and Range Province, the USGS organized a project to estimate vibratory ground motion for several earthquake scenarios affecting Yucca Mountain (Schneider et al. 1996). Participants in the study used established numerical modeling methods to simulate ground motions that were appropriate to the specific conditions at Yucca Mountain. As part of the modeling exercise, both median ground motion and its variability were estimated for each faulting scenario.

Six earthquake scenarios were evaluated (Table 12.3-16) based on two geologic criteria: the postulated sources are likely to have generated significant earthquakes in the past, and they are considered likely to produce ground motions that would impact seismic hazard estimates at Yucca Mountain. The six scenarios include four normal faulting events (M_w 6.3 to 6.6) at source-to-site distances of 1 to 15.5 km (0.6 to 9.6 mi.) and two strike-slip faulting events (M_w 6.7 and 7.0) at distances of 25 and 50 km (16 and 31 mi.), respectively.

Six modeling teams, each with a different preferred modeling approach, first validated their Yucca Mountain-specific models using records from the 1992 M_L 5.6 Little Skull Mountain earthquake. The teams were allowed to modify input parameters with the constraint that they be consistent with the observations and results of previous work. Slip distribution and other fault dynamics were unspecified and left to the modelers to define. Following the validation phase of the project, each team prepared ground motion estimates (median and uncertainty) for the six scenarios.

The six modeling approaches were the following:

- Specific barrier method (Chin and Aki)
- Stochastic method with ω^2 subevents (Silva)
- Stochastic slip functions method (Joyner)
- Composite fractal source method (Zeng and Anderson)
- Broadband Green's function method (Somerville)
- Empirical method using underground nuclear explosion sources (Bennett).

In the six modeling methods, the seismic source is prescribed only by the rupture geometry, seismic moment, and hypocenter. The manner in which the seismic slip is distributed and released on the fault plane varies between methods. The methods also vary significantly in their assumptions of wave propagation, site response, and overall level of complexity, but all the methods accommodate the essential aspects of seismic energy being generated from a finite source and propagated along a path to a site at the Earth's surface. A complete description of each modeling method is provided in Schneider et al. (1996).

Taken together, the six modeling methods represent the state of the art, and the differences in resulting predictions capture an important component of the uncertainty in ground motions in these scenario earthquakes that can be applied to the variability of other simulations.

Model Validation—In the validation phase of the project, the teams incorporated various Yucca Mountain source, path, and site parameters to calibrate their models to best fit ground motions from five sites that recorded the Little Skull Mountain earthquake. Most of the six methods had also been previously calibrated against recordings from recent earthquakes.

The computed 5 percent damped response spectra for each of the six modeling teams are plotted on Figure 12.3-26, along with an observed spectrum from the Little Skull Mountain earthquake. The comparisons are for the recording site (Lathrop Wells) nearest to the Little Skull Mountain main shock source.

The mean residual and standard deviation for all five sites were computed for each model. The average model bias for all groups is included on Figure 12.3-27. The models produced ground motion estimates that were comparatively unbiased for periods less than 1 s, indicating that they are applicable to estimating ground motions in the Basin and Range Province. However, the bias for periods greater than 1 s indicates that the numerical simulation models do not work well for this event at long periods.

The standard errors of the modeling misfits are plotted on Figure 12.3-28. This is the model uncertainty and represents the limitations of each model. This modeling uncertainty is part of the total uncertainty of numerical simulations discussed later in this section.

Computed Ground Motion—Using the Little Skull Mountain-calibrated models, the six teams proceeded to compute motions for the six faulting scenarios. Five of the teams whose models were numerical simulations (i.e., all except the empirical underground nuclear explosion model) ran multiple realizations of the source process and computed a mean spectrum for each scenario.

Nonlinear site response effects were incorporated in the scenario ground motions. Lacking information on the dynamic response of tuffs at Yucca Mountain, the nonlinear response of these materials was assumed to be similar to the response of tuffs from those tested (Wong et al. 1995, Section 6.2.3). The simulated ground motions were modified to account for the expected nonlinear response of the top 40 m (131 ft) of the tuff. For the nearby normal faulting event scenarios, the increase in damping from nonlinear effects reduced the high-frequency ground motion by about a factor of two as compared to the ground motions computed assuming linear site response. In the more distant strike-slip faulting scenarios, the ground motions were much lower, so the expected nonlinear response of the tuff is not significant.

The computed median spectral accelerations for the scenario events based on the team's models are shown on Figure 12.3-29. Ground motions computed for the normal faulting scenario events at close distances (Bow Ridge, Solitario Canyon, and Paintbrush Canyon faults) are large: 34-Hz spectral accelerations range from 0.5 to 1.0 g (490 to 981 cm/s²) at distances of 1 to 3 km (0.6 to 2 mi.). The more distant normal faulting scenario earthquakes (Bare Mountain and Rock Valley faults) resulted in ground motions with 34-Hz spectral accelerations from 0.2 to 0.3 g (196 to 294 cm/s²). The scenario event at farthest distance (Furnace Creek fault, a strike-slip scenario) produced the lowest high-frequency motion (less than 0.1 g [98 cm/s²] at 34 Hz); its long period motions are comparable to the Bare Mountain and Rock Valley fault events as a result of the larger magnitude of the Furnace Creek fault event.

Comparisons with Western U.S. Attenuation Relations—The model simulations were compared with several western U.S. empirical attenuation relations (Sadigh et al. 1993; Boore et al. 1994). The simulated median ground motions for the four normal faulting events exceed the western U.S. predictions by about 60 percent at distances less than 5 km (3 mi.) and by about 20 percent at 15 km (9 mi.). The differences are largest at high frequencies, attributable primarily to low damping (kappa effects) in the shallow rock at Yucca Mountain and to larger crustal amplification for the Basin and Range Province. At long periods, the difference is attributed to the larger crustal amplification and directivity effects.

For the more distant strike-slip faulting earthquakes, the simulated median ground motions are greater than the western U.S. attenuation predictions by about 30 percent at a distance of 25 km (16 mi.), also at the high frequencies. This increase is similarly attributed to low kappa and larger crustal amplification. At 50 km (31 mi.), the simulated longer period ground motions are consistent with western U.S. empirical attenuation predictions because the effect of kappa is not as significant.

The simulated higher ground motions at high frequencies are consistent with records from the 1992 Little Skull Mountain earthquake. The high-frequency ground motions from this event were significantly larger than those predicted by western U.S. empirical attenuation relations.

The variability of the simulated motions is also greater than that computed for western U.S. empirical attenuation relations. The standard error is about 0.15 natural log units larger than that found for empirical attenuation relations.

Ground Motion Variability—The variability of the ground motion was estimated in the Scenario Earthquake Modeling Project, including modeling, method, parametric, and geometric variability

(Schneider et al. 1996). The total variability is the combination of these sources of uncertainty. (The uncertainties in the ground motion part of the probabilistic seismic hazard analyses project were treated slightly differently [Wong and Stepp 1998].) Two types of uncertainty are considered: aleatory, representing random variations and captured in the standard deviation, and epistemic, representing scientific uncertainty due to limited data. Epistemic uncertainty is inherent in both median estimates and their aleatory variability.

The model variability (aleatory) is estimated from comparisons of the model predictions with recordings from actual earthquakes. In the Scenario Earthquake Modeling Project, this was captured in the Little Skull Mountain validation exercise and other validations each investigator had performed. Method variability (epistemic) is the uncertainty in the median ground motion introduced by the inability to know which numerical model will provide estimates closest to the correct median. Parametric variability (aleatory) is caused by variations in ground motion for future earthquakes due to variations in source, path, and site parameters in those events. It is computed by varying these parameters (optimized in the validation exercise) in other simulations. Geometric variability (epistemic) results from the inability to know what the geometry of a source truly is. For example, for a single fault, it is the uncertainty in the dip of that fault. In the Scenario Earthquake Modeling Project, geometric variability was included only in the computation of the total uncertainty, depending on the details of the individual simulations.

The uncertainty computed for all the simulations is included in Schneider et al. (1996). The four sources of uncertainty for the Paintbrush Canyon scenario event are shown on Figure 12.3-30. In general, the total uncertainty increases with period and the greatest contribution to the total uncertainty is the modeling uncertainty.

12.3.9.5 Ground Motion Characterization Supporting the Probabilistic Seismic Hazard Analysis Project

The most comprehensive evaluation of ground motions at Yucca Mountain was performed in support of the probabilistic seismic hazards analyses (Section 12.3.10). The goal of the evaluation was to formulate attenuation models describing vibratory ground motion at the potential repository. Expert elicitation methods were followed to integrate the range of scientific interpretations. Seven experts participated in the characterization, each with recognized technical expertise. The experts impartially evaluated various proponent models of ground motion based on information presented in a series of workshops. The characterization is documented in Wong and Stepp (1998).

The experts provided point estimates of ground motion for a suite of prescribed faulting cases, and these point estimates were subsequently regressed to attenuation equations. The ground motions constituted response spectral values (horizontal and vertical components) for specified spectral periods. The point estimates constituted an estimate of the median ground motion, its variability (aleatory variability), and the uncertainty in each (epistemic uncertainty). Each faulting case corresponded to a particular magnitude earthquake, fault geometry, and source-site distance. The cases were designed to sample the magnitude-distance-faulting space in sufficient detail to provide a robust regression.

The ground motion estimates and, thus, the resulting attenuation relations were developed for a free-field reference rock outcrop whose geotechnical conditions are the same as those at the depth of the buried repository, not those at the ground surface (Section 12.3.10).

In the course of the ground motion workshops, the results of all known relevant studies were presented. Among other issues, these workshops included discussions of several seismological parameters, including stress drop, crustal structure, Q, and site effects, including kappa, site response, and material nonlinearity. Workshop presentations covered seismological records from the 1992 Little Skull Mountain mainshock and aftershocks and the 1993 Rock Valley sequence. The experts were briefed on source focal mechanisms, event locations, and elements of the seismograms. The extensional regime data set and results (Spudich et al. 1997) and the scenario earthquake investigation (Schneider et al. 1996) were of direct relevance to the ground motion characterization. Ground motion estimation methods were also reviewed, including empirical attenuation relations, numerical simulations, and hybrid empirical numerical schemes.

Proponent Models—The experts computed their point estimates not from further analyses of measured strong ground motion data, but rather from existing proponent models. The proponent models fell into several classes: empirical attenuation relations, hybrid empirical, point source numerical simulations, finite-fault numerical simulations, and blast models. All ground motion modeling relations evaluated as part of this study are listed in Table 12.3-14.

Because no empirical attenuation models exist for the Yucca Mountain region or the Basin and Range Province, the empirical models used in this study resulted from regression analyses of strong motion records primarily from California earthquakes. Thus, all empirical relations required adjustments so they would better fit conditions in the Yucca Mountain region. The hybrid empirical model is derived from these relations and implicitly includes conversion factors that must be separately applied to the empirical relations.

The blast models are based on empirical records from underground nuclear explosions at the Nevada Test Site (Schneider et al. 1996, pp. 3-15 to 3-17). Three blast models were assessed, each with a different approach to account for differences in earthquake sources and explosion sources.

The numerical simulations were tailored to Yucca Mountain conditions and required no adjustments. The point source models are the simplest numerical models and also the best understood. The finite-fault numerical simulations were derived from the six models evaluated in the Scenario Earthquake Modeling Project previously described (Section 12.3.9.4). Three model approaches were chosen by the experts for their analyses:

- Stochastic method with ω^2 subevents (Silva)
- Composite fractal source method (Zeng and Anderson)
- Broadband Green's function method (Somerville).

Conversion Models—Depending on the nature of the data sets upon which they were based, the empirical relations often represented source, path, and site conditions different from those encountered at Yucca Mountain. Suites of conversion factors were consequently computed as part of the study. They were developed using the results of numerical finite fault simulations,

stochastic point source simulations, and empirical attenuation relations. Complete summaries of the conversion factors are presented in Wong and Stepp (1998). The factors included corrections for the following:

- Source: western U.S. transpressional seismic sources to Yucca Mountain extensional seismic sources
- Crust: western U.S. crust to Yucca Mountain crust
- Site: reference rock outcrop to Yucca Mountain surface conditions.

Eight conversion models for source and four for combined crust and site effects were available for application. The experts selected the conversions they wished to apply to the various empirical relations. If an empirical model did not require a correction term, then none was applied. For example, the numerical simulations were computed for Yucca Mountain conditions, so no crust or site correction was needed and none was applied.

Additionally, many of the proponent models did not include the full range of ground motion parameters required. For example, not all the empirical models included vertical ground motions. Thus, scaling factors were also developed in the same manner as the conversion models. The scaling factors include the following:

- Ratios of vertical motion to horizontal motion
- Ratios of peak velocity to peak spectral acceleration
- Ratios of peak velocity to 1-Hz spectral acceleration
- Component-to-component variability models
- Spectral acceleration interpolation models.

The scaling factors were applied in a manner analogous to the conversion models.

Attenuation Relations—Each expert developed a set of point estimates for the several cases representing different faulting styles, event magnitudes, source geometries, and source-site distances. The estimates comprised median ground motion, its variability, and the uncertainty in both. The estimates were derived directly from the models, the conversion factors, the adjustment factors described above, and other judgments by the experts.

These estimates were then parameterized using attenuation relations. The forms of the attenuation relations used by each expert are provided in Table 12.3-17. The experts constrained the relations, describing their estimates as much or as little as they chose. For example, each selected a distance measure for the regression. Some chose to constrain the degree of magnitude saturation at close distances. Some chose to regress hanging wall and footwall point estimates together rather than separately. Regression coefficients a_i , b_i , c_i , and d_i are listed in Wong and Stepp (1998, Appendix I).

During the course of the probabilistic seismic hazard analyses project, two faulting cases were identified that could not be captured by the cases for which the experts were developing point estimates. These special cases were (1) multiple rupture scenario on parallel faults and (2) a low-angle detachment zone rupture scenario. The experts addressed these scenarios by

providing rules for applying their attenuation equations in each specialized case. Their adjustment factors are provided in Wong and Stepp (1998, Appendix F).

As an example of the process, the point estimates for horizontal spectral acceleration for a case representing normal faulting (hanging wall) in a M_w 6.5 earthquake at a distance of 4 km are shown on Figure 12.3-31. Figures showing all four ground motion estimates, for all cases and for all experts, are contained in Wong and Stepp (1998, Section 5). All median estimates developed by a single expert were regressed using the median motion equation form (Table 12.3-17), subject to any constraints imposed by that expert.

Ground motion estimates for any of the four ground motion parameters may be computed using the sets of coefficients. Figure 12.3-32 presents one such set of estimates, corresponding to the median horizontal peak ground acceleration in a M_w 6.5 normal faulting earthquake on the hanging wall.

Typically, the seven sets of attenuation relations predict median ground motion, which differs by less than a factor of 1.5. The experts' horizontal aleatory estimates, the epistemic uncertainties in their median estimates, and the epistemic uncertainties in their aleatory estimates all vary by less than about 0.1 natural log unit.

12.3.10 Probabilistic Seismic Hazard Analysis

To assess the seismic hazards of vibratory ground motions and fault displacement at Yucca Mountain, a PSHA was performed (Wong and Stepp 1998; CRWMS M&O 2000e). The objectives of the PSHA are to provide quantitative hazard results to support a viability assessment of the potential repository's long-term performance with respect to waste containment and isolation and to form the basis for developing seismic design criteria for the license application. The hazard results are in the form of annual probabilities for the exceedance of various levels of fault displacement at selected locations in the preclosure controlled area and various levels of vibratory ground motion at a hypothetical rock outcrop at the ground surface.

The PSHA consists of three primary activities:

- Identification, evaluation, and characterization of seismic sources that will contribute to the fault displacement and vibratory ground motion hazard at Yucca Mountain
- Evaluation and characterization of vibratory ground motion attenuation, including earthquake source, wave propagation path, and rock site effects
- Analyses of probabilistic seismic hazards due to both fault displacement and vibratory ground motion.

Both the preclosure and postclosure performance periods of the potential repository are being addressed in the study.

By necessity, evaluations of seismic source characteristics, earthquake ground motions, and fault displacement involve interpretations of data. These interpretations have associated uncertainties related to the ability of data to fully resolve various hypotheses and models. In the PSHA, the

input includes both estimates of the parametric variability and uncertainty in the interpretations. To evaluate scientific uncertainty, seismic source characterizations have been made by six teams of three experts each, who together form a composite expertise in the seismicity, tectonics, and geology of the Yucca Mountain site and region. The ground motion assessments have been made by seven individual experts (Section 12.3.9.5).

Interpretations for hazard assessment have been coordinated and facilitated through a series of workshops. Each workshop was designed to accomplish a specific step in the overall interpretation and to ensure that the relevant data were fully considered and integrated into the evaluations.

The following sections present the PSHA methodology for both vibratory ground motions and fault displacement, the expert teams' seismic source characterization for analyses of vibratory ground motions and their fault displacement models, and the associated hazard results. The ground motion characterization performed by the PSHA ground motion experts was presented in Section 12.3.9.

12.3.10.1 Probabilistic Seismic Hazard Analysis Methodology

The PSHA methodology for vibratory ground motions was first developed by Cornell (1968, 1971) and has become standard practice in evaluating seismic hazards. The use of the methodology results in calculated annual probabilities that various measures of vibratory ground motion (e.g., peak horizontal acceleration) will be exceeded at a site (Figure 12.3-33). The resulting seismic hazard curve represents the integration over all earthquake sources and magnitudes of the probability of future earthquake occurrence and, given an occurrence, its effect at a site of interest. The methodology for evaluating fault displacement hazard probabilistically is very similar to that for vibratory ground motions.

The calculation of probabilistic ground motion hazard requires three basic inputs (Figure 12.3-33):

- Identification of relevant seismic sources and a characterization of their source geometry
- Rate of earthquake occurrence for each seismic source and its magnitude distribution
- Attenuation relationships that provide for the estimation of a specified ground motion parameter as a function of magnitude, source-to-site distance, local site conditions, and in some cases, seismic source characteristics.

For evaluating fault displacement hazard, the ground motion attenuation relationships are replaced by relationships that describe the distribution, sense, and amounts of displacement with earthquake occurrence. Both primary and secondary fault displacement are addressed. The three basic inputs for assessing both vibratory ground motions and fault displacement hazards are the products from the previously described characterization activities.

The mathematical formulation used for probabilistic seismic hazard analyses typically assumes that the occurrence of damaging earthquakes can be represented as a Poisson process. Under this

assumption, the probability that a ground motion parameter, Z , will exceed a specified value, z , in time period t is given by:

$$P(Z > z|t) = 1 - e^{-\bar{v}(z)t} \leq v(z) \cdot t \quad (\text{Eq. 12.3-2})$$

in which $v(z)$ is the average frequency during time period t at which the level of ground motion parameter z exceeds value Z at the site from all earthquakes on all sources in the region. The inequality at the right of Equation 12.3-2 is valid regardless of the probability model for earthquake occurrence, and $v(z) \cdot t$ gives an accurate and slightly conservative estimate of $P(Z > z)$ for probabilities of 0.1 or less, if $v(z)$ is the appropriate time-averaged value for the specific time period of interest.

The frequency of exceedance, $v(z)$, is a function of the frequency of earthquake occurrence, the randomness of size and location of future earthquakes, and the randomness in the level of ground motion they may produce at the site. It is computed by the expression:

$$v(z) = \sum_n \alpha_n (m^o)^m \int_m^{m^u} \left[\int_{r=0}^{r=\infty} f(r|m) \cdot P(Z > z|m, r) \cdot dr \right] \cdot dm \quad (\text{Eq. 12.3-3})$$

in which $\alpha_n (m^o)$ is the frequency of earthquakes on source n above a minimum magnitude of engineering significance, m^o ; m^u is the upper-bound magnitude event that can occur on the source; $f(r|m)$ is the probability density function for distance r to an earthquake of magnitude m occurring on source n ; and $P(Z > z | m, r)$ is the probability that, given the occurrence of an earthquake of magnitude m at distance r from the site, the peak ground motion will exceed level z .

An important aspect of the probabilistic seismic hazard calculations is the treatment of uncertainty. For the above inputs, uncertainties are quantified by the experts and included in their models. These uncertainties are propagated throughout the probabilistic analyses using a logic tree methodology resulting in a suite of hazard curves typically showing the mean, median, and various percentile curves.

The PSHA methodology shown on Figure 12.3-33 is formulated to represent the randomness inherent in the natural phenomena of earthquake generation and seismic wave propagation. The randomness in a physical process has come to be called aleatory uncertainty (Budnitz et al. 1997). In all assessments of the effects of rare phenomena, one faces uncertainty regarding the selection of the appropriate models and model parameters because the data are limited and/or alternative interpretations of the data exist. This uncertainty in knowledge has come to be called epistemic uncertainty (Budnitz et al. 1997). The seismic source experts placed a major emphasis on developing a quantitative description of the epistemic uncertainty.

The logic tree formulation for seismic hazard analysis involves setting out the logical sequence of assessments necessary to perform the analysis and addressing the uncertainties for each step in the assessment. Thus, it provides a convenient approach for breaking a large, complex assessment into a sequence of smaller, simpler components that can be addressed more easily.

Figures 12.3-34 and 12.3-35 show examples of logic trees composed of a series of nodes and branches from the nodes. Each node represents a state of nature or an input parameter that must be characterized to perform the analysis. Each branch from a node represents one possible alternative interpretation being evaluated. In practice, a sufficient number of branches are placed at a given node to represent the evaluator's uncertainty in estimating the parameter.

Assigned to each branch is a probability that is associated with the expert's evaluation that the branch represents the correct value or state of the input parameter. These probabilities are conditional on the assumption that all the branches from that node represent the true state of the preceding parameters. Because they are conditional probabilities for an assumed mutually exclusive and collectively exhaustive set of values, the sum of the conditional probabilities at each node is unity. The probabilities are often based on scientific expert judgment because the available data are often too limited to allow for objective statistical analysis and because scientific evaluation is needed to weigh alternative interpretations of the available data. The logic tree simplifies these evaluations because the uncertainty in each parameter is considered individually, conditional on assumed known states from prior evaluations. The nodes of the logic tree are sequenced to express conditional aspects or dependencies among the parameters and to provide a logical progression of evaluations, from general to specific, in characterizing the input parameters for PSHA.

12.3.10.2 Seismic Source Characterization for Vibratory Ground Motions

Two main types of seismic sources were characterized by the seismic source expert teams: fault sources and areal source zones. Fault sources are used to represent the occurrence of earthquakes along a known or suspected fault trace or traces. Uncertainty in the definition of fault sources is expressed by considering alternative rupture lengths, alternative fault dips, and possible linkages with other faults. In addition, an evaluation is made of the probability that a particular fault is active (Figure 12.3-35); that is, it produces earthquakes in the current tectonic regime.

Faults were represented in the PSHA by segmented planar features; the fault dip and the minimum and maximum depths of rupture on the fault plane were specified by the seismic source expert teams (Figure 12.3-35). Earthquake ruptures typically are considered to occur with equal likelihood at any point on the fault plane; the size of the rupture is specified by an empirical relationship between magnitude and rupture area.

Areal source zones represent regions of distributed seismicity that are not associated with specific known faults, such as "background earthquakes," and, therefore, the events are considered to be occurring on unidentified faults or structures whose areal extents are best characterized by zones. Areal zones may also be used to model the occurrence of earthquakes at great distances from a site when the details of the individual faults are not significant to the hazard assessment. The boundaries of regional source zones delineate areas that have relatively uniform seismic potential in terms of earthquake occurrence and maximum earthquake magnitude (Figure 12.3-36). Uncertainty in defining areal zones typically was expressed by considering alternative zonations of the region surrounding the Yucca Mountain site.

Two alternative approaches were used by the seismic source expert teams to characterize the spatial distribution of future earthquakes within the areal zones. The first considers equal likelihood of occurrence of earthquakes at all locations within the areal zone. The alternative interpretation was non-uniform spatial occurrence expressed by a non-uniform spatial density function for the areal zone based on the historical seismicity. This interpretation implies that future seismicity is more likely to occur near where it has in the past. This interpretation currently is being used to develop the national seismic hazard maps for the United States (Frankel 1995).

12.3.10.2.1 Assessment of Maximum Magnitude

The maximum magnitude (M_{\max}) for a seismic source represents the largest earthquake that can be generated by that source, regardless of its frequency of occurrence. The approach used to evaluate M_{\max} for a fault source was to estimate the maximum physical dimensions of rupture on the source and use relationships between rupture dimensions and earthquake magnitude. The types of empirical relationships available are magnitude versus surface- or subsurface-rupture length, rupture area, maximum surface displacement, average surface displacement, and slip rate. Some published empirical relationships include more than one parameter, such as rupture length and slip rate or the product of rupture length and displacement (e.g., Anderson, J.G. et al. 1996). Estimates of the rupture area and average slip on the fault can also be used to estimate the seismic moment of the M_{\max} , which is then converted to M_w using an empirical relationship, such as the one developed by Hanks and Kanamori (1979). The probabilistic seismic hazard analyses were conducted using M_w as the magnitude measure, and all estimates of M_{\max} were converted to this scale.

In estimating M_{\max} for faults, the seismic source expert teams considered multiple sources of uncertainty:

- The relative merit of alternative rupture characteristics for estimating magnitude (e.g., estimates based on rupture length versus estimates based on maximum displacement)
- The relative merit of alternative published empirical relationships
- Uncertainty in estimating the physical dimensions of the maximum rupture on a fault.

The logic tree on Figure 12.3-37 illustrates an example approach used to express these uncertainties. Alternative fault widths are assessed by considering a range of permissible maximum depths of rupture and alternative fault dips. Alternative maximum rupture lengths are assessed based on evidence for lasting segmentation points and differences in fault behavior. Alternative empirical relationships are considered: magnitude versus rupture length or rupture area from D.L. Wells and Coppersmith (1994), or magnitude versus rupture length and slip rate (Anderson, J.G. et al. 1996). If the J.G. Anderson et al. (1996) relationship is used, then a distribution of possible fault slip rates is assessed. The example logic tree (Figure 12.3-37) shows only some of the branches to illustrate the various evaluations. The complete logic tree leads to the discrete distribution for M_{\max} shown at the bottom of Figure 12.3-37.

Different approaches may be used to evaluate the M_{\max} for areal source zones. In cases where an areal source zone is used to model the occurrence of earthquakes at large distances from a site where the details of the individual fault sources are not significant to the hazard assessment, M_{\max} represents the largest earthquake determined to occur on any of the faults within the source zone. In cases where areal source zones are used to model the occurrence of earthquakes on unknown faults (there may be fault sources within the areal source zone that are modeled explicitly as separate sources in the hazard), M_{\max} for the areal zone is determined by the largest fault not explicitly considered within the zone or the largest earthquake that is not associated with surface faulting. The size of this fault will depend on the level of detailed mapping of the region and the identification of fault sources. Guidance for this evaluation is provided by studies that examine the frequency at which earthquakes of various magnitudes rupture the surface (e.g., Wells, D.L., and Coppersmith 1993; dePolo 1994b; Pezzopane and Dawson 1996). The data sets of dePolo (1994b) and Pezzopane and Dawson (1996) are specific to the Basin and Range Province.

12.3.10.2.2 Assessment of Earthquake Recurrence

Earthquake recurrence relationships for a seismic source describe the frequency at which earthquakes of various magnitudes occur. They are determined by estimating the overall frequency of earthquakes on the source, $\alpha_n(m^o)$, and the relative frequency of earthquakes of various sizes defined by the probability density of earthquake size, $f(m)$, between m^o (minimum magnitude) and m^u (maximum magnitude). Different approaches were used to determine the recurrence relationships for areal source zones and fault sources.

The earthquake recurrence relationships for areal zones were determined from the historical seismicity catalog compiled for the Yucca Mountain region (Section 12.3.2.2). The catalog was analyzed to identify and remove explosions and dependent events (earthquakes that were aftershocks or foreshocks of larger earthquakes) to produce data sets of earthquakes that can be considered to correspond to a Poisson process. Several alternative methods for identifying dependent events were used to express the uncertainty in the process. The seismic source expert teams used the alternative catalogs to develop alternative recurrence relationships for their areal zones.

The distribution of earthquake sizes in each areal source zone was interpreted to follow the Gutenberg and Richter (1954) exponential recurrence model. Because each source has a defined M_{\max} , the truncated exponential magnitude distribution was used to define the recurrence relationships.

The recurrence parameters needed for each areal source zone are $\alpha(m^o)$ and b (slope of the recurrence curve). The maximum likelihood procedure developed by Weichert (1980) was used to estimate these parameters from the recorded data. The likelihood function used in this study was modified from that presented by Weichert (1980) to allow for variable periods of complete reporting within the boundaries of the source, as well as variable magnitude intervals.

Two approaches were used to estimate the earthquake recurrence relationships for faults. The first involved estimating the frequency of large-magnitude surface-rupture earthquakes either by the use of recurrence intervals or by dividing an estimate of the average slip per event by an

estimate of the fault slip rate. The complete recurrence relationship for the fault is then specified by constraining a particular form of an earthquake recurrence model (magnitude distribution function) (Figure 12.3-38) to pass through the estimated frequency of large events. The second approach was to translate the estimated fault slip rate into seismic moment rate and then partition it into earthquakes of various magnitudes according to the recurrence model used. Both of these approaches constrain the earthquake recurrence relationship for the fault at the frequency of magnitudes near M_{max} . The frequency of smaller-magnitude earthquakes is then extrapolated from this frequency based on the form of the recurrence model used. Various recurrence models were considered by the seismic source expert teams, including the characteristic earthquake (Youngs and Coppersmith 1985), exponential, truncated exponential, and the maximum moment (Wesnousky et al. 1983) (Figure 12.3-38).

12.3.10.2.3 Summary of Experts' Seismic Source Characterization Assessments

The following section summarizes the range of interpretations made by the seismic source expert teams regarding key components of their seismic source characterization models. More detailed discussions are included in Wong and Stepp (1998).

Regional Faults—Regional faults were treated similarly by the seismic source expert teams. They were defined by most teams as Quaternary faults between about 15 and 100 km (9 and 62 mi.) from Yucca Mountain that were judged to be capable of generating earthquakes of M_w 5 and greater. Paleoseismic data from Piety (1996) and Whitney (1996) were used by all the teams to identify and characterize potential regional fault sources. Other sources, such as R.E. Anderson, Bucknam et al. (1995); R.E. Anderson, Crone et al. (1995); McKague et al. (1996); Keefer and Pezzopane (1996); and Pezzopane (1996) also were used to varying degrees by some of the teams. Some of the faults that McKague et al. (1996) identified as Type 1 faults were considered but not judged relevant to the hazard analysis and were not included by the teams because of their short lengths, distance from Yucca Mountain, and evidence indicating that many of these faults either have no significant Quaternary displacement or are much shorter than previously thought.

The number of regional faults considered by the expert teams ranged from 11 to 36 (e.g., Figure 12.3-39), reflecting in part the judgments of the teams regarding the activity of various faults, as well as the decision by some teams to also include potentially active faults. All of these faults are described in Section 12.3.7. One team included only faults that were judged to be active with a probability of 1.0, whereas other teams also included faults that were judged to be active with probabilities of less than 1.0. All of the teams modeled the regional faults as simple, planar faults to maximum seismogenic depth with generalized dips depending on the style of faulting (often 90° for strike-slip faults, 60° or 65° for normal-slip faults). Alternative fault lengths were included for most of the faults by all of the teams.

A variety of empirical relations was used by the teams to estimate M_{max} as previously described for both the regional and local fault sources. Two general approaches were used to estimate recurrence rates for the regional and local fault sources: slip rates and recurrence intervals. The four recurrence models previously described were used by the teams.

Local Faults—Varying fault behavioral and structural models were employed by the expert teams to capture the full range of complex rupture patterns and fault interactions in the characterization of local faults. Figure 12.3-40 shows an example of fault locations for an independent versus coalesced local fault model. A planar-fault block model was preferred by most teams, with linkages along strike or coalescence down dip considered by all teams. Some type of simultaneous rupture of multiple faults was included in all models (e.g., Figure 12.3-40b). In general, preferred models for multiple-fault rupture included two to four coalescing fault systems. Several teams used detachment models to constrain the extent and geometry of local fault sources. A seismogenic detachment fault was considered but not strongly favored by the teams as a source of large earthquakes. An example of the M_{max} distribution for several local faults estimated by one of the seismic source expert teams is shown on Figure 12.3-41.

The possibility that right-lateral shear is being accommodated in the Yucca Mountain region by a buried strike-slip fault was considered by all expert teams. Most of the teams included some variation of a regional buried strike-slip fault source, though with low probability.

Volcanic Sources—Seismicity related to volcanic processes, particularly seismicity related to basaltic volcanoes and dike-injection, was considered by all teams but explicitly modeled as distinct source zones by only two teams. Volcanic-related earthquakes were not modeled as a separate seismic source by the other four teams because the low magnitude and frequency of volcanic-related seismicity were assumed to be accounted for by earthquakes in the areal zones.

Areal Source Zones—Areal source zones were defined by the expert teams to account for background earthquakes that occur on potential buried faults or faults not explicitly included in their model. Some teams included alternative areal zone models within a 100-km (62-mi.) radius of the Yucca Mountain site in their characterization. The teams also defined areal zones that extended beyond a 100-km (62-mi.) radius of the Yucca Mountain site. Several teams defined a site area or zone solely for assigning a lower M_{max} to the area where more detailed investigations have been conducted and the inventory of fault sources is more complete. Examples of one team's alternative seismic source zones are shown on Figure 12.3-42.

All seismic source expert teams used the truncated exponential model to estimate earthquake recurrence rates within the areal source zones. All teams had their catalogs declustered to remove dependent events. Adjustments for underground nuclear explosions in relevant zones were also made. Varying treatments of the background seismicity were included: Uniform smoothing of seismicity was used solely or given significant weight by most teams, and non-uniform smoothing via Gaussian kernels with different smoothing distances was used by several teams.

Consideration of Tectonic Setting and Models—Each team of seismic source experts considered tectonic setting and models in developing their interpretations of seismic sources in the Yucca Mountain region. Information on the tectonics of the site area was presented to the experts at one of the workshops associated with the PSHA process (Wong and Stepp 1998, Appendix C, pp. C-39 to C-40). Most teams explicitly discussed the tectonic setting and models in their elicitation summary (Wong and Stepp 1998, Appendix E). In addition, teams also described how tectonic structure was incorporated into their interpretation of seismic sources. Tectonic models were employed to the degree that each team found them useful in characterizing

future sources of earthquakes. Brief summaries of each team's use of tectonic setting and models follows.

The Arabasz-R.E. Anderson-Ramelli team determined that Yucca Mountain lies in the Crater Flat domain and that simple (rotational) shear processes control the tectonics. They also allow the possibility that a northwest-southeast dextral shear structure might influence earthquake occurrence. Three options are considered for such a shear structure: a through-going regional dextral shear zone, a right-stepping shear zone that produces a pull-apart basin, and a right-stepping shear zone in which the pull-apart basin is underlain by a cross-basin dextral fault. While regional detachment faults are discounted, local detachments are accommodated in their interpretation of seismic sources. The local detachments are given low weight as seismogenic sources, but do constrain other elements of the seismic source interpretation (Wong and Stepp 1998, Appendix E, pp. AAR-1 to AAR-6).

The Ake-Slemmons-McCalpin team evaluated five classes of tectonic models (a caldera model, a volcanic-tectonic model, detachment models, planar fault blocks models, and lateral shear models) in interpreting seismic sources for the Yucca Mountain area. They found the caldera and lateral shear models unlikely; the planar fault block models plausible; evidence against the detachment models compelling, but not enough to rule out detachments at greater than 6 km; and that the volcanic-tectonic model may operate some of the time (Wong and Stepp 1998, Appendix E, pp. ASM-2 to ASM-8). In developing their seismic source interpretations, they employed a composite model based primarily on the planar fault model but incorporating elements of the detachment and lateral shear models.

The Doser-Fridrich-Swan team identified Yucca Mountain as a multiple-fault-block ridge in the eastern part of the extensional Crater Flat basin. They indicated that Crater Flat basin is a subbasin of the Amargosa trough and is bounded to the west by the Bare Mountain fault and to the east by the "gravity" fault. They also noted that the Timber Mountain caldera complex has influenced the development of structures in the northernmost part of the basin. The team observed that deformation in the Crater Flat basin is dominantly extensional, but includes a significant component of northwest-directed right-lateral strike-slip strain. They determined that the basin opened obliquely with greatest extension in its southwest corner. While the basin resembles a strike-slip pull-apart basin, evidence of master strike-slip faults is lacking. The strike-slip deformation is diffuse, rather than discrete (Wong and Stepp 1998, Appendix E, pp. DFS-1 to DFS-3). The Doser-Fridrich-Swan team considered detachment fault models and a caldera model. In interpreting seismic sources, the detachment model was given very low weight and the caldera model was given no weight. A planar fault model with high-angle faults extending to seismogenic depth was given the greatest weight (Wong and Stepp 1998, Appendix E, pp. DFS-34 to DFS-37).

The Rogers-Yount-L.W. Anderson team concluded that none of the tectonic models presented in the PSHA workshop provided a complete explanation of the available data. Therefore, they identified potential seismic sources and used geologic and geophysical constraints to characterize source properties. They concluded that Yucca Mountain faults are planar to listric and may coalesce to a small number of master faults at depth (Wong and Stepp 1998, Appendix E, pp. RYA-1 to RYA-2). Their interpretation of local seismic sources included pure planar faults that ruptured independently, faults that lie above a detachment or zone of decoupling and move in

response to slip on a buried fault, and faults that are planar to listric and coalesce down dip. They considered pure planar faults and detachment-decoupling model to be end-members of the coalescing fault model (Wong and Stepp 1998, Appendix E, pp. RYA-6 to RYA-7).

The K. Smith-Bruhn-Knuepfer team used tectonic models to constrain fault geometry and behavior and to estimate the characteristics of buried seismic sources. In evaluating tectonic models, the team considered several types of volcanic models. They concluded that a volcanic caldera model was not viable. A rift model is identified as an older structure that may provide part of the tectonic framework for current activity. A dike injection model is recognized as a potential influence on seismic strain rates; seismic sources related to volcanism are treated separately from primary faulting sources (Wong and Stepp 1998, Appendix E, pp. SBK-3 to SBK-6). The team concluded that detachment faults, which are a component of low-angle fault models, are not seismogenic sources. There is a small possibility, however, that they constrain the down-dip width of faults (Wong and Stepp 1998, Appendix E, pp. SBK-6 to SBK-7). A lateral-shear model involving a buried regional shear zone is given a low weight by the team. The model to which the team assigned the highest weight is a high-angle faulting model that includes a component of lateral shear related to Walker Lane deformation. The Yucca Mountain faults in this model are part of a half graben, which is bound on the west side by the Bare Mountain fault (Wong and Stepp 1998, Appendix E, pp. SBK-7 to SBK-8).

The R. Smith-dePolo-O'Leary team examined tectonic models characterized by dextral-shearing and buried strike-slip faults, detachment faults, and a half-graben structure. For dextral-shearing models they considered evidence that shearing is restricted to the Crater Flat basin and also that it is related to a northwest-striking strike-slip fault that projects into the basin from the southeast. They concluded that a buried strike-slip fault has a 40 percent likelihood of existing (Wong and Stepp 1998, Appendix E, pp. SDO-8 to SDO-9). The team determined that detachment fault models were not well supported by the available geologic, geophysical, and seismic evidence. Detachment models were not incorporated in their characterization of seismic sources (Wong and Stepp 1998, Appendix E, pp. SDO-10 to SDO-15). The team found the half-graben model to be most consistent with the available data. The model consists of two components: the half graben itself and a volcanic carapace that has collapsed into the graben. Defining two alternative realizations accommodates uncertainty on the role of the carapace. In one realization, all Yucca Mountain faults are planar faults that extend to seismogenic depth. In the other, only major, block-bounding faults extend through the crust; other faults are confined to the carapace or link to other faults at depth (Wong and Stepp 1998, Appendix E, pp. SDO-3 to SDO-4, SDO-15 to SDO-19). Interaction between the Paintbrush Canyon-Stagecoach Road fault and the Bare Mountain fault is identified as having a possible relation to basaltic dike intrusion (Wong and Stepp 1998, Appendix E, p. SDO-7).

In summary, when defining seismic sources the expert teams gave more weight to planar fault models than other models. Teams generally accommodated some component of dextral shear in their interpretations, but through-going, buried, strike-slip faults were usually given low weight. Detachment faults were weighted low as seismic sources, but were incorporated in some interpretations as possible constraints on the depth of faulting. Use of tectonic models by the expert teams is summarized in Wong and Stepp 1998 (Table 4-1, Appendix E).

Calculated Recurrence—An example of calculated earthquake recurrence relationships for one of the expert teams is shown on Figure 12.3-43. Part (a) shows the distribution of earthquake frequencies computed using the team's model for local fault sources. The team's local fault source model contains about 1.5 orders of magnitude uncertainty in the combined recurrence rate for the local sources. Part (b) shows the distribution of earthquake frequencies for regional faults. Occurrence rates were computed for those portions of the regional faults that lie within about 100 km (62 mi.) of the Yucca Mountain site. The uncertainty in the recurrence rate for the regional faults is significantly smaller than that for the local fault sources. It should be noted that for all of the expert teams' characterizations, the predicted recurrence rates for regional faults are dominated by those estimated for the Death Valley and Furnace Creek faults. Also shown on part (b) are the observed frequencies of historical earthquakes occurring within 100 km (62 mi.) of the Yucca Mountain site. Most of the smaller earthquakes are not close to the regional faults. Part (c) shows the computed recurrence for regional source zones for those portions of the regional source zones that lie within 100 km (62 mi.) of the Yucca Mountain site. The uncertainty in the recurrence rate for the regional source zones is also significantly smaller than that for the local fault sources. Also shown are the observed earthquake frequencies. The predicted earthquake frequencies for the regional zones are somewhat greater than the observed frequencies because they are based on larger source areas that include regions of higher seismicity rates that lie beyond the 100-km (62-mi.) circle. Part (d) shows the distribution of earthquake frequencies computed for all the seismic sources in this team's model for the region that lies within 100 km (62 mi.) of the Yucca Mountain site compared to the observed earthquake frequencies. The observed and predicted rates reasonably agree for magnitudes of interest to the ground motion hazard assessment.

Figure 12.3-44 compares the combined distribution for earthquake recurrence from all seismic sources and the mean results of the characterization by the six expert teams. Uncertainty in the estimation of regional seismicity rates ranges generally less than an order of magnitude. At smaller magnitudes, the range reflects the differences in how the teams characterized the regional source zones. The overprediction of the observed rate of M_w 4 to 5 earthquakes within 100 km (62 mi.) of the site reflects the teams' general assessment that larger regions are needed to characterize the seismicity rates. At larger magnitudes, the assessments from the individual teams lie within the uncertainty in the occurrence rates of earthquakes based on the historical record. Because the ground motion hazard is influenced largely (at least for high-frequency ground motions) by nearby seismic sources, the larger uncertainty in recurrence rates for the local sources, as typified by one team's interpretations on Figure 12.3-43, has a significant effect on the uncertainty in the ground motion hazard.

12.3.10.3 Vibratory Ground Motion Hazard

Vibratory ground motion hazard was computed at a defined reference rock outcrop having the properties of tuff at a depth of 300 m (984 ft) below the ground surface at Yucca Mountain—the waste emplacement depth. Ground motion was computed at this reference location as a control motion for later determination of seismic design bases motions for surface and potential waste-emplacement level locations.

Based on equally weighted inputs from the six seismic source expert teams and the seven ground motion experts, the probabilistic hazard for vibratory ground motion was calculated for

horizontal and vertical peak acceleration (defined at 100 Hz), spectral accelerations at frequencies of 0.3, 0.5, 1, 2, 5, 10, and 20 Hz, and peak velocity, and are expressed in terms of hazard curves (e.g., Figure 12.3-45). The hazard is also expressed in terms of uniform hazard spectra. Peak ground acceleration, 0.3- and 1.0-Hz spectral values, and peak velocity are summarized in Table 12.3-18 for the annual exceedance probabilities of 10^{-3} and 10^{-4} . The largest source of epistemic uncertainty in the hazard results is in the ground motion characterization.

Deaggregation of the mean hazard for an annual exceedance frequency of 10^{-4} shows that at 5 to 10 Hz (or other high frequencies), ground motions are dominated by earthquakes of smaller than M_w 6.5 occurring at distances less than 15 km (9 mi.) (Figure 12.3-46). Dominant events for low-frequency ground motions, such as at 1 to 2 Hz, display a bimodal distribution that includes large nearby events and M_w 7 and larger earthquakes beyond distances of 50 km (31 mi.) (Figure 12.3-46). The latter contribution is due mainly to the relatively higher activity rates for the Death Valley and Furnace Creek faults.

Extensive evaluations of parametric sensitivities of the ground motion hazard were performed. The recurrence approach (either slip rates or recurrence intervals) and recurrence model (e.g., characteristic, exponential, or maximum moment) are the parameters that contribute the most to uncertainty in the ground motion hazard, at the design basis hazard: 10^{-3} and 10^{-4} per year. M_{max} has a small effect on uncertainty, especially for 10 Hz, because a large fraction of the hazard at this frequency comes from more frequent moderate-magnitude events. Geometric fault parameters (e.g., rupture lengths, dips, maximum depths) are minor contributors to uncertainty. These parameters have a moderate effect on the locations of earthquakes and on M_{max} , but do not affect earthquake recurrence. Although the seismic source expert teams' results vary somewhat, the dominant sources for seismic hazard at 10-Hz ground motions are the Paintbrush Canyon-Stagecoach Road and Solitario Canyon faults (or coalesced fault systems including these two faults) and the host areal seismic source zone. For 1-Hz ground motions, the dominant seismic sources are the Death Valley and Furnace Creek faults and the same three sources mentioned above. Multiple-rupture interpretations of the type with comparable seismic moment release on more than one fault (i.e., those requiring modification of the attenuation equations) make a small contribution to the total hazard. Buried strike-slip faults, volcanic seismicity, and seismogenic detachments contribute negligibly to the total hazard.

The major contributor to epistemic uncertainty in the ground motion hazard is the expert-to-expert epistemic uncertainty in ground motion amplitude. Additional contributions to epistemic uncertainty arise from moderate differences among the seismic source expert teams and among the ground motion experts, as well as from the uncertainties expressed by the seismic source logic trees.

12.3.10.4 Fault Displacement Characterization

Several original approaches to characterize the fault displacement potential were developed by the seismic source expert teams, based primarily on empirical observations of the pattern of faulting at the site during past earthquakes determined from data collected during fault studies at Yucca Mountain. Empirical data were fit by statistical models to allow use by the experts.

The potential for fault displacement was categorized as either principal or distributed faulting. Principal faulting is the faulting along the main plane (or planes) of crustal weakness responsible for the primary release of seismic energy during the earthquake. Where the principal fault rupture extends to the surface, it may be represented by displacement along a single narrow trace or over a zone that is a few to many meters wide. Distributed faulting is defined as rupture that occurs on other faults in the vicinity of the principal rupture in response to the principal displacement. Distributed faulting may or may not be the source of seismic energy release, but it is assumed insignificant compared to the principal fault. It is expected that distributed faulting will be discontinuous in nature and occur over a zone that may extend outward several tens of meters to many kilometers from the principal rupture. A fault that can produce principal rupture may also undergo distributed faulting in response to principal rupture on other faults.

Both principal and distributed faulting are important to the assessment of the fault displacement hazard at the Yucca Mountain site. Nine locations within the preclosure controlled area were identified to demonstrate the fault displacement methodology (Figure 12.3-47). Two of the nine sites each had four identified faulting conditions. These locations were chosen to represent the range of potential faulting conditions. Some of these locations lie on faults that may experience both principal faulting and distributed faulting. The other points are sites of only potential distributed faulting.

The basic formulation for the probabilistic evaluation of fault displacement hazard is analogous to that for the ground motion hazard. The displacement hazard is represented probabilistically by a displacement hazard curve that is analogous to a ground motion hazard curve. Thus, the hazard curve is a plot of the frequency of exceeding a fault displacement value d , designated by $\nu(d)$. This frequency can be computed by the expression $\nu(d) = \lambda_{DE} \times P(D > d)$, in which λ_{DE} is the frequency at which displacement events occur on a feature at the site of interest and $P(D > d)$ is the conditional probability that the displacement in a single event will exceed value d .

The approaches developed by the seismic source expert teams for characterizing the frequency of displacement events, λ_{DE} , can be divided into two categories: the displacement approach and the earthquake approach. The displacement approach provides an estimate of the frequency of displacement events directly from observed feature-specific or point-specific data. The earthquake approach involves relating the frequency of slip events to the frequency of earthquakes on the various seismic sources defined by the seismic source characterization models for the ground motion assessment. Both approaches are used for assessing the fault displacement hazard for principal faulting and distributed faulting.

The conditional probability of exceedance, $P(D > d)$, can be considered to contain two parts: the variability of slip from event to event and the variability of slip along strike during a single event. The teams developed several approaches for evaluating the distribution of slip at a location given a principal faulting event. Some used the two-part representation of variability; others combined them into a single distribution function.

Principal faulting hazard was assessed for sites located on faults that the seismic source expert teams identified as being seismogenic. The preferred approach for estimating the frequency of displacement events is the use of slip rate divided by the average displacement per event. The slip rates were primarily based on the teams' seismic source characterization for the ground

motion hazard assessment. The teams used a number of approaches to evaluate the conditional probability of exceedance. These are based on empirical distributions derived from Yucca Mountain trenching data normalized by various parameters, including the expected maximum displacement in the maximum event, the average displacement estimated from displacement data, and the average and maximum displacements estimated from the length of the feature.

To characterize the frequency of displacement events, the teams used the frequency of earthquakes developed for the ground motion hazard assessment multiplied by the conditional probability that an event produces surface rupture at the site of interest. The along-strike intersection probability was computed using the rupture length estimated from the magnitude of the event randomly located along the fault length. Most teams used an empirical model based on historical ruptures to compute the probability of surface rupture. The approach used by most of the teams to assess the conditional probability of exceedance was to define a distribution for the maximum displacement, based either on the magnitude or the rupture length of the earthquake. This distribution is then convolved with a distribution for the ratio of the displacement to the maximum displacement to compute $P(D > d)$.

The majority of the seismic source expert teams considered the frequency of displacement events on features subject to only distributed faulting to be estimated by slip rate divided by the average displacement per event. The slip rates were based on the cumulative displacement and slip history. The teams used approaches for evaluating the conditional probability of exceedance that are similar to those used in the displacement approach for characterizing principal faulting hazard. The empirical distributions used were correlated with the scaling relationship used to estimate the average displacement per event.

The seismic source expert teams displayed the most variability in characterizing distributed faulting potential using the earthquake approach. The basic assessment of the frequency of earthquakes was derived from the seismic source characterization for ground motion hazard assessment defined by each team. The probability that an earthquake causes slip at the point of interest was assessed in a variety of ways. Most teams used the logistic regression model based on analyses of the pattern of historical ruptures. The widest variations in approaches were those for assessing the distribution for displacement per event on the distributed ruptures.

All of the teams considered the points on the Bow Ridge and Solitario Canyon faults as subject to principal faulting hazard. A few teams also considered some potential for principal faulting hazard at two locations on two intrablock faults. The teams varied widely in their assessments of the probability that distributed faulting could occur in future earthquakes at points that are located off of the block-bounding faults. These assessments were based on fault orientation, cumulative slip, and structural relationship. Four teams considered that the probability of displacement at a point in intact rock due to the occurrence of a future earthquake is essentially 0.

12.3.10.5 Fault Displacement Hazard

The probabilistic fault displacement hazard was calculated at nine demonstration sites within the preclosure controlled area (Figure 12.3-47). Two of the sites have four hypothetical conditions representative of the features encountered within the ESF. The integrated results provide a

representation of fault displacement hazard and its uncertainty at the nine sites, based on the interpretations and parameters developed by the six seismic source expert teams. Separate results were obtained for each site in the form of summary hazard curves (e.g., Figure 12.3-48). Table 12.3-19 summarizes the mean displacement hazard results for the two design basis annual exceedance probabilities, 10^{-4} and 10^{-5} , at the nine demonstration sites.

With the exception of the block-bounding Bow Ridge and Solitario Canyon faults (sites 1 and 2, respectively), the mean displacements are 0.1 cm (0.04 in.) or less at 10^{-5} annual exceedance frequency. At 10^{-5} annual frequency, the mean displacements are 7.8 and 32 cm (3.0 and 12.6 in.), respectively, for these two faults (Table 12.3-19). Thus, for sites not located on a block-bounding fault, such as the potential waste emplacement area, the average recurrence interval for displacements exceeding 0.1 cm (0.04 in.) is 100 k.y.

The fault displacement hazard results display significant uncertainty. This uncertainty is indicative of the state of practice in PSHA for fault displacement, which is less mature than probabilistic analysis for ground motions. Nonetheless, the results obtained here are considered robust by virtue of the large amount of empirical data for the site, extensive efforts at expert elicitation and feedback, as well as the methodological developments, that were undertaken as part of this study. Sites with the highest fault displacement hazard show uncertainties comparable to those obtained in ground motion PSHA. Sites with low hazard show much higher uncertainties.

Also, a not-unexpected correlation exists between the amount of geologic data available at a site and the uncertainty in the calculated hazard at that site. For sites with significant geologic data, the team-to-team uncertainty is less than one order of magnitude. For sites with little or no data, the individual team curves span three orders of magnitude. The larger uncertainty at these sites is considered to be due to data uncertainty (i.e., less certain constraints on the team's fault displacement characterization models).

12.3.11 Deterministic Seismic Hazard Analysis of Potential Type I Faults at Yucca Mountain

YMP scientists conducted a deterministic analysis of earthquake sources relevant to vibratory ground motion hazards at the Yucca Mountain site (USGS 2000). This analysis was designed to meet a U.S. Department of Energy commitment to the U.S. Nuclear Regulatory Commission to conduct deterministic analyses of Type I faults within 5 km (3 mi.) of the preclosure controlled area boundary as a supplement to the PSHA (Brocoum 1995, p. 3) (Section 12.3.10). The PSHA results provide the seismic hazard input to the repository design. The general methodology of the deterministic seismic hazard analysis consists of identification and characterization of Quaternary faults as independent seismic sources for maximum earthquakes (i.e., the largest possible earthquake that can reasonably be expected to occur in association with a fault in the present tectonic regime). Source characterization includes estimation of deterministic maximum magnitudes from fault parameters, such as rupture dimensions and single-event displacements. Critical ground motion parameters, such as horizontal spectral response and peak horizontal acceleration, are then calculated using ground motion attenuation equations. This deterministic analysis differs from the probabilistic methodology discussed in Section 12.3.10 primarily in that it does not include earthquake frequency information, fault slip rates and recurrence intervals,

and it uses conservative, but reasonable, single-value data as input that do not explicitly incorporate uncertainty.

An evaluation of Type I faults in the Yucca Mountain area, based on the definition of Type I faults in McConnell et al. (1992), is currently under way using the above approach. These faults are of sufficient length and location to potentially affect the design and performance of the potential repository. These faults are also potentially subject to displacement, based on either direct evidence for Quaternary displacement or one or more of the following indirect criteria:

- Association with seismicity
- Structural relations with other potential Type I faults
- Favorable orientation with respect to the contemporary stress field.

A fault is identified as a candidate Type I fault if it meets at least one of the subject-to-displacement criteria. A candidate Type I fault is then classified as a potential Type I fault for ground motion hazard if it meets the additional criterion that it is capable of generating an 84th percentile peak horizontal acceleration that equals or exceeds 0.1 g (98 cm/s^2) at the former conceptual controlled area boundary. This definition of a potential Type I fault approximately corresponds with the "potentially relevant" and "relevant" fault definition of Pezzopane (1996), as adapted from McConnell et al. (1992) and summarized in Section 12.3.8.

12.3.11.1 Methods

Compilation of Fault Characteristics—A list of 118 seismic sources was developed from several published compilations of known and suspected Quaternary faults within approximately a 100-km (62-mi.) radius of Yucca Mountain (Pezzopane 1996; Piety 1996; McKague et al. 1996). Thirty-eight are local sources inside or within 5 km (3 mi.) of the preclosure controlled area boundary; they consist of 32 individual faults and 6 fault rupture combinations that are possible sources of distributed ruptures (Figures 12.3-49 and 12.3-50). The latter distributed rupture sources are modified from the specific rupture scenarios described in Section 12.3.7.3, based on reevaluation of timing and geologic constraints for faulting events summarized in Table 12.3-9. Data for each source were compiled from published and unpublished literature sources. The compilation includes the following fault characteristics:

- The shortest horizontal distance between the nearest point on the surface trace of the fault and both a point in the center of the potential repository and the former conceptual controlled area boundary
- Documentation of Quaternary displacements
- Maximum fault lengths, used as a proxy for surface-rupture length without segmentation (see Section 12.3.7.5), as measured along the mapped fault trace
- Where paleoseismic data are available (for 30 percent of the faults), estimates of single-event displacements (Section 12.3.7.4), including the maximum (single largest measurement on the fault) and average (mean of measurements at all trench sites) displacements

- Fault geometry at seismogenic depth, including fault dips (estimated generically for various fault types from regional seismicity and geophysical data) and dip direction (based on surface outcrop)
- Sense of fault slip, determined from surface displacement patterns and slip indicators.

A 15-km (9-mi.) seismogenic depth was assigned to all faults, based on local and regional seismicity catalogs.

Calculation of Maximum Magnitude—A suite of four to seven maximum magnitudes (M_w) was calculated for each fault, depending on the type of available data. Six values were computed from the series of log-linear regression equations developed by D.L. Wells and Coppersmith (1994) from empirical data on all slip-types of historical earthquakes (Section 12.3.7.7). These regression equations relate M_w to surface-rupture length (here approximated by maximum fault length), average and maximum displacements per event, and three estimates of fault rupture area (the product of fault length and down-dip width—the latter derived from seismogenic depth and three estimates of fault dip). An additional M_w was converted with the regression of Hanks and Kanamori (1979) from direct estimates of the seismic moment, defined as the product of rupture area, average displacement, and the shear modulus. The arithmetic mean of these computed M_w estimates defines the deterministic maximum magnitude assigned to each fault or fault combination.

Calculation of Ground Motions—The vibratory ground motions were evaluated for each source by calculating horizontal acceleration response spectra and peak horizontal acceleration. Acceleration response spectra constitute the primary measure of the deterministic seismic hazard, whereas peak horizontal acceleration is used primarily for determining whether the maximum earthquake of the fault meets the 0.1-g (98-cm/s^2) criterion for potential Type I faults as defined earlier. The median (50th), 84th, and 16th percentile of both ground motion parameters are derived from the average of attenuation equations developed specifically for the probabilistic seismic hazard analyses project (Wong and Stepp 1998) (Section 12.3.9.5). These calculations use the mean M_w and minimum distance to the potential repository (for response spectra) and former conceptual controlled area boundary (for peak horizontal acceleration), as well as other input parameters (e.g., strike-slip versus normal faulting, hanging wall versus footwall position on normal faults, and single versus multiple-rupture fault). The seven-function average developed by the PSHA ground motion experts (for the reference rock outcrop) (Section 12.3.9.5) represents a significant improvement from the attenuation equations used in previous studies (Pezzopane 1996; McKague et al. 1996) because it emphasizes data from extensional tectonic regimes similar to the Yucca Mountain area, including region- and site-specific attenuation effects, and explicitly incorporates additional source and site parameters (e.g., fault type and multiple faults).

Identification of Candidate and Potential Type I Faults—Each seismic source was classified initially as a candidate Type I fault on the basis of data, such as evidence for Quaternary displacements, source-to-site distance, fault length, historical seismicity, mapped fault patterns, and general fault orientation, that address the subject-to-displacement criteria in NUREG-1451 (McConnell et al. 1992). Candidate Type I faults were then classified as potential Type I faults relevant to ground motion hazard on the basis of whether the average of the 84th percentile peak

horizontal acceleration calculated from the PSHA attenuation relations exceeds the 0.1-g (98-cm/s²) criterion, as shown by sources plotted below and to the right of the attenuation isopleth of the seven-function average in the magnitude-distance plot of Figure 12.3-51.

12.3.11.2 Deterministic Magnitudes-Ground Motions and Revised Potential Type I Faults

The deterministic maximum magnitudes calculated for the local seismic sources range from M_w 5.7 (e.g., Ghost Dance fault) to M_w 6.8 (e.g., the Paintbrush Canyon-Stagecoach Road-Bow Ridge fault combination) (Figure 12.3-51, Table 12.3-20). The largest magnitudes, in the range of M_w 6.6 to 6.8, are associated with either the three largest block-bounding faults (the Solitario, Paintbrush Canyon, and Windy Wash faults), or fault combinations on the eastern and western sides of the mountain that involve these faults. Most of the small-magnitude deterministic earthquakes are related to either short isolated Quaternary faults (e.g., the Black Cone, Lathrop Wells, and East Busted Butte faults) or short bedrock faults with no direct stratigraphic or geomorphic evidence for Quaternary displacements (e.g., the Boomerang Point and Simonds faults). Even if active, the latter faults probably do not extend to large seismogenic depths, based on their short lengths and proximity to the large principal block-bounding faults and, thus, are unlikely to act as independent seismic sources (Table 12.3-20). All sources with magnitudes greater than M_w 6.3 are associated with 21 faults or fault combinations identified as credible seismic sources (i.e., a probability of Quaternary activity greater than 0) by the seismic source expert teams (Table 12.3-20). The mean and median values of the distribution of M_{max} calculated for these sources in the deterministic seismic hazard analyses and the PSHA have small differences, averaging less than 0.1 magnitude units. The deterministic magnitude estimates of the remaining 17 faults that were not included as independent seismic sources by the PSHA expert teams are small, ranging from M_w 5.7 to 6.25, which were accounted for in the probabilistic analysis by a background earthquake.

Horizontal response spectra computed for the 38 local sources and three selected regional faults are summarized on Figure 12.3-52 and in Table 12.3-20. These data indicate four controlling deterministic earthquakes that are associated with four rupture scenarios involving mainly multiple parallel and colinear rupture combinations along three principal Quaternary block-bounding faults in the site area: Solitario Canyon, Paintbrush Canyon, and Windy Wash faults and their subordinates. The single most significant scenario is the three-fault multiple rupture of Solitario Canyon-Fatigue Wash-Windy Wash. The four controlling earthquake scenarios are predicted to produce peak horizontal spectral accelerations at approximately 10 Hz equal to or exceeding 1.0 g (981 cm/s²) at the median and 2.0 g (1,961 cm/s²) at the 84th percentile. The next most important deterministic earthquakes with slightly lower 10-Hz spectral accelerations are associated with the large Quaternary block-bounding faults modeled as independent sources. Local seismic sources identified by the PSHA expert teams could produce median horizontal 10-Hz spectral accelerations from 0.17 to 1.13 g (116 to 1,108 cm/s²) (Table 12.3-20), whereas similar ground motions for sources not characterized by expert teams are equal to or less than 0.63 g (618 cm/s²) (Table 12.3-20). All of these local deterministic earthquakes are rare events, in that they are associated with faults with recurrence intervals greater than 10⁴ years and slip rates less than or equal to 0.03 mm/yr. (1 × 10⁻³ in./yr.) (Sections 12.3.7.6 and 12.3.7.2).

Regional deterministic sources are predicted to produce median horizontal 10-Hz spectral accelerations no greater than 0.5 g (490 cm/s²) and 84th percentile values no greater than 0.9 g

(883 cm/s²). Eighteen regional sources are capable of exceeding median peak horizontal spectral accelerations of 0.1 g (98 cm/s²), and seven are capable of exceeding median values of 0.2 g (196 cm/s²). Roughly half of the regional faults are predicted to produce 84th percentile fractile horizontal acceleration spectra that exceed 0.1 g (98 cm/s²) across the frequency range from slightly below 1 Hz to approximately 50 Hz.

Of the 118 local and regional seismic sources considered in this study, 111 sources meet either the Quaternary displacement and/or indirect criteria for candidate Type I faults described in NUREG-1451 (see above; McConnell et al. 1992). However, only 53 faults meet the criterion for potential Type I faults, in that they are considered subject to displacement and have the potential to produce peak horizontal accelerations that equal or exceed 0.1 g (98 cm/s²) at the 84th percentile, using the deterministic mean maximum magnitudes, minimum horizontal distances, and the mean of the values derived from the average of the seven attenuation equations developed by the PSHA ground motion experts. All local sources (32 individual faults and 6 fault rupture combinations) characterized within 5 km (3 mi.) of the former conceptual controlled area boundary are included. Of the 32 faults, 21 lack evidence of Quaternary displacement and may not be independent sources of earthquakes, mainly because they seem to be too short to penetrate to large seismogenic depths. Fifteen of the 80 regional faults are potential Type I faults relevant to ground motion hazard. Ten of these faults have documented Quaternary displacements; activity on the remaining five is probably pre-Quaternary; therefore, they may not be earthquake sources.

The results of this deterministic analysis differ from those of previous studies of Type I relevant faults in the Yucca Mountain area presented in McKague et al. (1996) and Pezzopane (1996) (Section 12.3.8). The number of local potential Type I faults in the site area is larger in the deterministic seismic hazard analyses because the analysis includes all mutually exclusive candidate Type I faults identified in both previous studies, as well as several other faults and, particularly, fault combinations not included in either. All of the local sources are potential Type I sources, in a strict sense, because of their very close proximity to the site, irrespective of maximum magnitude size. However, a number of the sources (65 percent) of the individual faults are considered to be unlikely seismogenic sources because of lack of evidence for Quaternary activity, fault dimensions, and structural setting. The number of regional potential Type I faults is significantly less, primarily because this analysis uses attenuation equations developed specifically for the Yucca Mountain site by the PSHA ground motion experts. These relations predict that the ground motion effects at the site of far-field sources are markedly reduced, relative to the attenuation equations used in the previous studies.

The deterministic analysis of Type I faults employed the attenuation relationship developed for the PSHA. This relationship gives ground motion for the reference rock outcrop defined for the PSHA, an outcrop with rock properties found at a depth of about 300 m (984 ft) (Section 12.3.10.3). The results of the deterministic analysis do not, therefore, take into account the site response of the upper 300 m (984 ft) of rock. When calculation of the site response is completed (Section 12.3.12.4), this additional information can be incorporated into the deterministic analysis and a final evaluation of Type I faults can be carried out.

12.3.12 Development of Seismic Design Criteria

Proposed 10 CFR 63, Disposal of High-Level Radioactive Wastes in a Proposed Geologic Repository at Yucca Mountain, Nevada (64 FR 8640), requires that structures, systems, and components important to safety be designed so that natural phenomena and environmental conditions anticipated at the operations area of the potential geologic repository will not compromise necessary safety functions. Vibratory ground motion and fault displacement hazards are among the natural phenomena that must be considered in the design of structures, systems, and components important to safety. The results of the PSHA of both ground motion and fault displacement that have been performed for Yucca Mountain (Section 12.3.10) (Wong and Stepp 1998) have been used to develop preliminary seismic design inputs for the structures, systems, and components of the potential repository (CRWMS M&O 1998i).

In accordance with *Preclosure Seismic Design Methodology for a Geologic Repository at Yucca Mountain* (YMP 1997b), the seismic design is being developed for two levels of seismic hazard: Category 1 and Category 2. For vibratory ground motion, the reference annual frequencies of exceedance for these two categories are 10^{-3} and 10^{-4} , respectively. Hence, the seismic design ground motions reflect ground motion hazard with average return periods of 1 k.y. and 10 k.y. for Category 1 and Category 2, respectively.

Based on the probabilistic analysis for ground motion, uniform hazard spectra were generated for annual frequencies of exceedance of 10^{-3} and 10^{-4} for both horizontal and vertical motions (Figures 12.3-53 to 12.3-56) for the reference rock outcrop (Point A on Figure 12.3-57). These spectra were the starting point for the seismic design input calculations. For fault displacement, the annual exceedance frequencies are 10^{-4} and 10^{-5} , corresponding to displacement hazard return periods of 10 k.y. and 100 k.y., respectively.

The potential repository will have structures, systems, and components at multiple locations, including locations at the ground surface and within the subsurface. The seismic design ground motion values have been developed for each of these locations. Input ground motions are provided for a rock site at the surface (referred to as the tuff outcrop; Point C on Figure 12.3-57); for a location at 300 m (984 ft) depth (Point B on Figure 12.3-57), the approximate depth of the proposed waste emplacement area; and at the site of the proposed Waste Handling Building in Midway Valley (Point D on Figure 12.3-57). Design inputs for ground motion consist of peak values for acceleration and velocity, response spectra, and time histories. Results are presented for both vertical and horizontal components. In addition, strains and curvatures are presented as a function of depth from the surface to 300 m (984 ft).

The following section describes the methodology used to develop seismic design fault displacement and ground motion input for the safety-related structures, systems, and components of the potential repository. Implementation of the methodology is in process and thus is not reported here.

12.3.12.1 Seismic Design for Fault Displacement

According to the fault displacement hazard results described in Section 12.3.10.5, locations away from block-bounding faults have a low probability of experiencing significant displacement.

At the 10^{-5} annual exceedance probability, results for all such sites indicate displacements less than 1 cm (0.4 in.). For such sites, a specific design criterion for Category 1 and Category 2 structures, systems, and components will not be required.

For the two block-bounding faults considered (Solitario Canyon and Bow Ridge), the PSHA results indicate a higher fault displacement hazard. If safety-related structures, systems, and components cross these faults, they should be designed to accommodate displacements. For Category 2 structures, systems, and components that cross the Bow Ridge fault, design for a displacement of 7.8 cm (3 in.) is indicated, and for the Solitario Canyon fault, design should be for a displacement of 32 cm (12.6 in.). It should be noted, however, that the primary approach to seismic design for fault displacement is to avoid faults (YMP 1997b, Section 4.3).

If safety-related structures, systems, and components cross the Bow Ridge or Solitario Canyon faults, either at the surface or at the potential repository elevation, a local determination of the fault width must be made to determine the distance over which faulting may occur. Alternatively, the displacements indicated above can be considered to be knife-edge displacements. The sense of displacement (vertical, horizontal, or some combination) should be assumed to be in the most critical direction for each structure, system, and component being designed. For purposes of computing extension or compression on linear structures, systems, and components resulting from fault displacement, a dip angle of 45° can be assumed in lieu of a fault-specific determination.

In summary, fault displacement hazard results at sites located away from identified principal faults indicate a low hazard of displacement, even for a 10^{-5} annual exceedance probability. Therefore, structures, systems, and components located away from identified faults need not be designed for fault displacement.

12.3.12.2 Deaggregation of Vibratory Ground Motion Hazard

The deaggregation of probabilistic seismic hazard is the process of determining the contributions of combinations of magnitude (M), distance (R), and ground motion deviation (ϵ) to the annual frequency of exceeding a given ground motion amplitude (McGuire 1995). For this purpose, M is the moment magnitude (M_w) and ϵ is the difference between the logarithm of the ground motion amplitude and the mean logarithm of ground motion (for that M and R), measured in units of the standard deviation ϵ of log (ground motion). M, R, and ϵ combinations contribute differently, depending on the ground motion amplitude and the structural frequency of the ground motion measure.

The seismic hazard was deaggregated at ground motion amplitudes corresponding to 10^{-3} and 10^{-4} annual probabilities of exceedance. This deaggregation was done at frequencies of 10, 5, 2, and 1 Hz, and results for 5 and 10 Hz were averaged, as were results for 1 and 2 Hz, consistent with recommendations in Regulatory Guide 1.165.

Figures 12.3-58 and 12.3-59 show the relative contributions of M, R, and ϵ for 5- to 10-Hz horizontal motions corresponding to amplitudes with 10^{-3} and 10^{-4} annual probabilities of exceedance, respectively. The predominant contributions at these high frequencies come from magnitudes in the M_w 5 to 6 range and distances less than 15 km (9 mi.).

Figures 12.3-60 and 12.3-61 show the equivalent contributions for the 1- to 2-Hz horizontal motions. These plots show more contribution coming from large events (approximately M 7) at distances of about 50 km (31 mi.). The sources for these events are the Death Valley-Furnace Creek faults, which have a higher slip rate than do the local faults (Wong and Stepp 1998).

12.3.12.3 Reference Rock Outcrop Spectra

To derive horizontal spectra for seismic design, the deaggregation results were used to identify reference earthquakes at moderate frequencies (5 to 10 Hz) and low frequencies (1 to 2 Hz). Reference earthquakes for vertical motions were taken to be identical to those for horizontal motion for consistency. The deaggregation shows that the controlling event for moderate frequencies is M_w 5 to 6 at close distances, but for low frequencies, two events contribute significantly to the hazard. These results are summarized in Table 12.3-21.

For each event indicated in Table 12.3-21, acceleration response spectra were calculated based on the attenuation relationships provided by the ground motion experts in the probabilistic analysis (Section 12.3.9.5). The factors indicated in Table 12.3-21 are the multiplicative factors used to raise the spectra of the controlling events to match the uniform hazard spectra at the average of 5 to 10 Hz and 1 to 2 Hz, as appropriate. This scaling follows the procedure described in Regulatory Guide 1.165. For 1 to 2 Hz, the larger-magnitude events were used because they have a broader spectral shape at low frequencies; factors for the smaller magnitudes were not calculated.

Adjustments in M were made based on the results presented in Table 12.3-21, resulting in the reference earthquakes presented in Table 12.3-22, which represent the combined hazard due to all earthquakes represented by the uniform hazard spectra.

The M and R selections shown in Table 12.3-22 broaden the spectrum for the design earthquakes, result in slightly higher motion, and allow two reference earthquakes to represent all frequencies of the uniform hazard spectra (Figures 12.3-62 to 12.3-65). The revised multiplicative factors are also shown in Table 12.3-22.

In both comparisons, the two horizontal reference earthquake spectra envelop the uniform hazard spectra except in a narrow frequency range between 2 and 5 Hz (Figures 12.3-62 and 12.3-63). For 10^{-4} annual probability of exceedance, the design earthquake spectra are a maximum of 7 percent below the uniform hazard spectra; for 10^{-3} annual probability of exceedance they are a maximum of 10 percent below the uniform hazard spectra. This agreement is considered reasonable, given that the procedure outlined in Regulatory Guide 1.165 has been followed and that elsewhere the individual design earthquake spectra exceed the uniform hazard spectra, often by more than 10 percent. For consistency, the same design earthquakes are used for vertical motions as for horizontal motions (Figures 12.3-64 and 12.3-65).

These reference earthquakes, which have been determined at the reference rock outcrop, are used for two purposes. First, they represent individual earthquakes used in the site response studies to calculate equivalent response spectra for the repository interface, and at the surface, for both tuff and soil conditions. Second, they are the basis for generating time histories of ground motion at these locations that can be used in detailed checking of design levels.

12.3.12.4 Methodology to Develop Seismic Design Ground Motions

Site response, including peak motions and strains, is computed using specific earthquakes derived from the PSHA matching the outcrop uniform hazard spectra. Because the dynamic properties of the materials in the tuff overburden and soil are variable and have not been characterized in detail, the seismic design ground motions are obtained at a reference rock outcrop (hypothetical free surface) at the potential repository interface at an average depth of 300 m (984 ft). Available velocity measurements suggest surficial tuff and soil layers with shear-wave velocities as low as 300 to 400 m/s (984 to 1,312 ft/s). With maximum expected motions exceeding about 0.5 g (490 cm/s^2) at zero period, this shallow material may be expected to exhibit significant nonlinear response.

Defining the control point at the ground surface requires equivalent-linear deconvolution using broadband surface motions for the development of at-depth motions. This approach is generally considered undesirable, as motions can diverge (become unrealistically large) at depth due to anomalous high levels of strain induced by the use of a broadband surface control motion (CRWMS M&O 1998i, p. 3-1). Similarly, for the development of surface and repository-level motions, the use of broadband at-depth outcrop control motions is inappropriate. Accordingly, specific earthquakes (the reference earthquakes) have been identified by deaggregating the hazard at each target design level (uniform hazard spectra annual exceedance frequency of 10^{-3} and 10^{-4}) at the reference rock outcrop (Point A on Figure 12.3-57).

To properly represent the potential magnitude-dependence of site response spectra, three control motions, representing a range of earthquake magnitudes based on the hazard deaggregation, were also obtained for each of the two design levels (10^{-3} and 10^{-4} annual probabilities of exceedance) and two structural frequency ranges (5 to 10 Hz and 1 to 2 Hz). The three magnitudes M_{mean} , $M_{5\text{th}}$, and $M_{95\text{th}}$ represent magnitudes associated with the mean, 5th, and 95th percentile of the deaggregated hazard. Site response analyses are performed for each of these three control motions. These 12 earthquakes, three for each of the four reference earthquakes, are designated the deaggregation earthquakes.

For the computation of design spectra for a site with uncertain properties that exhibits a degree of lateral variability, a best-estimate base-case velocity profile is developed and used to simulate a number of shear-wave models (EPRI 1993, Volume 2, Appendix 6.A). Additionally, strain-dependent shear modulus and hysteretic damping are randomized about a best estimate base case. A large number of simulations can be required to achieve stable statistics on the response. The simulations attempt to capture the variability and uncertainty in the soil or rock parameters and layer thickness.

Given the variability and uncertainties of properties within the potential repository block, 60 randomized profiles were produced for the tuff overburden base case velocity profile. For each of the three deaggregation earthquakes (M_{mean} , $M_{5\text{th}}$, and $M_{95\text{th}}$), motions at each location, as well as strains and curvatures throughout the tuff overburden, are computed by equivalent-linear convolution analysis of each set of 60 simulations. The mean response spectra (based on analysis of the 60 convolutions) are divided by the control motion spectrum to produce a mean spectral amplification function for each deaggregation earthquake. The weighted average of the three mean spectral amplification functions, which reflect the distribution of

earthquake magnitudes contributing to the uniform hazard spectra, produce a magnitude-weighted mean spectral amplification function. The product of this spectral amplification function and the reference earthquake spectrum is taken as the design earthquake spectra. This process is repeated for each component of the four reference earthquakes.

For the repository interface and tuff overburden seismic design motions (Points B and C on Figure 12.3-57), design earthquake spectra are developed using a base case velocity profile. If necessary to represent the velocity variability of the emplacement block, multiple base case profiles can be used (e.g., best estimate, lower bound, and upper bound). The need for this approach will depend on the variability indicated by the velocity data available to characterize the emplacement block.

INTENTIONALLY LEFT BLANK

12.4 SUMMARY

Volcanic and seismic activity pose the tectonic hazards of concern in the evaluation of Yucca Mountain as the potential site for a geologic repository for high-level radioactive waste. Both volcanic and seismic events have occurred in the vicinity of Yucca Mountain during the Quaternary period. The hazard from possible volcanic and seismic events in the future was assessed probabilistically. Expert elicitation was used to interpret the large amount of data that was collected and to formulate inputs to probabilistic hazard calculations. The frequency of future seismic activity is taken into account in the design of a potential geologic repository at Yucca Mountain for the preclosure period (up to 300 yr.). Both volcanic and seismic effects are considered in assessing the long-term performance of such a repository.

Igneous Activity and Volcanic Hazard—Two major types of volcanism have occurred in the Yucca Mountain region: an early phase of Oligocene to Miocene silicic volcanism and a more recent phase of Miocene and post-Miocene basaltic volcanism. The silicic volcanism occurred primarily between about 15 and 11 Ma, forming the southwestern Nevada volcanic field. This activity was largely coincident with a major period of extension in the region. Yucca Mountain is an uplifted, erosional remnant of the voluminous ash-flow tuff deposits formed during the early phase of this silicic volcanism.

Basaltic volcanism commenced during the latter stages of the silicic volcanism phase and can be divided into two episodes: Miocene (eruptions between about 9 and 7.3 Ma) and post-Miocene (eruptions between about 4.8 and 0.08 Ma). While basaltic volcanism has continued into the Quaternary period, activity since about 7.5 Ma represents just 0.1 percent of the total eruptive volume of the southwestern Nevada volcanic field. In evaluating the volcanic hazard for Yucca Mountain, experts considered which periods of past activity were most relevant to determining the frequency of future activity.

Volcanic hazard at Yucca Mountain was assessed probabilistically. A panel of 10 volcanism experts evaluated available data to develop interpretations of the future spatial and temporal distribution of igneous events in the Yucca Mountain region. The experts also provided interpretations that allow the determination of whether an igneous event will result in an intersection of the potential repository by an associated dike, given the event occurs at some point in the Yucca Mountain region. The experts further provided quantitative descriptions of the uncertainties associated with their interpretations. The result of the probabilistic analysis was the annual frequency with which an igneous event resulted in a dike intersecting the repository footprint. A subsequent analysis recalculated the hazard for a revised repository footprint (Enhanced Design Alternative II) and used the experts' interpretations to address the frequency of a volcanic eruption through the potential repository.

To describe the temporal occurrence of future igneous activity, the probabilistic volcanic hazard analysis experts considered interpretations in which events occur randomly at a uniform rate (homogeneous), as well as those with a variable rate of activity (nonhomogeneous). Spatial models used by the experts to describe future volcanic activity in the Yucca Mountain region included homogeneous source zones, in which the likelihood of an igneous event was spatially uniform, and nonhomogeneous models, in which the likelihood of an event varied with location. Criteria used to define source zones included the distribution of observed basaltic volcanic

centers, geochemical affinities, and structural and tectonic attributes. Nonhomogeneous interpretations included representation by a bivariate Gaussian distribution and by kernel density estimation techniques that use various smoothing operators in combination with observed data.

Results of the probabilistic volcanic hazard analysis, recalculated for the Enhanced Design Alternative II repository footprint (primary plus contingency blocks), indicate that the mean annual frequency of intersection of the potential repository footprint by an igneous dike is 1.6×10^{-8} . For this case, 5th and 95th percentile values are 7.6×10^{-10} and 5.0×10^{-8} , respectively. Disaggregation of these results yields the distribution of dike orientation and length within the footprint of the emplacement area, which can be used to determine the number of waste packages that might be disrupted by an igneous dike.

To determine the annual frequency of a future volcanic eruption through the potential repository, it is necessary to evaluate the frequency of an eruptive vent forming through the repository, given that an igneous dike intersects the repository. The interpretations of the experts were examined to see how many eruptive vents they attributed to past events and the average spacing between eruptive vents. Alternative representations, based on different assumptions concerning the distribution of eruptive vents along a dike and the independence of vents, are included to determine the frequency of eruptive vents through the repository. Based on this analysis, the mean annual frequency of an eruptive vent forming through the combined primary and contingency emplacement areas is 7.7×10^{-9} . The 5th and 95th percentile values are 3.3×10^{-10} and 2.5×10^{-8} , respectively. These results are used to evaluate the effect on long-term performance of a volcanic eruption through the repository.

An understanding of the characteristics of potential future eruptive processes at Yucca Mountain is required to determine the effects of eruptive vents that may disrupt the potential repository and affect long-term performance. For some parameters, site-specific data are available and used to assess the range of values. In cases for which site-specific data are unavailable, eruptive processes are characterized by examining evidence from other locations. Based on such analyses, ranges of values are defined for parameters such as eruptive conduit width, physical and chemical properties of magma, bubble nucleation, fragmentation, duration, mass output, and bulk grain size.

The range of diameters for volcanic conduit width is defined on the basis of evidence from Kamchatka (Tobalchik) and New Mexico (Grants Ridge). A median width of 50 m (164 ft) is assessed, with an upper limit of 150 m (492 ft) and a lower limit of 15 m (49 ft). For dike width, based on data from the Yucca Mountain region, the mean is determined to be 1.5 m (4.9 ft). The number of dikes associated with an igneous event is determined to range from 1 to 10 with a mean value of 3.

Chemistry of future magmas is interpreted to follow that for the Lathrop Wells basalts. These deposits are the most recent and represent a composition associated with the more violent basaltic explosive eruptions in the Yucca Mountain region. Water content for future basalts in the Yucca Mountain region is based on inferences from basalts with similar composition. The assessed water content ranges from 0 to 4 percent. Mole percent concentrations of volcanic gases for Yucca Mountain region basalts are interpreted to follow concentrations measured for basalts world-wide.

Physical properties of future basalts in the Yucca Mountain region are determined from estimates of water content and the composition of Lathrop Wells basalt. For a range of water content and calculated saturation pressure values, magma temperature ranges from about 1,050° to 1,170°C (1,922° to 2,138°F), magma viscosity ranges from about 2.0 to 2.7 log poise, and magma density ranges from 2,474 to 2,663 kg/m³ (154 to 166 lb/ft³).

Eruptive styles documented for volcanoes in Crater Flat and at Lathrop Wells indicate that a range of styles characterize basaltic eruptions in the Yucca Mountain region. Styles include violent strombolian, strombolian, and effusive eruptions of aa lava flows. Key aspects of the eruptive process are the depth at which the magma fragments, its ascent velocity, and the duration of an eruption. For a model of magma ascent using an initial volatile content ranging from 0 to 4 percent, the depth at which the magma starts to fragment ranges from 200 to 900 m (656 to 2953 ft). The duration of an eruption lasts from 1 day to 15 yr., with a mean of 30 days, a duration that pertains to the formation of the entire volcano.

Studies of the amount of lithic fragments incorporated from the walls of volcanic conduits into erupted material provide some guidance on how radioactive waste from degraded waste packages might be entrained in ascending magma. The volume fraction of wall rock debris in erupted material varies with the style of eruption. For hydrovolcanic eruptions, the volume fraction of wall rock debris ranges from 0.32 to 0.91. For strombolian, Hawaiian, and effusive eruptive styles, the volume fraction of wall rock debris is much lower, generally ranging from 10⁻³ to 10⁻⁵.

To determine the consequences of a volcanic eruption through the potential repository, it is necessary to understand the characteristics of ash plumes and ash fallout sheets. Violent strombolian eruptions produce plumes that carry ash up into the atmosphere where it can be distributed by winds as it settles back to the ground. Its settling velocity in air depends on its bulk density, shape, and size. Based on the available data, particle size for future violent strombolian eruptions in the Yucca Mountain region are determined to range from 0.01 to 1 mm (0.0004 to 0.04 in.), with a mode value of 0.1 mm (0.004 in.). The density of particles varies with size.

Seismicity and Seismic Hazard—Studies to evaluate seismic hazards at Yucca Mountain focused on characterizing the contemporary seismic environment, the history of faults active during the Quaternary period, and the generation of ground motion from local and regional earthquakes. These studies formed the foundation for a probabilistic seismic hazard analysis (PSHA).

Contemporary seismic activity is documented through historical accounts of past earthquakes and through monitoring by seismometers. The number of seismometers monitoring earthquakes in the Yucca Mountain vicinity has varied with time and, thus, the size of earthquakes that could be detected has also varied. While present day monitoring can detect some events with magnitudes less than 1, monitoring for much of the 1900s could detect only earthquakes with magnitudes greater than 5.5 in the southern Great Basin.

Five earthquakes with magnitudes greater than 5.5 that are not located in regions of underground nuclear explosions are documented in the historical catalog as occurring within 100 km (62 mi.)

of Yucca Mountain. Except for the Little Skull Mountain earthquake, which occurred about 15 km (9 mi.) from Yucca Mountain, the larger documented events are located near the Death Valley-Furnace Creek fault system, more than 50 km (31 mi.) from Yucca Mountain.

Contemporary seismicity at Yucca Mountain is occurring at a low rate. Only a few microearthquakes have been detected in the immediate vicinity of the site. The Rock Valley fault zone to the southeast has had more seismicity spatially associated with it. The 1992 Little Skull Mountain earthquake occurred near the end of this zone, although it did not result from movement along the Rock Valley fault. Some of the smaller earthquakes associated with the Rock Valley fault zone exhibit focal mechanisms consistent with movement along the fault.

Contemporary earthquakes in the southern Great Basin occur predominantly at depths between 5 and 15 km (3 and 9 mi.). Modeling of seismograms for some larger events in the Basin and Range Province indicate that these earthquakes nucleate at depths between 10 and 20 km (6 and 12 mi.).

Focal mechanisms for earthquakes in the southern Great Basin indicate that right-lateral slip on northerly-trending faults is today the predominant mode of stress release near Yucca Mountain. Left-lateral faulting on east-northeast-striking faults and normal faulting on northeast-striking faults have also been observed, as well as oblique slip on structures of intermediate orientation with the appropriate dip angles. The principal extensional (minimum compression) stress axes inferred from earthquake focal mechanisms trend northwest and plunge approximately horizontal. The principal compressional (maximum compression) stress axes range from vertical (normal faulting) to northeast and horizontal (strike-slip faulting).

While Yucca Mountain shows quiescence with respect to contemporary seismicity, evidence from nearby faults indicates that some have experienced earthquakes in the Quaternary period. Faults with possible Quaternary movement have been investigated via trenching and mapping to document evidence of past events. Based on these studies, estimated slip rates for Quaternary faults near Yucca Mountain range from 0.001 to 0.07 mm/yr. These rates are generally low relative to rates observed elsewhere in the Basin and Range Province.

Preferred values for single-event displacements documented for Quaternary faults near Yucca Mountain vary from near 0 to 2.0 m (0 to 6.6 ft). Constraints on the timing of events are often insufficient to discriminate between independent earthquakes on single faults and distributed events on multiple faults. Given the close spacing of faults (0.5 to 2 km [0.3 to 1 mi.]), it would not be surprising if at least some past earthquakes involved rupture of more than one of the mapped surface faults.

Lengths determined from geologic mapping of faults near Yucca Mountain range from about 1 to 35 km (0.6 to about 22 mi.). These lengths represent the maximum fault rupture for future events if the faults rupture independently. Alternatively, only part of a fault may rupture in a single event, or multiple faults may rupture together, creating a longer combined length. Available data are generally insufficient to discriminate between these possibilities.

Average recurrence intervals for faults near Yucca Mountain range from about 5 to 270 k.y. Many values are uncertain because dated deposits bracket the features associated with the

earthquake rather than being from those features themselves. Recurrence interval estimates are also affected by whether each fault is considered to rupture independently or as part of an event in which multiple faults rupture at the same time.

In addition to information on the occurrence of current and past earthquakes in the Yucca Mountain vicinity, an analysis of seismic hazards for the site also must incorporate information on the ground motions that future earthquakes will generate. Ground motion characterization relies on both empirical and numerical studies. A key issue is how to apply to the Yucca Mountain site the ground motion relations determined primarily from data collected in California.

Site characterization studies have addressed a number of factors that affect ground motion. These factors include those that affect ground motion at its source, such as stress drop; along its travel path from the source to a site, such as damping (Q); and in the vicinity of the site, such as site attenuation (κ) and local rock and soil velocities.

Stress drops for earthquakes in extensional tectonic regimes, such as the southern Great Basin, average about 45 bars for normal faulting earthquakes and 55 bars for strike-slip earthquakes. This compares to stress drops for earthquakes in California that range from about 70 to 100 bars. The lower stress drops for earthquakes in an extensional regime result in lower, high-frequency ground motions relative to those observed in California.

Aftershocks from the Little Skull Mountain earthquake have been studied to determine site attenuation, as represented by the parameter κ . Measured values for different sites ranged from 0.005 to 0.03 s. These values are lower than those for typical soft rock, as observed in California. Thus, at higher frequencies, this factor contributes to higher ground motions at Yucca Mountain than in California for a given magnitude earthquake.

Ground motion is dependent on the velocity of the soil and rock underlying any particular site. Shallow velocities have been measured in six boreholes near Yucca Mountain using vertical seismic profiling. Measured velocities show borehole-to-borehole variability, which must be taken into account in developing seismic design inputs.

An empirical ground motion attenuation relation for extensional regimes was developed for potential use in the Yucca Mountain vicinity. Comparison of this relation to those developed for the western United States, primarily on the basis of data from California, shows that the relation for extensional regimes gives lower ground motions than those for the western United States.

Numerical methods were evaluated by using them to simulate ground motions for a suite of scenario earthquakes. Scenario earthquakes were defined to represent earthquakes that may have occurred on faults in the Yucca Mountain vicinity in the past. The different methods were first validated by simulating the ground motions for the Little Skull Mountain earthquake of 1992. Analysis of uncertainties for the different methods indicated that modeling uncertainty (our inability to know which model provides estimates closest to the true median) had the greatest contribution to total uncertainty.

Seismic hazard at Yucca Mountain was assessed probabilistically. Both ground motion and fault displacement hazards were evaluated. The PSHA employed an expert elicitation process

involving 25 experts to develop inputs on seismic sources, fault displacement, and ground motion. The interpretations were based on the results of site characterization activities and other available information. Uncertainties in interpretations were also documented and formed part of the input to the analyses. The analyses resulted in the annual frequencies with which various levels of ground motion and fault displacement would be exceeded at Yucca Mountain.

The experts defined two types of seismic sources. Fault sources were based on the known characteristics of Quaternary faults mapped at the surface in the vicinity of Yucca Mountain. Areal source zones were used to account for seismic activity that cannot be associated with specific faults. This type of source zone also was used, in some cases, to characterize faults whose distance from the site made the details of fault geometry unimportant. For all seismic sources, the experts provided interpretations of the rate of future earthquake occurrence and the maximum size of future events. Rates were based on fault slip rates, paleoearthquake recurrence intervals, and contemporary seismicity. Assessed fault length, rupture area, and past displacement were factors that contributed to the determination of maximum magnitude.

Ground motion experts developed interpretations of expected ground motion for a matrix of combinations involving magnitude, distance, fault type, location relative to the fault plane, and structural frequency. Their interpretations were based on empirical and numerical methods. For empirical methods, adjustments were made to account for differences between the site conditions at Yucca Mountain and those where the data were collected (primarily California). Ground motion values were developed for a hypothetical reference rock outcrop with properties of the rock found at a depth of 300 m below Yucca Mountain. Based on the experts' interpretations, attenuation relations were determined for the ground motion hazard analysis.

Ground motion hazard results were calculated for peak ground acceleration (taken as spectral acceleration at 100 Hz), peak ground velocity, and spectral acceleration at structural frequencies, ranging from 0.3 to 20 Hz. For horizontal acceleration with an annual frequency of exceedance of 10^{-4} , spectral acceleration ranges from 0.168 g (165 cm/sec²) at 0.3 Hz to 1.160 g (1138 cm/sec²) at 10 Hz to 0.534 g (524 cm/sec²) at peak ground acceleration. Deaggregation of the mean hazard indicates that ground motions at higher frequencies are dominated by earthquakes smaller than magnitude 6.5 at distances less than 15 km (9 mi.). Dominant events for lower frequencies include both large nearby events and magnitude 7 and larger events at distances greater than 50 km (31 mi.).

Fault displacement hazard was assessed for a suite of conditions spanning those existing in the site area. Nine sites were defined with conditions ranging from those on block-bounding Quaternary faults to those on unfractured rock. The experts addressed displacement hazard using two approaches. The displacement approach estimated displacement events from feature-specific or point-specific data. The earthquake approach related the frequency of displacement events to the frequency of earthquake occurrence on the source. Both principal faulting and distributed faulting were included in the analysis. Interpretations provided the rate of future surface faulting events, the distribution of displacements on primary and distributed faults, and the uncertainties in those evaluations.

Fault displacement hazard results indicate that, except for block-bounding faults, displacements with an annual frequency of exceedance of 10^{-5} are equal to or less than 0.1 cm (0.04 in.). For

block-bounding faults, such as the Bow Ridge and Solitario Canyon faults, displacements with an annual frequency of exceedance of 10^{-5} are 7.8 and 32 cm (3.0 and 12.6 in.), respectively.

To develop seismic design inputs for ground motion on the basis of the PSHA results, the rock and soil overlying the reference rock outcrop (used in the PSHA) must be taken into account. Seismic design inputs will be developed for a rock outcrop at the surface, a rock interface at the waste emplacement level, and the site of the Waste Handling Building located on soil. The methodology for developing the seismic design inputs generally consists of the following steps:

- Determine design earthquakes that represent the uniform hazard spectrum at 10^{-3} and 10^{-4} annual frequencies of exceedance.
- To account for the magnitude dependence of site response, determine deaggregation earthquakes that represent the mean, 5th, and 95th percentile magnitude contribution to the uniform hazard spectrum at a given frequency of exceedance and for structural frequency ranges of 1 to 2 Hz and 5 to 10 Hz.
- Perform site response analyses for each of the deaggregation earthquakes that incorporate randomization of the velocity profile for the overlying material, shear modulus reduction, and damping.
- For each deaggregation earthquake, develop a spectral amplification function from the site response analyses.
- Compute the weighted average of the spectral amplification function for the deaggregation earthquakes corresponding to each combination of frequency of exceedance (10^{-3} or 10^{-4}) and structural frequency range (1 to 2 Hz or 5 to 10 Hz).
- Multiply the weighted average spectral amplification function by the appropriate design earthquake reference rock outcrop spectrum and take the smooth envelope as the design spectrum.

If the velocity profile is uncertain, upper-bound and lower-bound base case profiles can also be used, weighted average spectral amplification functions determined for each, and the design spectrum determined by enveloping all the resulting spectra.

Seismic design inputs for fault displacement are based on hazard levels of 10^{-4} and 10^{-5} . Away from block-bounding faults, displacements with these annual frequencies of exceedance are 1 mm or less. Such small displacements do not need to be specifically addressed in the design. For the Bow Ridge and Solitario Canyon faults, any safety-related structures, systems, or components that need to accommodate displacements with a 10^{-5} annual probability of exceedance (Category 2) should use displacement values of 7.8 and 32 cm (3.0 and 12.6 in.), respectively, as design inputs.

INTENTIONALLY LEFT BLANK

12.5 REFERENCES

12.5.1 Documents Cited

Abrahamson, N.A. and Becker, A.M. 1996. "Estimation of Vibratory Ground Motion at Yucca Mountain." Chapter 10 of *Seismotectonic Framework and Characterization of Faulting at Yucca Mountain, Nevada*. Whitney, J.W., ed. Milestone 3GSH100M. Denver, Colorado: U.S. Geological Survey. TIC: 237980.

Abrahamson, N.A. and Silva, W.J. 1997. "Empirical Response Spectral Attenuation Relations for Shallow Crustal Earthquakes." *Seismological Research Letters*, 68, (1), 94-127. El Cerrito, California: Seismological Society of America. TIC: 240553.

Aki, K. 1979. "Characterization of Barriers on an Earthquake Fault." *Journal of Geophysical Research*, 84, (B11), 6140-6148. Washington, D.C.: American Geophysical Union. TIC: 234253.

Aki, K. 1984. "Asperities, Barriers, and Characteristic Earthquakes and Strong Motion Prediction." *Journal of Geophysical Research*, 89, (B7), 5867-5872. Washington, D.C.: American Geophysical Union. TIC: 234631.

Allen, C.R. 1986. "Seismological and Paleoseismological Techniques of Research in Active Tectonics." Chapter 9 of *Active Tectonics*. Studies in Geophysics. Washington, D.C.: National Academy Press. TIC: 209251.

Anderson, J.G. and Humphrey, J.R., Jr. 1991. "A Least Squares Method for Objective Determination of Earthquake Source Parameters." *Seismological Research Letters*, 62, (3-4), 201-209. El Cerrito, California: Seismological Society of America. TIC: 243235.

Anderson, J.G.; Wesnousky, S.G.; and Stirling, M.W. 1996. "Earthquake Size as a Function of Fault Slip Rate." *Bulletin of the Seismological Society of America*, 86, (3), 683-690. El Cerrito, California: Seismological Society of America. TIC: 240928.

Anderson, L.W. and Klinger, R.E. 1996. "Quaternary Faulting on the Bare Mountain Fault." Chapter 4.12 of *Seismotectonic Framework and Characterization of Faulting at Yucca Mountain, Nevada*. Whitney, J.W., ed. Milestone 3GSH100M. Denver, Colorado: U.S. Geological Survey. TIC: 237980.

Anderson, L.W.; Klinger, R.E.; and Anderson, D.S. 1997. "Quaternary Slip History of the Bare Mountain Fault (Nevada) from the Morphology and Distribution of Alluvial Fan Deposits: Comment and Reply." *Geology*, 25, 189. Boulder, Colorado: Geological Society of America. TIC: 234312.

Anderson, L.W. and O'Connell, D.R. 1993. *Seismotectonic Study of the Northern Portion of the Lower Colorado River, Arizona, California and Nevada*. USBR SR 93-4. Denver, Colorado: U.S. Department of the Interior, Bureau of Reclamation. TIC: 237904.

Anderson, R.E.; Bucknam, R.C.; Crone, A.J.; Haller, K.M.; Machette, M.N.; Personius, S.F.; Barnhard, T.P.; Cecil, M.J.; and Dart, R.L. 1995. *Characterization of Quaternary and Suspected Quaternary Faults, Regional Studies, Nevada and California*. Open-File Report 95-599. Denver, Colorado: U.S. Geological Survey. ACC: MOL.19960924.0562.

Anderson, R.E.; Crone, A.J.; Machette, M.N.; Bradley, L-A.; and Diehl, S.F. 1995. *Characterization of Quaternary and Suspected Quaternary Faults, Amargosa Area, Nevada and California*. Open-File Report 95-613. Denver, Colorado: U.S. Geological Survey. TIC: 246589.

Armstrong, R.L. and Ward, P. 1991. "Evolving Geographic Patterns of Cenozoic Magmatism in the North American Cordillera: The Temporal and Spatial Association of Magmatism and Metamorphic Core Complexes." *Journal of Geophysical Research*, 96, (B8), 13,201-13,224. Washington, D.C.: American Geophysical Union. TIC: 224968.

Atkinson, G.M. 1995. "Attenuation and Source Parameters of Earthquakes in the Cascadia Region." *Bulletin of the Seismological Society of America*, 85, (5), 1327-1342. El Cerrito, California: Seismological Society of America. TIC: 247913.

Axen, G.J.; Taylor, W.J.; and Bartley, J.M. 1993. "Space-Time Patterns and Tectonic Controls of Tertiary Extension and Magmatism in the Great Basin of the Western United States." *Geological Society of America Bulletin*, 105, 56-76. Boulder, Colorado: Geological Society of America. TIC: 224970.

Bailey, R.A. and Koeppen, R.P. 1977. *Preliminary Geologic Map of Long Valley Caldera, Mono County, California*. Open-File Report 77-468. Denver, Colorado: U.S. Geological Survey. TIC: 242720.

Balch, A.H. and Erdemir, C. 1996. *A Nine-Component, Multiple-Offset Vertical Seismic Profile at the UE-25 UZ#16 Borehole, Nevada Test Site, Nye County, Nevada: Taking VSPs to a New Level*. Milestone 3GUP622M. Denver, Colorado: U.S. Geological Survey. ACC: MOL.19990831.0049.

Beanland, S. and Clark, M.M. 1994. *The Owens Valley Fault Zone, Eastern California, and Surface Faulting Associated with the 1872 Earthquake*. Bulletin 1982. Denver, Colorado: U.S. Geological Survey. TIC: 234443.

Beaty, C.B. and dePolo, C.M. 1989. "Energetic Earthquakes and Boulders on Alluvial Fans: Is There a Connection." *Bulletin of the Seismological Society of America*, 79, (1), 219-224. El Cerrito, California: Seismological Society of America. TIC: 234259.

Beck, P.J. 1970. *The Southern Nevada-Utah Border Earthquakes August to December, 1966*. Master's thesis. Salt Lake City, Utah: University of Utah. TIC: 216837.

Bellier, O. and Zoback, M.L. 1995. "Recent State of Stress Change in the Walker Lane Zone, Western Basin and Range Province, United States." *Tectonics*, 14, (3), 564-593. Washington, D.C.: American Geophysical Union. TIC: 233037.

Best, M.G. and Christiansen, E.H. 1991. "Limited Extension During Peak Tertiary Volcanism, Great Basin of Nevada and Utah." *Journal of Geophysical Research*, 96, (B8), 13,509-13,528. Washington, D.C.: American Geophysical Union. TIC: 224978.

Biasi, G.P. 1996. *Teleseismic Tomographic Imaging of the Yucca Mountain Region*. Draft. Reno, Nevada: University of Nevada, Reno, Seismological Laboratory. TIC: 242401.

Birkeland, P.W. 1984. *Soils and Geomorphology*. New York, New York: Oxford University Press. TIC: 236909.

Blakely, R.J.; Langenheim, V.E.; Ponce, D.A.; and Dixon, G.L. 2000. *Aeromagnetic Survey of the Amargosa Desert, Nevada and California: A Tool for Understanding Near-Surface Geology and Hydrology*. Open-File Report 00-188. [Denver, Colorado]: U.S. Geological Survey. TIC: 248767.

Bodin, P. and Gomberg, J. 1994. "Triggered Seismicity and Deformation Between the Landers, California, and Little Skull Mountain, Nevada, Earthquakes." *Bulletin of the Seismological Society of America*, 84, (3), 835-843. El Cerrito, California: Seismological Society of America. TIC: 234274.

Bolt, B.A. and Miller, R.D. 1975. *Catalogue of Earthquakes in Northern California and Adjoining Areas 1 January 1910 - 31 December 1972*. Berkeley, California: University of California, Berkeley. TIC: 245759.

Boore, D.M.; Joyner, W.B.; and Fumal, T.E. 1994. *Estimation of Response Spectra and Peak Accelerations from Western North American Earthquakes: An Interim Report, Part 2*. Open-File Report 94-127. Menlo Park, California: U.S. Geological Survey. TIC: 246666.

Boore, D.M.; Joyner, W.B.; and Fumal, T.E. 1997. "Equations for Estimating Horizontal Response Spectra and Peak Acceleration from Western North American Earthquakes: A Summary of Recent Work." *Seismologic Research Letters*, 68, (1), 128-153. El Cerrito, California: Seismological Society of America. TIC: 240882.

Boucher, G.; Seeber, L.; Ward, P.; and Oliver, J. 1967. "Microaftershock Observations at the Epicenter of a Moderate-Sized Earthquake in Nevada." *Transactions of the American Geophysical Union*, 48, 205. Washington, D.C.: American Geophysical Union. TIC: 234477.

Bradshaw, T.K. and Smith, E.I. 1994. "Polygenetic Quaternary Volcanism at Crater Flat, Nevada." *Journal of Volcanology and Geothermal Research*, 63, 165-182. Amsterdam, The Netherlands: Elsevier Science Publishing Company. TIC: 224980.

Brocher, T.M.; Hunter, W.C.; and Langenheim, V.E. 1998. "Implications of Seismic Reflection and Potential Field Geophysical Data on the Structural Framework of the Yucca Mountain-Crater Flat Region, Nevada." *Geological Society of America Bulletin*, 110, (8), 947-971. Boulder, Colorado: Geological Society of America. TIC: 238643.

Brocoum, S.J. 1995. "Topical Report 'Methodology to Assess Fault Displacement and Vibratory Ground Motion Hazards at Yucca Mountain'." Letter from S.J. Brocoum (DOE/YMSCO) to M.J. Bell (NRC), March 16, 1995, with enclosure. ACC: MOL.19951031.0160.

Brune, J.N.; Nicks, W.; and Aburto, A. 1992. "Microearthquakes at Yucca Mountain, Nevada." *Bulletin of the Seismological Society of America*, 82, (1), 164-174. El Cerrito, California: Seismological Society of America. TIC: 212563.

Brune, J.N. and Smith, K.D. 1996. "Precarious Rocks and Seismic Shaking During and Before the 1992 M 5.6 Little Skull Mountain Earthquake." *Abstracts with Programs - Geological Society of America*, 28, (7), A-193. Boulder, Colorado: Geological Society of America. TIC: 234316.

Budnitz, R.J.; Apostolakis, G.; Boore, D.M.; Cluff, L.S.; Coppersmith, K.J.; Cornell, C.A.; and Morris, P.A. 1997. *Recommendations for Probabilistic Seismic Hazard Analysis: Guidance on the Uncertainty and Use of Experts*. NUREG/CR-6372. Two volumes. Washington, D.C.: U.S. Nuclear Regulatory Commission. TIC: 235076; 235074.

Bufe, C.G. 1992. "Recent Earthquakes and Historical California-Nevada Seismicity: The Big Picture." *Eos, Transactions (Supplement)*, 73, (43), 373. Washington, D.C.: American Geophysical Union. TIC: 210058.

Bufe, C.G. and Topozada, T.R. 1981. "California Earthquakes - End to Seismic Quiescence." *California Geology*, [34], ([6]), 111-116. [Sacramento, California]: California Division of Mines and Geology. TIC: 234309.

Buwalda, J.P. and Richter, C.F. 1948. "Movement on the Manix (California) Fault on April 10, 1947." *Abstracts of Papers Presented at Meeting in Pasadena, April 9-10, 1948, Cordilleran Section of the Geological Society of America*. [59], 1367. [New York, New York: Geological Society of America]. TIC: 234341.

Callaghan, E. and Gianella, V.P. 1935. "The Earthquake of January 30, 1934, at Excelsior Mountains, Nevada." *Bulletin of the Seismological Society of America*, 25, 161-168. El Cerrito, California: Seismological Society of America. TIC: 234305.

Campbell, K.W. 1981. "Near-Source Attenuation of Peak Horizontal Acceleration." *Bulletin of the Seismological Society of America*, 71, (6), 2039-2070. El Cerrito, California: Seismological Society of America. TIC: 221670.

Campbell, K.W. 1989. *Empirical Prediction of Near-Source Ground Motion for the Diablo Canyon Power Plant Site, San Luis Obispo County, California*. Open-File Report 89-484. Denver, Colorado: U.S. Geological Survey. TIC: 246582.

Campbell, K.W. 1990. *Empirical Prediction of Near-Source Soil and Soft-Rock Ground Motion for the Diablo Canyon Power Plant Site, San Luis Obispo County, California*. Evergreen, Colorado: Dames & Moore. TIC: 245324.

Campbell, K.W. 1993. "Empirical Prediction of Near-Source Ground Motion from Large Earthquakes." *Earthquake Hazard and Large Dams in the Himalaya*. Gaur, V.K., ed. Pages 93-103. New Delhi, India: Indian National Trust for Art and Cultural Heritage. TIC: 234475.

Campbell, K.W. 1997. "Empirical Near-Source Attenuation Relationships for Horizontal and Vertical Components of Peak Ground Acceleration, Peak Ground Velocity, and Pseudo-Absolute Acceleration Response Spectra." *Seismological Research Letters*, 68, (1), 154-179. El Cerrito, California: Seismological Society of America. TIC: 241762.

Campbell, K.W. and Bozorgnia, Y. 1994. "Near-Source Attenuation of Peak Horizontal Acceleration from Worldwide Accelerograms Recorded from 1957 to 1993." *Earthquake Awareness and Mitigation Across the Nation, Proceedings of the Fifth U.S. National Conference on Earthquake Engineering, July 10-14, 1994, Chicago, Illinois. III*, 238-292. Oakland, California: Earthquake Engineering Research Institute. TIC: 239121.

Carr, W.J. 1974. *Summary of Tectonic and Structural Evidence for Stress Orientation at the Nevada Test Site*. Open-File Report 74-176. Denver, Colorado: U.S. Geological Survey. ACC: HQS.19880517.1621.

Caskey, S.J.; Wesnousky, S.G.; Zhang, P.; and Slemmons, D.B. 1996. "Surface Faulting of the 1954 Fairview Peak ($M_s=7.2$) and Dixie Valley ($M_s=6.8$) Earthquakes, Central Nevada." *Bulletin of the Seismological Society of America*, 86, (3), 761-787. El Cerrito, California: Seismological Society of America. TIC: 234277.

Chavez, D.E. and Priestley, K.F. 1985. "ML Observations in the Great Basin and Mo Versus ML Relationships for the 1980 Mammoth Lakes, California Earthquake Sequence." *Bulletin of the Seismological Society of America*, 75, (6), 1583-1598. El Cerrito, California: Seismological Society of America. TIC: 234275.

Christiansen, R.L. and Lipman, P.W. 1972. "Cenozoic Volcanism and Plate Tectonic Evolution of the Western United States. II. Late Cenozoic." *Philosophical Transactions of the Royal Society of London, Series A, Mathematical and Physical Sciences*, 271, 249-284. London, England: Royal Society of London. TIC: 217617.

Christiansen, R.L. and McKee, E.H. 1978. "Late Cenozoic Volcanic and Tectonic Evolution of the Great Basin and Columbia Intermontane Regions." *Cenozoic Tectonics and Regional Geophysics of the Western Cordillera*. Memoir 152. Pages 283-311. Boulder, Colorado: Geological Society of America. TIC: 222151.

Clark, M.M.; Yount, J.C.; Vaughn, P.R.; and Zepeda, R.I. 1982. *Map Showing Surface Ruptures Associated with the Mammoth Lakes, California, Earthquake of May 1980*. Miscellaneous Field Studies Map MF-1396. Reston, Virginia: U.S. Geological Survey. TIC: 246594.

Cockerham, R.S. and Pitt, A.M. 1984. "Seismic Activity in the Long Valley Caldera, Eastern California, U.S.A.: June 1982 through July 1984." *Proceedings of Workshop XIX, Active Tectonic and Magmatic Processes Beneath Long Valley Caldera, Eastern California*. Hill, D.P.; Bailey, R.A.; and Ryall, A.S., eds. Open-File Report 84-939. Volume I. Pages 493-526. Menlo Park, California: U.S. Geological Survey. TIC: 234673.

Coe, J.A. 1996. "Preliminary Paleoearthquake Event Summary for the Northern Crater Flat Fault." Chapter 4.11 of *Seismotectonic Framework and Characterization of Faulting at Yucca Mountain, Nevada*. Whitney, J.W., ed. Milestone 3GSH100M. Denver, Colorado: U.S. Geological Survey. TIC: 237980.

Coe, J.A.; Oswald, J.; Vadurro, G.; and Lundstrom, S.C. 1996. "Quaternary Faulting on the Fatigue Wash Fault." Chapter 4.8 of *Seismotectonic Framework and Characterization of Faulting at Yucca Mountain, Nevada*. Whitney, J.W., ed. Milestone 3GSH100M. Denver, Colorado: U.S. Geological Survey. TIC: 237980.

Coe, J.A.; Oswald, J.A.; Vadurro, G.; Paces, J.B.; Ludwig, K.R.; Widmann, B.; Menges, C.M.; Lundstrom, S.C.; and de Fontaine, C.S. 1995. "Paleoseismic Investigations of the Fatigue Wash Fault, Crater Flat, Nye County, Nevada." *Transactions of the American Geophysical Union, 1995 Fall Meeting Supplement*. 318, F362. Washington, D.C.: American Geophysical Union. TIC: 234855.

Coe, J.A.; Taylor, E.M.; and Schilling, S.P. 1991. "Close-Range Geophotogrammetric Mapping of Trench Walls Using Multi-Model Stereo Restitution Software." *1991 ACSM-ASPRS Annual Convention, Baltimore, Maryland*. 5, 30-43. Bethesda, Maryland: American Society for Photogrammetry and Remote Sensing. TIC: 237576.

Coe, J.A.; Yount, J.C.; and O'Leary, D.W. 1996. "Preliminary Results of Paleoseismic Investigations of the Rock Valley Fault System." Chapter 4.13 of *Seismotectonic Framework and Characterization of Faulting at Yucca Mountain, Nevada*. Whitney, J.W., ed. Milestone 3GSH100M. Denver, Colorado: U.S. Geological Survey. TIC: 237980.

Coney, P.J. 1987. "The Regional Tectonic Setting and Possible Causes of Cenozoic Extension in the North American Cordillera." *Continental Extensional Tectonics*. Special Publication No. 28. Coward, M.P.; Dewey, J.F.; and Hancock, P.L., eds. Pages 177-186. [Oxford, England: Geological Society]. TIC: 224989.

Coney, P.J. and Reynolds, S.J. 1977. "Cordilleran Benioff Zones." *Nature*, 270, 403-406. London, England: Macmillan Journals. TIC: 224988.

Connor, C.B. and Hill, B.E. 1995. "Three Nonhomogeneous Poisson Models for the Probability of Basaltic Volcanism: Application to the Yucca Mountain Region, Nevada." *Journal of Geophysical Research*, 100, (B6), 10,107-10,125. Washington, D.C.: American Geophysical Union. TIC: 237682.

Connor, C.B.; Lane-Magsino, S.; Stamatakos, J.A.; Martin, R.H.; LaFemina, P.C.; Hill, B.E.; and Lieber, S. 1997. "Magnetic Surveys Help Reassess Volcanic Hazards at Yucca Mountain, Nevada." *Eos*, 78, (7), 73, 77 and 78. Washington, D.C.: American Geophysical Union. TIC: 234580.

Connor, C.B.; Stamatakos, J.A.; Ferrill, D.A.; Hill, B.E.; Ofoegbu, G.I.; Conway, F.M.; Sugar, B.; and Trapp, J. 2000. "Geologic Factors Controlling Patterns of Small-Volume Basaltic Volcanism: Application to a Volcanic Hazards Assessment at Yucca Mountain, Nevada."

Journal of Geophysical Research, 105, (B1), 417-432. Washington, D.C.: American Geophysical Union. TIC: 247906.

Coppersmith, K.J. 1991. "Seismic Source Characterization for Engineering Seismic Hazard Analysis." *Proceedings of the Fourth International Conference on Seismic Zonation, August 25th - 29th, 1991, Stanford University, Stanford, California*. 1, 3-60. Oakland, California: Earthquake Engineering Research Institute. TIC: 238247.

Cornell, C.A. 1968. "Engineering Seismic Risk Analysis." *Bulletin of the Seismological Society of America*, 58, (5), 1583-1606. El Cerrito, California: Seismological Society of America. TIC: 237493.

Cornell, C.A. 1971. "Probabilistic Analysis of Damage to Structures Under Seismic Loads." Chapter 27 of *Dynamic Waves in Civil Engineering*. Howells, D.A.; Haigh, I.P.; and Taylor, C., eds. New York, New York: Wiley-Interscience. TIC: 241003.

Cornwall, H.R. 1972. *Geology and Mineral Deposits of Southern Nye County, Nevada*. Bulletin 77. Reno, Nevada: Nevada Bureau of Mines and Geology. TIC: 207079.

Cross, T.A. and Pilger, R.H., Jr. 1978. "Constraints on Absolute Motion and Plate Interaction Inferred from Cenozoic Igneous Activity in the Western United States." *American Journal of Science*, 278, (7), 865-902. New Haven, Connecticut: Yale University, Kline Geology Laboratory. TIC: 217778.

Crowe, B.; Perry, F.; Geissman, J.; McFadden, L.; Wells, S.; Murrell, M.; Poths, J.; Valentine, G.A.; Bowker, L.; and Finnegan, K. 1995. *Status of Volcanism Studies for the Yucca Mountain Site Characterization Project*. LA-12908-MS. Los Alamos, New Mexico: Los Alamos National Laboratory. ACC: HQO.19951115.0017.

Crowe, B.; Self, S.; Vaniman, D.; Amos, R.; and Perry, F. 1983. "Aspects of Potential Magmatic Disruption of a High-Level Radioactive Waste Repository in Southern Nevada." *Journal of Geology*, 91, (3), 259-276. Chicago, Illinois: University of Chicago Press. TIC: 216959.

Crowe, B.M.; Johnson, M.E.; and Beckman, R.J. 1982. "Calculation of the Probability of Volcanic Disruption of a High-Level Radioactive Waste Repository Within Southern Nevada, USA." *Radioactive Waste Management and the Nuclear Fuel Cycle*, 3, (2), 167-190. New York, New York: Hardwood Academic Publishers. TIC: 222179.

Crowe, B.M. and Perry, F.V. 1990. "Volcanic Probability Calculations for the Yucca Mountain Site: Estimation of Volcanic Rates." *Proceedings of the Topical Meeting on Nuclear Waste Isolation in the Unsaturated Zone, FOCUS '89, September 17-21, 1989, Las Vegas, Nevada*. Pages 326-334. La Grange Park, Illinois: American Nuclear Society. TIC: 212738.

Crowe, B.M.; Perry, F.V.; Valentine, G.A.; Wallmann, P.C.; and Kossik, R. 1993. "Simulation Modeling of the Probability of Magmatic Disruption of the Potential Yucca Mountain Site." *Proceedings of the Topical Meeting on Site Characterization and Model Validation, FOCUS '93*,

September 26-29, 1993, Las Vegas, Nevada. Pages 182-191. La Grange Park, Illinois: American Nuclear Society. TIC: 102245.

Crowe, B.M.; Vaniman, D.T.; and Carr, W.J. 1983. *Status of Volcanic Hazard Studies for the Nevada Nuclear Waste Storage Investigations*. LA-9325-MS. Los Alamos, New Mexico: Los Alamos National Laboratory. ACC: HQS.19880517.1145.

CRWMS M&O 1996. *Probabilistic Volcanic Hazard Analysis for Yucca Mountain, Nevada*. BA0000000-01717-2200-00082 REV 0. Las Vegas, Nevada: CRWMS M&O. ACC: MOL.19971201.0221.

CRWMS M&O 1998a. Not used in text.

CRWMS M&O 1998b. "Disruptive Events." Chapter 10 of *Total System Performance Assessment-Viability Assessment (TSPA-VA) Analyses Technical Basis Document*. B00000000-01717-4301-00010 REV 00. Las Vegas, Nevada: CRWMS M&O. ACC: MOL.19980724.0399.

CRWMS M&O 1998c. "Tectonic Setting of the Yucca Mountain Region: Relationship to Episodes of Cenozoic Basaltic Volcanism." Chapter 3 of *Synthesis of Volcanism Studies for the Yucca Mountain Site Characterization Project*. Deliverable 3781MR1. Las Vegas, Nevada: CRWMS M&O. ACC: MOL.19990511.0400.

CRWMS M&O 1998d. "Probabilistic Modeling of Volcanism Data: Final Volcanic Hazard Studies for the Yucca Mountain Site." Chapter 6 of *Synthesis of Volcanism Studies for the Yucca Mountain Site Characterization Project*. Deliverable 3781MR1. Las Vegas, Nevada: CRWMS M&O. ACC: MOL.19990511.0400.

CRWMS M&O 1998e. "Geology and Geochronology of Basaltic Volcanism in the Yucca Mountain Region." Chapter 2 of *Synthesis of Volcanism Studies for the Yucca Mountain Site Characterization Project*. Deliverable 3781MR1. Las Vegas, Nevada: CRWMS M&O. ACC: MOL.19990511.0400.

CRWMS M&O 1998f. "Petrologic and Geochemical Constraints on Basaltic Volcanism in the Great Basin." Chapter 4 of *Synthesis of Volcanism Studies for the Yucca Mountain Site Characterization Project*. Deliverable 3781MR1. Las Vegas, Nevada: CRWMS M&O. ACC: MOL.19990511.0400.

CRWMS M&O 1998g. "Physical Processes of Magmatism and Effects on the Potential Repository: Synthesis of Technical Work through Fiscal Year 1995." Chapter 5 of *Synthesis of Volcanism Studies for the Yucca Mountain Site Characterization Project*. Deliverable 3781MR1. Las Vegas, Nevada: CRWMS M&O. ACC: MOL.19990511.0400.

CRWMS M&O 1998h. *Synthesis of Volcanism Studies for the Yucca Mountain Site Characterization Project*. Deliverable 3781MR1. Las Vegas, Nevada: CRWMS M&O. ACC: MOL.19990511.0400.

CRWMS M&O 1998i. *Seismic Design Basis Inputs for a High-Level Waste Repository at Yucca Mountain, Nevada*. B00000000-01727-5700-00018 REV 0. Las Vegas, Nevada: CRWMS M&O. ACC: MOL.19980806.0711.

CRWMS M&O 1999. *License Application Design Selection Report*. B00000000-01717-4600-00123 REV 01 ICN 01. Las Vegas, Nevada: CRWMS M&O. ACC: MOL.19990908.0319.

CRWMS M&O 2000a. *Characterize Framework for Igneous Activity at Yucca Mountain, Nevada (T0015)*. ANL-MGR-GS-000001 REV 00. Las Vegas, Nevada: CRWMS M&O. ACC: MOL.20000720.0541.

CRWMS M&O 2000b. *Characterize Eruptive Processes at Yucca Mountain, Nevada*. ANL-MGR-GS-000002 REV 00. Las Vegas, Nevada: CRWMS M&O. ACC: MOL.20000517.0259.

CRWMS M&O 2000c. *Yucca Mountain Historical Earthquake Catalog from 1868 to 1998*. Las Vegas, Nevada: CRWMS M&O. ACC: MOL.20000623.0302.

CRWMS M&O 2000d. *Disruptive Events Process Model Report*. TDR-NBS-MD-000002 REV 00 ICN 01. Las Vegas, Nevada: CRWMS M&O. ACC: MOL.20000727.0085.

CRWMS M&O 2000e. *Characterize Framework for Seismicity and Structural Deformation at Yucca Mountain, Nevada*. ANL-CRW-GS-000003 REV 00. Las Vegas, Nevada: CRWMS M&O. ACC: MOL.20000510.0175.

CRWMS M&O 2000f. *Dike Propagation Near Drifts*. ANL-WIS-MD-000015 REV 00. Las Vegas, Nevada: CRWMS M&O. ACC: MOL.20000523.0157.

CRWMS M&O 2000g. *Number of Waste Packages Hit by Igneous Intrusion*. CAL-WIS-PA-000001 REV 00. Las Vegas, Nevada: CRWMS M&O. ACC: MOL.20000602.0054.

CRWMS M&O 2000h. *Igneous Consequence Modeling for TSPA-SR*. ANL-WIS-MD-000017 REV 00. Las Vegas, Nevada: CRWMS M&O. ACC: MOL.20000501.0225.

CRWMS M&O 2000i. Not used in text.

CRWMS M&O 2000j. *Saturated Zone Flow and Transport Process Model Report*. TDR-NBS-HS-000001 REV 00 ICN 01. Las Vegas, Nevada: CRWMS M&O. ACC: MOL.20000821.0359.

CRWMS M&O 2000k. *Engineered Barrier System Degradation, Flow, and Transport Process Model Report*. TDR-EBS-MD-000006 REV 00 ICN 01. Las Vegas, Nevada: CRWMS M&O. ACC: MOL.20000724.0479.

CRWMS M&O 2000l. *Waste Package Degradation Process Model Report*. TDR-WIS-MD-000002 REV 00 ICN 01. Las Vegas, Nevada: CRWMS M&O. ACC: MOL.20000717.0005.

Day, W.C.; Dickerson, R.P.; Potter, C.J.; Sweetkind, D.S.; San Juan, C.A.; Drake, R.M., II; and Fridrich, C.J. 1998. *Bedrock Geologic Map of the Yucca Mountain Area, Nye County, Nevada*. Geologic Investigations Series Map I-2627. Denver, Colorado: U.S. Geological Survey. ACC: MOL.19981014.0301.

Day, W.C.; Potter, C.J.; Sweetkind, D.S.; Dickerson, R.P.; and Keefer, W.R. 1996. "Structural Geology of the Central Block of Yucca Mountain." Chapter 2-I of *Seismotectonic Framework and Characterization of Faulting at Yucca Mountain, Nevada*. Whitney, J.W., ed. Milestone 3GSH100M. Denver, Colorado: U.S. Geological Survey. TIC: 237980.

Delaney, P.T. and Gartner, A.E. 1997. "Physical Processes of Shallow Mafic Dike Emplacement Near the San Rafael Swell, Utah." *Geological Society of America Bulletin*, 109, (9), 1177-1192. Boulder, Colorado: Geological Society of America. TIC: 247421.

dePolo, C.M. 1994a. "Estimating Fault Slip Rates in the Great Basin, USA." *Proceedings of the Workshop on Paleoseismology, 18-22 September, 1994, Marshall, California*. Prentice, C.S.; Schwartz, D.P.; and Yeats, R.S., eds. Open-File Report 94-568. Pages 48-49. Menlo Park, California: U.S. Geological Survey. TIC: 234812.

dePolo, C.M. 1994b. "The Maximum Background Earthquake for the Basin and Range Province, Western North America." *Bulletin of the Seismological Society of America*, 84, (2), 466-472. El Cerrito, California: Seismological Society of America. TIC: 234991.

dePolo, C.M.; Peppin, W.A.; and Johnson, P.A. 1993. "Contemporary Tectonics, Seismicity, and Potential Earthquake Sources in the White Mountains Seismic Gap, West-Central Nevada and East-Central California." *Tectonophysics*, 225, 271-299. Amsterdam, The Netherlands: Elsevier Science Publishers. TIC: 234521.

dePolo, C.M. and Ramelli, A.R. 1987. "Preliminary Report on Surface Fractures Along the White Mountains Fault Zone Associated with the July 1986 Chalfant Valley Earthquake Sequence." *Bulletin of the Seismological Society of America*, 77, (1), 290-296. El Cerrito, California: Seismological Society of America. TIC: 234524.

dePolo, C.M.; Ramelli, A.R.; and Bell, J.W. 1994. "The 1932 Cedar Mountain Earthquake, Central Nevada, U.S.A.: A Major Basin and Range Province Earthquake that had a Widely Distributed Surface Faulting Pattern." *Proceedings of the Workshop on Paleoseismology, 18-22 September, 1994, Marshall, California*. Prentice, C.S.; Schwartz, D.P.; and Yeats, R.S., eds. Open-File Report 94-568. Pages 50-52. Menlo Park, California: U.S. Geological Survey. TIC: 234666.

dePolo, C.M. and Slemmons, D.B. 1990. "Estimation of Earthquake Size for Seismic Hazards." *Neotectonics in Earthquake Evaluation*. Krinitzsky, E.L. and Slemmons, D.B., eds. Reviews in Engineering Geology, Volume VIII. Pages 1-28. Boulder, Colorado: Geological Society of America. TIC: 234796.

Dickerson, R.P. and Spengler, R.W. 1994. "Structural Character of the Northern Segment of the Paintbrush Canyon Fault, Yucca Mountain, Nevada." *High Level Radioactive Waste Management, Proceedings of the Fifth Annual International Conference, Las Vegas, Nevada*,

May 22-26, 1994. 4, 2367-2372. La Grange Park, Illinois: American Nuclear Society. TIC: 210984.

Dohrenwend, J.C.; Menges, C.M.; Schell, B.A.; and Moring, B.C. 1991. *Reconnaissance Photogeologic Map of Young Faults in the Las Vegas 1° by 2° Quadrangle, Nevada, California, and Arizona*. Miscellaneous Field Studies Map MF-2182. Denver, Colorado: U.S. Geological Survey. ACC: NNA.19940524.0079.

Dohrenwend, J.C.; Schell, B.A.; McKittrick, M.A.; and Moring, B.C. 1992. *Reconnaissance Photogeologic Map of Young Faults in the Goldfield 1° by 2° Quadrangle, Nevada and California*. Miscellaneous Field Studies Map MF-2183. Denver, Colorado: U.S. Geological Survey. ACC: NNA.19940524.0080.

Doser, D.I. 1986. "Earthquake Processes in the Rainbow Mountain-Fairview Peak-Dixie Valley, Nevada, Region 1954-1959." *Journal of Geophysical Research*, 91, (B12), 12,572-12,586. Washington, D.C.: American Geophysical Union. TIC: 223278.

Doser, D.I. 1988. "Source Parameters of Earthquakes in the Nevada Seismic Zone, 1915-1943." *Journal of Geophysical Research*, 93, (B12), 15,001-15,015. Washington, D.C.: American Geophysical Union. TIC: 238889.

Doser, D.I. and Smith, R.B. 1989. "An Assessment of Source Parameters of Earthquakes in the Cordillera of the Western United States." *Bulletin of the Seismological Society of America*, 79, (5), 1383-1409. El Cerrito, California: Seismological Society of America. TIC: 236846.

Doubik, P. and Hill, B.E. 1999. "Magmatic and Hydromagmatic Conduit Development During the 1975 Tolbachik Eruption, Kamchatka, with Implications for Hazards Assessment at Yucca Mountain, NV." *Journal of Volcanology and Geothermal Research*, 91, 43-64. Amsterdam, The Netherlands: Elsevier Science B.V. TIC: 246029.

Dreger, D.S. 1994. "Investigation of the Rupture Process of the 28 June Landers Earthquake Utilizing TERRAScope." *Bulletin of the Seismological Society of America*, 84, (3), 713-724. El Cerrito, California: Seismological Society of America. TIC: 234529.

Dueker, K. and Humphreys, E. 1990. "Upper-Mantle Velocity Structure of the Great Basin." *Geophysical Research Letters*, 17, (9), 1327-1330. Washington, D.C.: American Geophysical Union. TIC: 225012.

Earthfield Technology 1995. *Summary Report Magnetic and Gravity Study of the Yucca Mountain Area, Nevada*. Houston, Texas: Earthfield Technology. ACC: MOL.20000228.0374.

Eaton, G.P. 1982. "The Basin and Range Province: Origin and Tectonic Significance." *Annual Review of Earth and Planetary Science*, 10, 409-440. Palo Alto, California: Annual Reviews. TIC: 225015.

Ellsworth, W.L. 1990. "Earthquake History, 1769-1989." Chapter 6 of *The San Andreas Fault System, California*. Professional Paper 1515. Denver, Colorado: U.S. Geological Survey. TIC: 234474.

Engdahl, E.R. and Rinehart, W.A. 1988. *Seismicity Map of North America*. Continent-Scale Map-004. Boulder, Colorado: Geological Society of America. TIC: 240261.

EPRI (Electric Power Research Institute) 1993. *Appendices for Ground Motion Estimation*. Volume 2 of *Guidelines for Determining Design Basis Ground Motions*. EPRI TR-102293. Palo Alto, California: Electric Power Research Institute. TIC: 226496.

Evans, J.R. and Smith, M., III 1992. "Teleseismic Tomography of the Yucca Mountain Region: Volcanism and Tectonism." *High Level Radioactive Waste Management, Proceedings of the Third International Conference, Las Vegas, Nevada, April 12-16, 1992*. 2, 2371-2380. La Grange Park, Illinois: American Nuclear Society. TIC: 204231.

Evernden, J.F. 1975. "Seismic Intensities, 'Size' of Earthquakes and Related Parameters." *Bulletin of the Seismological Society of America*, 65, (5), 1287-1313. El Cerrito, California: Seismological Society of America. TIC: 240820.

Fairer, G.M.; Whitney, J.W.; and Coe, J.A. 1989. "A Close-Range Photogrammetric Technique for Mapping Neotectonic Features in Trenches." *Bulletin of the Association of Engineering Geologists*, 26, (4), 521-530. College Station, Texas: Association of Engineering Geologists. TIC: 225428.

Farmer, G.L.; Perry, F.V.; Semken, S.; Crowe, B.; Curtis, D.; and DePaolo, D.J. 1989. "Isotopic Evidence on the Structure and Origin of Subcontinental Lithospheric Mantle in Southern Nevada." *Journal of Geophysical Research*, 94, (B6), 7885-7898. Washington, D.C.: American Geophysical Union. TIC: 201800.

Faulds, J.E.; Bell, J.W.; Feuerbach, D.L.; and Ramelli, A.R. 1994. *Geologic Map of the Crater Flat Area, Nevada*. Geophysical Investigations Map 101. Reno, Nevada: University of Nevada, Reno. TIC: 211484.

Feighner, M.A. and Majer, E.L. 1996. *Results of the Analysis of the Timber Mt., Lathrop Wells, and Yucca Mt. Aeromagnetic Data*. Milestone SPT23KM4. Berkeley, California: Lawrence Berkeley National Laboratory. ACC: MOL.19971204.0767.

Fernald, A.T.; Corchary, G.S.; Williams, W.P.; and Colton, R.B. 1968. "Surficial Deposits of the Yucca Flat Area, Nevada Test Site." *Nevada Test Site*. Eckel, E.B., ed. Memoir 110. Boulder, Colorado: Geological Society of America. TIC: 221562.

Ferrill, D.A.; Stamatakos, J.A.; Jones, S.M.; Rahe, B.; McKague, H.L.; Martin, R.H.; and Morris, A.P. 1996. "Quaternary Slip History of the Bare Mountain Fault (Nevada) from the Morphology and Distribution of Alluvial Fan Deposits." *Geology*, 24, (6), 559-562. Boulder, Colorado: Geological Society of America. TIC: 234557.

Ferrill, D.A.; Stamatakos, J.A.; and McKague, H.L. 1997. "Quaternary Slip History of the Bare Mountain Fault (Nevada) from the Morphology and Distribution of Alluvial Fan Deposits: Reply." *Geology*, 25, 190. Boulder, Colorado: Geological Society of America. TIC: 234625.

Fischer, F.G.; Papanek, P.J.; and Hamilton, R.M. 1972. *The Massachusetts Mountain Earthquake of 5 August 1971 and Its Aftershocks, Nevada Test Site*. USGS-474-149. Menlo Park, California: U.S. Geological Survey. ACC: HQS.19880517.1208.

Fitton, J.G.; James, D.; and Leeman, W.P. 1991. "Basic Magmatism Associated with Late Cenozoic Extension in the Western United States: Compositional Variations in Space and Time." *Journal of Geophysical Research*, 96, (B8), 13,693-13,713. Washington, D.C.: American Geophysical Union. TIC: 222420.

Fleck, R.J.; Turrin, B.D.; Sawyer, D.A.; Warren, R.G.; Champion, D.E.; Hudson, M.R.; and Minor, S.A. 1996. "Age and Character of Basaltic Rocks of the Yucca Mountain Region, Southern Nevada." *Journal of Geophysical Research*, 101, (B4), 8205-8227. Washington, D.C.: American Geophysical Union. TIC: 234626.

Fox, K.F., Jr. and Carr, M.D. 1989. "Neotectonics and Volcanism at Yucca Mountain and Vicinity, Nevada." *Radioactive Waste Management and the Nuclear Fuel Cycle*, 13, 37-50. New York, New York: Harwood Academic Publishers. TIC: 222276.

Frankel, A. 1995. "Mapping Seismic Hazard in the Central and Eastern United States." *Seismological Research Letters*, 66, (4), 8-21. El Cerrito, California: Seismological Society of America. TIC: 243318.

Fridrich, C.J. 1999. "Tectonic Evolution of the Crater Flat Basin, Yucca Mountain Region, Nevada." *Cenozoic Basins of the Death Valley Region*. Wright, L.A. and Troxel, B.W., eds. Special Paper 333. Pages 169-195. Boulder, Colorado: Geological Society of America. TIC: 248054.

Fridrich, C.J.; Whitney, J.W.; Hudson, M.R.; and Crowe, B.M. 1999. "Space-Time Patterns of Late Cenozoic Extension, Vertical Axis Rotation, and Volcanism in the Crater Flat Basin, Southwest Nevada." *Cenozoic Basins of the Death Valley Region*. Wright, L.A. and Troxel, B.W., eds. Special Paper 333. Pages 197-212. Boulder, Colorado: Geological Society of America. TIC: 248054.

Fridrich, C.J.; Whitney, J.W.; Hudson, M.R.; Keefer, W.R.; and Crowe, B.M. 1996. "Space-Time Patterns of Extension, Vertical-Axis Rotation, and Volcanism in the Crater Flat Basin." Chapter 2.II of *Seismotectonic Framework and Characterization of Faulting at Yucca Mountain, Nevada*. Whitney, J.W., ed. Milestone 3GSH100M. Denver, Colorado: U.S. Geological Survey. TIC: 237980.

Gans, P.B. and Bohrsen, W.A. 1998. "Suppression of Volcanism During Rapid Extension in the Basin and Range Province, United States." *Science*, 279, (5347), 66-68. [Washington, D.C.: American Association for the Advancement of Science]. TIC: 247964.

- Gianella, V.P. and Callaghan, E. 1934. "The Cedar Mountain, Nevada, Earthquake of December 20, 1932." *Bulletin of the Seismological Society of America*, 24, (4), 345-377. El Cerrito, California: Seismological Society of America. TIC: 217009.
- Gomberg, J. 1991a. "Seismicity and Detection/Location Threshold in the Southern Great Basin Seismic Network." *Journal of Geophysical Research*, 96, (B10), 16,401-16,414. Washington, D.C.: American Geophysical Union. TIC: 212627.
- Gomberg, J. 1991b. "Seismicity and Shear Strain in the Southern Great Basin of Nevada and California." *Journal of Geophysical Research*, 96, 16,383-16,399. Washington, D.C.: American Geophysical Union. TIC: 225033.
- Gomberg, J. and Bodin, P. 1994. "Triggering of the Ms = 5.4 Little Skull Mountain, Nevada, Earthquake with Dynamic Strains." *Bulletin of the Seismological Society of America*, 84, (3), 844-853. El Cerrito, California: Seismological Society of America. TIC: 240825.
- Gross, S. and Juamé, S. 1995. *Historical Seismicity in the Southern Great Basin of Nevada and California*. Denver, Colorado: U.S. Geological Survey. ACC: MOL.19980219.0840.
- Gutenberg, B. and Richter, C.F. 1954. *Seismicity of the Earth and Associated Phenomena*. Princeton, New Jersey: Princeton University Press. TIC: 246330.
- Hamilton, R.M.; Smith, B.E.; Fisher, F.G.; and Papanek, P.J. 1971. *Seismicity of the Pahute Mesa Area, Nevada Test Site, 8 December 1968 through 31 December 1970*. USGS-474-138. Menlo Park, California: U.S. Geological Survey. TIC: 217018.
- Hanks, T.C. and Kanamori, H. 1979. "A Moment Magnitude Scale." *Journal of Geophysical Research*, 84, (B5), 2348-2350. Washington, D.C.: American Geophysical Union. TIC: 212607.
- Harmsen, S.C. 1991. *Seismicity and Focal Mechanisms for the Southern Great Basin of Nevada and California in 1990*. Open-File Report 91-367. Denver, Colorado: U.S. Geological Survey. ACC: NNA.19920213.0219.
- Harmsen, S.C. 1993. *Seismicity and Focal Mechanisms for the Southern Great Basin of Nevada and California in 1991*. Open-File Report 92-340. Denver, Colorado: U.S. Geological Survey. ACC: NNA.19920629.0129.
- Harmsen, S.C. 1994a. *Preliminary Seismicity and Focal Mechanisms for the Southern Great Basin of Nevada and California: January 1992 through September 1992*. Open-File Report 93-369. Denver, Colorado: U.S. Geological Survey. ACC: NNA.19931215.0008.
- Harmsen, S.C. 1994b. "The Little Skull Mountain, Nevada, Earthquake of 29 June 1992: Aftershock Focal Mechanisms and Tectonic Stress Field Implications." *Bulletin of the Seismological Society of America*, 84, (5), 1484-1505. El Cerrito, California: Seismological Society of America. TIC: 237937.

Harmsen, S.C. and Bufe, C.G. 1992. *Seismicity and Focal Mechanisms for the Southern Great Basin of Nevada and California: 1987 through 1989*. Open-File Report 91-572. Denver, Colorado: U.S. Geological Survey. ACC: NNA.19920408.0001.

Harmsen, S.C. and Rogers, A.M. 1986. "Inferences About the Local Stress Field from Focal Mechanisms: Applications to Earthquakes in the Southern Great Basin of Nevada." *Bulletin of the Seismological Society of America*, 76, (6), 1560-1572. El Cerrito, California: Seismological Society of America. TIC: 237978.

Harmsen, S.C. and Rogers, A.M. 1987. *Earthquake Location Data for the Southern Great Basin of Nevada and California: 1984 through 1986*. Open-File Report 87-596. Denver, Colorado: U.S. Geological Survey. ACC: MOL.19950601.0076.

Hatheway, A.W. and Leighton, F.B. 1979. "Trenching as an Exploratory Method." *Geological Society of America Reviews in Engineering Geology*, 4, 169-195. Boulder, Colorado: Geological Society of America. TIC: 234889.

Hauksson, E.; Hutton, K.; Kanamori, H.; Jones, L.; Mori, J.; Hough, S.; and Roquemore, G. 1995. "Preliminary Report on the 1995 Ridgecrest Earthquake Sequence in Eastern California." *Seismological Research Letters*, 66, (6), 54-60. El Cerrito, California: Seismological Society of America. TIC: 234445.

Heizler, M.T.; Perry, F.V.; Crowe, B.M.; Peters, L.; and Appelt, R. 1999. "The Age of Lathrop Wells Volcanic Center: An $^{40}\text{Ar}/^{39}\text{Ar}$ Dating Investigation." *Journal of Geophysical Research*, 104, (B1), 767-804. Washington, D.C.: American Geophysical Union. TIC: 243399.

Hileman, J.A.; Allen, C.R.; and Nordquist, J.M. 1973. *Seismicity of the Southern California Region 1 January 1932 to 31 December 1972*. Pasadena, California: California Institute of Technology, Seismological Laboratory. TIC: 242404.

Hill, D.P.; Ellsworth, W.L.; Johnston, M.J.S.; Langbein, J.O.; Oppenheimer, D.H.; Pitt, A.M.; Reasenber, P.A.; Sorey, M.L.; and McNutt, S. 1990. "The 1989 Earthquake Swarm Beneath Mammoth Mountain, California: An Initial Look at the 4 May through 30 September Activity." *Bulletin of the Seismological Society of America*, 80, (2), 325-339. [El Cerrito, California]: Seismological Society of America. TIC: 234904.

Hill, D.P.; Reasenber, P.A.; Michael, A.; Arabaz, W.J.; Beroza, G.; Brumbaugh, D.; Brune, J.N.; Castro, R.; Davis, S.; dePolo, D.; Ellsworth, W.L.; Gomberg, J.; Harmsen, S.; House, L.; Jackson, S.M.; Johnston, M.J.S.; Jones, L.; Keller, R.; Malone, S.; Munguia, L.; Nava, S.; Pechmann, J.C.; Sanford, A.; Simpson, R.W.; Smith, R.B.; Stark, M.; Stickney, M.; Vidal, A.; Walter, S.; Wong, V.; and Zollweg, J. 1993. "Seismicity Remotely Triggered by the Magnitude 7.3 Landers, California Earthquake." *Science*, 260, 1617-1623. Washington, D.C.: American Association for the Advancement of Science. TIC: 234737.

Hill, D.P.; Wallace, R.E.; and Cockerham, R.S. 1985. "Review of Evidence on the Potential for Major Earthquakes and Volcanism in the Long Valley-Mono Craters-White Mountains Regions of Eastern California." *Earthquake Prediction Research*, 3, (3-4), 571-594. Tokyo, Japan: Terra Scientific Publishing. TIC: 217846.

Hill, R.L. and Beeby, D.J. 1977. "Surface Faulting Associated with the 5.2 Magnitude Galway Lake Earthquake of May 31, 1975: Mojave Desert, San Bernardino County, California." *Geological Society of America Bulletin*, 88, 1378-1384. Boulder, Colorado: Geological Society of America. TIC: 234738.

Hill, R.L.; Treiman, J.A.; Given, J.W.; Pechman, J.C.; McMillan, J.R.; and Ebel, J.E. 1980. "Geologic Study of the Homestead Valley Earthquake Swarm of March 15, 1979." *California Geology*, 33, 60-67. [Sacramento, California: California Division of Mines and Geology]. TIC: 234735.

Ho, C-H. and Smith, E.I. 1998. "A Spatial-Temporal/3-D Model for Volcanic Hazard Assessment: Application to the Yucca Mountain Region, Nevada." *Mathematical Geology*, 30, (5), 497-510. New York, New York: Plenum Publishing Corporation. TIC: 245110.

Hoffard, J.L. 1991. *Quaternary Tectonics and Basin History of Pahrump and Stewart Valleys, Nevada and California*. NWPO-TR-017-91. Reno, Nevada: State of Nevada, Agency for Nuclear Projects/Nuclear Waste Projects Office. TIC: 205071.

Hoover, D.L. 1989. *Preliminary Description of Quaternary and Late Pliocene Surficial Deposits at Yucca Mountain and Vicinity, Nye County, Nevada*. Open-File Report 89-359. Denver, Colorado: U.S. Geological Survey. ACC: NNA.19900403.0406.

Hudson, M.R.; Sawyer, D.A.; and Warren, R.G. 1994. "Paleomagnetism and Rotation Constraints for the Middle Miocene Southwestern Nevada Volcanic Field." *Tectonics*, 13, (2), 258-277. Washington, D.C.: American Geophysical Union. TIC: 232935.

Idriss, I. 1997. "Attenuation Relationships." Letter from I. Idriss (UC, Davis) to N. Abrahamson, May 1, 1997, with attachment. ACC: MOL.20000612.0014; MOL.20000612.0015.

Idriss, I.M. 1991. "Earthquake Ground Motions at Soft Soil Sites." *Second International Conference on Recent Advances in Geotechnical Earthquake Engineering and Soil Dynamics, March 11-15, 1991*. Prakash, S., ed. III, 2265-2272. Rolla, Missouri: University of Missouri-Rolla. TIC: 241773.

Idriss, I.M. 1993. *Procedures for Selecting Earthquake Ground Motions at Rock Sites (Revised)*. NIST GCR 93-625. Gaithersburg, Maryland: U.S. Department of Commerce, National Institute of Standards and Technology. TIC: 241629.

Jaques, A.L. and Green, D.H. 1980. "Anhydrous Melting of Peridotite at 0-15 Kb Pressure and the Genesis of Tholeiitic Basalts." *Contributions to Mineralogy and Petrology*, 73, 287-310. New York, New York: Springer-Verlag. TIC: 225050.

Johnson, C.M. 1991. "Large-Scale Crust Formation and Lithosphere Modification Beneath Middle to Late Cenozoic Calderas and Volcanic Fields, Western North America." *Journal of Geophysical Research*, 96, (B8), 13,485-13,507. Washington, D.C.: American Geophysical Union. TIC: 225051.

Johnston, M.J.S.; Hill, D.P.; Linde, A.T.; Langbein, J.; and Bilham, R. 1995. "Transient Deformation During Triggered Seismicity from the June 28, 1992 Mw = 7.3 Landers Earthquake at Long Valley Volcanic Caldera, California." *Bulletin of the Seismological Society of America*, 85, 787-795. El Cerrito, California: Seismological Society of America. TIC: 234686.

Jones, L.M. 2000. "Overview of the Mw7.1 Hector Mine, California Earthquake of October 16, 1999." *Seismological Research Letters, SSA 2000, Abstracts of the 95th Annual Meeting*, 71, (2), 205. El Cerrito, California: Seismological Society of America. TIC: 247896.

Joyner, W.B. and Boore, D.M. 1981. "Peak Horizontal Acceleration and Velocity from Strong-Motion Records Including Records from the 1979 Imperial Valley, California, Earthquake." *Bulletin of the Seismological Society of America*, 71, (6), 2011-2038. El Cerrito, California: Seismological Society of America. TIC: 221673.

Joyner, W.B. and Boore, D.M. 1988. "Measurement, Characterization, and Prediction of Strong Ground Motion." [*Earthquake Engineering and Soil Dynamics II: Recent Advances in Ground-Motion Evaluation, Park City, Utah, June 27-30, 1988*]. [Von Thun, J.L., ed.]. Pages 43-102. [New York, New York: American Society of Civil Engineers]. TIC: 241219.

Julian, B.R. and Sipken, S.A. 1985. "Earthquake Processes in the Long Valley Caldera Area, California." *Journal of Geophysical Research*, 90, (B13), 11,155-11,169. Washington, D.C.: American Geophysical Union. TIC: 234662.

Kane, M.F. and Bracken, R.E. 1983. *Aeromagnetic Map of Yucca Mountain and Surrounding Regions, Southwest Nevada*. Open-File Report 83-616. Denver, Colorado: U.S. Geological Survey. TIC: 201297.

Keefer, R. and Whitney, J.W., eds. 1996. "Summary of Midway Valley Studies." Chapter 4.3 of *Seismotectonic Framework and Characterization of Faulting at Yucca Mountain, Nevada*. Whitney, J.W., ed. Milestone 3GSH100M. Denver, Colorado: U.S. Geological Survey. TIC: 237980.

Keefer, W.R. and Pezzopane, S.K. 1996. "Quaternary Faults in the Yucca Mountain Region." Chapter 3 of *Seismotectonic Framework and Characterization of Faulting at Yucca Mountain, Nevada*. Whitney, J.W., ed. Milestone 3GSH100M. Denver, Colorado: U.S. Geological Survey. TIC: 237980.

King, K.W.; Bayer, K.C.; and Brockman, S.R. 1971. *Earthquakes On and Around the Nevada Test Site 1950 - 1971*. CGS-746-12. Washington, D.C.: U.S. Department of Commerce, National Oceanic and Atmospheric Administration. TIC: 204588.

Klinger, R.E. and Anderson, L.W. 1994. "Topographic Profiles and Their Implications for Late Quaternary Activity on the Bare Mountain Fault, Nye County, Nevada." *Abstracts with Programs - Geological Society of America*, 26, (2), 63-64. Boulder, Colorado: Geological Society of America. TIC: 224623.

Klinger, R.E. and Piety, L.A. 1996. "Late Quaternary Activity on the Furnace Creek Fault, Northern Death Valley, California." *Abstracts with Programs - Geological Society of America*, 28, (7), A-193. Boulder, Colorado: Geological Society of America. TIC: 234651.

Knutson, J. and Green, T.H. 1975. "Experimental Duplication of a High-Pressure Megacryst/Cumulate Assemblage in a Near-Saturated Hawaiiite." *Contributions to Mineralogy and Petrology*, 52, 121-132. Berlin, Germany: Springer-Verlag. TIC: 225057.

Kotra, J.P.; Lee, M.P.; Eisenberg, N.A.; and DeWispelare, A.R. 1996. *Branch Technical Position on the Use of Expert Elicitation in the High-Level Radioactive Waste Program*. NUREG-1563. Washington, D.C.: U.S. Nuclear Regulatory Commission. TIC: 226832.

Langenheim, V.E.; Kirchoff-Stein, K.S.; and Oliver, H.W. 1993. "Geophysical Investigations of Buried Volcanic Centers Near Yucca Mountain, Southwest Nevada." *High Level Radioactive Waste Management, Proceedings of the Fourth Annual International Conference, Las Vegas, Nevada, April 26-30, 1993*. 2, 1840-1846. La Grange Park, Illinois: American Nuclear Society. TIC: 208542.

Latham, A.G. 1995. "On the Principles of the U-Trend Method for Dating Quaternary Sediments, I: Model, Experimental Procedures and Data." *Quaternary Science Reviews (Quaternary Geochronology)*, 14, (4), 409-420. New York, New York: Pergamon Press. TIC: 237026.

Lienkaemper, J.J.; Pezzopane, S.K.; Clark, M.M.; and Rymer, M.J. 1987. "Fault Fractures Formed in Association with the 1986 Chalfant Valley, California, Earthquake Sequence: Preliminary Report." *Bulletin of the Seismological Society of America*, 77, (1), 297-305. El Cerrito, California: Seismological Society of America. TIC: 234659.

Lipman, P.W. 1980. "Cenozoic Volcanism in the Western United States: Implications for Continental Tectonics." Chapter 14 of *Continental Tectonics*. Studies in Geophysics. Washington, D.C.: National Academy of Sciences. TIC: 209284.

Lum, P.K. and Honda, K.K. 1992. *Processed Seismic Motion Records from Little Skull Mountain, Nevada Earthquake of June 29, 1992, Recorded at Stations in Southern Nevada*. JAB-10733-TM6. San Francisco, California: URS/John A. Blume & Associates. TIC: 207043.

Lundstrom, S.C.; Wesling, J.R.; Swan, F.H.; Taylor, E.M.; and Whitney, J.W. 1993. "Quaternary Allostratigraphy of Surficial Deposit Map Units at Yucca Mountain, Nevada: A Progress Report." *Abstracts with Programs - Geological Society of America*, 25, (5), A-112. Boulder, Colorado: Geological Society of America. TIC: 237811.

Magsino, S.L.; Connor, C.B.; Hill, B.E.; Stamatakos, J.A.; La Femina, P.C.; Sims, D.A.; and Martin, R.H. 1998. *CNWRA Ground Magnetic Surveys in the Yucca Mountain Region, Nevada (1996-1997)*. CNWRA 98-001. San Antonio, Texas: Center for Nuclear Waste Regulatory Analyses. TIC: 247807.

Mahood, G.A. and Baker, D.R. 1986. "Experimental Constraints on Depths of Fractionation of Mildly Alkalic Basalts and Associated Felsic Rocks: Pantelleria, Strait of Sicily." *Contributions to Mineralogy and Petrology*, 93, 251-264. New York, New York: Springer-Verlag. TIC: 225072.

Majer, E.L.; Feighner, M.; Johnson, L.; Daley, T.; Karageorgi, E.; Lee, K.H.; Williams, K.; and McEvelly, T. 1996b. *Surface Geophysics*. Volume I of *Synthesis of Borehole and Surface Geophysical Studies at Yucca Mountain, Nevada and Vicinity*. Milestone OB05M. Berkeley, California: Lawrence Berkeley National Laboratory. ACC: MOL.19970610.0150.

Majer, E.L.; Feighner, M.; Johnson, L.; Daley, T.; Williams, K.; Karageorgi, E.; and McEvelly, T. 1996a. *Level 4 Milestone Letter Report on Surface Geophysics Synthesis: Data Processing*. Berkeley, California: Lawrence Berkeley National Laboratory. ACC: MOL.19971224.0006.

McCalpin, J.P. 1995. "Short Notes Frequency Distribution of Geologically Determined Slip Rates for Normal Faults in the Western United States." *Bulletin of the Seismological Society of America*, 85, (6), 1867-1872. El Cerrito, California: Seismological Society of America. TIC: 236669.

McConnell, K.I.; Blackford, M.E.; and Ibrahim, A.B. 1992. *Staff Technical Position on Investigations to Identify Fault Displacement Hazards and Seismic Hazards at a Geological Repository*. NUREG-1451. Washington, D.C.: U.S. Nuclear Regulatory Commission. TIC: 204829.

McConnell, K.I. and Lee, M.P. 1994. *Staff Technical Position on Consideration of Fault Displacement Hazards in Geologic Repository Design*. NUREG-1494. Washington, D.C.: U.S. Nuclear Regulatory Commission. TIC: 212360.

McGarr, A. 1984. "Scaling of Ground Motion Parameters, State of Stress, and Focal Depth." *Journal of Geophysical Research*, 89, (B8), 6969-6979. Washington, D.C.: American Geophysical Union. TIC: 222577.

McGill, S.F. and Sieh, K. 1991. "Surficial Offsets on the Central and Eastern Garlock Fault Associated with Prehistoric Earthquakes." *Journal of Geophysical Research*, 96, (13), 21,597-21,621. Washington, D.C.: American Geophysical Union. TIC: 241013.

McGill, S.F. and Sieh, K. 1993. "Holocene Slip Rate of the Central Garlock Fault in Southeastern Searles Valley, California." *Journal of Geophysical Research*, 98, (B8), 14,217-14,231. Washington, D.C.: American Geophysical Union. TIC: 241008.

McGuire, R.K. 1995. "Probabilistic Seismic Hazard Analysis and Design Earthquakes: Closing the Loop." *Bulletin of the Seismological Society of America*, 85, (5), 1275-1284. El Cerrito, California: Seismological Society of America. TIC: 232947.

McKague, H.L.; Stamatakos, J.A.; and Ferrill, D.A. 1996. *Type I Faults in the Yucca Mountain Region*. CNWRA 96-007, Rev. 1. San Antonio, Texas: Center for Nuclear Waste Regulatory Analyses. TIC: 232061.

Menges, C.M.; Oswald, J.A.; Coe, J.A.; Lundstrom, S.C.; Paces, J.B.; Mahan, S.A.; Widmann, B.; and Murray, M. 1998. *Paleoseismic Investigations of Stagecoach Road Fault, Southeastern Yucca Mountain, Nye County, Nevada*. Open-File Report 96-417. Denver, Colorado: U.S. Geological Survey. ACC: MOL.19980330.0151.

Menges, C.M.; Wesling, J.R.; Whitney, J.W.; Swan, F.H.; Coe, J.A.; Thomas, A.P.; and Oswald, J.A. 1994. "Preliminary Results of Paleoseismic Investigations of Quaternary Faults on Eastern Yucca Mountain, Nye County, Nevada." *High Level Radioactive Waste Management, Proceedings of the Fifth Annual International Conference, Las Vegas, Nevada, May 22-26, 1994*. 4, 2373-2390. La Grange Park, Illinois: American Nuclear Society. TIC: 210984.

Menges, C.M. and Whitney, J.W. 1996a. "Distribution of Quaternary Faults in the Site Area." Chapter 4.2 of *Seismotectonic Framework and Characterization of Faulting at Yucca Mountain, Nevada*. Whitney, J.W., ed. Milestone 3GSH100M. Denver, Colorado: U.S. Geological Survey. TIC: 237980.

Menges, C.M. and Whitney, J.W. 1996b. "Summary of Quaternary Faulting on the Paintbrush Canyon, Stagecoach Road, and Bow Ridge Faults." Chapter 4.4 of *Seismotectonic Framework and Characterization of Faulting at Yucca Mountain, Nevada*. Whitney, J.W., ed. Milestone 3GSH100M. Denver, Colorado: U.S. Geological Survey. TIC: 237980.

Meremonte, M.E.; Cranswick, E.; Gomberg, J.; Worley, D.; Carver, D.; Brooks, J.; Banfill, R.; Overturf, D.; and Bice, T. 1993. *Report on the Seismological Field Investigations of the 29 June 1992 Little Skull Mountain Earthquake*. Open-File Report 93-555. Denver, Colorado: U.S. Geological Survey. ACC: NNA.19931117.0008.

Meremonte, M.E.; Gomberg, J.; and Cranswick, E. 1995. "Constraints on the 29 June 1992 Little Skull Mountain, Nevada Earthquake Sequence Provided by Robust Hypocentral Estimates." *Bulletin of the Seismological Society of America*, 85, (4), 1039-1049. El Cerrito, California: Seismological Society of America. TIC: 236659.

Meremonte, M.E. and Rogers, A.M. 1987. *Historical Catalog of Southern Great Basin Earthquakes 1868-1978*. Open File Report 87-80. Denver, Colorado: U.S. Geological Survey. TIC: 203189.

Monsen, S.A.; Carr, M.D.; Reheis, M.C.; and Orkild, P.P. 1992. *Geologic Map of Bare Mountain, Nye County, Nevada*. Miscellaneous Investigations Series Map I-2201. Denver, Colorado: U.S. Geological Survey. ACC: MOL.19941214.0060.

Mooney, W.D. and Schapper, S. 1995. "Seismic Refraction Investigations." Chapter 5 of *Major Results of Geophysical Investigations at Yucca Mountain and Vicinity, Southern Nevada*. Oliver, H.W.; Ponce, D.A.; and Hunter, W.C., eds. Open-File Report 95-74. Menlo Park, California: U.S. Geological Survey. ACC: MOL.19980305.0122.

Morgan, P.; Seager, W.R.; and Golombek, M.P. 1986. "Cenozoic Thermal, Mechanical and Tectonic Evolution of the Rio Grande Rift." *Journal of Geophysical Research*, 91, (B6), 6263-6276. Washington, D.C.: American Geophysical Union. TIC: 225085.

Nelson, A.R. 1992. "Lithofacies Analysis of Colluvial Sediments - Interpreting the Recent History of Quaternary Normal Faults in the Basin and Range Province, Western United States." *Journal of Sedimentary Petrology*, 62, (4), 611-621. Tulsa, Oklahoma: Society for Sedimentary Geology. TIC: 235045.

Nelson, S.T.; Sullivan, K.R.; and Davidson, J.P. 1992. "New Age Determinations of Central Colorado Plateau Laccoliths, Utah: Recognizing Disturbed K-Ar Systematics and Re-evaluating Tectonomagmatic Relationships." *Geological Society of America Bulletin*, 104, (12), 1547-1560. Boulder, Colorado: Geological Society of America. TIC: 247761.

Nelson, S.T. and Tingey, D.G. 1997. "Time-Transgressive and Extension-Related Basaltic Volcanism in Southwest Utah and Vicinity." *Geological Society of America Bulletin*, 109, (10), 1249-1265. Boulder, Colorado: Geological Society of America. TIC: 247915.

NRC (U.S. Nuclear Regulatory Commission) 1998. *Issue Resolution Status Report Key Technical Issue: Repository Design and Thermal-Mechanical Effects*. Rev. 1. Washington, D.C.: U.S. Nuclear Regulatory Commission. ACC: MOL.19981130.0219.

NRC (U.S. Nuclear Regulatory Commission) 1999. *Issue Resolution Status Report Key Technical Issue: Structural Deformation and Seismicity*. Rev. 2. Washington, D.C.: U.S. Nuclear Regulatory Commission. ACC: MOL.19991214.0623.

NRC (U.S. Nuclear Regulatory Commission) 2000. *Issue Resolution Status Report Key Technical Issue: Total System Performance Assessment and Integration*. Rev. 2. Washington, D.C.: U.S. Nuclear Regulatory Commission. TIC: 247614.

Paces, J.B.; Mahan, S.A.; Ludwig, K.R.; Kwak, L.M.; Neymark, L.A.; Simmons, K.R.; Nealey, L.D.; Marshall, B.D.; and Walker, A. 1995. *Progress Report on Dating Quaternary Surficial Deposits*. Milestone 3GCH510M. Final Draft. Denver, Colorado: U.S. Geological Survey. ACC: MOL.19960611.0220.

Paces, J.B.; Menges, C.M.; Widmann, B.; Wesling, J.R.; Bush, C.A.; Futa, K.; Millard, H.T.; Maat, P.B.; and Whitney, J.W. 1994. "Preliminary U-Series Disequilibrium and Thermoluminescence Ages of Surficial Deposits and Paleosols Associated with Quaternary Faults, Eastern Yucca Mountain." *High Level Radioactive Waste Management, Proceedings of the Fifth Annual International Conference, Las Vegas, Nevada, May 22-26, 1994*. 4, 2391-2401. La Grange Park, Illinois: American Nuclear Society. TIC: 210984.

Peltzer, G. and Rosen, P. 1995. "Surface Displacement of the 17 May 1993 Eureka Valley, California, Earthquake Observed by SAR Interferometry." *Science*, 268, 1333-1336. Washington, D.C.: American Association for the Advancement of Science. TIC: 235067.

Perry, F.V. and Crowe, B.M. 1992. "Geochemical Evidence for Waning Magmatism and Polycyclic Volcanism at Crater Flat, Nevada." *High Level Radioactive Waste Management, Proceedings of the Third International Conference, Las Vegas, Nevada, April 12-16, 1992*. 2, 2356-2365. La Grange Park, Illinois: American Nuclear Society. TIC: 204231.

Perry, F.V.; DePaolo, D.J.; and Baldrige, W.S. 1993. "Neodymium Isotopic Evidence for Decreasing Crustal Contributions to Cenozoic Ignimbrites of the Western United States: Implications for the Thermal Evolution of the Cordilleran Crust." *Geological Society of America Bulletin*, 105, 872-882. Boulder, Colorado: Geological Society of America. TIC: 225116.

Perry, F.V. and Straub, K.T. 1996. *Geochemistry of the Lathrop Wells Volcanic Center*. LA-13113-MS. Los Alamos, New Mexico: Los Alamos National Laboratory. ACC: MOL.19961015.0079.

Peterson, F.F. 1988. "Consultant's Report: Soil-Geomorphology Studies in the Crater Flat, Nevada, Area." Appendix B of *Quaternary Geology and Active Faulting at and Near Yucca Mountain*. [Reno, Nevada: Nevada Bureau of Mines and Geology]. TIC: 222315.

Peterson, F.F.; Bell, J.W.; Dorn, R.I.; Ramelli, A.R.; and Ku, T.L. 1995. "Late Quaternary Geomorphology and Soils in Crater Flat, Yucca Mountain Area, Southern Nevada." *Geological Society of America Bulletin*, 107, (4), 379-395. Boulder, Colorado: Geological Society of America. TIC: 235112.

Pezzopane, S.K. 1996. "Relevant Earthquake Sources." Chapter 11 of *Seismotectonic Framework and Characterization of Faulting at Yucca Mountain, Nevada*. Whitney, J.W., ed. Milestone 3GSH100M. Denver, Colorado: U.S. Geological Survey. TIC: 237980.

Pezzopane, S.K.; Bufe, C.G.; Dawson, T.E.; Wong, I.G.; and Bott, J.D.J. 1996. "Historical Seismicity in the Yucca Mountain Region." Chapter 7 of *Seismotectonic Framework and Characterization of Faulting at Yucca Mountain, Nevada*. Whitney, J.W., ed. Milestone 3GSH100M. Denver, Colorado: U.S. Geological Survey. TIC: 237980.

Pezzopane, S.K. and Dawson, T.E. 1996. "Fault Displacement Hazard: A Summary of Issues and Information." Chapter 9 of *Seismotectonic Framework and Characterization of Faulting at Yucca Mountain, Nevada*. Whitney, J.W., ed. Milestone 3GSH100M. Denver, Colorado: U.S. Geological Survey. TIC: 237980.

Pezzopane, S.K.; Whitney, J.W.; and Dawson, T.E. 1996. "Models of Earthquake Recurrence and Preliminary Paleoearthquake Magnitudes at Yucca Mountain." Chapter 5 of *Seismotectonic Framework and Characterization of Faulting at Yucca Mountain, Nevada*. Whitney, J.W., ed. Milestone 3GSH100M. Denver, Colorado: U.S. Geological Survey. TIC: 237980.

Piety, L.A. 1996. *Compilation of Known or Suspected Quaternary Faults Within 100 km of Yucca Mountain, Nevada and California*. Open-File Report 94-112. Denver, Colorado: U.S. Geological Survey. ACC: MOL.19971009.0003.

Pitt, A.M. and Hill, D.P. 1994. "Long-Period Earthquakes in the Long Valley Caldera Region, Eastern California." *Geophysical Research Letters*, 21, (16), 1679-1682. Washington, D.C.: American Geophysical Union. TIC: 234820.

Ponce, D.A. 1993. "Geophysical Investigations of Concealed Faults Near Yucca Mountain, Southwest Nevada." *High Level Radioactive Waste Management, Proceedings of the Fourth*

Annual International Conference, Las Vegas, Nevada, April 26-30, 1993. 1, 168-174. La Grange Park, Illinois: American Nuclear Society. TIC: 208542.

Priestley, K.F.; Smith, K.D.; and Cockerham, R.S. 1988. "The 1984 Round Valley, California Earthquake Sequence." *Geophysical Journal*, 95, 215-235. Oxford, England: Blackwell Scientific Publications. TIC: 234814.

Ramelli, A.R.; Bell, J.W.; and dePolo, C.M. 1991. "Late Quaternary Faulting at Crater Flat, Yucca Mountain, Southern Nevada." Appendix E of *Evaluation of the Geologic Relations and Seismotectonic Stability of the Yucca Mountain Area, Nevada Nuclear Waste Site Investigation Progress Report*. Reno, Nevada: University of Nevada-Reno, Mackay School of Mines, Center for Neotectonic Studies. TIC: 236005.

Ramelli, A.R.; Oswald, J.A.; Vadurro, G.; Menges, C.M.; and Paces, J.B. 1996. "Quaternary Faulting on the Solitario Canyon Fault." Chapter 4.7 of *Seismotectonic Framework and Characterization of Faulting at Yucca Mountain, Nevada*. Whitney, J.W., ed. Milestone 3GSH100M. Denver, Colorado: U.S. Geological Survey. TIC: 237980.

Reamer, C.W. 1999. "Issue Resolution Status Report (Key Technical Issue: Igneous Activity, Revision 2)." Letter from C.W. Reamer (NRC) to Dr. S. Brocoum (DOE), July 16, 1999, with enclosure. ACC: MOL.19990810.0639.

Reheis, M.C. 1988. "Preliminary Study of Quaternary Faulting on the East Side of Bare Mountain, Nye County, Nevada." Chapter 8 of *Geologic and Hydrologic Investigations of a Potential Nuclear Waste Disposal Site at Yucca Mountain, Southern Nevada*. Carr, M.D. and Yount, J.C., eds. Bulletin 1790. Denver, Colorado: U.S. Geological Survey. TIC: 203085.

Reheis, M.C. 1991. *Aerial Photographic Interpretation of Lineaments and Faults in Late Cenozoic Deposits in the Eastern Parts of the Saline Valley 1:100,000 Quadrangle, Nevada and California, and the Darwin Hills 1:100,000 Quadrangle, California*. Open-File Report 90-500. Denver, Colorado: U.S. Geological Survey. ACC: NNA.19910507.0001.

Reheis, M.C. 1992. *Aerial Photographic Interpretation of Lineaments and Faults in Late Cenozoic Deposits in the Cactus Flat and Pahute Mesa 1:100,000 Quadrangles and the Western Parts of the Timpahute Range, Pahrnagat Range, Indian Springs, and Las Vegas 1:100,000 Quadrangles, Nevada*. Open-File Report 92-193. Denver, Colorado: U.S. Geological Survey. ACC: NNA.19940524.0085.

Reheis, M.C. 1994. "Holocene Faulting Along the Central Fish Lake Valley Fault Zone, California and Nevada." *Abstracts with Programs - Geological Society of America*, 26, (2), 83. Boulder, Colorado: Geological Society of America. TIC: 246689.

Reheis, M.C. and Noller, J.S. 1991. *Aerial Photographic Interpretation of Lineaments and Faults in Late Cenozoic Deposits in the Eastern Part of the Benton Range 1:100,000 Quadrangle and the Goldfield, Last Chance Range, Beatty, and Death Valley Junction 1:100,000 Quadrangles, Nevada and California*. Open-File Report 90-41. Denver, Colorado: U.S. Geological Survey. ACC: NNA.19901031.0001.

- Reiter, L. 1990. *Earthquake Hazard Analysis, Issues and Insights*. New York, New York: Columbia University Press. TIC: 236929.
- Richter, C.F. 1947. "The Manix (California) Earthquake of April 10, 1947." *Bulletin of the Seismological Society of America*, 37, 171-179. El Cerrito, California: Seismological Society of America. TIC: 234925.
- Rogers, A.M.; Harmsen, S.C.; and Carr, W.J. 1981. *Southern Great Basin Seismological Data Report for 1980 and Preliminary Data Analysis*. Open-File Report 81-1086. Denver, Colorado: U.S. Geological Survey. ACC: NNA.19870518.0068.
- Rogers, A.M.; Harmsen, S.C.; Corbett, E.J.; Priestly, K.; and dePolo, D. 1991. "The Seismicity of Nevada and Some Adjacent Parts of the Great Basin." Chapter 10 of *The Geology of North America Decade Map*. Volume 1. Boulder, Colorado: Geological Society of America. TIC: 243190.
- Rogers, A.M.; Harmsen, S.C.; and Meremonte, M.E. 1987. *Evaluation of the Seismicity of the Southern Great Basin and Its Relationship to the Tectonic Framework of the Region*. Open-File Report 87-408. Denver, Colorado: U.S. Geological Survey. ACC: HQX.19880315.0004.
- Rogers, A.M. and Lee, W.H.K. 1976. "Seismic Study of Earthquakes in the Lake Mead, Nevada-Arizona Region." *Bulletin of the Seismological Society of America*, 66, (5), 1657-1681. El Cerrito, California: Seismological Society of America. TIC: 218413.
- Rogers, A.M.; Wuollet, G.M.; and Covington, P.A. 1977. *Seismicity of the Pahute Mesa Area, Nevada Test Site, 8 October 1975 to 30 June 1976*. USGS-474-184. Reston, Virginia: U.S. Geological Survey. TIC: 217121.
- Romanowicz, B.; Dreger, D.; Pasyanos, M.; and Uhrhammer, R. 1993. "Monitoring of Strain Release in Central and Northern California Using Broadband Data." *Geophysical Research Letters*, 20, (15), 1643-1646. Washington, D.C.: American Geophysical Union. TIC: 236627.
- Roquemore, G.R. and Simila, G.W. 1994. "Aftershocks from the 28 June 1992 Landers Earthquake: Northern Mojave Desert to Coso Volcanic Field, California." *Bulletin of the Seismological Society of America*, 84, (3), 854-862. El Cerrito, California: Seismological Society of America. TIC: 236673.
- Roquemore, G.R.; Simila, G.W.; and Mori, J. 1996. "The 1995 Ridgecrest Earthquake Sequence: New Clues to the Neotectonic Development of Indian Wells Valley and the Coso Range, Eastern California." *Abstracts with Programs - Geological Society of America*, 28, (5), 106. Boulder, Colorado: Geological Society of America. TIC: 236678.
- Rosenbaum, J.G.; Hudson, M.R.; and Scott, R.B. 1991. "Paleomagnetic Constraints on the Geometry and Timing of Deformation at Yucca Mountain, Nevada." *Journal of Geophysical Research*, 96, (B2), 1963-1979. Washington, D.C.: American Geophysical Union. TIC: 225126.

Sabetta, F. and Pugliese, A. 1996. "Estimation of Response Spectra and Simulation of Nonstationary Earthquake Ground Motions." *Bulletin of the Seismological Society of America*, 86, (2), 337-352. El Cerrito, California: Seismological Society of America. TIC: 241042.

Sadigh, K.; Chang, C.-Y.; Abrahamson, N.A.; Chiou, S.J.; and Power, M.S. 1993. "Specification of Long-Period Ground Motions: Updated Attenuation Relationships for Rock Site Conditions and Adjustment Factors for Near-Fault Effects." *Proceedings of ATC 17-1 Seminar on Seismic Isolation, Passive Energy Dissipation, and Active Control, San Francisco, California, March 11-12, 1993*. 1, 59-70. Redwood City, California: Applied Technology Council. TIC: 238494.

Sadigh, K.; Chang, C.-Y.; Egan, J.A.; Makdisi, F.; and Youngs, R.R. 1997. "Attenuation Relationships for Shallow Crustal Earthquakes Based on California Strong Motion Data." *Seismological Research Letters*, 68, (1), 180-189. El Cerrito, California: Seismological Society of America. TIC: 240552.

Savage, J.C. and Clark, M.M. 1982. "Magmatic Resurgence in Long Valley Caldera, California: Possible Cause of the 1980 Mammoth Lakes Earthquakes." *Science*, 217, (6), 531-533. Washington, D.C.: American Association for the Advancement of Science. TIC: 236652.

Savage, J.C. and Gross, W.K. 1995. "Short Notes, Revised Dislocation Model of the 1986 Chalfant Valley Earthquake, Eastern California." *Bulletin of the Seismological Society of America*, 85, (2), 629-631. El Cerrito, California: Seismological Society of America. TIC: 235750.

Savage, J.C.; Lisowski, M.; and Prescott, W.H. 1990. "An Apparent Shear Zone Trending North-Northwest Across the Mojave Desert into Owens Valley, Eastern California." *Geophysical Research Letters*, 17, (12), 2113-2116. Washington, D.C.: American Geophysical Union. TIC: 235680.

Sawyer, D.A.; Fleck, R.J.; Lanphere, M.A.; Warren, R.G.; Broxton, D.E.; and Hudson, M.R. 1994. "Episodic Caldera Volcanism in the Miocene Southwestern Nevada Volcanic Field: Revised Stratigraphic Framework, $^{40}\text{Ar}/^{39}\text{Ar}$ Geochronology, and Implications for Magmatism and Extension." *Geological Society of America Bulletin*, 106, (10), 1304-1318. Boulder, Colorado: Geological Society of America. TIC: 222523.

Schneider, J.F.; Abrahamson, N.A.; and Hanks, T.C. 1996. *Ground Motion Modeling of Scenario Earthquakes at Yucca Mountain, Final Report for Activity 8.3.1.17.3.3*. Volume 1. Denver, Colorado: U.S. Geological Survey. ACC: MOL.19980617.0477.

Schwartz, D.P. 1988. "Geologic Characterization of Seismic Sources: Moving into the 1990s." *Earthquake Engineering and Soil Dynamics II: Recent Advances in Ground-Motion Evaluation, Park City, Utah, June 27-30, 1988*. Von Thun, J.L., ed. 20, 1-42. New York, New York: American Society of Civil Engineers. TIC: 235723.

Schwartz, D.P. and Coppersmith, K.J. 1984. "Fault Behavior and Characteristic Earthquakes: Examples from the Wasatch and San Andreas Fault Zones." *Journal of Geophysical Research*, 89, (B7), 5681-5698. Washington, D.C.: American Geophysical Union. TIC: 235753.

Schwartz, D.P. and Coppersmith, K.J. 1986. "Seismic Hazards: New Trends in Analysis Using Geologic Data." Chapter 14 of *Active Tectonics*. Studies in Geophysics. Washington, D.C.: National Academy Press. TIC: 209251.

Scott, R.B. 1990. "Tectonic Setting of Yucca Mountain, Southwest Nevada." Chapter 12 of *Basin and Range Extensional Tectonics Near the Latitude of Las Vegas Nevada*. Wernicke, B.P., ed. Memoir 176. Boulder, Colorado: Geological Society of America. TIC: 222540.

Scott, R.B. 1992. *Preliminary Geologic Map of Southern Yucca Mountain, Nye County, Nevada*. Open-File Report 92-266. Denver, Colorado: U.S. Geological Survey. ACC: MOL.19960416.0311.

Scott, R.B. and Bonk, J. 1984. *Preliminary Geologic Map of Yucca Mountain, Nye County, Nevada, with Geologic Sections*. Open-File Report 84-494. Denver, Colorado: U.S. Geological Survey. TIC: 203162.

Sheehan, A.F.; Smith, K.D.; and Savage, M.K. 1994. *Data Package on Seismological Field Investigations of the 29 June 1992 Little Skull Mountain Earthquake*. Reno, Nevada: University of Nevada, Reno. ACC: NNA.19940608.0276.

Shields, G.; Smith, K.; and Brune, J. 1995. "Source Parameters of a Sequence of Very Shallow Earthquakes in the Rock Valley Fault Zone, Southern Nevada Test Site." *Transactions of the American Geophysical Union*, 76, F426. Washington, D.C.: American Geophysical Union. TIC: 235738.

Shroba, R.R.; Muhs, D.R.; and Rosholt, J.N. 1988a. *Physical Properties and Radiometric Age Estimates of Surficial and Fracture-Fill Deposits Along a Portion of the Carpetbag Fault System, Nevada Test Site, Nye County, Nevada*. DOE/NV/10583-1. Denver, Colorado: U.S. Geological Survey. ACC: NNA.19900502.0076.

Shroba, R.R.; Muhs, D.R.; and Rosholt, J.N. 1988b. "Uranium-Trend and Uranium-Series Age Estimates of Surficial and Fracture-Fill Deposits on the Carpetbag Fault System, Nevada Test Site, Nye County, Nevada." *Abstracts with Programs - Geological Society of America*, 20, 231. Boulder, Colorado: Geological Society of America. TIC: 245862.

Sieh, K.; Jones, L.; Hauksson, E.; Hudnut, K.; Eberhart-Phillips, D.; Heaton, T.; Hough, S.; Hutton, K.; Kanamori, H.; Lilje, A.; Lindvall, S.; McGill, S.F.; Mori, J.; Rubin, C.; Spotila, J.A.; Stock, J.; Thio, H.K.; Theiman, J.; Wernicke, B.; and Zachariasen, J. 1993. "Near-Field Investigations of the Landers Earthquake Sequence, April to July 1992." *Science*, 260, 171-176. Washington, D.C.: American Association for the Advancement of Science. TIC: 235760.

Sieh, K.E. 1978. "Prehistoric Large Earthquakes Produced by Slip on the San Andreas Fault at Pallett Creek, California." *Journal of Geophysical Research*, 83, (B8), 3907-3939. Washington, D.C.: American Geophysical Union. TIC: 239586.

Simonds, F.W.; Whitney, J.W.; Fox, K.F.; Ramelli, A.R.; Yount, J.C.; Carr, M.D.; Menges, C.M.; Dickerson, R.P.; and Scott, R.B. 1995. *Map Showing Fault Activity in the Yucca*

Mountain Area, Nye County, Nevada. Miscellaneous Investigations Series Map I-2520. Denver, Colorado: U.S. Geological Survey. TIC: 232483.

Slemmons, B. 1997b. "Yucca Mountain Aerial Reconnaissance on January 10, 1997 by David B. Slemmons and Norma Biggar, Geologists, and Cady Johnson, Pilot and Geologist." Memorandum from B. Slemmons to R. Quittmeyer, February 3, 1997. ACC: MOL.20000831.0068.

Slemmons, D.B. 1957. "Geological Effects of the Dixie Valley-Fairview Peak, Nevada, Earthquakes of December 16, 1954." *Bulletin of the Seismological Society of America*, 47, (3), 353-375. El Cerrito, California: Seismological Society of America. TIC: 234933.

Slemmons, D.B. 1997a. "Carrara Fault, in Southern Nevada from Paleoseismic, Geologic and Geophysical Evidence: Implications to the Earthquake Hazards and Tectonics near Yucca Mountain, Nevada." *Eos, Transactions (Supplement)*, 78, (46), F453. [Washington, D.C.]: American Geophysical Union. TIC: 248765.

Slemmons, D.B. and dePolo, C.M. 1986. "Evaluation of Active Faulting and Associated Hazards." Chapter 3 of *Active Tectonics. Studies in Geophysics*. Washington, D.C.: National Academy Press. TIC: 209251.

Slemmons D.B.; Jones, A.E.; and Gimlett, J.I. 1965. "Catalog of Nevada Earthquakes, 1852-1960." *Bulletin of the Seismological Society of America*, 55, (2), 519-566. El Cerrito, California: Seismological Society of America. TIC: 217161.

Smith, B.E.; Hamilton, R.M.; and Jackson, W.H. 1971. *Seismicity of the Central Nevada Test Area, 26 September 1969 - 1 October 1970*. USGS-474-109. Menlo Park, California: U.S. Geological Survey. ACC: NNA.19910405.0045.

Smith, E.I.; Blaylock, J.; Boland, K.; Morikawa, S.; and Sanchez, A. 1996. "Complex Behavior of Low-Volume Mafic Magma Systems: Polycyclic, Polygenetic, and Complex Monogenetic Quaternary Cinder Cones in the Western US and Mexico." *Abstracts with Programs - Geological Society of America*. Page A-502. Boulder, Colorado: Geological Society of America. TIC: 234932.

Smith, E.I.; Feuerbach, D.L.; Naumann, T.R.; and Faulds, J.E. 1990. "The Area of Most Recent Volcanism Near Yucca Mountain, Nevada: Implications for Volcanic Risk Assessment." *High Level Radioactive Waste Management, Proceedings of the International Topical Meeting, Las Vegas, Nevada, April 8-12, 1990. 1*, 81-90. La Grange Park, Illinois: American Nuclear Society. TIC: 202058.

Smith, K. 2000. "Scotty's Junction and Frenchman Flat Earthquakes." E-mail from K. Smith (UNR) to R. Quittmeyer (CRWMS M&O), June 7, 2000, with attachment. ACC: MOL.20000609.0302.

Smith, K.D.; Brune, J.N.; dePolo, D.; Savage, M.K.; Anosheepoor, R.; and Sheehan, A.F. [n.d.]. *The 1992 Little Skull Mountain Earthquake Sequence, Southern Nevada Test Site*. Reno, Nevada: University of Nevada, Reno, Seismological Laboratory. ACC: MOL.20000531.0007.

Smith, K.D. and Priestley, K.F. 1988. "The Foreshock Sequence of the 1986 Chalfant, California Earthquake." *Bulletin of the Seismological Society of America*, 78, 172-187. El Cerrito, California: Seismological Society of America. TIC: 234907.

Smith, K.D.; Shields, G.; von Seggern, D.; Biasi, G.P.; Brune, J.N.; and Pezzopane, S.K. 1996. "Small Earthquakes at Yucca Mountain." *Abstracts with Programs - Geological Society of America*, 28, (7), A-193. Boulder, Colorado: Geological Society of America. TIC: 234940.

Smith, R.L. and Luedke, R.G. 1984. "Potentially Active Volcanic Lineaments and Loci in Western Conterminous United States." Chapter 4 of *Studies in Geophysics, Explosive Volcanism: Inception, Evolution, and Hazards*. Washington, D.C.: National Academy Press. TIC: 246871.

Smith, R.S.U. 1979. "Holocene Offset and Seismicity Along the Panamint Valley Fault Zone, Western Basin-and-Range Province, California." *Tectonophysics*, 52, 411-415. Amsterdam, The Netherlands: Elsevier Science Publishers. TIC: 225835.

Spence, W. and Gross, R.S. 1990. "A Tomographic Glimpse of the Upper Mantle Source of Magmas of the Jemez Lineament, New Mexico." *Journal of Geophysical Research*, 95, (B7), 10,829-10,849. Washington, D.C.: American Geophysical Union. TIC: 225150.

Spengler, R.W.; Braun, C.A.; Linden, R.M.; Martin, L.G.; Ross-Brown, D.M.; and Blackburn, R.L. 1993. "Structural Character of the Ghost Dance Fault, Yucca Mountain, Nevada." *High Level Radioactive Waste Management, Proceedings of the Fourth Annual International Conference, Las Vegas, Nevada, April 26-30, 1993*. 1, 653-659. La Grange Park, Illinois: American Nuclear Society. TIC: 208542.

Spengler, R.W.; Braun, C.A.; Martin, L.G.; and Weisenberg, C.W. 1994. *The Sundance Fault: A Newly Recognized Shear Zone at Yucca Mountain, Nevada*. Open-File Report 94-49. Denver, Colorado: U.S. Geological Survey. ACC: NNA.19940128.0119.

Spudich, P.; Fletcher, J.B.; Hellweg, M.; Boatwright, J.; Sullivan, C.; Joyner, W.B.; Hanks, T.C.; Boore, D.M.; McGarr, A.; Baker, L.M.; and Lindh, A.G. 1996. *Earthquake Ground Motions in Extensional Tectonic Regimes*. Open-File Report 96-292. Menlo Park, California: U.S. Geological Survey. TIC: 245279.

Spudich, P.; Fletcher, J.B.; Hellweg, M.; Boatwright, J.; Sullivan, C.; Joyner, W.B.; Hanks, T.C.; Boore, D.M.; McGarr, A.; Baker, L.M.; and Lindh, A.G. 1997. "SEA96—A New Predictive Relation for Earthquake Ground Motions in Extensional Tectonic Regimes." *Seismological Research Letters*, 68, (1), 190-198. El Cerrito, California: Seismological Society of America. TIC: 234935.

Stamatakos, J.A.; Connor, C.B.; Hill, B.E.; Magsino, S.L.; Ferrill, D.A.; Kodama, K.P.; and Justus, P.S. 1997a. "The Carrara Fault in Southwestern Nevada Revealed from Detailed Gravity and Magnetic Results -- Implications for Seismicity, Volcanism and Tectonics Near Yucca Mountain." *AGU 1997 Fall Meeting, December 8-12, 1997, San Francisco, California*. F453. Washington, D.C.: American Geophysical Union. TIC: 246064.

Stamatakos, J.A.; Connor, C.B.; and Martin, R.H. 1997b. "Quaternary Basin Evolution and Basaltic Volcanism of Crater Flat, Nevada, from Detailed Ground Magnetic Surveys of the Little Cones." *Journal of Geology*, 105, 319-330. Chicago, Illinois: University of Chicago. TIC: 245108.

Stewart, J.H. 1988. "Tectonics of the Walker Lane Belt, Western Great Basin: Mesozoic and Cenozoic Deformation in a Zone of Shear." *Metamorphism and Crustal Evolution of the Western United States*. Ernst, W.G., ed. Rubey Volume 7. Pages 683-713. Englewood Cliffs, New Jersey: Prentice-Hall. TIC: 218183.

Stewart, J.H.; Moore, W.J.; and Zietz, I. 1977. "East-West Patterns of Cenozoic Igneous Rocks, Aeromagnetic Anomalies, and Mineral Deposits, Nevada and Utah." *Geological Society of America Bulletin*, 88, 67-77. Boulder, Colorado: Geological Society of America. TIC: 217235.

Stover, C.W. and Coffman, J.L. 1993. *Seismicity of the United States, 1568-1989 (Revised)*. Professional Paper 1527. Denver, Colorado: U.S. Geological Survey. TIC: 234929.

Su, F.; Anderson, J.G.; Brune, J.N.; and Yuehua, Z. 1996. "A Comparison of Direct S-Wave and Coda-Wave Site Amplification Determined from Aftershocks of the Little Skull Mountain Earthquake." *Bulletin of the Seismological Society of America*, 86, (4), 1006-1018. El Cerrito, California: Seismological Society of America. TIC: 236585.

Swadley, WC and Hoover, D.L. 1990. *Geologic Map of the Surficial Deposits of the Yucca Flat Area, Nye County, Nevada*. Miscellaneous Investigations Series Map I-2047. Denver, Colorado: U.S. Geological Survey. ACC: NNA.19940113.0040.

Swadley, WC; Hoover, D.L.; and Rosholt, J.N. 1984. *Preliminary Report on Late Cenozoic Faulting and Stratigraphy in the Vicinity of Yucca Mountain, Nye County, Nevada*. Open-File Report 84-788. Denver, Colorado: U.S. Geological Survey. ACC: NNA.19870519.0104.

Swan, F.H.; Schwartz, D.P.; and Cluff, L.S. 1980. "Recurrence of Moderate to Large Magnitude Earthquakes Produced by Surface Faulting on the Wasatch Fault Zone, Utah." *Bulletin of the Seismological Society of America*, 70, (5), 1431-1462. El Cerrito, California: Seismological Society of America. TIC: 221557.

Swan, F.W.; Wesling, J.R.; Angell, M.M.; Thomas, A.P.; Whitney, J.W.; and Gibson, J.D. 1994. *Evaluation of the Location and Recency of Faulting Near Prospective Surface Facilities in Midway Valley, Yucca Mountain Project, Nye County, Nevada*. Draft. San Francisco, California: Geomatrix Consultants. TIC: 216525.

Takahashi, E. 1980. "Melting Relations of an Alkali-Olivine Basalt to 30 Kbar, and Their Bearing on the Origin of Alkali Basalt Magmas." *Carnegie Institution of Washington, Year Book 79*, 271-276. Washington, D.C.: Carnegie Institution of Washington. TIC: 234936.

Takahashi, E. and Kushiro, I. 1983. "Melting of a Dry Peridotite at High Pressures and Basalt Magma Genesis." *American Mineralogist*, 68, 859-879. Washington, D.C.: Mineralogical Society of America. TIC: 225157.

Taylor, E.M. 1986. *Impact of Time and Climate on Quaternary Soils in the Yucca Mountain Area of the Nevada Test Site*. Master's thesis. Lakewood, Colorado: University of Colorado. TIC: 218287.

Taylor, E.M. 1996. "Quaternary Faulting on the Southern Crater Flat Fault." Chapter 4.10 of *Seismotectonic Framework and Characterization of Faulting at Yucca Mountain, Nevada*. Whitney, J.W., ed. Milestone 3GSH100M. Denver, Colorado: U.S. Geological Survey. TIC: 237980.

Taylor, E.M.; Menges, C.M.; de Fontaine, C.S.; Buesch, D.C.; Mundo, B.O.; and Murray, M. 1996. "Preliminary Results of Paleoseismic Investigations on the Ghost Dance Fault." Chapter 4.5 of *Seismotectonic Framework and Characterization of Faulting at Yucca Mountain, Nevada*. Whitney, J.W., ed. Milestone 3GSH100M. Denver, Colorado: U.S. Geological Survey. TIC: 237980.

Townley, S.D. and Allen, M.W. 1939. "Descriptive Catalog of Earthquakes of the Pacific Coast of the United States 1769 to 1928." *Bulletin of the Seismological Society of America*, 29, (1), 1-297. Berkeley, California: University of California Press. TIC: 239409.

Turrin, B.D.; Champion, D.; and Fleck, R.J. 1991. "⁴⁰Ar/³⁹Ar Age of the Lathrop Wells Volcanic Center, Yucca Mountain, Nevada." *Science*, 253, (5020), 654-657. Washington, D.C.: American Association for the Advancement of Science. TIC: 225167.

Turrin, B.D.; Champion, D.E.; and Fleck, R.J. 1992. "Measuring the Age of the Lathrop Wells Volcanic Center at Yucca Mountain." *Science*, 257, 555-558. Washington, D.C.: American Association for the Advancement of Science. TIC: 225168.

USGS (U.S. Geological Survey) 1988. *Probabilities of Large Earthquakes Occurring in California on the San Andreas Fault*. Open File Report 88-398. Menlo Park, California: U.S. Geological Survey. TIC: 246664.

USGS (U.S. Geological Survey) 2000. *Deterministic Seismic Hazard Analysis of Potential Type I Faults in the Yucca Mountain Area*. Input Transmittal 00288.T. Las Vegas, Nevada: U.S. Geological Survey. ACC: MOL.20000606.0003.

Valentine, G.A. and Groves, K.R. 1996. "Entrainment of Country Rock During Basaltic Eruptions of the Lucero Volcanic Field, New Mexico." *Journal of Geology*, 104, 71-90. Chicago, Illinois: University of Chicago Press. TIC: 246146.

Vaniman, D.T.; Crowe, B.M.; and Gladney, E.S. 1982. "Petrology and Geochemistry of Hawaiite Lavas from Crater Flat, Nevada." *Contributions to Mineralogy and Petrology*, 80, 341-357. Berlin, Germany: Springer-Verlag. TIC: 201799.

Vittori, E.; Michetti, A.M.; Slemmons, D.B.; and Carver, G. 1993. "Style of Recent Surface Deformation at the South End of the Owens Valley Fault Zone, Eastern California." *Abstracts with Programs - Geological Society of America*, 25, 159. Boulder, Colorado: Geological Society of America. TIC: 234944.

von Seggern, D.H. and Brune, J.H. 1994. "Seismicity in the Southern Great Basin, 1868-1992." *Yucca Mountain Tectonics Workshop, January 24-26, 1994*. Draft. [Reno, Nevada]: University of Nevada-Reno, Seismological Laboratory. ACC: MOL.19960318.0596.

von Seggern, D.H. and dePolo, D.M. 1998. *Seismicity in the Vicinity of Yucca Mountain, Nevada, for the Period October 1, 1996, to September 30, 1997*. Milestone Report SP32BTM4. [Reno], Nevada: University of Nevada, Reno, Seismological Laboratory. ACC: MOL.19990503.0147.

Vortman, L.J. 1991. *An Evaluation of the Seismicity of the Nevada Test Site and Vicinity*. SAND86-7006. Albuquerque, New Mexico: Sandia National Laboratories. ACC: NNA.19911118.0084.

Walck, M.C. and Phillips, J.S. 1990. *Two-Dimensional Velocity Models for Paths from Pahute Mesa and Yucca Flat to Yucca Mountain*. SAND88-3033. Albuquerque, New Mexico: Sandia National Laboratories. ACC: NNA.19901005.0051.

Wallace, R.E. 1984. "Patterns and Timing of Late Quaternary Faulting in the Great Basin Province and Relation to Some Regional Tectonic Features." *Journal of Geophysical Research*, 89, (B7), 5763-5769. Washington, D.C.: American Geophysical Union. TIC: 218113.

Wallace, R.E. 1987. "Grouping and Migration of Surface Faulting and Variations in Slip Rates on Faults in the Great Basin Province." *Bulletin of the Seismological Society of America*, 77, (3), 868-876. El Cerrito, California: Seismological Society of America. TIC: 234948.

Wallace, T.C.; Helmberger, D.V.; and Engen, G.R. 1983. "Evidence of Tectonic Release from Underground Nuclear Explosions in Long-Period P Waves." *Bulletin of Seismological Society of America*, 73, (2), 593-613. El Cerrito, California: Seismological Society of America. TIC: 218114.

Wallace, T.C.; Helmberger, D.V.; and Engen, G.R. 1985. "Evidence of Tectonic Release from Underground Nuclear Explosions in Long-Period S Waves." *Bulletin of the Seismological Society of America*, 75, (1), 157-174. El Cerrito, California: Seismological Society of America. TIC: 218116.

Walter, W.R. 1993. "Source Parameters of the June 29, 1992 Little Skull Mountain Earthquake from Complete Regional Waveforms at a Single Station." *Geophysical Research Letters*, 20, (5), 403-406. Washington, D.C.: American Geophysical Union. TIC: 236889.

Weichert, D.H. 1980. "Estimation of the Earthquake Recurrence Parameters for Unequal Observation Periods for Different Magnitudes." *Bulletin of the Seismological Society of America*, 70, (4), 1337-1346. El Cerrito, California: Seismological Society of America. TIC: 237642.

Wells, D.L. and Coppersmith, K.J. 1993. "Likelihood of Surface Rupture as a Function of Magnitude." *Seismological Research Letters*, 64, (1), 54. El Cerrito, California: Seismological Society of America. TIC: 243234.

Wells, D.L. and Coppersmith, K.J. 1994. "New Empirical Relationships Among Magnitude, Rupture Length, Rupture Width, Rupture Area, and Surface Displacement." *Bulletin of the Seismological Society of America*, 84, (4), 974-1002. El Cerrito, California: Seismological Society of America. TIC: 226273.

Wells, S.G.; Crowe, B.M.; McFadden, L.D.; Turrin, B.D.; Champion, D.E.; and Fleck, R.J. 1992. "Measuring the Age of the Lathrop Wells Volcanic Center at Yucca Mountain." *Science*, 257, 556-558. Washington, D.C.: American Association for the Advancement of Science. TIC: 231868.

Wells, S.G.; McFadden, L.D.; Renault, C.E.; and Crowe, B.M. 1990. "Geomorphic Assessment of Late Quaternary Volcanism in the Yucca Mountain Area, Southern Nevada: Implications for the Proposed High-Level Radioactive Waste Repository." *Geology*, 18, 549-553. Boulder, Colorado: Geological Society of America. TIC: 218564.

Wesling, J.R.; Bullard, T.F.; Swan, F.H.; Perman, R.C.; Angell, M.M.; and Gibson, J.D. 1992. *Preliminary Mapping of Surficial Geology of Midway Valley Yucca Mountain Project, Nye County, Nevada Interim Data Report*. SAND91-0607. Albuquerque, New Mexico: Sandia National Laboratories. ACC: NNA.19920410.0053.

Wesnousky, S.G.; Scholz, C.H.; Shimazaki, K.; and Matsuda, T. 1983. "Earthquake Frequency Distribution and the Mechanics of Faulting." *Journal of Geophysical Research*, 88, (B11), 9331-9340. Washington, D.C.: American Geophysical Union. TIC: 241700.

Whitney, J.W., ed. 1996. *Seismotectonic Framework and Characterization of Faulting at Yucca Mountain, Nevada*. Milestone 3GSH100M. Denver, Colorado: U.S. Geological Survey. ACC: MOL.19970129.0041; MOL.19970129.0042; MOL.19970129.0043; MOL.19970129.0044; MOL.19970129.0045; MOL.19970129.0046; MOL.19970129.0047; MOL.19970129.0048; MOL.19970129.0049; MOL.19970129.0050; MOL.19970129.0051; MOL.19970129.0052; MOL.19970129.0053; MOL.19970129.0054; MOL.19970129.0055; MOL.19970129.0056; MOL.19970129.0057; MOL.19970129.0058; MOL.19970129.0059; MOL.19970129.0060; MOL.19970129.0061; MOL.19970129.0062.

Whitney, J.W.; Menges, C.M.; Berger, D.L.; and de Fontaine, C. 1996. "Comparison of Late Tertiary and Quaternary Slip Rates on the Stagecoach Road and Windy Wash Faults, Yucca Mountain, Nevada." *Abstracts with Programs - Geological Society of America*, 28, (7), A-194. Boulder, Colorado: Geological Society of America. TIC: 234931.

Whitney, J.W.; Simonds, F.W.; Shroba, R.R.; and Murray, M. 1996. "Quaternary Faulting on the Windy Wash Fault." Chapter 4.9 of *Seismotectonic Framework and Characterization of Faulting at Yucca Mountain, Nevada*. Whitney, J.W., ed. Milestone 3GSH100M. Denver, Colorado: U.S. Geological Survey. TIC: 237980.

Whitney, J.W. and Taylor, E.M., eds. 1996. "Quaternary Paleoseismology and Stratigraphy of the Yucca Mountain Site Area." Chapter 4 of *Seismotectonic Framework and Characterization of Faulting at Yucca Mountain, Nevada*. Whitney, J.W., ed. Milestone 3GSH100M. Denver, Colorado: U.S. Geological Survey. TIC: 237980.

Whitney, J.W.; Taylor, E.M.; and Wesling, J.R. 1996. "Quaternary Mapping and Stratigraphy." Chapter 4.1 of *Seismotectonic Framework and Characterization of Faulting at Yucca Mountain, Nevada*. Whitney, J.W., ed. Milestone 3GSH100M. Denver, Colorado: U.S. Geological Survey. TIC: 237980.

Wilson, L. and Head, J.W., III 1981. "Ascent and Eruption of Basaltic Magma on the Earth and Moon." *Journal of Geophysical Research*, 86, (B4), 2971-3001. Washington, D.C.: American Geophysical Union. TIC: 225185.

Wong, I.; Kelson, K.; Olig, S.; Kolbe, T.; Hemphill-Haley, M.; Bott, J.; Green, R.; Kanakari, H.; Sawyer, J.; Silva, W.; Stark, C.; Haraden, C.; Fenton, C.; Unruh, J.; Gardner, J.; Reneau, S.; and House, L. 1995. *Seismic Hazards Evaluation of the Los Alamos National Laboratory*. Volume 1. Oakland, California: Woodward-Clyde Federal Services. TIC: 247191.

Wong, I.; Pezzopane, S.K.; Menges, C.M.; Green, R.K.; and Quittmeyer, R.C. 1996. "Probabilistic Seismic Hazard Analysis of the Exploratory Studies Facility at Yucca Mountain, Nevada." *Proceedings of the Topical Meeting on Methods of Seismic Hazards Evaluation, FOCUS '95, September 18-20, 1995, Las Vegas, Nevada*. Pages 51-63. La Grange Park, Illinois: American Nuclear Society. TIC: 232628.

Wong, I.G. and Stepp, C. 1998. *Probabilistic Seismic Hazard Analyses for Fault Displacement and Vibratory Ground Motion at Yucca Mountain, Nevada*. Milestone SP32IM3, September 23, 1998. Three volumes. Oakland, California: U.S. Geological Survey. ACC: MOL.19981207.0393.

YMP (Yucca Mountain Site Characterization Project) 1997a. *Methodology to Assess Fault Displacement and Vibratory Ground Motion Hazards at Yucca Mountain*. Topical Report YMP/TR-002-NP, Rev. 1. Las Vegas, Nevada: Yucca Mountain Site Characterization Office. ACC: MOL.19971016.0777.

YMP (Yucca Mountain Site Characterization Project) 1997b. *Preclosure Seismic Design Methodology for a Geologic Repository at Yucca Mountain*. Topical Report YMP/TR-003-NP, Rev. 2. Las Vegas, Nevada: Yucca Mountain Site Characterization Office. ACC: MOL.19971009.0412.

YMP (Yucca Mountain Site Characterization Project) 1999. *Monitored Geologic Repository Requirements Document*. YMP/CM-0025, Rev. 3, DCN 01. Las Vegas, Nevada: Yucca Mountain Site Characterization Office. ACC: MOL.19990429.0228.

Yokoyama, I. and de la Cruz-Reyna, S. 1990. "Precursory Earthquakes of the 1943 Eruption of Paricutin Volcano, Michoacan, Mexico." *Journal of Volcanology and Geothermal Research*, 44, 265-281. Amsterdam, The Netherlands: Elsevier Science Publishers. TIC: 234990.

Youngs, R.R. and Coppersmith, K.J. 1985. "Implications of Fault Slip Rates and Earthquake Recurrence Models to Probabilistic Seismic Hazard Estimates." *Bulletin of the Seismological Society of America*, 75, (4), 939-964. El Cerrito, California: Seismological Society of America. TIC: 237426.

Yount, J.C.; Shroba, R.R.; McMasters, C.R.; Huckins, H.E.; and Rodriguez, E.A. 1987. *Trench Logs from a Strand of the Rock Valley Fault System, Nevada Test Site, Nye County, Nevada*. Miscellaneous Field Studies Map MF-1824. Reston, Virginia: U.S. Geological Survey. TIC: 203093.

Zhang, P.; Ellis, M.; Slemmons, D.B.; and Mao, F. 1990. "Right-Lateral Displacements and the Holocene Slip Rate Associated with Prehistoric Earthquakes Along the Southern Panamint Valley Fault Zone: Implications for Southern Basin and Range Tectonics and Coastal California Deformation." *Journal of Geophysical Research*, 95, (B4), 4857-4872. Washington, D.C.: American Geophysical Union. TIC: 237567.

Zhao, L-S. and Helmberger, D.V. 1994. "Source Estimation from Broadband Regional Seismograms." *Bulletin of Seismological Society of America*, 84, 91-104. El Cerrito, California: Seismological Society of America. TIC: 239122.

Zreda, M.G.; Phillips, F.M.; Kubik, P.W.; Sharma, P.; and Elmore, D. 1993. "Cosmogenic (36)Cl Dating for a Young Basaltic Eruption Complex, Lathrop Wells, Nevada." *Geology*, 21, 57-60. Boulder, Colorado: Geological Society of America. TIC: 225192.

12.5.2 Codes, Standards, Regulations, and Procedures

64 FR 8640. Disposal of High-Level Radioactive Wastes in a Proposed Geologic Repository at Yucca Mountain, Nevada. Proposed rule 10 CFR 63. Readily available.

Regulatory Guide 1.165. 1997. *Identification and Characterization of Seismic Sources and Determination of Safe Shutdown Earthquake Ground Motion*. Washington, D.C.: U.S. Nuclear Regulatory Commission. Readily available.

12.5.3 Source Data, Listed by Data Tracking Number

LB960808314212.003. Borehole Seismic Recordings VSP and Velocity Survey from Boreholes: NRG-6, WT-2, RF-4, RF-7A, SD-12, G-2, G-4. Submittal date: 08/30/1996.

MO0003YMP98126.001. Quaternary and Pliocene Basalt. Submittal date: 03/02/2000.

MO0004YMP00024.000. Fault Displacement Hazard Assessment. Submittal date: 04/18/2000.

MO0004YMP00026.000. Borehole Locations for Vertical Seismic Profile Surveys. Submittal date: 04/14/2000.

MO0005SEPECINT.001. Estimated Completeness Intervals for the Southern Great Basin. Submittal date: 05/24/2000.

MO0005SMALLEQD.002. Small Earthquake Data. Submittal date: 05/30/2000.

MO0006YMP00025.000. Seismographs Stations in the Southwestern United States. Submittal date: 06/28/2000.

MO0006YMP00062.000. Seismograph Stations Operating in the Southwestern United States, 1980 and 1996. Submittal date: 06/26/2000.

MO0006YMP98125.002. Historical Earthquake Epicenters Within 300 Kilometers of Yucca Mountain. Submittal date: 06/26/2000.

MO0006YMP98136.002. Historical Seismicity Within 100 Kilometers of Yucca Mountain. Submittal date: 06/28/2000.

MO0006YMP98137.002. Seismic Regions Within 300 Kilometers of Yucca Mountain. Submittal date: 06/28/2000.

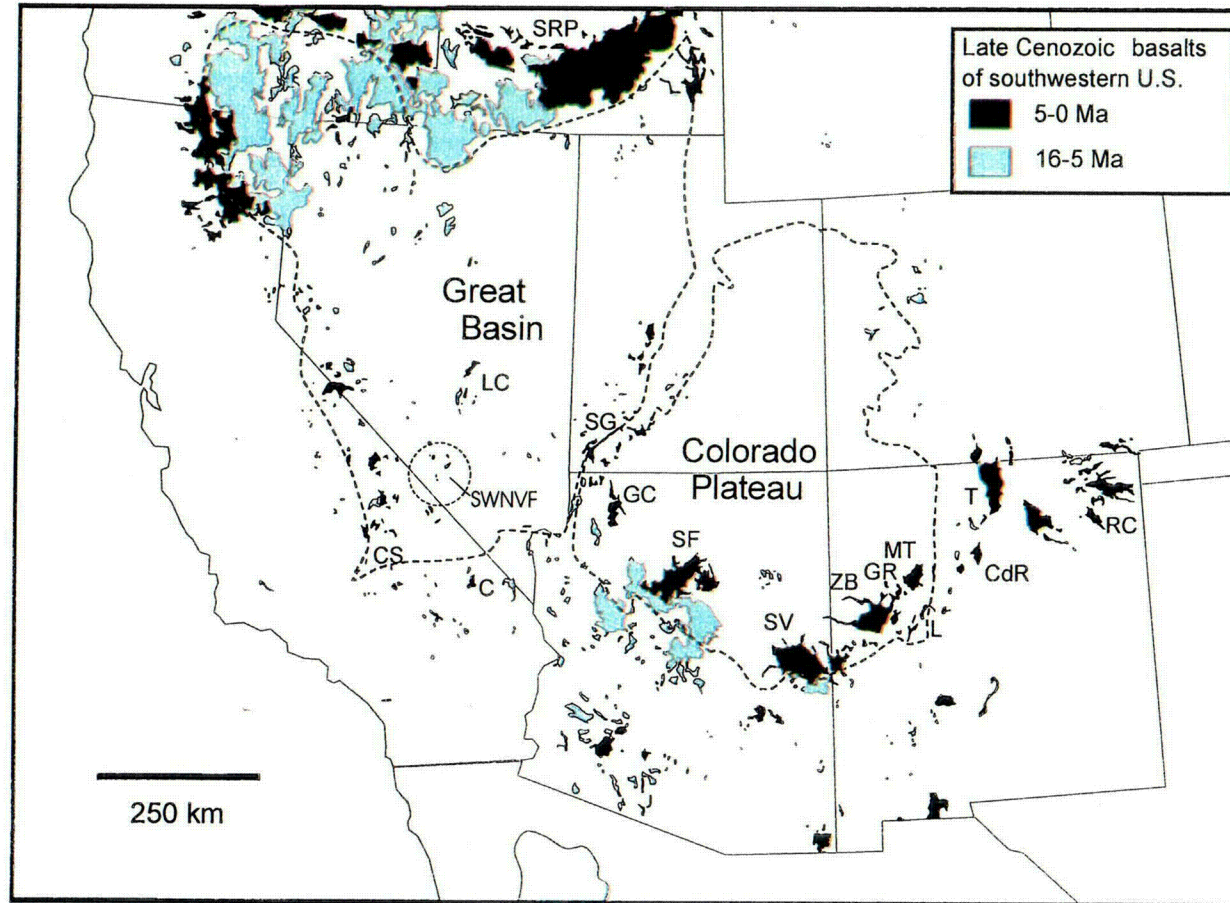
MO0008SEPFMECH.001. Focal Mechanisms for Earthquakes of Local Magnitude Greater than 3.5 in the Vicinity of Yucca Mountain from 1987 to 1997. Submittal date: 08/29/2000.

MO0009YMP98131.002. Miocene and Post-Miocene Basaltic Vent Locations in the Yucca Mountain Region. Submittal date: 09/08/2000.

MO970483117412.002. Seismicity in the Vicinity of Yucca Mountain, Nevada for the Period October 1, 1995 to September 30, 1996. Submittal date: 04/02/1997.

MO98PRECLOSURE.000. Design Event Spectra Based on the Results of Probabilistic Seismic Hazard Analyses for Yucca Mountain and a Velocity Profile for the Repository Block to Support Development of Ground Motion Design Inputs. Submittal date: 02/20/1998.

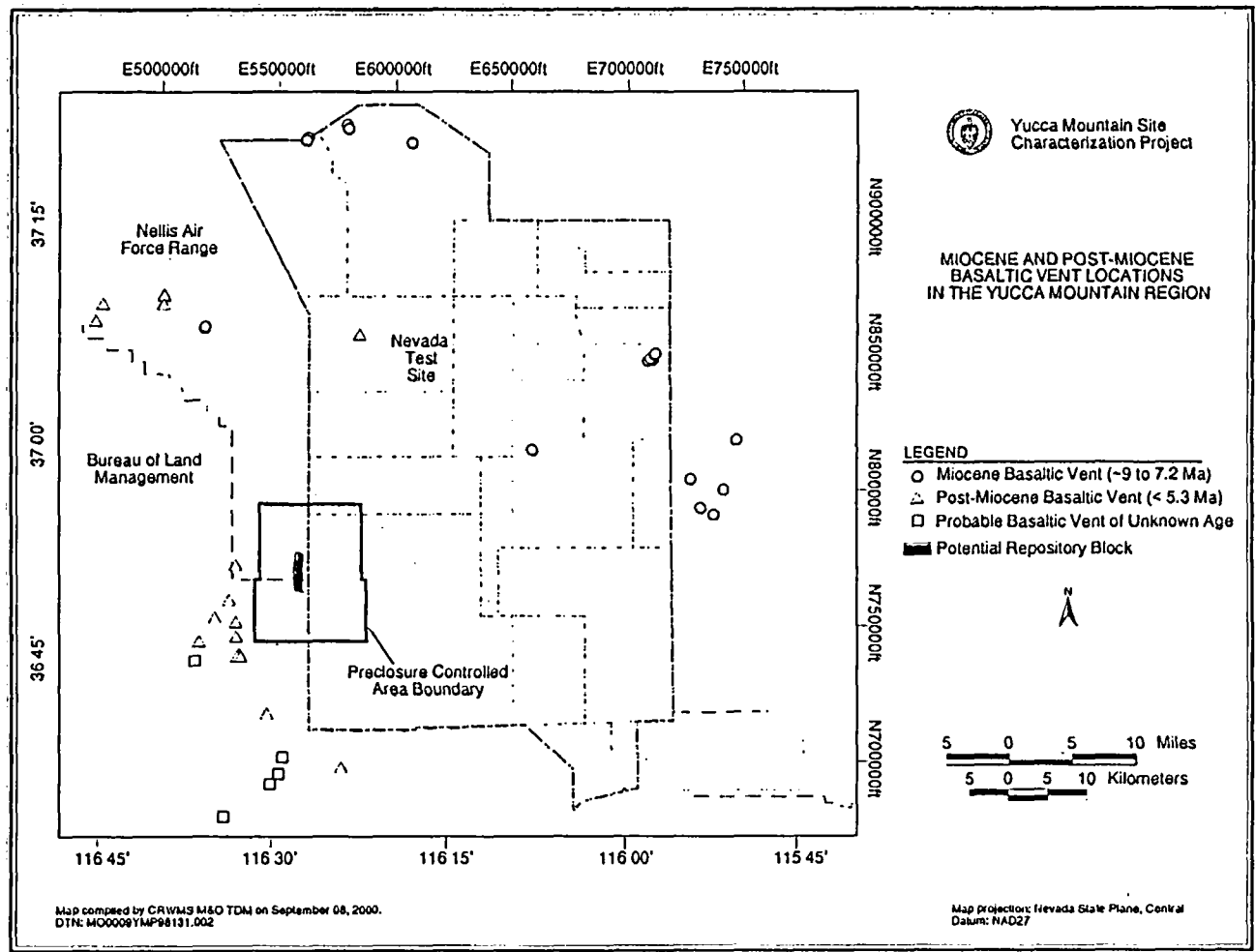
INTENTIONALLY LEFT BLANK



Source: Fitton et al. (1991, Figures 3 and 4)

NOTE: The distribution of volcanic rocks of silicic and intermediate composition is not shown. The location of the Southwestern Nevada Volcanic Field (SWNVF), within which Yucca Mountain is located, is indicated as a circle of 50 km radius centered on Yucca Mountain. The circle encompasses post-5 Ma basaltic centers of the Yucca Mountain region. Other labeled volcanic fields are: C: Cima; CdR: Cerros Del Rio; CS: Coso; GC: Grand Canyon; GR: Grants Ridge; LC: Lunar Crater; L: Lucero; MT: Mount Taylor; RC: Raton-Clayton; SF: San Francisco; SG: St. George; SRP: Snake River Plain; SV: Springerville; T: Taos; ZB: Zuni-Bandera.

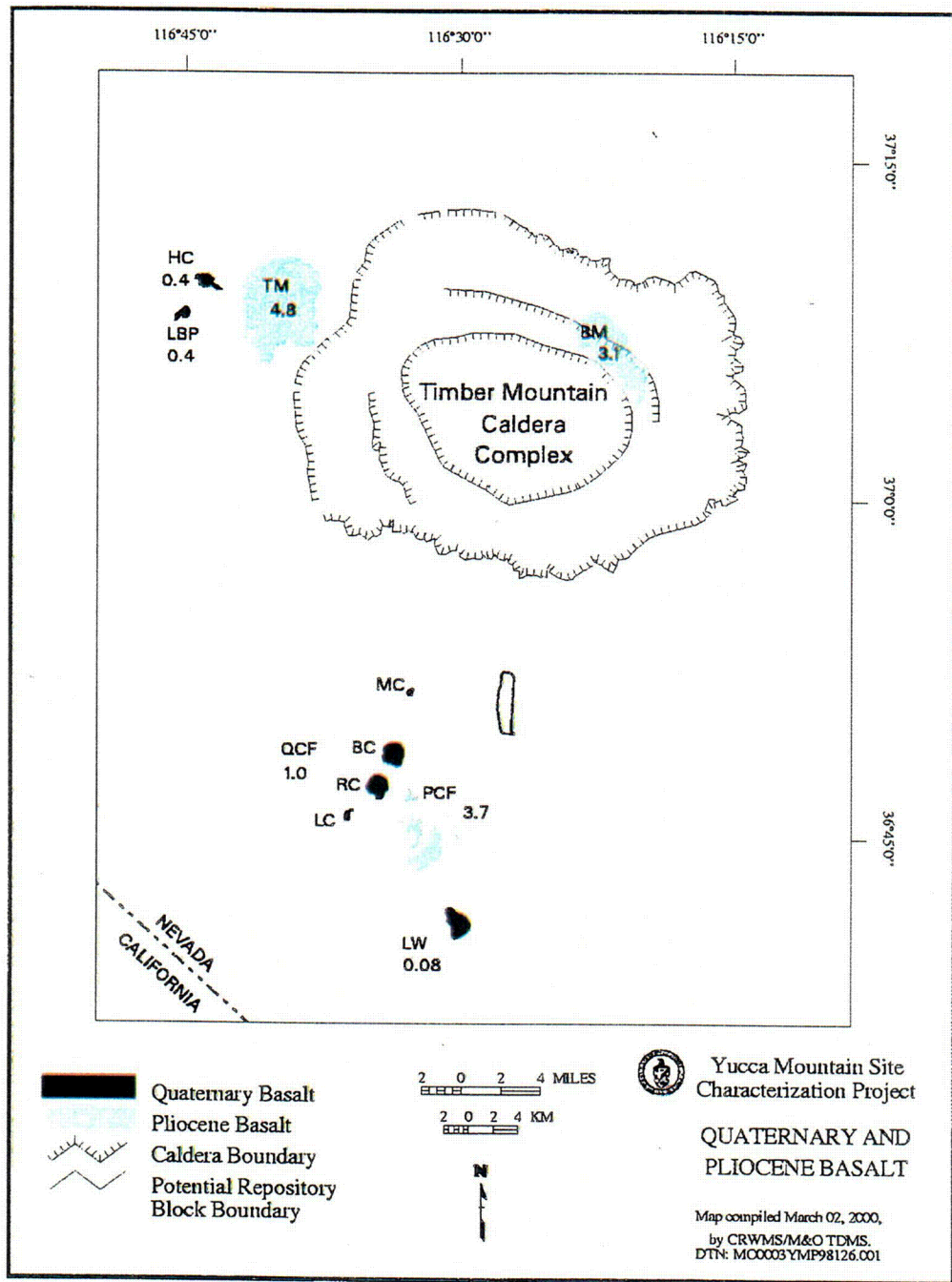
Figure 12.2-1. Distribution of Late Cenozoic Basaltic Rocks in the Western United States



39-06 CDR 123.81EDEC
12.2-2 CDR 31EDEC-001 CN 01

Source: Modified from CRWMS M&O (1998c, Figure 3.14) and Reamer (1999, p. 98, Figure 7)

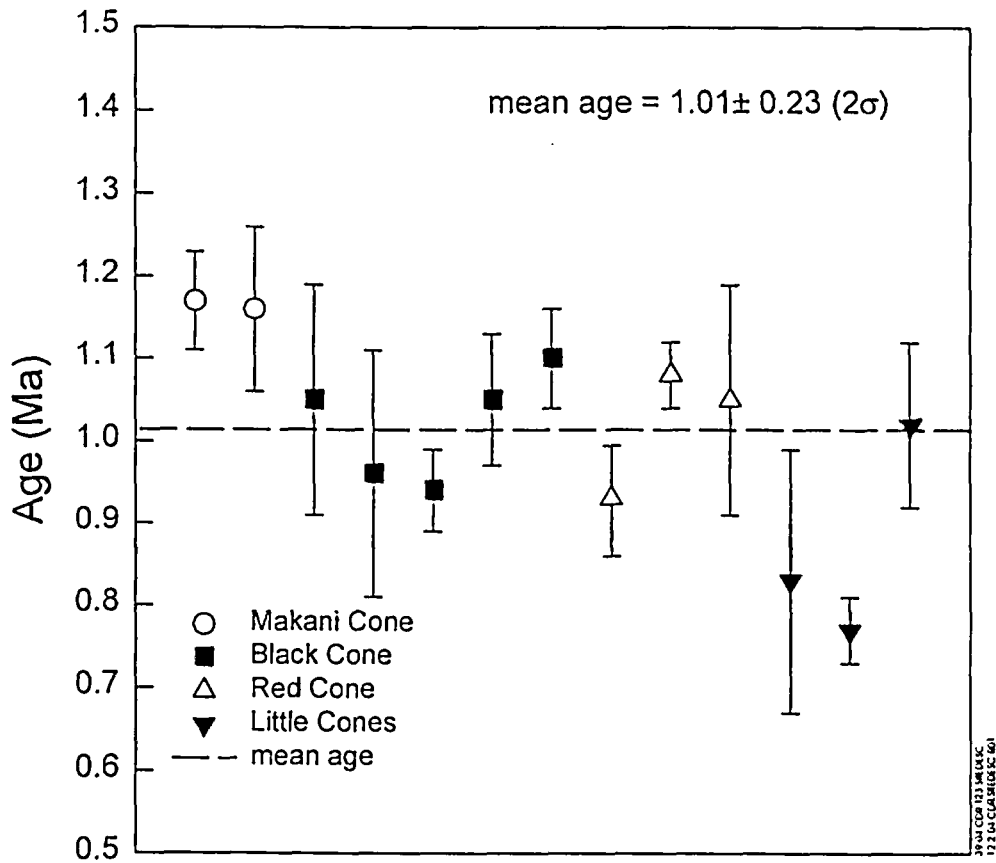
Figure 12.2-2. Location of Miocene and Post-Miocene Basaltic Vents, as Well as Probable Basaltic Vents of Unknown Age, in the Yucca Mountain Region



Source: CRWMS M&O (2000a, Figure 3)

NOTE: Numbers by each volcanic center indicate approximate age in millions of years. TM: Thirsty Mesa; PCF: Pliocene Crater Flat; BM: Buckboard Mesa; QCF: Quaternary Crater Flat (MC: Makani Cone; BC: Black Cone; RC: Red Cone; LC: Little Cones); HC: Hidden Cone; LBP: Little Black Peak; LW: Lathrop Wells.

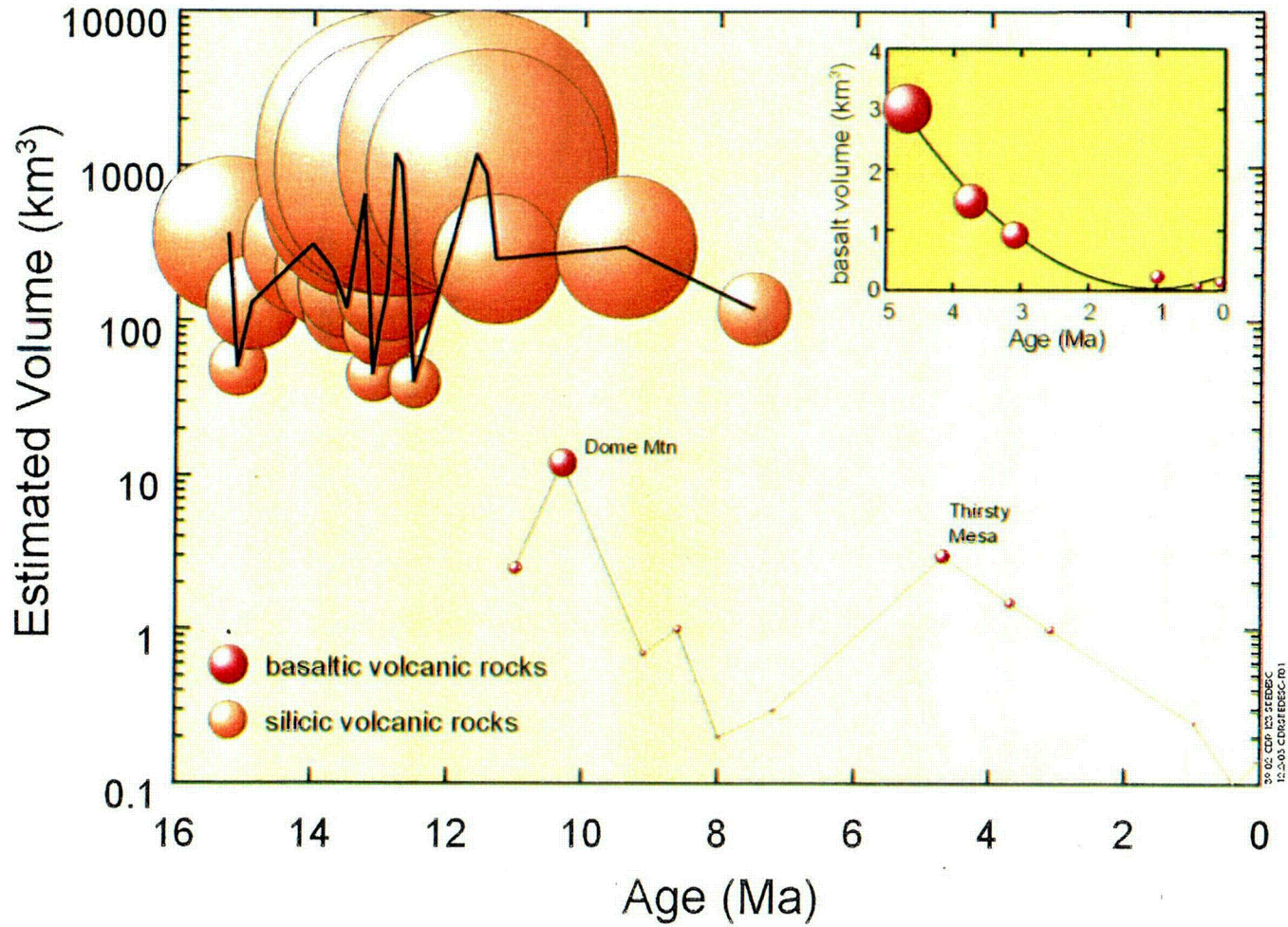
Figure 12.2-3. Post-Miocene Volcanoes in the Yucca Mountain Region



Source: CRWMS M&O (1998e, Table 2.B, p. 2-13)

NOTE: Left to right on the figure corresponds to north to south for the location of basalt centers within Crater Flat.

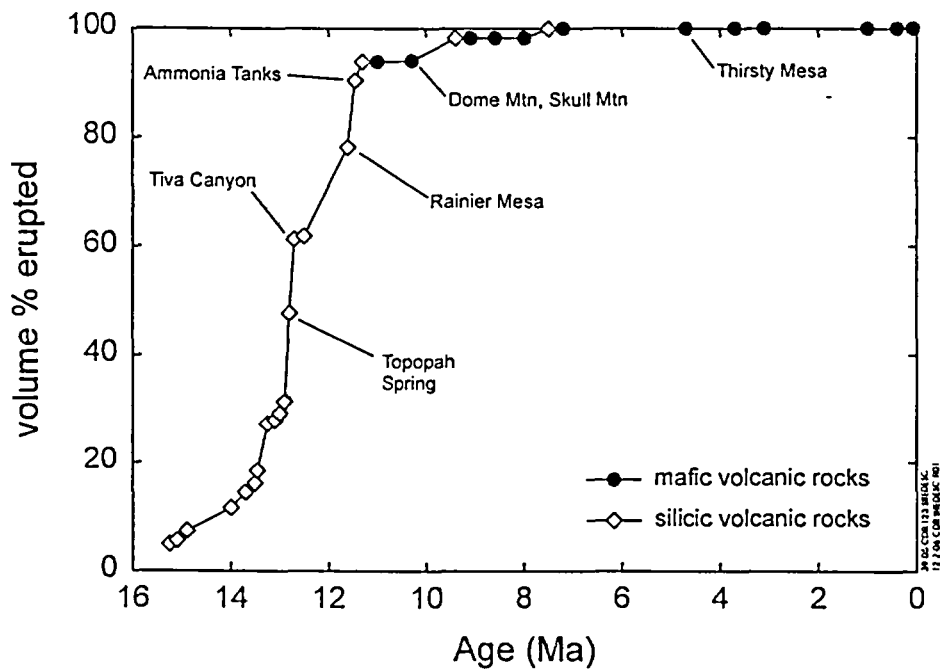
Figure 12.2-4. Argon-40/Argon-39 Ages from Quaternary Basalt Centers of Crater Flat



Source: Data are from Sawyer et al. (1994, Table 1) and CRWMS M&O (1998h, Tables 3.1 and 6.12).

NOTE: Inset shows volume versus age of the post-Miocene basalts of the Yucca Mountain region. Area symbols are proportional to the estimated volume of each eruptive unit.

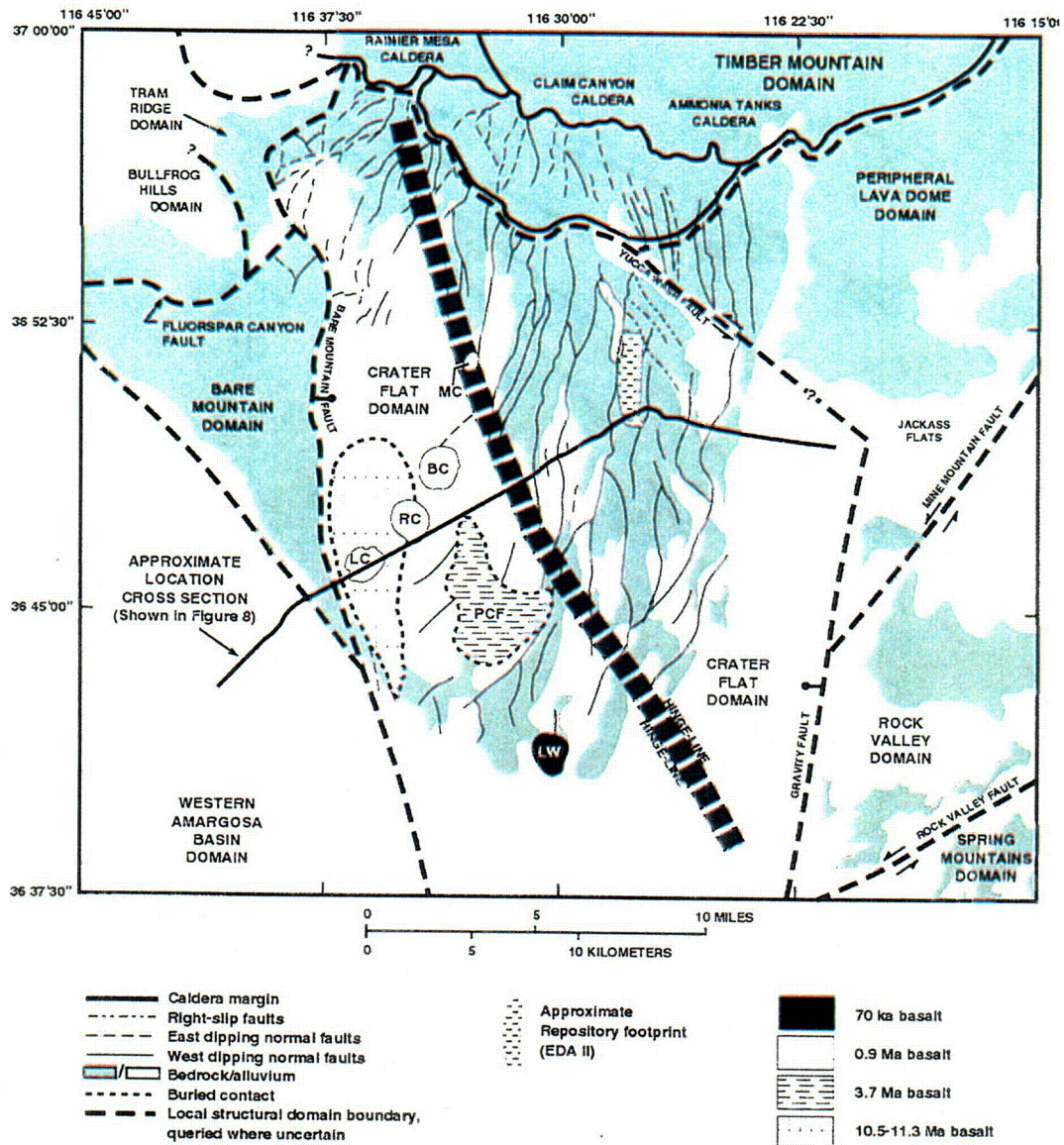
Figure 12.2-5. Estimated Volume versus Age for Volcanic Rocks of the Southwestern Nevada Volcanic Field



Source: Data are from Sawyer et al. (1994, Table 1) and CRWMS M&O (1998h, Tables 3.1 and 6.12).

NOTE: Most of the volume of the southwestern Nevada volcanic field consists of early erupted silicic volcanic rocks. Compare with Figure 12.2-5.

Figure 12.2-6. Percent Cumulative Volume Erupted versus Age of Volcanic Units of the Southwestern Nevada Volcanic Field

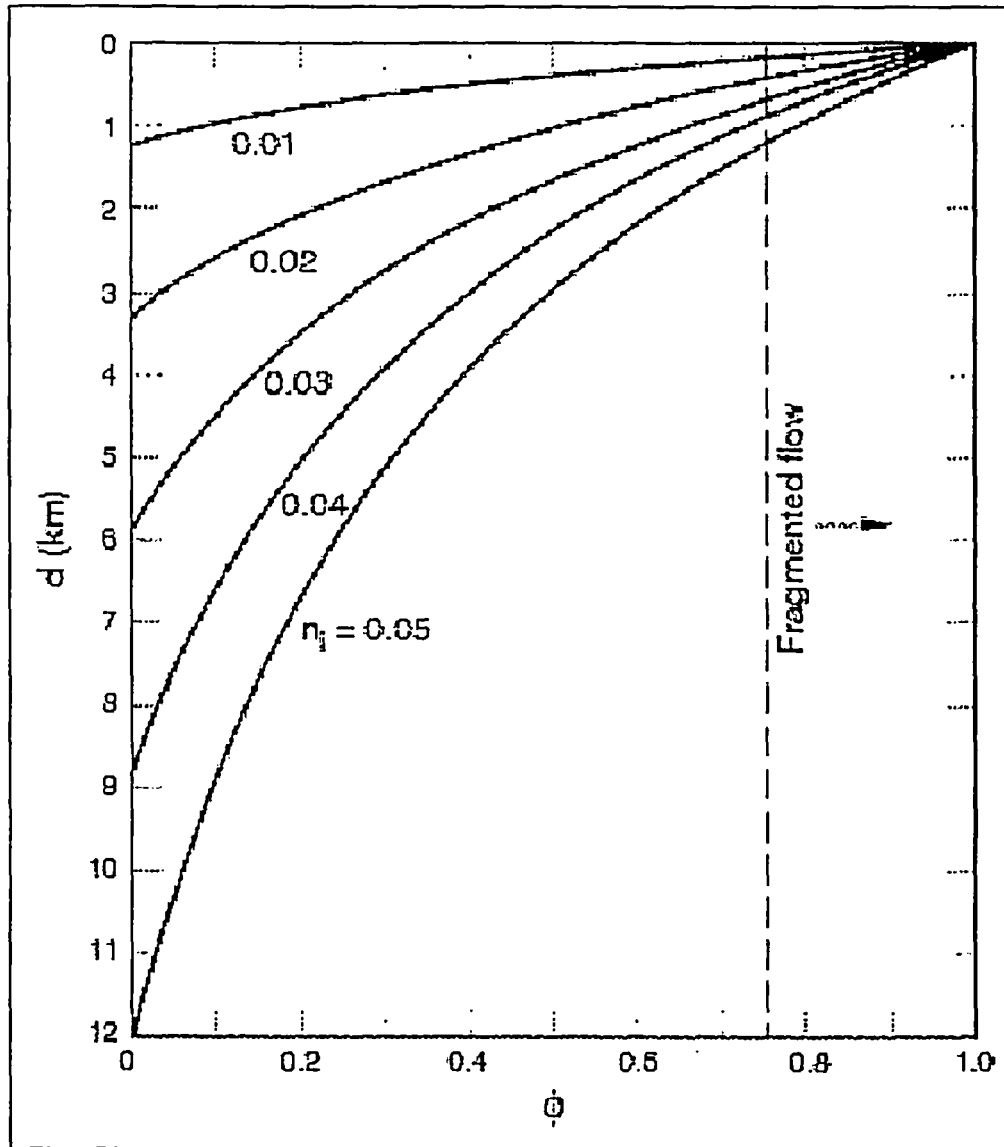


12.2-07.DOC.SITEDESC-R01

Source: After CRWMS M&O (2000a, Figure 7)

NOTES: Basalts of different ages are shown in relation to basin structure.
 MC = Makani Cone, BC = Black Cone, RC = Red Cone, LC = Little Cones, LW = Lathrop Wells Cone,
 PCF = Pliocene Crater Flat, EDA II = Enhanced Design Alternative II

Figure 12.2-7. Local Structural Domains and Domain Boundaries of the Yucca Mountain Region, and Internal Structures of the Crater Flat Basin and Selected Parts of Adjacent Domains

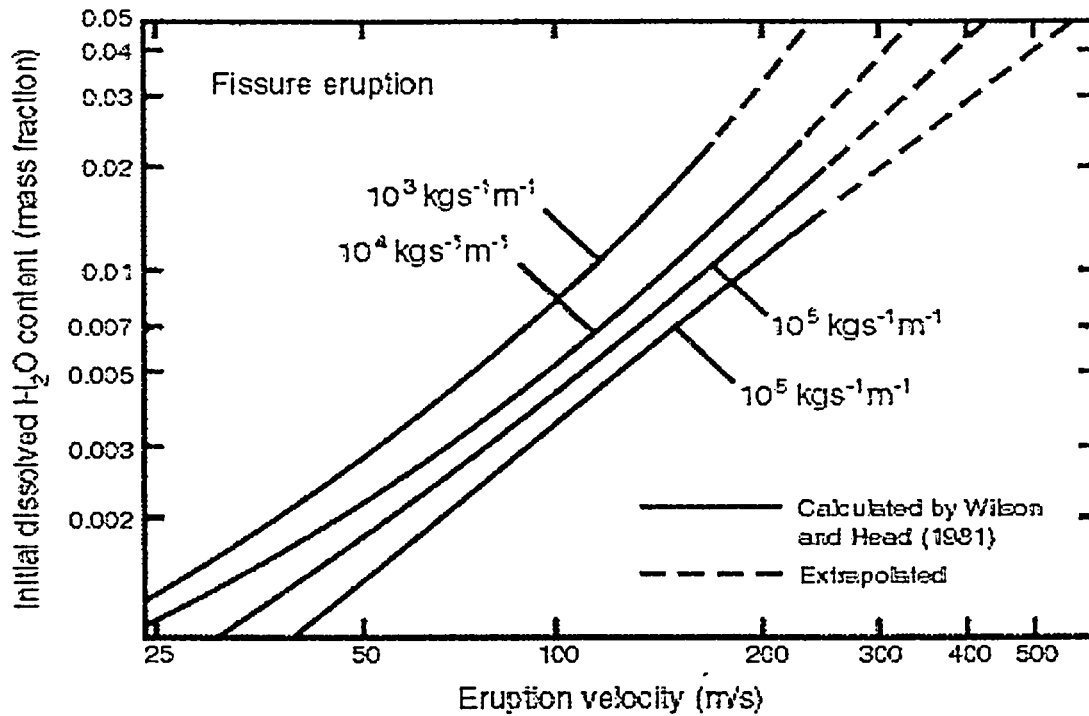


12.2-08.CDR.SITEDESC-R01

Source: After CRWMS M&O (2000b, Figure 2)

NOTES: Calculations assume $\rho_c = 2,000 \text{ kg/m}^3$, $\rho_m = 3,000 \text{ kg/m}^3$, $T = 1,300 \text{ K}$, and $R = 461 \text{ J/kg/K}$. The dashed line defines a critical gas volume fraction of 0.75, which is assumed to be the threshold for fragmentation of the magma. ρ_c = wall-rock density; ρ_m = melt density (no bubbles); T = temperature; R = gas constant for water, n_i = initial dissolved water content.

Figure 12.2-8. Variation of Gas Volume Fraction with Depth

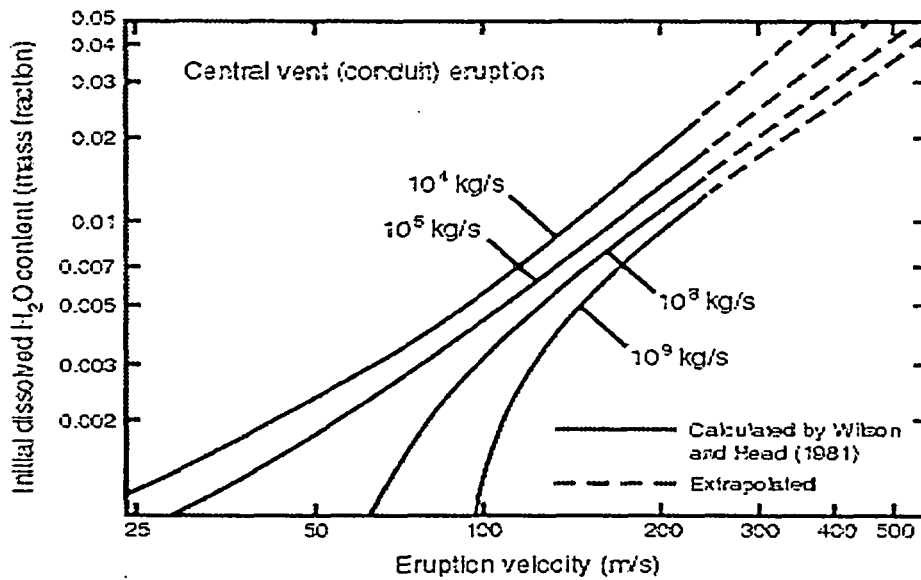


12.2-09.DOC.SITEDESC-R01

Source: CRWMS M&O (2000b, Figure 3)

NOTE: Solid curves show values calculated by Wilson and Head (1981), whereas dashed lines are graphical extrapolations to include the range of initial volatile contents of concern for Yucca Mountain. Calculations assume homogeneous flow and lithostatic pressure in the rising magma column.

Figure 12.2-9. Variation of Eruption Velocity with Initial Dissolved Water Content for Various Mass Discharge Rates along a Fissure

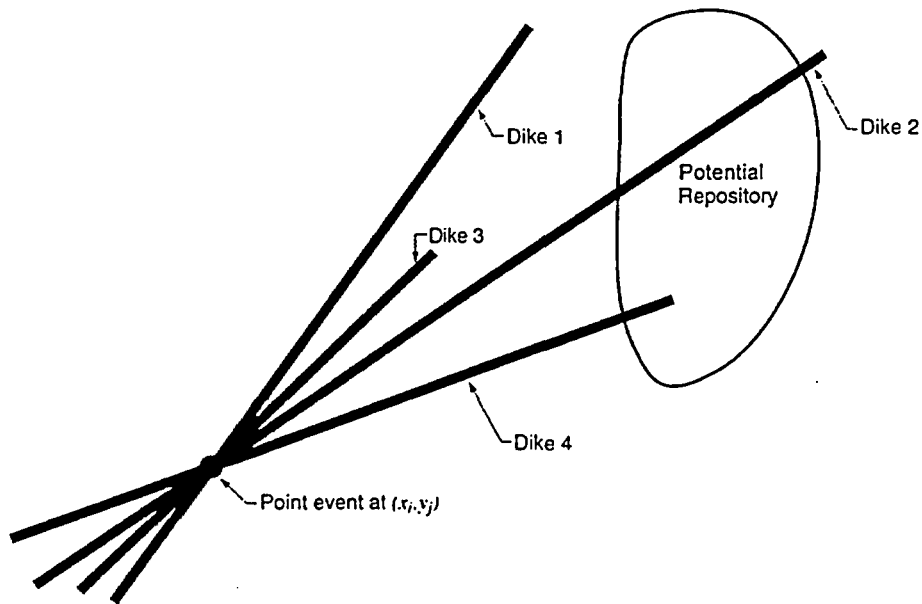


12.2-10.DOC.SITEDESC-R01

Source: CRWMS M&O (2000b, Figure 4)

NOTE: Solid curves show values calculated by Wilson and Head (1981), whereas dashed lines are graphical extrapolations to include the range of initial volatile contents of concern for Yucca Mountain. Calculations assume homogeneous flow and lithostatic pressure in the rising magma column.

Figure 12.2-10. Variation of Eruption Velocity with Initial Dissolved Water Content for Various Mass Discharge Rates from a Circular Conduit

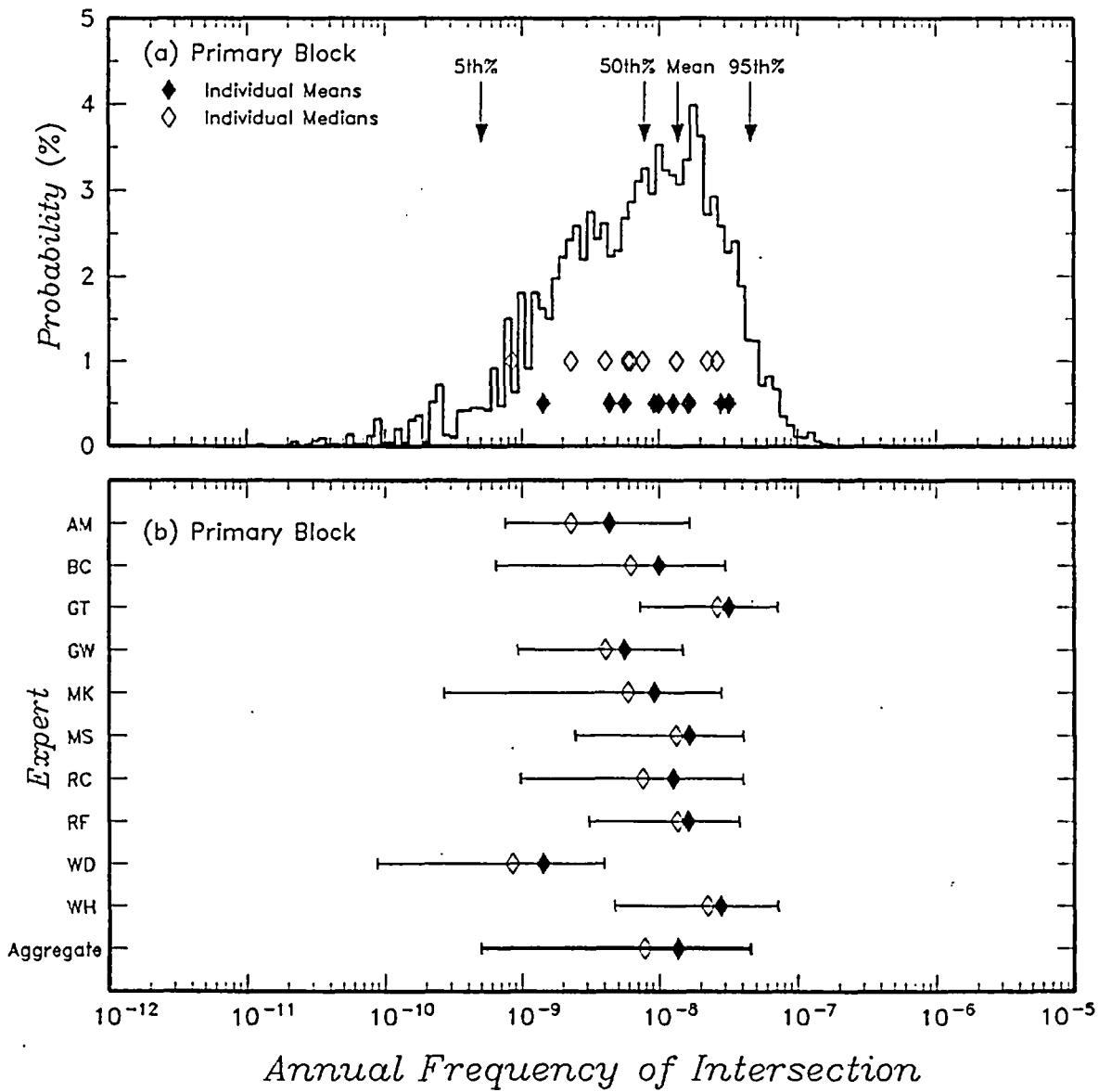


12.2-11.DOC.SITEDESC-R01

Source: CRWMS M&O (2000a, Figure 10)

NOTE: The models for specifying the spatial and temporal distributions for volcanic events define the occurrence rate for events at a point. Associated with this point "event" is a dike system of uncertain length and azimuth. The distance from the point event to the end of the dike system, d , and the azimuth of the dike system, f , determine whether or not a volcanic event occurring at a point will result in an intersection of the repository. Distributions for d and f were specified by the probabilistic volcanic hazard analysis experts.

Figure 12.2-11. Schematic Illustrating Procedure for Computing the Frequency of Intersection of the Potential Repository by a Volcanic Event



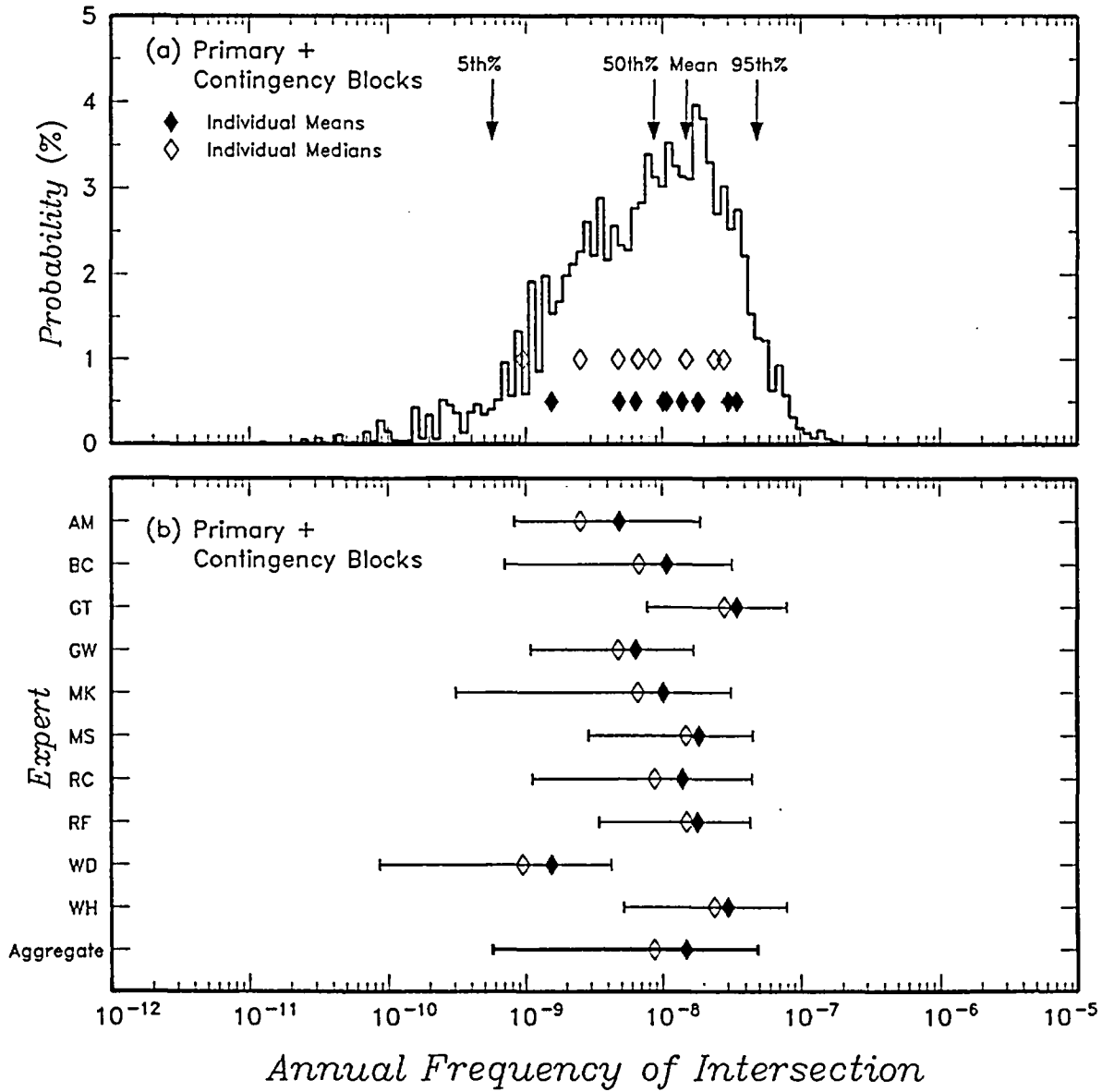
12.2-12.DOC.SITEDESC-R01

Source: CRWMS M&O (2000a, Figure 20)

NOTES: (a) Aggregate distribution and median and means for individual probabilistic volcanic hazard analysis expert hazard models for the primary block case. (b) Range for 5th and 95th percentiles for results from individual probabilistic volcanic hazard analysis expert hazard models compared to range for aggregate distribution for the primary block case.

Two-letter code indicates initials of experts identified in Table 12.2-6.

Figure 12.2-12. Annual Frequency of Intersecting the Potential Repository Footprint for the Primary Block Case



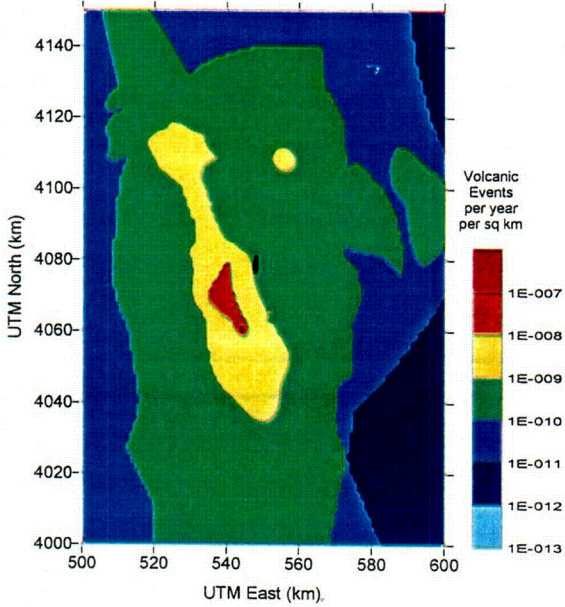
12.2-13.DOC.SITEDESC-R01

Source: CRWMS M&O (2000a, Figure 21)

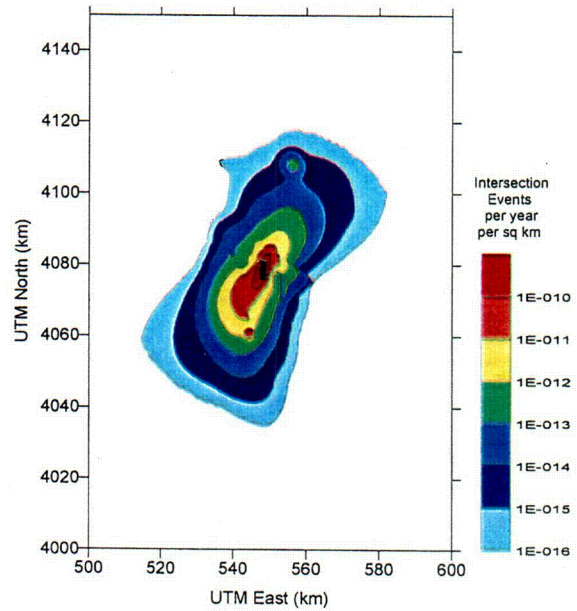
NOTES: (a) Aggregate distribution and median and means for individual probabilistic volcanic hazard analysis expert interpretations for the primary + contingency blocks case. (b) Range for 5th and 95th percentiles for results from individual probabilistic volcanic hazard analysis expert interpretations compared to range for aggregate distribution for the primary + contingency blocks case. Two-letter code indicates initials of experts identified in Table 12.2-6.

Figure 12.2-13. Annual Frequency of Intersecting the Potential Repository Footprint for the Primary Plus Contingency Blocks Case

(a) Mean Volcanic Event Frequency



(b) Spatial Disaggregation of Intersection Frequency



12.2-14.DOC.SITEDESC-R01

Source: CRWMS M&O (2000a, Figure 17)

NOTE: The maps represent the mean results averaged over 10 experts and over each expert's logic tree (CRWMS M&O 1996, Appendix E). Black area in center of maps is the potential repository footprint.

Figure 12.2-14. Spatial Distribution of Volcanic Hazard Defined by the Probabilistic Volcanic Hazard Analysis Expert Panel

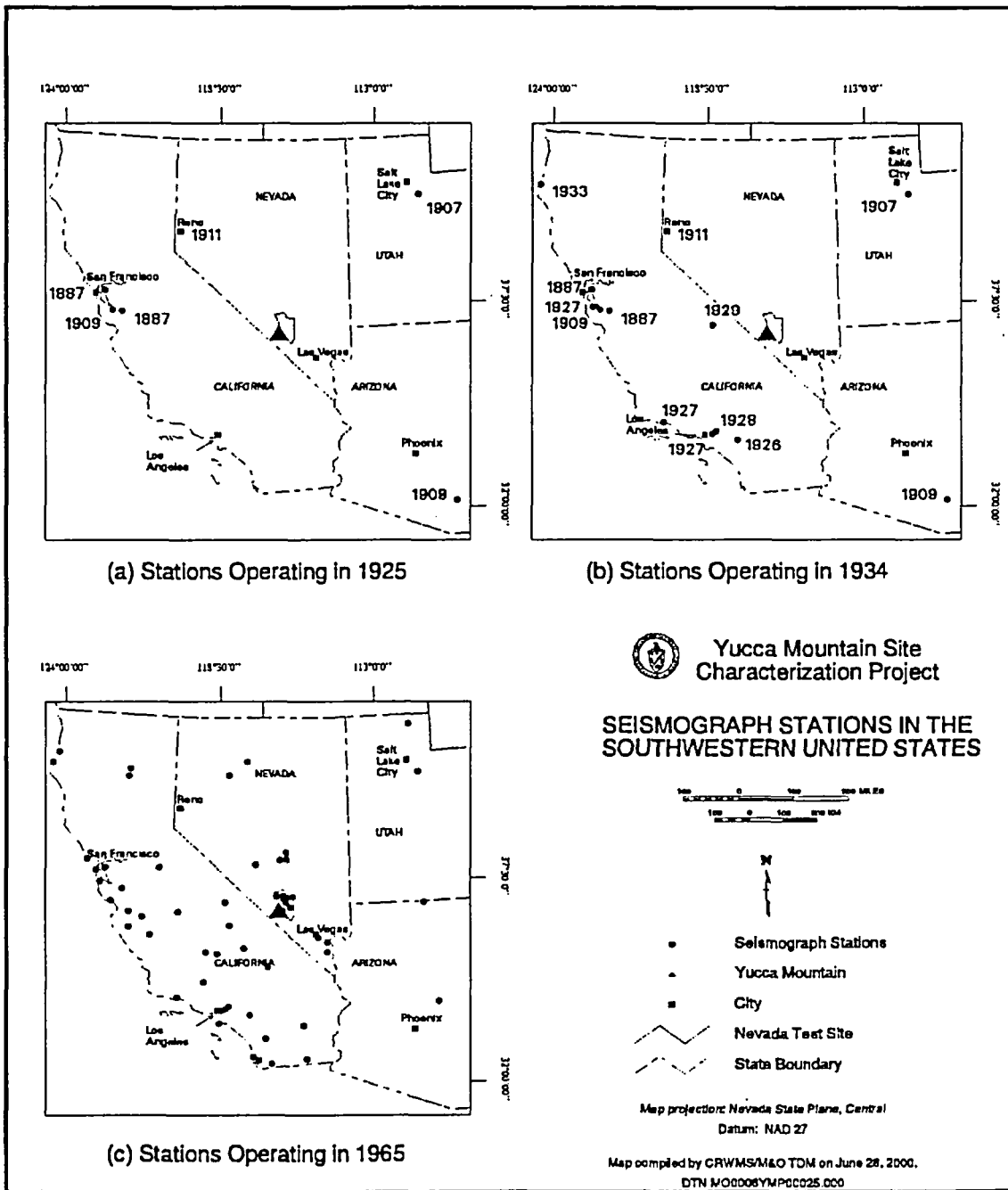
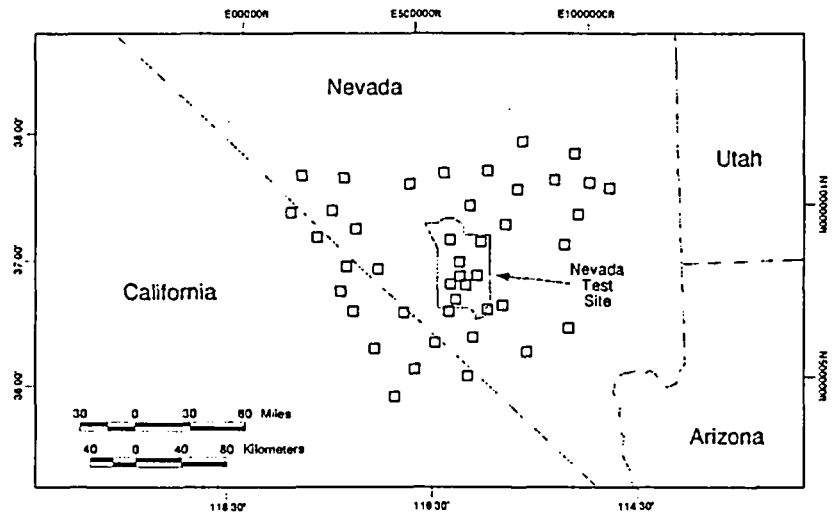
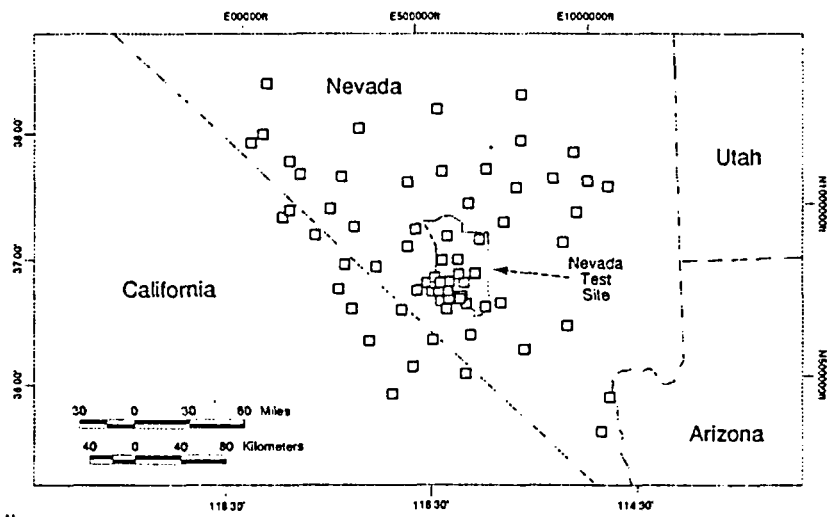


Figure 12.3-1. Seismograph Stations Operating in the Western United States



Seismograph Stations Operating in 1980



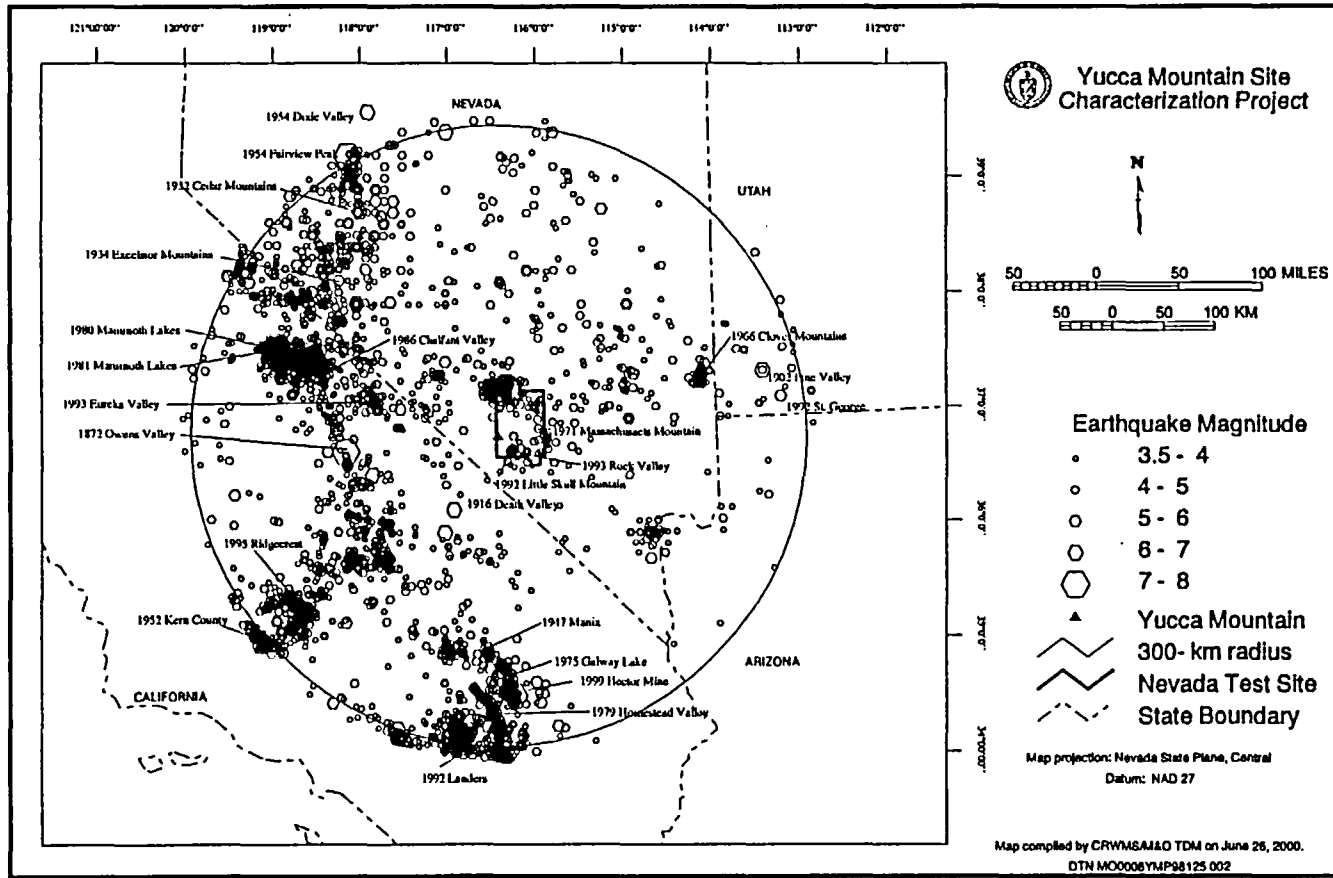
Seismograph Stations Operating in 1996

Map compiled by CRWMS/M&O TDM on June 22, 2000
DTN M00006YMP00062.000

Map projection: Nevada State Plane, Central
Datum: NAD27

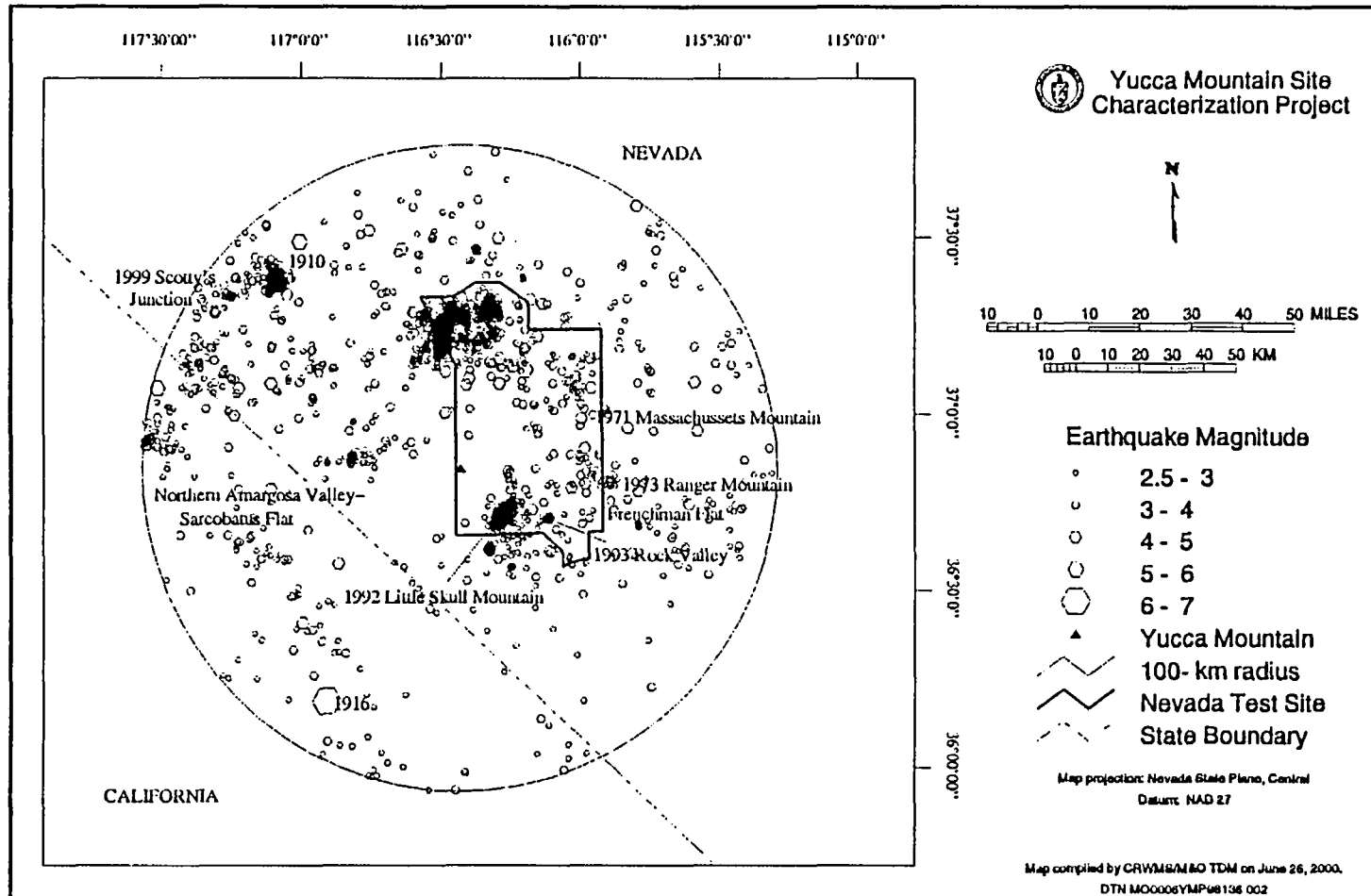
12.3-02 CRW/REDESC 001

Figure 12.3-2. Seismograph Stations Operating in the Southern Great Basin



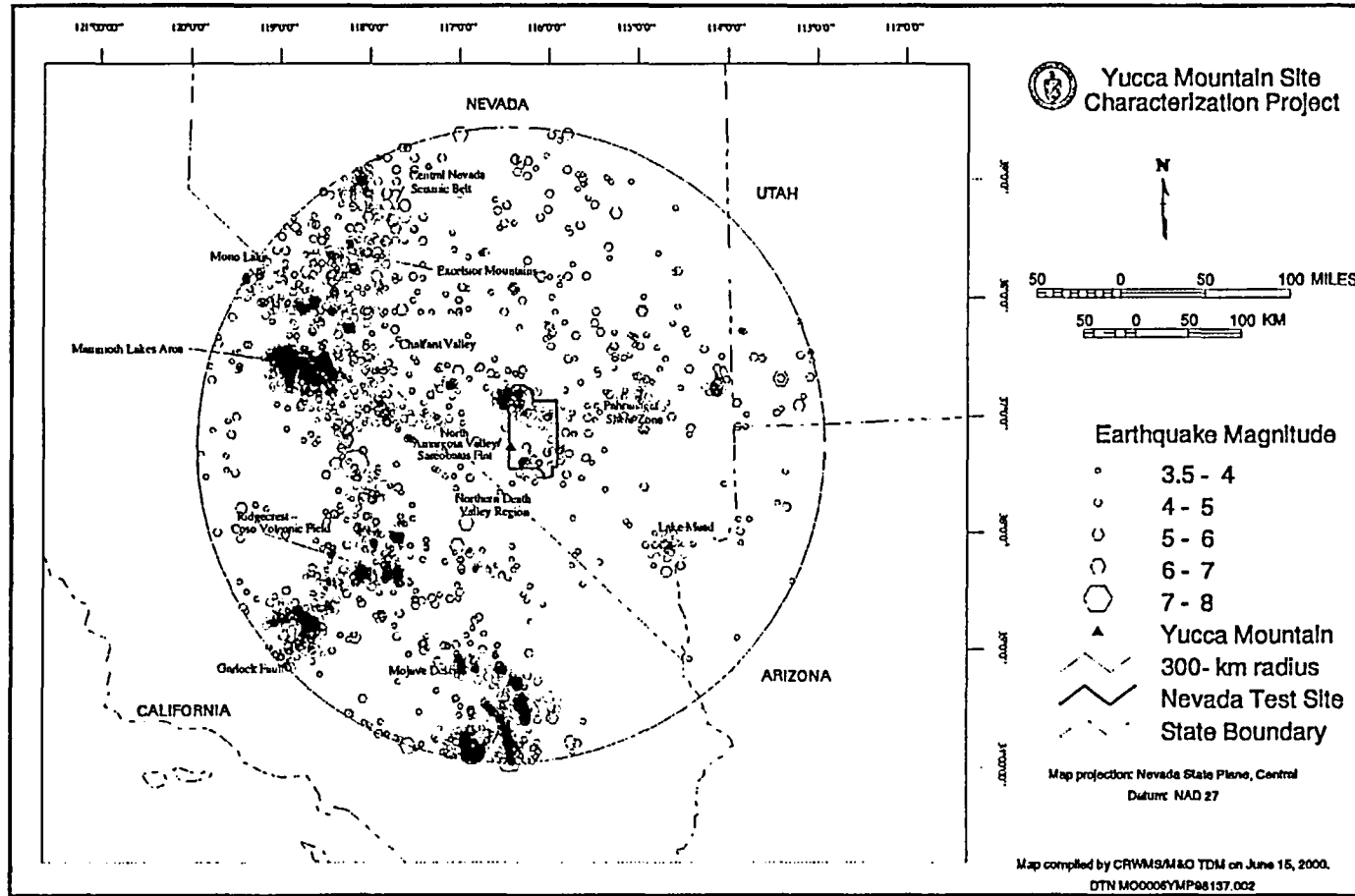
NOTE: Shown are earthquakes from 1868 to 1998. In addition, earthquakes of the 1999 Hector Mine sequence are shown. Significant earthquakes are labeled with years of occurrence.

Figure 12.3-3. Historical Earthquake Epicenters within 300 Kilometers of Yucca Mountain



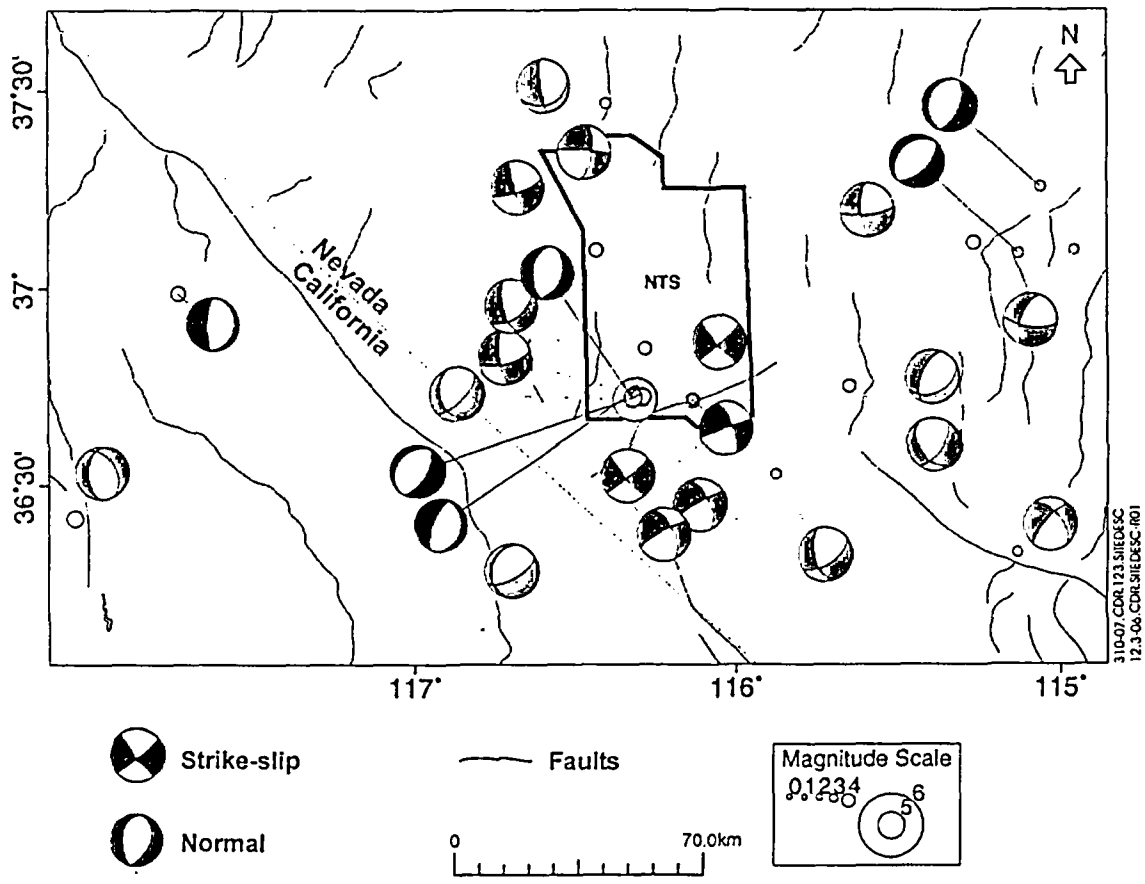
NOTE: Shown are earthquakes from 1904 to 1998. Significant earthquakes or earthquake sequences are shown with years of occurrence.

Figure 12.3-4. Historical Seismicity within 100 Kilometers of Yucca Mountain



NOTE: Shown are earthquakes from 1868 to 1998. In addition, earthquakes of the 1999 Hector Mine sequence are shown.

Figure 12.3-5. Regions of Seismicity within 300 Kilometers of Yucca Mountain

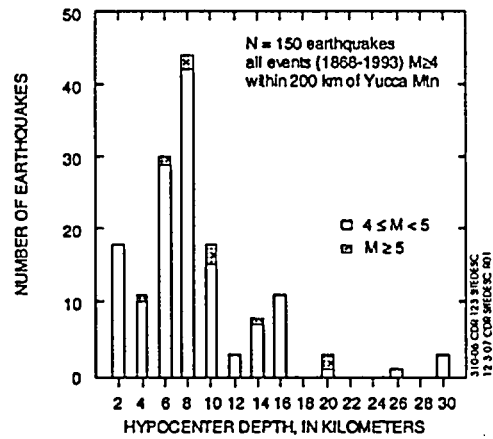
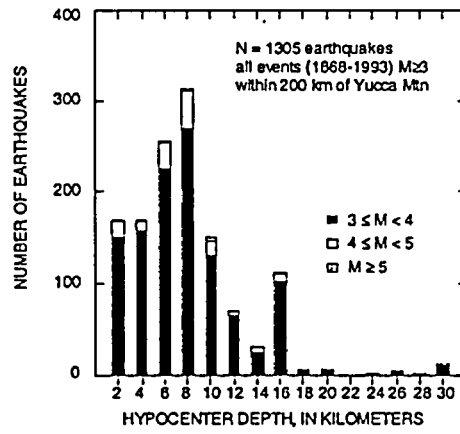
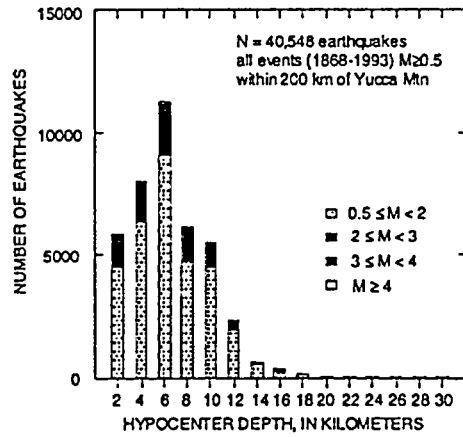


316-07.CDR.123.SI.EDESC
12.3-06.CDR.SI.EDESC-R01

FIG1-23E8.CDR
12.3-07.CDR.SI.EDESC-R01

DTN: MO0008SEPFMECH.001

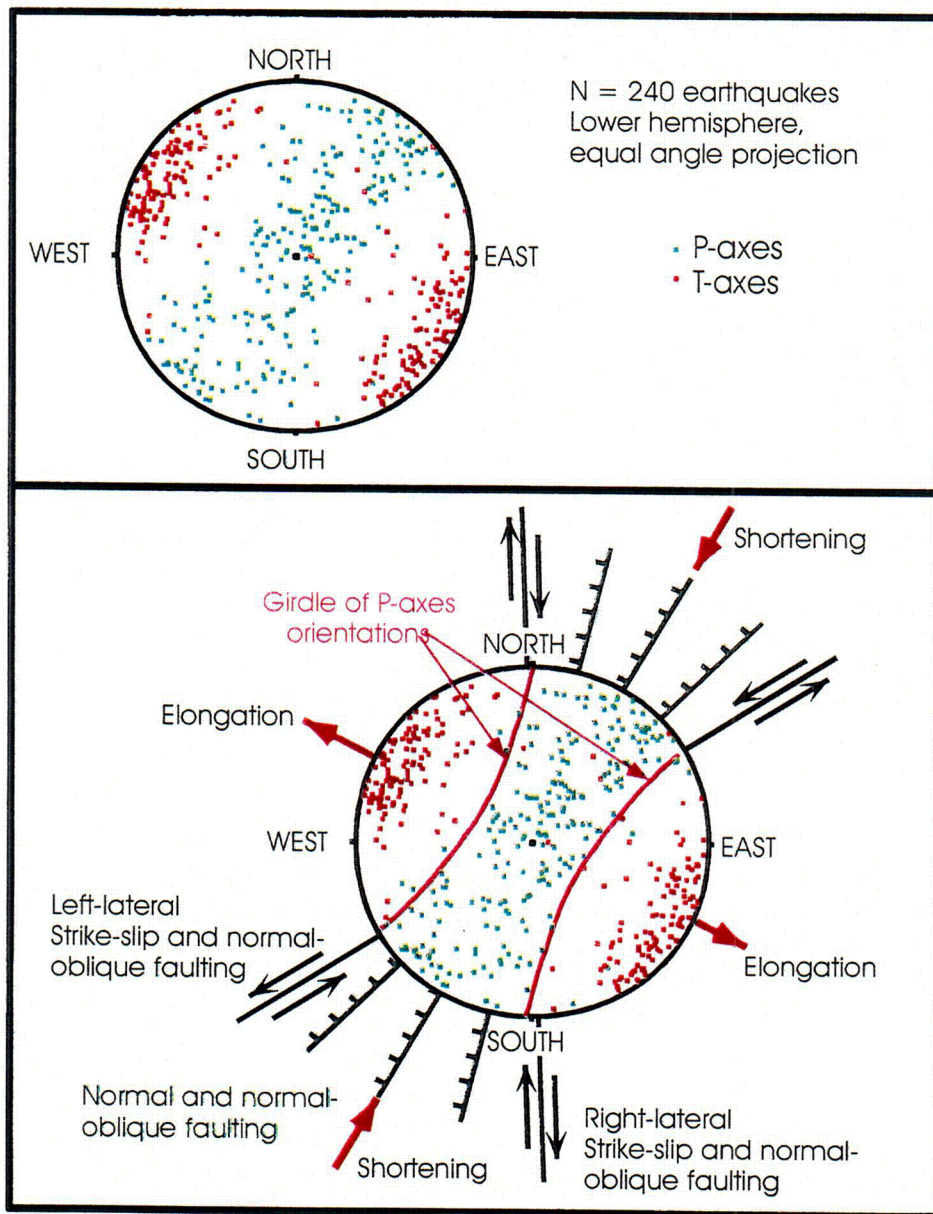
Figure 12.3-6. Focal Mechanisms for Earthquakes of M_L Greater Than 3.5 in the Vicinity of Yucca Mountain from 1987 to 1997



Source: Pezzopane, Bufe et al. (1996, Figure 7-6)

NOTE: Top graph: earthquakes with $M \geq 0.5$; center graph: earthquakes $M \geq 3.0$; bottom graph: earthquakes $M \geq 4.0$.

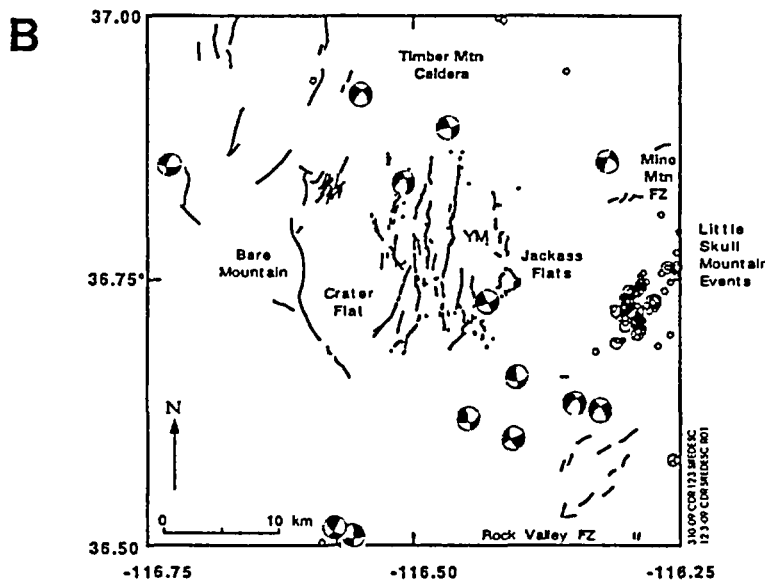
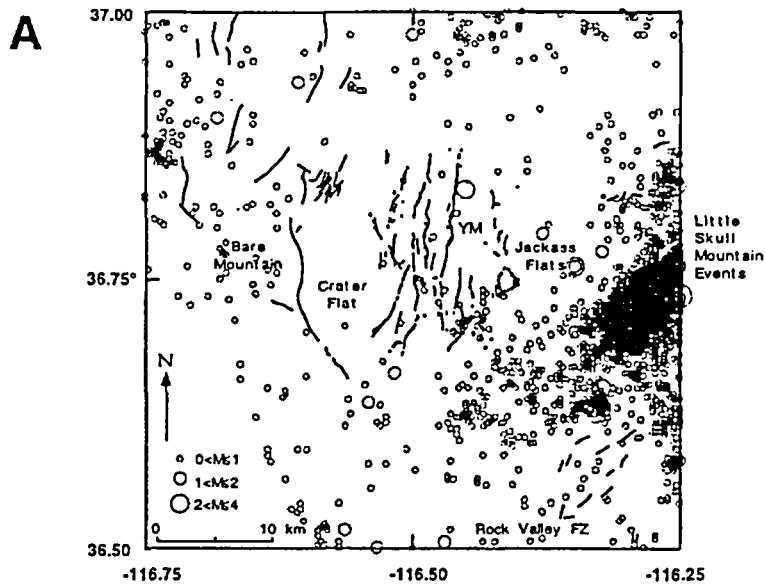
Figure 12.3-7. Focal Depth Distribution of Earthquakes (1868 to 1993) within 200 Kilometers of Yucca Mountain



Source: Pezzopane, Bufe et al. (1996, Figure 7-5)

NOTE: Lower hemisphere equal angle projection of the principal stress axes. Upper plot shows the data, and the lower plot shows the inferred orientations of faulting consistent with the stress orientations. Maximum relative compression (P) axes form a girdle from vertical to northeast-southwest orientations, whereas extensional (minimum relative compression) (T) axes trend northwest-southeast.

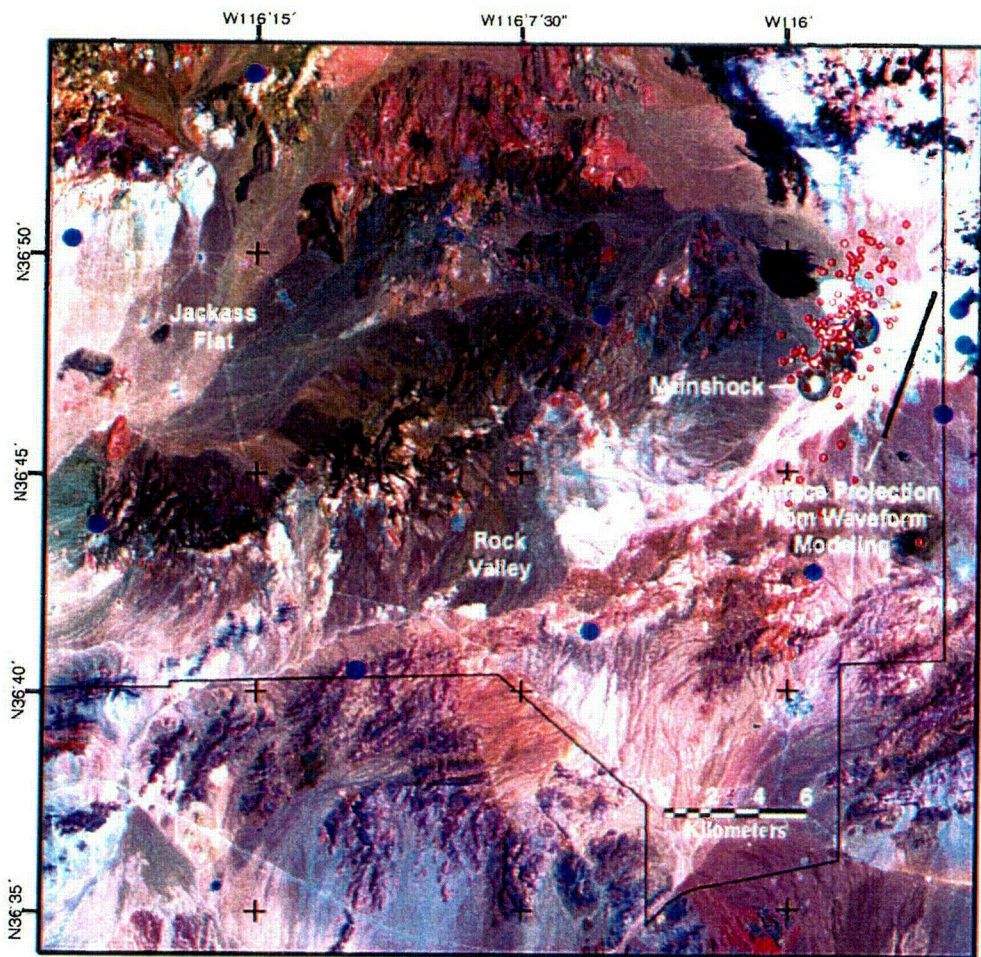
Figure 12.3-8. Principal Stress Axes from Focal Mechanisms of Southern Great Basin Earthquakes



Source: Pezzopane, Bufe et al. (1996, Figure 7-4)

NOTE: Epicenters are represented by open circles. Focal mechanisms show lower hemisphere projections.

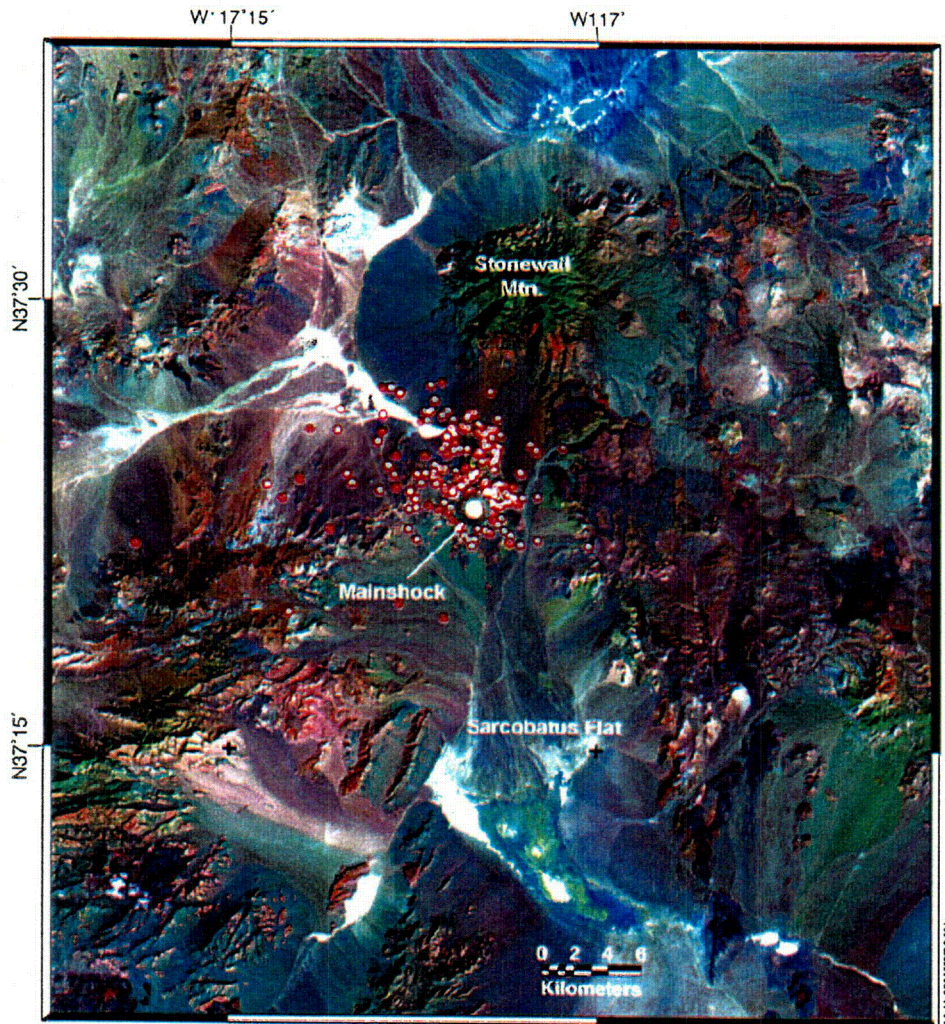
Figure 12.3-9. Epicenters and Focal Mechanisms of Earthquakes and Known or Suspected Quaternary Faults near Yucca Mountain



Source: Smith, K. (2000)

NOTE: Filled blue circles show locations of permanent and temporary seismic stations. Larger earthquakes are shown by white circles. Small red circles represent foreshocks and aftershocks. The solid line shows the southeastern boundary of the Nevada Test Site.

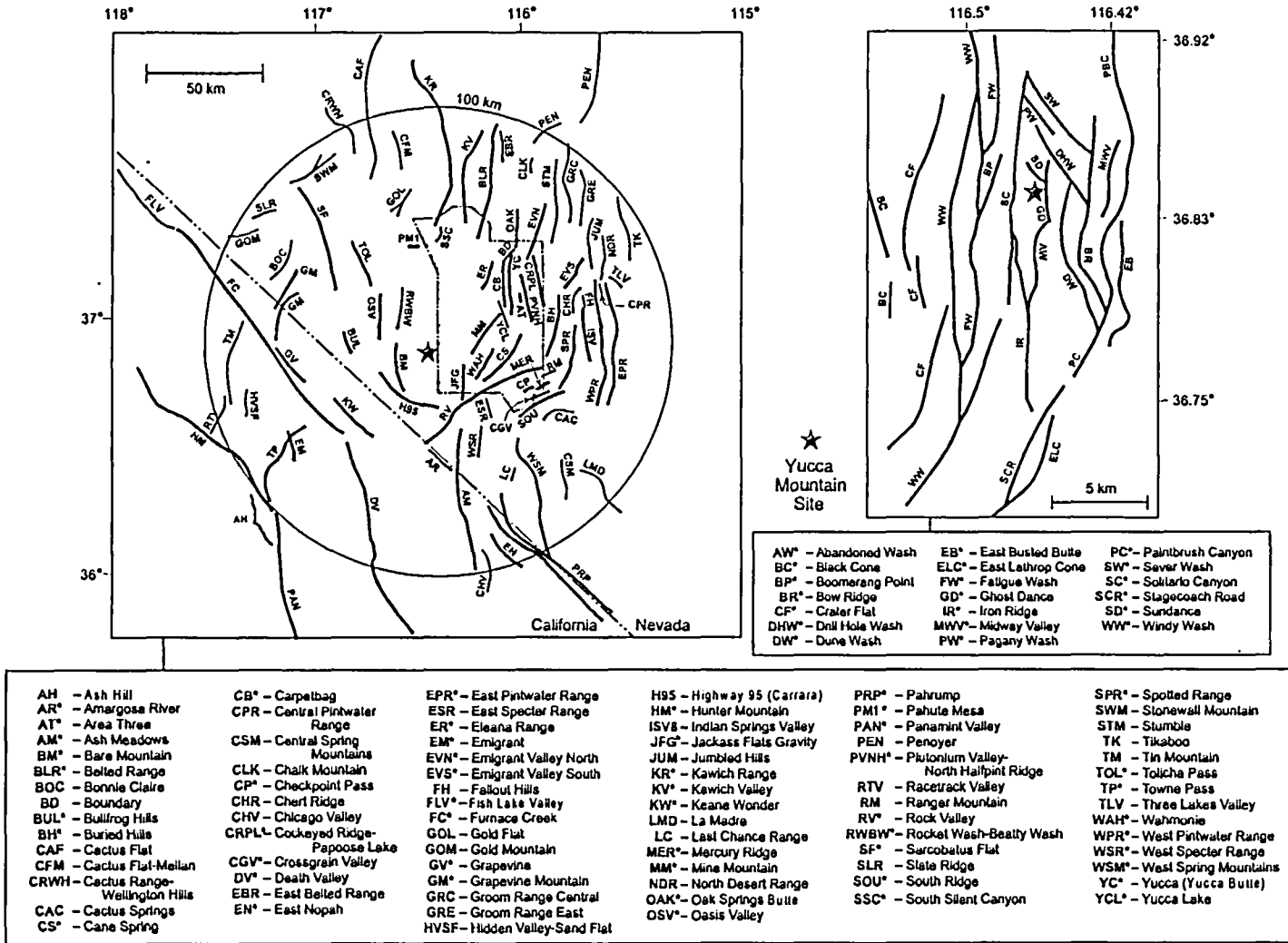
Figure 12.3-10. Frenchman Flat Earthquake Sequence of 1999



Source: Smith, K. (2000)

NOTE: Aftershocks are shown by small red circles. Aftershock locations are poorly constrained due to limited station coverage in the area.

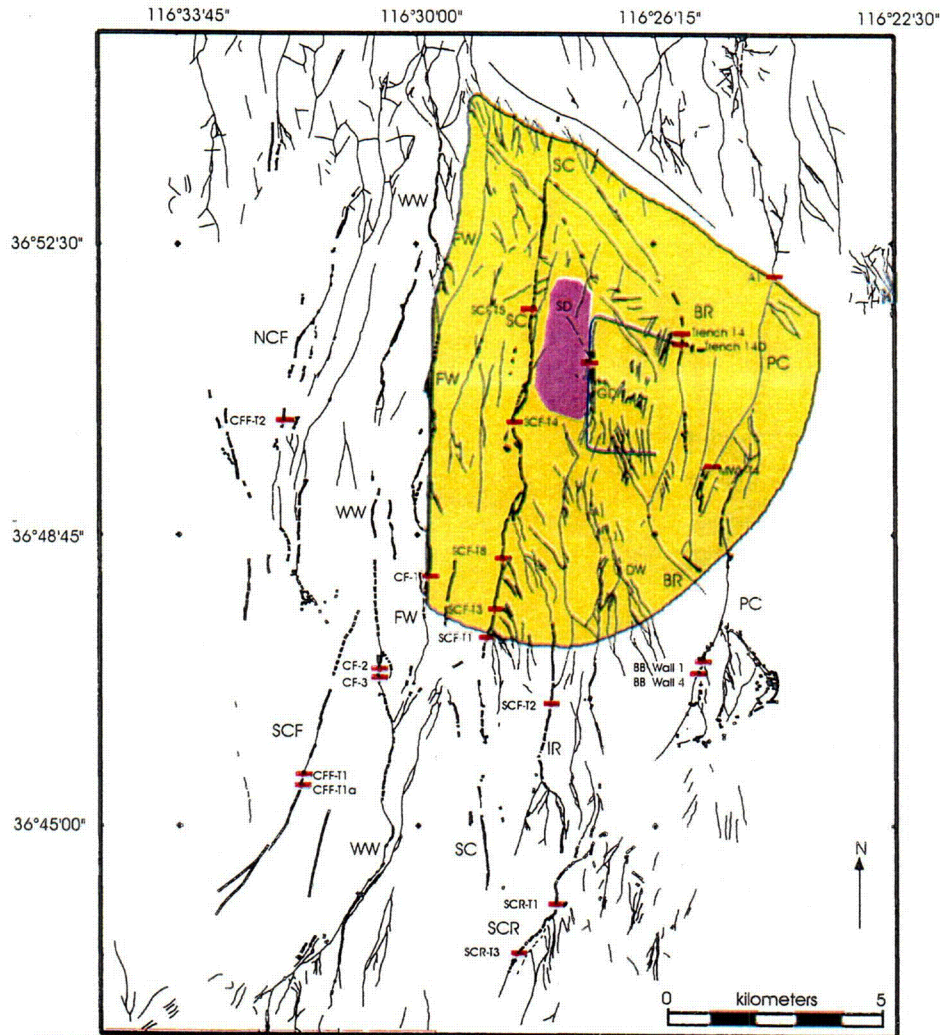
Figure 12.3-11. Scotty's Junction Earthquake Sequence of 1999



310-10 COR 123 SITEDESC
12.3-12 COR SITEDESC-R01

Source: Faults included in the probabilistic seismic hazard analyses (Wong and Stepp 1998) and/or considered relevant by Pezzopane (1996)

Figure 12.3-12. Known or Suspected Quaternary Faults and Significant Local Faults within 100 Kilometers of Yucca Mountain

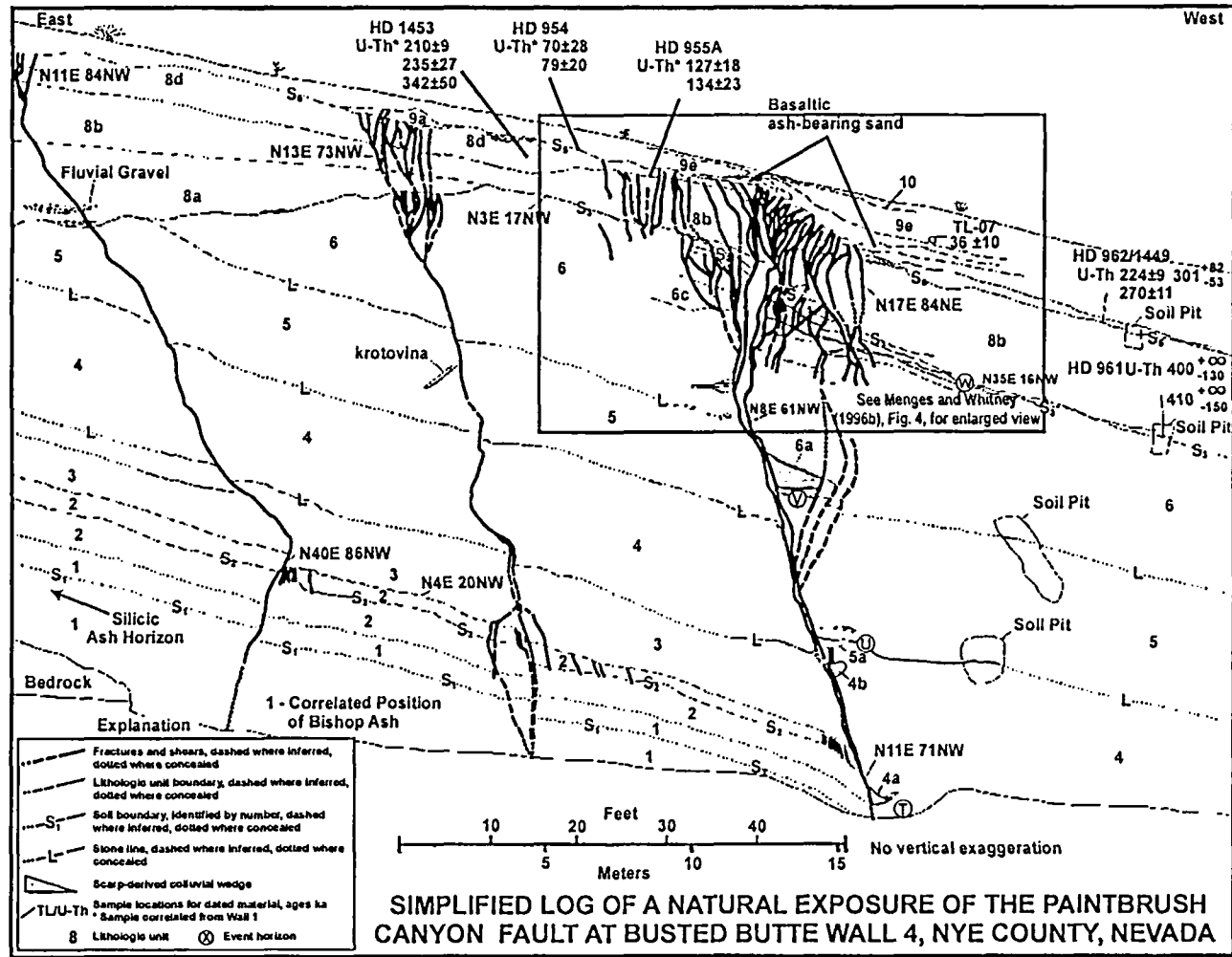


EXPLANATION	
	Paleoseismic Trench Locations
	Faults; Quaternary and suspected Quaternary age of last movement
	Faults; pre-Quaternary or undetermined age of last movement
	Approximate Potential Repository Area and Exploratory Studies Facility
	Approximate Former Conceptual Controlled Area Boundary
	BR = Bow Ridge
	DW = Dune Wash
	FW = Fatigue Wash
	GD = Ghost Dance
	IR = Iron Ridge
	NCF = Northern Crater Flat
	PC = Paintbrush Canyon
	SD = Sundance
	SC = Solitario Canyon
	SCF = Southern Crater Flat
	SCR = Stagecoach Road
	WW = Windy Wash

310-11 CDK 123 SHEDEC
12.3-13 CDK SHEDEC-101

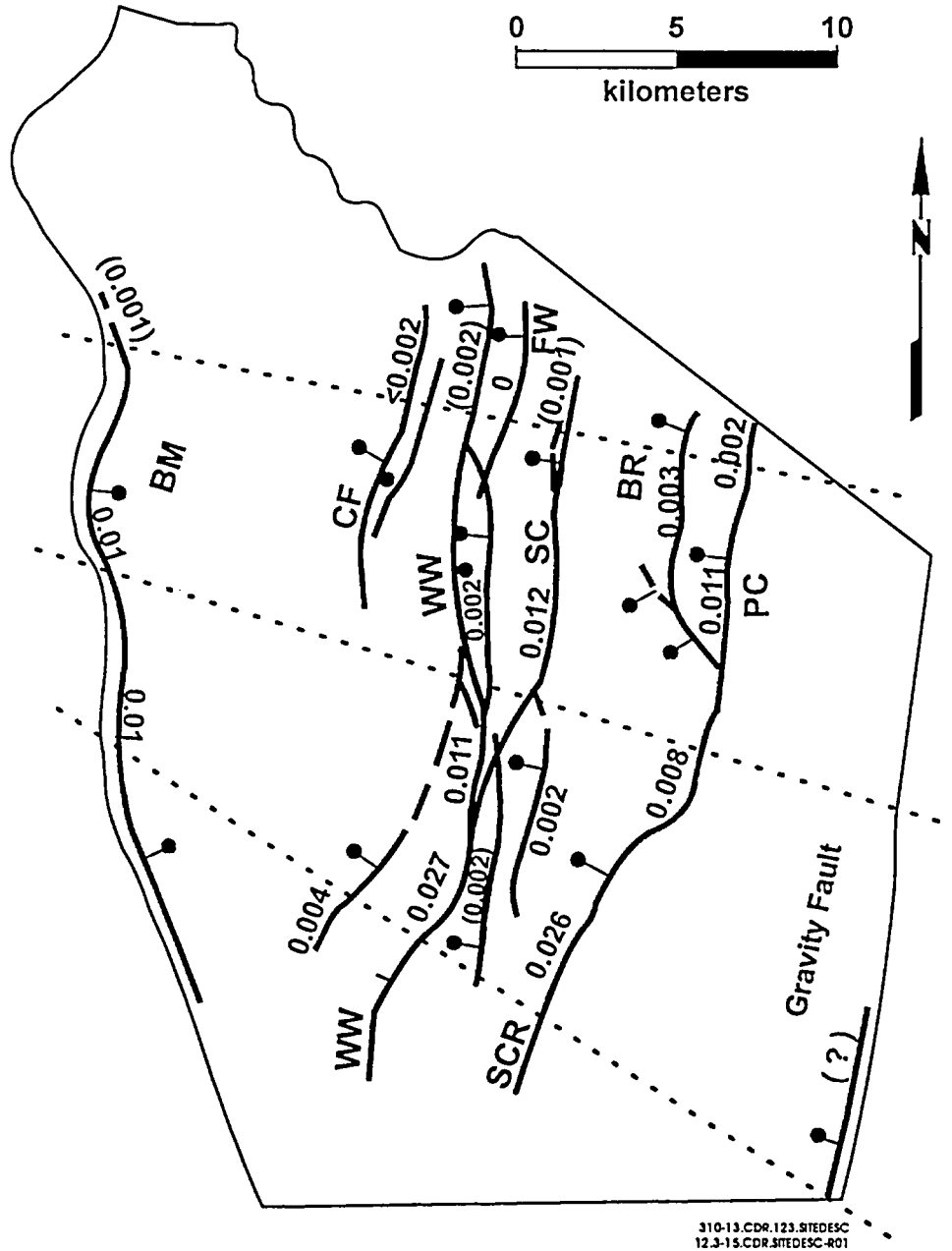
Source: Fault map is modified from Simonds et al. (1995); Pezzopane, Whitney et al. (1996)

Figure 12.3-13. Local Faults and Paleoseismic Study Sites at Yucca Mountain



Source: Menges and Whitney (1996b, Figure 4.4.1)

Figure 12.3-14. Example Trench Log from Paleoseismic Studies of Late Quaternary Faults near Yucca Mountain: Paintbrush Canyon Fault at Busted Butte

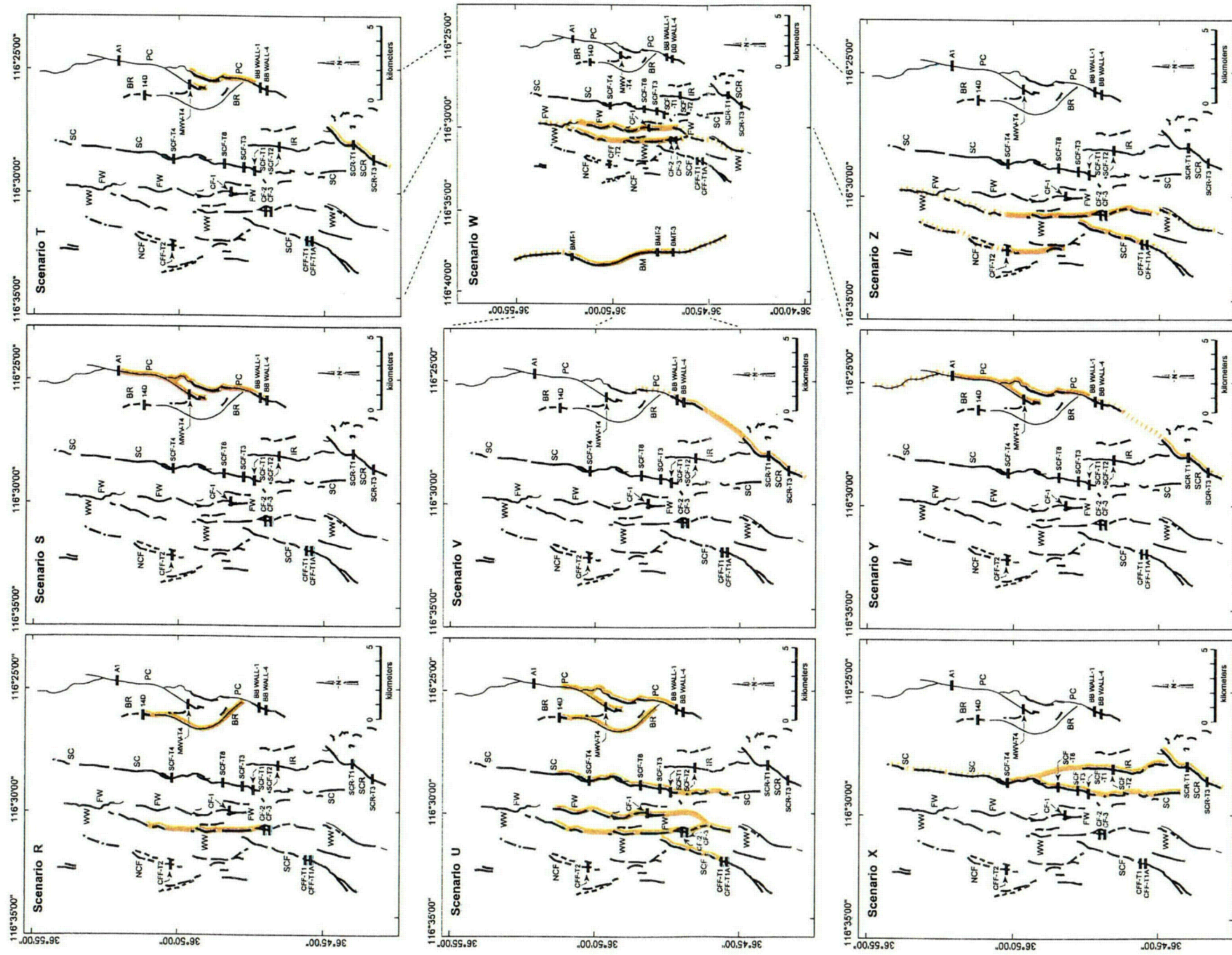


Source: Adapted from Fridrich et al. (1996)

NOTE: Slip rates are in millimeters per year. Values in parentheses are inferred. Fault abbreviations are from Figure 12.3-10.

Figure 12.3-15. Late Quaternary Faults with Slip Rates near Yucca Mountain

INTENTIONALLY LEFT BLANK



EXPLANATION

- Scenario minimum surface rupture length
- Scenario maximum surface rupture length
- Trench locations (labelled with trench designation)
- Faults; Quaternary and suspected Quaternary age of last movement
- Faults; pre-Quaternary or undetermined age of last movement

Fault Abbreviations

BM	Bare Mountain	PC	Paintbrush Canyon
BR	Bow Ridge	SC	Solitario Canyon
FW	Fatigue Wash	SCF	Southern Crater Flat
IR	Iron Ridge	SCR	Stegococh Road
NCF	Northern Crater Flat	WW	Windy Wash

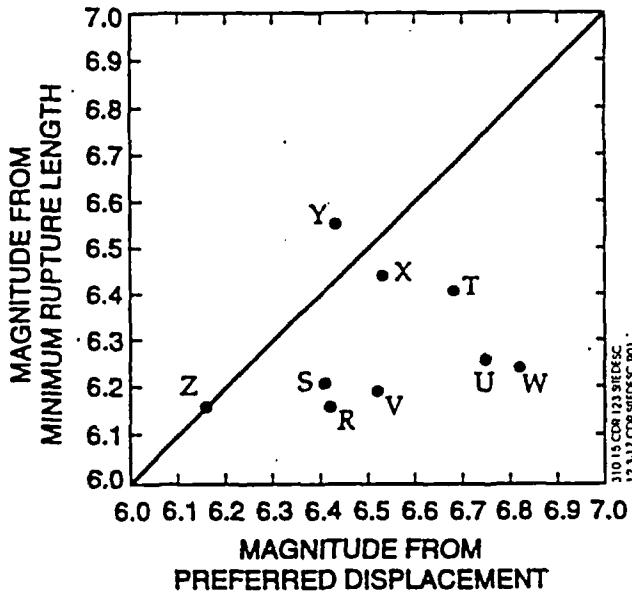
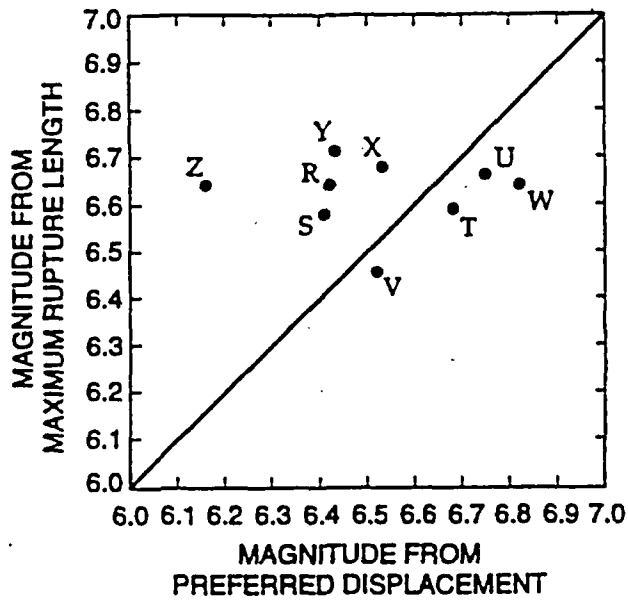
310-16 CDR 123.5REDESC
12-3-16 CDR STEBEC-001

Source: Pezzopane, Whitney, and Dawson (1996, Figure 5-8)

NOTE: Trench designations do not always follow fault abbreviations used for this figure

Figure 12.3-16. Surface Rupture Length Scenarios

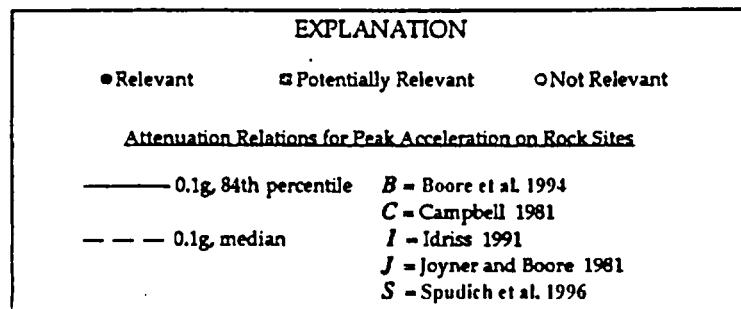
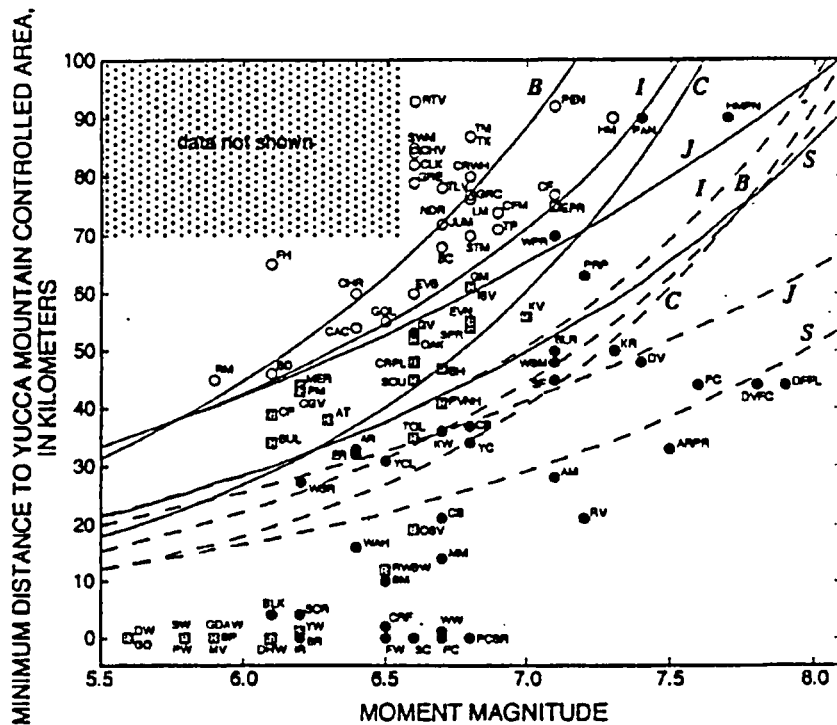
INTENTIONALLY LEFT BLANK



Source: Pezzopane, Whitney, and Dawson (1996, Figure 5-10)

NOTE: Letters correspond to rupture scenarios (Figure 12.3-16, Table 12.3-10).

Figure 12.3-17. Magnitudes Calculated for Rupture Scenarios at Yucca Mountain

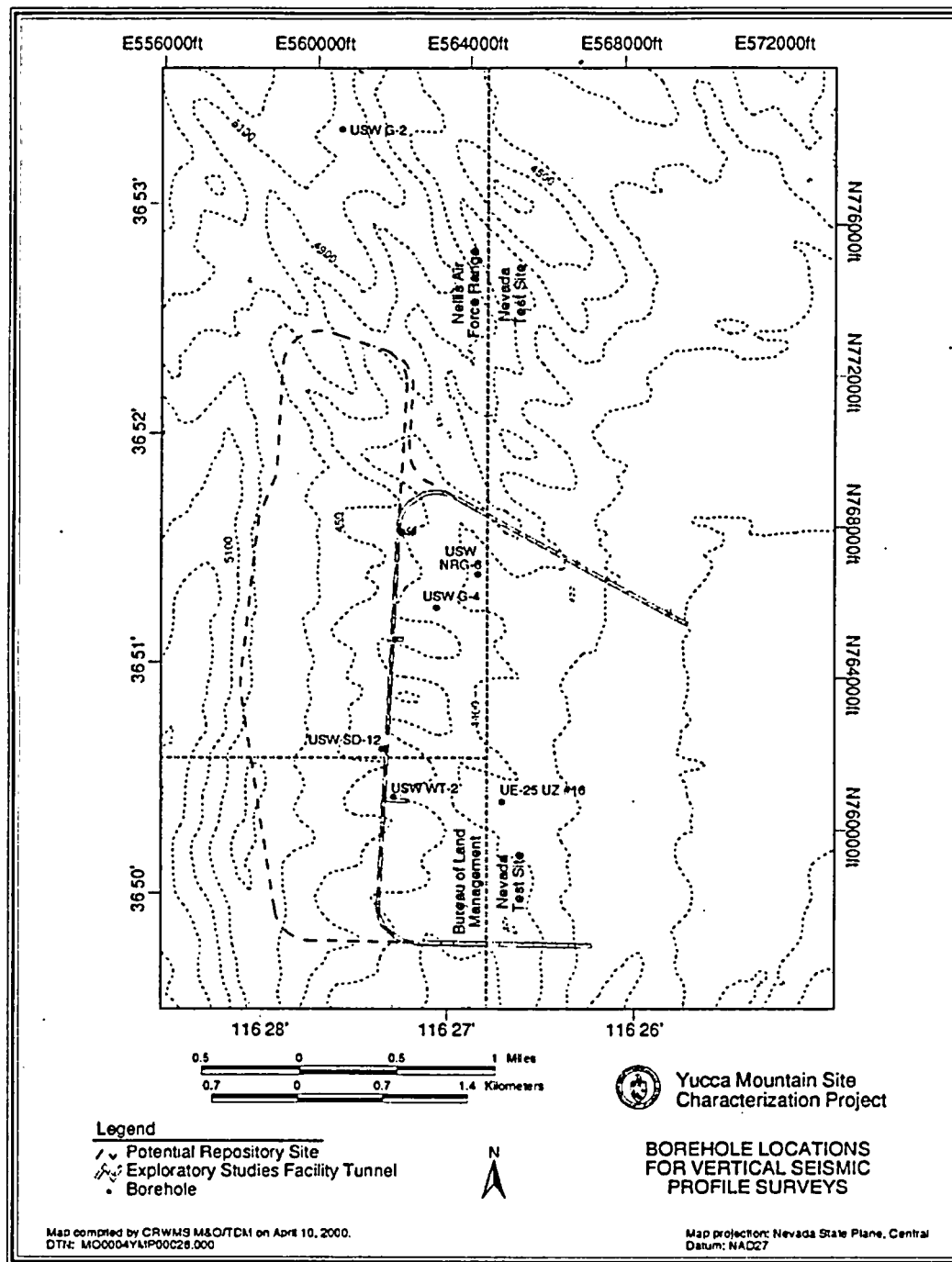


1101A, CDR, 1101, 1101, 1101
 1101, 1101, 1101, 1101, 1101

Source: Pezzopane (1996, Figure 11-3)

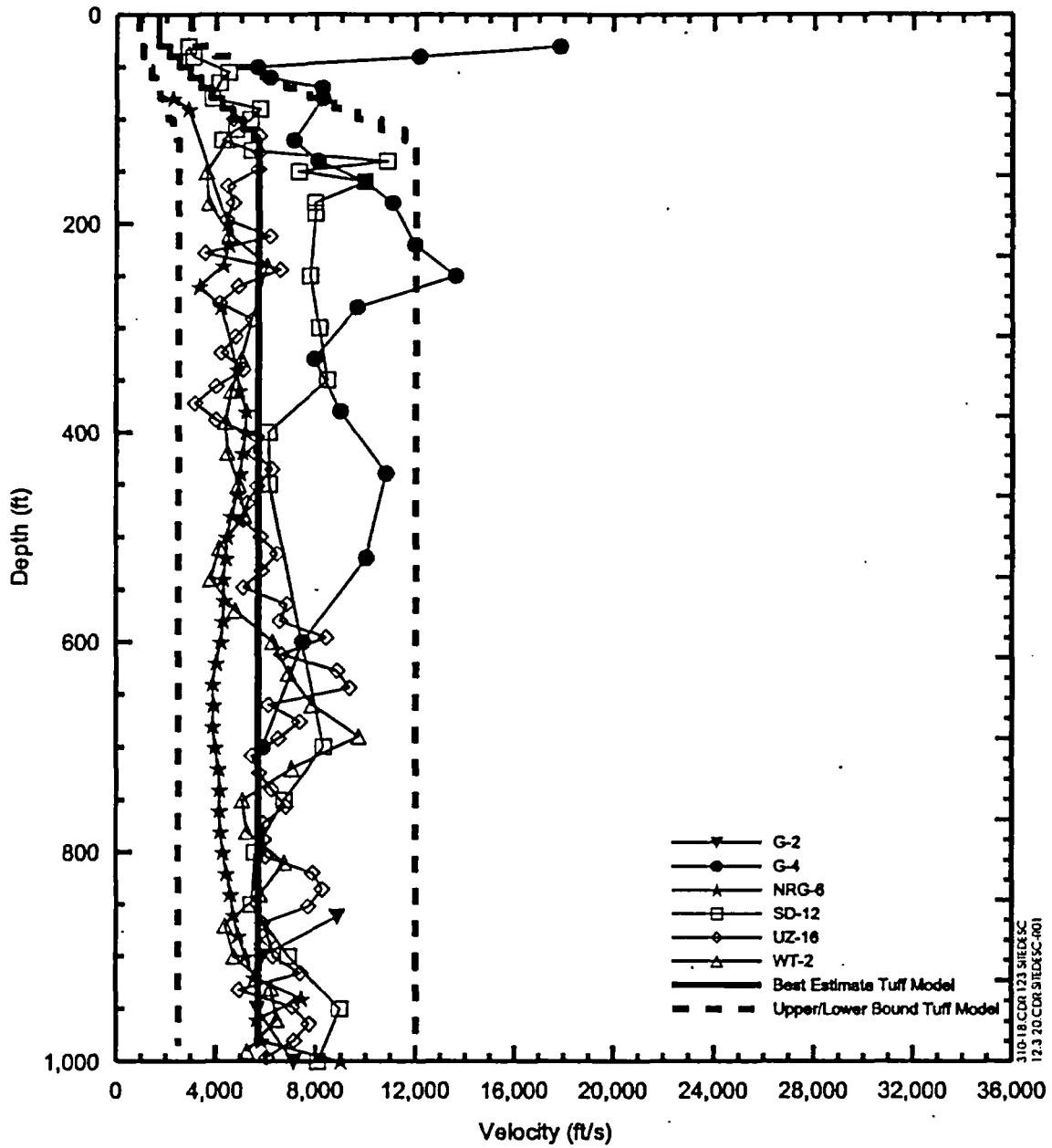
NOTES: Candidate seismic sources are plotted as a function of their closest distance to the former Conceptual Controlled Area and their estimated maximum magnitude. In general, fault abbreviations are found in Figure 12.3-10. Additional abbreviations are: ARPR = Amargosa River-Pahrump; BLK = Black Cone; BC = Bonnie Clair; CF = Cactus Flat; CFM = Cactus Flat-Mellan; CRF = Crater Flat; DFFL = Death Valley-Furnace Creek-Fish Lake Valley; DVFC = Death Valley-Furnace Creek; GDAW = Ghost Dance-Abandoned Wash; GM = Grapevine Mountains; HMPN = Hunter Mountain-Panamint Valley; ISV = Indian Springs Valley; LM = La Madre; MV = Midway Valley; PCSR = Paintbrush Canyon-Stage Coach Road; PM = Pahute Mesa; YW = Yucca Wash

Figure 12.3-18. Assessment of Relevant and Potentially Relevant Earthquake Sources for the Yucca Mountain Region



NOTE: Vertical seismic profile data are shown on Figure 12.3-20.

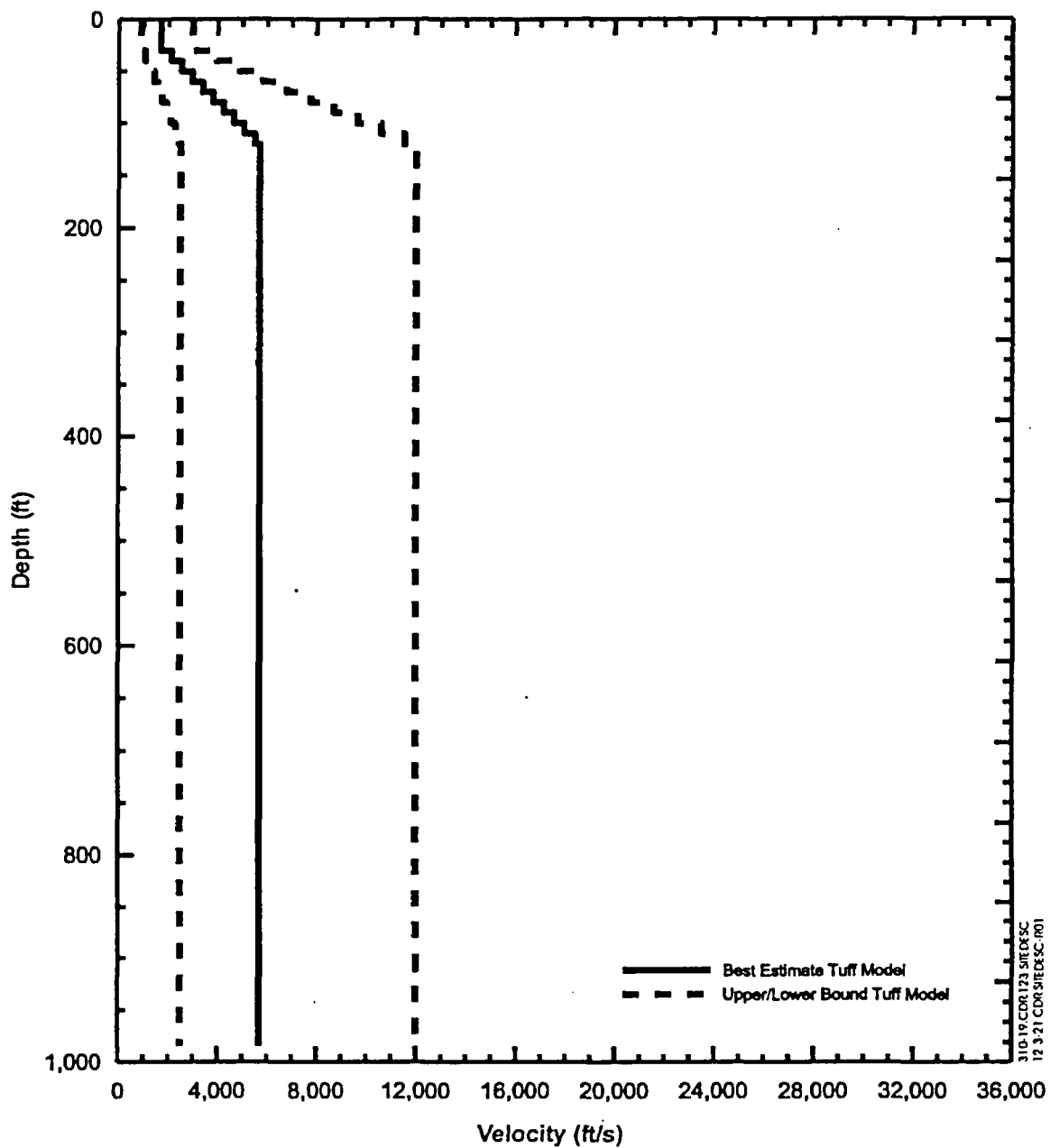
Figure 12.3-19. Borehole Locations for Vertical Seismic Profile Surveys



DTNs: LB960808314212.003, MO98PRECLOSURE.000

NOTE: Borehole locations are shown on Figure 12.3-19. To convert ft/s to km/s, multiply by 3.048×10^{-4} .

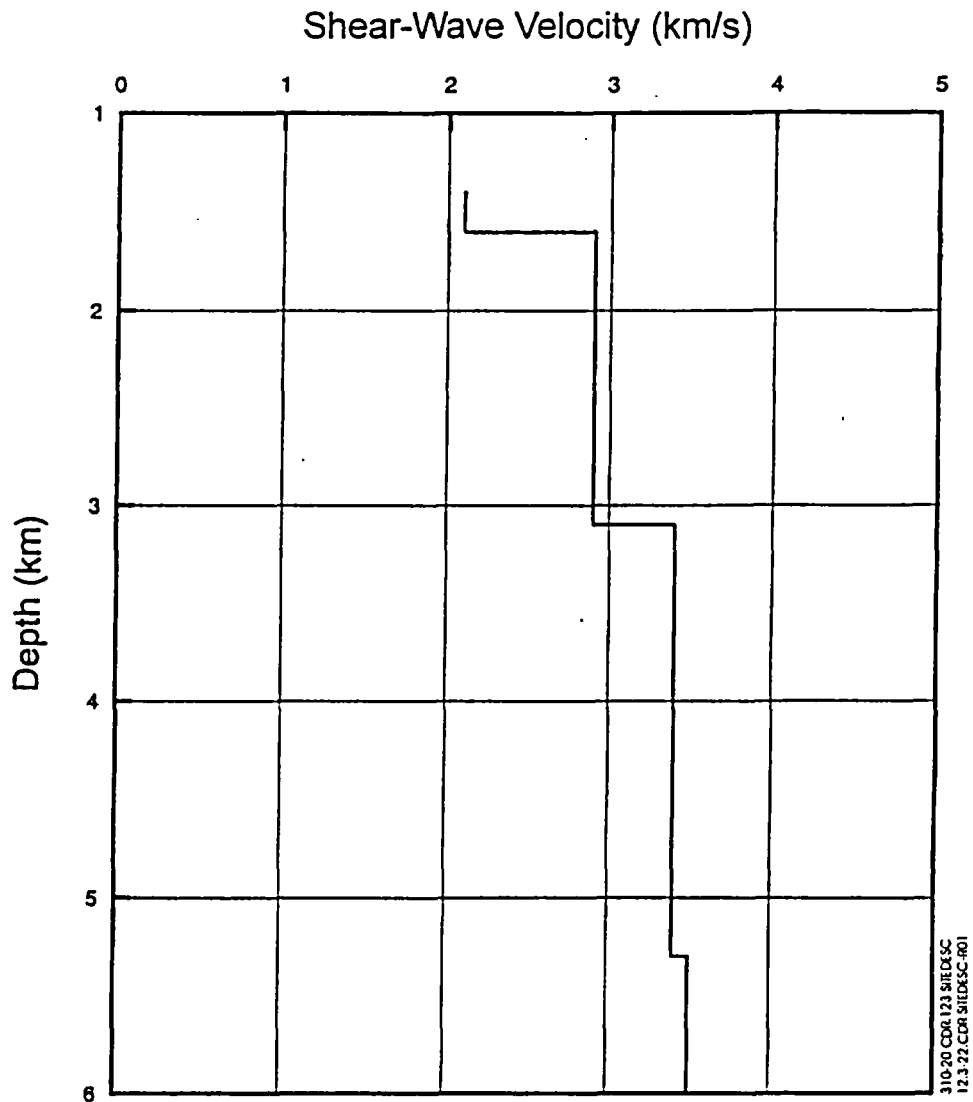
Figure 12.3-20. Shear-Wave Interval Velocities Interpreted from Vertical Seismic Profile Surveys at Six Boreholes



DTN: MO98PRECLOSURE.000

NOTE: To convert ft/s to km/s, multiply by 3.048×10^{-4} .

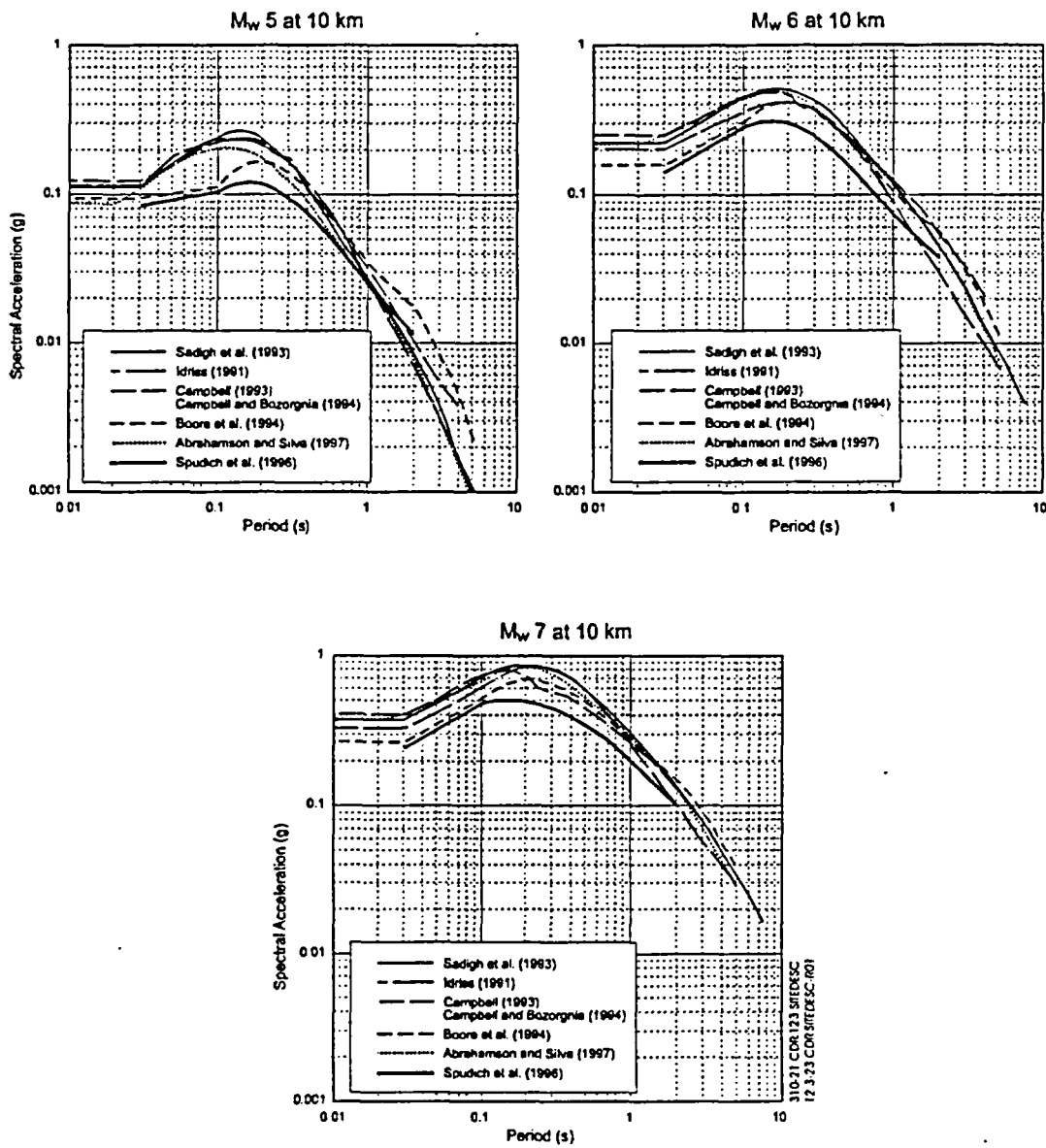
Figure 12.3-21. Shallow Shear-Wave Seismic Velocity Model for Yucca Mountain and Thermal-Mechanical Layer Velocities



Source: Schneider et al. (1996, Table 5.2)

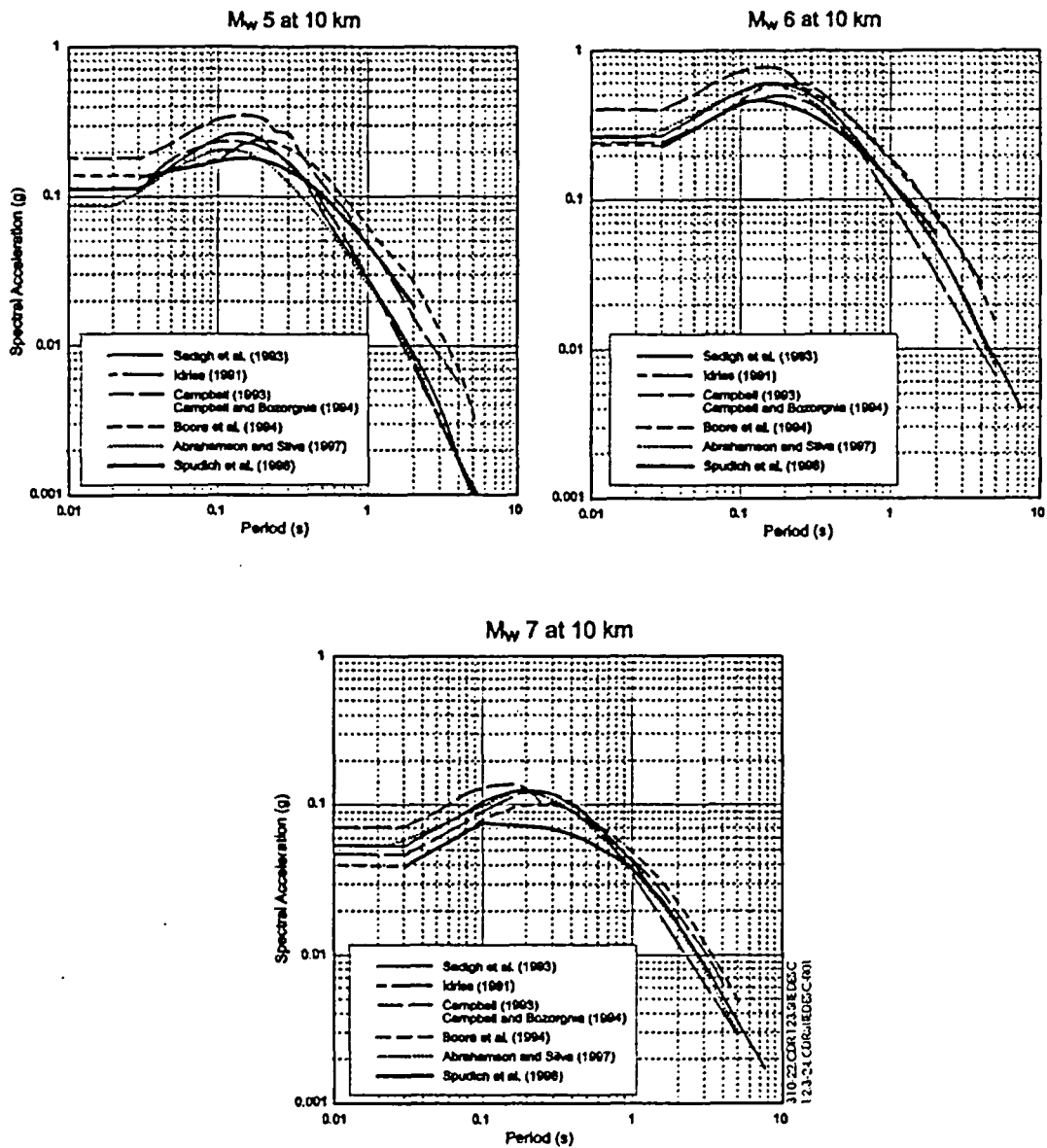
NOTE: To convert km/s to ft/s, multiply by 3280.8.

Figure 12.3-22. Deep Shear-Wave Seismic Velocity Model for Yucca Mountain



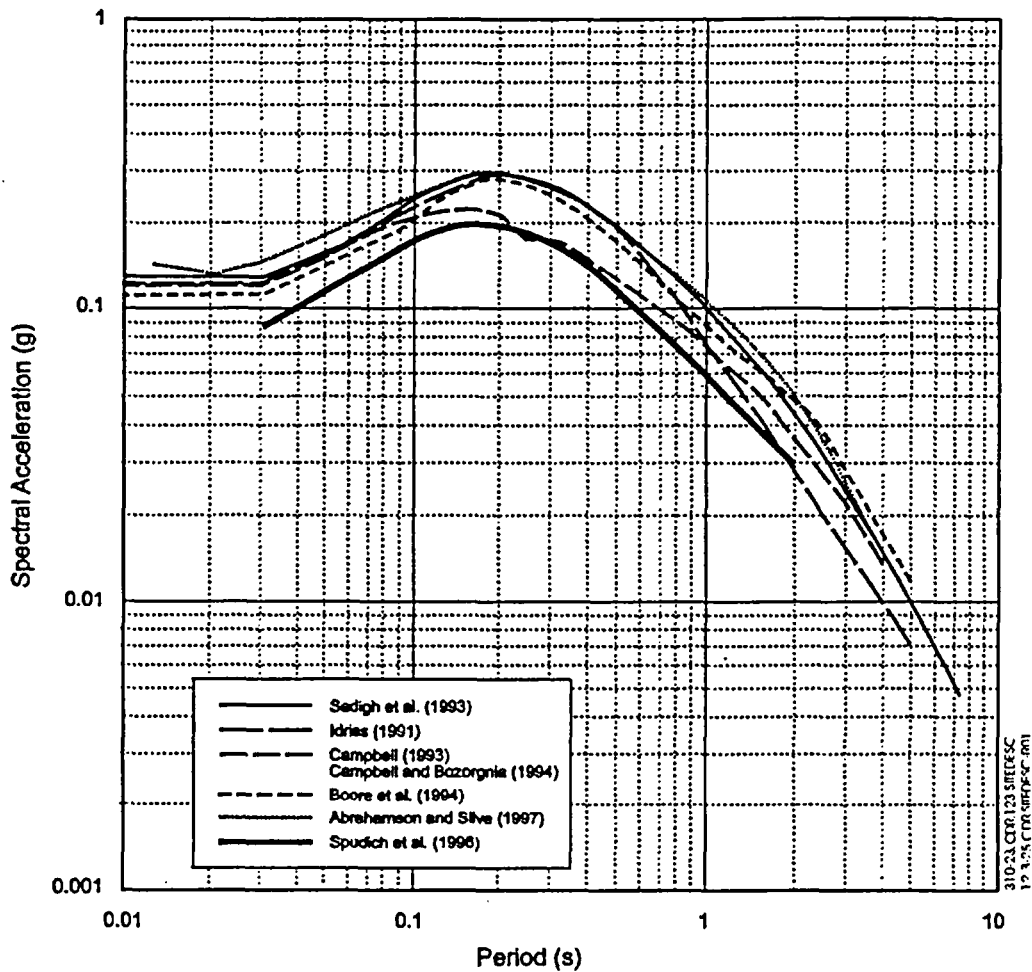
Source: Abrahamson and Becker (1996, Figure 10.6-1)

Figure 12.3-23. Median Spectral Accelerations for Rock on the Footwall of a Normal Fault



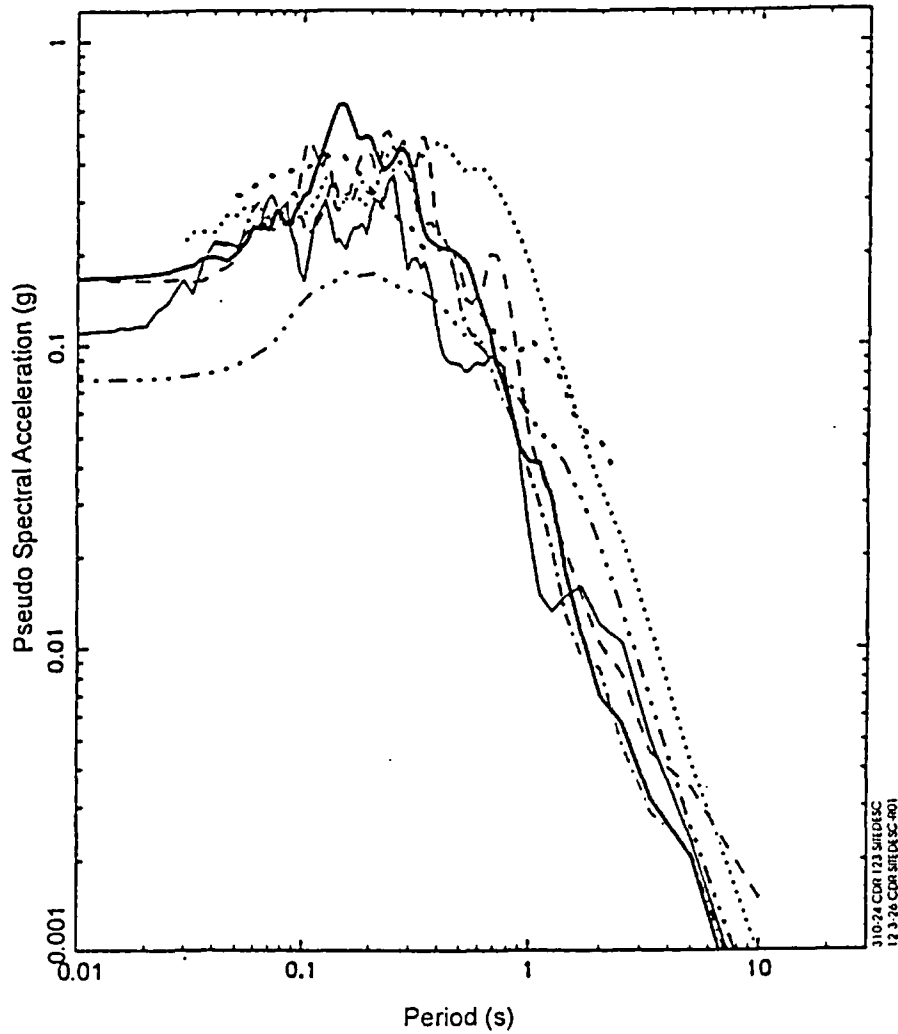
Source: Abrahamson and Becker (1996, Figure 10.6-2)

Figure 12.3-24. Median Spectral Accelerations for Rock in the Hanging Wall of a Normal Fault



Source: Abrahamson and Becker (1996, Figure 10.6-3)

Figure 12.3-25. Median Spectral Accelerations on Rock for a M_w 6.5 Strike-Slip Earthquake at a Distance of 25 Kilometers



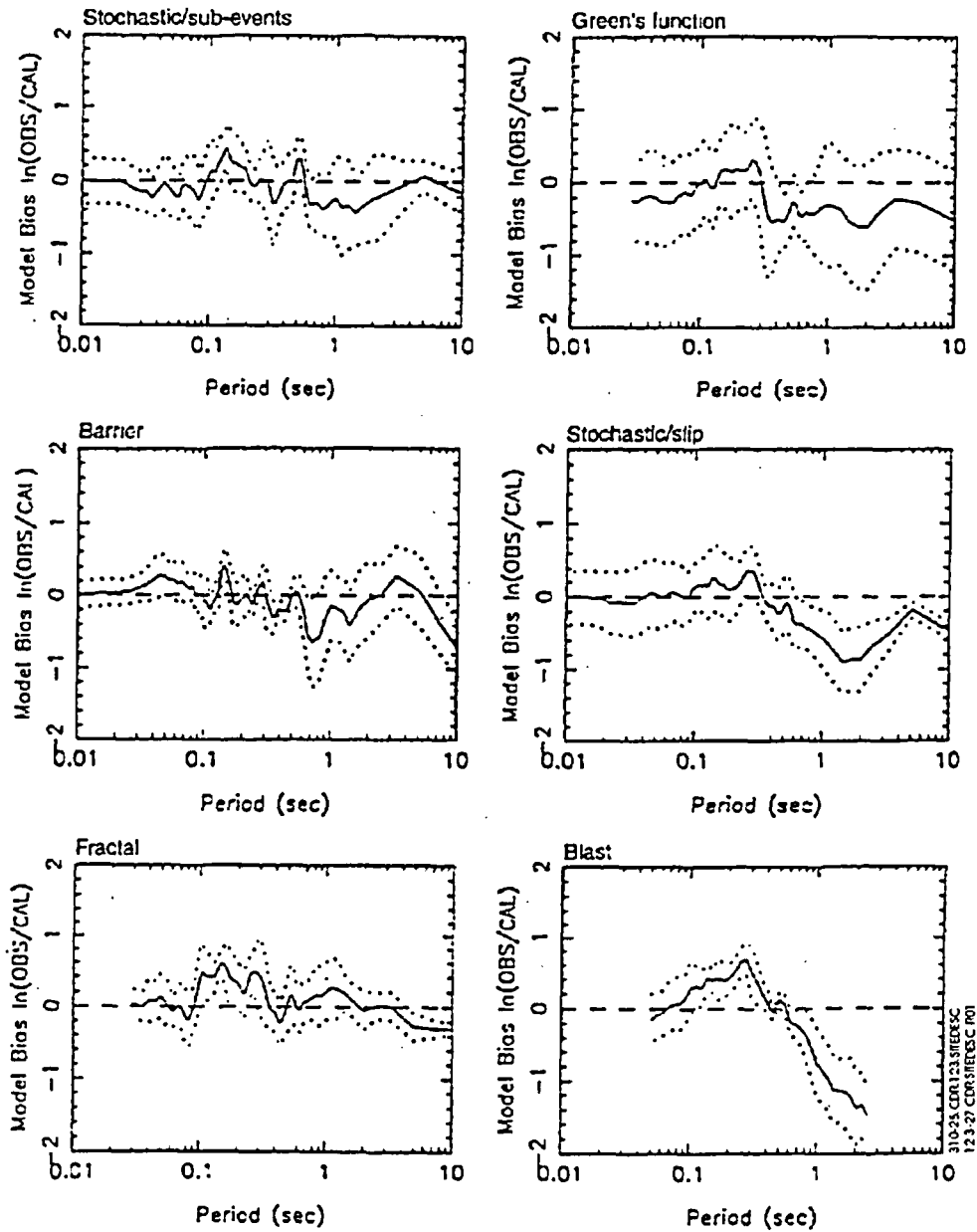
LEGEND

- | | |
|-------------------------------|---------------------------|
| ————— : Observed | : Green's function |
| ————— : Stochastic/sub-events | — · — · : Stochastic/slip |
| - - - - - : Barrier | · · · · · : Blast |
| - · - · - : Fractal | |

Source: Abrahamson and Becker (1996, Figure 10.7-4a)

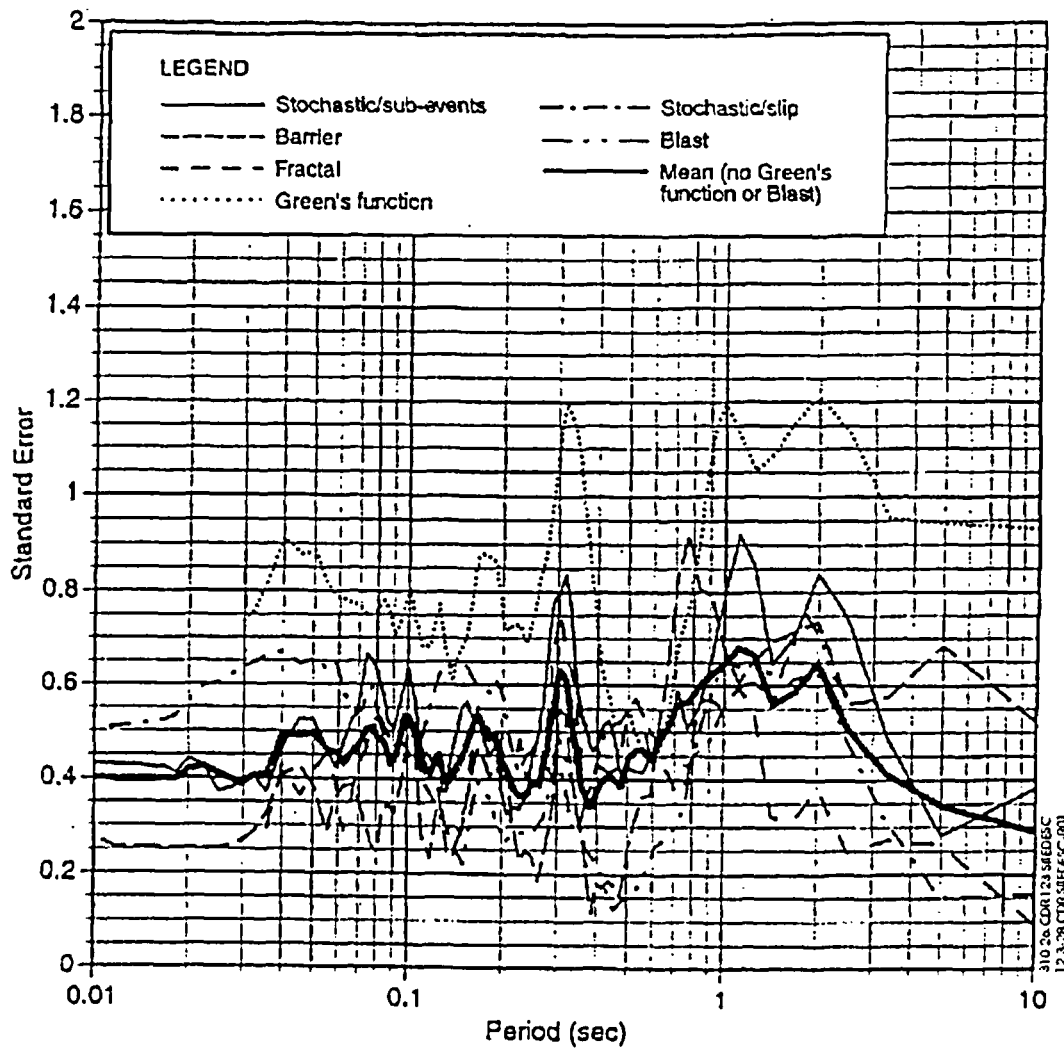
NOTE: Shown is an observed spectrum (5 percent damping) for a recorded motion from the Little Skull Mountain earthquake (Lathrop Wells Station) and spectra calculated by six teams using different modeling methods.

Figure 12.3-26. Results of Validation Studies in the Scenario Earthquake Modeling Study



Source: Abrahamson and Becker (1996, Figure 10.7-5)

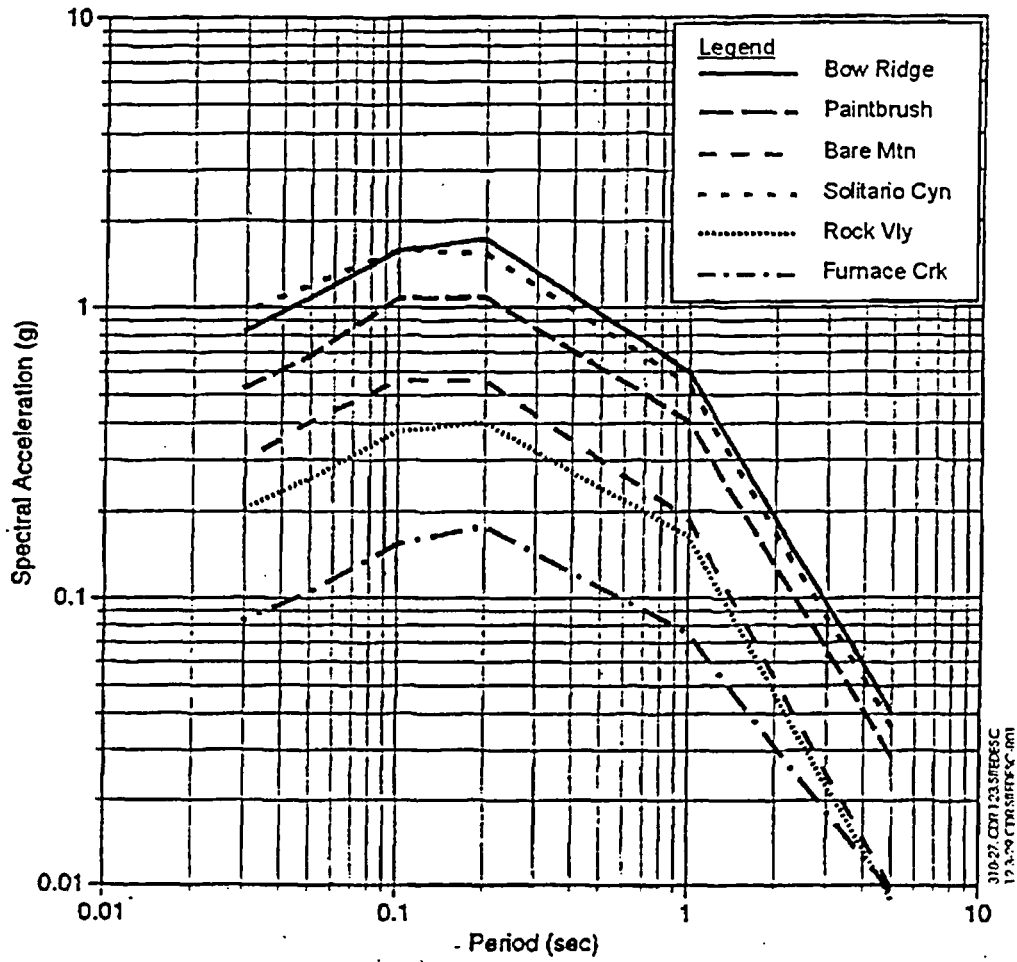
Figure 12.3-27. Model Bias of Observed Spectra to Calculated Spectra for the Little Skull Mountain Earthquake Validation



Source: Abrahamson and Becker (1996, Figure 10.7-6)

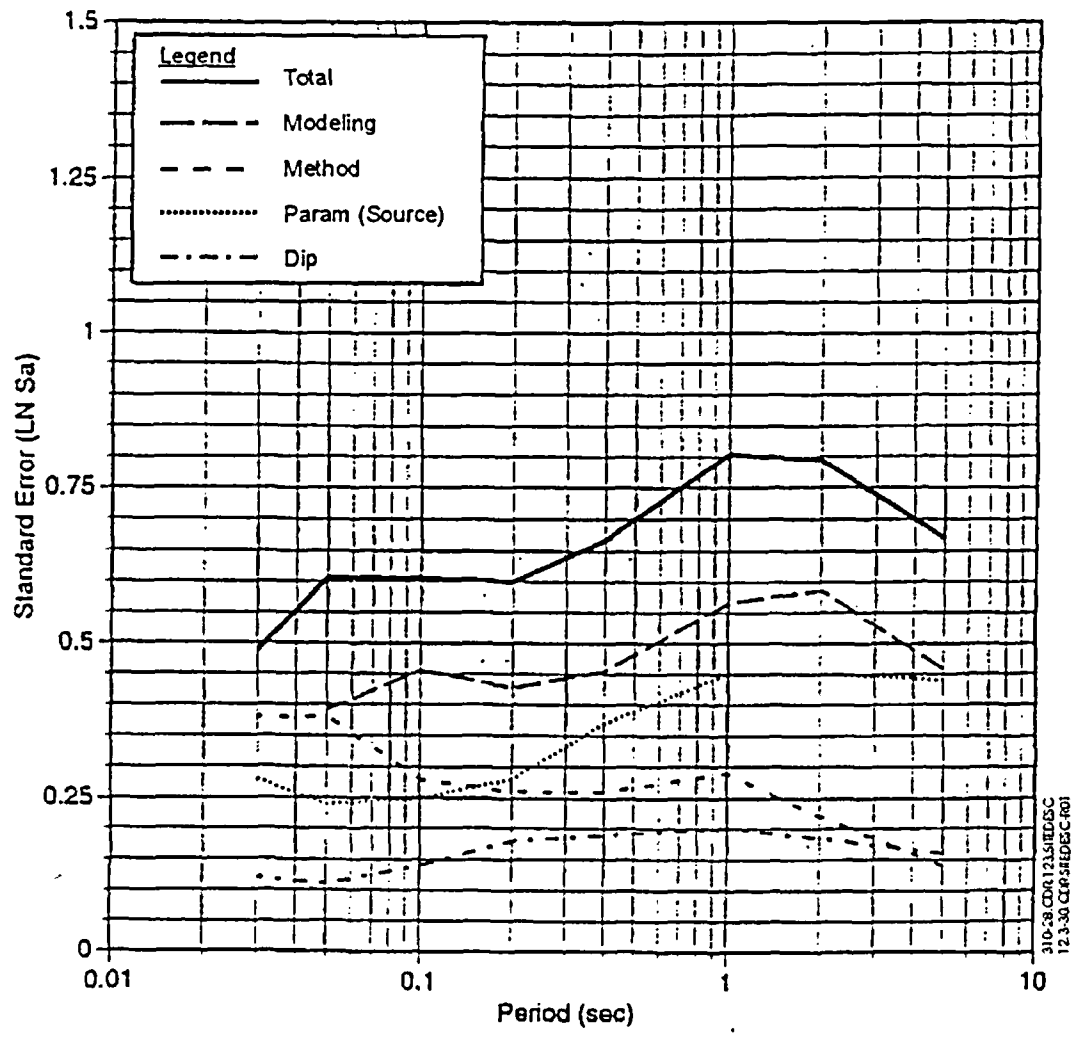
NOTE: The mean excludes the empirical blast model and the Green's function model.

Figure 12.3-28. Model Standard Errors for the Little Skull Mountain Earthquake Validation



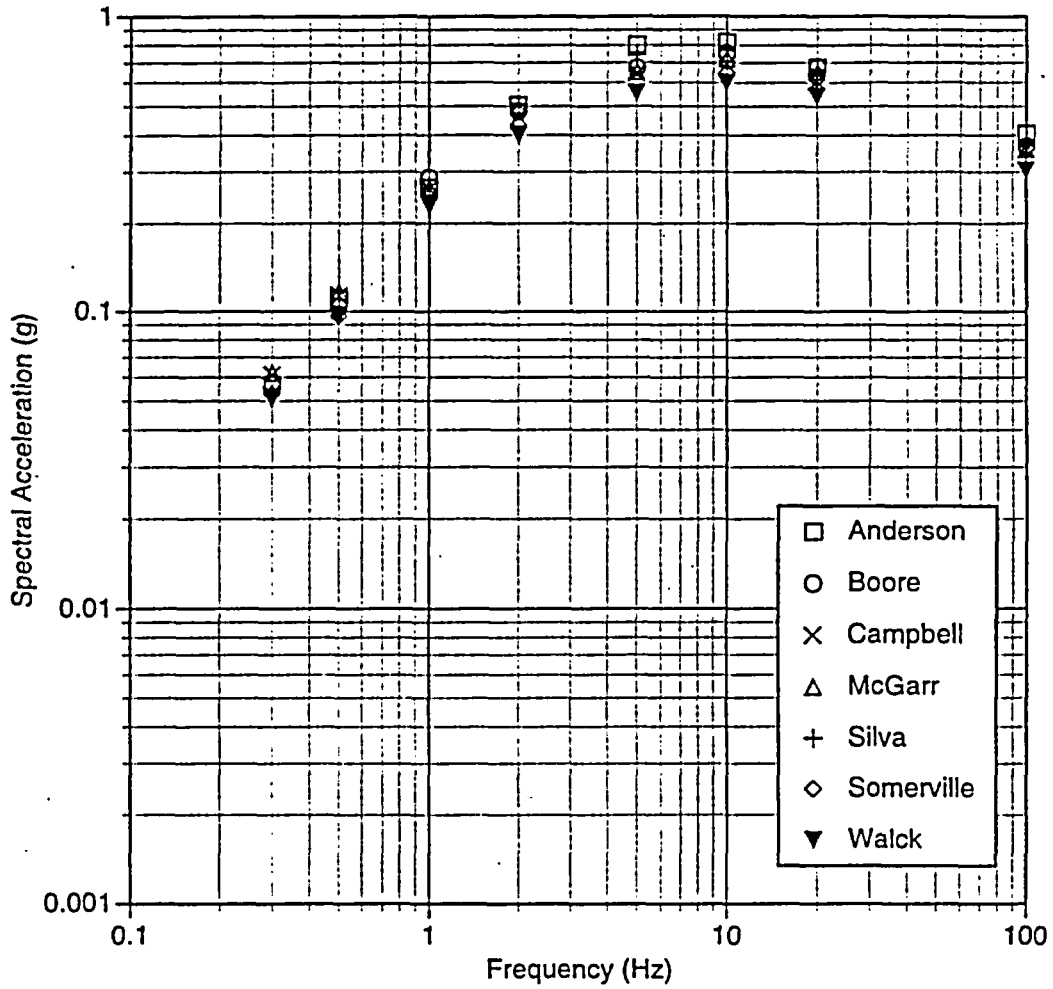
Source: Abrahamson and Becker (1996, Figure 10.8-15)

Figure 12.3-29. Median Spectral Acceleration for Scenario Earthquakes



Source: Abrahamson and Becker (1996, Figure 10.8-13)

Figure 12.3-30. Example of Total Uncertainty and Its Components (for the Paintbrush Canyon Earthquake Scenario)

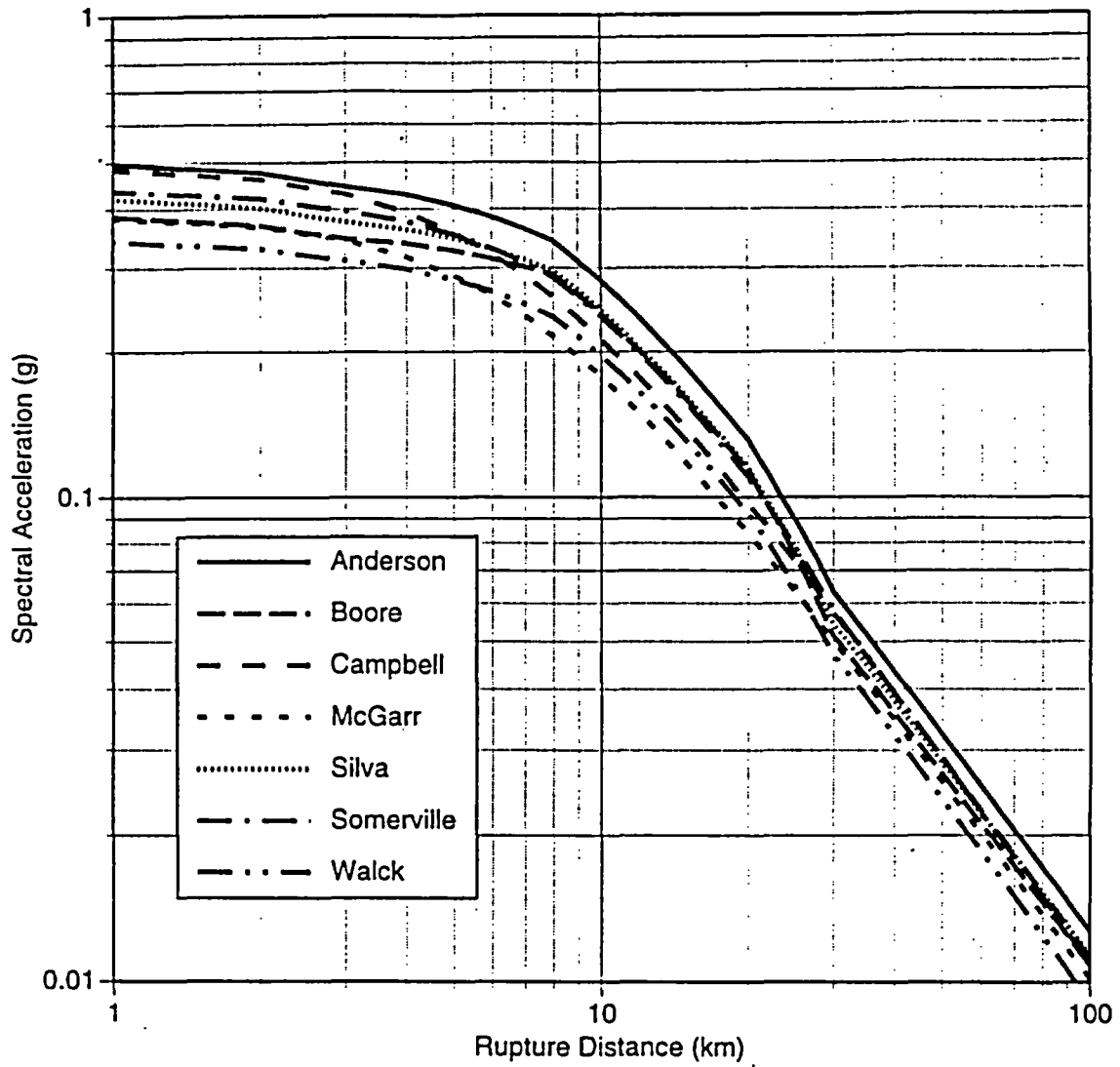


12.3-31 DOC.SITEDESC-R01

Source: Wong and Stepp (1998, Figure 5-5)

NOTE: Legend gives names of the probabilistic seismic hazard analysis ground motion experts.

Figure 12.3-31. Point Estimates for Median Horizontal Spectral Acceleration for a M_w 6.5 Earthquake at 4 Kilometers on the Hanging Wall of a Normal Fault



12.3-32.DOC.SITEDESC-R01

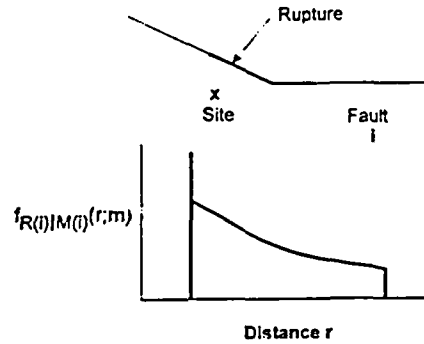
Source: Wong and Stepp (1998, Figure 6-1)

NOTE: These estimates are computed from the probabilistic seismic hazard analysis ground motion experts' attenuation relations.

Figure 12.3-32. Median Horizontal Peak Ground Acceleration for a M_w 6.5 Earthquake on the Hanging Wall of a Normal Fault

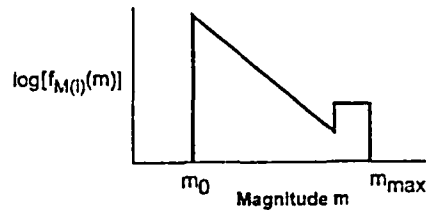
- a) Seismic source *i*
 Earthquake locations in space (and magnitude-dependent rupture dimensions) lead to a distribution of distance

$$f_{R(i)|M(i)}(r;m)$$



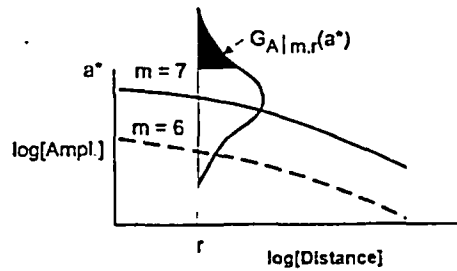
- b) Magnitude distribution and rate of occurrence for source *i*

$$f_{M(i)}(m), \nu_i$$



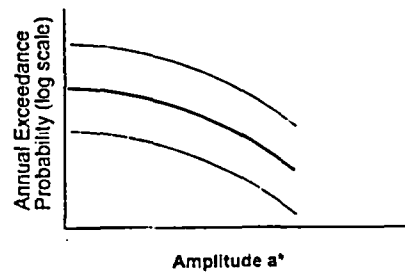
- c) Ground-motion attenuation equation

$$G_{A|m,r}(a^*)$$



- d) Probability analysis:
 annual exceedance probability

$$\approx \sum_i \nu_i \int_r \int_m G_{A|m,r}(a^*) f_{M(i)}(m) f_{R(i)|M(i)}(r;m) \delta m \delta r$$

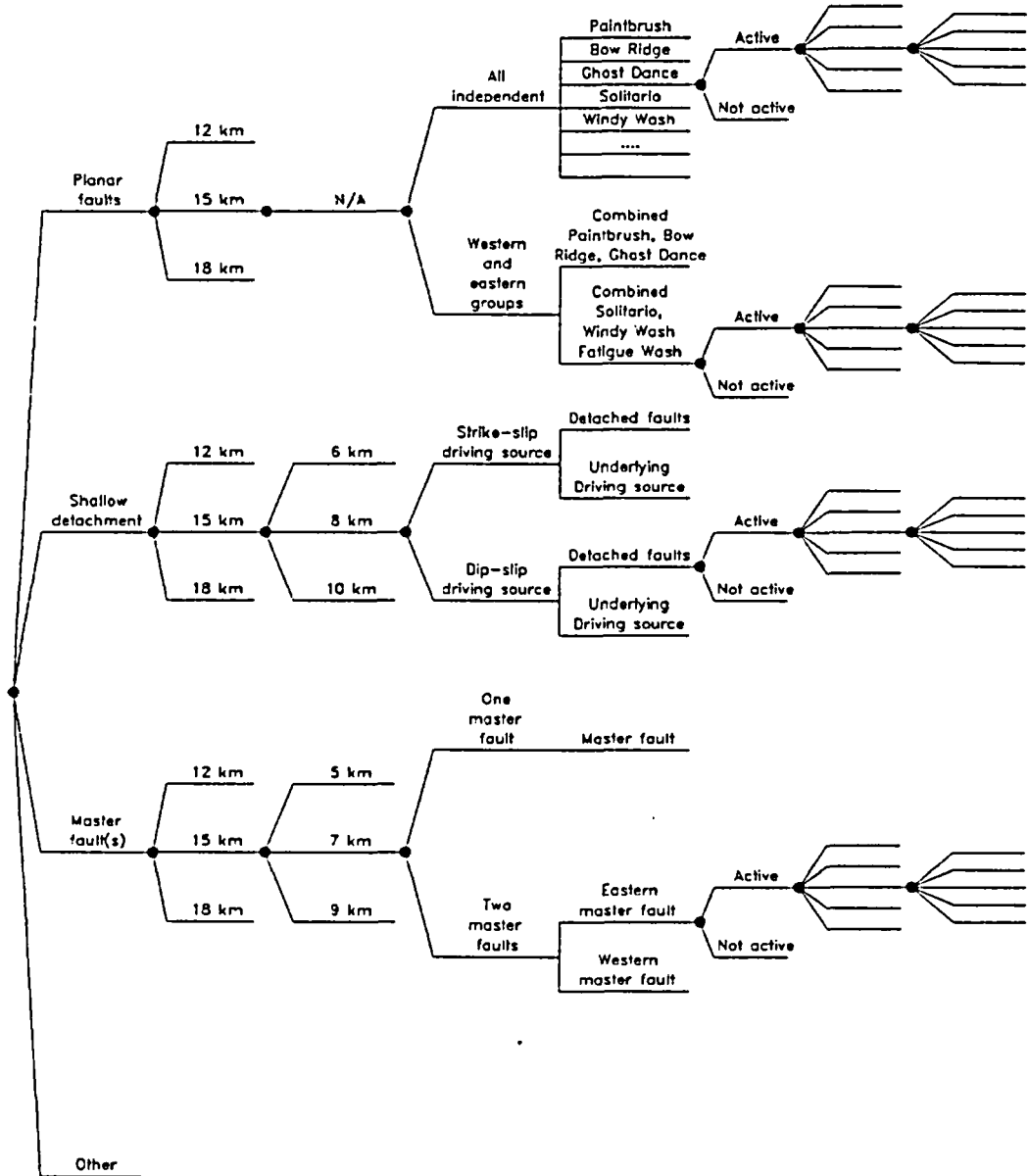


310-31 CDR 123 SITEDESC
 12 3-33 CDR SITEDESC-R01

Source: Wong and Stepp (1998, Figure 7-1)

Figure 12.3-33. Schematic Diagram of the Elements of a Probabilistic Seismic Hazard Analysis for Vibratory Ground Motions

Alternative Tectonic/Faulting Models	Maximum Depth of Rupture	Depth of Detachment or Master Fault	Alternative Fault Configurations	Sources	Fault Activity	Maximum Magnitude	Seismicity Parameters
--------------------------------------	--------------------------	-------------------------------------	----------------------------------	---------	----------------	-------------------	-----------------------

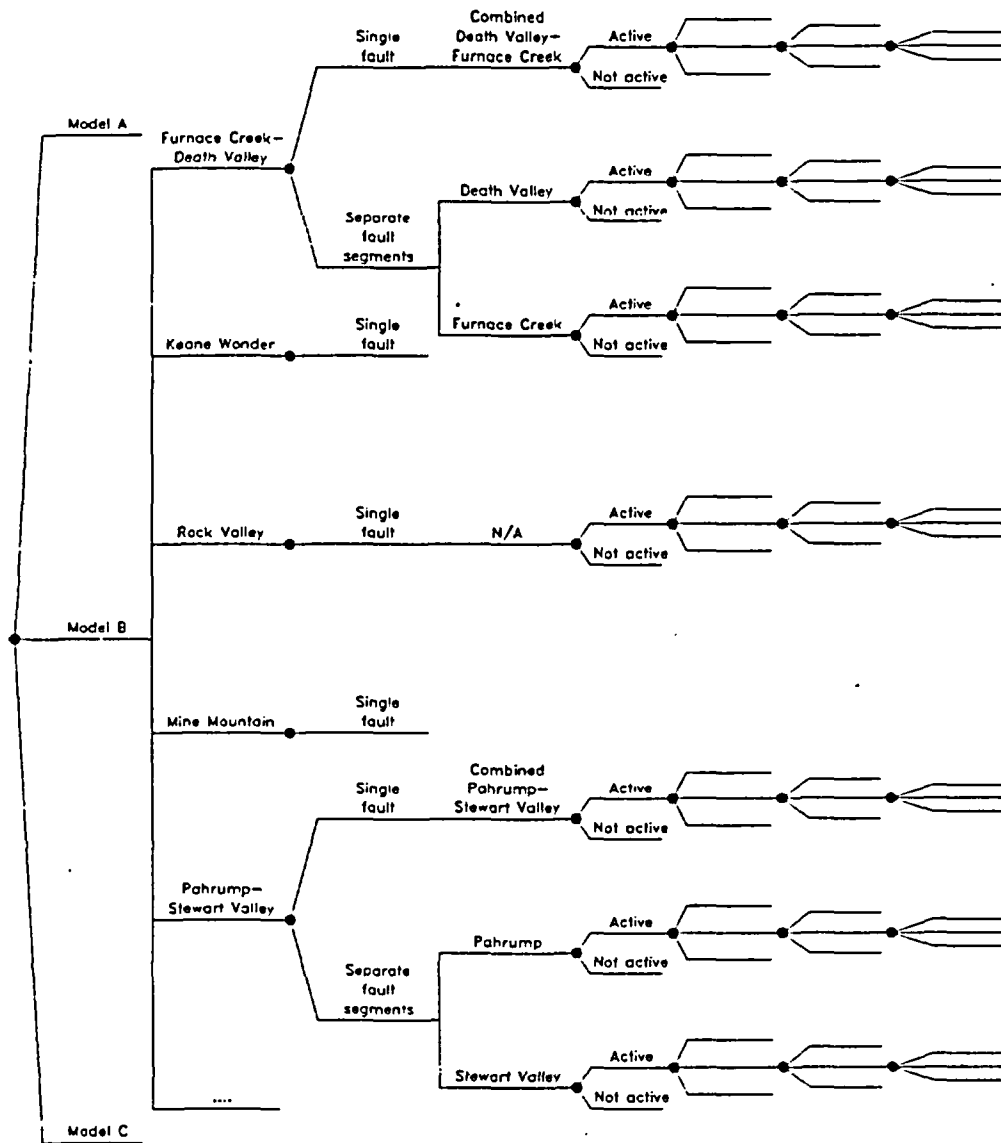


12.3-34 DOC.SITEDESC-R01

Source: Wong and Stepp (1998, Figure 4-2)

Figure 12.3-34. Example Logic Tree for Expressing the Uncertainty in Characterizing Local Fault Sources

Alternative Regional Tectonic Models	Sources	Fault Zone Segmentation	Individual Sources	Fault Activity	Maximum Depth of Rupture	Maximum Magnitude	Seismicity Parameters
--------------------------------------	---------	-------------------------	--------------------	----------------	--------------------------	-------------------	-----------------------

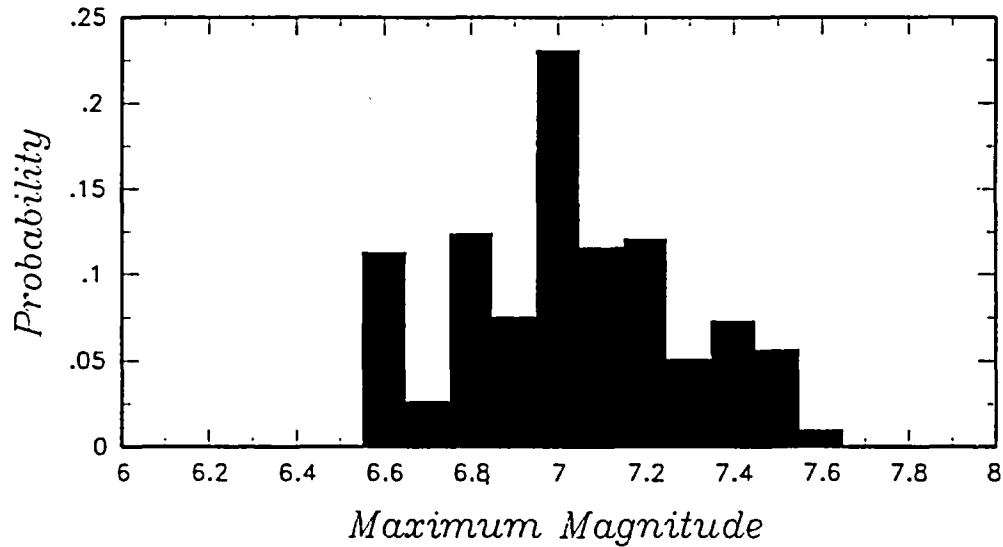
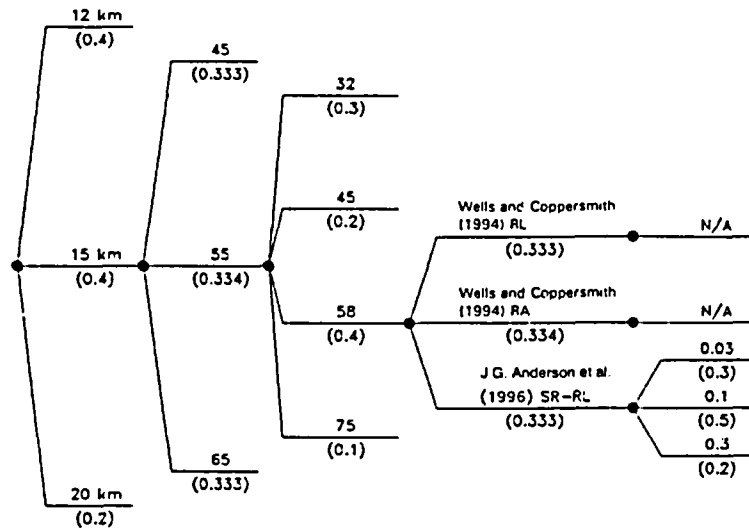


12.3-35 DOC.SITEDESC-R01

Source: Wong and Stepp (1998, Figure 4-3)

Figure 12.3-35. Example Logic Tree for Expressing the Uncertainty in Characterizing Regional Fault Sources

Maximum Depth of Rupture	Fault Dip (deg)	Maximum Rupture Length (km)	Maximum Magnitude Approach	Slip Rate (mm/yr)
--------------------------	-----------------	-----------------------------	----------------------------	-------------------

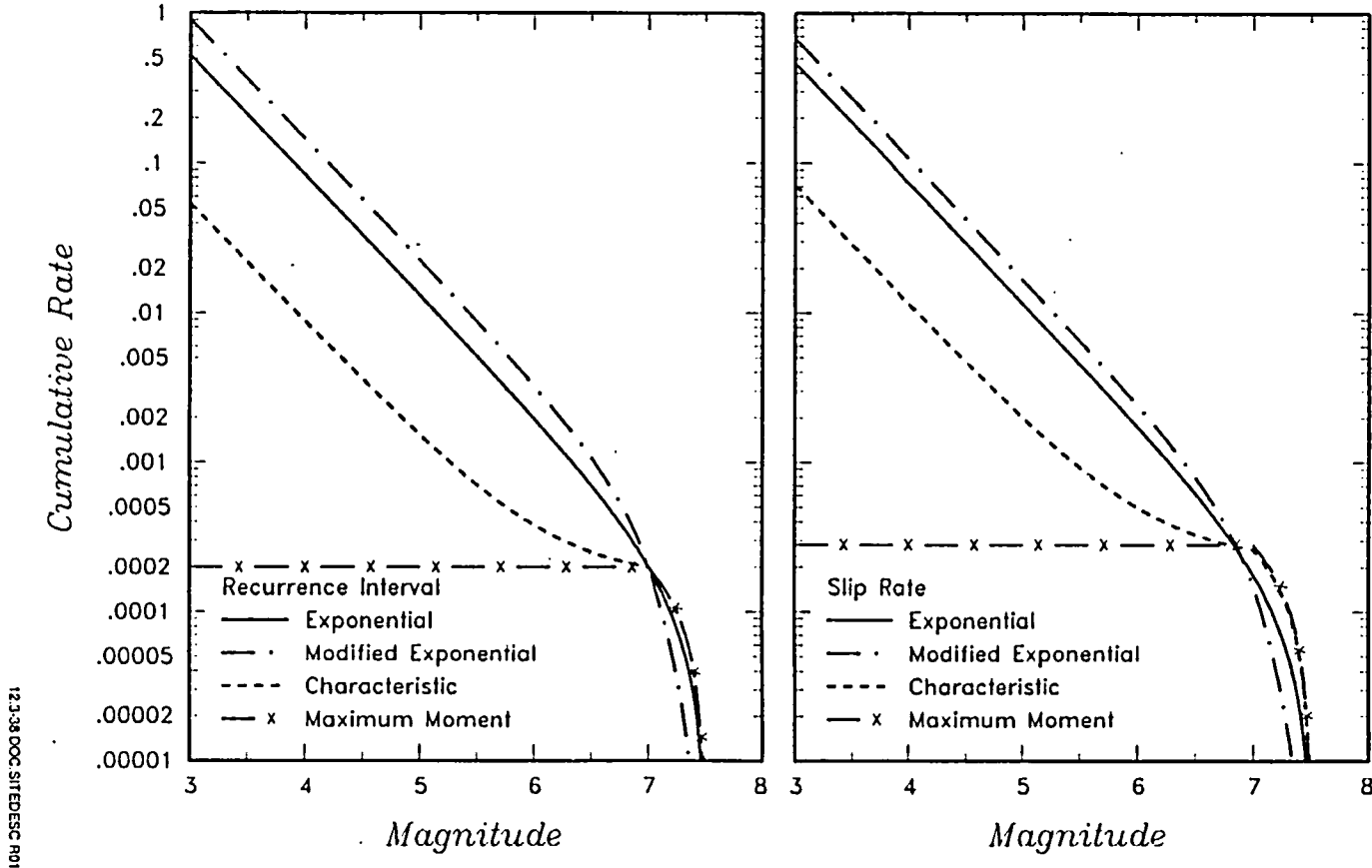


12.3-37.DOC.SITEDESC.R01

Source: Wong and Stepp (1998, Figure 4-5)

NOTE: The top graphic is a logic tree for uncertainty assessment. The bottom graphic is the resulting discrete distribution for maximum magnitude.

Figure 12.3-37. Example Assessment of Maximum Magnitude for a Fault Source

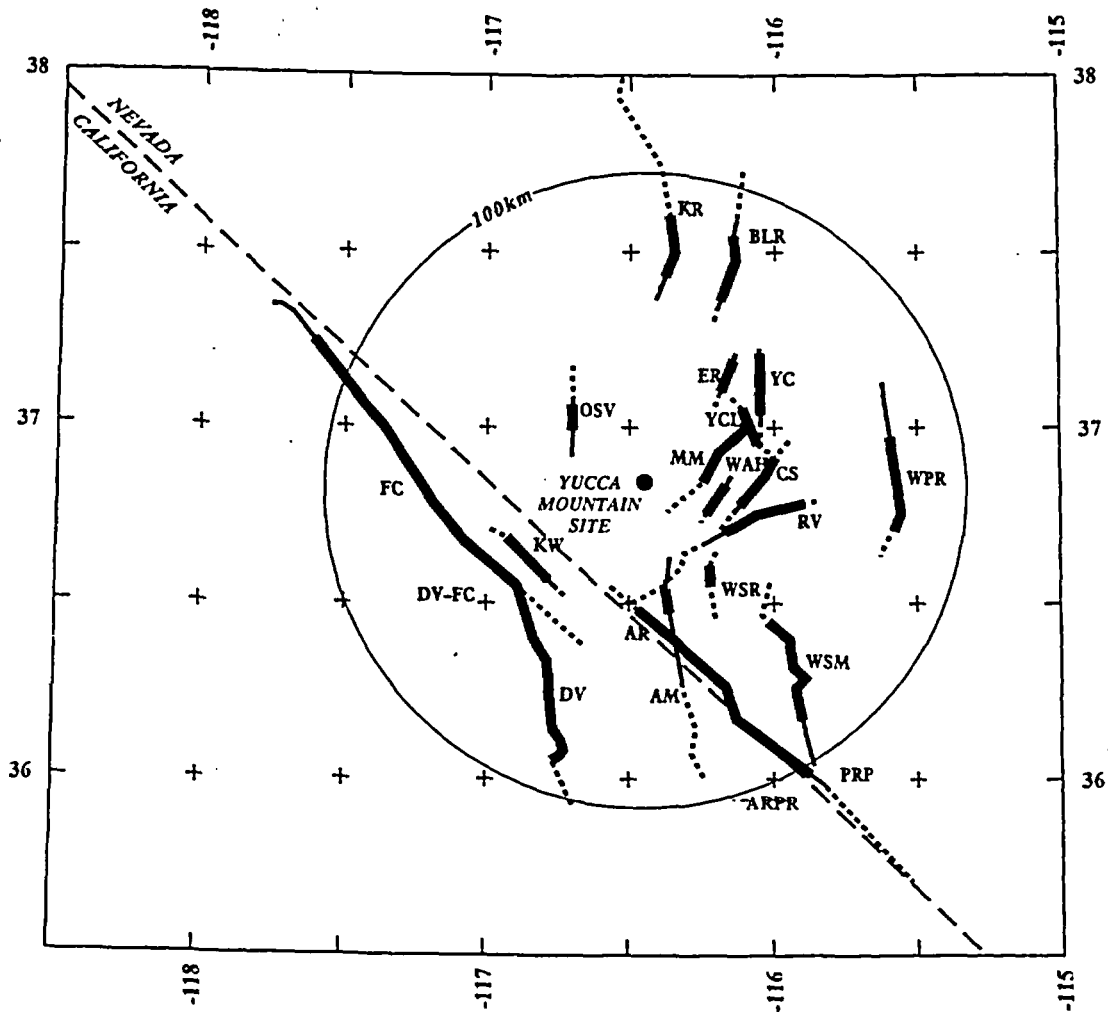


12.3-38 DOC SITEDESC R01

Source: Wong and Stepp (1998, Figure 4-7)

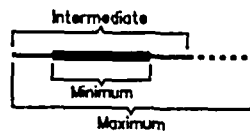
NOTE: Recurrence model is constrained by recurrence interval or slip rate.

Figure 12.3-38. Alternative Recurrence Models for Large-Magnitude Events

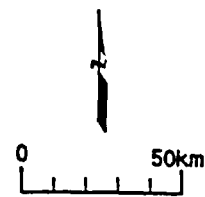


EXPLANATION

Fault Lengths:



NOTE: Fault names are listed in Table 12.3-12

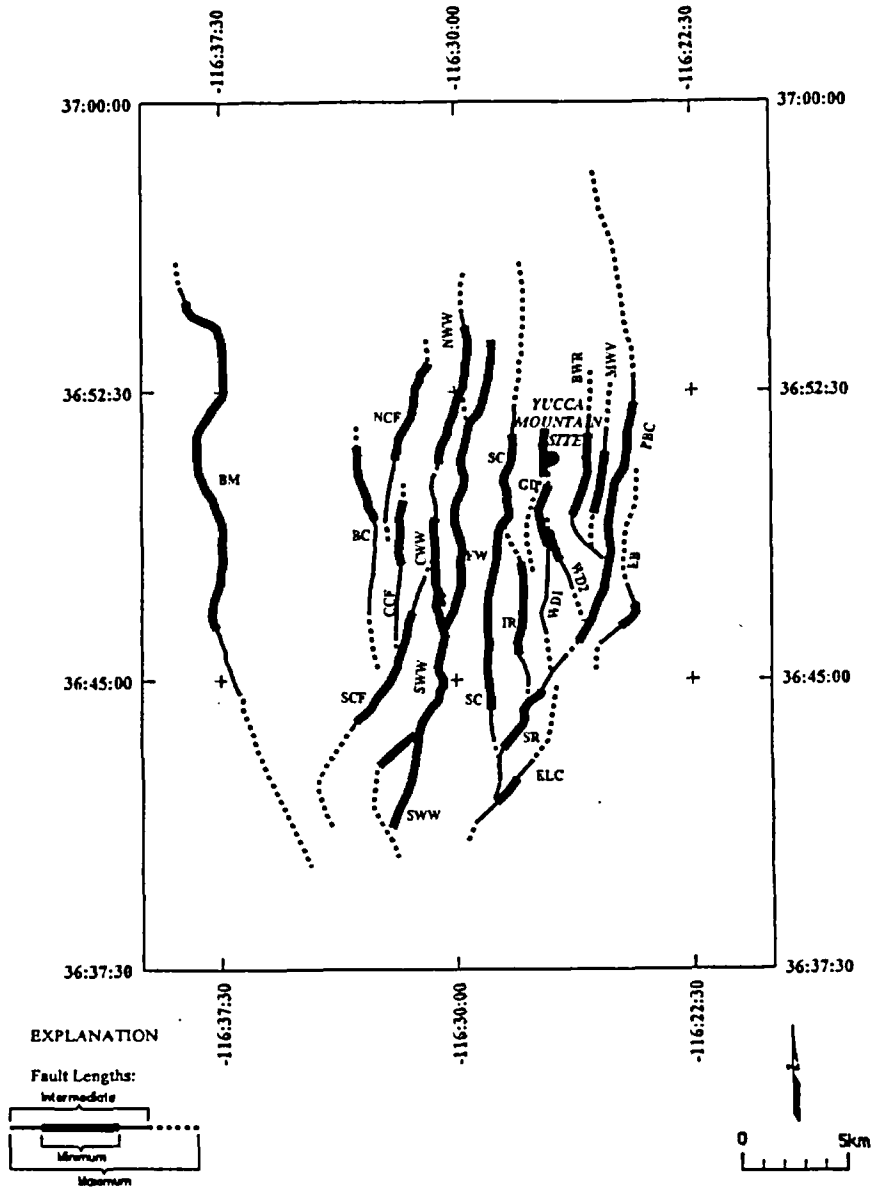


12.3-39.DOC.SITEDESC-R01

Source: Wong and Stepp (1998, Figure 4-21)

Figure 12.3-39. Regional Fault Sources Considered by One Seismic Source Expert Team

(a) Local Faults Considered as Independent Faults



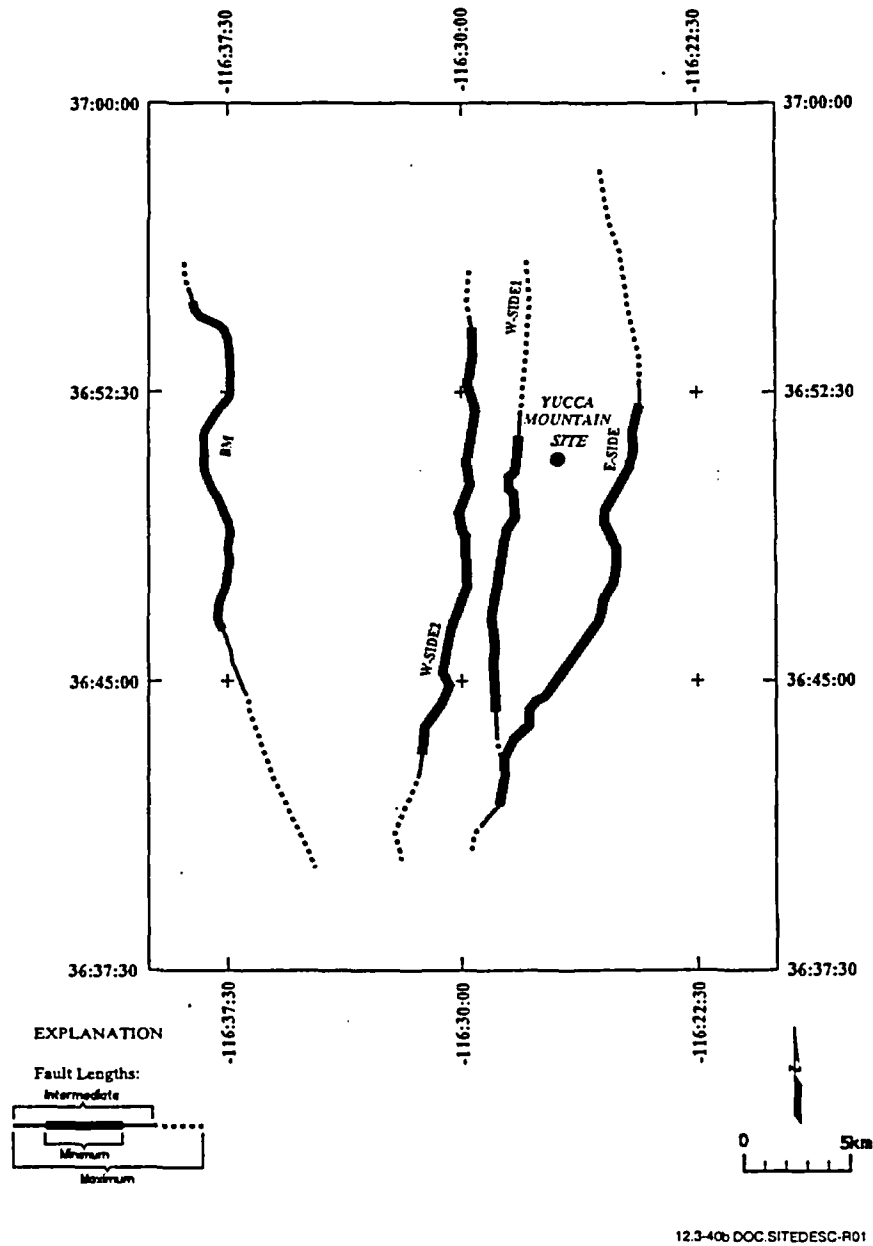
12.3-40a DOC SITEDESC-R01

Source: Wong and Stepp (1998, Figure 4-18)

NOTE: Fault names are listed on Figure 12.3-12. Exceptions are NCF, CCF, and SCF, which refer to the North, Central, and Southern Crater Flat faults; NWW, CWW, and SWW, which refer to the North, Central, and Southern Windy Wash faults; and WD1 and WD2, which refer to the West Dune Wash fault.

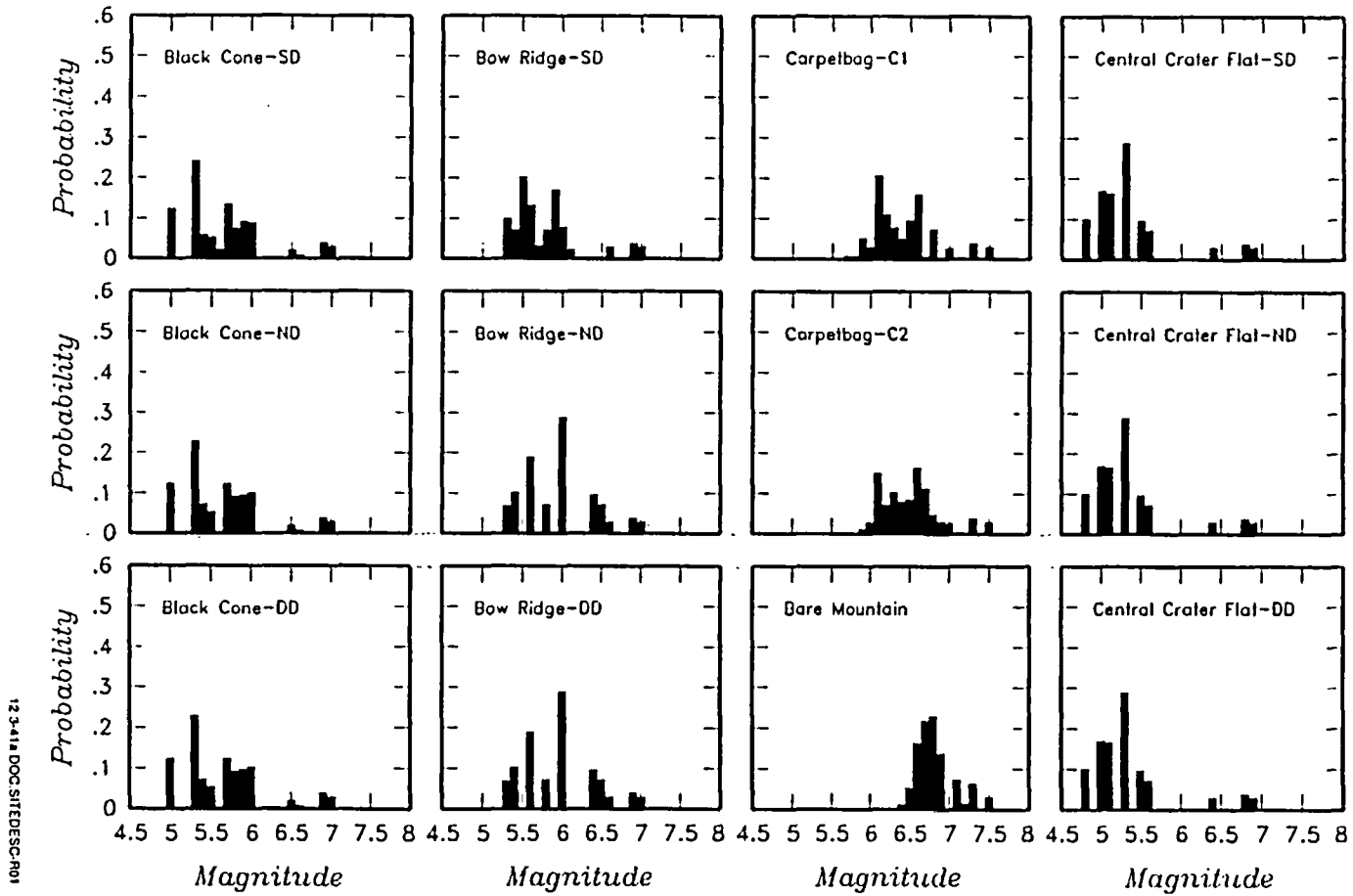
Figure 12.3-40. Example of Local Faults Considered as Independent Faults and Coalesced Faults

(b) Local Faults Considered as Coalesced Faults



Source: Wong and Stepp (1998, Figure 4-19)

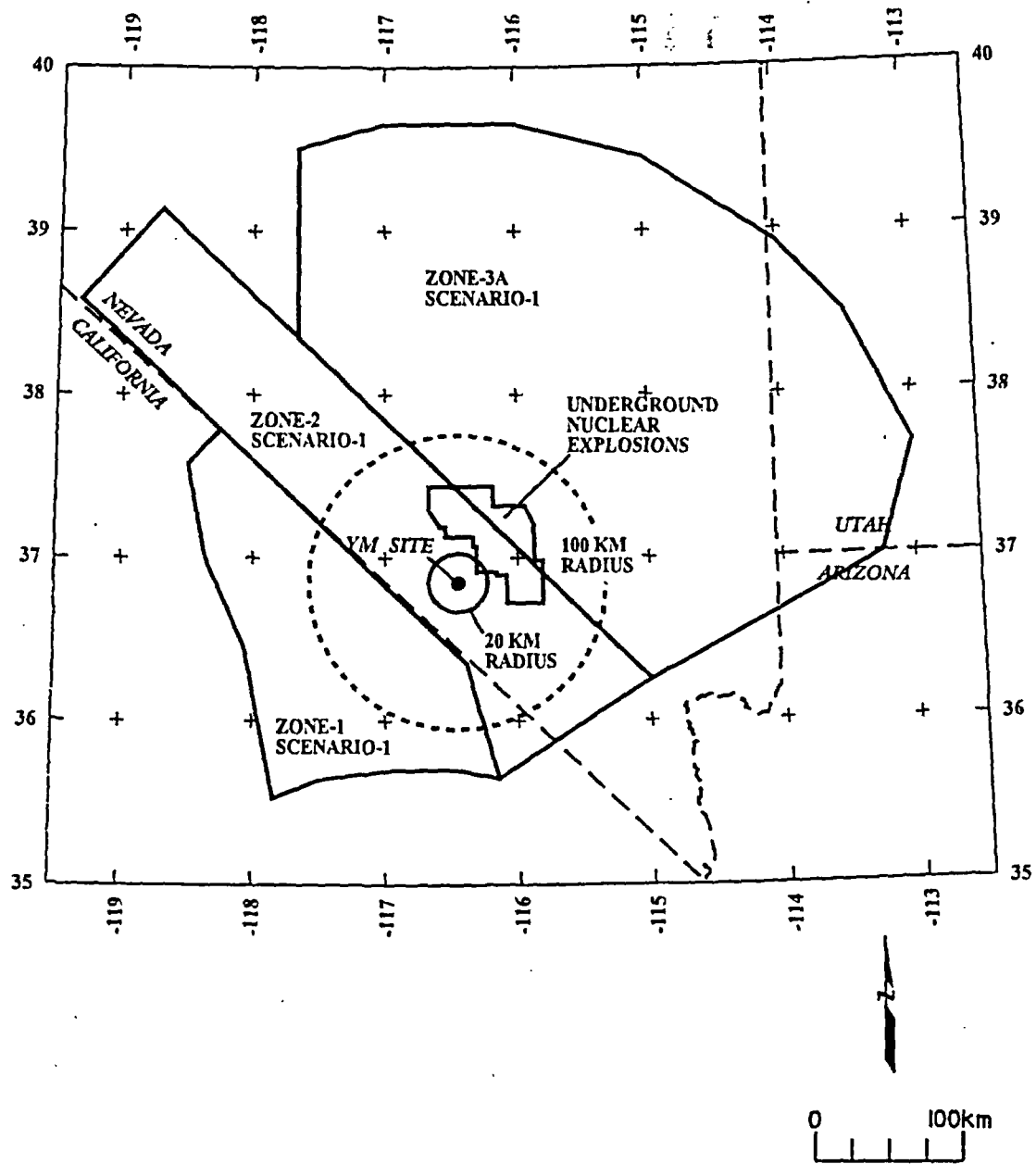
Figure 12.3-40. Example of Local Faults Considered as Independent Faults and Coalesced Faults (Continued)



12-3-41 DOC SITEDESC.R01

Source: Wong and Stepp (1998, Figure 4-20)

Figure 12.3-41. Example of Maximum Magnitude Distributions for Local Faults from One Seismic Source Expert Team

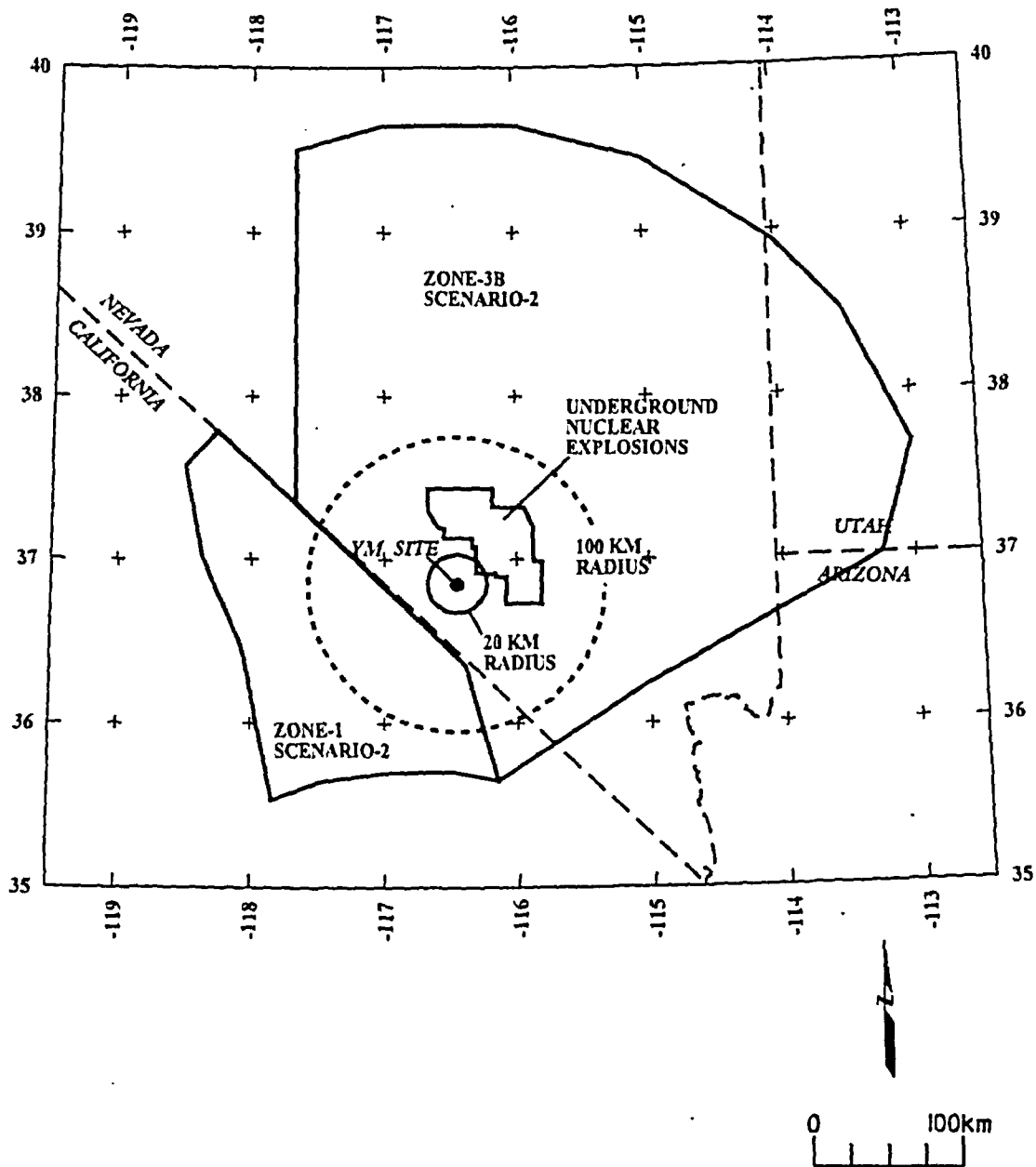


12.3-42a.DOC.SITEDESC-R01, ICN 01

Source: Wong and Stepp (1998, Figure 4-24)

NOTE: YM = Yucca Mountain

Figure 12.3-42. Alternative Regional Source Zone Models Considered by One Seismic Source Expert Team

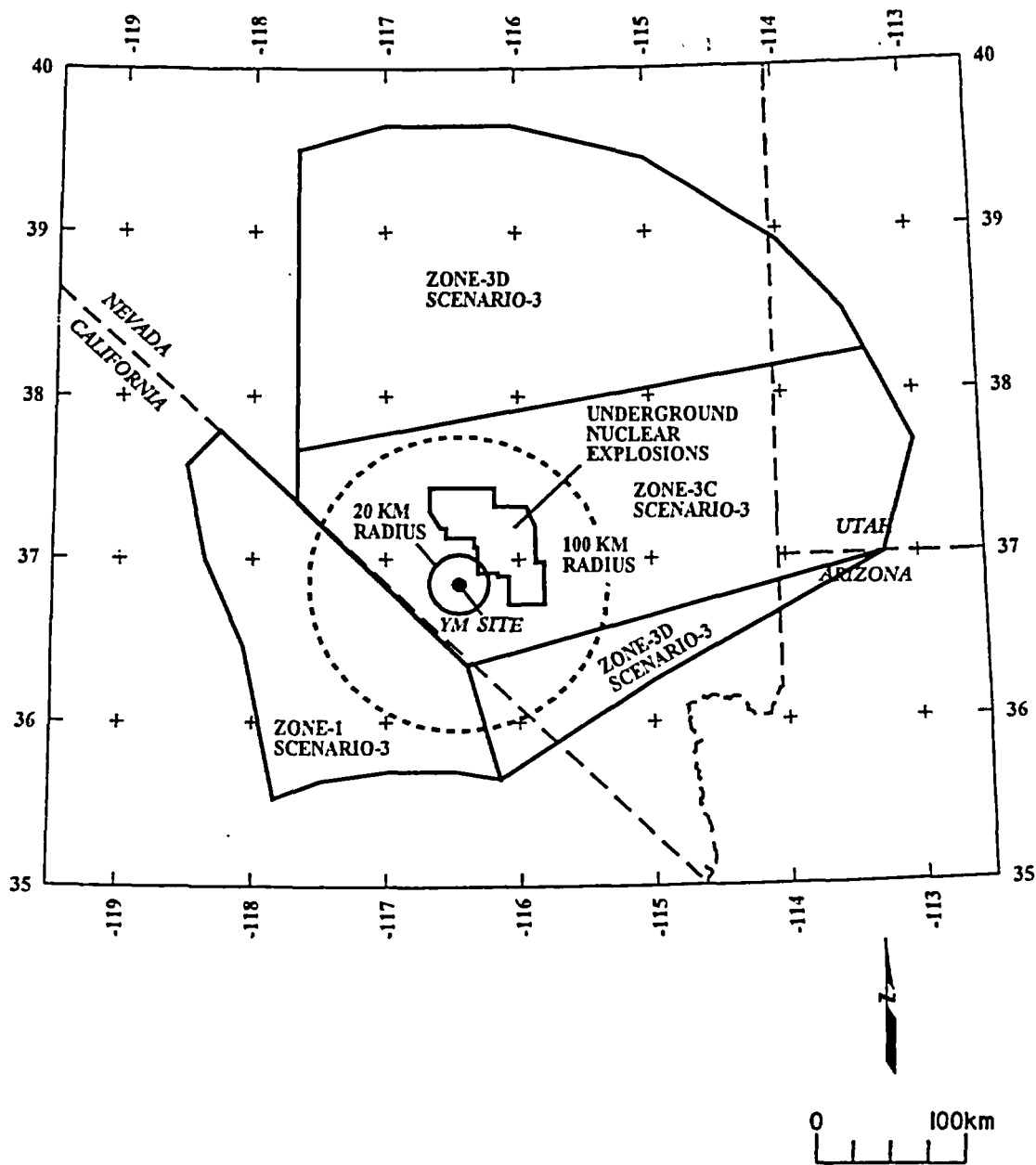


12.3-42b.DOC.SITEDESC-R01, ICN 01

Source: Wong and Stepp (1998, Figure 4-24)

NOTE: YM = Yucca Mountain

Figure 12.3-42. Alternative Regional Source Zone Models Considered by One Seismic Source Expert Team (Continued)

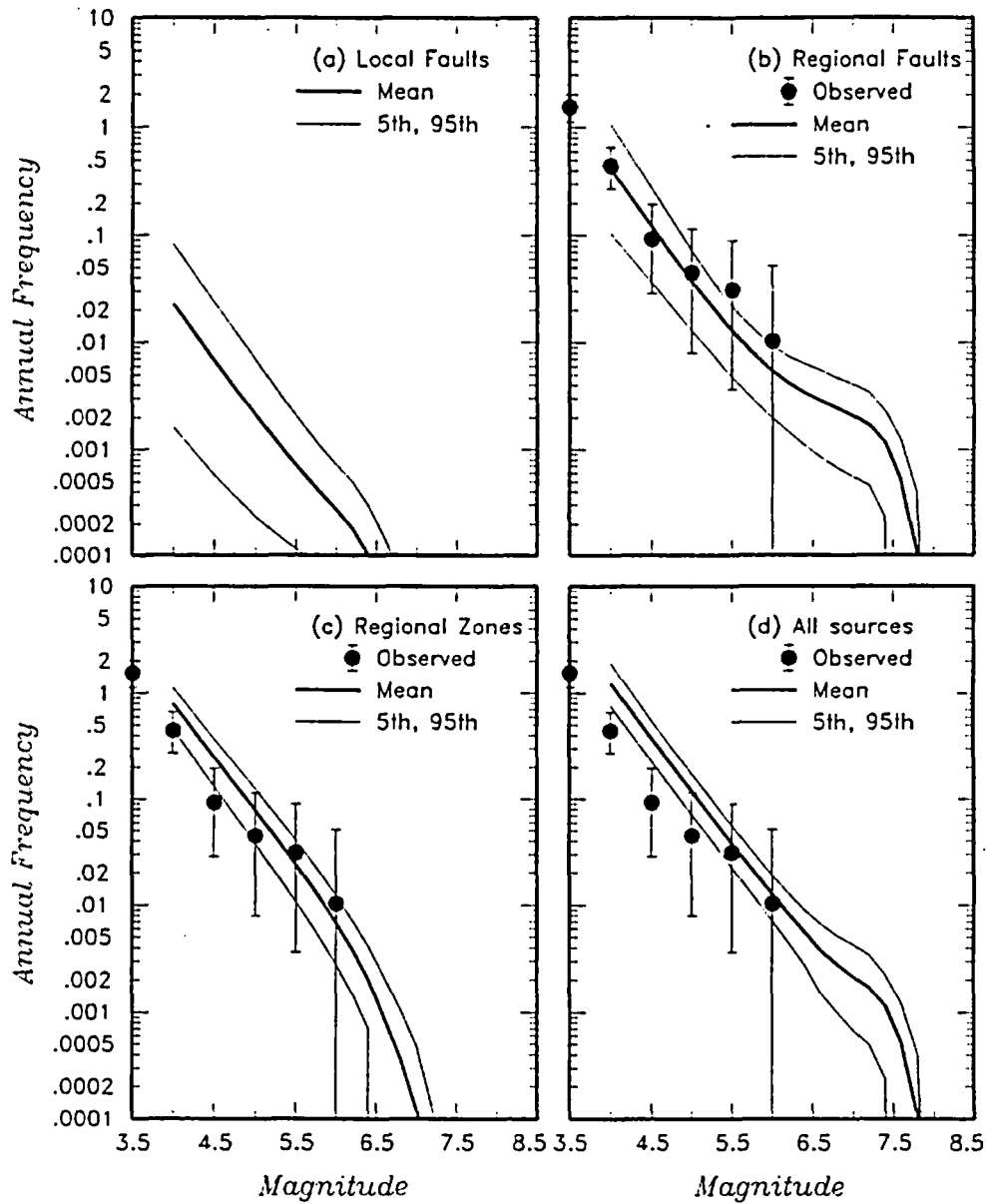


12.3-42c.DOC.SITEDESC-R01, ICN 01

Source: Wong and Stepp (1998, Figure 4-24)

NOTE: YM = Yucca Mountain

Figure 12.3-42. Alternative Regional Source Zone Models Considered by One Seismic Source Expert Team (Continued)

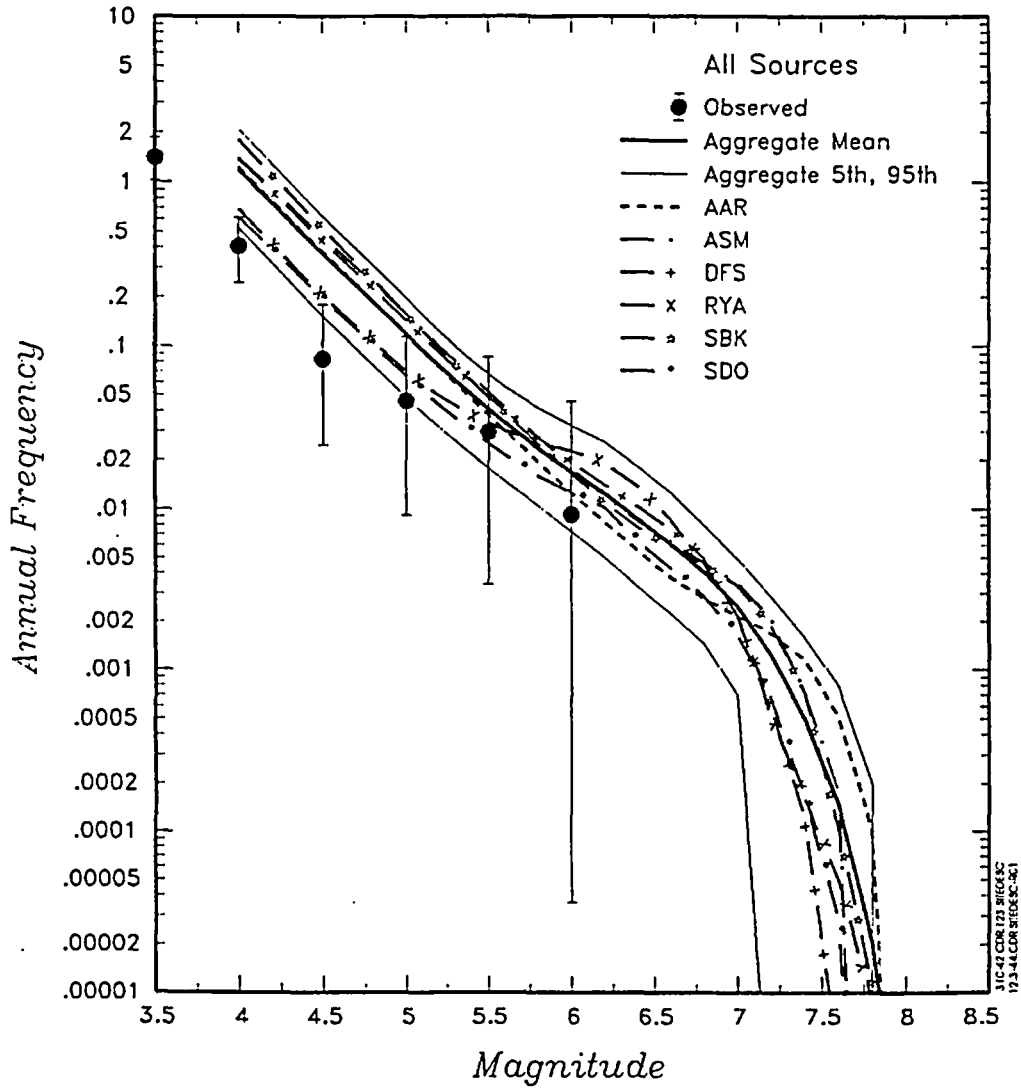


12.3-43 DOC SITEDESC-R01

Source: Wong and Stepp (1998, Figure 4-26)

NOTE: The solid dots with vertical error bars represent the observed frequency of earthquakes occurring within 100 km of the Yucca Mountain site.

Figure 12.3-43. Earthquake Recurrence Rates Determined by One Seismic Source Expert Team

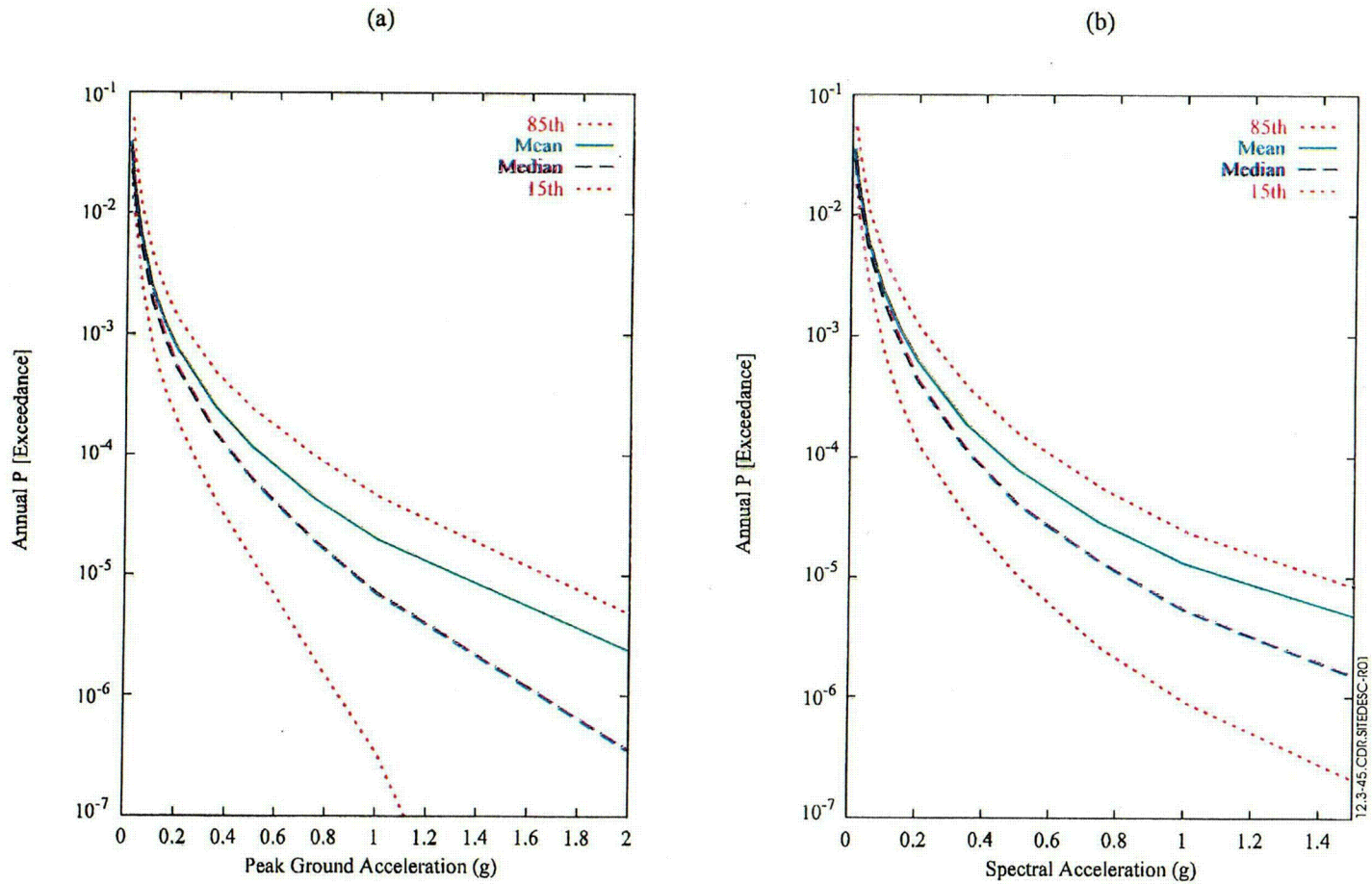


Source: Wong and Stepp (1998, Figure 4-77)

NOTE: The solid dots with vertical error bars represent the observed frequency of earthquakes occurring within 100 km of the Yucca Mountain site. The three-letter abbreviations designate the seismic source expert teams. See Wong and Stepp (1998) for more information.

Figure 12.3-44. Earthquake Recurrence Rates for All Sources Combined Predicted by All Teams Combined and by Individual Seismic Source Expert Teams

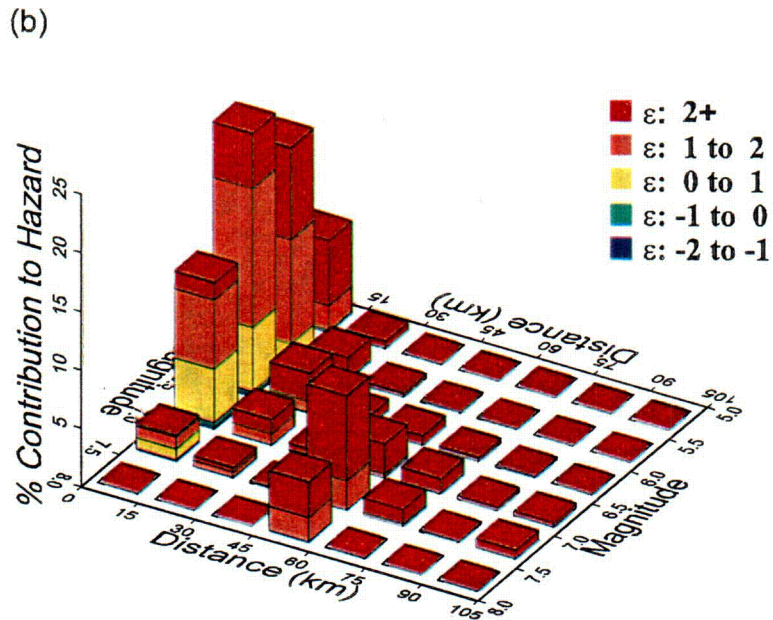
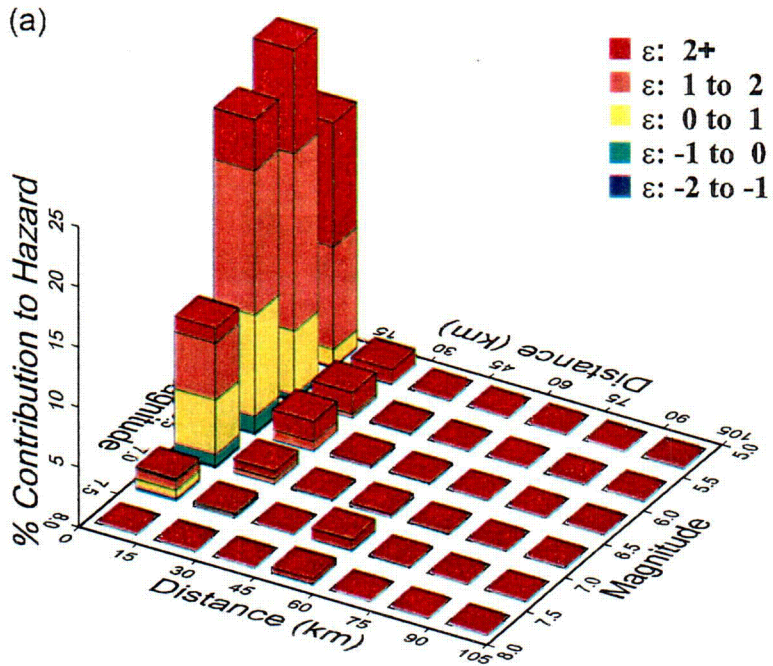
C11



Source: Wong and Stepp (1998, Figures 7-10 and 7-12)

NOTE: Plot (a) shows horizontal peak ground acceleration; plot (b) shows 1-Hz spectral acceleration.

Figure 12.3-45. Summary Hazard Curves for Horizontal Peak Ground Acceleration and 1-Hertz Spectral Acceleration

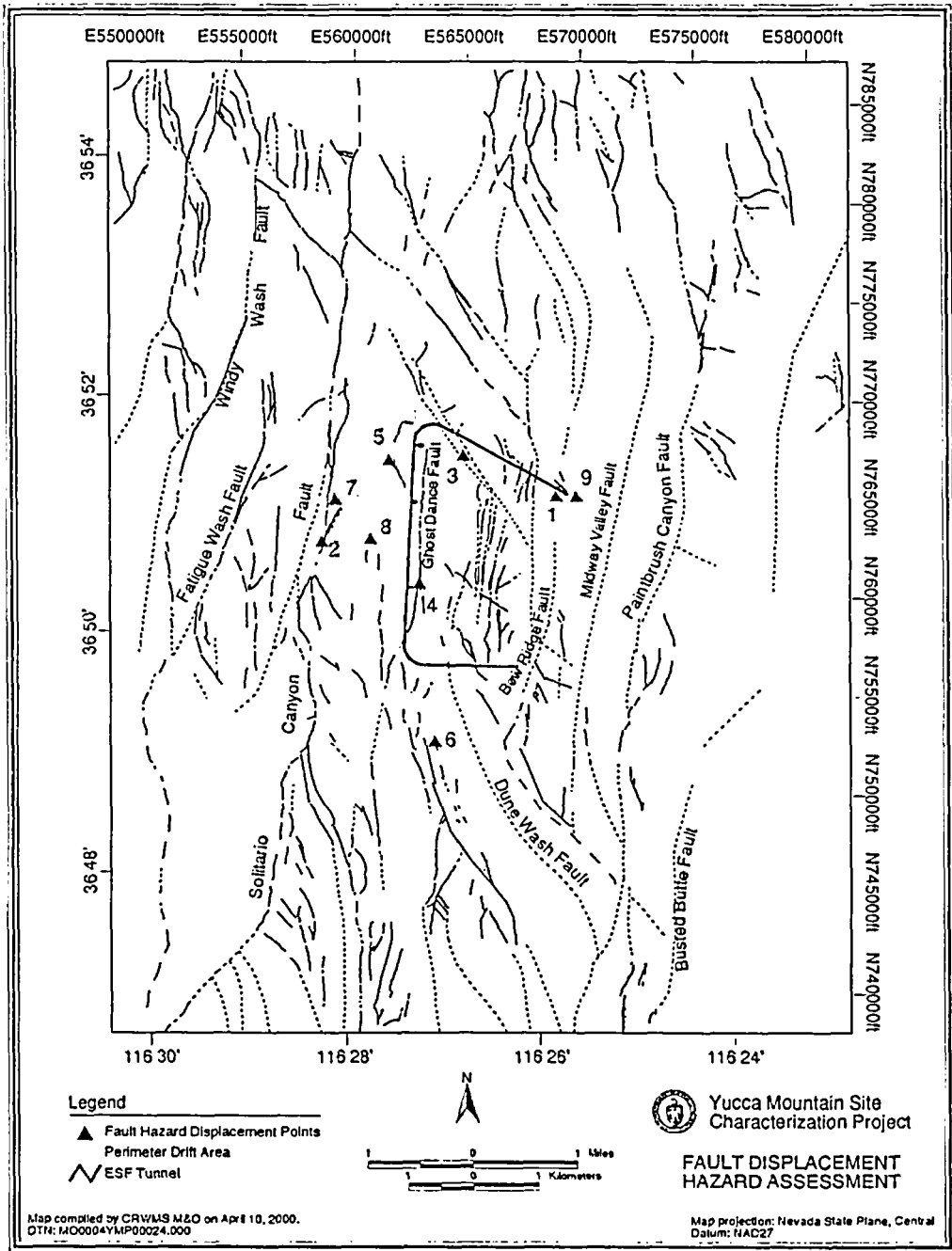


12.3-46.CDR SITEDESC-R01

Source: Wong and Stepp (1998, Figures 7-15 and 7-16)

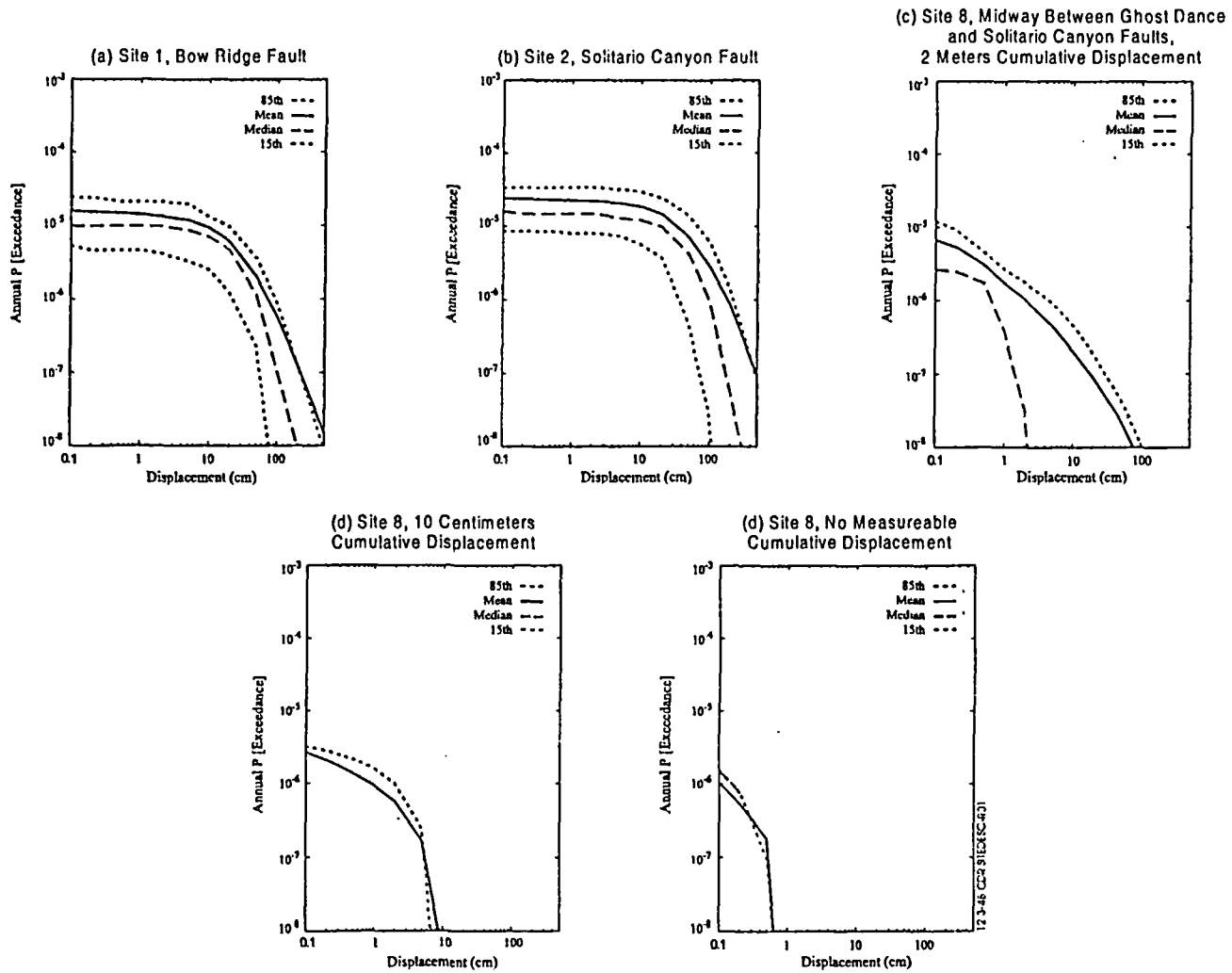
NOTE: Graph (a) is for 5- to 10-Hz horizontal spectral acceleration; graph (b) is for 1- to 2-Hz horizontal spectral acceleration

Figure 12.3-46. Deaggregation of Mean Seismic Hazard for Horizontal Spectral Acceleration at 10^{-4} Annual Exceedance Probability



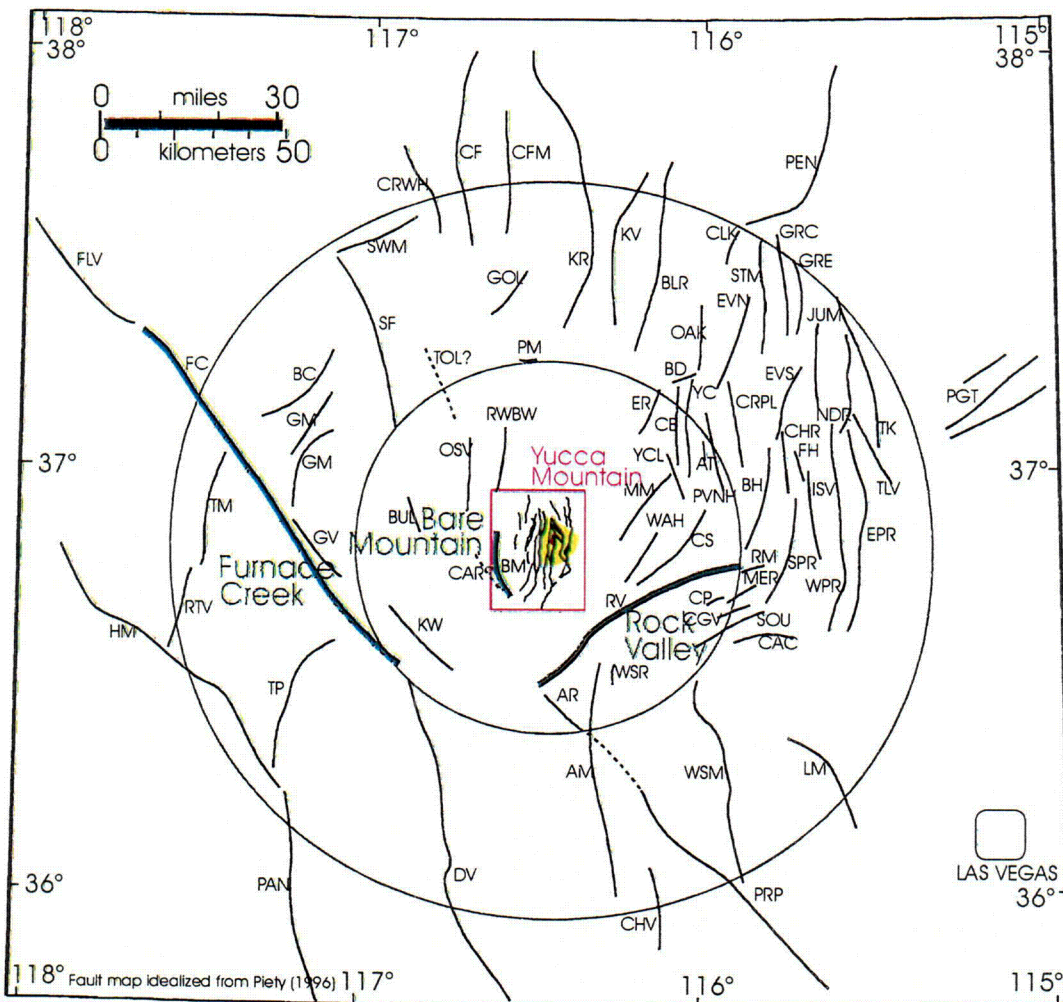
Source: Wong and Stepp (1998, Figure 4-9)

Figure 12.3-47. Location of Nine Demonstration Sites Used in Fault Displacement Hazard Assessment



Source: Wong and Stepp (1998, Figures 8-2, 8-3, 8-12, and 8-13)

Figure 12.3-48. Summary Fault Displacement Hazard Curves Site 8, No Measurable Cumulative Displacement



Fault map idealized from Piety (1996)

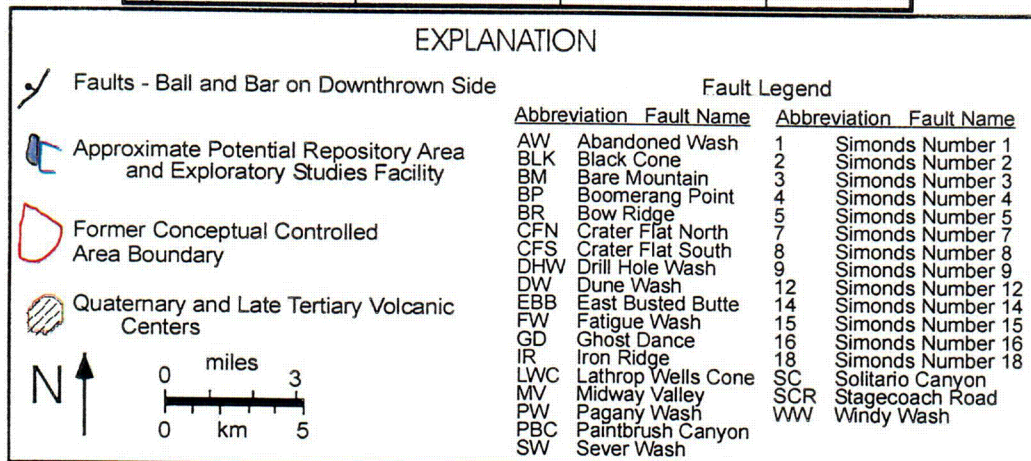
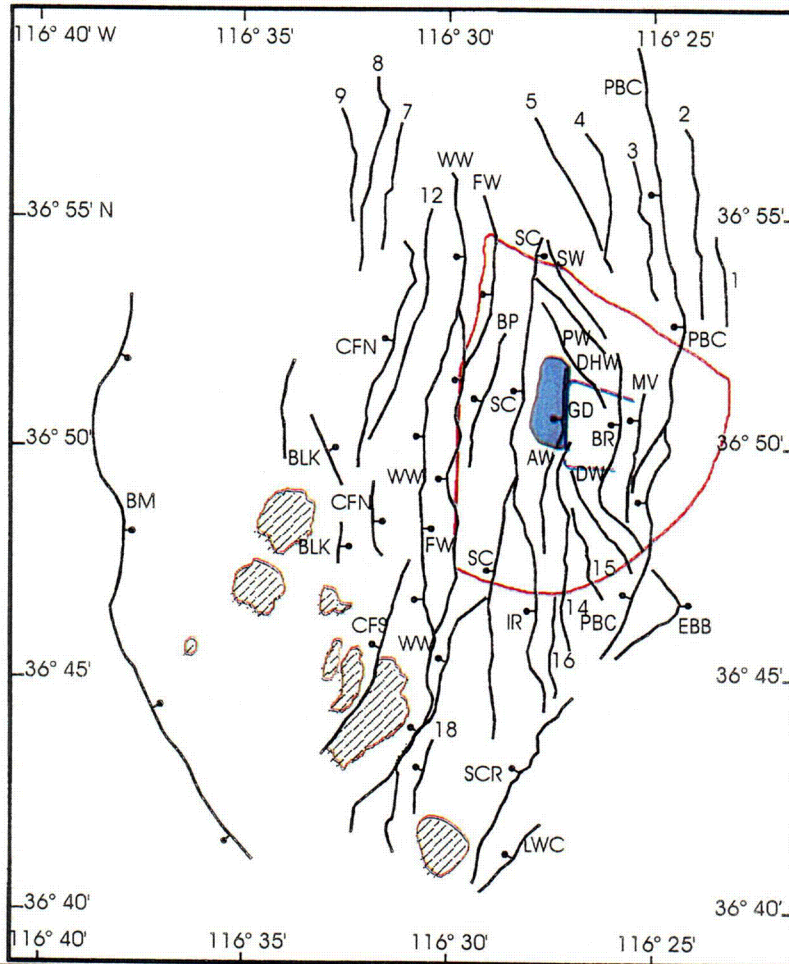
AM	Ash Meadows	CRPL	Cockeyed Ridge-Papoose Lake	ISV	Inchian Springs Valley	RV	Rock Valley
AR	Amargosa River	CSWH	Cactus Range-Wellington Hills	JUM	Jumbled Hills	RWBW	Rock Wash-Beatty Wash
AT	Area Three	DV	Death Valley	KV	Kawich Range	SOU	Sarcobatus Flat
BC	Bonnie Claire	DVFC	DV and FC	KW	Kawich Valley	SPR	South Range
BD	Buried Hills	ER	East Pintwater Range	LV	Leona Valley	STM	Spotted Range
BE	Belted Range	EVN	Leona Range	MER	Mercury Ridge	SWM	Stonewall Mountain
BU	Bare Mountain	GOI	Emigrant Valley North	MM	Mine Mountain	TK	Tikaboo
BUL	Bullfrog Hills	GOV	Emigrant Valley South	NOR	North Desert Range	TLV	Three Lakes Valley
CC	Cactus Springs	GV	Furnace Creek	OAK	Oak Spring Butte	TM	Tin Mountain
CCAC	Carrara	HM	Fallout Hills	OSV	Oasis Valley	TOL	Tolicha Peak
CCB	Carpetbag	TP	Fish Lake Valley	PAN	Panamint Valley	TP	Towne Pass
CCF	Cactus Flat	TP	Grapevine Mountains	PEN	Penover	WAH	Wahmonie
CCFM	Cactus Flat-Mellon	TP	Gold Flat	PGT	Pahranaagat	WPR	West Pintwater Range
CCG	Cossagain Valley	TP	Groom Range Central	PM	Pahrump	WSM	West Springs Mountain
CCIR	Chert Ridge	TP	Groom Range East	PVNH	Platinum Valley	WSR	West Specter Range
CCV	Chicago Valley	TP	Grapevine	RV	N Halfant Range	YCL	Yucca Lake
CCW	Chalk Mountain	TP	Hunter Mountain	RM	Ranger Mountains		
CP	Checkpoint Pass	TP		RTV	Racetrack Valley		

310-43.CDR.123.SIEDSC
12.3-49.CDR.SIEDSC-R01

Source: USGS (2000, Figure 1)

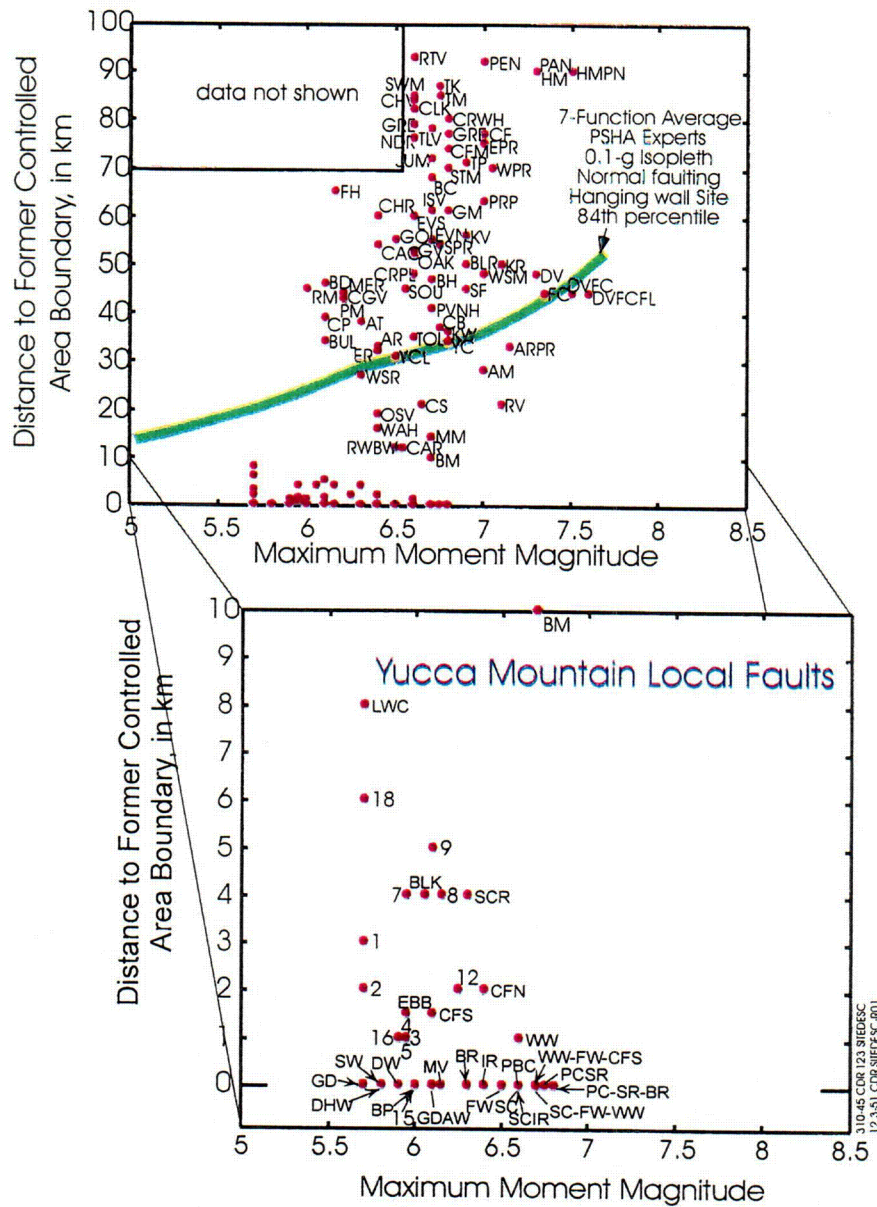
NOTE: Three regional faults (BM, FC, and RV) included in Table 12.3-20 are highlighted. The two large circles show 50 and 100 km (31 and 62 mi.) from Yucca Mountain.

Figure 12.3-49. Faults within 100 Kilometers of Yucca Mountain Considered in the Deterministic Seismic Hazard Analysis



Source: USGS (2000, Figure 2)

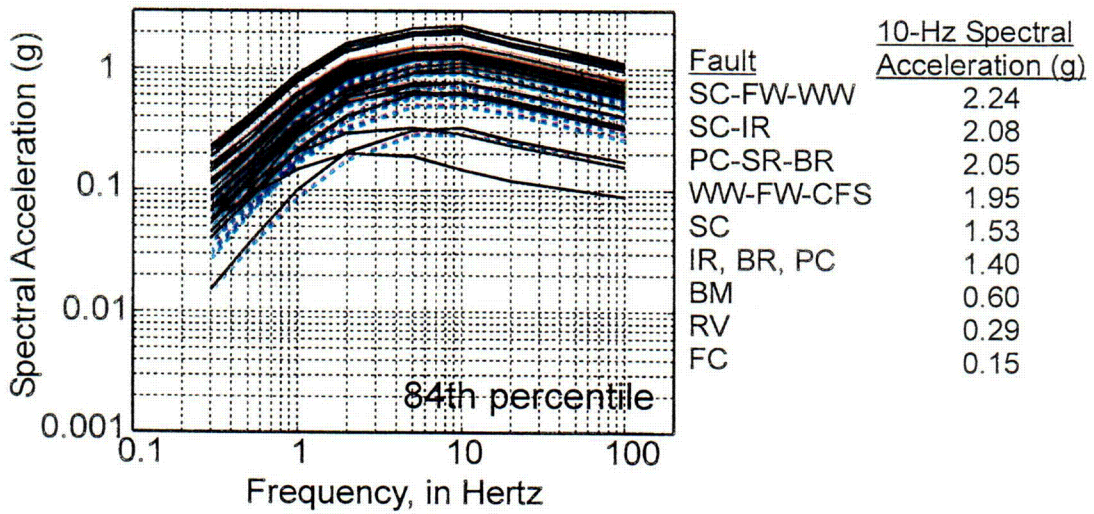
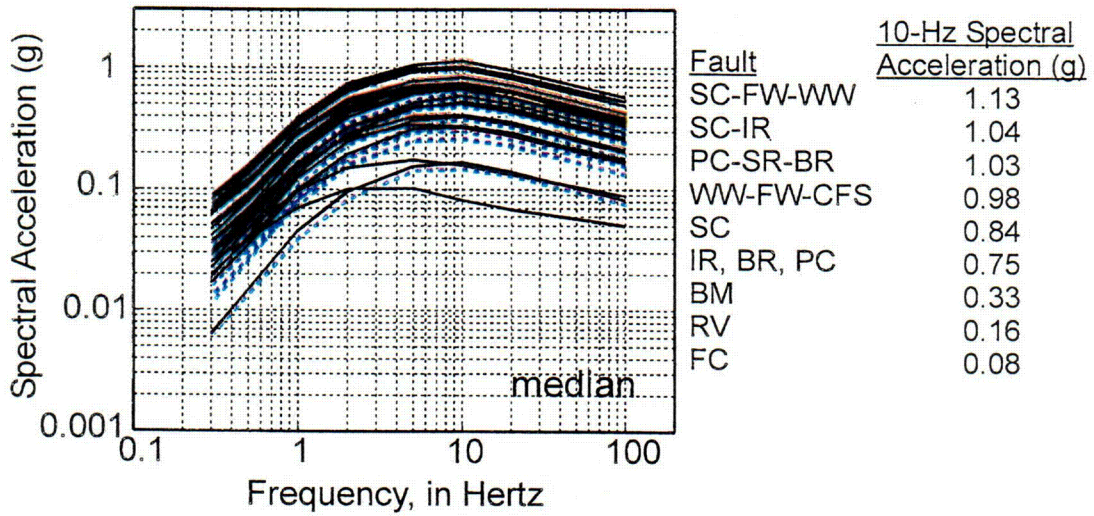
Figure 12.3-50. Local Faults Considered in the Deterministic Seismic Hazard Analysis



Source: After USGS (2000, Figure 3)

NOTE: Fault abbreviations are, in general, defined in Figures 12.3-49 and 12.3-50. In addition to the definitions given on those figures, the following additional abbreviations are used: ARPR = Amargosa Valley-Pahrump; DVFCFL = Death Valley-Furnace Creek-Fish Lake Valley; GDAW = Ghost Dance-Abandoned Wash; NDR = North Desert Range; PCSR = Paintbrush Canyon-Stagecoach Road; PC-SR-BR = Paintbrush Canyon-Stagecoach Road-Bow Ridge; SC-FW-WW = Solitario Canyon-Fatigue Wash-Windy Wash; SCIR = Solitario Canyon-Iron Ridge; WW-FW-CFS = Windy Wash-Fatigue Wash-Crater Flat South. PSHA = Probabilistic Seismic Hazard Analysis

Figure 12.3-51. Deterministic Maximum Magnitudes in Relation to Minimum Distance to the Former Conceptual Controlled Area Boundary for Fault Sources within 100 Kilometers of the Yucca Mountain Site

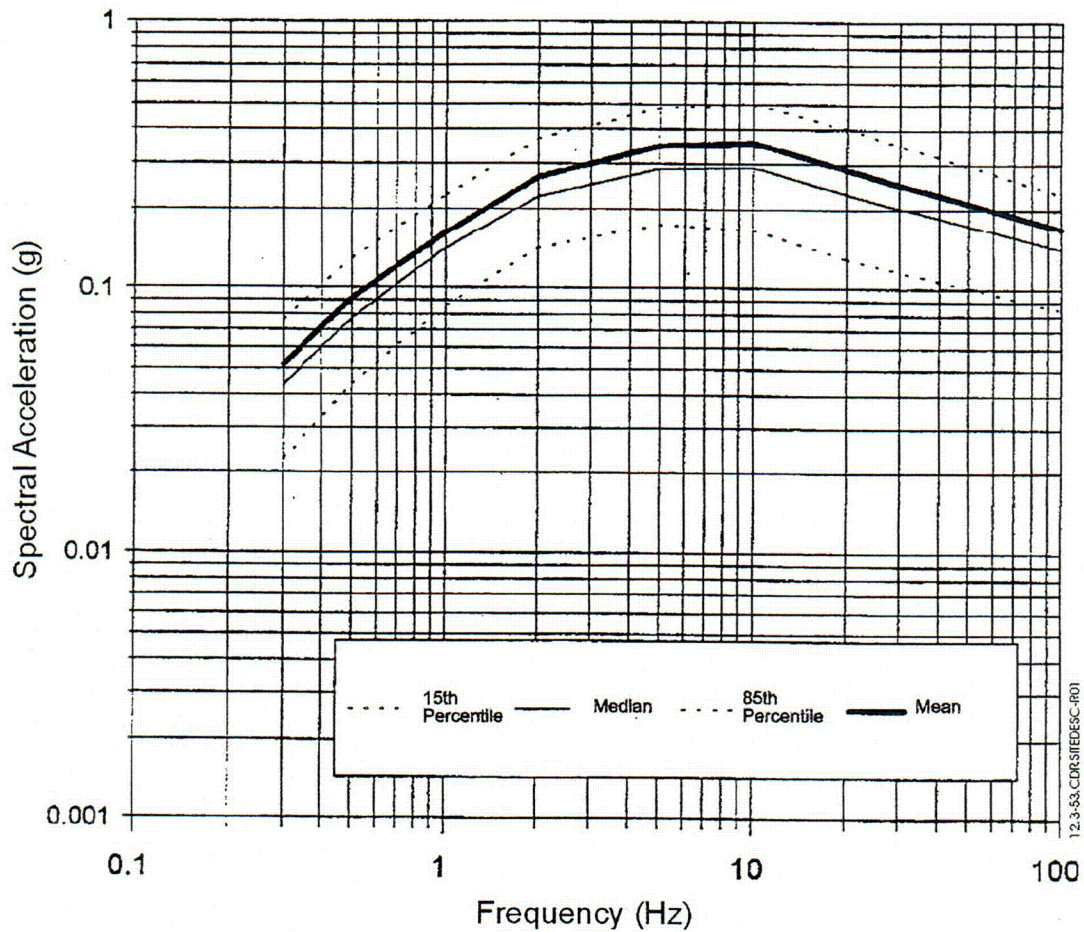


310-46.CDR.123.SITEDESC
12.3-52.CDR.SITEDESC-R01

Source: After USGS (2000, Figure 6)

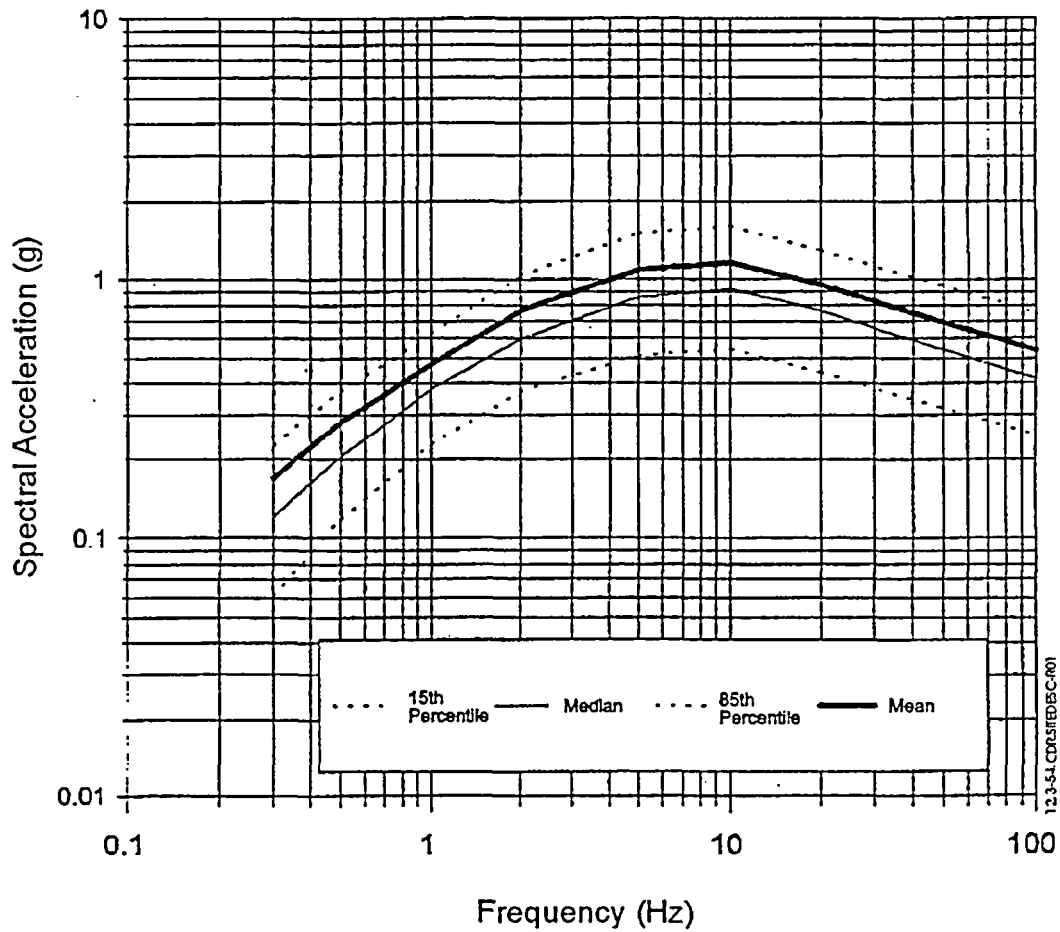
NOTE: Fault names are listed in Figures 12.3-49 and 12.3-50 and the Note to Figure 12.3-51.

Figure 12.3-52. Acceleration Response Spectra for 38 Local and 3 Selected Regional Deterministic Earthquakes



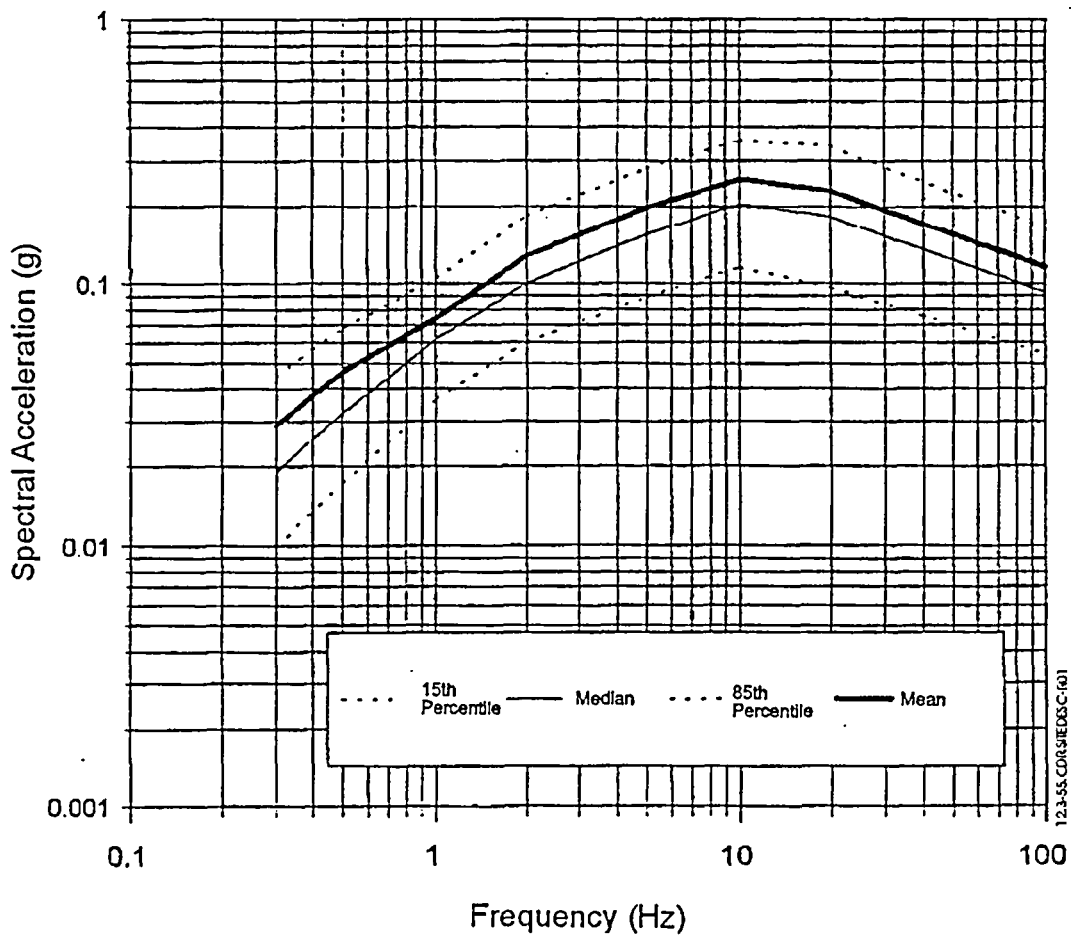
Source: CRWMS M&O (1998i, Figure 2.4-1)

Figure 12.3-53. Uniform Hazard Spectrum for Horizontal Motions at Reference Rock Outcrop, 10^{-3} Annual Probability of Exceedance



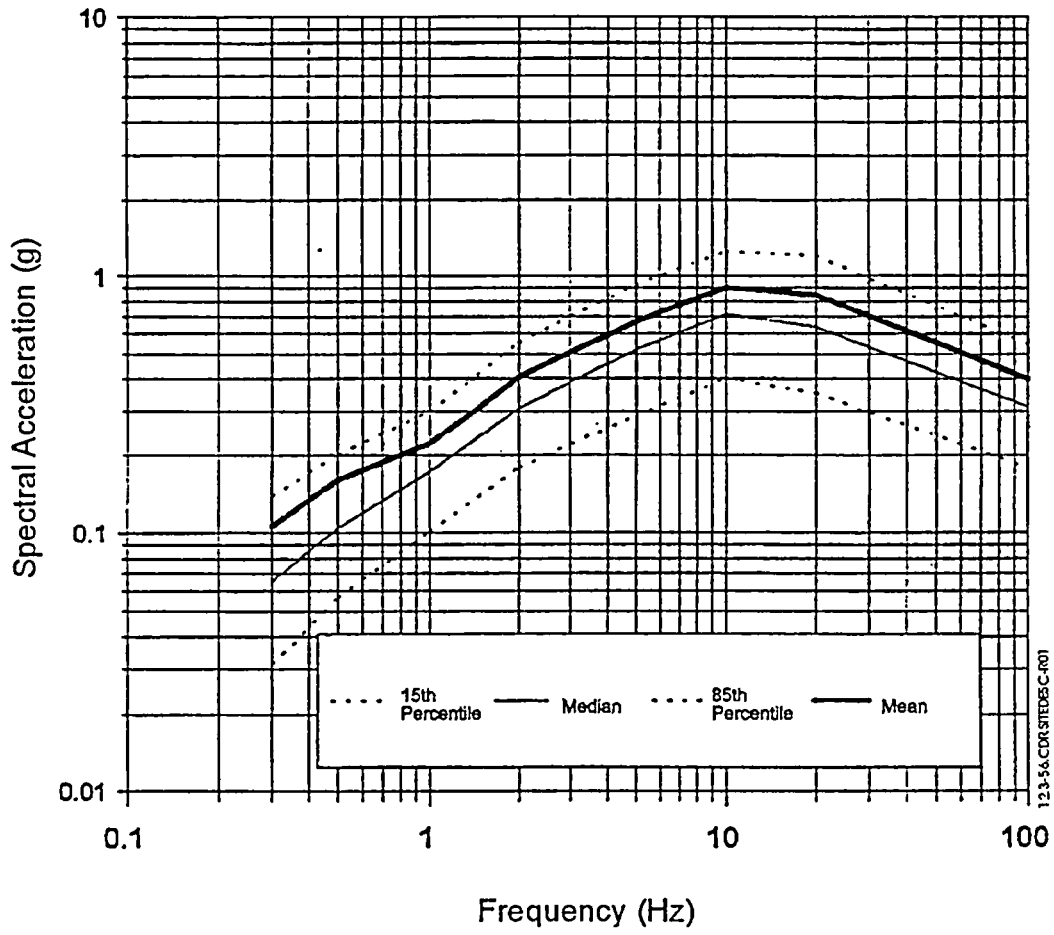
Source: CRWMS M&O (1998i, Figure 2.4-2)

Figure 12.3-54. Uniform Hazard Spectrum for Horizontal Motions at Reference Rock Outcrop, 10^{-4} Annual Probability of Exceedance



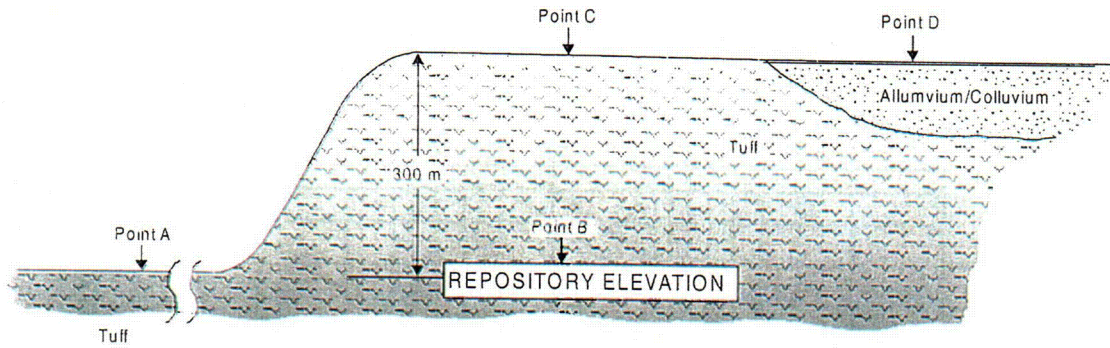
Source: CRWMS M&O (1998i, Figure 2.4-3)

Figure 12.3-55. Uniform Hazard Spectrum for Vertical Motions at Reference Rock Outcrop, 10^{-3} Annual Probability of Exceedance



Source: CRWMS M&O (1998i, Figure 2.4-4)

Figure 12.3-56. Uniform Hazard Spectrum for Vertical Motions at Reference Rock Outcrop, 10^{-4} Annual Probability of Exceedance



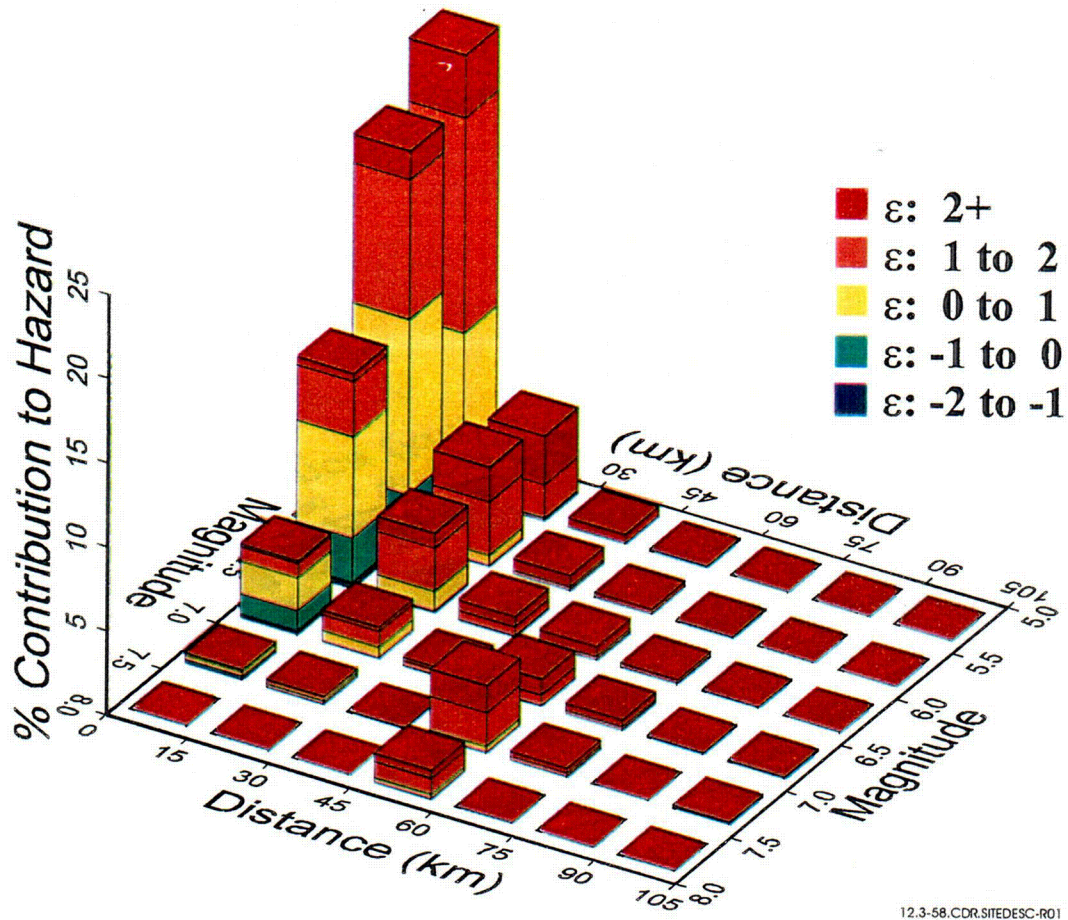
LEGEND

- Point A — Reference rock outcrop at repository elevation
- Point B — Repository elevation with tuff overburden
- Point C — Rock surface
- Point D — Soil surface

12.3-57.CDR.SITEDESC-R01

Source: After Wong and Stepp (1998, Figure 1-1)

Figure 12.3-57. General Locations of Specified Design Earthquake Ground Motions

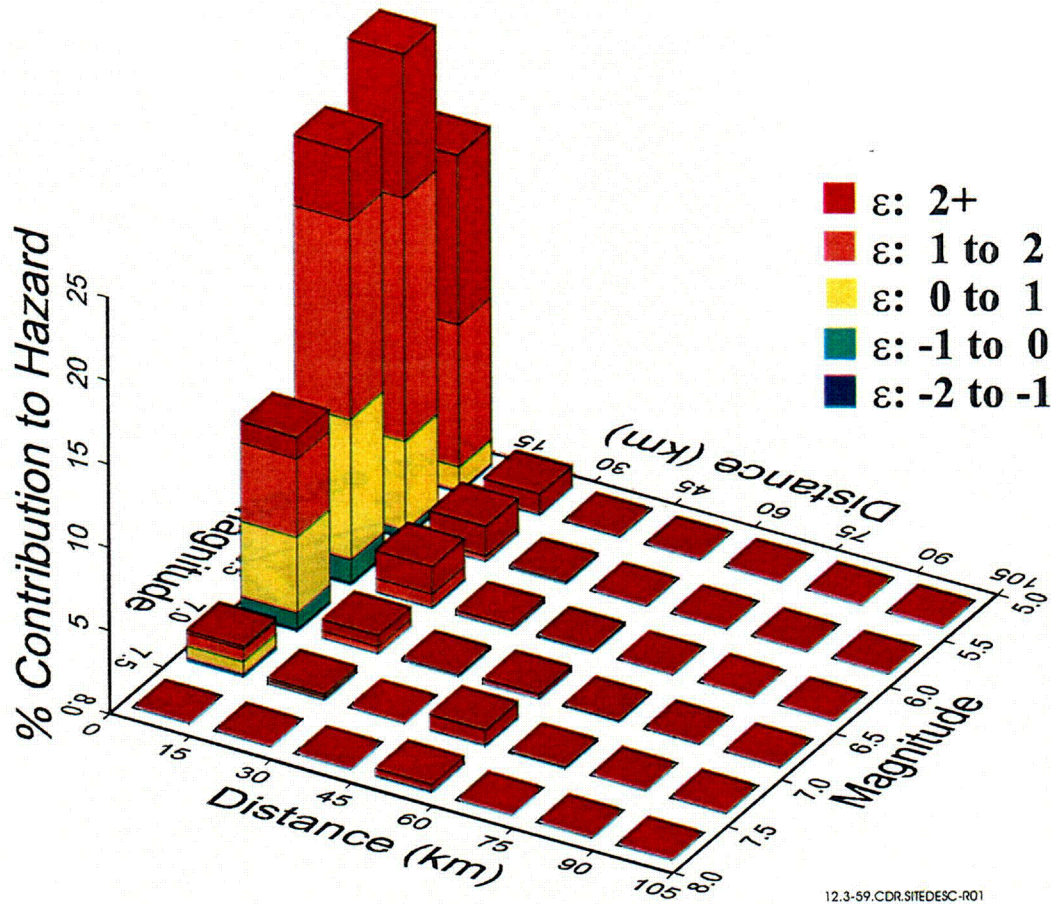


12.3-58.CDR.SITEDESC-R01

Source: CRWMS M&O (1998i, Figure 2.5-1)

NOTE: Moment magnitude is used. Epsilon (ϵ) is in units of standard deviation.

Figure 12.3-58. Contribution to Ground Motion Hazard as a Function of Magnitude, Distance, and Ground Motion Deviation: 5- to 10-Hertz Horizontal Spectral Acceleration, 10^{-3} Annual Frequency of Exceedance

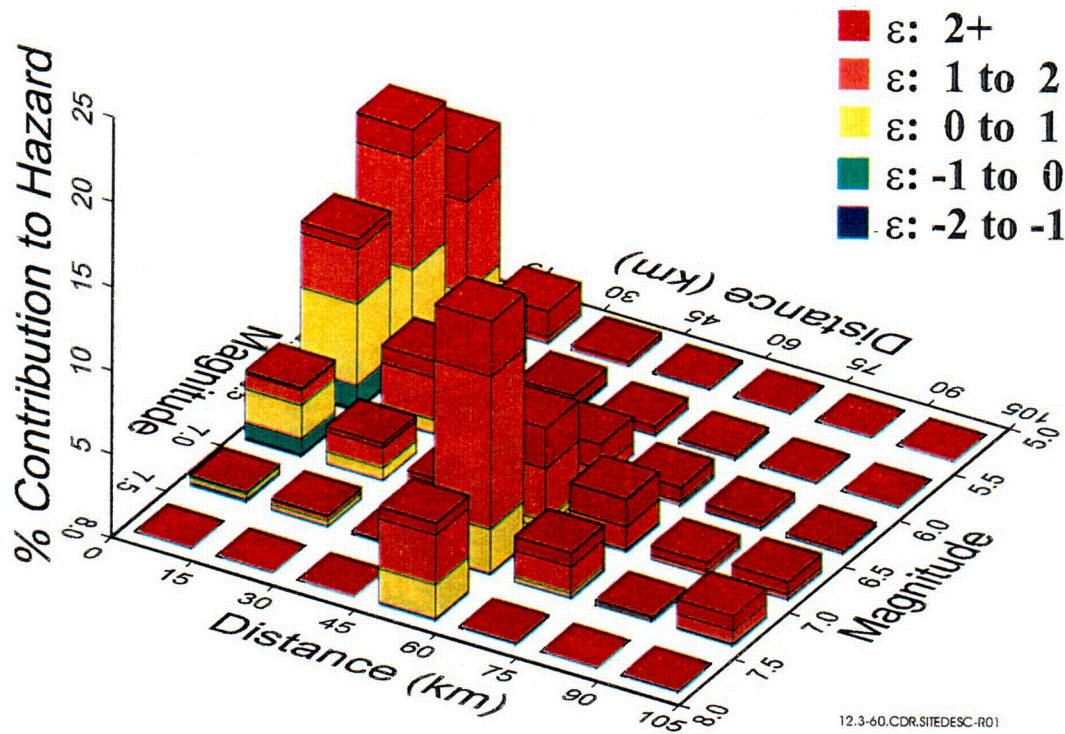


12.3-59.CDR.SITEDESC-R01

Source: CRWMS M&O (1998i, Figure 2.5-2)

NOTE: Moment magnitude is used. Epsilon (ϵ) is in units of standard deviation.

Figure 12.3-59. Contribution to Ground Motion Hazard as a Function of Magnitude, Distance, and Ground Motion Deviation: 5- to 10-Hertz Horizontal Spectral Acceleration, 10^{-4} Annual Frequency of Exceedance

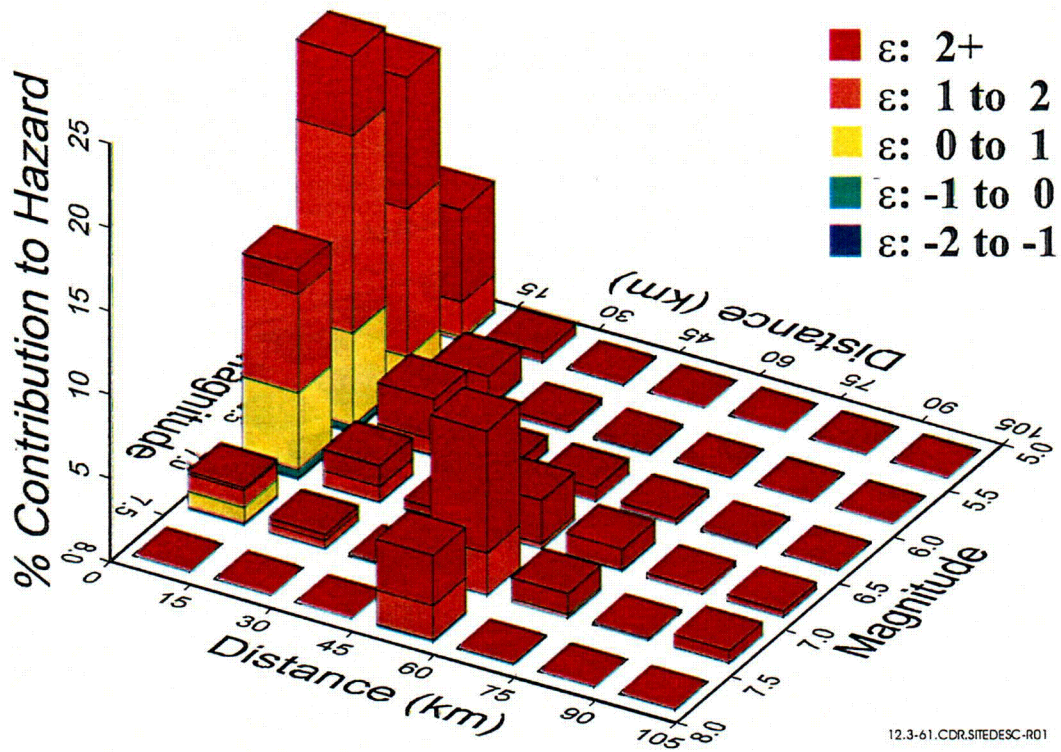


12.3-60.COR.SITEDESC-R01

Source: CRWMS M&O (1998i, Figure 2.5-3)

NOTE: Moment magnitude is used. Epsilon (ε) is in units of standard deviation.

Figure 12.3-60. Contribution to Ground Motion Hazard as a Function of Magnitude, Distance, and Ground Motion Deviation: 1- to 2-Hertz Horizontal Spectral Acceleration, 10⁻³ Annual Frequency of Exceedance

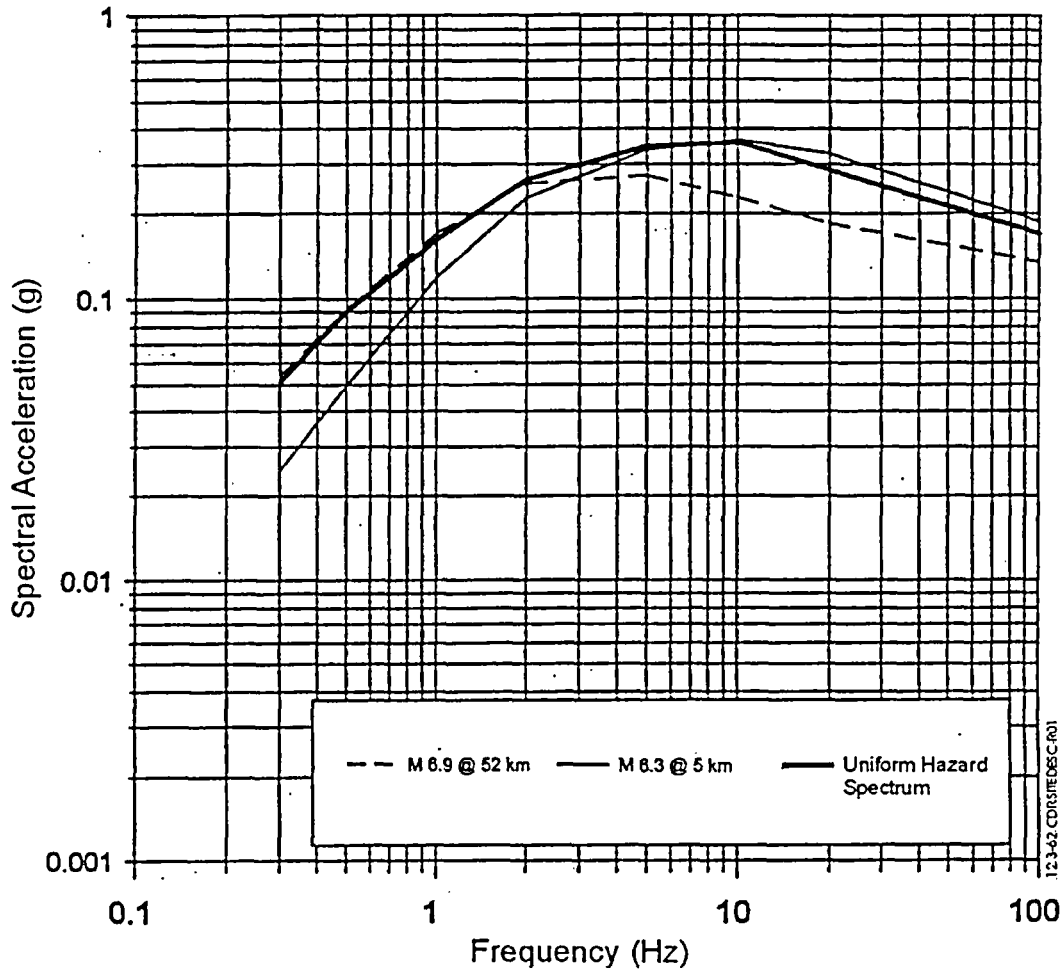


12.3-61.CDR.SITEDESC-R01

Source: CRWMS M&O (1998i, Figure 2.5-4)

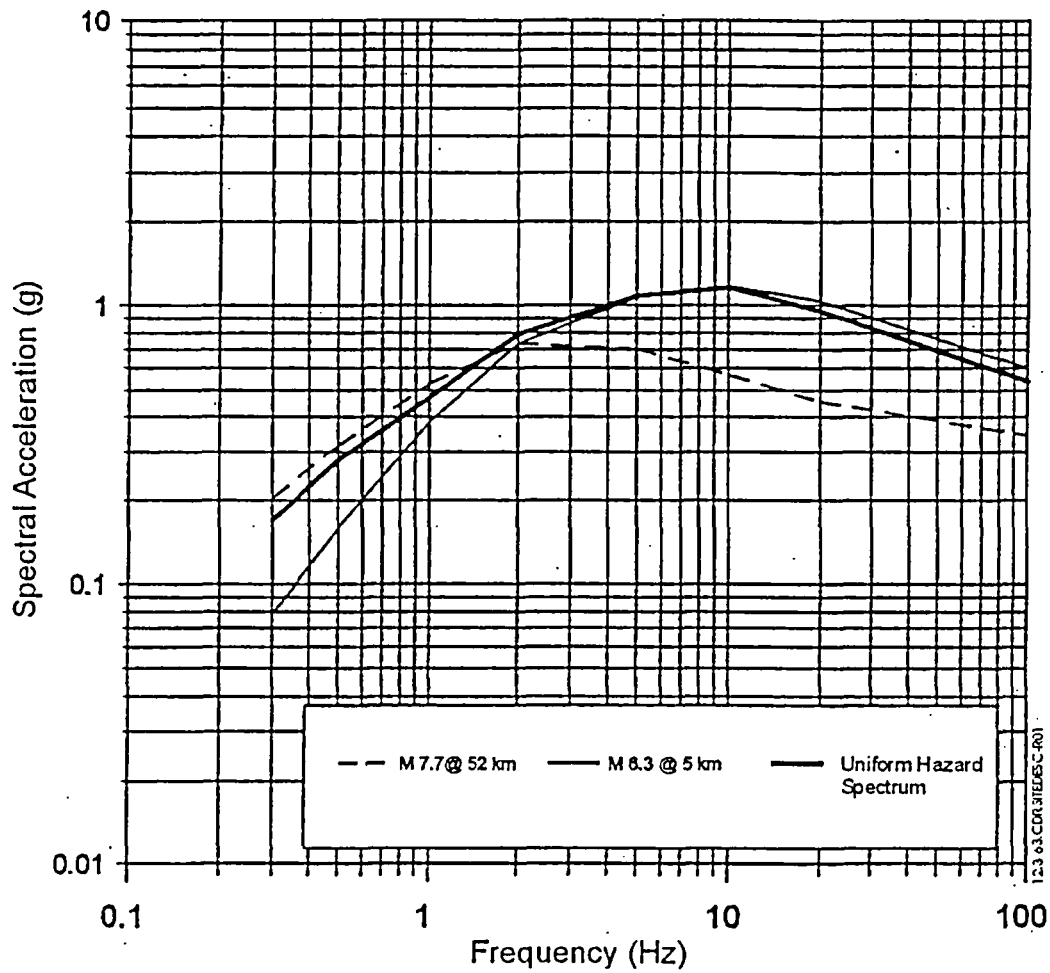
NOTE: Moment magnitude is used. Epsilon (ϵ) is in units of standard deviation.

Figure 12.3-61. Contribution to Ground Motion Hazard as a Function of Magnitude, Distance, and Ground Motion Deviation: 1- to 2-Hertz Horizontal Spectral Acceleration, 10^{-4} Annual Frequency of Exceedance



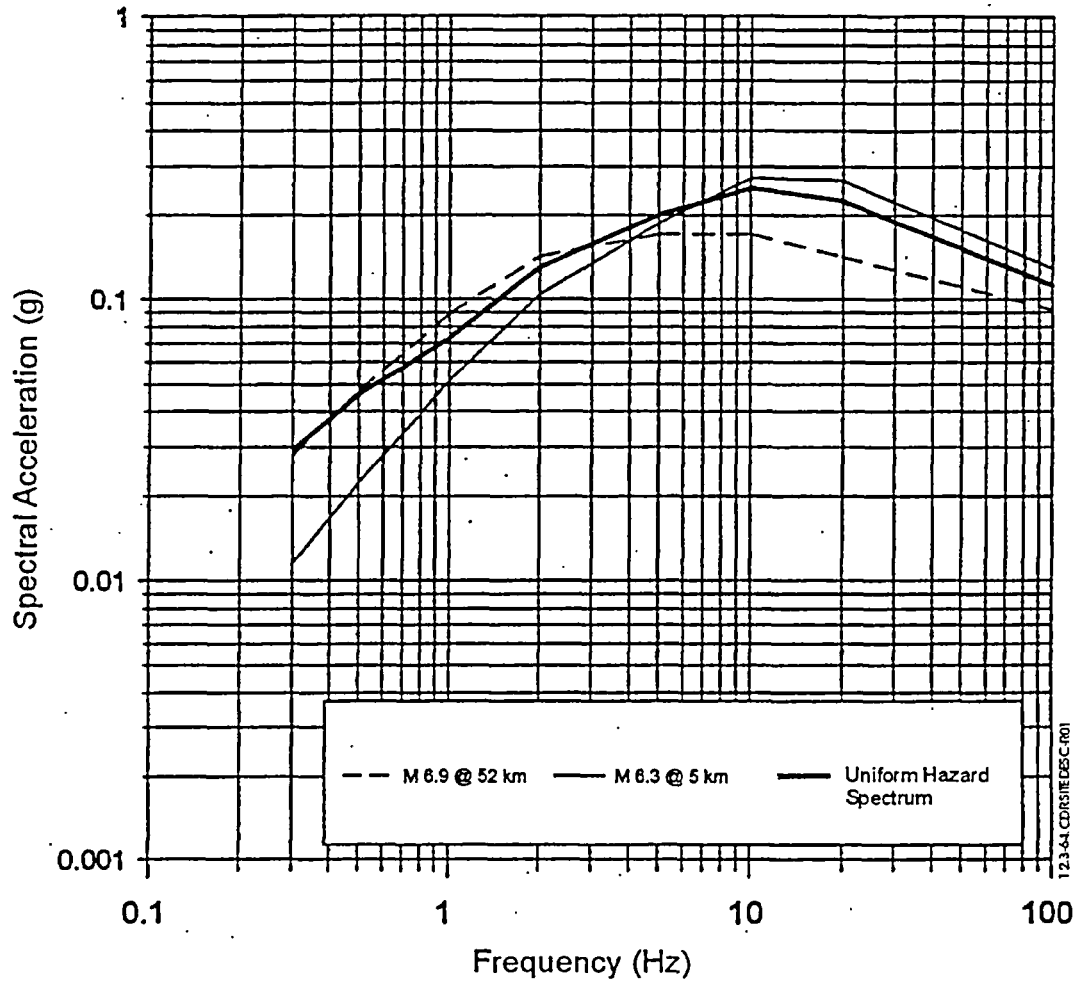
Source: CRWMS M&O (1998i, Figure 2.6-1)

Figure 12.3-62. Comparison of the Uniform Hazard Spectrum with Spectra for Two Reference Earthquakes: Horizontal Spectral Acceleration, 10^{-3} Annual Frequency of Exceedance



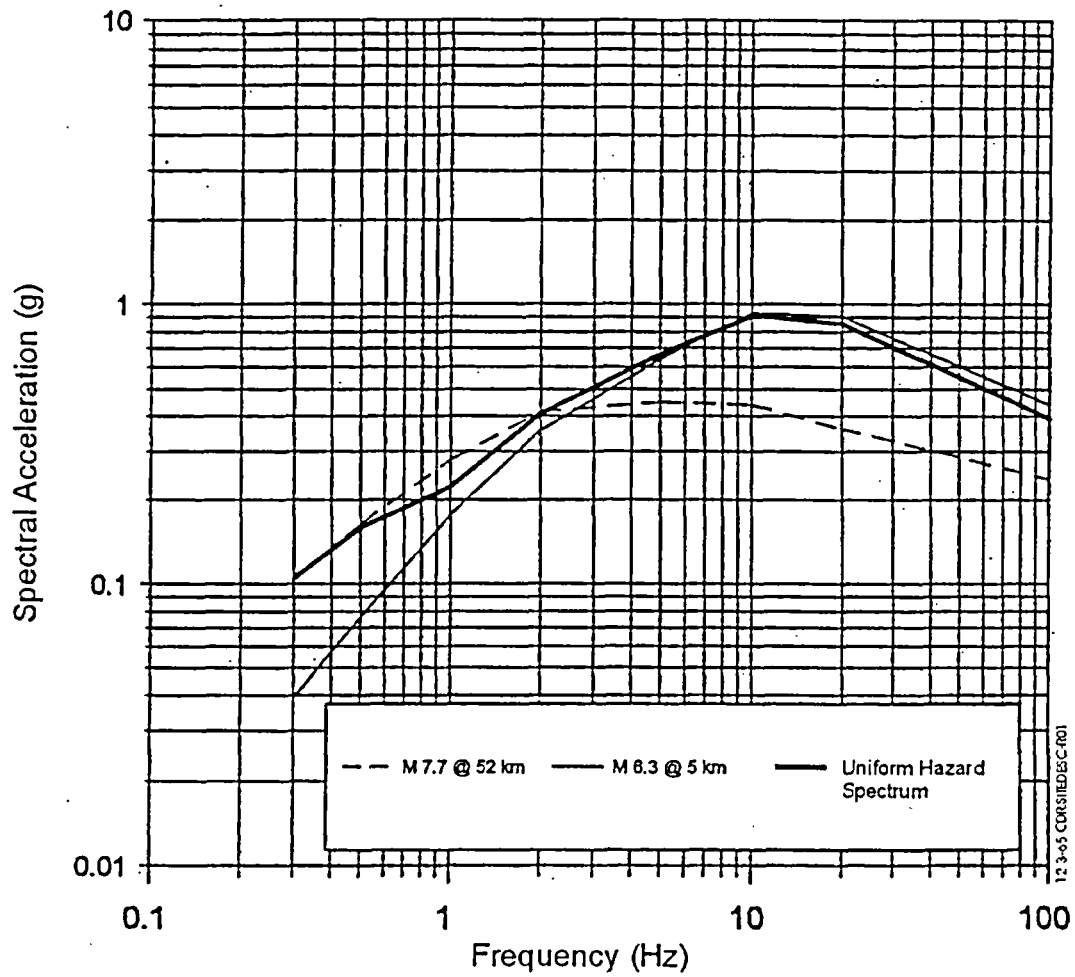
Source: CRWMS M&O (1998i, Figure 2.6-2)

Figure 12.3-63. Comparison of the Uniform Hazard Spectrum with Spectra for Two Reference Earthquakes: Horizontal Spectral Acceleration, 10^{-4} Annual Frequency of Exceedance



Source: CRWMS M&O (1998i, Figure 2.6-3)

Figure 12.3-64. Comparison of the Uniform Hazard Spectrum with Spectra for Two Referen Earthquakes: Vertical Spectral Acceleration, 10^{-3} Annual Frequency of Exceedance



Source: CRWMS M&O (1998i, Figure 2.6-4)

Figure 12.3-65. Comparison of the Uniform Hazard Spectrum with Spectra for Two Reference Earthquakes: Vertical Spectral Acceleration, 10^{-4} Annual Frequency of Exceedance

Table 12.2-1. Comparison of Potassium-Argon and Argon-40/Argon-39 Ages of Volcanic Episodes in the Yucca Mountain Region

Volcanic Episode	K-Ar Age (M.y.)	⁴⁰ Ar/ ³⁹ Ar Age ^c (M.y.)	Percent Difference
Thirsty Mesa	4.63 ^a	4.78	3.24
SE Crater Flat	3.73 ^a	3.75	0.54
Buckboard Mesa	2.87 ^a	3.11	8.36
Quaternary Crater Flat	1.025 ^b	1.014	-1.07
Sleeping Butte	0.338 ^b	0.410	21.30
Lathrop Wells	0.119 ^b	0.08	-32.77

Sources: ^aFleck et al. (1996, Table 1)

^bFleck et al. (1996, Table 2, weighted mean data)

^cCRWMS M&O (1998e, Tables 2.B and 2.C)

NOTE: Percent difference is relative to K-Ar age.

K-Ar ages from Fleck et al. (1996) assume LWI and LWII determinations are the same eruptive age, Little Black Peak and Hidden Cone erupted at the same time, and all Crater Flat centers erupted at the same time. Values in table are calculated as weighted means as follows:

$$Age_{best} = \frac{\sum_{i=1}^n \left(\frac{1}{\sigma_i^2} \right) \times Age_i}{\sum_{i=1}^n \frac{1}{\sigma_i^2}}$$

Table 12.2-2. Estimated Volume and Argon-40/Argon-39 Age of Quaternary Volcanoes in the Yucca Mountain Region

Volcano	Volume (km ³) ^a	Volume (km ³) ^b	Age (M.y.) ^d
Makani Cone	0.006	—	1.16 to 1.17
Black Cone	0.105	0.07	0.94 to 1.10
Red Cone	0.105	—	0.92 to 1.08
Little Cones	0.002	>0.01 ^c	0.77 to 1.02
Hidden Cone	0.03	—	0.32 to 0.56
Little Black Peak	0.03	—	0.36 to 0.39
Lathrop Wells Cone	0.14	—	0.074 to 0.084

Source: CRWMS M&O (2000a, Table 4)

NOTES: ^aCRWMS M&O (1998c, Chapter 3, Table 3.1)

^bStamatakis et al. (1997b, p. 327)

^cAccounts for volume of buried flows detected by ground magnetic surveys

^dRange of ages from CRWMS M&O (1998e, Table 2.B). Lathrop Wells ages (Heizler et al. 1999, Table 3) represent the range of plateau ages measured, except for sample LW157, a statistical outlier.

⁴⁰Ar/³⁹Ar dates provide the most complete and self-consistent chronology data set for Quaternary volcanoes of the YMR. A full discussion of other chronology methods used to date basaltic rocks in the YMR can be found in CRWMS M&O (1998e). Other chronology methods may not provide consistent or accurate estimates of the time of eruption.

To convert km³ to mi.³, multiply by 0.240.

Table 12.2-3. Lathrop Wells Lava Chemistry with Associated Statistics

Parameter	SiO ₂	TiO ₂	Al ₂ O ₃	Fe ₂ O ₃ T ^a	Fe ₂ O ₃ ^b	FeO ^b	MnO	MgO	CaO	Na ₂ O	K ₂ O	P ₂ O ₅
Mean	48.50	1.93	16.74	11.63	1.74	8.90	0.17	5.83	8.60	3.53	1.84	1.22
Standard Error	0.09	0.01	0.03	0.03	0.00	0.02	0.00	0.02	0.03	0.01	0.01	0.00
Median	48.57	1.93	16.75	11.58	1.74	8.86	0.17	5.83	8.55	3.55	1.84	1.22
Mode	48.55	1.97	16.87	11.56	1.73	8.84	0.17	5.88	8.41	3.59	1.84	1.21
Standard Deviation	0.58	0.06	0.22	0.22	0.03	0.17	0.00	0.11	0.22	0.09	0.04	0.03
Sample Variance	0.34	0.00	0.05	0.05	0.00	0.03	0.00	0.01	0.05	0.01	0.00	0.00
Count	45	45	45	45	45	45	45	45	45	45	45	45

Source: CRWMS M&O (2000b, Table 2)

NOTES: ^aTotal iron is reported as Fe₂O₃T.

^bFe₂O₃ and FeO were recalculated assuming a 0.15 mole fraction of ferric iron (Fe₂O₃).
Values are in weight percent (excluding count).

Table 12.2-4. Concentration of Constituents in Volcanic Gases

Constituent	Mean (mole percent) ^a	Square Root of the Sum of the Squares ^b	Standard Deviation ^c
H ₂ O	73.16	17.97	19.81
H ₂	1.17	0.89	0.67
CO ₂	14.28	16.03	15.32
CO	0.57	0.59	0.75
SO ₂	9.45	8.90	8.95
S ₂	0.41	0.63	0.40
HCl	0.87	0.21	1.12
HF	0.17	0.04	0.08
H ₂ S	0.74	1.04	0.69
fO ₂	-10.63 (log bars)	1.92	1.80

Source: CRWMS M&O (2000b, Table 3)

NOTES: ^a Concentrations are given in mole percent, except for oxygen fugacity (fO₂) which is given in log bars

^b Square root of the sum of the squares of individual standard deviations for individual volcanic centers

^c Standard deviation of the individual means for individual volcanic centers

Table 12.2-5. Calculated Saturation Pressures, Temperatures, Viscosities, and Densities as a Function of Water Content for Lathrop Wells Magmas

Water Content (wt. %)	Saturation Pressure (Pa)	Temperature (°C)	Viscosity (log poise)	Density (kg/m ³)
0	1 x 10 ⁵	1169	2.678	2,663
0.5	9.0 x 10 ⁶	1153	2.572	2,633
1	2.4 x 10 ⁷	1137	2.472	2,605
2	6.5 x 10 ⁷	1106	2.284	2,556
3	1.2 x 10 ⁸	1076	2.112	2,512
4	1.7 x 10 ⁸	1046	1.957	2,474

Source: CRWMS M&O (2000b, Table 4)

NOTE: To convert Pa to lb./in.², multiply by 1.450 x 10⁻⁴.
 To convert kg/m³ to lb./ft³, multiply by 0.0624.
 To convert °C to °F, use the formula: °F = (°C x 1.8) + 32.

Table 12.2-6. Probabilistic Volcanic Hazard Analysis Panel Members

Expert	Abbreviation	Affiliation
Dr. Richard W. Carlson	RC	Carnegie Institute of Washington
Dr. Bruce M. Crowe	BC	Los Alamos National Laboratory
Dr. Wendell A. Duffield	WD	United States Geological Survey, Flagstaff
Dr. Richard V. Fisher	RF	University of California, Santa Barbara (Emeritus)
Dr. William R. Hackett	WH	WRH Associates, Salt Lake City
Dr. Mel A. Kuntz	MK	United States Geological Survey, Denver
Dr. Alexander R. McBirney	AM	University of Oregon (Emeritus)
Dr. Michael F. Sheridan	MS	State University of New York, Buffalo
Dr. George A. Thompson	GT	Stanford University
Dr. George P.L. Walker	GW	University of Hawaii, Honolulu

Source: CRWMS M&O (2000a, Table 5)

Table 12.2-7. Reported Probabilities that the Potential Yucca Mountain Repository Will Be Intersected by a Volcanic Event

Reference	Intersection Probability (per year)	Comment	Event Representation
Crowe et al. (1982, pp. 184 to 185)	3.3×10^{-10} to 4.7×10^{-8}	–	point
Crowe et al. (1993, p. 188)	2.6×10^{-8}	Median value of probability distribution	point
Connor and Hill (1995, pp. 10,121)	1 to 5×10^{-8}	Range of 3 alternative models	point
Crowe et al. (1995, Table 7.22)	1.8×10^{-8}	Median value of 22 alternative probability models	point
Ho and Smith (1998, pp. 507 to 508)	(1) 1.5×10^{-8} (2) 1.09×10^{-8} , 2.83×10^{-8} (3) 3.14×10^{-7}	Three alternative models; third model assumes a spatial intersection ratio (using a Bayesian prior) of 8/75 or 0.11, approximately one order of magnitude higher than other published estimates, because volcanic events are forced to occur within a small zone enclosing Yucca Mountain	point
CRWMS M&O (1998c, p. 6-84)	2.5×10^{-8}	Sensitivity analysis that conservatively assumes all aeromagnetic anomalies in Amargosa Valley are Quaternary age	point
Reamer (1999, pp. 61, 131, Figures 29, 30)	10^{-8} to 10^{-7}	Value of 10^{-7} assumes event length of 20 km and that crustal density variations contribute to event location.	line

Source: CRWMS M&O (2000a, Table 6)

Table 12.2-8. Summary Frequencies of Disruptive Volcanic Events

Potential Repository Footprint	Hazard Level	Annual Frequency of Intersection of Potential Repository by a Dike	Weighted Conditional Probability of No Eruptive Centers	Annual Frequency of Occurrence of One or More Eruptive Centers within Potential Repository
Primary Block	5th percentile	6.6×10^{-10}	0.58	2.8×10^{-10}
	Mean	1.4×10^{-8}	0.53	6.7×10^{-9}
	95th percentile	4.7×10^{-8}	0.53	2.2×10^{-8}
Primary+Contingency Blocks	5th percentile	7.6×10^{-10}	0.56	3.3×10^{-10}
	Mean	1.6×10^{-8}	0.50	7.7×10^{-9}
	95th percentile	5.0×10^{-8}	0.51	2.5×10^{-8}

Source: CRWMS M&O (2000a, Table 13)

Table 12.3-1. Key Milestones for Earthquake Reporting in the Southern Great Basin

Date	Milestone
Pre-1925	Historical compilations (Townley and Allen 1939; Slemmons et al. 1965; Meremonte and Rogers 1987); no systematic reporting, some low-gain seismographs (e.g., at Reno, Nevada; Mt. Hamilton and Berkeley, California; and Tucson, Arizona) with detection capability of larger events ($M_L > 5.5$) in the southern Great Basin (e.g., 1916 Death Valley earthquake). The University of California, Berkeley, began systematic reporting of western Nevada earthquakes north of 37° latitude in 1910 (Bolt and Miller 1975).
1925	U.S. Coast and Geodetic Survey began systematic compilation of earthquake felt reports.
1932	Felt reports and instrumental locations for larger earthquakes computed by California Institute of Technology (CIT). First seismograph station installed in the southern Great Basin at Tinemaha in Owens Valley, California, by CIT in 1931 (Hileman et al. 1973). Four stations installed (1938-1941) by U.S. Bureau of Reclamation in vicinity of Lake Mead, Nevada, to monitor for reservoir induced seismicity. Detection threshold reduced to about $M_L 4.0$ in southern Great Basin (Anderson and O'Connell 1993).
1960	Worldwide Standardized Seismographic Network (WWSSN) in operation-location capability (routine operations) (Engdahl and Rinehart 1988) and detection threshold about $M_L 3.5$ for southern Nevada.
1961	Regional network installed around the Nevada Test Site (NTS) by U.S. Coast and Geodetic Survey, Earth Science Laboratories, to monitor NTS activity (King et al. 1971). No significant improvement in detection threshold.
1968	Short-duration local networks sponsored by the Department of Defense in and around the NTS. Detection threshold decreased to about $M_L 2.5$ (Rogers et al. 1991).
1972	Regional network installed and operated by the Seismological Laboratory at the University of Nevada, Reno, for the State of Nevada; however, no seismographs installed in southern Nevada (Rogers et al. 1991). No significant change in detection threshold.
1978	The U.S. Geological Survey Southern Great Basin network began operation-location capability (routine operations) about $M_L < 1.0$ in the vicinity of Yucca Mountain and $M_L 1.3$ regionally (Gomberg 1991a). Network operation taken over by University of Nevada, Reno, in 1992 (Wong and Stepp 1998, p. G-5).
1995	University of Nevada, Reno, installed 3-component high-dynamic-range digital network and redesigned station configuration-detection capability $M_L -0.5$ in Yucca Mountain block and $M_L 1.0$ regionally (von Seggern and dePolo 1998, pp. 40 to 41).

Source: See references listed in Table.

Table 12.3-2. Networks Relevant to Assessing Seismicity in the Southern Great Basin

Network	Dates of Operation	Detection Threshold in Southern Great Basin	Location Accuracy	References
Only a few isolated seismograph stations	Pre-1932	M_L 5.5 regionally	Depends on population distribution and density	Townley and Allen (1939); Slemmons et al. (1965); Meremonte and Rogers (1987)
California networks operated by University of California, Berkeley, and the California Institute of Technology	UCB 1910-1997 CIT 1932-1997	M_L 4.0 regionally	\pm 50 km in epicenter early on and no depth control: improved to \pm 10 km epicentrally	Bolt and Miller (1975); Hileman et al. (1973)
Worldwide Standardized Seismographic Network (WWSSN)	1960-1997	M_L 3.5 regionally	\pm 20 km in 1960s, now \pm 5 km. Poor depth control. (Data not used after 1977.)	Meremonte and Rogers (1987)
Local Nevada Test Site networks supported by the Department of Defense	1968-1978	M_L 3.5 regionally, M_L \sim 1.0 locally	\pm 1 km in epicenter and \pm 2 km in depth locally	Hamilton, R.M. et al. (1971); Smith, B.E. et al. (1971); Fischer et al. (1972); Rogers, A.M., Wuolett, and Covington (1977); King et al. (1971)
Southern Great Basin network operated by U.S. Geological Survey until 1992; then by the University of Nevada, Reno, from 1992-1995	1978-1995	M_L 1.3 regionally, M_L $<$ 1.0 in the vicinity of Yucca Mountain	\pm 1 km in epicenter, \pm 2 km in depth	Rogers et al. (1987); Harmsen and Rogers (1987); Harmsen and Bufe (1992); Harmsen (1991, 1993, 1994a)
Southern Great Basin digital network operated by University of Nevada, Reno	1995-1999	M_L 1.0 regionally, M_L -0.5 in the vicinity of Yucca Mountain	\pm 1 km in epicenter, \pm 2 km in depth around Yucca Mountain, \pm 1 km regionally $>$ 2 km in depth	von Seggern and dePolo (1998, pp. 40 to 41)

Source: See References column in table.

NOTE: To convert km to mi., multiply by 0.621.

Table 12.3-3. Regional Seismicity Catalogs Used for the Yucca Mountain Seismicity Catalog

Regional Seismicity Catalog	Date	Reference
Southern Great Basin Earthquake Catalog	1868 to 1978	Meremonte and Rogers (1987)
Southern Great Basin Network Catalog	1978 to 1992	Rogers et al. (1987); Harmsen and Bufe (1992); Harmsen (1991, 1993, 1994a); and Harmsen and Rogers (1987)
California Division of Mines and Geology Catalog for California	1868 to 1932	--
California Institute of Technology Seismological Laboratory and U.S. Geological Survey (USGS) Catalog for Southern California	1932 to 1996	--
University of California at Berkeley Seismographic Station Catalog for Northern California	1910 to 1972	--
USGS Catalog for Northern and Central California	1969 to 1996	--
Seismological Laboratory of the University of Nevada, Reno, Catalog for Nevada (including the Southern Great Basin network data for 1992 to 1994)	1874 to 1996	--
Decade of North American Geology Catalog	1868 to 1985	Engdahl and Rinehart (1988)
Northern Arizona University Catalog for Arizona	1891 to 1992	--
Stover, Reagor, and Algermissen State Catalogs for Utah and Arizona compiled by the National Earthquake Information Center (NEIC)	1881 to 1985	--
University of Utah Seismographic Stations Catalog for Utah	1881 to 1996	--
NEIC Preliminary Determination of Epicenters Catalog for Utah and Arizona	1938 to 1996	--

Source: Wong and Stepp (1998, Appendix G)

Table 12.3-4. Time Period as a Function of Magnitude for Which the Earthquake Catalog Is Estimated To Be Complete

Magnitude (M_L)	Estimated Completeness Interval
1.5	1995-1999
2.0	1985-1999
2.5	1979-1999
3.0	1979-1999
3.5	1961-1999
4.0	1934-1999
4.5	1934-1999
5.0	1924-1999
5.5	1924-1999
6.0	1914-1999
6.5	1880-1999

Source: DTN: MO0005SEPECINT.001

Table 12.3-5. Significant Earthquakes within 300 Kilometers of the Yucca Mountain Region

Date	Oirgin Time (GMT) (hr:min:sec)	Latitude (degrees)	Longitude (degrees)	Depth (km)	Magnitude (M _w)	Location
March 26, 1872	10:30:00	36.70	-118.10	-	7 3/4	Owens Valley, CA
November 17, 1902	19:50:00	37.39	-113.52	-	6	Pine Valley, NV
November 10, 1916	09:11:00	36.20	-116.90	-	6.1	Death Valley, CA
December 21, 1932	06:10:04	38.80	-117.98	-	6.8	Cedar Mountain, NV
January 30, 1934	20:16:35	38.28	-118.37	-	6.1	Excelsior Mountain, NV
April 10, 1947	15:58:06	34.98	-116.55	-	6.5	Manix, CA
December 16, 1954	11:07:11	39.28	-118.12	15	7.1	Fairview Peak, CA
December 16, 1954	11:11:00	39.67	-117.90	12	6.8	Dixie Valley, NV
September 22, 1966	18:57:34	37.37	-114.18	7	5.7	Clover Mountain, NV
June 1, 1975	01:38:49	34.52	-116.50	4.5	5.2	Galway Lake, CA
March 15, 1979	21:07:17	34.33	-116.44	2.5	5.5	Homestead Valley, CA
May 25, 1980	16:33:44	37.59	-118.85	10.2	6.2	Mammoth Lakes, CA
May 25, 1980	16:49:27	37.67	-118.92	8.9	5.9	Mammoth Lakes, CA
May 25, 1980	20:35:48	37.63	-118.84	8.2	5.6	Mammoth Lakes, CA
May 27, 1980	14:50:57	37.49	-118.81	16.1	5.9	Mammoth Lakes, CA
September 30, 1981	11:53:26	37.59	-118.87	5.7	5.6	Mammoth Lakes, CA
November 23, 1984	18:08:25	37.46	-118.61	11.5	5.8	Round Valley, CA
July 20, 1986	14:29:45	37.57	-118.44	6.7	5.8	Chalfant Valley, CA
July 21, 1986	14:42:26	37.54	-118.44	10.5	6.3	Chalfant Valley, CA
July 21, 1986	14:51:09	37.49	-118.43	11.8	5.5	Chalfant Valley, CA
July 31, 1986	07:22:40	37.47	-118.37	8.1	5.5	Chalfant Valley, CA
June 28, 1992	11:57:34	34.20	-116.44	1.0	7.3	Landers, CA
June 29, 1992	10:14:20	36.72	-116.29	11.8	5.6	Little Skull Mountain, NV
September 2, 1992	10:26:19	37.17	-113.33	9.6	5.9	St. George, UT
May 17, 1993	23:20:50	37.18	-117.83	9.1	6.1	Eureka Valley, CA
August 17, 1995	22:39:58	35.77	-117.65	10.5	5.2	Ridgecrest, CA
September 20, 1995	23:27:36	35.75	-117.64	8.3	5.3	Ridgecrest, CA
Octcber 16, 1999	09:46:44	34.59	-116.27	5.0	7.1	Hector Mine, CA

Source: CRWMS M&O (2000c)

NOTE: GMT = Greenwich Mean Time; M_w = moment magnitude. To convert km to mi., multiply by 0.621.

Table 12.3-6. 1992 Little Skull Mountain Mainshock Source Parameters

Information Source	Strike	Dip	Rake ^a	Seismic Moment (10 ²⁴ dyne-cm)
Smith, K.D. et al. ([n.d.], Table 1)	N60°±15°	70°±13°SE	-70°±10°	Not calculated
Meremonte, Gomberg, and Cranswick (1995)	N55°E	56°SE	-72°	Not calculated
Romanowicz et al. (1993)	N43°E	66°SE	-73°	3.5
Romanowicz et al. (1993)	N34°E	44°SE	-70°	2.6
Zhao and Helmberger (1994)	N45°E	55°SE	-60°	3.0
Walter (1993)	N35°E	54°SE	-87°	4.1
Harmsen (1994b)	N55°E	56°SE	-72°	Not calculated

Source: Modified from Schneider et al. (1996, Table 6-2)

NOTE: ^aRake is the angle between the strike direction and the slip vector. The negative sign indicates that this is a normal fault.

Table 12.3-7. Small-Magnitude Earthquakes at Yucca Mountain

Date (yr/mo/day)	Origin (hr./min.)	Time (s)	Latitude (deg/min)	Longitude (deg/min)	Depth (km)	M _L
950505	1321	33.13	36 50.65	116 24.01	6.08	0.58
950701	1526	56.69	36 40.84	116 30.88	8.65	-0.96
950707	0758	59.68	36 49.74	116 24.75	6.06	-0.27
950728	0618	51.42	36 54.12	116 30.51	4.79	-0.48
950904	1239	47.12	36 44.46	116 29.98	4.44	0.72
951119	2216	24.90	36 50.79	116 23.66	6.32	-0.25
951120	0226	57.39	36 50.83	116 23.74	6.44	-0.43
951125	1501	23.04	36 46.39	116 21.68	8.20	-0.35
951206	2327	15.85	36 43.58	116 28.83	8.12	0.29
960101	0755	12.56	36 47.70	116 20.19	9.01	-0.14
960129	1020	32.32	36 44.23	116 29.44	9.90	-0.35
960330	1957	28.63	36 48.60	116 27.98	7.24	-0.59
960408	0714	49.64	36 49.94	116 25.19	8.26	-0.58
960602	1015	33.29	36 49.25	116 29.43	9.81	0.01
960602	1646	15.29	36 49.09	116 29.15	8.79	-0.69
960731	0357	37.30	36 45.91	116 34.54	8.55	-0.76
960812	0422	50.68	36 48.48	116 23.09	5.02	-0.62
961026	0211	34.17	36 54.89	116 27.59	5.49	0.39
970225	0604	11.76	36 53.03	116 26.17	2.86	-0.32
970614	2026	46.94	36 50.05	116 24.60	4.27	0.18
970616	2203	31.89	36 49.86	116 24.18	3.89	-0.64
970707	1536	53.26	36 42.18	116 28.68	5.22	0.07
970731	1754	50.68	36 42.29	116 26.98	9.53	1.18
980402	1218	27.99	36 43.15	116 33.49	8.58	0.12
980725	0635	50.59	36 51.52	116 32.20	5.67	-0.51
980727	0223	44.74	36 44.77	116 24.56	6.98	-0.76
990220	1936	57.34	36 57.16	116 29.21	3.59	-0.21
990329	1602	57.20	36 49.10	116 22.94	6.17	-0.09

Sources: DTNs: MO970483117412.002 and MO0005SMALLEQD.002

NOTE: To convert km to mi., multiply by 0.621

Table 12.3-8a. Event Displacements and Timing Data from Paleoseismic Studies of Yucca Mountain Faults: Summary

Fault	Sense of Slip	Fault Strike at Surface	Fault Dip at Surface	Fault Length (km)			Number of Possible Fault Segments	Number of Trenches ^a
				Min	Pref	Max		
Bare Mountain	Normal-right lateral	N-S	60-80°E	-	20	-	1	3
Bow Ridge	Normal-left lateral	N5-15°E	65-85°W	6	8	10	1	7
Northern Crater Flat	Normal-left lateral	N5-20°E	70°W	1	11	20	1	1
Southern Crater Flat	Normal-left lateral	N4-28°E	82-89°W	4	8	20	1	2
Fatigue Wash	Normal-left lateral	N9°E	73°W	10	16	17	1	2
Ghost Dance	Normal	N-S	>65°W	3	6	9	1	4
Iron Ridge	Normal-left lateral	N-S	70°W	-	-	21	1	1
Paintbrush Canyon	Normal-left lateral	N10°E	70°W	10	19	26	2-3	6 (plus 4 natural exposures)
Rock Valley	Left lateral-oblique	N60°E	90°	-	30	-	3	10
Solitario Canyon	Normal-left lateral	N8°E	72°W	13	18	22	3	11 (plus 1 natural exposure)
Stagecoach Road	Normal-left lateral	N30°E	73°W	4	-	5	1	3
Windy Wash	Normal-left lateral	N4-20°E	77-90°W	3	22	35	3	3

Source: See source line of Table 12.3-8b.

NOTE: ^aTrenches with limited or no data are not included in this compilation; for information on excluded trenches, see Whitney, Taylor, and Wesling (1996, Chapter 4).

To convert km to mi., multiply by 0.621.

Table 12.3-8b. Event Displacements and Timing Data from Paleoseismic Studies of Yucca Mountain Faults: Detailed Data

Fault Name	Sense of Slip	Displacement			Fault Strike at Surface	Fault Dip at Surface	Fault Length (km)			Number of Possible Fault Segments		Number of Trenches
							Min	Pref	Max			
Bare Mountain (Anderson and Klinger 1996; Pezzopane, Whitney et al. 1996)	Normal-right-lateral				N-S	60-80°E		20		1		3
	Trench BMT-1											
	Event ^k	Displacement (cm) ^b			Event Criteria ⁹	Event Confidence ^h	Event Timing (ka)			Dating Method ⁱ	Dating Reliability ^h	Shape of Timing Distribution
		Min	Pref	Max			Min	Pref	Max			
	Z	-	150	-	D, F, T, U	NS ^j	14	-	100	T, S, Ar	NS ^j	Trapezoid
	Trench BMT-2											
	Event ^k	Displacement (cm) ^b			Event Criteria ⁹	Event Confidence ^h	Event Timing (ka)			Dating Method ⁱ	Dating Reliability ^h	Shape of Timing Distribution
		Min	Pref	Max			Min	Pref	Max			
	Z	-	-	-	F,W	NS ^j	14	-	100	S	NS ^j	Trapezoid
	Y	-	-	-	F,W	-	-	-	-	-	-	Triangle
	Trench BMT-3											
	Event ^k	Displacement (cm) ^b			Event Criteria ⁹	Event Confidence ^h	Event Timing (ka)			Dating Method ⁱ	Dating Reliability ^h	Shape of Timing Distribution
Min		Pref	Max	Min			Pref	Max				
Z	-	80	-	D, F, U	NS ^j	14	-	100	S	NS ^j	Trapezoid	
Y	-	150	300	D, F	-	-	-	-	S	-	Triangle	
Bow Ridge (Menges and Whitney 1996a; Pezzopane, Whitney et al. 1996)	Normal-left-lateral				N5-15°E	65-85°E	6	8	10	1		5
	Trench (T-14)											
	Event ^k	Displacement (cm) ^b			Event Criteria ⁹	Event Confidence ^h	Event Timing (ka)			Dating Method ⁱ	Dating Reliability ^h	Shape of Timing Distribution
		Min	Pref	Max			Min	Pref	Max			
	Z	-	-	-	F	NS ^j	30	40-60	130	A	NS ^j	Triangle
	Trench (T-14D)											
	Event ^k	Displacement (cm) ^b			Event Criteria ⁹	Event Confidence ^h	Event Timing (ka)			Dating Method ⁱ	Dating Reliability ^h	Shape of Timing Distribution
		Min	Pref	Max			Min	Pref	Max			
Z	15	44	80	D,F,U,W	NS ^j	30	40-60	130	T,U,S	NS ^j	Triangle	
Y	4	13	45	D,F,U,W	-	130	-	150	T,U,S	-	Triangle	
X	1	14	40	D,W	-	250	340	460	U	-	Triangle	

Table 12.3-8b. Event Displacements and Timing Data from Paleoseismic Studies of Yucca Mountain Faults: Detailed Data (Continued)

Fault Name	Sense of Slip	Displacement			Fault Strike at Surface	Fault Dip at Surface	Fault Length (km)			Number of Possible Fault Segments		Number of Trenches
							Min	Pref	Max			
Bow Ridge (Continued)	Trench (T A/BR-3)											
	Event ^k	Displacement (cm) ^b			Event Criteria ^g	Event Confidence ^h	Event Timing (ka)			Dating Method ⁱ	Dating Reliability ^h	Shape of Timing Distribution
		Min	Pref	Max			Min	Pref	Max			
-	-	-	-	-	-	-	-	-	-	-	-	-
Northern Crater Flat (Coe 1996; Menges and Whitney 1996b; Pezzopane, Whitney et al. 1996)	Normal-left-lateral				N5-20°E	70°W	1	11	20	1		2
	Trench (CFF-T2a)											
	Event ^k	Displacement (cm) ^b			Event Criteria ^g	Event Confidence ^h	Event Timing (ka)			Dating Method ⁱ	Dating Reliability ^h	Shape of Timing Distribution
		Min	Pref	Max			Min	Pref	Max			
	Z	0	-	5	D,F,T	H	4	8	10	T	NS ^j	Triangle
	Y	0	-	5	U	M	10	150-200	433	T,S	-	Trapezoid
	X	-	40	-	U,D,W	H	-	>433	-	S	-	-
W	-	50	-	D	H	-	>>433	-	S	-	-	
V	-	50	-	D	M	-	>>>433	-	S	-	-	
Southern Crater Flat (Taylor 1996; Menges and Whitney 1996b; Pezzopane, Whitney et al. 1996)	Normal-left-lateral				N4-28°E	82-89°W	4	8	20	1		2
	Trench (CFF-1)											
	Event ^k	Displacement (cm) ^b			Event Criteria ^g	Event Confidence ^h	Event Timing (ka)			Dating Method ⁱ	Dating Reliability ^h	Shape of Timing Distribution
		Min	Pref	Max			Min	Pref	Max			
	Z	5	-	10	D	M	2	3-4	8	S	H	Triangle
	Y	5	-	10	D,U,F	H	-	< 60	-	S	H	Triangle
	X	10	-	15	-	-	-	>250	-	S	-	Triangle
Trench (CFF-1a)												
Event ^k	Displacement (cm) ^{ba}			Event Criteria ^g	Event Confidence ^h	Event Timing (ka)			Dating Method ⁱ	Dating Reliability ^h	Shape of Timing Distribution	
	Min	Pref	Max			Min	Pref	Max				
Z	-	18	-	D,W	H	2	2-6	8	T	M	Triangle	
Y	5	10	15	D,U,T,F	H	8	-	>60	S	H	Triangle	
X	17	20	32	D,U,T	L	130	-	>250	S	H	Triangle	

Table 12.3-8b. Event Displacements and Timing Data from Paleoseismic Studies of Yucca Mountain Faults: Detailed Data (Continued)

Fault Name	Sense of Slip	Displacement			Fault Strike at Surface	Fault Dip at Surface	Fault Length (km)			Number of Possible Fault Segments		Number of Trenches
							Min	Pref	Max			
Fatigue Wash (Menges and Whitney 1996b; Coe, Oswald et al. 1996; Pezzopane, Whitney et al. 1996)	Normal-left-lateral				N9°E	73°W	10	16	17	1		2
	Trench (CFF-1)											
	Event ^k	Displacement (cm) ^b			Event Criteria ^g	Event Confidence ^h	Event Timing (ka)			Dating Method ⁱ	Dating Reliability ^h	Shape of Timing Distribution
		Min	Pref	Max			Min	Pref	Max			
	Z	20	30	40	U	L	8	20-60	70	T,U,S	NS ^j	Trapezoid
	Y	15	25	35	F,D	NS	15	60-70	100	T,U,S,A	-	Trapezoid
	X	25	-	125	F,W,U,T,D	NS	-	-	450	T,U,S	-	Trapezoid
W	-	54	-	W,D	L	450	-	730	T,U,S	-	Boxcar	
Pre-W	-	-	-	U	-	-	>730	-	-	-	-	
Ghost Dance (Taylor, Menges et al. 1996)	Normal				N-S	N65°W	3	6	9	1		4
	Trench (T2 Drill Hole Wash)											
	Event ^k	Displacement (cm) ^b			Event Criteria ^g	Event Confidence ^h	Event Timing (ka)			Dating Method ⁱ	Dating Reliability ^h	Shape of Timing Distribution
		Min	Pref	Max			Min	Pref	Max			
	-	-	-	-	-	-	-	-	-	-	-	-
	Trench (BMT-3)											
	Event ^k	Displacement (cm) ^b			Event Criteria ^g	Event Confidence ^h	Event Timing (ka)			Dating Method ⁱ	Dating Reliability ^h	Shape of Timing Distribution
		Min	Pref	Max			Min	Pref	Max			
	-	-	-	-	-	-	-	-	-	-	-	-
	Trench (T4a-Split Wash)											
Event ^k	Displacement (cm) ^b			Event Criteria ^g	Event Confidence ^h	Event Timing (ka)			Dating Method ⁱ	Dating Reliability ^h	Shape of Timing Distribution	
	Min	Pref	Max			Min	Pref	Max				
Z	-	Fracture	-	L	NS ^j	-	>265	-	U	NS ^j	None	
Trench (WBR)												
Event ^k	Displacement (cm) ^b			Event Criteria ^g	Event Confidence ^h	Event Timing (ka)			Dating Method ⁱ	Dating Reliability ^h	Shape of Timing Distribution	
	Min	Pref	Max			Min	Pref	Max				
Z	-	Fracture	-	U	L	-	-	-	U	NS ^j	None	

Table 12.3-8b. Event Displacements and Timing Data from Paleoseismic Studies of Yucca Mountain Faults: Detailed Data (Continued)

Fault Name	Sense of Slip	Displacement			Fault Strike at Surface	Fault Dip at Surface	Fault Length (km)			Number of Possible Fault Segments		Number of Trenches
							Min	Pref	Max			
Paintbrush Canyon (Continued)	Trench (BB1)	Correlated to BB4										
	Event ^k	Displacement (cm) ^b			Event Criteria ^g	Event Confidence ^h	Event Timing (ka)			Dating Method ⁱ	Dating Reliability ^h	Shape of Timing Distribution
		Min	Pref	Max			Min	Pref	Max			
	Z	0	44	72	D,W	NS ^j	35	40-50	90	U,T,S,A	NS ^j	Trapezoid
	Y	16	28	56	D,W,U	-	80	80-150	300	U,T,S	-	Triangle
	X	35	47	69	D	-	150	-	300	U,T,S	-	Triangle
	W	88	167	205	E,W	-	-	270-400	-	U,T,S	-	Triangle
	V	0	142	222	W	-	-	650-700	-	U,T,A	-	-
	U	12	105	257	-	-	-	650-700	-	U,T,A	-	-
	T	75	94	201	U,D	-	-	650-700	-	U,T,A	-	-
	S	-	-	-	D	-	-	-	-	-	-	-
	R	-	-	-	D	-	-	-	-	-	-	-
	Trench (BB4)											
	Event ^k	Displacement (cm) ^b			Event Criteria ^g	Event Confidence ^h	Event Timing (ka)			Dating Method ⁱ	Dating Reliability ^h	Shape of Timing Distribution
Min		Pref	Max	Min			Pref	Max				
Z	0	44	72	D,W	NS ^j	35	40-50	90	U,T,S,A	NS ^j	Trapezoid	
Y	16	28	56	D,W,U	-	80	80-150	300	U,T,S	-	Triangle	
X	35	47	69	D	-	150	-	300	U,T,S	-	Triangle	
W	88	167	205	E,W	-	-	270-400	-	U,T,S	-	Triangle	
V	0	142	222	W	-	-	650-700	-	U,T,A	-	-	
U	12	105	257	-	-	-	650-700	-	U,T,A	-	-	
T	75	94	201	U,D	-	-	650-700	-	U,T,A	-	-	
Trench (MWW-T4)												
Event ^k	Displacement (cm) ^b			Event Criteria ^g	Event Confidence ^h	Event Timing (ka)			Dating Method ⁱ	Dating Reliability ^h	Shape of Timing Distribution	
	Min	Pref	Max			Min	Pref	Max				
Z	-	20	-	W,U	NS ^j	6	-	40	NS ^j	NS ^j	-	
Y	44	62	77	W,U	-	65	-	100	-	-	-	
X	53	98	143	W,U	-	-	-	-	-	-	-	
W	0	40	140	W	-	-	-	-	-	-	-	

Table 12.3-8b. Event Displacements and Timing Data from Paleoseismic Studies of Yucca Mountain Faults: Detailed Data (Continued)

Fault Name	Sense of Slip	Displacement			Fault Strike at Surface	Fault Dip at Surface	Fault Length (km)			Number of Possible Fault Segments		Number of Trenches
							Min	Pref	Max			
Paintbrush Canyon (Continued)	Trench (16)											
	Event ^k	Displacement (cm) ^b			Event Criteria ^g	Event Confidence ^h	Event Timing (ka)			Dating Method ⁱ	Dating Reliability ^h	Shape of Timing Distribution
		Min	Pref	Max			Min	Pref	Max			
	-	-	-	-	-	-	-	-	-	-	-	-
	Trench (16b)											
	Event ^k	Displacement (cm) ^b			Event Criteria ^g	Event Confidence ^h	Event Timing (ka)			Dating Method ⁱ	Dating Reliability ^h	Shape of Timing Distribution
Min		Pref	Max	Min			Pref	Max				
-	-	-	-	-	-	-	-	-	-	-	-	
Rock Valley Fault System (Coe, Yount, and O'Leary 1996)	Left-lateral-oblique				N60°E	90°	-	30	-	3		5
	Trench (RV-1)											
	Event ^k	Displacement (cm) ^b			Event Criteria ^g	Event Confidence ^h	Event Timing (ka)			Dating Method ⁱ	Dating Reliability ^h	Shape of Timing Distribution
		Min	Pref	Max			Min	Pref	Max			
	Z	10	-	31	D,U	NS ^j	-	-	-	TR	NS ^j	-
	Trench (RV-2)											
	Event ^k	Displacement (cm) ^b			Event Criteria ^g	Event Confidence ^h	Event Timing (ka)			Dating Method ⁱ	Dating Reliability ^h	Shape of Timing Distribution
		Min	Pref	Max			Min	Pref	Max			
	Z	10	-	31	D,U	NS ^j	-	-	-	TR	NS ^j	-
	Y	-	-	-	D,F,U	-	-	-	-	-	-	-
Trench (RV-3)												
Event ^k	Displacement (cm) ^b			Event Criteria ^g	Event Confidence ^h	Event Timing (ka)			Dating Method ⁱ	Dating Reliability ^h	Shape of Timing Distribution	
	Min	Pref	Max			Min	Pref	Max				
Y	-	<51	<609	F,U,W	H	4	-	17	T,U	NS ^j	-	
X	-	<69	<824	W	M-H	17	-	-	T,U	-	-	
W	-	<39	<466	W,D	M	pend	pend	pend	T,U	-	-	
V	-	<63	<753	W	M	pend	pend	pend	-	-	-	

Table 12.3-8b. Event Displacements and Timing Data from Paleoseismic Studies of Yucca Mountain Faults: Detailed Data (Continued)

Fault Name	Sense of Slip	Displacement			Fault Strike at Surface	Fault Dip at Surface	Fault Length (km)			Number of Possible Fault Segments		Number of Trenches	
							Min	Pref	Max				
Rock Valley Fault System (Continued)	Trench (RV-4)												
	Event ^k	Displacement (cm) ^b			Event Criteria ^g	Event Confidence ^h	Event Timing (ka)			Dating Method ⁱ	Dating Reliability ^h	Shape of Timing Distribution	
		Min	Pref	Max			Min	Pref	Max				
		Z	0	-	10	D,U,T	H	<2	2.5	3	T	NS ^j	-
		Y	0	-	10	F,U	M	2	-	27	T	-	-
	X	0	-	10	U,D	M	>>2	-	27	T	-	-	
	Trench (RV-5)												
	Event ^k	Displacement (cm) ^b			Event Criteria ^g	Event Confidence ^h	Event Timing (ka)			Dating Method ⁱ	Dating Reliability ^h	Shape of Timing Distribution	
		Min	Pref	Max			Min	Pref	Max				
		Z	-	Fractures	-	U	L-M	5	6	7	T	NS ^j	-
Y		-	58	-	F	H	9	10	10	T	-	-	
X	-	-	-	U	H	-	-	-	T	-	-		
Solitario Canyon (Ramelli et al. 1996; Menges and Whitney 1996a; Pezzopane, Whitney et al. 1996)	Normal-left-lateral				N8°E	72°W	13	18	22	3		11 trenches 1 natural exposure	
	Trench (SCF-T1)												
	Event ^k	Displacement (cm) ^b			Event Criteria ^g	Event Confidence ^h	Event Timing (ka)			Dating Method ⁱ	Dating Reliability ^h	Shape of Timing Distribution	
		Min	Pref	Max			Min	Pref	Max				
		Z	-	-	-	U	NS ^j	20	20-30	40	R	L	Triangle
		Y	50	-	120	F	-	60	70	80	R	M	Triangle
	X	-	-	-	-	-	-	-	-	-	-	-	
	W	-	-	-	-	-	-	-	-	-	-	-	
	Trench (SCF-T3)												
	Event ^k	Displacement (cm) ^b			Event Criteria ^g	Event Confidence ^h	Event Timing (ka)			Dating Method ⁱ	Dating Reliability ^h	Shape of Timing Distribution	
Min		Pref	Max	Min			Pref	Max					
Z		0	-	10?	U	NS ^j	20	20-30	40	R	L	Triangle	
Y		60	-	120	F	-	60	70	80	R	M	Triangle	
X	-	-	-	-	-	-	-	-	-	-	-		
W	20	-	40	-	-	150	200	250	R	L	Triangle		

Table 12.3-8b. Event Displacements and Timing Data from Paleoseismic Studies of Yucca Mountain Faults: Detailed Data (Continued)

Fault Name	Sense of Slip	Displacement			Fault Strike at Surface	Fault Dip at Surface	Fault Length (km)			Number of Possible Fault Segments		Number of Trenches
							Min	Pref	Max			
Solitario Canyon (Continued)	Trench (SCF-T4)											
	Event ^k	Displacement (cm) ^b			Event Criteria ^g	Event Confidence ^h	Event Timing (ka)			Dating Method ⁱ	Dating Reliability ^h	Shape of Timing Distribution
		Min	Pref	Max			Min	Pref	Max			
	Z	0	-	10?	U	L	20	20-30	40	R	L	Triangle
	Y	20	-	30	F	H	60	70	80	R	M	Triangle
	X	-	-	-	-	-	-	-	-	-	-	-
	W	15	-	30	F	H	150	200	250	R	L	Triangle
	Trench (SCF-T8)											
	Event ^k	Displacement (cm) ^b			Event Criteria ^g	Event Confidence ^h	Event Timing (ka)			Dating Method ⁱ	Dating Reliability ^h	Shape of Timing Distribution
		Min	Pref	Max			Min	Pref	Max			
	Z	10	-	20	U, dragged ash	M	14	15	17	U	L	Triangle
	Y	110	-	130	F	H	31	-	65-124	R,U,T	M	Triangle
	X	20	-	40	F	L	112	-	150-250	U	M	Triangle
W	30	-	60	F	H	-	-	-	R	L	Triangle	
Trench (T13)												
Event ^k	Displacement (cm) ^b			Event Criteria ^g	Event Confidence ^h	Event Timing (ka)			Dating Method ⁱ	Dating Reliability ^h	Shape of Timing Distribution	
	Min	Pref	Max			Min	Pref	Max				
-	-	-	-	-	-	-	-	-	-	-	-	
Stagecoach Road (Menges and Whitney 1996a, 1996b; Pezzopane, Whitney et al. 1996)	Normal-left-lateral				N30°E	73°W	4	-	5	1		3
	Trench (SCR-T1)											
	Event ^k	Displacement (cm) ^b			Event Criteria ^g	Event Confidence ^h	Event Timing (ka)			Dating Method ⁱ	Dating Reliability ^h	Shape of Timing Distribution
		Min	Pref	Max			Min	Pref	Max			
	Z	40	40	82	D,W	H	5	-	17	T,U,R	NS ^j	Triangle
	Y	20	42	70	W,F,U,T	H	10	-	14	T,U,R	-	Triangle
X	14	47	99	U,T,W,F	M	24	-	32	T,U,R	-	Trapezoid	
W	24	51	74	U,T,W	M	>32	-	<38	T,U,R	-	Trapezoid	

Table 12.3-8b. Event Displacements and Timing Data from Paleoseismic Studies of Yucca Mountain Faults: Detailed Data (Continued)

Fault Name	Sense of Slip	Displacement			Fault Strike at Surface	Fault Dip at Surface	Fault Length (km)			Number of Possible Fault Segments		Number of Trenches
							Min	Pref	Max			
Stagecoach Road (Continued)	Trench (SCR-T2)											
	Event ^k	Displacement (cm) ^b			Event Criteria ^g	Event Confidence ^h	Event Timing (ka)			Dating Method ⁱ	Dating Reliability ^h	Shape of Timing Distribution
		Min	Pref	Max			Min	Pref	Max			
	-	-	-	-	-	-	-	-	-	-	-	-
	Trench (SCR-T3)											
	Event ^k	Displacement (cm) ^b			Event Criteria ^g	Event Confidence ^h	Event Timing (ka)			Dating Method ⁱ	Dating Reliability ^h	Shape of Timing Distribution
		Min	Pref	Max			Min	Pref	Max			
	Z	25	43	66	W,F	H	<22	-	<28	T,U,R	NS ^j	Triangle
Y	20	59	77	U,T,W	H	22	-	28	T,U,R	-	Triangle	
X	25	57	84	U,W	M	-	-	-	T,U,R	-	Trapezoid	
W	26	67	87	T,W	-	69	-	118	T,U,R	-	Trapezoid	
Windy Wash (Whitney, Simonds et al. 1996; Menges and Whitney 1996a; Pezzopane, Whitney et al. 1996)	Normal-left-lateral				N4-20°E	77-90°W	3	22	35	3		3
	Trench (CF-2-northwall)											
	Event ^k	Displacement (cm) ^b			Event Criteria ^g	Event Confidence ^h	Event Timing (ka)			Dating Method ⁱ	Dating Reliability ^h	Shape of Timing Distribution
		Min	Pref	Max			Min	Pref	Max			
	Z	0	4	10	F	H	2	-	3	T	H	Triangle
	Y	-	-	-	F,D,U	M	30	40	60	U	M	Triangle
	X	45	50	53	W,U	L	70	75	120	U,A	M	Triangle
	W	18	-	25	W,U	M	120	150	160	U	M	Triangle
	V	70	-	83	W,F	M	180	200	220	R	L	Triangle
U	40	30	60	W,F	M-L	220	240	260	R	L	Triangle	
T	48	-	60	W,U	M	300	340	370	U	M	Triangle	

Table 12.3-8b. Event Displacements and Timing Data from Paleoseismic Studies of Yucca Mountain Faults: Detailed Data (Continued)

Fault Name	Sense of Slip	Displacement			Fault Strike at Surface	Fault Dip at Surface	Fault Length (km)			Number of Possible Fault Segments		Number of Trenches
							Min	Pref	Max			
Windy Wash (Continued)	Trench (CF-2 southwall)											
		Event ^k	Displacement (cm) ^b			Event Criteria ^g	Event Confidence ^h	Event Timing (ka)			Dating Method ⁱ	Dating Reliability ^h
	Min		Pref	Max	Min			Pref	Max			
	Z	0	4	10	F	H	2	-	3	T	H	Triangle
	Y	8	-	18	F,D	M	30	40	60	U	M	Triangle
	X	45	50	53	W	M	70	75	120	U,A	M	Triangle
	W	38	-	52	W,U	M	130	150	160	U	M	Triangle
	V	24	-	30	W	M	180	200	220	R	L	Triangle
	U	15	19	24	W	L	220	240	260	R	L	Triangle
	T	55	60	65	W,U	M	300	340	370	U	M	Triangle
	S	45	65?	95?	W,F	M	390	400	>400	R	L	Triangle
	Trench (CF-2.5)											
		Event ^k	Displacement (cm) ^b			Event Criteria ^g	Event Confidence ^h	Event Timing (ka)			Dating Method ⁱ	Dating Reliability ^h
	Min		Pref	Max	Min			Pref	Max			
	Z	0	4	10	F,D	H	2	-	3	T	H	Triangle
	Y	-	-	-	F,D	M-H	30	40	60	U	M	Triangle
	X	33	-	54	D,W	H	70	75	120	U	M	Triangle
	W	25	35	50	D,F,U	M	130	150	160	U	M	Triangle
	V	-	-	-	W	H	180	200	220	S,R	L	Triangle
Trench (CF-3 northwall)												
	Event ^k	Displacement (cm) ^b			Event Criteria ^g	Event Confidence ^h	Event Timing (ka)			Dating Method ⁱ	Dating Reliability ^h	Shape of Timing Distribution
Min		Pref	Max	Min			Pref	Max				
Z	0	4	10	F,D	M	2	-	3	T	H	Triangle	
Y	-	-	-	F,D	M-H	30	40	60	U	M	Triangle	
X	71	-	96	D,W	H	70	75	120	U	M	Triangle	
W	-	-	-	D	H	130	150	160	U	M	Triangle	
V	-	-	-	D,W	H	180	200	220	U	L	Triangle	

Table 12.3-8b. Event Displacements and Timing Data from Paleoseismic Studies of Yucca Mountain Faults: Detailed Data (Continued)

Fault Name	Sense of Slip	Displacement			Fault Strike at Surface	Fault Dip at Surface	Fault Length (km)			Number of Possible Fault Segments		Number of Trenches
							Min	Pref	Max			
Windy Wash (Continued)	Trench (CF-3 southwall)											
		Displacement (cm) ^b			Event Criteria ^g	Event Confidence ^h	Event Timing (ka)			Dating Method ⁱ	Dating Reliability ^h	Shape of Timing Distribution
	Min	Pref	Max	Min			Pref	Max				
	Z	0	4	10	F,D	M	2	-	3	T	H	Triangle
	Y	25	-	45	D	M-H	30	40	60	U	M	Triangle
X	78	-	98	D,U	H	70	75	120	U	M	Triangle	

Source: For each fault, source(s) provided in the column labeled "Fault Name."

NOTES: ^aTrenches with limited or no data are not included in this compilation; for information on excluded trenches see Whitney, Taylor, and Wesling (1996, Chapter 4).

^bVertical displacement, corrected for local deformation effects such as backtilting and graben formation

^cNet tectonic displacement, adjusted from dip-slip values by including (a) oblique-slip components and and/or (b) removal of local deformation effects such as backtilting and graben formation

^dApparent vertical displacement, not adjusted for local deformation effects or oblique-slip components

^eApparent dip-slip displacement, displacement measured along the fault zone, not corrected for oblique-slip components or local deformation

^fDip-slip displacements, slip along the fault zone, not adjusted for oblique components of slip

^gD = displacement of unit; F = fault-related fissure; W = fault-related colluvial wedge; U = upward termination of fractures; T = tilted and/or deformed units

^hH = high; M = moderate; L = low

ⁱT = thermoluminescence; U = U-series; S = soil development; A = ash; R = relative correlation; Ar = archaeological; TR = U-trend

^jNS = not specified by principal investigation

^kEvent Scenarios are defined in Table 12.3-10

To convert km to mi., multiply by 0.621.

Table 12.3-9. Summary of Paleoseismic Data for Quaternary Faults in the Yucca Mountain Area

Fault	Number of Events	Displacement/Event (cm)		Most Recent Event (ka)		Average Recurrence Interval (k.y.)		Slip Rate (mm/yr.)	
		Range	Pref.	Range	Pref.	Range	Pref.	Range	Preferred Value
Bare Mountain	1-2	80-300	80-150	14-100	14-100	10-200 ^a	100-200	0.06-0.01	0.01
Bow Ridge	2-3	1-80	14-44	30-130	40-60	70-215	100-140	0.002-0.007	0.003
Northern Crater Flat	3-5	0-50	0-50	4-10	4.1-10	120-160	120-160	0.002-0.003	0.002-0.003
Southern Crater Flat	2-3	5-32	18-20	2-8	2-8	NA	5-60	NA	0.002
Fatigue Wash	3-6	0-125	25-125	8-70 (Z) 15-100 (Y)	20-60 (Z) ^b 60-70 (Y)	120-250	185	0.001-0.015	0.003-0.015
Iron Ridge	1-4	5-200	5-200	<20	<20	ND	ND	ND	ND
Paintbrush Canyon	3-7	0-257	6-167	7-20 (N) 35-90 (S)	7-20 (N) ^c 40-50 (S) ^d	20-270	20-120	0.001-0.03	0.002-0.015
Rock Valley	2-5	0-824	<39-<63	4-17 (N) 2-3 (S)	4-17 (N) ^e 2-3 (S) ^f	5->10	10 ^a	0.002-0.05	0.02-0.05
Solitario Canyon	4-6	0-130	0-130	14-40	15-30	35-100	50-70	0.01-0.02	0.01
Stagecoach Road	2-7	14-99	40-67	<28	-	5-50	10-30	0.006-0.07	0.03-0.05
Windy Wash	3-8	0-98	65	3-7	2-3	40-57	40-45	0.009-0.01	0.011

Source: See sources for Table 12.3-8.

NOTES: Range = maximum and minimum range of values; Pref. = preferred range of values

ND = no data; NA = not applicable; paleoseismic parameters are defined in Section 12.7.

^aOrder of magnitude estimate made from sparse data.

^bAge constraint for possible event Z, which, if it exists, is the most recent event. Otherwise most recent event is Y, with age constraint below.

^cAge constraints for most recent event on northern end of fault.

^dAge constraints for most recent event on southern end of fault.

^eAge constraints for most recent event on northern strand of fault.

^fAge constraints for most recent event on southern strand of fault.

To convert cm to in., multiply by 0.394.

To convert mm/yr. to in./yr., multiply by 0.0394.

Table 12.3-10. Preliminary Ages, Rupture Lengths, Displacements, and Magnitudes of Proposed Prehistoric Earthquake Rupture Scenarios at Yucca Mountain

Scenario	Faults ^a	Preferred Age ^b (k.y.)	Correlation Confidence ^c	Rupture Length ^d (km)		Rupture Displacement ^e (cm)	Estimated Magnitude ^f			Preferred Scenario Magnitude ^g
				Min.	Max.		Min. RL	Max. RL	Displ.	
Z	WW, SCF, NCF	5 ± 2	H	8.5	22	18	6.16	6.64	6.16	6.2
Y	PC, SCR	13 ± 3	H	18.5	25.5	43	6.55	6.71	6.43	6.5
X	SC, SCR, IR	26 ± 5	M	15	24	59	6.44	6.68	6.53	6.4
W	BM, WW, FW	40 ± 5	M	10	22	150	6.24	6.64	6.82	6.8
V	PC, SCR	59 ± 5	M	9	15.5	57	6.19	6.46	6.52	6.5
U	SCF, WW, FW, SC, BR, PC	75 ± 10	H	10.5	23	120	6.26	6.66	6.75	6.7 - 6.9 ^h
T	PC, SCR	99 ± 10	M	14	20	98	6.41	6.59	6.68	6.6
S	PC, SCR?	120 ± 13	L-M	9.5	19.5	40	6.21	6.58	6.41	6.6
R	WW, BR	140 ± 10	L	8.5	22	42	6.16	6.64	6.42	6.5

Source: Pezzopane, Whitney, and Dawson (1996, Table 5-3)

NOTES: ^aFault abbreviations are as follows: BM = Bare Mountain; BR = Bow Ridge; FW = Fatigue Wash; IR = Iron Ridge; NCF = Northern Crater Flat; PC = Paintbrush Canyon; SC = Solitario Canyon; SCF = Southern Crater Flat; SCR = Stagecoach Road; WW = Windy Wash.

^bPreferred age is the estimated age (in k.y.) of each rupture scenario based on the overlap of the timing distributions. The preferred age and a standard error are given; however, a better description of the age uncertainties is provided by the cumulative timing curves shown in the different plots of Figure 5-6 of Pezzopane, Whitney, and Dawson (1996).

^cCorrelation confidence is a subjective assessment of confidence in the correlation of individual paleoevents to form a rupture scenario: H = high, M = moderate, L = low.

^dMinimum (Min.) and maximum (Max.) rupture lengths are derived for each scenario on the basis of the trench locations with evidence of correlative events, as well as locations that lack evidence of the correlative event.

^eRupture displacement is the largest preferred displacement value (in centimeters) measured on an individual fault or at a single site involved in each rupture scenario.

^fEstimated magnitudes (moment magnitude) are derived from scenario rupture lengths (Max. RL = maximum rupture length; Min. RL = minimum rupture length) and rupture displacements (Displ. = rupture displacement; see Note "e") using the appropriate empirical relation of Wells, D.L. and Coppersmith (1994).

^gPreferred scenario magnitude (moment magnitude) is the preferred magnitude for the scenario rupture.

^hPreferred value based on maximum rupture length is M 6.7; if slip is summed across all west-side faults (assumes surface faults merge to a single rupture plane at seismogenic depth), a value of M 6.9 is preferred.

To convert km to mi., multiply by 0.621.

To convert cm to in., multiply by 0.394.

Table 12.3-11. Fault Data Interpretations and Ground Motion Estimates for the Relevant Earthquake Source Evaluation by Pezzopane (1996)

Minimum Distance to CAB ^a (km)	Minimum Distance to YMPP ^b (km)	Fault Name and Abbreviation	Relevant Fault ^c	Documented Quaternary Displacement ^d	Maximum Fault Length ^e (km)	Reference ^f	Maximum Moment Magnitude ^g (M _w)	Average Peak Acceleration ^h Median - 84th Percentile (g)	SEA96h Peak Acceleration ⁱ Median - 84th Percentile (g)
0	0	Ghost Dance GD	Yes?	No?	3	1, 2, 3, 24	5.6	0.44 - 0.74	0.23 - 0.38
0	0	Ghost Dance-Abandoned Wash GDAW	Yes?	No?	5 ^j	1, 2, 3, 24	5.9	0.48 - 0.79	0.27 - 0.44
0	0	Sundance SD	Yes?	No?	1	1, 3, 4, 24	5.1	0.38 - 0.66	0.18 - 0.29
0	1	Solitario Canyon SC	Yes	Yes	28	1, 2, 5, 24	6.6	0.58 - 0.94	0.39 - 0.64
0	1.5	Drill Hole Wash DHW	Yes?	No?	4	1, 2, 6, 24	5.8	0.46 - 0.77	0.25 - 0.42
0	2	Dune Wash DW	Yes?	No?	3	1, 2, 24	5.6	0.44 - 0.74	0.23 - 0.38
0	2.5	Bow Ridge BWR	Yes	Yes	10	1, 2, 5, 7	6.2	0.52 - 0.85	0.31 - 0.52
0	2.5	Pagany Wash PW	Yes?	No?	4	1, 2, 6, 24	5.8	0.46 - 0.77	0.25 - 0.42
0	2.5	Iron Ridge IR	Yes	Yes	9	1, 2	6.2	0.52 - 0.85	0.31 - 0.52
0	2.5	Boomerang Point BP	Yes?	No?	5	1, 2	5.9	0.48 - 0.79	0.27 - 0.44
0	3	Sever Wash SW	Yes?	No?	4	1, 2, 6, 24	5.8	0.46 - 0.77	0.25 - 0.42
0	3	Midway Valley MWV	Yes?	Yes?	5	1, 2, 25	6.1	0.50 - 0.83	0.30 - 0.49
0	3.5	Fatigue Wash FW	Yes	Yes	17	1, 2, 5, 8	6.5	0.56 - 0.92	0.37 - 0.60
0	4	Paintbrush Canyon PC	Yes	Yes	28	1, 2, 5, 7, 9	6.7	0.60 - 0.97	0.41 - 0.67
0	4	Paintbrush Canyon-Stagecoach Road PCSR	Yes	Yes	33 ^j	1, 2, 5, 7, 9	6.8	0.62 - 1.00	0.43 - 0.71
1	4.5	Windy Wash WW	Yes	Yes	25	1, 2, 5	6.7	0.56 - 0.91	0.40 - 0.66
2	6	Crater Flat CF	Yes	Yes	18	1, 10, 23	6.5	0.48 - 0.79	0.35 - 0.57
4	8.5	Black Cone BC	Yes	Yes	7	1, 5, 10	6.1	0.35 - 0.58	0.24 - 0.40
4	10	Stagecoach Road SR	Yes	Yes	9	1, 2, 5, 7	6.2	0.36 - 0.60	0.26 - 0.42
10	14	Bare Mountain BM	Yes	Yes	16	5, 11, 20	6.5	0.27 - 0.44	0.19 - 0.31

Table 12.3-11. Fault Data Interpretations and Ground Motion Estimates for the Relevant Earthquake Source Evaluation by Pezzopane (1996) (Continued)

Minimum Distance to CAB ^a (km)	Minimum Distance to YMPR ^b (km)	Fault Name and Abbreviation	Relevant Fault ^c	Documented Quaternary Displacement ^d	Maximum Fault Length ^e (km)	Reference ^f	Maximum Moment Magnitude ^g (M _w)	Average Peak Acceleration ^h Median - 84th Percentile (g)	SEA96h Peak Acceleration ⁱ Median - 84th Percentile (g)
12	19	Rocket Wash-Beatty Wash RWBW	Yes?	Yes?	17	5, 18	6.5	0.23 - 0.39	0.16 - 0.27
14	19	Mine Mountain MM	(Yes)	Yes?	27	5, 21	6.7	0.23 - 0.38	0.16 - 0.26
16	22	Wahmonie WAH	(Yes)	Yes?	15	5, 21	6.4	0.18 - 0.30	0.12 - 0.20
19	24	Oasis Valley OSV	Yes?	Yes?	20	5, 18	6.6	0.17 - 0.28	0.12 - 0.19
21	27	Rock Valley RV	Yes	Yes	65	5, 19, 21	7.2	0.22 - 0.35	0.15 - 0.24
21	29	Cane Spring CS	(Yes)	No?	27	5, 21	6.7	0.17 - 0.27	0.11 - 0.19
27	33	West Specter Range WSR	Yes	Yes	9	18	6.2	0.10 - 0.16	0.07 - 0.11
28	34	Ash Meadows AM	Yes	Yes	60	5, 19	7.1	0.16 - 0.26	0.11 - 0.18
31	36	Yucca Lake YCL	(Yes)	Yes?	17	5	6.5	0.10 - 0.17	0.07 - 0.12
32	37	Eleana Range ER	Yes	Yes	13	5	6.4	0.09 - 0.16	0.07 - 0.11
33	38	Amargosa River AR	Yes	Yes	15	5, 19	6.4	0.09 - 0.15	0.06 - 0.11
33	38	Amargosa River -Pahrump ARPR	Yes	Yes	130 ^{j,k}	5, 19	7.5	0.18 - 0.28	0.11 - 0.19
34	38	Bullfrog Hills BUL	Yes?	Yes?	7	5	6.1	0.07 - 0.12	0.05 - 0.09
34	40	Yucca YC	Yes	Yes	32	5	6.8	0.11 - 0.18	0.08 - 0.13
35	42	Tolicha Pass TOL	Yes?	Yes?	22	5, 18	6.6	0.10 - 0.16	0.07 - 0.11
36	43	Keane Wonder KW	Yes	Yes	25	5, 18	6.7	0.10 - 0.16	0.07 - 0.11
37	43	Carpetbag CB	Yes	Yes	30	5	6.8	0.10 - 0.17	0.07 - 0.12
38	44	Area Three AT	Yes?	Yes?	12	5	6.3	0.07 - 0.12	0.05 - 0.09
39	44	Checkpoint Pass CP	Yes?	No?	8 ^l	5	6.1	0.06 - 0.11	0.05 - 0.08
41	46	Plutonium Valley - N Halfpint Ridge PVNH	Yes?	No?	26	5	6.7	0.09 - 0.14	0.06 - 0.10
43	48	Crossgrain Valley CGV	Yes?	Yes?	9	5	6.2	0.06 - 0.10	0.04 - 0.07
43	48	Pahute Mesa PM	Yes?	Yes?	9	5	6.2	0.06 - 0.10	0.04 - 0.07

Table 12.3-11. Fault Data Interpretations and Ground Motion Estimates for the Relevant Earthquake Source Evaluation by Pezzopane (1996) (Continued)

Minimum Distance to CAB ^a (km)	Minimum Distance to YMPR ^b (km)	Fault Name and Abbreviation	Relevant Fault ^c	Documented Quaternary Displacement ^d	Maximum Fault Length ^e (km)	Reference ^f	Maximum Moment Magnitude ^g (M _w)	Average Peak Acceleration ^h Median - 84th Percentile (g)	SEA96h Peak Acceleration ⁱ Median - 84th Percentile (g)
44	48	Mercury Ridge MER	Yes?	No?	10	5	6.2	0.06 - 0.10	0.04 - 0.07
44	50	Furnace Creek FC	Yes	Yes	145 ^m	5, 22	7.6	0.14 - 0.23	0.09 - 0.15
44	50	Death Valley-Furnace Creek DVFC	Yes	Yes	205 ^{l,n}	5, 22	7.8	0.16 - 0.26	0.10 - 0.17
44	50	Death Valley-Furnace Creek-Fish Lake Valley DFFL	Yes	Yes	288 ^{l,o}	5, 12, 22	7.9	0.17 - 0.27	0.11 - 0.18
45	49	Ranger Mountain RM	No	Yes?	5	5	5.9	0.05 - 0.08	0.04 - 0.06
45	50	South Ridge SOU	Yes?	Yes?	19	5	6.6	0.08 - 0.12	0.05 - 0.09
45	52	Sarcobatus Flat SF	(Yes)	Yes?	51	5, 18	7.1	0.10 - 0.17	0.07 - 0.11
46	51	Boundary BD	No	Yes	7	5	6.1	0.05 - 0.09	0.04 - 0.07
47	53	Buried Hills BH	Yes?	Yes?	26	5	6.7	0.08 - 0.13	0.05 - 0.09
48	53	West Spring Mountains WSM	Yes	Yes	60	5, 18	7.1	0.10 - 0.16	0.07 - 0.11
48	53	Cockeyed Ridge-Papoose Lake CRPL	Yes?	Yes?	21	5	6.6	0.07 - 0.12	0.05 - 0.08
48	55	Death Valley DV	Yes	Yes	100 ^p	5, 22	7.4	0.12 - 0.19	0.08 - 0.13
50	55	Belted Range BLR	Yes	Yes	54	5, 18	7.1	0.09 - 0.15	0.06 - 0.10
50	57	Kawich Range KR	Yes	Yes	84	5, 18	7.3	0.11 - 0.17	0.07 - 0.11
52	57	Oak Springs OAK	Yes?	Yes?	21	5	6.6	0.06 - 0.11	0.05 - 0.08
53	58	Grapevine GV	Yes	Yes	20	5	6.6	0.06 - 0.10	0.05 - 0.08
54	59	Spotted Range SPR	Yes?	Yes?	30	5	6.8	0.07 - 0.12	0.05 - 0.08
54	59	Cactus Springs CAC	No	Yes?	14	5	6.4	0.05 - 0.09	0.04 - 0.07
55	60	Emigrant Valley North EVN	Yes?	Yes?	28	5	6.8	0.07 - 0.11	0.05 - 0.08
55	60	Gold Flat GOL	No	Yes?	16	5	6.5	0.06 - 0.09	0.04 - 0.07
56	61	Kawich Valley KV	Yes?	Yes?	43	5	7.0	0.08 - 0.13	0.05 - 0.09

Table 12.3-11. Fault Data Interpretations and Ground Motion Estimates for the Relevant Earthquake Source Evaluation by Pezzopane (1996) (Continued)

Minimum Distance to CAB ^a (km)	Minimum Distance to YMPR ^b (km)	Fault Name and Abbreviation	Relevant Fault ^c	Documented Quaternary Displacement ^d	Maximum Fault Length ^e (km)	Reference ^f	Maximum Moment Magnitude ^g (M _w)	Average Peak Acceleration ^h Median - 84th Percentile (g)	SEA96h Peak Acceleration ⁱ Median - 84th Percentile (g)
60	66	Emigrant Valley South EVS	No	Yes?	20	5	6.6	0.06 - 0.09	0.04 - 0.07
60	65	Chert Ridge CHR	No	Yes?	14	5	6.4	0.05 - 0.08	0.04 - 0.06
61	67	Indian Springs Valley ISV	Yes?	Yes?	28	5	6.8	0.06 - 0.10	0.04 - 0.07
61	67	Grapevine Mountains GM	Yes?	Yes?	31 ^q	5	6.8	0.06 - 0.10	0.04 - 0.07
63	70	Pahrump PRP	Yes	Yes	70 ^k	5	7.2	0.08 - 0.12	0.05 - 0.09
65	70	Fallout Hills FH	No	Yes?	8	5	6.1	0.04 - 0.06	0.03 - 0.05
68	74	Bonnie Claire BOC	No	Yes?	27	5	6.7	0.05 - 0.08	0.04 - 0.06
70	74	Stumble STM	No	Yes?	33	5	6.8	0.05 - 0.09	0.04 - 0.06
70	76	West Pintwater Range WPR	Yes	Yes	82	5	7.1	0.07 - 0.11	0.05 - 0.08
71	76	Towne Pass TP	No	Yes	38	5	6.9	0.06 - 0.09	0.04 - 0.07
72	77	Jumbled Hills JUM	No	Yes?	27	5	6.7	0.05 - 0.08	0.04 - 0.06
74	80	Cactus Flat-Mellan CFM	No	Yes?	35	5	6.9	0.05 - 0.09	0.04 - 0.06
75	81	East Pintwater Range EPR	Yes?	Yes?	58	5	7.1	0.06 - 0.10	0.04 - 0.07
76	81	North Desert Range NDR	No	Yes?	24	5	6.7	0.05 - 0.07	0.03 - 0.06
76	82	La Madre LMD	No	Yes?	33	5	6.8	0.05 - 0.08	0.04 - 0.06
77	84	Cactus Flat CAF	No	Yes?	50	5	7.1	0.06 - 0.09	0.04 - 0.07
77	82	Groom Range Central GRC	No	Yes?	31	5	6.8	0.05 - 0.08	0.04 - 0.06
78	84	Three Lakes Valley TLV	No	No?	27	5	6.7	0.04 - 0.07	0.03 - 0.06
79	85	Groom Range East GRE	No	No?	20	5	6.6	0.04 - 0.07	0.03 - 0.05

Table 12.3-11. Fault Data Interpretations and Ground Motion Estimates for the Relevant Earthquake Source Evaluation by Pezzopane (1996) (Continued)

Minimum Distance to CAB ^a (km)	Minimum Distance to YMPR ^b (km)	Fault Name and Abbreviation	Relevant Fault ^c	Documented Quaternary Displacement ^d	Maximum Fault Length ^e (km)	Reference ^f	Maximum Moment Magnitude ^g (M _w)	Average Peak Acceleration ^h Median - 84th Percentile (g)	SEA96h Peak Acceleration ⁱ Median - 84th Percentile (g)
80	87	Cactus Range -Wellington Hills CRWH	No	No?	29	5	6.8	0.05 - 0.07	0.03 - 0.06
82	87	Chalk Mountain CLK	No	Yes?	20	5	6.6	0.04 - 0.06	0.03 - 0.05
84	90	Chicago Valley CHV	No	Yes	20	5	6.6	0.04 - 0.06	0.03 - 0.05
85	90	Tin Mountain TM	No	Yes	29	5	6.8	0.04 - 0.07	0.03 - 0.05
87	92	Tikaboo TK	No	Yes	33	5	6.8	0.04 - 0.07	0.03 - 0.05
85	92	Stonewall Mountain SWM	No	Yes	22	5	6.6	0.04 - 0.06	0.03 - 0.05
90	95	Hunter Mountain HM	No	Yes	85	5	7.3	0.06 - 0.09	0.04 - 0.07
90	95	Panamint Valley PAN	Yes	Yes	100	5	7.4	0.06 - 0.10	0.04 - 0.07
90	95	Hunter Mountain - Panamint Valley HMPN	Yes	Yes	185 ^j	5	7.7	0.07 - 0.12	0.05 - 0.08
92	97	Penoyer PEN	No	Yes	56	5	7.1	0.05 - 0.08	0.04 - 0.06
93	97	Racetrack Valley RTV	No	Yes?	22	5	6.6	0.03 - 0.06	0.03 - 0.04
101	106	Pahranagat PGT	No	Yes	91 ^r	5	7.4	0.05 - 0.09	0.04 - 0.06
122	126	Owens Valley OWV	No	Yes	110	5	7.4	0.04 - 0.07	0.03 - 0.05
130	135	Fish Lake Valley FLV	No	Yes	83	5, 12	7.3	0.04 - 0.06	0.03 - 0.05
145	150	Garlock GAR	No	Yes	251 ^s	13, 14	7.9	0.05 - 0.08	0.04 - 0.06
180	185	White Mountains and Cedar Mountain WMCM	No	Yes	115 ^t	5, 15	7.5	0.03 - 0.05	0.02 - 0.04
285	291	San Andreas SAF	No	Yes	420 ^u	16, 17	8.1	0.03 - 0.05	0.02 - 0.03

Source: Pezzopane (1996, Table 1)

NOTES: ^aMinimum distance to the controlled area boundary refers to the closest distance (in kilometers) from a point on the surface trace of the fault to the boundary of the area. The controlled area boundary extends approximately 5 to 7 km from the potential repository outline. Thus, most faults are from 7 to 9 km farther from the center of the potential repository (approximately latitude 36.85°N. and longitude 116.45°W.) than the minimum distance indicates. (See footnote b.)

Table 12.3-11. Fault Data Interpretations and Ground Motion Estimates for the Relevant Earthquake Source Evaluation by Pezzopane (1996) (Continued)

- ^b Minimum distance to Yucca Mountain potential repository refers to the closest distance (in kilometers) from a point on the surface trace of the fault to the center of the Yucca Mountain potential repository (approximately latitude 36.85°N. and longitude 116.45°W.).
- ^c Relevant faults (indicated with "Yes") are those with documented Quaternary activity and the potential to generate average 84th percentile peak accelerations that equal or exceed 10 percent of gravity (0.1 g) at the controlled area boundary of the Yucca Mountain site (see footnote h). Potentially relevant faults ("Yes?") are those with suspected or questionable Quaternary activity ("Yes?" or "No?" in column 5 of this table) and the capability to produce at least 0.1 g peak acceleration at the 84th percentile level. Potentially relevant faults that are considered subject to displacement on the basis of potential structural associations with seismicity or other Quaternary faults are tentatively identified as relevant faults (indicated with parentheses ("Yes")). Nonrelevant faults ("No") are those that cannot produce at least 0.1 g average peak acceleration (84th percentile), regardless of their Quaternary activity.
- ^d Documented Quaternary displacement designates the status of evidence for Quaternary fault activity with three alternatives, "Yes", "Yes?", and "No?", depending upon whether published studies document Quaternary (<2 Ma) displacement, or other compelling evidence supports Quaternary displacement potential, such as associated seismicity or field studies. Faults with a "Yes" are those with demonstrated Quaternary displacement. Faults with a "Yes?" are those for which evidence suspects Quaternary displacement, but the faults have not been studied in sufficient detail to either document or disprove such displacement. Also, complete stratigraphic sections, including older Quaternary deposits, may not be preserved over the fault traces. Faults with a "No?" are those that lack evidence of Quaternary displacement or for which the data are inconclusive.
- ^e Maximum fault length is the along-trace length of the fault zone (in kilometers) as reported in published references or as estimated from maps and plates in cited references (Simonds et al. 1995; Scott and Bonk 1984; Piety 1996). The maximum length represents the entire length of the mapped or inferred fault zone, including sections portrayed as concealed, discontinuous, or both.
- ^f References for maximum fault length and Quaternary activity are keyed by number: (1) is Simonds et al. (1995); (2) Scott and Bonk (1984); (3) Spengler et al. (1993); (4) Spengler et al. (1994); (5) Piety (1996); (6) Scott and Bonk (1984); (7) Menges et al. (1994); (8) Coe et al. (1995); (9) Dickerson and Spengler (1994); (10) Faulds et al. (1994); (11) Klinger and Anderson (1994); (12) Reheis (1994); (13) McGill and Sieh (1993); (14) McGill and Sieh (1991); (15) dePolo et al. (1993); (16) Sieh (1978); (17) USGS (1988); (18) Anderson, R.E., Bucknam et al. (1995); (19) Anderson, R.E., Crone et al. (1995); (20) Anderson, L.W. and Klinger (1996); (21) Coe, Yount, and O'Leary (1996); (22) Klinger and Piety (1996); (23) Ramelli et al. (1991); (24) Day et al. (1998); (25) Swan, F.W. et al. (1994).
- ^g Maximum moment magnitude (M_w) is the size of the earthquake associated with rupture of the maximum fault length. Moment magnitude is calculated using maximum fault lengths and the empirical relation between surface-rupture length and moment magnitude derived by Wells, D.L. and Coppersmith (1994) for all fault types.
- ^h Average peak acceleration (median and 84th percentile) is the average of four empirical attenuation relations appropriate for rock sites (Boore et al. 1994; Campbell 1981; Idriss 1991; Joyner and Boore 1981) calculated using the maximum moment magnitude and the minimum distance from the source to the controlled area boundary. The value on the left is the average of the median peak accelerations derived from the four attenuation relations, and on the right is the average of the 84th percentile peak acceleration.
- ⁱ SEA96h peak acceleration (median and 84th percentile) are calculated using the minimum distance from the source to the controlled area boundary, the maximum moment magnitudes, and the attenuation relation for extensional regimes and rock sites derived by Spudich et al. (1996). These ground motion values are listed for comparison and are not used to determine relevant faults.
- ^j Faults are assumed to join in a compound rupture of the entire zone.

Table 12.3-11. Fault Data Interpretations and Ground Motion Estimates for the Relevant Earthquake Source Evaluation by Pezzopane (1996) (Continued)

- ^kThe maximum length of the Pahrump fault zone, combined with other along-strike faults, has been interpreted to be 130 km (summarized in Piety [1996]). To obtain this length, the fault is projected across long reaches where no surface trace is mapped. The total length of projection is approximately 60 km, almost one-half of the total Pahrump fault length. The northernmost projection of this 130-km-long zone may merge or intersect with the Amargosa River, Ash Meadows, and Rock Valley fault zones. The analysis considers this possibility by including the Amargosa River (AR) fault as the northern continuation of the Pahrump fault zone. Even with this interpretation (ARPR), an additional 40 km of unmapped fault length is at the southeastern projection of the Pahrump fault zone.
- ^lMaximum length is the sum of the northern and southern traces of the western half of the Checkpoint Pass fault (see Piety 1996).
- ^mMaximum fault length is measured from Cucomungo Canyon at the northern end southward along the base of the Funeral Mountains east of Death Valley, almost to the town of Death Valley, California, at the southeastern end of Furnace Creek Wash.
- ⁿMaximum fault length is measured from Cucomungo Canyon at the northern end of the Furnace Creek fault to the southern end of the southern Death Valley fault, almost to the Garlock fault.
- ^oMaximum fault length combines the maximum lengths of the Death Valley and Fish Lake Valley faults and includes 105 km for the Furnace Creek fault. The Furnace Creek fault length is measured from the southern end of the Fish Lake Valley fault in Cucomungo Canyon to the northern end of the Death Valley fault.
- ^pMaximum length of the Death Valley fault includes the southernmost part of the Southern Death Valley fault almost to the Garlock fault.
- ^qThe Grapevine Mountains fault zone consists of an eastern and a western fault (Piety 1996). The maximum fault length is measured from the southern end of the eastern fault to the northern end of the western fault.
- ^rMaximum length is for the Maynard Lake fault (see MAY in Piety [1996]), which includes the northeastward fault continuation inferred to lie beneath Tertiary volcanic rocks.
- ^sMaximum fault length for the Garlock fault assumes rupture of the entire fault (McGill and Sieh 1991). The minimum distance to the site is measured from latitude 35.6°N. and longitude 117°W., at the eastern end of the Garlock fault. This location, east of its junction with the Panamint Valley fault, is near paleoseismic study sites that document the fault's Quaternary activity (McGill and Sieh 1991, 1993).
- ^tThe White Mountains - Cedar Mountain zone is an idealized seismic source that represents several large faults in a broad area located between the 1872 Owens Valley, California, and 1932 Cedar Mountain, Nevada, earthquakes. Normal and oblique-slip Quaternary faults in this area have lengths between 20 and 70 km and are considered capable of M_w 6.8 to 7.4 earthquakes (dePolo et al. 1993). This table considers an idealized fault source with an assumed M_w of 7.5, which is larger than the expected magnitudes of the largest faults in the region, such as M 7.3 on the White Mountains fault zone (dePolo et al. 1993) and the historical M 7.2 Cedar Mountain earthquake. The minimum distance of 185 km is measured from latitude 37.5°N. and longitude 118°W., which is slightly closer to Yucca Mountain than the minimum distances from the 1932 Cedar Mountain earthquake ruptures and from the White Mountains fault zone.
- ^uThe 420-km rupture length for the San Andreas fault represents an event equivalent to, or slightly larger than, the 1857 and 1906 earthquakes; both were larger than M 8 (Sieh 1978; USGS 1988). The 1857 event ruptured SAF segments closest to the Yucca Mountain site. The minimum distance was measured to a point near Pallet Creek at latitude 34.5°N. and longitude 118°W., a paleoseismic study site that provides evidence for the fault's Quaternary activity (Sieh 1978).

Table 12.3-11. Fault Data Interpretations and Ground Motion Estimates for the Relevant Earthquake Source Evaluation by Pezzopane (1996) (Continued)

CAB = controlled area boundary; YMPR = Yucca Mountain potential repository

This table lists faults that may be relevant to seismic hazards at the potential waste repository at Yucca Mountain. Potential seismic sources are listed in order of their minimum distance to the boundary of the Yucca Mountain conceptual controlled area and to the center of the Yucca Mountain potential repository. To the right of the fault name are supporting data and estimates of potential peak accelerations that could be produced at the Yucca Mountain site, given maximum-magnitude earthquakes on faults in the region. The footnotes and text provide additional explanation.

To convert km to mi., multiply by 0.621.

To convert g to cm/s^2 , multiply by 980.7.

Table 12.3-12. Average Recurrence Intervals and Estimated Magnitudes for Different Recurrence Models Developed for Yucca Mountain Faults

Recurrence Model ^a	Average Recurrence Interval (k.y.) ^b	Estimated Magnitude ^c
1 (<500 k.y.)*	44 (+10, -7)	6.7 ± 0.4
1 (<150 k.y.)	19 (+8, -4)	6.7 ± 0.4
2 (<500 k.y.)*	13 (±5?)	6.4 (+0.5, -0.8)
2 (<150 k.y.)	35 (+15, -10)	6.4 (+0.5, -0.8)
3 (<150 k.y.)	17 (± 5?)	6.5 (+0.4, -0.3)

Source: Pezzopane, Whitney, and Dawson (1996, Table 5-4)

NOTES: ^aTwo different versions of models 1 and 2 are for two different time intervals, using all of the 500-k.y. paleoseismic record (those shown with an [asterisk]) or only the past 150-k.y. record, which is more complete. Model 3 is the the recurrence model preferred by the source authors.

^bAverage recurrence intervals (in k.y.) are calculated in different ways, as described in Pezzopane, Whitney, and Dawson (1996). The uncertainties are 1-sigma values; queries (?) indicate rough approximation.

^cEstimated magnitude is moment magnitude derived from the Wells, D.L. and Coppersmith (1994) relation, as described in Pezzopane, Whitney, and Dawson (1996).

Table 12.3-13. Seismic Velocity Structure Developed for Application at Potential Yucca Mountain Repository

Depth (ft)	S-Wave Velocity (ft/s)			Poisson's Ratio
	Lower Bound	Median	Upper Bound	
0 - 30	900	1,700	3,000	0.35 ± 0.10
30-125 (gradient layer)	900 to 2,500	1,700 to 5,700	3,000 to 12,000	0.30 ± 0.10
125-1,000	2,500	5,700	12,000	0.25 ± 0.10

DTN: MO98PRECLOSURE.000

NOTE: To convert ft to m, multiply by 0.305.
To convert ft/s to m/s, multiply by 0.305.

Table 12.3-14. Empirical Attenuation Models Evaluated in the Probabilistic Seismic Hazard Analysis Ground Motion Characterization Study

Investigator	Date	Site Conditions
Abrahamson and Silva	1997	Rock
Boore, Joyner, and Fumal	1997	Vs categories
Boore, Joyner, and Fumal	1994	Classes A and B
Campbell	1997	Soft and hard rock
Campbell, Campbell and Bozorgnia	1993, 1994	Hard rock
Campbell, Campbell and Bozorgnia	1990, 1994	Soft rock
Campbell	1990	Soil, soft rock
Idriss	1993	Rock, stiff soil
Idriss	1997	Rock, stiff soil
Joyner and Boore	1988	Rock
McGarr	1984	Rock
Sabetta and Pugliese	1996	Rock
Sadigh et al.	1997	Rock
Spudich et al.	1996	Rock

Source: Wong and Stepp (1998, Table 5-3)

Table 12.3-15. Source Parameters for the 1992 Little Skull Mountain Earthquake and Two Major Aftershocks

Event	Stress Drop (bar)
29 June mainshock	37 ± 11
5 July aftershock	23 ± 8
13 September aftershock	34 ± 14

Source: Schneider et al. (1996, Table 6-7)

NOTE: To convert bars to MPa, multiply by 0.1.

Table 12.3-16. Definition of Earthquake Scenarios

Scenario	Fault	M	Rupture Distance (km)	Mechanism
1	Paintbrush Canyon-Bow Ridge	6.3	Paintbrush Canyon branch: 4.5 Bow Ridge branch: 2.5	Normal
2	Solitario Canyon	6.5	1.0	Normal
3	Rock Valley	6.7	25	Strike-Slip
4	Bare Mountain	6.4	15.5	Normal
5	Furnace Creek	7.0	50	Strike-Slip
6	Solitario Canyon-Fatigue Wash-Windy Wash	6.6	1.0	Normal

Source: Schneider et al. (1996, Tables 8-1 and 9-2)

NOTE: M = Magnitude
To convert km to mi., multiply by 0.621.

Table 12.3-17. Form of Attenuation Equations Adopted in Probabilistic Seismic Hazard Analysis Ground Motion Characterization Study

	For $M < m_1$	For $M \geq m_1$
Median motion (μ)	$\mu = a_1 + a_2 (M-m_1) + a_6 (8.5-M)^2 + [a_3 + a_5 (M-m_1)] \ln(R^2 + a_8^2)^{1/2} + a_7 F + a_9 W_H f_1(M,R) + a_{10} W_F f_1(M,R)$	$\mu = a_1 + a_4 (M-m_1) + a_6 (8.5-M)^2 + [a_3 + a_5 (M-m_1)] \ln(R^2 + a_8^2)^{1/2} + a_7 F + a_9 W_H f_1(M,R) + a_{10} W_F f_1(M,R)$
	For $M < b_4$	For $M \geq b_4$
Aleatory variability (σ_{al})	$\sigma_{al} = b_1 + b_2 (M-b_4)$	$\sigma_{al} = b_1$
Epistemic Uncertainty in the Median (σ_μ)	$\sigma_\mu = c_1 + c_2 (M-c_6) + c_3 \ln(R+1) + c_4 [\ln(R+1)]^2 + c_5 F$	$\sigma_\mu = c_1 + c_2 (M-c_6) + c_3 \ln(R+1) + c_4 [\ln(R+1)]^2 + c_5 F$
	For $M < d_4$	For $M \geq d_4$
Epistemic Uncertainty in the Aleatory Variability (σ_σ)	$\sigma_\sigma = d_1 + d_2 (M-d_4)$	$\sigma_\sigma = d_1$

Source: Wong and Stepp (1998, pp. 6-2 to 6-3)

NOTE:

$$f(M, R) = \begin{cases} \frac{0}{R-x_1} \\ \frac{x_2-x_1}{x_2-x_1} \\ 1 \\ \frac{x_4-R}{x_4-x_3} \\ 0 \end{cases} \quad \begin{array}{l} \text{For } R \leq x_1 \\ x_1 < R < x_2 \\ x_2 \leq R \leq x_3 \\ x_3 < R < x_4 \\ R \geq x_4 \end{array} \quad x \begin{cases} 0 \\ \frac{M-a_{11}}{a_{12}-a_{11}} \\ 1 \end{cases} \quad \begin{array}{l} \text{For } M \leq a_{11} \\ a_{11} \leq M \\ M > a_{12} \end{array}$$

In all cases,

$$x_1 = 3, x_2 = 8, x_3 = 10, x_4 = 30, m_1 = 6.25$$

For normal faulting, $W_F = 1$ for footwall case and $W_H = 1$ for hanging wall case (0 for no footwall or hanging wall).

Table 12.3-18. Mean Ground Motion Hazard at 10⁻³ and 10⁻⁴ Annual Exceedance

Frequency (Hz)	Horizontal		Vertical	
	10 ⁻³	10 ⁻⁴	10 ⁻³	10 ⁻⁴
PGA	0.169 g	0.534 g	0.112 g	0.391 g
0.3	0.051 g	0.168 g	0.029 g	0.105 g
1.0	0.162 g	0.471 g	0.073 g	0.222 g
PGV	15.3 cm/s	47.6 cm/s	7.4 cm/s	23.4 cm/s

Source: Wong and Stepp (1998, Table 7-1)

NOTE: PGA = peak ground acceleration; PGV = peak ground velocity
 To convert g to cm/s², multiply by 980.7.
 To convert cm/s to in./s, multiply by 0.394.

Table 12.3-19. Mean Displacement Hazard at Nine Demonstration Sites

Site	Location	Mean Displacement (cm)	
		Annual Exceedance Probability	
		10 ⁻⁴	10 ⁻⁵
1	Bow Ridge fault	<0.1	7.8
2	Solitario Canyon fault	<0.1	32
3	Drill Hole Wash fault	<0.1	<0.1
4	Ghost Dance fault	<0.1	<0.1
5	Sundance fault	<0.1	<0.1
6	Unnamed fault west of Dune Wash	<0.1	<0.1
7	100 m east of Solitario Canyon fault	-	-
7a	2-m small fault	<0.1	<0.1
7b	10-cm shear	<0.1	<0.1
7c	fracture	<0.1	<0.1
7d	intact rock	<0.1	<0.1
8	Between Solitario Canyon and Ghost Dance faults	-	-
8a	2-m small fault	0.1	0.1
8b	10-cm shear	0.1	0.1
8c	fracture	0.1	0.1
8d	intact rock	0.1	0.1
9	Midway Valley	<0.1	0.1

Source: Wong and Stepp (1998, Table 8-1)

NOTE: To convert cm to in., multiply by 0.394.

Table 12.3-20. Summary Deterministic Seismic Hazard Analysis for Yucca Mountain

Fault Name and Abbreviation (Combined Faults ^a)	Minimum Distance to CAB ^b (km)	Minimum Distance to YMPR ^c (km)	Potential Type I Fault ^d	Documented Quaternary Displacement ^e	Fault Length ^f (km)	Fault Dip ^g (deg)	Fault-Slip Type ^h	Mean Maximum Magnitude ⁱ (M _w)	Horizontal Spectral Acceleration (g)			
									Frequency-1 Hz		Frequency-10 Hz	
									Median	84th Percentile	Median	84th Percentile
Faults Selected as Credible Independent Sources By at Least One Probabilistic Seismic Hazard Analysis Expert Team												
Black Cone (BLK)	4	8.5	Yes	Yes	6	60	N, H	6.05	0.12	0.27	0.40	0.75
Bow Ridge (BR)	0	2.5	Yes	Yes	13 (8)	60	N, H	6.3	0.23	0.50	0.74	1.38
Crater Flat North (CFN)	2	6	Yes	Yes	13	60	N, F	6.4	0.17	0.36	0.50	0.92
Crater Flat South (CFS)	1.5	8	Yes	Yes	8	60	N, F	6.1	0.10	0.22	0.32	0.60
Dune Wash (DW)	0	2	Yes?	No?	5	80	N, H	5.9	0.16	0.34	0.58	1.11
East Busted Butte (EBB)	1.5	7	Yes	Yes	5	60	N, F	5.95	0.09	0.21	0.33	0.63
Fatigue Wash (FW)	0	3.5	Yes	Yes	17	60	N, F	6.5	0.24	0.51	0.71	1.31
Ghost Dance (GD)	0	0	Yes?	No?	3	70	N, H	5.7	0.13	0.30	0.53	1.02
Ghost Dance-Abandoned Wash (GDAW)	0	0	Yes?	No?	7	70	N, H	6.1	0.21	0.45	0.70	1.32
Iron Ridge (IR)	0	2.5	Yes	Yes	9	60	N, F	6.4	0.25	0.53	0.76	1.40
Lathrop Wells Cone (LWC)	8	14	Yes	Yes	3	60	N, H	5.7	0.05	0.10	0.17	0.32
Midway Valley (MV)	0	3	Yes?	No?	8	60	N, H	6.15	0.19	0.42	0.66	1.24
Paintbrush Canyon (PBC)	0	4	Yes	Yes	24 (15)	60	N, H	6.7	0.28	0.58	0.75	1.37
Paintbrush Canyon-Stagecoach Road (PC-SR) ^j	0	4	Yes	Yes	33 (24)	60	N, H	6.75	0.28	0.60	0.76	1.38
Paintbrush Canyon-Stagecoach Road-Bow Ridge (PC-SR-BR) ^j	0	2.5	Yes	Yes	33 (24)	60	N, H	6.8	0.37	0.85	1.03	2.05
Solitario Canyon (SC)	0	1	Yes	Yes	19	60	N, F	6.6	0.30	0.63	0.84	1.53
Solitario Canyon-Iron Ridge (SC-IR) ^j	0	1	Yes	Yes	18	60	N, F	6.6	0.53	0.82	1.04	2.08
Solitario Canyon-Fatigue Wash-Windy Wash (SC-FW-WWW) ^j	0	1	Yes	Yes	25	60	N, F	6.7	0.39	0.90	1.13	2.24

Table 12.3-20. Summary Deterministic Seismic Hazard Analysis for Yucca Mountain (Continued)

Fault Name and Abbreviation (Combined Faults ^a)	Minimum Distance to CAB ^b (km)	Minimum Distance to YMPR ^c (km)	Potential Type I Fault ^d	Documented Quaternary Displacement ^e	Fault Length ^f (km)	Fault Dip ^g (deg)	Fault-Slip Type ^h	Mean Maximum Magnitude ⁱ (M _w)	Horizontal Spectral Acceleration (g)			
									Frequency-1 Hz		Frequency-10 Hz	
									Median	84th Percentile	Median	84th Percentile
Stagecoach Road (SCR)	4	10	Yes	Yes	9	60	N, H	6.3	0.15	0.32	0.41	0.76
Windy Wash (WW)	1	4.5	Yes	Yes	25 (21)	60	N, F	6.6	0.23	0.48	0.65	1.18
Windy Wash-Fatigue Wash-Crater Flat South (WW-FW-CFS) ^j	0	3.5	Yes	Yes	25 (21)	60	N, F	6.7	0.33	0.77	0.98	1.95
Bare Mountain (BM)	10	14	Yes	Yes	20	60	N, H	6.7	0.15	0.32	0.33	0.60
Furnace Creek (FC)	44	50	Yes	Yes	115 (105)	90	S	7.35	0.07	0.15	0.08	0.15
Rock Valley (RV)	21	27	Yes	Yes	65-48	80	S	7.1	0.10	0.20	0.16	0.29
Faults Not Selected As Credible Independent Sources By at Least One Probabilistic Seismic Hazard Analysis Expert Team												
Boomerang Point (BP)	0	2.5	Yes?	No?	5	60	N, F	6.0	0.17	0.37	0.61	1.16
Drill Hole Wash (DHW)	0	1.5	Yes?	No?	4	80	S	5.8	0.15	0.33	0.55	1.06
Pagany Wash (PW)	0	2.5	Yes?	No?	4	80	S	5.8	0.14	0.31	0.53	1.01
Sever Wash (SW)	0	3	Yes?	No?	4	80	S	5.8	0.16	0.38	0.63	1.33
Simonds Number 1	3	7	Yes?	No?	3	60	N, H	5.7	0.08	0.18	0.34	0.66
Simonds Number 2	2	6	Yes?	No?	3	60	N, H	5.7	0.09	0.20	0.37	0.72
Simonds Number 3	1	5	Yes?	No?	5	60	N, H	5.95	0.15	0.32	0.52	0.98
Simonds Number 4	1	5	Yes?	No?	5	60	N, H	5.95	0.14	0.30	0.50	0.95
Simonds Number 5	1	5	Yes?	No?	5	60	N, H	5.95	0.14	0.30	0.50	0.95
Simonds Number 7	4	9	Yes?	No?	5	60	N, F	5.95	0.08	0.17	0.26	0.49
Simonds Number 8	4	9	Yes?	No?	8	60	N, F	6.15	0.10	0.21	0.30	0.56
Simonds Number 9	5	10	Yes?	No?	7	60	N, F	6.1	0.08	0.18	0.26	0.49
Simonds Number 12	2	6	Yes?	No?	10	60	N, F	6.25	0.15	0.32	0.48	0.90
Simonds Number 14	0	4	Yes?	No?	5	60	N, H	6.0	0.15	0.34	0.56	1.06
Simonds Number 15 (East Ridge-EAR)	0	2	Yes?	No?	5	60	N, H	6.0	0.18	0.38	0.62	1.18
Simonds Number 16	1	7	Yes?	No?	4	60	N, H	5.9	0.11	0.24	0.40	0.77
Simonds Number 18	6	13	Yes?	No?	3	60	N, F	5.7	0.04	0.09	0.15	0.29

Source: USGS (2000, Tables 1, 2, 4)

Table 12.3-20. Summary of Deterministic Seismic Hazard Analysis for Yucca Mountain (Continued)

- NOTES: ^aFault names and abbreviations are listed following nomenclature of Piety (1996) and Pezzopane (1996). Faults located within 5 km of the conceptual controlled area boundary of the site (see column 2 and footnote b) that have been selected as a credible source by at least one probabilistic seismic hazard analysis expert team are listed alphabetically.
- ^bMinimum distance to conceptual controlled area boundary refers to the shortest distance from a point on the surface trace of the fault to the controlled area boundary at Yucca Mountain, consistent with guidance in NUREG-1451 (McConnell et al. 1992). The conceptual controlled area boundary extends outward approximately 5 to 7 km from the potential repository outline. Thus, most faults are from 7 to 9 km farther from the center of the potential repository (approximately latitude 36.85°N. and longitude 116.45°W.) than the minimum distance indicates. (See footnote c.)
- ^cMinimum distance to Yucca Mountain potential repository refers to the shortest distance from a point on the surface trace of the fault to the center of the Yucca Mountain potential repository (approximately latitude 36.85°N. and longitude 116.45°W.).
- ^dThis column indicates whether a candidate Type I fault meets the criteria for a potential Type I fault relevant to vibratory ground motion hazard based on the criteria presented in NUREG-1451 (McConnell et al. 1992). Potential Type I faults indicated with "Yes" are those with documented Quaternary activity ("Yes" in column 5 of this table) and the potential to generate average 84th percentile peak accelerations that equal or exceed 10 percent of gravity (0.1 g) at the conceptual controlled area boundary of the Yucca Mountain site. Potential Type I faults with a "Yes?" are those with questionable or indeterminate documentation of Quaternary activity ("No?" in column 5 of this table) and the capability to produce at least 0.1 g peak acceleration at the 84th percentile level.
- ^eDocumented Quaternary displacement designates the status of evidence for Quaternary fault activity with two alternatives, "Yes" and "No?", depending upon whether there are published studies that document Quaternary displacement or other compelling evidence for Quaternary displacement potential, such as associated seismicity or field studies. This is the primary criterion for classifying candidate and potential Type I faults. Faults with a "Yes" are those with demonstrated Quaternary displacement. Faults with a "No?" are those that lack evidence of Quaternary displacement or for which the data are inconclusive
- ^fMaximum fault length is the length of the fault zone as reported in published references or as estimated from maps and plates in cited references (Simonds et al. 1995; Scott and Bonk 1984; Piety 1996). The maximum length represents the entire length of the mapped or inferred fault zone, including sections portrayed as concealed or discontinuous or both. Values in parentheses indicate the probable length of late Quaternary rupture where it can be estimated from either paleoseismic data in trenches or, more commonly, by the extent of Quaternary fault scarps developed along the fault trace. The maximum length was used for M_w calculations. Lengths for combined faults are measured along the single longest combination of faults in the system, based on the assumption that the individual faults are joined in a compound rupture of the entire zone.
- ^gThe preferred dips for faults are generally assigned according to type of fault, based on regional seismic and geophysical data.
- ^hThis column indicates the slip type of the fault source entered into the ground motion attenuation equations developed by the ground motion experts for the probabilistic seismic hazard analysis (USGS 1998) (see text). These equations differentiate between strike-slip and normal-slip faults, and subdivide the latter into whether the site is located on the hanging wall or footwall of the fault. Symbols are N = normal-slip; S = strike-slip; H = hanging wall; F = footwall.
- ⁱThis column contains the deterministic mean M_w assigned to each fault. It is the mean of a suite of M_w calculated from fault length, displacement per event, seismic moment, and rupture area data.
- ^jIndividual faults that are combined together into one earthquake source; this includes, but is not limited to, the combined faults near the site with distributed ruptures.

Table 12.3-20. Summary of Deterministic Seismic Hazard Analysis for Yucca Mountain (Continued)

CAB = conceptual controlled area boundary (used previously on the YMP, but not currently in use); YMPR = Yucca Mountain potential repository.

A seismogenic depth of 15 km is assumed for all fault widths.

To convert km to mi., multiply by 0.621.

To convert g to cm/s^2 , multiply by 980.7.

Table 12.3-21. Reference Earthquakes at the Reference Rock Outcrop from Deaggregation of Seismic Hazard

Frequency	10 ⁻³ Annual Probability of Exceedance	Factor	10 ⁻⁴ Annual Probability of Exceedance	Factor
5 to 10 Hz	M _w 5.1, R = 10 km	2.665	M _w 5.9, R = 5 km	2.484
1 to 2 Hz	M _w 5.9, R = 5 km	(Not calculated or used)	M _w 6.3, R = 5 km	(Not calculated or used)
	M _w 7.4, R = 52 km	2.568	M _w 7.7, R = 52 km	5.761

Source: CRWMS M&O (1998i, Section 2.6)

NOTE: R = distance, M_w = moment magnitude
To convert km to mi., multiply by 0.621.

Table 12.3-22. Adjusted Reference Earthquakes Representing the Uniform Hazard Spectra

Frequency	10 ⁻³ Annual Probability of Exceedance	Factor	10 ⁻⁴ Annual Probability of Exceedance	Factor
5 to 10 Hz	M _w 6.3, R = 5 km	0.574	M _w 6.3, R = 5 km	1.837
1 to 2 Hz	M _w 6.9, R = 52 km	3.858	M _w 7.7, R = 52 km	5.631

Source: CRWMS M&O (1998i, Section 2.6)

NOTE: R = distance, M_w = moment magnitude
To convert km to mi., multiply by 0.621.

13. NATURAL ANALOGS

13.1 INTRODUCTION

Reasoning by analogy relates the likeness of a process or set of properties to a similar process or set of properties, either in another location or a different time frame. Analogs provide an important temporal and spatial dimension to the understanding of processes that may take place in a radioactive waste repository and the surrounding area. In this section, analogs are considered for the natural and engineered barrier systems at the potential Yucca Mountain repository, and descriptions are given as to how each selected analog is used to test and build confidence in process models that are used as input to total system performance assessment (TSPA).

13.1.1 Purpose

The purpose of this section is to synthesize previous natural analog studies and to document cases in which the Yucca Mountain Site Characterization Project (YMP) has used this analog information, in order to identify and recommend areas where natural analogs could bring additional confidence for the Site Recommendation-License Application (SR-LA), and to provide an approach for selecting and applying natural analog information for future use in the SR-LA and for performance confirmation.

Results of the analog studies will be used to corroborate estimates of the magnitude and limitation of operative processes, thus building realism into conceptual and numerical process models that underlie performance assessment in the representative case of postclosure safety. The approach followed in this section is consistent with the U.S. Department of Energy philosophy (DOE 1995) on the use of natural analogs (defined in Section 13.1.2) and is based on factors important to performance and safety that are identified and prioritized in the *Repository Safety Strategy: Plan to Prepare the Safety Case to Support Yucca Mountain Site Recommendation and Licensing Considerations* (CRWMS M&O 2000d).

One of the important applications of natural analogs is for illustrative purposes (i.e., to make complex processes understandable). In this way, analogs have a significant function in the education of the public about how geologic repository processes work over time spans of thousands of years. Although public confidence in this process is vital, it is not part of the purpose of this section, and is addressed only briefly with particular analogs that might be especially suitable examples for illustrative purposes.

13.1.2 Definition of Natural Analogs

Natural analogs refer to both natural and anthropogenic (human-induced) systems in which processes, similar to those that might be expected to occur in a radioactive waste repository, are considered to have occurred over long time periods (decades to millennia) and over large spatial scales (up to tens of kilometers) that are not accessible to ordinary laboratory experiments. The primary purpose for using natural analogs is to obtain an understanding of a system's unknown component by comparing known components in order to determine whether something pertinent can be said of the unknown component by analogy (comparison) with the known.

The use of analogy has been endorsed by the international radioactive waste community as a means of demonstrating confidence in the operation of systems, components, and processes that are related to radioactive waste disposal (e.g., publications of the International Atomic Energy Agency and the Natural Analog Working Group of the European Community).

The role of a natural analog should...be to confirm: (a) that the process is, in fact, something which can or will occur in practice, as well as in theory, and in nature, as well as in the laboratory; (b) where, when, and under what conditions it [the process] can occur; (c) that the effects of the process are those envisaged in the model; and (d) that the magnitude of the effects, in terms of scale and time, are similar to those predicted for a similar set of conditions (Chapman and Smellie 1986).

Use of analogy is also encouraged by the U.S. National Research Council (National Research Council 1990, pp. 27 to 28) and by the U.S. Nuclear Regulatory Commission, in 10 CFR 60 and in proposed 10 CFR 63 (64 FR 8640).

As pointed out by Percy and Murphy (Ababou et al. 1990, p. 7-2), the 10-k.y. period required for high-level radioactive waste isolation is a difficult period to approximate using natural analogs. Most ore deposits are on the order of a million to a billion years in age, whereas anthropogenic sites are generally on the order of a few thousand years, or less. Most helpful in terms of long-term processes relevant to a high-level radioactive waste repository would be finding analogs on the order of 1 k.y. to 1 m.y.

13.1.3 Role of Natural Analogs in Process Models and Performance Assessment

Natural analogs may be applied in a quantitative manner or in a qualitative, descriptive manner, depending on the purpose to which they are applied and on the specific analog. The analogs can provide descriptive information about the occurrence of various processes, or they may be able to provide boundaries to those processes. Natural analogs allow testing of the pertinence of individual processes over geologic time and space scales, as well as providing an assessment of the relative importance of various processes and the effects of the coupling of various processes. For some processes (e.g., those that are thermally coupled), natural analogs may be the only means of providing the required understanding of long-term and large-scale behavior that is needed to provide scientific confidence in process models for input to TSPA. Through analog investigations, conditions under which the processes occur and the effects of the processes, as well as the magnitude and duration of the phenomena, may be determined.

Analog information can provide databases for the testing of codes and for the validation of conceptual and numerical models. Natural analog information may also be used to build confidence in the databases themselves. Because natural analogs can be used to test conceptual and numerical models over long distances and time scales that are not reproducible by laboratory or field experiments, analogs are uniquely suited to building confidence in process models. In this manner, they can be used as a means of model validation, or confidence building. Each of the process model reports supporting SR will include a section on validation that may use testing against natural analog information (Section 13.2.5).

Natural analogs can be used to evaluate the validity of extrapolating from temporally limited field-scale experiments to longer time scales, when field-scale experiments are impractical; to add confidence when extrapolating from laboratory and intermediate-scale experiments to tests of larger spatial scales; and to effectively critique performance assessment model assumptions and parameter ranges, as well as the strength, vigor, and consistency of process models. Natural analogs may also be used (though less often) to assist and support the selection of scenarios and to establish the probability that selected scenarios will occur.

Natural analogs do not reduce uncertainty, per se (i.e., the uncertainty bounds on a given parameter value may remain unchanged). However, they can build confidence that the bounds are set appropriately. Since some uncertainties are greater in natural analogs than at the site being characterized, information from natural analogs must always be used with other information so that laboratory and field data can be evaluated consistently.

YMP has stressed (DOE 1995) that natural analog studies should be process-oriented. In this regard, analogs can be used to gain a better understanding of operative processes and their bounds for testing conceptual models, or they can be used for testing and building confidence in numerical models that represent processes. Natural analogs provide the following with respect to process models (Petit 1990, p. 186):

- Quantitative natural experiments that replicate a process or group of processes that are used in a model
- Specific parameter values for determining parameter bounds
- Qualitative indicators of which phenomena can occur in a system being modeled, by reference to a parallel or similar system
- Methods for integrating the results of many processes at one site over long time periods.

Given the uncertainties in analog studies, analogs may not be able to validate models in the strictest sense, but they can be used to test models of long-term processes. Comparison of model predictions with the results of natural analog investigations will, in general, only permit confirmation that the model takes into account the relevant processes in appropriate ways. Validation of a predictive model by such comparison can result in reasonable assurance that the model reflects future behavior. This is the level of confidence required by proposed 10 CFR 63 (64 FR 8640), which, in 10 CFR 63.101(a)(2), states: "Demonstrating compliance will involve the use of complex predictive models that are supported by limited data from field and laboratory tests, site-specific monitoring, and natural analog studies that may be supplemented by prevalent expert judgment."

Care must be taken in selecting an appropriate analog to correctly represent the process of interest (e.g., all uranium deposits are not categorically good analogs for the stability of a radioactive waste repository). Some uranium deposits may indicate the long-term stability of some geologic environments, but some of the same ore deposits could be used to argue for the massive transport of radioactive materials over large distances by natural processes. The substantial quantity of uranium contained in these types of deposits was originally dispersed throughout a larger geologic volume but was transported and concentrated at the site of the

present deposit (e.g., the Oklo analog in Section 13.4.3.2.3). Furthermore, evidence exists for migration away from some ore deposits after their emplacement (e.g., the Koongarra deposit in the Alligator Rivers analog, Section 13.4.3.2.1). Therefore, uranium ore deposits also provide implicit evidence of potential mobility of this ore in some environments.

13.1.4 Criteria for Selection of Analogs Used in Model Validation

Because no single site will be a perfect analog to all ongoing and anticipated processes at Yucca Mountain, focus is placed on sites having analogous processes rather than total system analogs. However, it is still worthwhile to attempt to match as many features and characteristics as possible when identifying suitable analog sites. An ideal analog site for long-term radionuclide transport at Yucca Mountain would have to possess the following characteristics (DOE 1995): (1) a known source term, (2) a similar set of radionuclides, (3) well-characterized, with site data, (4) similar geologic conditions, (5) observable long-term conditions, (6) identifiable boundaries of the system, and (7) a clear-cut process that can be decoupled from other processes. It would also be useful if the proposed analog had been in place for at least thousands of years so that the results of long-term behavior were observable.

In addition to the use of analogs for long-term predictions, models must be able to explain (and match) the transport times and pathways from contaminated sites that provide anthropogenic analogs, such as Hanford, Washington; the Idaho National Engineering and Environmental Laboratory; and the Nevada Test Site. Anthropogenic analog sites will be a challenge to constrain in models because they often occur in highly heterogeneous formations, and often contain numerous contaminated areas, sometimes with poorly identified source terms, a complex mixture of radionuclides and other contaminants.

When choosing different geochemical transport analogs, Chapman and Smellie (1986, p. 167) recommend:

- The process involved should be clear cut. (Other processes that may have been involved in the geochemical system should be identifiable and amenable to quantitative assessment as well, so that their effects can be accountable.)
- The chemical analogy should be good. (It is not always possible to study the behavior of a mineral system, chemical element, or isotope identical to that whose behavior requires assessing. The limitations of this should be fully understood.)
- The magnitude of the various physicochemical parameters involved (pressure (P), temperature (T), oxidation potential (Eh), concentration) should be determinable, preferably by independent means.
- The boundaries of the system should be identifiable (whether the system is open or closed, and, consequently, how much material has been involved in the process being studied).
- The time-scale of the process must be measurable, since this factor is of the greatest significance for a natural analog.

However, care must be exercised in the selection of appropriate analogs to exclude those for which initial or boundary conditions are poorly known and where important data, such as the source term, are poorly constrained or may not be obtainable. A given site will usually be analogous only to some portion of a repository or to a subset of processes that will occur in a repository. Furthermore, additional processes will have occurred that are not characteristic of the repository. Therefore, processes of the greatest relevance and processes that can be isolated for study should be chosen, as demonstrated for Yucca Mountain in Section 13.2. The long-term nature of analogs introduces some limitations and uncertainties, but, notwithstanding, analogs can still be used effectively if rigorous selection criteria are applied.

13.1.5 Scope of Natural Analog Section

Section 13 considers a breadth of analogs that encompasses both the engineered barriers and natural system components of the potential geological repository at Yucca Mountain. System components and their analogs are discussed in this order, working from the repository outward to the natural environment:

- Waste form
- Waste package
- Other engineered barrier system and repository materials
- Thermally coupled processes
- Unsaturated flow and transport
- Saturated flow and transport.

First, the role of each component in conceptual models of Yucca Mountain or in the disposal concept is presented. Second, examples are provided of analog studies relevant to the operative processes in the conceptual models. Each analog study is discussed at only a moderate level of detail. For many of the sites mentioned, a voluminous body of literature exists.

In general, there are no total system analogs and none have been identified for Yucca Mountain. However, one exception to the general rule of having no total system analogs is Cigar Lake, in Canada (Section 13.5). The Cigar Lake analog study was able to tie its components to virtually all system components of the Canadian disposal concept. For this reason, Cigar Lake stands out as being unique among analog studies and is discussed here, even though the hydrogeological-chemical system is different from Yucca Mountain and the Canadian disposal concept is different from that proposed by the United States.

After the relevant analog is described, a discussion of how the analog information could be applied to testing process models and building confidence in their applications is given. Where this has already been done for Yucca Mountain, it is noted. From the TSPA-Viability Assessment, areas are drawn that were cited as potentially benefiting from natural analog studies, or, more commonly, areas of uncertainty in performance assessment that, based on the natural analogs for this section, could address some of the uncertainties in process models used for performance assessment. Finally, insights gained from surveying many natural and anthropogenic analogs were used to recommend the direction for application of analog information to SR-LA and performance confirmation. The recommendations are made on the

basis of the repository safety strategy (Section 13.2.6) and needs identified by performance assessment.

13.2 BACKGROUND

13.2.1 Introduction

This section provides the framework for discussing natural analogs. First, the role played by natural analogs is presented, based on the views of oversight groups and their licensing roles as regulated by the U.S. Nuclear Regulatory Commission. Second, the U.S. Department of Energy (DOE) Yucca Mountain Site Characterization Project (YMP) philosophy regarding definition, scope, and application of natural analogs is described. Third, a brief summary of the current repository design and waste package concept follows, providing an understanding of the role natural analogs play with regard to materials and thermal considerations. Fourth, areas of process model uncertainty or sensitivity addressed by the 1998 total system performance assessment (TSPA) for the Viability Assessment (VA) and areas where natural analogs may contribute to reducing those uncertainties are described. Finally, the processes and analogs that will be discussed are placed in a context that assigns them a priority for the License Application (LA), based on principal and other factors that are components of the repository safety strategy (CRWMS M&O 2000d).

13.2.2 Role of Natural Analogs in the License Application

The National Research Council endorsed the use of natural analogs as natural test cases, geological settings in which naturally occurring radioactive materials have been subjected to environmental forces for millions of years (National Research Council 1990, p. 27). The National Research Council indicated that natural analogs are essential for validating performance assessment models of geologic repositories over thousands or millions of years, as well as forming the basis for communicating the safety of a deep geologic repository in terms the public can understand. The Nuclear Waste Technical Review Board concurred in these recommendations (NWTRB 1990, p. 27; 2000, p. 20).

Proposed 10 CFR 63 (64 FR 8640) does not require a license applicant to incorporate the use of natural analogs into a case for demonstrating public health and safety. Instead, the regulation allows for the demonstration of reasonable assurance of repository performance for thousands of years by means of a number of different approaches, including data collection from accelerated tests and models that are supported by such measures as field and laboratory tests, monitoring data, and natural analog studies.

13.2.3 Yucca Mountain Site Characterization Project Philosophy on the Role of Natural Analogs

In the early 1990s, the DOE convened a panel of international experts in natural analogs to provide guidance in the use and selection of natural analogs for implementation by the YMP. The Natural Analog Review Group report recommended that natural analogs be process-oriented and address the issues resulting from the perturbation of a natural system (the geologic site) by the introduction of a technological system (the repository) (DOE 1995, p. 2). The Natural Analog Review Group explicitly stated that such studies should clearly be distinguished from those that, following the classical approach of earth sciences, are based on the comparative study of geological sites or situations. In particular, all investigations normally part of site

characterization, even when considering comparisons with similar remote sites, such as (paleo)hydrology, should not be considered as natural analog studies (DOE 1995, p. 2). Continued use of the DOE-adopted, Natural Analog Review Group clarification of what constitutes a natural analog is endorsed in this section.

The Natural Analog Review Group (DOE 1995, pp. 15 to 18) further provided a useful set of selection guidelines for natural analog studies. Used in conjunction with Table 13.2-1, which relates process models and natural analogs, the guidelines provide a clear-cut and defensible rationale for selection of a natural analog study. A paraphrase of the Natural Analog Review Group selection guidelines follows:

- Define the specific information requirements from natural analog studies
- Define the end-user and means of application of the information
- Define the preferred methodology
- Define the types of environment that could provide such information
- Use a checklist set of criteria to aid comparison of alternative sites and selection of the best sites
- Evaluate the feasibility of obtaining the data required from the sites
- Prepare a plan for implementing a study at the selected sites.

The Natural Analog Review Group guidelines were used to select natural analogs for study and continue to form the basis for selection of natural analog sites. For example, the checklist set of criteria (Section 13.1.4) was applied in the selection of Peña Blanca as the most promising overall candidate for a flow and transport analog, as well as a spent nuclear fuel alteration analog, to Yucca Mountain.

In April 1998, DOE convened a group of project personnel knowledgeable in natural analogs and asked them for recommendations regarding future analog studies. This ad hoc group, the Natural Analog Group, has met on occasion to integrate suppliers and users of natural analog information and to provide direction. One of the main outcomes of the April 1998 meeting was the consensus that limited work investigating analogs may be possible during the LA time frame, but more detailed or thorough analog examination would have to be undertaken as part of performance confirmation. It was also decided then that process modelers, as users of analog information, should play an important role in determining how analogs can best be used to support performance assessment and design groups in reducing uncertainties in the long-term behavior of natural and engineered systems. Subsequently, a number of events have taken place that helped to focus the direction of future analog investigations:

- Process models supporting TSPA were defined for the TSPA-VA
- The License Application Design Selection study identified a preferred suite of conditions and materials for repository design

- The YMP developed a safety strategy for the Site Recommendation-License Application that relied on factors important to performance.

13.2.4 License Application Design Selection and Its Relation to Applicable Analogs

The License Application Design Selection study was conducted with the goal of developing and evaluating a range of conceptual repository designs and of recommending an initial design concept for the Site Recommendation-License Application. The following information on the recommended design is taken from the *License Application Design Selection Report* (CRWMS M&O 1999, p. viii to ix).

The recommended repository concept, called Enhanced Design Alternative II differs from the VA design in a number of areas, and has a low thermal-impact design. This design uses extensive thermal management techniques to limit the impact of heat released by the waste. These thermal management techniques include the following:

- Thermal blending of spent nuclear fuel assemblies
- Closer spacing of the waste packages
- Wider spacing of the waste emplacement drifts
- Preclosure ventilation.

Thermal blending of spent nuclear fuel assemblies reduces the peak heat output of the waste packages, making it easier to limit temperatures in the rock around the waste packages, although the drift wall temperature may reach, but not exceed, 200°C. Close spacing of the waste packages within the emplacement drifts reduces temperature variations in the drifts, simplifies the analysis of heat effects, and reduces the total length of drifts excavated.

Spacing the drifts farther apart reduces the effects of heat from each drift on its neighbors, leaves a wide region of rock between drifts that remains below the boiling point of water (97°C at the repository horizon), allowing water to circulate around the drifts, and limits the long-term heat-induced alterations to the repository rock. Preclosure ventilation makes it possible to stay within temperature limits in the rock and around the waste packages during operation, despite the much closer waste package spacing, and reduces maximum temperatures after closure.

The recommended design differs from the VA design in a number of other aspects. While both use a two-layer waste package, the recommended Enhanced Design Alternative II places the corrosion-resistant material on the outside rather than the inside to provide long-term protection to the more corrosion-susceptible structural material inside. The recommended design also adds defense in depth with a drip shield covered by backfill to protect the waste packages from dripping water while they are hot enough to be susceptible to localized corrosion. (It should be noted that backfill has been removed since the study was completed.) The recommended design also uses steel structural materials in the drifts, instead of concrete evaluated in the VA design, to avoid the possible chemical impacts of concrete on mobilization and movement of radionuclides. Neither design incorporates the use of sorptive filler in backfill.

License application design selection projections of performance using TSPA models indicate that the recommended design would perform very well with respect to a screening criterion of

25 mrem/yr. to an average member of a critical group living 20 km from the potential repository during the first 10 k.y. A calculated dose of 25 mrem/yr. would not be reached for more than 300 k.y., and the dose rate at any time would be less than 100 mrem/yr. The calculated time of the first corrosion failure of a waste package is about 100 k.y. (CRWMS M&O 1999, p. 7-2).

The recommended design reduces or avoids uncertainties associated with the thermal pulse, and is intended to reduce perceived uncertainties from postulated ponding of water above the repository. Such ponding could cause water to flow into the drifts to corrode the hot drip shields or waste packages. This is accomplished, first, by keeping larger areas of very wide pillars cool enough to allow water to move around the drifts and drain through the pillars. Second, by allowing only a small amount (several meters) of the rock mass around the drifts to exceed the boiling point of water for several hundred years, the design localizes the area affected by elevated kinetics in the presence of water. This in turn reduces the potential for long-term hydrological and geochemical alteration of the host rock, which, in turn, should reduce uncertainties associated with modeling coupled processes in host-rock performance. Third, the wide drift spacing reduces the analytical complexities resulting from temperature interactions among closely spaced drifts, thus simplifying the analysis of repository performance. Fourth, the design does not subject the waste package material to temperature and humidity conditions conducive to aggressive crevice corrosion. As a result of both thermal conditions and the diversion of water by the drip shield, the waste package material is subject only to very slow general corrosion.

The concept waste package consists of a 2-cm layer of corrosion-resistant Alloy-22 protecting a 5-cm inner structural shell of stainless steel 316L. Alloy-22 is a nickel-based alloy with 22 percent chromium. The assumed inventory is 63,000 metric tons of heavy metal of commercial spent nuclear fuel and a total of 7,000 metric tons of heavy-metal equivalent of DOE spent nuclear fuel and high-level radioactive waste. As an additional defense-in-depth measure, drip shields made of the titanium alloy grade-7 would be used to prevent water from contacting waste packages. Additional enhancements that could be added to the design during future refinement include (CRWMS M&O 1999, p. O-10):

- Ceramic coating on waste packages
- Backfill
- Filler inside the waste package
- A dual corrosion-resistant materials waste package
- Richards Barrier
- Canistered assemblies
- A trench with lid.

Analog studies of metals are discussed in Section 13.3.5; analogs related to concrete and alkaline plumes are discussed in Section 13.3.6; and the effects of radiolysis are considered in Section 13.3.7.

13.2.5 Building Confidence in Total System Performance Assessment for the Viability Assessment through Natural Analogs

The 1998 TSPA-VA (DOE 1998b) made one specific recommendation for the use of natural analogs. This was in regard to saturated zone flow and transport, discussed below. In addition to that recommendation, the TSPA-VA discussed processes that were sensitive in TSPA calculations and that need to be understood with greater certainty. In researching information for this section, areas were considered where TSPA-VA indicated the need for improved understanding of the bounds of operative processes and their effects.

The TSPA-VA indicated that for peak dose rates, the fraction of waste packages contacted by seepage water was the most important parameter in each of the three simulation periods—10, 100, and 1,000 k.y. (DOE 1998a, p. 2-10). The effect of seepage water becomes more dominant over time, because an increase in the number of waste packages contacted by water leads to an increase in radionuclide releases from the repository.

The seepage model for TSPA-VA assumed steady-state conditions. Drift collapse and thermal alteration of matrix hydrologic properties were not considered, nor was the possibility of episodic flow at the repository horizon and its effect on seepage needs or the effect of discrete fracture flow on seepage. Natural (or anthropogenic) analogs may contribute to understanding the effects of drift collapse and thermal alteration of hydrologic properties on drift seepage. Seepage analogs are discussed in Section 13.4.2.2.3.

The TSPA-VA model of unsaturated zone transport did not account for a number of processes, including alteration of the unsaturated zone caused by thermal alteration of minerals, chemical interactions of repository materials, mineral dissolution, and precipitation. Should thermal-chemical alteration occur, reduced matrix sorption and fracture-matrix interaction could result, thereby causing increased radionuclide release rates from the unsaturated zone. Other processes not accounted for include colloid filtration by the host rock and fracture sorption. However, the assumptions of no colloid filtration and no radionuclide sorption onto fracture surfaces are conservative for transport in the unsaturated zone. Although sensitivity studies conducted to date have found that transport is not highly sensitive to fracture sorption, this result would require further investigation to better define the appropriate range of parameters for fracture sorption. Radionuclide transport in the unsaturated zone is sensitive to changes in matrix diffusion, which suggests that further effort is needed to bound the magnitude of matrix diffusion (CRWMS M&O 1998d, p. 7-102). Natural analogs provide insights into fracture sorption and matrix diffusion processes and may be used to place bounding conditions on their importance to various environmental conditions. The role of fracture minerals in retarding radionuclides and the role of colloids are discussed in Sections 13.4.2, 13.4.3, and 13.5.1.

TSPA-VA noted that process-level modeling of chemical alteration of fracture hydrologic properties should be considered in the LA time frame. Formation of a mineral cap surrounding the emplacement drift has been suggested in modeling studies (Hardin 1998, pp. 5.57 to 5.58) as a result of phase-change processes during thermal loading. This issue is addressed by geothermal and fossil hydrothermal analogs in Section 13.4.1. The fracture-matrix interaction parameter is potentially a key factor in describing the processes altered by chemistry and, subsequently, the manner in which fractures and matrix rock interact. The TSPA noted

(CRWMS M&O 1998a, p.3-191) that it is essential that flow processes be accurately represented so that an assessment can be made as to whether the development of mineral deposits is physically realistic. Natural analogs of carefully selected systems may help to place bounds and add realism to the conceptualization of these coupled thermohydrologic-chemical effects.

Thermohydrologic-mechanical processes were not considered in the TSPA-VA. Although natural analogs to thermohydrologic-mechanical effects are not addressed in this section, except in Table 13.2-1, this topic is considered for future work in Section 13.7.

TSPA-VA sensitivity analysis results indicate that uncertainty in calculated peak dose rates in all three simulation periods is primarily dominated by that fraction of waste packages in contact with seepage water. Waste package corrosion rate is also an important contributor to uncertainty in peak dose rates. In particular, the mean Alloy-22 corrosion rate is an important contributor to uncertainty, but to a lesser extent than the fraction of waste packages contacted by seepage water, particularly in the 1-m.y. period. In that time period, the saturated zone dilution factor and biosphere dose-conversion factors were found to be slightly more important than the Alloy-22 mean corrosion rate. Finally, sensitivity analysis results also indicate that neptunium solubility is an important contributor to uncertainty in peak dose rates once uncertainties in seepage and waste package parameters are reduced or removed (CRWMS M&O 1998c, p. 5-63). Metal corrosion analogs are addressed in Section 13.3.5, and biosphere analogs may be a topic of future research.

The dilution factor in the saturated zone was shown to be a sensitive parameter for the TSPA-VA. The appropriate range of uncertainty for dilution and transverse dispersivity is also an open topic. TSPA-VA stated that reducing the uncertainty of these parameters will probably depend on inferences from analog sites or, potentially, from analysis of natural solute tracers in the saturated zone at the site (CRWMS M&O 1998e, p. 120). The TSPA-VA recommended that additional effort should be devoted to an evaluation of potential analog systems of saturated flow in fractured media or in highly heterogeneous porous media (CRWMS M&O 1998e, p. 120). Analogous to radionuclide transport regarding dilution in the saturated zone are addressed in Section 13.4.3.3.

13.2.6 Strategy for Establishing Priorities of Processes and Analog

The DOE repository safety strategy (CRWMS M&O 2000d) provides a pathway to licensing that is based on five elements:

- TSPA
- Safety margin and defense in depth
- Consideration of potentially disruptive events and processes
- Natural analog insights
- Long-term performance evaluation and confirmation.

The strategy then builds a case for postclosure safety around these five elements by identifying factors that contribute to waste isolation and setting priorities of their importance, based on

design and performance assessment considerations. The factors (see Table 13.2-1) are based on the repository safety strategy (CRWMS M&O 2000d).

As indicated above, the fourth element of the postclosure safety case (CRWMS M&O 2000d) calls for an assessment of insights gained from the study of natural analogs.

Relevant information about the possible system performance of the site can be gleaned from analysis of natural processes that share characteristics with the repository system. ...These data may provide a degree of independent validation of the reasonableness of selected aspects of the assessments of repository performance (CRWMS M&O 2000d, p. 15).

The principal factors upon which the safety case is based, as well as the other factors that will be bounded, may be strengthened from building confidence through natural analogs.

Because the factors identified as important to safety were based in part on process model and TSPA sensitivities, that list of factors was used to prepare Table 13.2-1. This table serves as an organizing framework for discussing natural analogs based on process models and as a schematic way of setting priorities for the processes that need to be further bounded and quantified. Table 13.2-1 serves as a guideline for identifying future natural analog work that can be used in a semiquantitative or quantitative way to improve confidence in models that are important to performance and safety. The use of natural analogs for building public confidence is not intended through this schematic.

In preparing Table 13.2-1 as a framework for synthesizing and applying natural analog information, various sources were used. One source was the major body of literature about past analog projects in the United States and other countries. Also relied on heavily were TSPA recommendations from the TSPA-VA report and from informal memoranda and discussions with performance assessment staff. The needs identified by performance assessment and the factors listed in Table 13.2-1 were used to guide the natural analog studies for fiscal years 1999 and 2000 and to provide direction for future work. Section 13 covers a wide variety of relevant analogs that meet to varying degrees the selection criteria listed in Section 13.1.4. This means some individual analog studies were not included because they were poorly constrained to meet the selection criteria.

One major factor important to performance listed in Table 13.2-1 that is not discussed in this section is analogs to disturbed-case scenarios (i.e., volcanism, seismicity, human intrusion, and criticality). Of these four scenarios, only criticality lends itself well to natural analog studies. Criticality has been studied with regard to the Oklo natural reactors (Section 13.4.3.2.3), and criticality calculations were made for TSPA. There are no natural analogs for human intrusion scenarios. Volcanism and seismicity scenarios are included in the area of natural analog studies by the U.S. Nuclear Regulatory Commission, but are categorized by DOE under normal site characterization and have been addressed extensively in other DOE topical reports.

INTENTIONALLY LEFT BLANK

13.3 WASTE FORM, ENGINEERED BARRIER SYSTEM, AND REPOSITORY MATERIALS ANALOGS

This section addresses analogs to spent nuclear fuel and glass waste forms intended for geologic disposal. It also includes components of the engineered barrier system (i.e., waste package materials and other introduced engineered barrier system components). Radiolysis effects are discussed in Section 13.3.7. Also briefly discussed are cements, even though they play a limited role in the current repository design. Bentonite clay as backfill material is not currently planned for use in the United States, though it plays a role in repository programs of many other countries—as backfill and, in some cases, as a candidate disposal medium. Because bentonite is not considered in the Yucca Mountain repository concept, it is not discussed in this section.

Sites that are addressed as analogs to spent nuclear fuel alteration frequently are discussed as analogs to radionuclide transport as well. In Section 13.3.2, sites where most of the research has been in the area of mineral studies are described. In Sections 13.4.2 and 13.4.3, sites are discussed for which most of the characterization has been related to transport phenomena. Palmottu and Poços de Caldas are examples of sites that have had more emphasis placed on transport and site characterization. Sites that have been studied extensively from both perspectives (e.g., Oklo and Peña Blanca) are discussed in Sections 13.3.2, 13.4.2, and 13.4.3.

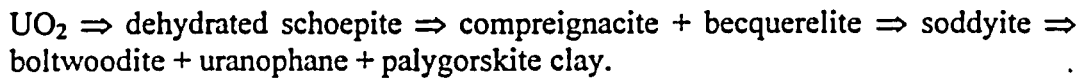
13.3.1 Role of Waste Form Dissolution in the Disposal Concept

Spent nuclear reactor fuel that would be disposed at Yucca Mountain consists predominantly of uranium dioxide (UO_2) with a cubic crystalline structure. Other radioactive isotopes make up several percent of spent nuclear fuel, occurring as impurities in the UO_2 structure, as phase segregations, and as grain-boundary precipitates. Spent nuclear fuel with uranium in reduced valence (U^{+4}) is thermodynamically unstable in oxidizing conditions such as Yucca Mountain and will oxidize eventually to stable phases that incorporate the uranyl (U^{+6}) ion. Natural analog studies provide some indication as to the time scale over which secondary-phase formation can be expected to occur. However, there is a limitation in using the naturally occurring uranium mineral, uraninite (UO_{2+x}), as an analog to spent fuel. It does not contain the internal phase segregations present in spent nuclear fuel, nor does it include a substantial transuranic component.

Most of the uranium released to solution during the dissolution of UO_2 combines with ions in water to form secondary alteration phases. Both natural and experimental uranium systems display a paragenetic sequence of mineral phase formation that is characterized by the following general trend (Stout and Leider 1997, pp. 2.1.3.5-21, 2.1.3.5-22):

$\text{UO}_2 \Rightarrow$ uranyl oxide hydrates \Rightarrow alkali- and alkaline-earth uranyl oxide hydrates
 \Rightarrow uranyl silicates \Rightarrow alkali- and alkaline-earth uranyl silicates + palygorskite clay.

Specifically, mineralization in the paragenetic sequence of alteration phases is (Wronkiewicz et al. 1996, p. 94):



The phases that form depend on the chemical composition of the water with which the uraninite is in contact, which, in turn, depends on the mineralogy of the surrounding host rocks and the hydrological environment (i.e., reducing or oxidizing). This mineral sequence appears to be controlled by precipitation kinetics and is nearly identical to alteration patterns observed during the weathering of naturally occurring uraninite (e.g., that which occurs at the Nopal I uranium deposit [Peña Blanca]; see Section 13.3.2.2.1).

The alkali- and alkaline-earth uranyl silicates represent the long-term solubility-limiting phases for uranium in laboratory UO_2 tests and in the natural uranium deposits at Nopal I. This similarity suggests that the experiments and the natural analog reactions may simulate the long-term reaction progress of spent UO_2 fuel following potential disposal at Yucca Mountain. This similarity was noted in the TSPA-VA (CRWMS M&O 1998c, p. 6-100). Uranium transport generally occurs in oxidizing surface water and groundwater as uranyl species, most often as UO_2^{2+} or as uranyl fluoride, phosphate, hydroxyl, or carbonate species. The background concentration of uranium in uranium mine waters is about 15 to 400 ppb. At Nopal I, uranium concentrations in groundwater and seepage are much lower and ranged from 170 ppt to 5 ppb (Pickett and Murphy 1999, Table II). The upper part of this range is similar to concentrations seen in spent nuclear fuel dissolution experiments (Stout and Leider 1997).

Spent nuclear fuel plays an important role in the disposal concept at Yucca Mountain because it determines the source term of radionuclides that could be released from a repository, whether the radionuclides are solubility-limited, and whether they could be retained in alteration products of spent nuclear fuel. Therefore, it is important to understand how spent nuclear fuel corrodes through time. As previously stated, in an oxidizing environment, uraninite instability will proceed to form uranyl (U^{+6}) oxide hydrates as alteration products. The corrosion products will have significant impact on the mobility of actinides and fission products in the fuel assembly. The composition of schoepite ($\text{UO}_3 \cdot 2\text{H}_2\text{O}$) is often used to represent an alteration product in models of spent nuclear fuel alteration, but this is an oversimplification, based on observations in nature. Many studies have shown that uraninite oxidizes in nature, as discussed in Section 13.3.2.2.

Focus was placed on U deposits that have been studied as natural analogs to spent nuclear fuel alteration, because these studies often included important additional characterization information necessary to understand the larger geologic system, which is sometimes missing in mining reports. The entire body of literature regarding uranium oxidation was not surveyed. Additional information could be obtained from studies of uranium ore deposits, such as the Colorado Plateau ore roll-type deposits, and countless other studies of uranium mines.

Approximately 10 percent of the waste would be encapsulated in borosilicate glass derived from defense waste. Analogs to nuclear waste glass are discussed in Section 13.3.3.

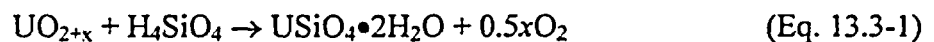
13.3.2 Spent Nuclear Fuel Alteration and Dissolution

This section summarizes five localities where studies related to spent nuclear fuel have been conducted. They are grouped according to the relative oxidation potentials to which the analog sites are exposed. However, this grouping is somewhat arbitrary, as some degree of oxidation is apparent in nearly all the sites described below.

13.3.2.1 Reducing Environments

In the presence of liquid water around a waste package, a water chemistry with reducing potential may form, but reducing conditions would be temporary. Reducing environments are discussed briefly to point out the contrasting sequence of alteration products that form in comparison to those that form in oxidizing environments. Oklo and Cigar Lake are two natural analog sites where uraninite exists under reducing conditions, although some of the reactors at Oklo (see discussion of Bangombé in Section 13.4.3.2.3.6) are found under oxidizing conditions.

Uraninite under reducing conditions, in the presence of saline hydrothermal solutions, may be altered through dissolution, preferential loss of Pb or Y and lanthanides, and coffinitization (Janeczek and Ewing 1992, p. 157). Coffinitization is the formation of the hydrated uranium silicate coffinite ($USiO_4 \cdot nH_2O$) by the reaction



Janeczek and Ewing (1992) pointed out the strong similarity between alteration textures and phase chemistries at Oklo and Cigar Lake. Dissolution of uraninite at both sites was associated with precipitation of illite. The authors attribute this to saline, moderately acidic solutions with temperatures of about 200°C. In addition to uraninite dissolution, coffinitization resulted in uranium, lead, and lanthanide element release (Janeczek and Ewing 1992, p. 157). The formation of Pb-rich and lead-depleted uraninites at both Oklo (Section 13.4.3.2.3) and Cigar Lake (Section 13.5) resulted from the loss of lead due to episodic diffusion related to regional geologic events and unrelated to uranium mobilization.

13.3.2.2 Oxidizing Environments

Uraninite will form under reducing conditions with uranium as U^{4+} , as previously stated. The uraninite structure can accommodate some degree of oxidation; in highly oxidizing aqueous environments, however, uraninite is unstable and decomposes (Finch and Ewing 1991, p. 392). Hydrated uranyl phases precipitate on the surface of the corroding uraninite, and a rind of corrosion products forms. The impurities often contained in uraninite, such as Pb, Ca, Si, U^{+6} , Th, Zr, and lanthanides, affect the thermodynamic properties of uraninite, the rate of uraninite alteration, and the composition of the corrosion products (Finch and Ewing 1991, p. 392).

The uranyl oxide hydrates are common initial-corrosion products of uraninite during weathering. In the presence of dissolved silica, these early phases alter to uranyl silicates, most commonly soddyite, $U_2SiO_8 \cdot 2H_2O$, and uranophane, $CaU_2Si_2O_{11} \cdot 6H_2O$ (see Section 13.3.1). Uraninite usually contains radiogenic lead (Finch and Ewing 1992, p. 465), and the early-formed lead-poor uranyl oxide hydrates alter incongruently to uranyl silicates plus lead-enriched uranyl oxide

hydrates, such as curite (Finch and Ewing 1992, p. 465). Radiogenic lead may serve to limit the mobility of uranium in nature by fixing uranium in solid phases, such as curite. Curite may also play an important role in the formation of uranyl phosphates, which are significantly less soluble than the uranyl silicates and control uranium solubility in many groundwaters associated with altered uranium ore (Finch and Ewing 1992, p. 465). In the absence of lead, schoepite and becquerelite are the common initial corrosion products. The reaction path for the alteration of lead-free uraninite results in the formation of uranyl silicates. Thus, the long-term oxidation behavior for ancient, lead-bearing uraninite is different from young, lead-free uraninite, which is similar to spent nuclear fuel. Because the presence of lead effectively reduces the mobility of uranium in oxidizing waters, the concentration of uranium in groundwater associated with oxidized uranium ore deposits will depend in part on the age of the primary uraninite (Finch and Ewing 1991, p. 396).

13.3.2.2.1 Nopal I Mine, Peña Blanca, Chihuahua, Mexico

At Nopal I, uraninite occurs in rhyolite tuff in a semiarid environment, where it has been exposed to oxidizing conditions for more than 8 ± 5 m.y. (Pearcy et al. 1993, p. 724). (See Section 13.4.2.3.1 for a description of the Nopal I site.) Uranium was initially deposited as uraninite at Nopal I. Geologic, petrographic, and geochemical analyses indicate that primary uraninite at Nopal I has been almost entirely altered to hydrated oxides and silicates containing uranium in the oxidized (uranyl) form. Because of its young geologic age, the deposit is low in radiogenic lead. The formation sequence of uranyl minerals by alteration of uraninite at Nopal I is shown in Figure 13.3-1 and is similar to many geologically young uranium deposits located in oxidizing environments.

Leslie et al. (1993) and Pearcy et al. (1993) compared the alteration of uraninite from Nopal I to laboratory experiments of degradation of spent nuclear fuel at Yucca Mountain. They found that uraninite from the Nopal I deposit should be a good natural analog to spent nuclear fuel because long-term experiments on spent nuclear fuel show alteration paragenesis, intergrowths, and morphologies very similar to those observed at Nopal I (Wronkiewicz et al. 1996, p. 92). Oxidation of the uraninite at Nopal I has produced an ordered suite of minerals, first forming schoepite, a uranyl oxyhydroxide, followed by hydrated uranyl silicates, such as soddyite (Figure 13.3-1). Consistent with a high-Ca abundance in Nopal I groundwater, the dominant secondary uranium phase is uranophane, a hydrated calcium-uranyl silicate. Due to abundance of calcite at Yucca Mountain, uranophane would be a potential secondary phase there as well. In comparison, laboratory experiments find that the general trend is to form mixed uranium oxides, followed by uranyl oxyhydroxides, and, finally, uranium silicates, mostly uranophane with lesser amounts of soddyite (Wronkiewicz et al. 1996). In addition, uraninite at Nopal I has a low trace-element component (average of 3 percent by weight) that compares well with that of spent nuclear fuel (typically less than 5 percent by weight).

13.3.2.2.2 Koongarra Uranium Deposit, Alligator Rivers, Northern Territories, Australia

A number of uranium deposits in the Alligator Rivers region of northern Australia have been studied as natural analogs for radionuclide migration from a spent nuclear fuel repository (Airey 1986). Of these studies, the Koongarra deposit has received the most attention. Like other

Alligator Rivers uranium deposits, the Koongarra deposit is an unconformity-type deposit, with a genesis similar to uranium deposits in the Athabasca Basin in northern Saskatchewan, Canada (e.g., Cigar Lake, Section 13.5). However, Koongarra has been exposed to strongly oxidizing conditions near the surface. (Transport features of the Koongarra deposit are described in Section 13.4.3.2.1.)

The uranium mineralogy of Koongarra was described by Snelling (1980), Isobe et al. (1992), and Murakami et al. (1997). Two distinct types of uraninite were identified: low Ca (1 to 3 percent by weight) vein-type uraninite, and high Ca (3 to 5 percent by weight) hydrothermal uraninite. The vein-type uraninites are more oxidized than the hydrothermal uraninites. Two periods of remobilization are apparent from the uraninite in the ore zone. The first remobilization event partially dissolved much of the originally euhedral uraninite grains, redepositing them as veinlets and masses but without any significant change in their chemistry. The second remobilization resulted in the precipitation of low-temperature, supergene uraninite, with increased Si, P, Ca, and O, and decreased U and Pb relative to the vein-type uraninites. Alteration of the primary-ore zone also produced uranyl oxyhydroxides and uranyl silicates at depth. Often, uraninite grains or entire veins are pseudomorphously replaced by lead-uranyl minerals vandendriesscheite, fourmarierite, and curite. The uranyl oxyhydroxides are, in turn, replaced by uranyl silicates uranophane, sklodowskite, and kasolite. In several areas, uraninite has completely altered to uranyl silicates.

Koongarra is one of the most studied occurrences of uranyl phosphates in the world. The alteration of uraninite and the genesis of uranyl phosphates at Koongarra have been examined extensively by Snelling (1980, 1992) and Isobe et al. (1992, 1994). A variety of uranyl phosphates have been identified among the Koongarra uranium minerals, including saléeite, dewindtite, sabugalite, torbernite, and renardite. Saléeite is the predominant uranyl phosphate in the weathered zone at Koongarra. Three mineralogical zones are defined at Koongarra, based on the predominant types of uranium minerals that occur within them: a uranium oxide zone, a uranyl silicate zone, and a uranyl phosphate zone (Snelling 1980, p. 487). Dissolved uranium is transported roughly from the uranium oxide zone at depth to the silicate zone, also at depth, then upward to the phosphate zone. The uranyl phosphate zone exists in the most oxidized weathered zone near the surface.

13.3.2.2.3 Poços de Caldas, Minas Gerais, Brazil

No secondary uranyl minerals are reported in any studies at either of the two mines in the Poços de Caldas caldera. See Section 13.4.3.2.2 for a more complete discussion of actinide and trace element transport at Poços de Caldas.

13.3.2.2.4 Shinkolobwe Mine, Shaba, Democratic Republic of Congo

Finch and Ewing (1991) studied uraninite alteration products at the 1,800-Ma Shinkolobwe deposit as an analog to the weathering of spent nuclear fuel. The deposit occurs under near-surface, highly oxidizing conditions. The host rocks at Shinkolobwe are dolomitic shales, siliceous dolostones, and chloritic siltstones. The host rocks contribute to significant concentrations of silica, carbonate, and sulfate in the groundwater, which form complexes with the uranyl ion. Dissolved metal cations in groundwater are Ca^{2+} , Ba^{2+} , Mg^{2+} , Cu^{2+} , and some

lanthanides as rare earth element-carbonate complexes. Recrystallization of uraninite and loss of radiogenic lead occurred 600 Ma to 720 Ma because of a thermal event that generated hydrothermal fluids. Some oxidative alteration of uraninite may have occurred then (Finch and Ewing 1991).

The uraninite at Shinkolobwe lacks many impurities (e.g., Th, lanthanides) common in uraninite (Finch and Ewing 1991, p. 393). The deposit has been exposed at the surface since the beginning of the Tertiary Period (approximately 60 Ma), and extensive weathering has altered or replaced much of the original uraninite. The deposit is found in a monsoonal climate; large annual rainfall accumulates during half the year, thus exposing the uranium minerals to extremes of wet and dry conditions. Uranium(VI) mineralization occurs along fracture zones, along which meteoric waters have penetrated 80 m or more. Uraninite crystals at Shinkolobwe are commonly surrounded by dense rinds of corrosion products, mostly uranyl oxyhydroxides, as well as uranyl silicates and rutherfordine, a uranyl carbonate. Uranyl phosphates are also common within fractures throughout the host rocks, but are rare or absent from corrosion rinds.

Uranyl minerals that make up the corrosion rinds surrounding many uraninite crystals undergo continuous alteration through repeated interaction with carbonate- and silica-bearing groundwater, combined with periodic dehydration of (especially) schoepite and metaschoepite (Finch and Ewing 1991, p. 396). Such secondary alteration occurs along small (approximately 0.1 to 1 mm) veins within the corrosion rinds. Grain size generally decreases as alteration proceeds, most commonly along veins. Schoepite, however, is not observed to re-precipitate where in contact with dehydrated schoepite (Finch and Ewing 1991, p. 396). Thus, while the early formation of schoepite during the corrosion of uraninite may be favored, schoepite is not a long-term solubility-limiting phase for oxidized uranium in natural groundwater containing dissolved silica or carbonate (e.g., the type of groundwater at Yucca Mountain).

The following conclusions are presented on the alteration paragenesis of uraninite from Shinkolobwe (Finch and Ewing 1991, p. 396):

- Becquerelite (Ca-bearing), Pb-bearing vandendriesscheite and fourmarierite, schoepite [UO₃•2H₂O], billietite (Ba-bearing), and compreignacite (K-bearing) are formed relatively early in the alteration sequence.
- Pb-bearing curite and masuyite tend to be formed later.
- The uranyl silicates uranophane and cuprosklodowskite appear to be the last phases to be formed.

13.3.2.2.5 Krunkebach Mine, Menzenschwand, Germany

At the Krunkebach Mine, U-bearing, quartz-barite-fluorite veins several centimeters to a few meters wide occur in a highly differentiated two-mica granite, near the contact of the granite and juxtaposed gneisses and metasediments (Hofmann 1989, p. 921). The veins were formed about 310 Ma and were subject to hydrothermal alteration during Tertiary time and to low-temperature oxidation since uplift in Quaternary time (less than 2 Ma) (Hofmann 1989, p. 921). The vein of the ore body lies parallel to, and only a few meters away from, a fracture zone that acts as a

major groundwater channel. The ore is oxidized to a depth of at least 240 m (Hofmann 1989, p. 921). At present, uranium migration is retarded by sorption onto iron oxyhydroxides, gorceixite $[\text{BaAl}_3(\text{PO}_4)(\text{PO}_3\text{OH})(\text{OH})_6]$, and clays; Ra is fixed in barite (Hofmann 1989, p. 923). The Ba-uranyl minerals (uranocircite and heinrichite) are much more common than their Ca-uranyl equivalents, autunite and uranospinite.

A late Tertiary or early Quaternary hydrothermal event (approximately 150°C) is thought to have mobilized SO_4^{2-} , with sulfur derived from pyrite oxidation (Hofmann 1989, p. 921). The increased SO_4^{2-} dissolved primary barite, increasing the Ba concentration in solution and precipitated Ba-uranyl phosphates. Suspended material composed of clays (illite > kaolinite > smectites), quartz, gorceixite, and amorphous iron oxyhydroxides constitutes 0.006 to 5.9 ppm of the groundwater. These particles appear to have been transported 1 to 2 km under the ambient, oxidizing near-neutral pH conditions (Dearlove et al. 1989, p. 932). Over a distance of only a few meters, the concentration of dissolved uranium drops about two orders of magnitude, the major uranium species change from carbonate to phosphate, the secondary uranium sulfates precipitate, and the uranium is accumulated by gorceixite, smectite, and chlorite clays (Dearlove et al. 1989, p. 929).

13.3.2.2.6 Summary of Spent Nuclear Fuel Alteration Analogs

The paragenesis of uraninite alteration phases depends on the mineralogy of surrounding host rocks and on groundwater composition, pH, and oxidation-reduction (redox) potential. In general, the progression of phases will be to uranyl silicates, with coffinite in a reducing environment and uranophane in an oxidizing environment. Numerous compositional variations are caused by trace elements present in the system. As shown by Finch and Ewing (1991, p. 396), the formation of intermediate-phase schoepite may be favored early during the corrosion of uraninite, but schoepite is not a long-term, solubility-limiting phase for oxidized uranium in natural groundwater containing dissolved silica or carbonate (i.e., the type of groundwater at Yucca Mountain).

Uraninite alteration products that form in reducing environments are not relevant to the assemblage that would form at Yucca Mountain. The most analogous suite of alteration products is found at Nopal I, where groundwater is oxidizing and nearly neutral in pH, and the host rhyolitic tuffs are similar to Yucca Mountain tuffs. The unusual Ba-rich composition of alteration products at the Krunkelbach Mine makes it a less useful analog to Yucca Mountain. Phosphate-rich conditions at Koongarra produce a different suite of minerals than those anticipated at Yucca Mountain. Alteration of Proterozoic (approximately 2,400 Ma to 700 Ma) uranium deposits, such as Koongarra and Shinkolobwe, introduces the important Pb-bearing phases, such as curite, that play a role in the development of other stable phases in the system. Because of the very young age of repository spent nuclear fuel, the presence of radiogenic lead will not be an issue at Yucca Mountain. The young age of the Nopal I deposit is another similarity to Yucca Mountain in regard to the absence of Pb-bearing phases.

13.3.3 Nuclear Waste Glass Analogs

Among the natural volcanic glasses, basalt glasses are compositionally the most similar to nuclear waste glasses (Lutze et al. 1987, p. 142). Basalt glass and nuclear waste glass are similar

in silica content, alteration products, alteration layer morphologies, and alteration rates in laboratory experiments (Grambow et al. 1986; Arai et al. 1989; Cowan and Ewing 1989). However, there are substantial compositional differences, as shown in Table 13.3-1. Basalt glass alteration has been studied in a number of environments, including ocean floor, subglacial, hydrothermal, and surface conditions (Grambow et al. 1986; Jercinovic et al. 1986; Arai et al. 1989; Cowan and Ewing 1989). Inferred alteration rates, as calculated from alteration rinds, range from 0.001 $\mu\text{m}/\text{k.y.}$ to 30 $\mu\text{m}/\text{k.y.}$ (Arai et al. 1989, p. 73).

Byers et al. (1987, p. 2) reported results of a study of natural basalt glasses that were collected from a wide range of continental and oceanic environments. Ages of the samples ranged from a few million to 350 Ma. All of the samples had altered to palagonite and exhibited dissolution textures. (Palagonite is a vitreous, yellow-orange to red-brown alteration product that forms as a surface gel layer on fresh basaltic glass.) The alteration products were mainly smectite clays, zeolites, and calcite. The paragenetic sequence of the alteration minerals was largely a function of the altering fluid composition. Byers et al. (1987) found no simple connection between the thickness of the alteration rinds and age or general alteration environments. Jercinovic et al. (1986, p. 671) reported that basaltic glass from the Wanapum Basalt near Hanford, Washington, is replaced by surface layers of palagonite that are 10 to 350 μm thick. The palagonite chemically resembles nontronite, an Fe-rich smectite. Later alteration causes formation of Mg-rich clays, such as saponites. In palagonites that formed as alteration rinds in Icelandic basalts, Jercinovic and Ewing (1987, p. xiv) showed that the formed layers were not completely amorphous, but contained a high proportion of clays, and that channels formed in the leached layer allowed solutions to reach the fresh glass/alteration interface so that it was not protected from further alteration.

Basaltic glass that had weathered for the past 12 to 28 k.y. at Hanauma Bay, Hawaii, had altered partially to palagonite and zeolites (Cowan and Ewing 1989, p. 49). Zeolites were formed in the following order: analcime to phillipsite to chabazite. The rate of alteration was less than predicted by experiments, which led the authors to infer that the difference was a result of the episodic presence of the groundwater over the years.

Grambow et al. (1986) demonstrated that a glass-and-water reaction model could be used to model the long-term reaction of basaltic glass from a variety of aqueous environments. Their study pointed out the important role of metastable phases in controlling solution compositions. They also noted that the reaction rate can vary by five orders of magnitude, depending on environment, and that the reaction rate is a factor of 100 lower under silica-saturated conditions. They concluded that the long-term stability of glass is related to low temperatures and sealing of the glass against circulating water. According to these authors, basalt glass could be preserved under these conditions for hundreds of millions of years, whereas under more aggressive conditions, the glass could be altered much sooner.

Hydration rates of rhyolitic glass were determined by Ericson (1981, p. 283) using obsidians from California and Oregon in conjunction with archaeological data. This author found that laboratory alteration rates were much lower than the rates of natural hydration, in contrast to comparative hydration rates of basaltic glasses found by Cowan and Ewing (1989, p. 49). The calculated rate of hydration of high-silica glasses is about 30 $\mu\text{m}/\text{m.y.}$ at 20°C (Zielinski 1980,

p. 198). It was observed that as the temperature increased, the devitrification rate also increased. At 120°C, the process was found to be faster by four orders of magnitude.

Malow and Ewing (1981) compared the thermal and chemical stabilities of two borosilicate glasses and one glass ceramic to those of three natural (volcanic) rhyolitic glasses, through a variety of laboratory tests and observations of natural weathering. They concluded that natural glasses are much more stable than waste-form glasses, as a result of higher silica contents in the natural glasses (75 percent versus 28 to 51 percent in waste form glasses [Malow and Ewing 1981, p. 317]). No difference in weathering was observed among the natural samples, which ranged in age from 500 yr. to 670 k.y. At elevated temperatures, the waste glasses tended to form new phases and to recrystallize, whereas the natural glasses did not display this tendency. They noted that most volcanic glasses are less than 2 Ma, suggesting stability up to a few million years at ambient weathering conditions.

Tektites (nonvolcanic glass of extraterrestrial or impact origin) range in age from approximately 100 ka to 35 Ma. They rarely show signs of alteration, dehydration, or devitrification (Lutze et al. 1987, p. 143). Their great durability may be a result of their high silica and alumina (approximately 30 percent) contents and their low (less than 4 percent) alkali contents (Lutze et al. 1987, p. 144).

The degradation of archaeological glass has also been the subject of study. Glass was first manufactured in approximately 1500 B.C. (Kaplan 1980, p. 85). The earliest glass was rich in soda and lime. Later, lead glass came into being, followed by potassium-lime glass. Some of the earliest glass has survived 3,500 yr. with little degradation (Kaplan and Mendel 1982, p. 24; Miller and Chapman 1995, p. 34), even though it has high alkali concentrations that would tend to make it reactive. Kaplan and Mendel (1982) identified five styles of structural decomposition in the ancient glasses: weeping, pitting, crizzling (formation of a tiny network of cracks), layering, and crusting. Some of these types of decomposition could be relevant to decomposition of borosilicate glass.

A Japanese study examined the development of alteration products on the surfaces of glasses deposited 280 to 2,800 yr. ago and produced by ancient volcanic eruptions on Mt. Fuji and as scorias on Izuoshima Island (Yamato et al. 1992). The glasses had been subjected to weathering by highly oxidizing rainwater. The water on Izuoshima is also enriched in salts. Under conditions that were favorable for leaching, the glasses appeared to deteriorate at slow rates, between 0.2 to 3.1 $\mu\text{m}/\text{k.y.}$ for the Mt. Fuji glasses, and 1.7 to 1.8 $\mu\text{m}/\text{k.y.}$ for the Izuoshima glasses (Yamato et al. 1992, p. 47).

In summary, natural glass studies suggest that the rate of devitrification is too slow for the process to be significant in the repository, although these studies have not considered the effect of radiation. The compositions of the glasses used in natural analog studies differ somewhat from borosilicate glasses, however, and this makes a simple analogy dubious for quantitative purposes. High silica and alumina contents, along with low alkali contents, are favorable for long-term preservation. For illustrative purposes, glass studies may be quite useful.

13.3.4 Archaeological Analogs to Burial in an Unsaturated Environment

Illustrative archaeological analogs are introduced in this section, in connection with the studies of glasses just described and the studies of metals that follow in Section 13.3.5. Although they may not provide suitable data sets for testing in Yucca Mountain models, the types of archaeological analogs described by Winograd (1986, p. 4-6) should not be overlooked in demonstrating the efficacy of an unsaturated environment in isolating radioactive waste. Winograd (1986) cited numerous examples of delicate objects preserved by burial in arid and semiarid unsaturated zones, including caves. He noted the preservation of cave art as old as 35 ka and archaeological finds that included ivory animal statuettes and molded clay bison from caves in France and Germany, respectively. The caves provided a well-drained environment with a relatively constant annual temperature and humidity. These conditions were apparently favorable for preserving artifacts, in spite of the presence of oxidizing conditions and high humidity. Other examples from Winograd's (1986) much more extensive list, not limited to caves, included the following:

- A heap of preserved horse-bean seeds in Israel, dated 6500 to 6000 B.C.
- 10-ka wood and textiles in a Peruvian cave
- 4 to 8-ka Chilean mummies in shallow burial pits
- The 2-ka Dead Sea scrolls
- The 1-ka manuscripts in Chinese cave temples in the Gobi Desert.

The main point is that considerable evidence points to the preservation of delicate materials over many millennia in dry, unsaturated environments. An example closer to home is at Spirit Cave, Nevada where a 9.4-ka mummy was discovered (Dansie 1997). The body was well preserved, with clothing and hair remaining. Stuckless (2000) has cited evidence from Paleolithic to Neolithic paintings in caves and rock shelters in Europe and paintings and artifacts preserved in man-made rock shelters in Turkey that support models in which flow occurs around openings in the unsaturated zone over long time periods and in varied climates and geologic media.

Winograd (1986, p. 5-6) recommended that a detailed synthesis of preserved materials and objects be prepared to attempt to determine the environmental conditions that led to preservation. The archaeological record, like the paleontological record, is subject to bias, in that only some objects are preserved. Furthermore, the environmental record of the distant past may be difficult to determine. However, synthesizing the archeological record with past environmental data could provide a valuable qualitative supplement to numerical models and be more easily demonstrated to the public.

Archaeological and industrial analog studies of materials, such as glasses and cements, have tended to provide qualitative information that can be used to infer long-term stability of these materials. Although these studies may not provide quantitative data themselves, they can be used to support extrapolated values from short-term laboratory experiments. Such studies may also yield important information concerning the nature of the degradation processes (i.e., whether radionuclides may be retained by secondary alteration products through sorption or precipitation).

13.3.5 Metal Analogs to Waste Package Materials: Their Role in the Disposal Concept

The current reference design is a two-layer barrier system, with a 2-cm layer of Alloy-22 (Ni-based, high-Cr) as the corrosion-resistant material, over a 5-cm layer of stainless steel (316L) as the corrosion-allowance material. No carbon steel will be used except in the interior basket. Because the canister is thinner than in previous designs, it is not self-shielded, so radiation will be higher. It is not certain whether radiolysis will be a problem (CRWMS M&O 1999, p. 5-39). Although failure of the canister will most likely occur in the form of perforations created by localized corrosion of the corrosion-resistant layer, the high-performance, corrosion-resistant alloys could undergo degradation predominantly by general corrosion (CRWMS M&O 1998c, pp. 5.1, 5.2).

Many factors influence the potential corrosion modes of the candidate materials. These include:

- Metallurgical factors (alloy composition and microstructure)
- Physical factors (temperature, relative humidity, and water contact mode)
- Chemical factors (pH and concentration of aggressive species, such as chloride, sulfate, nitrate, and carbonate ions)
- Mechanical stress (McCright 1998, p. xv).

Under the near-field environmental conditions expected in the unsaturated zone at Yucca Mountain, the majority of waste packages are expected to be exposed to humid air conditions during the emplacement period. In the absence of a drip shield, some fraction of the waste packages that are emplaced in areas where seepage occurs could be dripped on during the emplacement period. Therefore, the significant contributors to the degradation mode of the waste package are the temperature and relative humidity in the drift and the water-contact mode. The frequency of the seepage and its chemistry (especially pH and chloride concentration) will also significantly affect the degradation of the waste packages (CRWMS M&O 1998c, p. 5.1-2; McCright 1998).

The durability of metals is discussed briefly. This discussion is brief because typically the metals that have been studied as analogs to waste package materials are not very similar in composition to the high-Cr, Alloy-22 composition that is planned for use in waste package canisters or the titanium planned for drip shields in the repository. Nevertheless, it may be possible to use information regarding degradation of common metals (e.g., iron and copper) as evidence of their longevity, provided environmental conditions are taken into consideration.

13.3.5.1 Iron

13.3.5.1.1 Buried Nails at Inchtuthil, Scotland

An ancient hoard of buried nails has been used in a study of the corrosion of iron. These nails were found on the site of the most northerly fortress of the Roman Empire at Inchtuthil, Scotland. An estimated total of more than 1 million nails had been buried in a 5-m-deep pit and covered with 3 m of compacted earth in a successful attempt to hide the nails from Pictish tribes

when the fortress was abandoned in 87 A.D. (Miller et al. 1994, p. 336). The fortress was excavated in the 1950s, when the surviving nails (about 850,000) were unearthed. Although the nails were composed of iron, they were heterogeneous in composition, with regions of high and low carbon content. The surfaces of all the nails exhibited some corrosion, but the degree of corrosion was greatly controlled by the location within the hoard. The nails toward the inside of the hoard showed minimal corrosion, limited to the formation of a thin, corroded layer, whereas the nails toward the outside of the hoard, especially those near the top, were corroded to such an extent that they formed a solid crust. This example serves to illustrate the protective role of a corrosion-formed crust in reducing or preventing further corrosion.

13.3.5.1.2 Meteorites and Iron Artifacts

It has been suggested that iron meteorites may be good analogs of steel-alloy waste package canisters. Iron meteorites are essentially Ni-Fe alloys (Ni content usually ranges between 5 and 11 percent by weight, with a maximum of 60 percent by weight), with minor amounts of Co (0.3 to 1.0 percent) and traces of Cr (5 to 2,500 ppm), Cl (1 to 10 ppm), and Ti and V (0.5 to 5.0 ppm) (Johnson and Francis 1980, p. 4.2). Iron meteorites lack the high Cr concentration of Alloy-22 used in the YMP design. Nevertheless, if iron meteorites were to be studied for the purpose of extrapolating their corrosion rates to those of a waste package canister material, it would be necessary to select meteorites of datable terrestrial ages. Furthermore, their validity as an analog would be increased by the ability to monitor the present environmental parameters, such as pH, Eh, or soil moisture, and to estimate past environmental parameters in the setting where they fell to Earth. This means that only meteorites that can be traced to their depositional sites would yield useful information for such a study.

The presence or absence of a fusion crust (i.e., a magnetite $[\text{Fe}_3\text{O}_4]$ -wüstite $[\text{Fe}_{1-x}\text{O}]$ rind formed by rapid oxidation during atmospheric descent) may be a factor in the range of weathering that occurs at sites where meteorites fragment on descent as well as on impact. At Canyon Diablo, Arizona, meteoric material that developed a fusion crust during descent was, with the exception of silica-coated metal particles, more resistant to weathering than masses formed on impact, which developed a thin fusion crust, if any (Johnson and Francis 1980, p. 4.20).

The nickel content of a meteorite appears to affect its resistance to corrosion. Phases with 20 to 30 percent by weight Ni (ataxites) have frequently shown superior resistance to terrestrial corrosion than phases with less Ni. By measuring potentials between selected phases, Buddhue (in Johnson and Francis 1980, p. 6.4) determined that corrosion over a period of centuries consumed kamacite (Fe, 7.5 percent Ni), while preserving phases such as taenite (Fe, 25 percent Ni), schreibersite $(\text{Fe, Ni})_3\text{P}$ (identified by Buchwald [in Johnson and Francis 1980, p. 6.4] as the meteorite mineral most resistant to corrosion), and draubreelite $(\text{FeCr}_2\text{S}_4)$. The better preserved phases are higher in Cr and Ni.

The durability of the iron pillar (99.7 percent Fe) of Asoka, India, is attributed to its location in a relatively dry environment and to its fabrication with minimal impurities. Johnson and Francis (1980, p. 6.5) indicated that the pillar was constructed by forge-welding together many solid disks. They suggested that conditions during welding may have been favorable for formation of corrosion-resistant oxides.

Johnson and Francis (1980, p. 3.4) investigated general, as opposed to localized, corrosion of more than 40 Fe artifacts and a few meteorites and obtained a rate of uniform corrosion of 0.1 to 10 $\mu\text{m}/\text{yr.}$ over a range of environmental conditions, excluding sea water. Chapman et al. (1984, p. 39) used a corrosion rate of 1 $\mu\text{m}/\text{yr.}$ (in the middle of this range) to obtain a lifetime of 50 k.y. for the mechanical stability of the Swiss waste package container.

Johnson and Francis (1980, p. 6.7) noted that dry and tomb-like environments were the most benign to all ancient materials, because lack of moisture condensation suppressed corrosion. They further suggested that if temperatures are below the range where rapid oxidation occurs (varying by metal), elevated temperatures (above the dew point) are an advantage to the preservation of metals.

13.3.5.2 Copper

13.3.5.2.1 Kronan Submerged Bronze Cannon

A bronze cannon salvaged from the Swedish man-of-war ship *Kronan*, which sank in the Baltic Sea in 1676, was the subject of an investigation of the rate and mechanism of copper corrosion (Neretnieks 1986). The cannon had been partly buried in a vertical position in clay since the ship sank. This is a close analogy to the copper canisters used in the Swedish KBS-3 spent nuclear fuel repository design (Miller et al. 1994, p. 336), in that the cannon had a high Cu content and the montmorillonitic clay surrounding it was tightly packed and water-saturated. Chemical analysis showed that the copper from the cannon had diffused 4 cm into the clay, causing a 1 percent reduction in the copper content at the surface of the cannon. The sediment pore waters around the cannon had neutral pH with variable Eh. Pore waters nearest the top of the sediments were more strongly oxidizing, as a result of oxygen diffusion from sea water. Corrosion products included Cu_2O and Fe_2O_3 , which confirm a generally oxidizing environment. A corrosion rate of 0.15 $\mu\text{m}/\text{yr.}$ was calculated, and this was uniform over the bronze surface.

13.3.5.2.2 Copper Artifacts

Tylecote (1977, 1979) investigated archaeological artifacts, including those from shipwrecks of various ages, to determine the durability of copper over long periods of time. The author found that, under aggressive conditions, the most corrosion-resistant materials were the tin-bronzes, and he was able to calculate an average corrosion rate of 0.225 $\mu\text{m}/\text{yr.}$ for these in mildly alkaline soil. Johnson and Francis (1980) conducted a more comprehensive analysis of 34 artifacts composed of copper or copper alloys and determined from them a range of copper corrosion rates of 0.025 to 3.0 $\mu\text{m}/\text{yr.}$, with an average rate of approximately 0.3 $\mu\text{m}/\text{yr.}$ If this rate were related to corrosion of a 10-cm-thick copper canister (e.g., of the type planned for disposal in the Swedish radioactive waste program), it would correspond to a canister lifetime on the order of 800 k.y. to 4 m.y. However, a simple extrapolation such as this neglects consideration of different manufacturing techniques and compositions of modern copper alloys compared to those found in the ancient historical record.

13.3.5.3 Titanium

Johnson and Francis (1980, p. 2.3) indicated that titanium was not discovered until the end of the eighteenth century and was first produced as a pure metal in 1910. Therefore, it will not be possible to find ancient materials that used titanium. Any future studies would need to consider its occurrence and stability in rocks. The one analog study that has considered titanium, with respect to the Canadian disposal concept, is Cigar Lake (see Section 13.5).

13.3.6 Concrete and Alkaline Plumes: Their Role in the Disposal Concept

The interaction of water with concrete support components in emplacement drifts was considered in the TSPA-VA, but concrete is not part of the license application design selection repository design except as grout around rock bolts. The TSPA-VA analyses indicate that water interacting with concrete would have a pH near 11 for at least 10 k.y. but for much less than 100 k.y. This pH change represents a substantial change to ambient water composition and may affect the ability of the engineered barrier system to contain radionuclides within the drift. This would, in turn, change the source term for TSPA. In addition, higher pH fluids migrating into the geosphere could react more readily with the host rock (CRWMS M&O 1998b, p. 4.7-4).

Such alkaline fluids can alter the siliceous host rock along the fracture pathways and in the matrix. The mineralogical changes, the distance over which they may occur, and the distribution of such alterations are still very uncertain, but they could produce changes in the amount of fracture-matrix interaction and the sorption of radionuclides within the unsaturated zone host rock. Because of the complex and uncertain nature of this alteration, current process models do not include any explicit representation of these potential changes to minerals along radionuclide migration pathways. The potential impacts from concrete-modified water compositions assessed in the TSPA-VA sensitivity results appear to be greatest for the 10-k.y. period, because earlier and more frequent waste package failures allow greater exposure of the waste form inventories at earlier times (CRWMS M&O 1998b, p. 4.7-5).

13.3.6.1 Oman

The Oman investigation was a natural analog study of hyperalkaline groundwaters concerned with the effect of hyperalkaline conditions on radionuclide transport processes, including solubility and speciation, colloids, and microbial populations. A primary aim of the study was to test the ability of thermodynamic codes to represent and predict hyperalkaline rock-groundwater equilibrium conditions. Details of the investigations are given by Bath et al. (1987b) and are summarized in Bath et al. (1987a) and McKinley et al. (1988).

The Oman natural analog site is located in the Semail Ophiolite Nappe of northern Oman (Figure 13.3-2). The ophiolite represents a complete 15-km-thick cross section of obducted oceanic crust and upper mantle rocks (Lippard et al. 1986, p. 153). The original mineralogy of the upper-mantle harzburgites was predominantly olivine, with lesser amounts of pyroxenes, whereas in the gabbros and basalts of the oceanic crust, the original mineralogy was predominantly pyroxenes with lesser amounts of olivine. The Mg- and Fe-rich olivine has been substantially hydrated by reaction with large volumes of meteoric water to form serpentine and iron oxide phases, with the effect of increasing matrix porosity. Serpentinization causes the

northern Oman groundwater to become both strongly alkaline and reducing. The hyperalkaline groundwater tends to flow in the mantle-derived rocks and reach the surface at springs located at the contact between the crustal and mantle-derived rocks. At the surface, the groundwater degases large volumes of dissolved hydrogen. Seven springs were sampled, and the groundwater was found to be a Na-Cl-Ca-OH solution, with pH levels between 10 and 12. This unusual chemistry is reflected in the minerals precipitated at the springs, which include brucite ($\text{Mg}(\text{OH})_2$) and portlandite ($\text{Ca}(\text{OH})_2$). The concentration of trace elements in the groundwater was very low (Bath et al. 1987b).

13.3.6.2 Maqarin, Jordan

The Maqarin study site is located at the hyperalkaline (pH 12 to 13) natural springs of the Maqarin area of northern Jordan (Figure 13.3-3). The rock formations of interest are Cretaceous marls and bituminous limestones, known locally as the Bituminous Marl Formation. The geology of the site is described by Khoury et al. (1992). The rocks are composed essentially of calcite, with accessory quartz, dolomite, apatite, pyrite, and clay minerals, and have a high organic content (up to 20 percent). This rock formation is of interest because it contains an assemblage of naturally formed cement minerals. Both high- and low-temperature mineral assemblages have been identified. High-temperature minerals include graphite, apatite, diopside, wollastonite, and anorthite. Low-temperature minerals include gypsum, ettringite, tobermorite, and, most importantly, portlandite as a rock-forming mineral. The portlandite forms by a two-stage process. First, lime forms as the rock spontaneously combusts if quartz is absent, and second, the lime hydrates to form the portlandite as groundwater is introduced. The high pH of the groundwater is controlled by the solubility of portlandite and other cement phases. This is analogous to the situation in a cementitious low-and-intermediate-level waste repository of the type planned in the United Kingdom, and it is different from the system at the Oman natural analog site, where the hyperalkaline conditions relate to the alteration of ultramafic minerals (see Section 13.3.6.1).

High trace-element concentrations were measured in the Maqarin groundwater. High concentrations of major ions were also measured, which likely result from the subsurface dissolution of sodium and potassium oxides. The order of source-rock leachates appears to be the same as predicted by models of cement degradation (i.e., NaOH and KOH, followed by $\text{Ca}(\text{OH})_2$) (Maqarin Natural Analogue Site Study Group 1992, p. 130).

The principal use made of the Maqarin natural analog has been in blind testing of solubility and speciation thermodynamic databases and, to a lesser extent, thermodynamic codes. Microbiological and colloidal populations have also come under investigation. Full details of these investigations are given in Khoury et al. (1992), Maqarin Natural Analogue Site Study Group (1992, Chapter 5), and Tweed and Milodowski (1994). Although this natural analog has only been used in model testing, the close analogy between the groundwater at Maqarin, and that expected in a cementitious low- and intermediate-level waste repository, make this an ideal natural analog for the study of other processes in a hyperalkaline environment. A two-volume report that encompasses the entire body of work conducted at Maqarin was published by the Swedish Nuclear Fuel and Waste Management Company (Smellie 1998).

13.3.6.3 Gallo-Roman Cements

Cement studies have shown that calcium silicate hydrate compounds provide the strength and stability in modern Portland cements. Calcium silicate hydrate compounds were formed early in the development of Roman cement, which used crushed vitreous fireclay as a pozzolan in the concrete mixture (e.g., Hadrian's wall in northern England) (Miller et al. 1994, p. 140; Miller and Chapman 1995, p. 39). The calcium silicate hydrate compounds reduced the porosity and permeability of the concrete and helped to ensure its preservation for more than 2,000 years with no loss of mechanical strength. Similar results were obtained from the earliest reinforced concrete structures in Britain and in the earliest Portland cements used in sea defenses 150 years ago (Miller and Chapman 1995, p. 40).

However, the interaction between cements and materials with which cement is in contact is important to examine. One industrial analog study looked at interaction between cement and rock in a tunnel driven into marls. The concrete was found to be completely recrystallized at the contact zone, resulting in a significant increase in porosity and loss of mechanical strength (Miller and Chapman 1995, p. 42). It would be useful to investigate other pairs of potential repository materials, because the effect of material stability may be unexpected. Such a study could be conducted at the Krasnoyarsk-26 site in Russia, where a 1-km-long tunnel constructed in granodiorite is lined with 1-m-thick concrete. The excavation has been subjected to heating by nuclear reactor processes. The site would also afford the opportunity to investigate the effect of thermally coupled processes on concrete stability.

13.3.7 Effects of Radiolysis

Radiolysis is chemical decomposition caused by radiation, and its effects on both the waste form and the waste package deserve examination. The effects of radiolysis in the Oklo ore deposit are discussed by Curtis and Gancarz (1983). The authors calculated the alpha- and beta-particle doses in the critical reaction zones during criticality and the energy provided to the fluid phase by these particles. The energy caused radiolysis of water and the production of reductants and oxidants. The effect of these reductants and oxidants on the transport of radionuclides within and outside the reactors has been difficult to quantify. Iron is most reduced in the samples that show the greatest ^{235}U depletion. Curtis and Gancarz (1983, p. 32) suggested that the reduction of iron in the reactor zones and oxidation of U^{+4} in uraninite was contemporaneous with the nuclear reactions and not a later supergene phenomenon of secondary enrichment. Curtis and Gancarz (1983) suggested that radiolysis of water resulted in the reduction of Fe^{+3} in the reactor zones and the oxidation of uranium. Furthermore, the authors suggested that the oxidized uranium was transported out of the critical reaction zones and precipitated through reduction processes in the host rocks immediately outside the zones. The reduction processes likely involved organics or sulfides present in the host rocks. However, if the host rocks around the natural reactor cores had not contained species capable of reducing the oxidized uranium transported out of the cores, the uranium could have been transported much farther from the critical reaction zones. The important point is that, even with intensive radiolysis, very little (only several percent) of the uranium in the natural reactors was mobilized (Naudet 1978, p. 590).

13.3.8 Summary of Waste Package Metal and Concrete Analogs

The analogs to metals presented in Section 13.3.5 serve mainly to demonstrate that under ambient to slightly elevated temperatures, the metals will be stable for thousands of years, even under oxidizing conditions. Because the historical record is unlikely to offer analogs to titanium stability, Ti-bearing minerals such as sphene and rutile may offer insights. For cements, important considerations are the effects of elevated temperatures on stability of cement minerals and reactions at the interface between cement and other materials. Radiolysis deserves consideration because it is uncertain if radiolysis will be a potential problem around waste packages in the Yucca Mountain Site Characterization Project Enhanced Design Alternative II design scenario, in which waste packages are not self-shielded. Under criticality conditions at Oklo, several percent of uranium was estimated to have been mobilized, but the conditions were far more extreme than those anticipated at Yucca Mountain.

INTENTIONALLY LEFT BLANK

13.4 NATURAL SYSTEM ANALOGS

This section considers analogs to natural system processes, working from the direction of the potential repository and near-field environment (Section 13.4.1) to the unsaturated zone (Section 3.4.2) and out to the saturated zone (Section 13.4.3).

13.4.1 Analogs to Coupled Thermal-Hydrologic-Chemical Processes

13.4.1.1 Introduction

The emplacement of heat-generating waste in a geologic repository located in the unsaturated zone will cause perturbations to the natural environment through heat transfer, resulting from convection and conduction, as well as by associated geochemical and geomechanical changes taking place in the repository near-field and altered rock zones (Section 11 of this report). Although data collected from heater tests have significantly advanced understanding of thermohydrologic processes and coupled behavior, it will be difficult to measure thermohydrologic behavior deterministically, because the experiments would be too limited for the time frame over which the processes take place and thus cannot represent time and rate scales. Natural analogs, on the other hand, provide opportunities for testing models and building understanding in thermally coupled processes by providing data from fossil hydrothermal systems, by observations from ongoing processes in geothermal fields, and by using data from geothermal systems to test and build confidence in numerical modeling codes and in thermodynamic and kinetic databases. Sections 13.4.1.2 and 13.4.1.3 discuss these three opportunities for application of natural analogs.

13.4.1.2 Fossil Hydrothermal and Intrusive Contacts

The effects of shallow (less than 500 m) magmatic intrusions into unsaturated rocks can be quite different from the effects associated with deeper hydrothermal, saturated systems. This section examines the thermally coupled hydrologic-chemical processes that are relevant to thermal-hydrologic-chemical interactions during the repository postclosure period and identifies natural analog cases where the effects of magmatic intrusion and attendant heating have been studied in both saturated and unsaturated systems. Processes that are relevant to thermal-hydrologic-chemical interactions during the repository postclosure period include:

- Zeolitization of volcanic glass, affecting transport pathways and sorption
- Potential dehydration of zeolites and vitrophyre, causing water release and affecting heat and fluid flow
- Thermal reduction of sorptive mineral properties
- Changes in water chemistry resulting from interactions between engineered barriers and groundwater, which may affect seepage and flow
- Fracture permeability changes caused by dissolution or precipitation of minerals, including formation of mineral caps.

A good analogy for understanding future potential repository behavior is the fossil hydrothermal system at Yucca Mountain itself (Bish and Aronson 1993). Detailed mineralogical examination of Yucca Mountain tuffs showed that most zeolitic alteration occurred between 13 to 11.6 Ma, at about the same time as tuff emplacement. After formation of the major zeolitic horizons, deep-seated hydrothermal activity persisted until about 10 Ma. This activity was limited to temperatures between 90° and 100°C, the zeolite stability limit. At prolonged exposure to temperatures greater than 90°C, the sorptive zeolites clinoptilolite and mordenite are altered to the nonsorptive zeolite analcime, plus quartz and calcite.

Conceptual models for mineral evolution at Yucca Mountain (DOE 1998a, p. 2-67) suggest that the most likely mineralogical reactions caused by repository heating would include the following:

- Dissolution of volcanic glass and precipitation of clinoptilolite, clay, and opal-CT (i.e., opal with cristobalite- and tridymite-type stacking)
- Dissolution and precipitation of silica polymorphs (cristobalite, opal-CT, tridymite, and quartz)
- Alteration of feldspars to clays
- Reactions involving calcite and zeolites.

Figure 13.4-1a illustrates paleotemperatures that were inferred from mineralogical data in several drillholes at Yucca Mountain (Bish and Aronson 1993, p. 154). Measured, present-day temperature profiles are shown for comparison. It can be seen from Figure 13.4-1a that present-day temperatures in drillhole G-3, which is within the potential repository block, compare closely to inferred paleotemperatures. In contrast, increasingly higher paleotemperatures are inferred for drillholes G-1 and G-2, which are closer to the center of the Timber Mountain caldera source of eruption (G-2 being the farthest north). Figure 13.4-1b shows mineral and glass abundance and clay mineralogy from GU-3/G-3 drill core which were used to infer the paleotemperatures. Similar mineral abundance diagrams for G-1 and G-2 drill cores indicate a northward progression of an increasing abundance of clays and zeolites, along with decreased glass abundance. This is in keeping with the reactions stated above.

Results from thermodynamic modeling indicate that the stability of various zeolites is a function of silica activity, temperature, aqueous Na concentration, and the mineralogy of silica polymorphs (Carey et al. 1997). Increasing temperature or Na concentration causes the alteration of zeolites to other phases. Kinetic effects are, however, important in assessing the significance of thermodynamic and natural analog study conclusions. Kinetic data suggest that saturated conditions are necessary for notable progress in these reactions, as discussed by Carey et al. (1997). Therefore, under ambient conditions, the reactions are likely to proceed more slowly in the Yucca Mountain unsaturated zone (excluding perched water zones) than below the water table. Similarly, the persistence of opal-CT below the water table indicates that silica reaction kinetics at Yucca Mountain are slower than laboratory studies suggest. However, if prolonged boiling occurred in saturated tuffs, significant progress in all these reactions could occur. The thermal design of the potential repository would limit temperatures above 100°C

within the Topopah Spring welded unit, and, in any case, the current Enhanced Design Alternative II design scenario calls for sufficient drift spacing such that temperatures between drifts will remain below boiling (CRWMS M&O 1999).

In addition to considering Yucca Mountain as a self-analog, contacts between igneous intrusions and the host rock may provide useful information as coupled process analogs. Numerous igneous intrusion contact zones have been examined with the objective of understanding chemical reactions and the migration of elements away from the heated contact zone, as well as understanding thermal-hydrologic-chemical effects, both in saturated and unsaturated systems. In early studies, elemental migration across a 2-m-wide contact zone around the Eldora Stock in Colorado was investigated as an analog to elemental transfer in a crystalline repository during heating by waste canisters (Brookins 1986; Wollenberg and Flexser 1986). Oxygen isotope data showed a distinct contrast between the 58-Ma quartz monzonite stock and the Precambrian metamorphic country rock, which Wollenberg and Flexser (1986) interpreted to indicate a lack of hydrothermal convective cooling. No systematic uranium enrichment or depletion was detected in rocks that could be related to distance from the contact (Wollenberg and Flexser 1986), but data were insufficient to ascertain whether uranium mineralization occurred before or after emplacement of the stock.

In contrast to the Eldora stock, intrusion of the Alamosa River, Colorado, stock, a monzonite body that intruded tuffaceous and andesitic volcanic rocks about 30 Ma (Brookins 1984), appears to have established a large-scale convecting hydrothermal system (Brookins 1986). Alteration of the tuffs is observable to 60 m from the contact with the occurrence of calcite intergrown with the rock matrix, chlorite and sericite, quartz overgrowths, and epidote (Wollenberg and Flexser 1986). The contact itself contains a dense intergrowth of epidote, sphene, and fine hematite-filled fractures. Concentration gradients of Cs, Th, and Co in the tuff increase toward the contact, but other trace elements show no indication of migration between the stock and the tuff (Wollenberg and Flexser 1986).

The effects of shallow (less than 500 m) magmatic intrusions into unsaturated host rocks can be quite different from the effects associated with deeper hydrothermal systems (which have been studied more extensively) and of which the two previously mentioned studies are examples. One site in an unsaturated environment was the contact between the Banco Bonito obsidian flow and the underlying Battleship Rock Tuff in a steep-walled canyon on the southwest rim of the Valles Caldera, New Mexico. This has been the focus of a number of analog studies (Krumhansl and Stockman 1988; Stockman et al. 1994). The Banco Bonito flow filled a steep-walled canyon cut in the Battleship Rock Tuff about 400 ka. Present hydrologic conditions are unsaturated. The obsidian, initially at temperatures of 850°C, heated the porous tuff in the canyon walls to 150° to 350°C for decades, and, according to models, vaporized much of the pore water, causing refluxing of water. Contact effects include a reddish baked zone, extending tens of feet into the tuffs. No evidence of hydrothermal alteration was noted, suggesting that the area was unsaturated at the time of contact.

The Valles analog site presents several interesting features. First, the Battleship Rock Tuff is very homogeneous in major- and trace-element composition, so that it would be possible to detect distinct elemental differences caused by heating at the contact. Second, there is no evidence of a later hydrothermal overprint that could blur the effect caused by deposition of the

obsidian flow. Based on a detailed mineralogical, chemical, and isotopic study, Stockman et al. (1994, p. 88) concluded that the overall effects of heating in this unsaturated environment appeared to have been slight and were limited to the tuff nearest the contact. Some evidence existed for devitrification and migration of volatiles in the tuff within 10 m of the contact, but variations in major- and trace-element chemistry were small and difficult to distinguish from the natural variability of these elements in the rock. Apart from devitrification, the principal mineralogic change in tuff near the contact was the development of feldspar-silica linings on voids in the pumiceous-tuff matrix. No significant development of zeolites was found.

The influence of a shallow, basaltic intrusion into pyroclastic deposits at Grants Ridge, New Mexico, was studied by WoldeGabriel et al. (1999). At Grants Ridge, a 2.6-Ma basalt plug intruded into 3.3-Ma nonwelded, pumice-rich, compositionally homogeneous rhyolitic tuff and volcanoclastic sediments. A 10-m-wide aureole, characterized by color variation, contact welding, brecciation, partial melting, and stoping, developed around the 150-m-wide basalt plug. Despite the high-temperature basaltic intrusion, there was no evidence of pervasive hydrothermal circulation and consequent alteration of the country rock that could have occurred had there been extensive, fluid-driven, convective heat transfer. WoldeGabriel et al. (1999) found that the proportion of volcanic glass, volatile species, Fe, and some trace-element and lanthanide-element contents in the host rocks were somewhat depleted at the contact of the intrusion. In contrast, the degree of devitrification and K content were higher along the contact. The authors postulated that vapor-phase expulsion of elemental species could have been responsible for the minor depletion of elements during devitrification of the silicic glass at near-solidus temperature related to the basaltic intrusion.

The WoldeGabriel et al. (1999) study performed finite difference numerical modeling to model the Grants Ridge intrusion as a dry, conduction-dominated system. Model results were compared to an analytical solution and to results using the heat and mass transport code FEHM (Zyvoloski et al. 1992, 1997). Modeling results, which agreed well with geochemical and mineralogical data, indicated that contact welding of the host rocks apparently occurred at temperatures greater than 700°C under a lateral load of approximately 1 MPa, corresponding to the observed depth below the former ground surface of approximately 100 m (WoldeGabriel et al. 1999). Because devitrification is generally enhanced by the presence of aqueous fluids, the abundance of volcanic glass within a short distance (approximately 10 m) from the plug is consistent with the inference that the plug intruded into an unsaturated environment. Although no apparent hydrothermal alteration was recognized in the contact zone, this field study and others like it provide an upper-temperature-bound natural analog to evaluate the effects of heat from decay of radioactive waste. In fact, the temperatures in these studies far exceed the highest temperatures anticipated in a repository. Field and laboratory data from this analog study can also be used to build confidence and to calibrate models of such processes within similar physical and chemical environments.

In the Paiute Ridge area of the Nevada Test Site, late Miocene basaltic magma intruded a sequence of 22- to 11- Ma tuffs (Lichtner et al. 1999, p. 5). The intrusions formed as dikes, sills, and lopoliths. The original depth of the intrusions was on the order of 150 to 200 m (Crowe et al. 1983, p. 266). A contact aureole approximately 3 m wide surrounds the intrusions. Matyskiela (1997) studied alteration surrounding one intrusion, the 50-m-wide Papoose Lake sill, in proposing the Paiute Ridge intrusive complex as a natural analog for thermal-hydrologic-

chemical processes at Yucca Mountain. The analysis by Matyskiela (1997) was based on a pure heat-conduction model. The model results from Matyskiela (1997, p. 1116) indicated maximum temperatures in the tuff host rock of 550°C and cooling times ranging from 10 to 400 years following the intrusive event. These results contrast strongly with much longer cooling times, on the order of several thousand years, calculated by Lichtner et al. (1999, p. 21). The major finding by Matyskiela (1997) was alteration of glass shards to cristobalite and clinoptilolite in the host tuff within 60 m of the intrusion. He interpreted the alteration as being hydrothermal in origin, resulting from emplacement of the intrusion, although he never conclusively demonstrated that the alteration postdated the intrusion. Most significant was his observation of complete filling of pore spaces with silica at fracture-matrix interfaces, thus creating open conduits for infiltrating fluid flow along fractures.

Matyskiela (1997, p. 1117) estimated enhanced fracture-flow in the open conduits to be as much as five times that of ambient conditions. This is opposite to the behavior that would occur with formation of a silica cap, as predicted by simulations conducted for Yucca Mountain (Hardin 1998, pp. 5.57, 5.58), in which fractures would become filled with quartz or chalcedony, thus inhibiting further flow. More recently YMP modeling results based on current fracture porosity estimates indicate no formation of a silica cap (CRWMS M&O 2000c). At issue is the extent to which a fracture can be filled by the silica contained in matrix-pore water. The two-phase numerical simulation results by Lichtner et al. (1999) suggest that at distances of tens of meters from the larger of the Paiute Ridge intrusions his group studied (width greater than or equal to 39 m), prolonged boiling conditions were established for as long as several thousand years. Their analysis assumes that, as pore fluid in the matrix is brought into equilibrium with respect to a particular silica polymorph (e.g., amorphous silica) at boiling conditions, the matrix fluid boils and escapes into the surrounding fracture network. Amorphous silica, with its higher solubility, provides the largest fracture filling, followed by chalcedony and quartz. For the complete sealing of a fracture, only a very small fracture-volume fraction is needed.

Thermal-hydrologic-chemical processes can be better constrained through analysis of selected intrusive complexes hosted in unsaturated tuffaceous rock. The ideal intrusion to serve as a natural analog to thermal-hydrologic-chemical processes anticipated at a Yucca Mountain repository should be emplaced above the water table, should be of sufficient size to produce enough heat to sustain boiling conditions for times on the order of several thousand years (approximately 30 m wide), and should occur in host rock of similar composition and characteristics to the Topopah Spring Tuff. The Paiute Ridge intrusive complex satisfies the first two criteria, but the tuff host rock into which it has intruded is a nonwelded vitric tuff. Nevertheless, this does not exclude it as a meaningful analog.

In summary, in both the Banco Bonito study and the Grants Ridge basalt-intrusion study, the effects of high-temperature intrusions into unsaturated environments appear:

- To have been slight
- To have been limited to within approximately 10 m of the contact
- To show no evidence of fluid-driven convective heat transfer or pervasive hydrothermal alteration of the country rock.

These field studies, along with the Paiute Ridge field studies, provide data for assessment of magmatic intrusions into or near a potential repository. But just as importantly, they provide a limiting, high-temperature-case natural analog for evaluating thermal-hydrologic-chemical processes introduced by decay of radioactive waste in an unsaturated environment.

13.4.1.3 Geothermal Systems

Many processes that are expected to take place under repository conditions are the same as those that occur in geothermal fields. These processes include evaporation, boiling, condensation, one- and two-phase fluid flow, mineral alteration and reaction, mineral precipitation and dissolution, and consequent potential changes in fracture-matrix interaction. Coupled processes related to geothermal systems have been observed, measured, and simulated for more than two decades in the geothermal industry. Data and analyses from geothermal analogs yield important information about expected thermohydrologic conditions at Yucca Mountain and about perturbations caused by thermally induced geochemical and mechanical changes in the rock mass. Geothermal analogs are one of the major ways of building confidence in understanding the thermohydrologic behavior of the repository system, as it is coupled to chemical processes, over long time periods. Data from geothermal fields can be used to test coupled process-modeling codes used by the YMP in order to match observations (e.g., chemical reactions, occurrence of heat pipes) in geothermal fields with those predicted by the code.

The versatility of geothermal reservoir simulators has made possible their application to a wide range of fluid and heat-flow problems. Main areas in which numerical simulation studies have produced significant advances in understanding geothermal systems include the following:

- Pressure decline in the depletion of boiling reservoirs
- Evaluation of boiling and condensation zones
- Reservoir exploitation strategies
- Vapor-dominated and liquid-dominated heat pipes
- Transition from liquid-dominated to vapor-dominated systems
- Natural evolution of hydrothermal convection systems
- Fluid and heat transfer in fractured porous media
- Nonisothermal and two-phase well testing
- Effects of reinjection and natural recharge
- Noncondensable gas effects.

To produce an adequate model, numerical codes must be able to handle processes of heat transfer; two-phase flow under nonisothermal conditions in one, two, and three dimensions (with varying degrees of nonlinearity); coupling of fluid and heat flows; and complex boundary conditions. Modeling of geothermal systems has provided major advances toward this goal, which adds confidence in the numerical models of Yucca Mountain.

Table 13.4-1 compares issues important to assessing coupled processes that may occur at Yucca Mountain and processes that take place in geothermal reservoir systems. Some issues that are important for assessing Yucca Mountain (i.e., water saturation near the heater, localized seepage), have been omitted from the list because they are not of concern in geothermal reservoir engineering. Table 13.4-1 shows geothermal fields that could be used as potential analogs to

study thermal-hydrologic-chemical processes. Corresponding to each issue, geothermal sites are listed that may, upon further evaluation, provide added confidence in modeling thermally coupled processes at Yucca Mountain, using approaches suggested in column 4.

Conflicting conclusions regarding the effect of mineral precipitation on fracture permeability, reported in Section 13.4.1.2 and identified by performance assessment as having uncertainty, point toward thermal-hydrologic-chemical processes as having high priority for additional study in active geothermal systems. Many active geothermal fields throughout the world could serve as potential analog sites to some hydrothermal conditions expected to occur at Yucca Mountain. An appropriate candidate site would have a high similarity factor to Yucca Mountain (Table 13.4-1) and would include features such as temperatures ranging from 25° to 300°C, a broad range of phenomena and features available for study, a range of water chemistries that would bound those expected to occur at Yucca Mountain, a range of hydrologic properties (e.g., porosity, permeability, fracture characteristics) similar to those at Yucca Mountain, water-saturated and unsaturated environments, a suite of hydrothermal alteration minerals similar to those expected to form at Yucca Mountain (e.g., zeolites and clays), evidence of fracture-matrix interactions, an active monitoring system, and access to extensive data sets from the recorded history of the field.

The capabilities and limitations of geochemical modeling codes, such as the solubility, speciation, and reaction-path code EQ3/6 (Wolery and Daveler 1992), and thermodynamic databases have been tested by analyzing natural hydrothermal systems with mineralogical and environmental similarities to Yucca Mountain. One example is the Yellowstone caldera. The Yellowstone caldera closely duplicates characteristics of the volcanic sequence at Yucca Mountain, as well as the temperatures anticipated at the candidate repository horizon. The Yellowstone volcanic sequence is dominated by Quaternary, silicic-welded ash-flow tuffs and rhyolite flows. Geothermal activity is reflected in hundreds of hot springs and geysers that emit waters that have circulated through the volcanic rocks and have formed a variety of hydrothermal mineral assemblages. Using data from 13 U.S. Geological Survey drill cores as a basis for deriving paragenetic sequences of mineral deposition in the Yellowstone geothermal systems, Meijer (1987) conducted preliminary thermodynamic simulations using an early version of EQ3/6. His evaluation suggested that the most significant effects of the thermal pulse on the chemical environment at the repository horizon would be the transport and redeposition of silica along hydrologic and thermal gradients and the precipitation of clays in the groundmass of the devitrified repository host rock. Secondary effects could include the deposition of clays and zeolites in fractures and cavities adjacent to the repository and in the underlying vitrophyre. These horizons should remain stable unless acidic groundwater conditions are generated in association with the repository. Results of the Carey et al. (1997) model of mineral evolution at Yucca Mountain compared favorably with earlier simulations by Meijer (1987).

Bruton et al. (1995) cataloged a survey of literature and data for many geothermal fields as a means of selecting a field-analog site for thermohydrologic-chemical studies. The sites in their survey included many of the better-known geothermal fields: The Geysers, California; Krafla (and other geothermal areas) in Iceland; Cerro Prieto, Mexico; Valles Caldera, New Mexico; Larderello, Italy; Long Valley Caldera, California; Yellowstone, Wyoming; and the Wairakei and Ohaaki-Broadlands fields of New Zealand. Some fields were considered unsuitable because they occur in rock types dissimilar to those at Yucca Mountain, lack sufficient data, have access

problems, or are entirely liquid- or vapor-dominated fields. The geothermal system at Wairakei was endorsed by the YMP as the site most amenable to the study of thermal-hydrologic-chemical processes, because it possesses the greatest number of features similar to Yucca Mountain (Bruton et al. 1995, p. 8), because of logistic practicalities, and because of the potential for collaborative research.

EQ3/6 was used to simulate mineral-fluid relations in Wairakei and other New Zealand geothermal fields (Glassley and Christensen 1992; Bruton et al. 1993). Comparisons between observed mineral assemblages and model simulations of equilibria were used to evaluate the thermodynamic database for various environmental conditions encompassing the possible range of temperatures and water conditions anticipated in a Yucca Mountain repository system. The results of these modeling studies are generally consistent with observed vein and matrix mineral equilibria at Wairakei for fluids at temperatures greater than 240°C. Both field data and model results indicate that stable mineral assemblages can be significantly impacted by small differences in fluid chemistry, temperature, or pressure. Comparison of laboratory data with field data from natural hydrothermal waters at Wairakei for amorphous silica precipitation has shown that significant discrepancies exist between results obtained with different test conditions (Carroll et al. 1995). Rates measured in the field were 400 times faster than those obtained in laboratory measurements. Silica precipitation under repository conditions at Yucca Mountain could exhibit rate behavior somewhere in the range between the laboratory and field experiments.

The results of these studies emphasize two points necessary for use of geothermal systems in model validation. First, the natural systems must be thoroughly understood and quantitatively characterized, if rigorous testing of simulations is to be completed. Second, simulations must be capable of providing predictive results that can be tested in an active field setting. Thus, the chemical and hydrological features associated with actively evolving systems must be amenable to measurement and study, if kinetically controlled systems are to be rigorously simulated.

13.4.2 Unsaturated Zone Flow and Transport

Section 13.4.2 considers the role of the flow and transport of radionuclides in the unsaturated zone under the ambient temperatures of the far field. Examined first are analogs to unsaturated zone infiltration, seepage, and flow, with specific examples, including an analog study at Box Canyon. Analogs to unsaturated zone transport of radionuclides, including a uranium-series study at Peña Blanca, Mexico, are discussed next.

13.4.2.1 Conceptual Model of Unsaturated Zone Flow and Transport at Yucca Mountain

The unsaturated zone at Yucca Mountain is divided into five hydrogeologic units of alternating welded and nonwelded tuffs, with contrasting hydraulic properties. Overlying these tuffs are surficial deposits, designated Quaternary alluvium, and consisting of irregularly distributed deposits of alluvium and colluvium up to 30 m thick. These surficial alluvial deposits may be absent over large areas of the site, particularly on ridgetops and side slopes. The presence or absence of Quaternary alluvium and the slope aspect exert significant control over net infiltration at the site, with areas of thin or absent alluvium conducting moisture rapidly to the underlying tuff.

Underlying the Quaternary alluvium is the Tiva Canyon welded hydrogeologic unit, a moderately to densely welded, devitrified ash-flow tuff that may vary from 0 to 150 m in thickness (Montazer and Wilson 1984, pp. 12, 14). The fractured nature of the Tiva Canyon welded unit and its relatively low porosity may facilitate moisture flux from the surface to below the zone of evapotranspiration. Below the Tiva Canyon welded unit is the Paintbrush nonwelded unit, a 20- to 100-m-thick sequence of partially welded to nonwelded, vitric, and occasionally devitrified, tuffs (Montazer and Wilson 1984, p. 14). Because it has significantly less fracturing and higher storage capability than the welded units, the Paintbrush nonwelded unit may moderate moisture and gas-phase fluxes between the surface and the potential repository horizon.

Underlying the Paintbrush nonwelded unit is the potential repository host rock, the Topopah Spring welded hydrostratigraphic unit. The 290- to 360-m-thick Topopah Spring welded unit is composed of moderately to densely welded, devitrified ash flow tuff. Average porosity of the Topopah Spring welded units is low, except for the vitric caprock and basal vitrophyre. Below the Topopah Spring welded unit is the Calico Hills nonwelded unit, a 100- to 400-m-thick sequence of nonwelded to partially welded ash-flow tuffs. The Calico Hills nonwelded unit is divided into vitric and zeolitic facies. Perched water zones are generally found high in the Calico Hills nonwelded unit at the top of the zeolitic facies or at the Topopah Spring welded unit/Calico Hills nonwelded unit contact.

The deepest of the six unsaturated zone hydrostratigraphic units is the Crater Flat undifferentiated unit, which consists of 0 to 200 m of undifferentiated welded and nonwelded, vitric, devitrified, and zeolitized ash-flow and airfall tuffs. The Crater Flat undifferentiated unit hydrofacies lies above the water table under the western margin and the southernmost half of the potential repository block. Toward the east and north, the unit lies below the water table, as does the Calico Hills nonwelded unit.

Matrix saturated hydraulic conductivities measured on laboratory samples are small for the welded units (on the order of 10^{-10} to 10^{-12} m/s for the Tiva Canyon welded unit; 10^{-11} m/s for the Topopah Spring welded unit) and higher for the moderately welded to nonwelded units (on the order of 10^{-7} m/s for the Paintbrush nonwelded unit; 10^{-9} m/s for the Tiva Canyon moderately welded unit) (Flint 1998, pp. 3-4, 44-45). It is because of high bulk conductivities that fractures are thought to be well connected. Bulk conductivities are higher for the moderately to highly fractured welded units. Estimates of fracture densities for welded units are 10 to 20/m³ (Tiva Canyon welded unit), and 8 to 40/m³ (Topopah Spring welded unit), while moderately welded units range from 1/m³ in the Paintbrush nonwelded unit to 2 to 3/m³ in the Calico Hills nonwelded unit (Montazer and Wilson 1984, pp. 1, 12). The fractures seem to have little interaction with the matrix. High water potentials measured throughout much of the unsaturated zone indicate the absence of strong water potential gradients needed for matrix imbibition of fracture water (DOE 1998a, p. 2-51).

Hydrologic properties of the potential repository block-bounding faults are poorly understood. It is not known whether they act as pathways, or barriers, or are neutral to moisture flow. Based on results of detecting bomb-pulse ³⁶Cl at the potential repository horizon, fault zones may act as fast pathways (see Section 5.3 of this report). Ahlers et al. (1999) showed pneumatic-response data indicating that faults act as fast pathways for gas flow in the Paintbrush nonwelded and Topopah Spring welded units.

Precipitation in the vicinity of Yucca Mountain is approximately 17 cm/yr. (Hevesi et al. 1992, p. 677). Net infiltration is variable but averages approximately 8 mm/yr. (DOE 1998a, p. 2-5). Percolation-flux estimates vary from 0.01 to 21.1 mm/yr., depending upon location and method of estimation, but average around 7 mm/yr. (DOE 1998a, p. 2-5). At the repository horizon, percolation flux ranges from 1 to 20 mm/yr. (DOE 1998a, p. 2-6). Even though the average percolation flux may vary within this range over a scale of tens of meters, local fluxes at the centimeter scale of individual fractures could be many times the average values. The seepage into drifts depends on percolation flux, which may focus flow to cause localized, variable seepage. The key parameter is seepage threshold—the value below which seepage cannot occur. This value has been determined to be 200 mm/yr. (CRWMS M&O 2000a, p. 70).

Percolating water that could penetrate a waste package and contact waste materials could acquire and transport radionuclides, either in solution, suspension, or as colloids. The radionuclide-carrying water would then migrate toward engineered barriers, such as backfill, where it could be retarded before reaching the near-field heated region of the rock surrounding the drift. Gaseous transport is also part of the conceptual model for radionuclide transport, but is not discussed further, because it is difficult to evaluate through natural analogs. Transport of dissolved or colloidal species depends on factors that include the water chemical composition, pH, Eh, and temperature; the type and distribution of mineral fracture coatings (especially sorptive minerals such as zeolites, clays, and Fe/Mn oxides); and the nature and extent of fracture-matrix interaction.

Fracture flow has been shown to be the most likely mode of transport in the Topopah Spring welded unit, but water continuing downward would encounter different hydrologic conditions and flow properties when it reached the Calico Hills nonwelded unit (DOE 1998a, p. 2-38). In some regions of the Calico Hills nonwelded unit, it is expected that percolating water would contact both zeolitic and vitric tuffs. Flow in the zeolitic units would probably retard sorbing radionuclides, such as neptunium, cesium, and strontium. In other areas, perched water zones resulting from low-matrix permeabilities or hydrologic discontinuities may result in lateral diversion. Depending on the extent of the perched zone, water either may be laterally diverted for short distances before returning to the unsaturated zone or flowing vertically down faults, or may continue laterally to the water table, bypassing the lower unsaturated zone.

13.4.2.2 Analogs to Unsaturated Zone Infiltration, Seepage, and Flow

This section examines analogs to unsaturated zone infiltration, seepage, and flow. Section 13.4.2.2.1 presents results of a modeling study that used data from Box Canyon, Idaho, to build confidence in modeling approaches to unsaturated zone flow employed in Yucca Mountain process models. Section 13.4.2.2.2 considers aspects of seepage and flow at Rainier Mesa analogous to those at Yucca Mountain. Section 13.4.2.2.3 addresses aspects of the Apache Leap site that may be used as an analog to processes occurring at Yucca Mountain.

13.4.2.2.1 Box Canyon, Idaho

13.4.2.2.1.1 Introduction

The variably saturated, fractured-basalt hydrogeological system at Box Canyon, Idaho, was chosen for study (CRWMS M&O 2000b) in order to examine the applicability of conceptual and numerical modeling methodologies used at Yucca Mountain to similar hydrogeological systems. Confirmation of the applicability of these approaches at natural analog sites serves to substantiate use of the analogs as predictive tools for the potential Yucca Mountain repository. Box Canyon was chosen for the study, because a considerable body of hydrologic data was available from studies at the Idaho National Engineering and Environmental Laboratory of unsaturated fracture flow in fractured basalts. The studies had been conducted at scales ranging from core sample measurements (centimeter-scale) and meter-scale laboratory tests, to field tests that covered tens of meters, to a kilometer-scale aquifer pumping test. The Box Canyon tests were in the intermediate-scale range.

The Box Canyon site is located on the Eastern Snake River Plain near the Idaho National Engineering and Environmental Laboratory (Figure 13.4-2) and is adjacent to the Big Lost River, a tributary of the Snake River. The Snake River Plain is composed primarily of fractured Quaternary basalt flows, interbedded with sedimentary deposits. Sedimentary interbeds may separate basalt flow units that were formed at disparate times, and their thickness may range from a few centimeters to as much as 15 m. Basalt flow units are comprised of a number of basalt flows from the same eruptive event. Individual basalt flows are from 3 to 12 m thick, elongated in one direction, and 20 to 60 m wide. The total basalt thickness in the Snake River Plain may exceed 3 km (Faybishenko et al. 1999, p. 5; Knutson et al. 1993). The Box Canyon site is located on a basalt flow that is approximately 10 to 12 m thick, with a nearby cliff-face exposure at the Big Lost River. Additional basalt flows underlie the upper basalt flow directly beneath the experimental site.

Several infiltration experiments were conducted at the Box Canyon site to study the flow of water in the variably saturated fractured basalt (Faybishenko et al. 1998, 1999). Instrumentation was used to delineate the subset of fractures that actively conducted the infiltrating water. The purpose of the Box Canyon analog study was to construct and calibrate a numerical model to simulate the observed infiltration behavior of water at the Box Canyon site. The methodology adopted to simulate the Box Canyon site was based on the dual-permeability numerical approach used to characterize variably saturated flow at Yucca Mountain (Bandurraga and Bodvarsson 1999). Hydrogeological parameters used to calibrate the Box Canyon model could then be used to substantiate values for the same parameters obtained during calibration of the Yucca Mountain site. Direct comparison of parameters obtained from Yucca Mountain is problematic at best, given that Box Canyon has a scale of tens of meters, whereas Yucca Mountain is on a scale of thousands of meters. Therefore, upscaling of parameters was an issue. The investigation (CRWMS M&O 2000b) involved identifying physical processes and calibrating parameters controlling the observed infiltration of water at the Box Canyon site.

13.4.2.2.1.2 Geological Model Conceptualization

Conceptualization of the geological model for the Box Canyon site followed directly from Faybishenko et al. (1999). The site consists of layered basalt flows containing horizontal and vertical columnar fractures resulting from cooling of the basalt. The water table (a perched water body) at the Box Canyon site is approximately 20 m below the ground surface (Faybishenko et al. 1999, p. 7). Field data consisted of monitoring pneumatic and infiltration tests almost entirely within the upper-basalt flow, which had an average thickness of 12 m. Columnar cooling fractures, originating from the top and bottom of the basalt, reach an identical spacing where the two cooling fronts met at the dimensionless depth (the dimensionless depth is defined as the depth from the ground surface divided by the thickness of the upper-basalt flow) of 0.6 (Grossenbacher and Faybishenko 1997, p. 7).

The conceptual geological model addressed issues related to the geometry of fast preferential flow paths of infiltrating water in the basalt hydrogeological system. To do this, fractures were identified that actively conducted water during the 1996 and 1997 infiltration tests (Faybishenko et al. 1998, 1999), and these data were then used to determine an interconnected fracture network. The locations in plan view of these water-conducting fracture and borehole intersections are provided in Figure 13.4-3.

13.4.2.2.1.3 Numerical Model Conceptualization

Calibration of the model was performed in two steps, using air-injection and infiltration test data. The conceptual geological model was used to develop a numerical model to simulate the physics of water- and gas-phase advection through the fractured basalt at Box Canyon. The numerical modeling effort was conducted using TOUGH2 (Pruess 1991) with the EOS3 module, which involves both mobile water and gas phases.

The fracture-matrix system of the basalt was simulated using a dual-permeability grid in a manner analogous to that used to simulate the site-scale unsaturated zone flow field at Yucca Mountain. A three-dimensional visualization of the model structure, including the zonation of the upper basalt, inclusion of the rubble zone, and a portion of the lower basalt, is shown in Figure 13.4-4. Two separate views of the model are shown to illustrate the variable thickness of the upper basalt flow. Based on the observations of active water flow features, a conceptual fracture network was constructed and mapped onto a plan view of the mesh. Details on how this was done are explained in CRWMS M&O (2000b).

The fracture network was then used to condition the permeability and porosity of the fracture-continuum nodes that were calculated from the fracture aperture. The fracture aperture was calculated from fitting to the air permeability test data. Weighting factors were used to subjectively increase the permeability and porosity of nodes where flow was actually observed to occur relative to the unconditioned background nodes. Flow of water and gas occurs between the fracture and matrix continuum according to the mass conservation laws discretized by TOUGH2 (Pruess 1991). This formulation is consistent with that used in the dual-permeability simulations of the Yucca Mountain site-scale unsaturated zone flow model.

13.4.2.2.1.4 Pneumatic Test Analysis

Pneumatic tests were conducted at the Box Canyon site (Benito et al. 1998) to assess the permeability of the basalt. The intent of these tests was to delineate vertical variations in the permeability of the upper basalt flow. The pneumatic tests were simulated using the three-dimensional model in order to calibrate the permeability of the fracture continuum nodes. To calibrate the model, only steady-state pressure responses within the injection intervals were used. An initial estimate of fracture permeability surrounding the injection interval for each pneumatic test was obtained using an analytical solution. To calibrate the permeability of the fracture continuum nodes, the injected air is assumed to flow entirely through the fractures. This procedure is consistent with the calibration methodology employed at Yucca Mountain (Huang et al. 1999).

13.4.2.2.1.5 Infiltration Test Analysis

Two sets of infiltration experiments were conducted at Box Canyon in 1996 and 1997 (Faybishenko et al. 1998, 1999). Subsequent analysis of the infiltration experiments involved calibrating hydrogeological parameters in the dual-permeability model of the Box Canyon site to match the arrival times of the infiltration front at various monitoring points (CRWMS M&O 2000b). Simulations were also performed to determine whether the fracture pattern inferred from active water flow features in the subsurface acts to preferentially redistribute the infiltrating water within the computational domain. Furthermore, the model was used to examine the influence of the fracture density zonation within the basalt flow and rubble zone on flow patterns of the infiltrating water. The permeability of the fracture-continuum nodes for the dual-permeability model was taken directly from the pneumatic test calibration (CRWMS M&O 2000b).

Calibration of hydrogeological parameters controlling the infiltration rate of water in the fracture-matrix basalt system involved manually adjusting the porosity of the fracture continuum, the permeability of the matrix continuum, and the interfacial area between the fracture and matrix continua (CRWMS M&O 2000b). These parameters were modified until the infiltration-front arrival times, simulated by the numerical model, matched field data obtained at sampling intervals during the infiltration events. The arrival times of the infiltration front were inferred from the first significant increase in bromide concentration in water samples, taken as part of the tracer tests conducted during each infiltration test. It was assumed that the bromide tracer was conservative and advected at the same velocity as the infiltration front in the fracture continuum. The bromide data were used to constrain parameters controlling variably saturated groundwater flow, but were not used to simulate transport.

The model was calibrated by extracting one-dimensional, vertical columns from beneath the infiltration pond where the bromide data indicated boreholes intersected with fractures that actively conducted water. Fracture continuum porosity was a sensitive parameter controlling the arrival time of the infiltration front. The resulting fracture-continuum porosity for the upper basalt ranged from 0.01 to 0.02.

Results of the analyses of the one-dimensional vertical columns indicated that the ability to simulate preferential flow of infiltrating water in a specific columnar fracture relative to another could be achieved only using the full three-dimensional site model.

Simulation of the three-dimensional infiltration front indicated that the front is relatively uniform, both laterally and vertically. It shows little, if any, influence from either the zoned distribution of hydrogeological parameters in the upper basalt or the fracture network that was meant to channel the flow of infiltrating water. This may be a consequence of equally distributing the water that was observed to infiltrate from the pond during the various infiltration tests to all surface nodes within the perimeter of the pond. Alternatively, the bias applied to the fracture nodes may have provided an insufficient permeability contrast to preferentially channel the infiltrating water as expected.

In general, a consistent set of parameters was obtained that allowed the dual-permeability model to replicate the field data. Although the dual-permeability approach is also applied to explain groundwater flow at Yucca Mountain, the vastly different scales of Box Canyon and Yucca Mountain imply that upscaling is an issue when comparing parameter values.

13.4.2.2.2 Rainier Mesa, Nevada

Rainier Mesa is approximately 20 miles northeast of Yucca Mountain. The Rainier Mesa area contains a number of tunnels that were excavated for the underground nuclear weapons testing program. Before construction of the Exploratory Studies Facility at Yucca Mountain, the hydrogeologic data collected at Rainier Mesa provided the only extensive underground observations in tuff units similar to those of Yucca Mountain.

Rainier Mesa is situated at a higher elevation than Yucca Mountain and has a mean annual precipitation of approximately 320 mm/yr., approximately double the Yucca Mountain mean (Wang et al. 1993, p. 676). About 8 percent of the measured Rainier Mesa mean precipitation was observed to be infiltrating a tunnel constructed in zeolitic tuffs. The seepage was associated with a small number of faults and fractures (Wang 1991, p. 79). These structural features are thought to be a pathway for flow from perched water above the zeolitic horizon (Wang 1991, p. 82). The seepage is geochemically similar to meteoric water (Wang et al. 1993). Tracer tests and tritium samples indicate that the likely rate of fast pathway flow is from 1 to 6 yr. to move from the surface to the water table at a depth of 1,000 m. The travel time is orders of magnitude less than the matrix travel time calculated using measured matrix-sample conductivities. This is supported by measurements of bomb-pulse ^{36}Cl in several samples from one tunnel (Wang et al. 1993, p. 677).

The stratigraphy of both Rainier Mesa and Yucca Mountain consists of alternating welded and nonwelded tuffs. The zeolitic Tunnel Bed tuffs at Rainier Mesa show a range of mineral compositions similar to those in the Calico Hills nonwelded zeolitic tuff at Yucca Mountain. Also, the higher Rainier Mesa mean precipitation is similar to the long-term average predicted for Yucca Mountain. However, the relative thicknesses of the welded and nonwelded tuff units at the two sites differ significantly (Figure 13.4-5). Below the welded tuff caprock at Rainier Mesa lies the approximately 150-m-thick nonwelded Paintbrush Tuff. The bottom third of this unit is extensively zeolitized due to hydrothermal alteration of the tuff shortly after its

emplacement. At Yucca Mountain, the Paintbrush nonwelded unit is mostly vitric, with thin, localized lenses of clays and zeolites. Seepage at Rainier Mesa occurs in tunnels constructed in the zeolites; for the tunnel constructed in nonzeolitized nonwelded tuff, no seepage is observed.

Tuff matrix permeabilities at Rainier Mesa are reported to be a few orders of magnitude higher than those of corresponding units at Yucca Mountain. Since the tuffs at the two sites have similar origins, mineralogy, and porosity, there is no apparent reason why their permeabilities should be different. Wang et al. (1993, p. 676) suggested that the differences could be an artifact of different measurement methods. Now that extensive matrix permeability data are available for Yucca Mountain tuffs, this issue should be readily resolved by repeating the permeability measurement procedure on Rainier Mesa samples by using the same methods.

In spite of differences in thickness of stratigraphic units and reported permeabilities, Rainier Mesa provides one of the best opportunities to study a number of processes analogous to Yucca Mountain. These include the following:

- Episodic pulses, such as those that affect the Paintbrush nonwelded unit
- Flow patterns and percolation fluxes, based on geochemical signatures
- Seepage into drifts
- Sorption in vitric and zeolitic units.

Substantial data already exist that could be applied in the unsaturated zone flow and transport model to evaluate seepage and percolation under wetter climate scenarios. Additional tests would have to be conducted to evaluate sorption and retardation. An aspect of the Rainier Mesa site that affects its suitability as an analog is the perturbation from nearby underground nuclear weapons testing that may have affected the Paintbrush nonwelded unit and increased the number of structural features that act as fast flow pathways. This effect will need to be evaluated before the Rainier Mesa data can be used to develop long-term predictions of the Yucca Mountain response to climate perturbations.

13.4.2.2.3 Other Flow and Seepage Analogs

In addition to the sites discussed above, other locations may be suitable analogs to infiltration and flow processes at Yucca Mountain. One already used in Yucca Mountain analyses is the U.S. Nuclear Regulatory Commission Apache Leap site in Arizona. Saturated and unsaturated flow parameters from tuff at the site were compared to Yucca Mountain data (Wang 1992). Based on the differences between the flow parameters, a relationship between the pore-size distribution index and saturated permeability was developed. The relationship could be applied to test its potential utility in scaling hydrologic parameters of Yucca Mountain faults or fractures, based on measured data from other sites.

Mitchell Caverns is an unsaturated limestone site in the East Mojave National Park, California, where speleothems (mineral deposits created by dripping water) have formed and where the National Park Service reportedly has data pertaining to the rate of speleothem formation and water infiltration. These data may be useful for future confidence-building in seepage models by providing bounds to initial model conditions and by providing a check on seepage threshold.

13.4.2.3 Analogs to Radionuclide Transport in the Unsaturated Zone

Most natural analogs to radionuclide transport are located in saturated environments (e.g., Oklo, Gabon; Cigar Lake, Canada) or in shallow, weathered, saturated or unsaturated sites (e.g., Alligator Rivers, Australia; Bangombé, Gabon). In this section, only three unsaturated zone analogs are considered: the Nopal I uranium deposit at Peña Blanca, Chihuahua, Mexico; the collective northwestern Nevada-southeastern Oregon uranium deposits; and the trace-metal migration study at Santorini, Greece. Other sites that are mainly in the saturated zone, but are subject to weathering under oxidizing conditions in the unsaturated zone, are discussed in Section 13.4.3.

13.4.2.3.1 Natural Analog Studies of Nopal I at Peña Blanca, Mexico

This section summarizes the analysis of data from Peña Blanca, Mexico (CRWMS M&O 2000b) relevant to radionuclide retention in the unsaturated zone. In the analysis model report, new U-series disequilibria data are applied to evaluate this site regarding open- versus closed-system U-series evolution, and recommendations are made for application of information from Peña Blanca to test and build confidence in Yucca Mountain unsaturated zone flow and transport models.

13.4.2.3.1.1 Background Setting

In the 1980s, the Peña Blanca U deposits in Chihuahua, Mexico, were recognized as a possible natural analog for the potential Yucca Mountain repository (Goodell 1985; Murphy 1995). Since that time, the Nopal I deposit at Peña Blanca has been extensively studied by U.S. and European researchers as an analog for evaluating the fate of spent nuclear fuel, associated actinides, and fission products at a geologic repository. CRWMS M&O (2000b) includes a bibliography of natural analog work conducted at Peña Blanca.

The Nopal I uranium deposit represents an environment that closely approximates the potential high-level radioactive waste repository at Yucca Mountain, in the following ways:

- Climatologically, both are located in semiarid to arid regions.
- Structurally, both are part of a basin-and-range horst structure composed of Tertiary rhyolitic tuffs overlying carbonate rocks.
- Hydrologically, both are located in a chemically oxidizing, unsaturated zone 100 m or more above the water table.
- Chemically, the alteration of uraninite to secondary uranium minerals at Nopal I may be similar to the eventual fate of uranium fuel rods in a potential geologic repository like Yucca Mountain (see Section 13.3.2.2.1).

The Peña Blanca uranium district is located in the northern part of the Sierra Peña Blanca, in central Chihuahua, Mexico (Figure 13.4-6), approximately 50 km north of Chihuahua City, Mexico. The region is part of the Chihuahua tectonic belt, which is characterized by northwesterly vergent folds and thrust faults in Mesozoic and lower Tertiary rocks. A regionally

extensive sequence of Tertiary volcanic rock unconformably overlies the older units. The region was affected by north-south-trending normal faulting, which is thought to be the southern manifestation of the Rio Grande Rift tectonism. North-south oriented basin-and-range topography now characterizes the region (Goodell 1985).

The Peña Blanca uranium district consisted of three exploration camps: El Nopal, Margaritas, and El Cuervo. Many of the uranium deposits in the district were drilled or developed by underground or open-pit mining, but there has been no mining activity at Peña Blanca since 1985. Combined, these deposits contained more than 2,000 metric tons of U_3O_8 and constitute the bulk of Mexican uranium sources. The deposits occur close to the eastern edge of the Sierra Peña Blanca range and are generally concentrated in the lower part of the Tertiary volcanic section. Uranium mineralization locally extends downward into the upper part of the Cretaceous limestone.

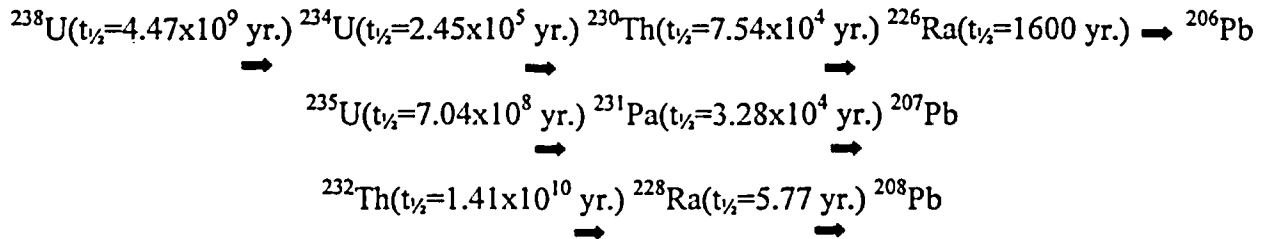
The oldest rocks in the vicinity of the Peña Blanca district are Early to Late Cretaceous reef, back-reef, and basinal, thinly bedded to massive limestones. The limestone is unconformably overlain by a sequence of Tertiary volcanic and lesser sedimentary rocks. From older to younger, these Tertiary units are the Pozos conglomerate and rhyolitic ignimbrite of the Corrales, Coloradas, Nopal, and Escuadra Formations. Locally, the Piloncillos fanglomerate separates the Nopal and Escuadra Formations. The Nopal Formation was dated at 44 Ma (K-Ar age) (Alba and Chavez 1974; Percy et al. 1994).

Nopal I is a small, high-grade uranium deposit located in a highly brecciated zone that occurs at the intersection of two steep faults (Figure 13.4-7). The Nopal I deposit is interpreted to have formed by hydrothermal solutions that precipitated uraninite as they moved through a subvertical, highly fractured zone within welded silicic tuff (Percy et al. 1994, p. 714). This deposit is roughly cylindrical, with approximate horizontal dimensions of 18 m by 30 m, with a nominal ore zone extending approximately 100 m vertically (Figure 13.4-7) (Percy et al. 1995, p. 685). Currently, about 300 metric tons of oxidized uranium remains on site. The upper, highest-grade portion of the deposit is hosted by heavily fractured, silicic tuffs of the Nopal and Coloradas Formations. The deposit extends into the underlying Pozos Formation, although the grade decreases significantly. In the vicinity of the ore body, the Nopal Formation is a densely welded, crystal-lithic rhyolitic tuff, with phenocrysts of quartz, sanidine, and biotite. A highly altered vitrophyre occurs at the base of the formation. The Coloradas Formation is a lithic-crystal, densely welded tuff, with phenocrysts of quartz, sanidine, plagioclase, and biotite.

Uraninite occurs only very locally in highly silicified pods near the center of the ore body. The uraninite is interpreted to be part of a relict ore assemblage that was altered by oxidizing fluids that produced the secondary suite of uranyl oxyhydroxides (schoepite) and uranyl silicates (uranophane) (Percy et al. 1994) (see Figure 13.3-1). Uranophane is the primary ore mineral, but at least seven other uranium-bearing minerals have been identified (Percy et al. 1994). Uranophane occurs as euhedral needles, as well as granular masses in highly oxidized zones that are also enriched in kaolinite, limonite, and chalcedony. As noted in Section 13.3.2.2.1, the sequence of uranium-bearing oxidation products observed at Nopal I is very similar to those produced in laboratory experiments of uranium oxide exposed to oxidizing conditions in the presence of simulated groundwater (Wronkiewicz et al. 1996).

13.4.2.3.1.2 Characterization of Radionuclide Transport Using Uranium-Series Disequilibria

Uranium-series isotope activity ratios can be used to determine the apparent age of samples based on isotopic disequilibria (Ivanovich and Harmon 1992). Samples from Peña Blanca have been analyzed to estimate margin mobility in an environment similar to Yucca Mountain. The relevant decay series are shown below:



13.4.2.3.1.2.1 Previous Work

The Center for Nuclear Waste Regulatory Analyses at the Southwest Research Institute has conducted studies to consider using Peña Blanca as an analog to Yucca Mountain. Many of these studies are discussed in this section.

To determine the relative mobility of uranium along fractures and in the rock matrix, Percy et al. (1993, 1995) mapped and sampled portions of the Nopal I deposit. Fracture mapping carried out at a scale of 1:25, included 11,374 individual fractures. Distribution of uranium in the host tuff, examined at scales ranging from 10^{-6} to 10 m, indicates that uranium occurs outside the primary deposit, mainly along fractures in secondary minerals (iron hydroxides, oxides, and silicates). Uranium-rich caliche, located at an elevation of about 3 m outside the limit of uranium mineral occurrence, has been dated by U-series isochron techniques at 53.6 ± 0.8 ka, suggesting that weathering of the deposit has been the dominant mode of alteration for at least that period (Percy et al. 1994, p. 714). Major conclusions from this work (Percy et al. 1995), based on both field study and ${}^{234}\text{U}$ analyses, include the following:

- Transport of uranium away from the deposit occurred mainly along fracture paths.
- Transport along mesofractures (aperture greater than 1 mm and trace length greater than 10 m) (Percy et al. 1995, p. 693) occurred at 20 times greater distance (up to 30 m) than along microfractures (aperture less than 1 mm).
- Mobilization of uranium from the deposit occurred within the last 1 m.y.
- Matrix transport was limited to distances of less than 1 mm.

Prikryl et al. (1997) reported electron microprobe analyses of uranium concentration in fracture-filling minerals, as well as ${}^{238}\text{U}/{}^{234}\text{U}/{}^{230}\text{Th}$ alpha spectrometry data on bulk-fracture samples from the major east-west trending fracture at 13.5 m north (fracture B in Figure 13.4-8). Uranium concentrations in bulk-fracture materials and in goethite and hematite show a decreasing trend away from the ore body. This trend suggests that uranium was mobilized and transported away from the deposit, most likely by episodic infiltration of meteoric water.

Uranium and Th isotopic data on the 13.5 m north fracture also revealed a $^{234}\text{U}/^{238}\text{U}$ ratio greater than unity, both within and outside the deposit. This suggests that uranium mobilization was relatively recent (less than 1 Ma) and is related to uptake of uranium from fracture fluids that carried excess ^{234}U . Variations in $^{234}\text{U}/^{238}\text{U}$ were interpreted as resulting from a multistage mobilization process.

Pickett and Murphy (1997) obtained additional $^{238}\text{U}/^{234}\text{U}/^{230}\text{Th}$ data for other fractures at Nopal I. Most of their data for fracture-filling materials plots in the forbidden zone (e.g., Figure 13.4-9), which is the region on a Concordia diagram where there is no finite single-stage age solution. Pickett and Murphy (1997) explained the data by invoking multiple U-mobilization events, involving both enrichment and removal, over the past few hundred thousand years. Three samples of uranophane gave $^{238}\text{U}/^{206}\text{Pb}$ and $^{235}\text{U}/^{207}\text{Pb}$ internal and external isochron ages of 3.4 and 3.2 m.y., respectively (Pickett and Murphy 1997). The isotopic and chemical data indicate the following history:

- Primary uraninite mineralization occurred approximately 8 Ma.
- Deposition of uranyl silicates occurred during a single period around 3 Ma.
- Complex episodic uranium mobilization and remobilization, including dispersion of uranium via aqueous transport into the surrounding fractured tuff, took place over the past few hundred thousand years.

Complementary to studies of fracture-filling materials, Pickett and Murphy (1999) recently presented measurements of U-Th isotope composition and concentration in samples from perched water, seep water, and groundwater collected near the Nopal I uranium deposit. The U and Th concentrations generally correlate with concentrations of major cations and anions and total conductivity, which may reflect evaporation followed by dilution or rock dissolution effects on all of these species. Thorium and U concentrations also correlate strongly with each other. Pickett and Murphy (1999) interpret these concentrations in the context of solubility control by various uranium silicate minerals (haiweeite, soddyite) and thorianite.

Activity ratios for $^{234}\text{U}/^{238}\text{U}$ are highest for the seep water (2.85 to 5.07), lower for the perched water (2.19), and still lower for the groundwater (1.39) (Pickett and Murphy 1999, pp. 4 and 7). A positive correlation between $1/\text{U}$ concentration and $^{234}\text{U}/^{238}\text{U}$ for the perched and seep waters is consistent with selective leaching of ^{234}U in dilute seep waters versus greater dissolution for the perched waters. This interpretation is also consistent with results for the major element concentrations and Th. Activity ratios for $^{230}\text{Th}/^{232}\text{Th}$ are also highest for the seep water, which, along with the higher $^{234}\text{U}/^{238}\text{U}$, may reflect greater influence of selective leaching and recoil effects. Activity ratios for $^{230}\text{Th}/^{234}\text{U}$ are quite low (less than 0.01) relative to typical values in the rock of 1 to 1.5, indicating that thorium is significantly less mobile than uranium (Pickett and Murphy 1999, p. 8).

Wong (1998) studied U-series disequilibria using gamma spectrometry for fracture-filling materials at Nopal I. The $^{230}\text{Th}/^{238}\text{U}$ and $^{226}\text{Ra}/^{230}\text{Th}$ activity ratios ranged from 0.58 to 1.74 and 0.85 to 1.54, respectively (Wong 1998, pp. 87, 93). Samples with higher uranium concentrations within the deposit had narrower ranges in $^{230}\text{Th}/^{238}\text{U}$ and $^{226}\text{Ra}/^{230}\text{Th}$ with activity ratios of

approximately 1.0 to 1.2 and 0.87 to 1.2, respectively. Because errors in gamma spectrometry data are fairly large (± 10 percent or more; this is the reason for error bars on Figure 13.4-9), it is difficult to draw strong conclusions from these data. However, the observations of disequilibria for both $^{230}\text{Th}/^{238}\text{U}$ and $^{226}\text{Ra}/^{230}\text{Th}$ led Wong to conclude that there had been open-system behavior for these nuclides—within the past 8 k.y. for Ra/Th and within the past 300 k.y. for Th/U.

Using electron paramagnetic resonance, Allard and Muller (1998) tested the potential use of point-defect centers (essentially, radiation damage from absorbed dose) in kaolinite to detect uranium mobilization. They compared integrated defects to current uranium distribution to infer the past distributions of uranium at Peña Blanca. This investigation indicated two major migration events:

1. Past accumulation of uranium outside the mineralized zone, followed by leaching
2. A late-stage accumulation of uranium in the area of the primary uranium deposit.

Previous work on U-series thermal ionization mass spectrometry by YMP found closed-system behavior in fracture-filling material for U, Th, and Pa for the last 100 to 400 k.y. (Murrell et al. 1997). In an effort to settle the apparent discrepancies with Pickett and Murphy's (1997) results and to learn the extent of uranium mobility at Peña Blanca, additional samples were analyzed from four prominent uranium mineralized fractures emanating into surrounding silicic tuff.

YMP measured ^{238}U - ^{234}U - ^{230}Th - ^{226}Ra and ^{235}U - ^{231}Pa in 18 samples obtained from the Center for Nuclear Waste Regulatory Analyses from fractures that emanate from the primary U-bearing zone of the deposit. Details of sample preparation are provided in CRWMS M&O (2000b). All samples were analyzed by thermal ionization mass spectrometry.

13.4.2.3.1.2.2 New Uranium and Thorium Isotopic Results

Results for uranium and thorium isotopes for the samples and standards are provided in CRWMS M&O (2000b). The sampling locations referred to in this section are shown on Figure 13.4-8. Uranium concentrations for the samples generally decrease from the outer margin of the deposit to the far end of the fractures, in general agreement with prior studies (Pearcy et al. 1995; Wong 1998). The absolute concentrations for the powders agreed well with the results obtained by Pickett and Murphy (1997).

The $^{234}\text{U}/^{238}\text{U}$ activity ratios are shown in Figure 13.4-10 and range from 0.94 to 1.49, with a mean of about 1.2. There is no obvious systematic spatial trend for these data within the fractures. These results are also similar to values reported by Pickett and Murphy (1997, p. 118). The $^{234}\text{U}/^{238}\text{U}$ results are generally consistent with an old ^{234}U enrichment (approximately 100 to 1,000 ka) (Ivanovich and Harmon 1992, p. 77), produced during dissolution processes and preserved in precipitated minerals. However, as can be seen from Figure 13.4-10, there appears to be a small-scale, post-depositional loss and gain of ^{234}U to the fracture materials that have spread the distribution about the mean.

Figure 13.4-9 has been modified from Pickett and Murphy (1997) by the addition of typical error bars and data (shown as orange dots) from Murrell et al. (1997). Pickett and Murphy (1997) used decay-counting methods. Murrell et al. (1997) used more precise thermal ionization mass spectrometry. In this type of plot, known as a Concordia plot, the evolution of a closed system through time is shown by the curved arrow labeled "time." Most of the data of Pickett and Murphy (1997) fall in the "forbidden zone," the region of no finite, single-stage age solution. These values led Pickett and Murphy (1997) and Wong (1998) to invoke multiple U-mobilization events involving both U-enrichment and removal over the past few hundred thousand years to explain their data. The values that fall in the forbidden zone are a consequence of their higher $^{230}\text{Th}/^{234}\text{U}$ and variable $^{226}\text{Ra}/^{230}\text{Th}$ measurements, which cannot be explained by a simple model of closed system evolution.

The $^{230}\text{Th}/^{234}\text{U}$ activity ratios measured by Murrell et al. (1997) are generally close to 1 and fall along the curved time arrow. These values differ significantly from those obtained by Pickett and Murphy (1997). These latter values are difficult to discern from secular equilibrium using the decay-counting methods employed by previous studies. This difficulty may be the reason for the difference between the more precise thermal ionization mass spectrometry data and Pickett and Murphy's (1997) results and conclusions. Because the thermal ionization mass spectrometry data are more precise, the closed system interpretation is preferred.

Because the fracture minerals were deposited by aqueous solutions, the ages of the mineral phases are related to the timing of the primary fluid flow. Subsequent alteration of these mineral phases during more recent fluid movement can also be evaluated using U-series disequilibria data. As shown in Figure 13.4-11, the majority of the U-Th data provide finite solutions to the age equation, and, although most points plot very near the forbidden zone, only two points actually fall in this area. The data for these two samples are consistent with the small amounts of ^{234}U loss. Model U-Th ages for the other samples indicate ages of greater than 300 k.y., with the exception of discordant sample NOPI 320, at an age of 88 k.y. which also indicated ^{234}U loss.

The U-Th ages are calculated using zero initial ^{230}Th in the samples. While this is a reasonable assumption for these samples, since their U concentrations are so high, a correlation observed for fracture B is related to the Th/U of the sample, with highest ages for samples with the lowest authigenic component and greatest Th/U. Since the ages appear to be affected by the relative abundances of authigenic and nonauthigenic components in the samples, a correction is needed to obtain an age for only the authigenic component (Ivanovich and Harmon 1992). The measured Th/U ratios were used to correct the measured $^{230}\text{Th}/^{234}\text{U}$ and $^{234}\text{U}/^{238}\text{U}$ ratios for the nonauthigenic component within these samples. Based on these ratios, the calculated age for the authigenic component is 425 ± 80 k.y. (based on 7 data values). Based on this age, initial $^{234}\text{U}/^{238}\text{U}$ activity ratios are approximately 2, in reasonable agreement with typical values for the modern water samples near Nopal I (Pickett and Murphy 1999). While this isochron age for fracture B agrees with the uncorrected data from sample NOPI-418 (398 ± 20 k.y.), the sample with the highest U concentration, the fit is not exact, suggesting that there have been small degrees of secondary ^{234}U redistribution along the fracture that have disturbed, but not completely reset, the isochron.

The $^{231}\text{Pa}/^{235}\text{U}$ activity ratios are either at, or very near, secular equilibrium (sample mean = 0.996 ± 0.007 [CRWMS M&O 2000b]). Analytical errors are smaller than the data points and

are typically less than 1 percent. This means that $^{231}\text{Pa}/^{235}\text{U}$ (and ^{238}U since the 238/235 ratios are natural) have behaved as a closed system in the fractures over the last 200 k.y. From these observations, it can be concluded that U (235, 238) has remained in the fractures over the last 200 k.y. Based on these results, the mobility of U discussed above seems limited to ^{234}U .

One sample (NOPI-320) is younger, with a U-Pa model age of 47 ± 2 k.y. This sample also has an anomalously low U-Th model age of 88 ± 4 k.y. The U-Pa model age is similar to U-Th ages for caliche (Pearcy et al. 1995, p. 714) and opal of about 50 k.y. This event caused a resetting of sample NOPI-320 but had no measurable effect on ^{235}U or ^{238}U , Th, or Pa mobility in the vast majority of fracture samples.

The $^{226}\text{Ra}/^{230}\text{Th}$ activity ratios range from 0.7 to 1.1 (CRWMS M&O 2000b). These results are similar to values reported by Wong (1998, pp. 87, 93). The $^{226}\text{Ra}/^{230}\text{Th}$ results are consistent with open-system radium behavior and demonstrate that fluids have occupied the fractures over the last 5 k.y., which implies that U has had ample opportunity for fluid interactions. Furthermore, a variety of plant (*Phacelia robusta*) growing in the vicinity has very high radium content (Leslie et al. 1999, p. 833).

13.4.2.3.1.3 Discussion and Conclusions of Uranium-Series Analyses

Transport of U-series nuclides at Peña Blanca has occurred over a range of time scales. From the U-Th age data, it appears that the primary transport of U to the fractures occurred more than 300 ka. Subsequently, there has not been significant ^{238}U or ^{235}U redistribution. The $^{231}\text{Pa}/^{235}\text{U}$ activity ratios for the fracture samples support this conclusion. Results for one anomalous sample, along with U-Th ages for opal and caliche, suggest enhanced aqueous fluxes at approximately 50 to 90 ka and local uranium mobility. The enhanced flux had no effect on ^{235}U or ^{238}U , Th, or Pa distribution in the remainder of the fracture samples. The $^{226}\text{Ra}/^{230}\text{Th}$ activity ratios indicate redistribution of radium within the last 5 k.y. as a result of secondary fluid events. The fluid events appear to have also produced small redistributions of ^{234}U . Presumably, this reflects the preferential mobility of ^{234}U resulting from selective leaching and direct-recoil effects. Such effects are well documented in rock-water systems (e.g., Ivanovich and Harmon 1992). In an analog sense, this stability should extend to transuranics and the lanthanide elements. The high mobility of Ra is also remarkable and should be considered in modeling transport of strontium and cesium.

The 300-k.y. stability of ^{235}U , ^{238}U , Th, and Pa in the fracture-filling minerals has apparently survived even recent hydrologic disturbances from surface-water infiltration of the fracture because of mining activities, as well as the infiltration of rainwater, since the fractured rock was uplifted above the water table (Pearcy et al. 1994, p. 714). Hence, U, Th, and Pa in secondary fracture materials appear to be unaffected by surface-water infiltration and, perhaps, saturated groundwater flow over approximately 100-k.y. time scales.

The two data sets discussed above (Pickett and Murphy 1997; Murrell et al. 1997) directly contrast with each other in their final interpretations. The major implication of the Pickett and Murphy (1997) and Wong (1998) data is that the host rhyolitic tuffs around Nopal I have not effectively retained the uranium mobilized from uraninite alteration. In contrast, the more precise thermal ionization mass spectrometry data (Murrell et al. 1997; CRWMS M&O 2000b)

indicate that the geochemical system at Nopal I restricts actinide mobility in the unsaturated environment. By analogy, the tuffs at Yucca Mountain should have similar retentive properties to impede oxidized uranium mobility. The accumulation of natural analog data from Peña Blanca and similar sites would be of particular importance if they demonstrate the general validity (or lack thereof) of low actinide mobility in unsaturated siliceous tuffs under semiarid climate conditions.

13.4.2.3.2 Uranium Deposits in Northwestern Nevada and Southeastern Oregon

The McDermitt caldera uranium deposits, and other uranium deposits in northwestern Nevada and southeastern Oregon, have been suggested as possible analogs to potential radionuclide transport processes at Yucca Mountain (Alexander and Van Luik 1991) and were the focus of a field trip by YMP representatives in 1995. As a follow-up, Castor et al. (1996) compared features of 16 of the deposits, five of which are located in settings having a thin vadose zone. These are the Moonlight, Bretz, and Opalite mines of the McDermitt caldera, Virgin Valley deposits of northwestern Nevada, and Painted Hills deposits near Reno, Nevada (Figure 13.4-12). Mines in the Lakeview and Steens Mountain uranium districts of southeastern Oregon all occur in saturated rhyolite flows, bedded tuff, or mafic volcanic rock. Mineralization of the McDermitt caldera is discussed in Wallace and Roper (1981). More details on these deposits can be found in Castor et al. (1996).

Tuffs in the McDermitt caldera and Virgin Valley are 15.7 to 16.5 Ma (Castor et al. 1996). Distance to the water table is 38 to 50 m. At the Moonlight Mine, uranium deposition has occurred along faults. Host rocks are dacite flows and rhyolite ash-flow tuffs in the footwall and biotite rhyolite breccias in the hanging wall. Ore deposition was associated with epithermal fluids and occurs mainly in the rhyolite breccias. The Moonlight Mine is the only area at McDermitt with recorded U production (approximately 700 kg of U_3O_8 , with an average grade of approximately 0.13 percent U_3O_8) (Dayvault et al. 1985, p. 383).

At the Bretz and Opalite mines, mineralization is associated with mercury (1.6 percent Hg) in hot springs and caldera ring-fracture faults in silicified breccia. Uranium deposition is genetically related to magmatic systematics in Virgin Valley and is associated with airfall and minor ash-flow tuffs and lacustrine sediments (including diatomite and lignite). Stratiform opal deposits contain uranium, which is also found along fractures in rhyolitic breccia. In the Painted Hills district near Reno, Nevada, uranium mineralization is associated with late-stage mineralization within a caldera. Notable concentration is found at the contact between rhyolitic ash-flow tuff and a basalt dike, and as fracture-filling in the tuffs. Of the sites discussed above, zeolites are observed only in the Virgin Valley area but have been reported at the Bretz and Moonlight mines (Castor et al. 1996). In all of the deposits mentioned, uranium is found as U^{+6} ; only at the Moonlight Mine is it also found as U^{+4} , in association with zircon.

Some of the uranium mineralization at McDermitt caldera and the other northern Nevada deposits may seem to be good analogs to aspects of radionuclide transport at Yucca Mountain, but this is questionable for several reasons. One reason is that the host volcanic rocks for these deposits are somewhat different (i.e., peralkaline rhyolite and trachyandesite flows, bedded tuffs, lacustrine sediments, and basalt dikes). Another reason is that the uranium mineralization is fine-grained and low in concentration in these deposits. Age of deposition is poorly constrained

for most of the deposits. Drilling has taken place in only two of the areas, which could provide solid samples for analyses; hydrologic data are sparse. Previous characterization has included the geologic setting of uranium deposition, uranium oxidation state, primary and secondary mineral assemblages, and water chemistry for a few locations (Table 13.4-2).

Furthermore, the origin of the Virgin Valley and Painted Hills deposits is uncertain. Deposition by ascending fluids along dike barriers is suggested for Painted Hills, since mineralization occurs almost exclusively along footwalls of mafic dikes. At both the Painted Hills deposits and at Virgin Valley, evidence suggests remobilization and redeposition of uranyl minerals to account for local enrichment. Source-term information needed for models is lacking. In spite of their appealing proximity to Yucca Mountain for ease of study, the northern Nevada uranium deposits would require extensive additional characterization before data could be used, in any sense, for building confidence in flow and transport process models.

13.4.2.3.3 Akrotiri, Santorini, Greece

Murphy et al. (1998) conducted a study of trace-element transport at the Akrotiri archaeological site on the island of Santorini, Greece, to evaluate the use of natural analog data in support of long-term performance-predictive modeling for a potential Yucca Mountain repository. This analog study produced primarily qualitative results. Akrotiri is similar to Yucca Mountain in its silicic volcanic rocks, dry climate, and oxidizing, hydrologically unsaturated subsurface conditions. Bronze and lead artifacts were buried under 1.5 to 2.0 m of volcanic ash 3.6 ka (1645 B.C.) (Murphy et al. 1998) by the Minoan eruption.

The Minoan eruption buried settlements under 30 m of volcanic sediment. Evidence for a plume of copper, tin, and lead was indicated through selective leaching of packed earth and bedrock samples collected directly beneath the site where bronze and lead artifacts were excavated. Field data indicated that little of the bronze material had been transported away from its primary location. Original textures and patterns were preserved in fine detail, even on artifacts that were apparently crushed by compacting volcanic ash. The total amount of copper predicted to have been removed from the artifacts is approximately 38 cm³, roughly three orders of magnitude smaller than the volume of the artifacts (Murphy et al. 1998, p. 273). Neither copper nor lead was detected below a depth of 45 cm.

A numerical model of elemental transport was developed that used geological characteristics and hydraulic properties of the enclosing tuff. The well-constrained location of the contaminant source, well-constrained time scale for transport processes, and relatively well-known physical characteristics of the site facilitated development of the transport model. Some of the model results were qualitatively consistent with the field data, including the small amount of material transported, limited amounts of sorbed material, and relatively elevated sorption on a packed-earth layer. System heterogeneity and complexity also played an important role in the distribution of contaminants on solids in the excavated area. The Akrotiri study shows preservation of artifacts for a long period of time in an oxidizing environment, leading Murphy et al. (1998) to conclude that unsaturated systems in arid environments may provide favorable sites for geologic disposal of radioactive waste.

13.4.2.4 Summary of Unsaturated Zone Transport Analogs

Although aspects of some uranium deposits in northwestern Nevada may be suitable for study as analogs to unsaturated zone transport at Yucca Mountain, considerable additional site characterization would be required at all of them before the strength of the analogy could be demonstrated. Both the Peña Blanca and Akrotiri sites demonstrate that arid, unsaturated, oxidizing environments may provide suitable conditions for limiting the migration of radionuclides and metals over thousands of years. Peña Blanca further shows that migration of U-series isotopes has been limited at Nopal I over the past 300 to 400 k.y., with only small amounts of migration along fractures.

13.4.3 Saturated Zone Flow and Transport

Section 13.4.3 considers analogs to saturated zone flow and transport at Yucca Mountain. First, natural analogs are considered at six sites: Alligator Rivers, Poços de Caldas, Oklo, Bangombé, Tono, and Palmottu. Various anthropogenic sites in Russia, Ukraine, and the United States are then examined.

13.4.3.1 Conceptual Model of Saturated Zone Flow and Transport

The water table near the potential Yucca Mountain repository block is currently at an elevation of approximately 730 m, more than 300 m below the potential repository horizon (DOE 1998a, p. 2-56). Water infiltrating the unsaturated zone becomes recharged to the regional flow system. Water moves generally southeast beneath the site before flowing south out of the volcanic rocks and into the thick valley fill of the Amargosa Desert. The hydraulic gradient is very low (approximately 0.0001) (Fridrich et al. 1994) downgradient from Yucca Mountain so that the travel time of groundwater may be long. Near Yucca Mountain, volcanic rocks up to several thousand meters thick cover the Paleozoic and older rocks of the region (DOE 1998a, p. 2-58). Their hydrologic properties change dramatically over short distances, which produces a complex hydrogeology. The volcanic rock section becomes thinner to the south and is not an important component of the saturated zone flow system in southern Amargosa Valley, where the major aquifer consists of Quaternary-Tertiary heterogeneous valley-fill deposits.

The dominant regional aquifer is the carbonate aquifer. This consists of Paleozoic marine limestones, dolomites, and minor clastic sediments that are thousands of meters thick. Fractures enlarged by dissolution provide the large permeability associated with this aquifer, which underlies most of the Ash Meadows and part of the Alkali Flat-Furnace Creek subbasins that make up the regional saturated zone flow system. In the Yucca Mountain area, the carbonate aquifer is not tapped as a groundwater source because of its great depth below the surface (DOE 1998a, p. 2-58).

Luckey et al. (1996) divided the volcanic rocks below the water table into four hydrogeologic units. From top to bottom, these are the upper volcanic aquifer, the upper volcanic confining unit, the lower volcanic aquifer, and the lower volcanic confining unit. The upper volcanic aquifer is composed of the Topopah Spring Tuff, which occurs in the unsaturated zone near the repository, but is also present beneath the water table to the east and south of the potential repository and in Crater Flat. The upper volcanic confining unit includes the Calico Hills

nonwelded unit and the uppermost, unfractured part of the Prow Pass Tuff, in areas where they are saturated. The lower volcanic aquifer includes most of the Crater Flat Group (Luckey et al. 1996, p. 18-20), and the lower volcanic confining unit includes the lowermost Crater Flat Group and deeper tuffs, lavas, and flow breccias. The upper volcanic aquifer underlying Yucca Mountain is generally productive and provides a groundwater source for the site. The main distinction between saturated zone volcanic aquifers and confining units is that the aquifers tend to be more welded and contain more permeable fractures. However, alteration of the tuffs to zeolites and clays, which reduces permeability, is more pronounced at depth, where greater pressure reduces fracture permeability.

The chemistry of saturated zone waters beneath Yucca Mountain (Oliver and Root 1997) reflects processes that affected these waters as they flowed to the Yucca Mountain area from recharge areas to the north (McKinley et al. 1991). In general, these dilute, sodium-bicarbonate waters are neutral to mildly alkaline and mildly oxidizing. Similarities between the composition of saturated zone waters in the recharge areas north of and beneath Yucca Mountain suggest that water compositions primarily reflect water-rock interactions in the recharge areas (DOE 1998a, p. 2-60).

After reaching the water table, flow continues downgradient (generally to the southeast) away from the repository. The majority of saturated flow occurs in zones with enhanced permeabilities caused by fractures. Retardation processes, such as sorption, matrix diffusion, and dispersion, would also function in the saturated zone. Water may contact sorbing zeolites in the Calico Hills and Prow Pass tuffs, and, as in the unsaturated zone, fracture minerals may have a significant effect on both the hydrology and transport properties of the repository system.

At Yucca Mountain, the major control on fracture mineralogy is the location above or below the water table. Fracture minerals in the unsaturated zone are more varied than in the saturated zone. Fracture minerals in the unsaturated zone include clays, zeolites, manganese oxides, hematite, calcite, fluorite, opal, and the silica polymorphs (cristobalite, tridymite, and quartz) (Carey et al. 1997). Calcite and opal are the most characteristic fracture minerals deposited by percolation in the unsaturated zone. Below the water table, the variety of fracture minerals decreases. Smectite is the only common clay. Manganese oxide minerals occur, and hematite is more common than in the unsaturated zone. The only common silica minerals in saturated zone fractures are quartz and opal-CT. The only common zeolites in saturated zone fractures are clinoptilolite and mordenite, the same zeolites that characterize the altered-rock matrix below the water table (Carey et al. 1997). The differences between saturated zone and unsaturated zone fracture mineralogy may affect transport properties above and below the water table (Vaniman and Chipera 1996). Laboratory experiments have shown that fractures containing smectite, manganese oxides, and calcite show particular affinity for plutonium retention (DOE 1998a, p. 2-66).

13.4.3.2 Natural Analogs of Saturated Zone Flow and Transport

Section 13.4.3.2 discusses some of the major analog studies that have been conducted in saturated environments. All occur in uranium ore deposits and rare-earth (lanthanide) deposits in varying types of host rocks. The sites are relevant to the degree that they demonstrate something about the potential transport of radionuclides in particular environments. Sites in strongly

reducing environments, such as Tono, have little relevance to groundwater conditions at Yucca Mountain, but the uranium deposits that display a redox front (e.g., Poços de Caldas, Oklo, and Palmottu) or that are subject to weathering and periodic influx of water (e.g., Alligator Rivers and Bangombé) are somewhat more relevant. The saturated zone transport analogs that are perhaps most relevant to Yucca Mountain are the anthropogenic analogs that are discussed in Section 13.4.3.3.

13.4.3.2.1 Alligator Rivers, Australia

The Alligator Rivers Analog Project, 1987 to 1992, involved agencies from five countries (including the U.S. Department of Energy [DOE] Office of Civilian Radioactive Waste Management) under the auspices of the Organization for Economic Cooperation and Development, Nuclear Energy Agency. The Alligator Rivers Analog Project was an investigation of the Koongarra secondary enriched-uranium deposit in the Northern Territory of Australia (Figure 13.4-13). Investigations at Alligator Rivers were designed to study the migration of radionuclides away from a uranium deposit so that it could be used as an analog to migration from a waste repository. The Alligator Rivers Analog Project focused on the Koongarra deposit because it contains high uranium concentrations, its hydrology has been undisturbed by mining, and elemental migration has occurred. The Alligator Rivers uranium deposits are the most significant mineralization in the Pine Creek Geosyncline, which comprises an approximately 14-km thickness of Lower Proterozoic metasediments (carbonaceous shales, sandstones, and carbonates), together with interlayered tuffs that were deformed and metamorphosed around 1,800 Ma (Airey 1986). These Lower Proterozoic rocks rest on late Archean granites and are overlain by the Kombolgie Sandstone of Middle Proterozoic age. The uranium deposits lie at the base of the Cahill Formation schists and are located in extensively chloritized zones adjacent to massive dolomites (Figure 13.4-14).

Numerous reports and papers discussing the analog characteristics and project goals have been published (e.g., Duerden et al. 1987; Hardy and Duerden 1989; Airey and Ivanovich 1985; Airey et al. 1987; Airey 1986). Results from the Alligator Rivers Analog Project were presented at the Fifth Natural Analog Working Group Meeting (von Maravic and Smellie 1994).

The Koongarra uranium deposit was discovered in the early 1970s by airborne geophysical measurements. More than 40 boreholes were drilled to characterize the ore body. The deposit was never exploited and, hence, is relatively undisturbed. The natural analog study had two broad objectives: to investigate the processes leading to the decomposition and leaching of the primary ore (uraninite and pitchblende) and to investigate the processes of radionuclide transport and retardation in the system, including the effect of colloids. As part of this program, techniques for in situ distribution coefficient measurements were improved as was testing of thermodynamic solubility and speciation codes.

The Koongarra ore body lies in two distinct parts, separated by a barren zone. The two parts are composed of uraninite- and pitchblende-bearing veins within a zone of steeply dipping, sheared, quartz-chlorite schists and a fault that brings the ore body in contact with the Kombolgie sandstone (Figure 13.4-14). The primary ore at depth is being leached by groundwater to form a secondary mineralization (Isobe et al. 1992) that extends from the ground surface to the base of

the weathered zone at about 30 m. This leaching process has resulted in the ore body, and the region above it, forming four zones:

1. The primary ore of uraninite and pitchblende
2. A uranium silicate zone formed by in situ alteration of the primary ore
3. A zone of secondary uranyl phosphate minerals that are currently being leached by the groundwater
4. A shallow dispersed uranium zone, with the uranium in association with clays and iron oxyhydroxides.

Distinctive zones of weathering are apparent at Koongarra, differing only in the relative intensity of weathering. As a result of the weathering front, a dispersion fan has developed in the weathering zone, where uranium has been mobilized. Secondary minerals are found as far as 50 m downstream from the ore body, with detectable concentrations of U-series nuclides for about 300 m downstream in the dispersion fan. The age of the dispersion fan has been estimated from 0.5 to 3.0 m.y., with a median age in the range of 1 to 1.5 m.y. (Golian and Lever 1992, pp. 245 to 250). These estimates are based on a number of assumptions about the variation of the U addition to the fan over time.

The uppermost of the four weathering zones (above approximately 20 m) is the most weathered. Here, chlorite has been altered to kaolinite, minor amounts of smectite, hematite, and various iron oxyhydroxides. A transitional zone (20 to 25 m) of less-weathered rock consists predominantly of vermiculite derived from primary chlorite (present below approximately 24 m) and altering to kaolinite and iron oxides. Weathering of the quartz-chlorite schist produces different mineral assemblages according to the degree of alteration. The migration behavior of nuclides at each depth is thought to be related to the chlorite alteration mineral assemblage (Ohnuki et al. 1990). The zone of lowest uranium concentration corresponds to the chlorite-rich zone, that of intermediate U concentration to the vermiculite-rich zone, and that of the greatest uranium concentration to the kaolinite-rich zone. The highest uranium concentrations in the dispersion fan are associated with the lower part of the kaolinite-weathered zone (Ohnuki et al. 1990; Isobe et al. 1992; Murakami et al. 1997, pp. 889 to 897).

Isobe et al. (1992) describe uranium redistribution associated with weathering. Uranium activity closely follows oxidation fronts in the slightly weathered zone and advances most readily along cracks and fissures in which percolation of oxidizing groundwater is most enhanced. Significant flow occurs as fracture flow, rather than as porous media flow. Uranium distribution in the most strongly weathered rocks depends only on the mineralogy present and is not controlled by the presence of fissures, as is the case for the more moderately weathered rocks. In the dispersion fan, processes that control the amount of radionuclides removed from groundwater include equilibrium sorption, chemical incorporation into iron oxides, uranium minerals or other crystalline phases, and recoil transfer of daughter products caused by alpha-particle decay (Golian and Lever 1992).

The groundwater is slightly acidic to neutral in pH, oxidizing, and relatively dilute, with the major ion chemistry dominated by Mg and bicarbonate. Water from the weathered zone is

undersaturated with respect to a number of U-bearing minerals. This is consistent with the idea that the present groundwater may be dissolving and dispersing the uranium in the deposit's phosphate zone (Sverjensky et al. 1992).

Groundwater samples from Koongarra drillholes were studied for colloidal content (Airey 1986; Ivanovich et al. 1987). Drillholes closest to faults were found to have the greatest variety of colloids (Ivanovich et al. 1987). Identified colloids included particles of Fe, kaolinite, chlorite, silica, Pb, U, and Ti. All colloid samples were dominated by Fe-rich particles, and uranium was only found in Fe-rich species (Ivanovich et al. 1987). Low colloid concentrations (approximately 10^6 particles/L or less) and the absence of radionuclides in colloids outside the center of the ore body indicated that colloidal transport of radionuclides is minor at Koongarra (Payne et al. 1992).

In summary, Koongarra may represent a worst-case scenario for transport, with its near-surface exposure to oxidizing weathering conditions and monsoonal climate. The dissolution and reprecipitation of U in the dispersion fan is especially notable. Its relevance would be greater as a total system analog for a shallow repository or as a disturbed case rather than as an analog to deep unsaturated disposal. However, it might be very instructive to use data associated with the migration rate and dispersion pattern in the Koongarra dispersion fan in testing models of saturated zone plume dispersion at Yucca Mountain.

13.4.3.2.2 Poços de Caldas, Brazil

The Poços de Caldas plateau is located in the state of Minas Gerais in Brazil (Figure 13.4-15). This area has been investigated for about 20 yr. because of its high levels of natural radiation. Morro do Ferro, in particular, has been identified as among the most naturally radioactive places on earth (Miller et al. 1994). The area was identified as a promising site for a natural analog study, and a 3-yr. project was undertaken (1986 to 1989). The project was cofunded by the Swedish Nuclear Fuel Waste Management Company (Sweden), NAGRA (Switzerland), the U.S. DOE, and the United Kingdom Department of Energy and was supported by Urânio de Brasil. The project generated a series of technical reports that were published in 15 volumes, of which the summary volume is Chapman et al. (1991). A collection of papers appeared in a special issue of *Journal of Geochemical Exploration* (Chapman et al. 1992). The project aims were focused on performance assessment requirements. The above-mentioned reports include the data collected, their interpretation, and the predictive modeling and relationship to radioactive waste disposal, particularly to performance assessments.

The objectives of the Poços de Caldas project, as discussed in detail by Smellie et al. (1989), were:

1. To assist in the validation of equilibrium thermodynamic codes and databases used to evaluate rock-water interactions, and solubility and speciation of elements in an environment rich in natural radionuclides and lanthanides
2. To determine interactions of natural groundwater colloids, radionuclides, and mineral surfaces with respect to radionuclide transport processes and colloid stability

3. To produce a model of the geochemical evolution of redox fronts specifically aimed at understanding long-term, large-scale movements of redox-sensitive natural-series radionuclides
4. To model the migration of lanthanide and U-Th series radionuclides during hydrothermal activity, similar to that anticipated in the very-near-field of some spent nuclear fuel repositories.

The Poços de Caldas caldera is a ring structure approximately 53 km in diameter, composed of alkaline volcanic and plutonic rocks, mainly phonolites, carbonatites, and nepheline syenites of Cretaceous age (Schorscher and Shea 1991; Miller et al. 1994). Two major hydrothermal events that affected the caldera led to widespread argillization (alteration to clay minerals) and zeolite formation. Local magmatic brecciation occurred in association with intense hydrothermal potassium and sulfur-rich alteration (Schorscher and Shea 1991). The second hydrothermal event was more localized than the first and is believed to be responsible for the formation of the numerous ore bodies within the caldera complex. The mineralizing events ended about 76 Ma (Schorscher and Shea 1991).

Two of these ore bodies were the focus of the Poços de Caldas natural analog study: (1) the Osamu Utsumi Mine, which is a uranium-ore body with subsidiary thorium, zirconium, and lanthanide enrichment, and (2) Morro do Ferro, which, in contrast, is a thorium and lanthanide element ore body, with subsidiary uranium. The Osamu Utsumi uranium mine is known for its well-developed redox front within the uranium ore (Figure 13.4-16). At Osamu Utsumi, research was directed toward the behavior of natural decay-series nuclides at the redox fronts, whereas at Morro do Ferro, attempts were made to relate the distributions of Th, U, and light rare-earth elements to the groundwater flow patterns in order to evaluate the extent of mobilization of these elements (MacKenzie et al. 1991). In addition to the analytical aspects of the study, much attention was paid to testing thermodynamic solubility and speciation codes and databases in blind predictions at both sites.

The Osamu Utsumi open pit mine is about 100 m deep, 1 km long, and 0.5 km wide. The mine consists of an upper weathered zone (laterite soil, top 40 m) that is completely argillized, depleted in Si and K, and enriched in alumina. The underlying oxidized zone is approximately 150 m thick and consists of alternating areas of oxidized and reduced bedrock. The reduced zone consists of essentially altered phonolites (62 percent potassium-feldspar, 37 percent clay minerals, with accessory pyrite, fluorite, and barite). The primary mineralogical difference between the oxidized and reduced rocks is the presence of pyrite in the reduced rocks (Smellie et al. 1989).

Primary mineralization is mostly low-grade and is disseminated throughout the rock. The redox front is generally very sharp but irregular in profile, as it follows the dips of faults and fractures along which oxidizing waters have penetrated (see Figure 13.4-16). Uranium mineralization occurs at the redox front itself in the form of pitchblende accumulations several centimeters across. The mine has been excavated to the level of the redox front.

Morro do Ferro is a roundish hill that stands about 140 m above the surrounding plateau and is 5 km north of the Osamu Utsumi Mine (Figure 13.4-15). It has been weathered to a much

greater degree than the Osamu Utsumi Mine, to a depth of at least 100 m, so that now the hill is composed of gibbsite, kaolinite, and illite, with additional veins of magnetite and manganese hydroxides that tend to form distinct layers. The thorium and rare earth element ore occurs as elongated mineralized lenses that extend down the hill slope. Major ore minerals include bastnaesite, monazite, cheralite, goyazite, thorianite, and thorite (Waber 1991). Thorium and lanthanide element mineralization are very enriched, with up to 3 percent by weight ThO_2 and up to 20 percent by weight total rare-earth elements, in some soils and weathered rocks (Chapman et al. 1992). No uranium mineralization is present at Morro do Ferro.

Groundwaters in the Poços de Caldas area typically have low concentrations (less than 1 mg/L) of colloids (Miekeley et al. 1989, 1991a). Most of the colloids are composed of iron and organic species. Only minor amounts of uranium are associated with colloids, but greater amounts of thorium and rare-earth elements are transported in the colloidal fraction. The suspended particle concentration is 5 to 10 times greater at Morro do Ferro than at Osamu Utsumi, but there appears to be very little thorium transport at Morro do Ferro, either by colloids or true solution. Filtration of particulate material, even in the highly fractured and porous rocks of the Poços de Caldas plateau, seems to be an efficient process (Smellie et al. 1989). The colloidal material acts as a largely irreversible sink for many elements (especially as they are immobile).

Groundwater at Morro do Ferro is lower in most major- and trace-element concentrations than groundwater at the Osamu Utsumi Mine (Miekeley et al. 1989). However, high concentrations of manganese in groundwaters are an exception and result from the presence of nodular Mn-oxides.

The groundwaters at Osamu Utsumi have high concentrations of uranium (up to 24 mg/L [Nordstrom et al. 1990]), whereas those from Morro do Ferro are much lower (Miekeley et al. 1991b). Concentrations of ^{232}Th are low in groundwaters from both sites (less than 0.1 $\mu\text{g/L}$), but are occasionally higher (up to 100 times) in surficial waters with abundant humic compounds or sulfate. Disequilibria is noted between ^{234}U and ^{238}U in the groundwaters from both sites (Miekeley et al. 1991a).

The groundwaters in the Poços de Caldas area have an unusual K-Fe- SO_4 composition because of the weathering of the altered, mineralized, K-rich rocks (Nordstrom et al. 1990). Also, relatively high concentrations of Ba and SO_4 detected in the Osamu Utsumi Mine groundwater may be important, since microcrystalline barite can act as a scavenger for radionuclides. The Osamu Utsumi Mine groundwater flow is upward from depth, except for the upper 10 to 15 m, where lateral surface-flow predominates. All groundwaters appear to be of meteoric origin, as indicated by tritium and stable isotope measurements (Nordstrom et al. 1990). Shallow groundwaters are less than 40 yr. old, but deeper waters may be a mixture of younger and older fluids, producing an apparent age of 40 to 60 yr. (Nordstrom et al. 1990).

Microbial activity is important for the pyrite oxidation and may be responsible for uraninite mobilization and reprecipitation at the redox front. At Poços de Caldas, microbes were found in all core and groundwater samples, independent of depth (West et al. 1989, 1990). West et al. (1989) reported that microbes are enhancing the supply of oxidants from the rock mass, thereby accelerating the rate of advance of the redox front. This could explain the observation that the

redox front is moving faster than would be expected, simply on the basis of dissolved oxygen concentration.

The natural plutonium concentration in a centimeter-sized pitchblende nodule was measured. Neither ^{238}Pu nor ^{240}Pu was detected. The concentration of ^{239}Pu was calculated to be $2.3 \pm 0.7 \times 10^8$ atoms/g, with the uranium concentration 43 ± 2 percent (Chapman et al. 1991, pp. 37, 39). The presence of natural plutonium (formed via neutron capture by uranium) is a function of host-rock composition and the length of time the system has been open to loss or gain of U or Pu. In a system that has been closed for about 100 k.y. (several half-lives of Pu), a state of secular equilibrium is reached between the parent U and the daughter Pu. In such a system, the Pu/U ratio is independent of time. The Pu/U in the pitchblende nodule is consistent with a state of secular equilibrium with the matrix phonolite. Based on the Pu/U ratio in the nodule, it appears that the two elements have resided, unfractionated, in the most highly uraniferous rock in the deposit for the last 100 k.y. Even if alteration has occurred more recently, the processes did not significantly fractionate Pu from U (Chapman et al. 1991, pp. 37, 39).

The Poços de Caldas project, in common with other natural analog studies, illustrates the complexity of natural groundwater systems. In particular, it highlighted the importance of amorphous phases in suspension, or as coatings on rock, as the principal reactive surfaces for many trace elements in solution. The presence of amorphous phases tends to reduce the concentration and mobility of trace elements in solution. Some of the fixing processes appear to be irreversible over long time scales, compared to reversible sorption used in performance assessment models, which tends to make these models conservative (Chapman et al. 1991).

Study of the redox front provided direct evidence of the operation of flow channeling in fractures and solute transport in the rock matrix as the key controls on the shape and movement of these fronts. A consistent picture emerged of very slow front movement and solute transport over the front dominated by diffusion. The front plays a significant role in retarding a wide spectrum of trace elements.

13.4.3.2.3 Oklo, Gabon

13.4.3.2.3.1 Introduction

The Oklo uranium mine contains the only known examples of natural fission reactors and is perhaps the best known natural analog. Most of the early investigations at Oklo were performed under the auspices of the International Atomic Energy Agency, which organized two symposia (IAEA 1975, 1978). The Commission of European Communities sponsored an international program at Oklo that began in 1991: Phase III ended in January 1999. A vast amount of literature about the Oklo natural fission reactors has been published. The literature review by Jakubick and Church (1986), although dated, provides an introduction to all aspects of work conducted to that date. More recent summaries of the investigations on radiolysis and the behavior of the radionuclides in the reactors are given by Curtis et al. (1989), Loss et al. (1989), and Brookins (1990). The Commission of European Communities program results are summarized by Chapuis and Blanc (1993), Gauthier-Lafaye et al. (1996), and Louvat and Davies (1998).

13.4.3.2.3.2 Background

Oklo is located in the southeast part of the Republic of Gabon (Figure 13.4-17) in the Franceville Basin. The Franceville Basin rocks are of Early Proterozoic age (approximately 2,000 Ma). They consist predominantly of deltaic sandstones, conglomerates, and marine black shales with interbedded dolomites, cherts, and some rhyolitic tuffs in the upper strata. Despite their ancient age, the rocks have survived virtually unmetamorphosed, with only brittle deformation. Sixteen reactor zones have been identified among three uranium deposits in the Franceville Basin (Smellie 1995). The uranium deposits containing the natural fission reactors are located at the top of the basal sandstone-conglomerate unit, the FA sandstone of the Francevillian Series (Gauthier-Lafaye et al. 1989; Gauthier-Lafaye and Weber 1989). The FA-Sandstone is immediately overlain by a carbon-rich mudstone (green pelite) that belongs to the FB-Formation of the Francevillian Series.

Two grades of ore, associated with two different occurrences of uranium, are distinguished in the Franceville Basin, a schematic of which is shown in Figure 13.4-18. The low-grade ore contains 0.1 to 1.0 percent uranium and the high-grade ore (greater than 1.0 percent) commonly contains up to 10 percent uranium (Gauthier-Lafaye et al. 1989). The low-grade ore is primary and is the most widespread. It occurs in disseminated blanket- or pod-like concentrations within black silicified sandstones containing secondary silica, chlorite, and illite, and is always associated with hydrocarbon material (Gauthier-Lafaye and Weber 1989). Common sulfides include pyrite and galena. The uranium exists predominantly as fine-grained botryoidal uraninite (pitchblende) with sporadic coffinite surrounding the pitchblende. Uranyl minerals are rare or absent, but when present these minerals are always associated with recent alteration.

The high-grade ore is secondary and occurs within fractured sandstones that have been interpreted as hydraulic breccias associated with faults or joints in the sandstone (Gauthier-Lafaye et al. 1989). As with the low-grade ore, uranium occurs as pitchblende with rare coffinite, but the high-grade ore usually occurs within secondary porosity caused by the dissolution of detrital quartz. The formation of the high-grade ore is attributed to the remobilization of low-grade ore by oxidizing hydrothermal fluids, which transported the uranium along the faults, followed by precipitation within the fracture zones when conditions became more reducing. In places, the uranium ore in this secondary type of deposit is extremely enriched (up to 70 percent uranium oxide) so that, at the time of formation, a critical mass of ^{235}U was formed, which initiated the natural fission reactions.

13.4.3.2.3.3 Evidence for Natural Fission

In 1972, French scientists from the Pierrelatte Diffusion Plant found an isotopic anomaly in the Oklo ore. The ^{235}U content was depleted from the normal 0.72 percent down to 0.62 percent. The discrepancy in ^{235}U was small, but significant, and led to an investigation that discovered other samples with depletions to as low as 0.296 percent. The occurrence of ancient nuclear chain reactions was confirmed when substantial quantities of fission products were found in the depleted ores (Naudet 1978).

Today, ^{235}U constitutes only 0.72 percent of natural uranium, because ^{235}U has a shorter half-life (700 m.y.) than ^{238}U (4,500 m.y.). In the past, the proportion was higher. The fission reactions

were possible because the $^{235}\text{U}/^{238}\text{U}$ ratio 2,000 Ma was approximately 3.5 percent (a value similar to ^{235}U enrichment for modern nuclear fuel). This concentration, and the presence of an appropriate moderator (probably groundwater), allowed the formation of a self-sustaining nuclear reaction (Cowan 1976). The conditions leading up to spontaneous nuclear fission were discussed by Naudet (1978), who showed that criticality and subsequent nuclear reaction may occur spontaneously if the uranium content reaches 10 percent within a 2-cm-thick layer. Such concentrations occur within the high-grade ores at Oklo. The fission reactions may have occurred spontaneously in relatively small volumes within the high-grade ore. Heat generated by these fission reactions would have resulted in local convective circulation of groundwater that, in turn, caused U migration to some of the reactor zones, thereby sustaining fission reactions for several thousands of years. It is unlikely that Oklo is the only place where natural nuclear chain reactions have occurred, but searches have turned up no other sites (Cramer 1986).

According to Holliger (1993), criticality was reached approximately $1,968 \pm 50$ Ma and lasted intermittently for 0.1 to 0.8 m.y. Roughly 1,000 to 2,000 metric tons of uranium were initially present as fuel, of which about 6 to 12 metric tons consisted of ^{235}U , which underwent fission and produced some 4 metric tons of plutonium (Naudet 1978).

13.4.3.2.3.4 The Oklo Reactor Ore Bodies

Mineralogy of the reactors consists of uraninite, chlorite, illite, and carbonates. There is little organic carbon or quartz in the reactor zones. Figure 13.4-19 shows a schematic of an idealized reactor zone. The mineralized regions are usually less than 10 m thick, from 10 to 20 m in length, and, normally, have a maximum ore grade of 1 to 2 percent (Jensen et al. 1997). The reactors consist of an inner core and an outer aureole. The core contains only uraninite, while the aureole contains uraninite with coffinite and pitchblende. The loss of quartz is due to heat generated by the reactions (temperatures to 350°C). The type of clay mineralization within the reactor zones is related to the temperature regime (Gauthier-Lafaye et al. 1989).

13.4.3.2.3.5 Retention of Radionuclides

Early natural analog investigations at Oklo concentrated on the mobility of the fission product elements during the 2,000 m.y. since their production. Some fission products are the same as radioelements to be emplaced in a radioactive waste repository (e.g., Tc, Np, Pu, Am). The fission products originally collected in the crystalline uraninite of the reactor zones as the nuclear reaction proceeded. Radiometric dating and modeling of the nuclear reaction allow estimates to be made of the production and decay of fission products at the site (Curtis et al. 1981). Although little alteration of uraninite occurred subsequent to its formation, some of the fission products have escaped from the uraninite, probably by solid-state diffusion (Curtis et al. 1981), and transport of some radionuclides has occurred subsequent to their release from the uraninite.

Palladium and Te appear to have been retained in the reactor zones, whereas Ag, Sn, and Cd were lost, and Ag and Sn may have been retained in the surrounding host rock (De Laeter et al. 1980). According to Gancarz et al. (1980) and Curtis et al. (1981), Ru, Tc, and Nd were dispersed into rocks surrounding the reactor zones, but appear to have been contained within a few tens of meters of their source. Curtis (1986) postulated that increased temperatures and greater oxidizing conditions in the reactors led to dissolution of Tc in hydrothermal fluids and

migration to the surrounding rocks, where the Tc precipitated in response to a drop in temperature and more reducing conditions. Curtis et al. (1989, p. 49) suggested that a portion of the fission-produced Te, Ru, Pd, Tc, Cd, and Mo was retained, essentially at the site of production and the portion that escaped the uraninite crystals of origin was completely removed from the reactor zone. Curtis et al. (1989) presented evidence that Nd and Sn were removed from the site of their production, but were retained within the reactor zone.

Because the reactions ended nearly 2,000 Ma, the short-lived radionuclides have decayed to more stable daughter nuclides. Analysis of the behavior of these short-lived radionuclides is problematic. According to Brookins (1978), Pu, Np, and Am were likely retained within the reactor, while Bi and Pb would have been redistributed locally without substantial migration (Brookins 1978). Most geochemical observations at Oklo support these predictions to varying degrees. Curtis et al. (1989) conclude that the retention of fission products is related to their partitioning into uraninite or secondary mineral assemblages. Those fission products that partitioned into the secondary mineral assemblages were largely lost over time, pointing to the importance of small uraninite grains in controlling the chemical microenvironment.

13.4.3.2.3.6 **Bangombé**

The Bangombé uranium deposit is located approximately 25 km west-northwest of Franceville and is strongly affected by near-surface ferralitic (Fe-rich) weathering (Bros et al. 1998). The reactor zone consists of an approximately 5-cm-thick reactor core, overlain by an up to 0.3-m-thick hydrothermal clay mantle (Bros et al. 1993 p. 1352). Immediately above this mantle lie black shales and green pelites of the FB-formation (Figure 13.4-19).

The Bangombé uranium deposit is located within the saturated zone (groundwater is within 4 to 6 m of the surface in the vicinity of the reactor zone). Smellie et al. (1993) interpreted the deposit as being located in a groundwater discharge area (Figure 13.4-20). Field measurements of pH, Eh, and alkalinity suggest three groundwater types that are broadly related to geological units intercepted by the boreholes. Surface waters have low pH (5.08 to 5.76) and high Eh (322 to 455 mV). Groundwaters of deeper origin have higher pH (6.00 to 6.14) and lower Eh (189 to 225 mV), and a second groundwater of deep origin has high pH (6.80 to 6.90) and moderate Eh (241 to 284 mV) (Smellie et al. 1993). These authors concluded that preservation of the Bangombé mineralization is attributable to the discharging groundwater that is less oxidizing than surface waters and that the green pelites act not only as a potential hydraulic barrier, preventing large-scale penetration of surface and near-surface oxidizing waters from reaching the mineralization, but also as a trap for the U-rich solutions reaching the surface. In short, at the Oklo and Bangombé uranium deposits, retention of uranium and fission products in the reactor zone appears to rely on reducing conditions in groundwater, sequestration within small uraninite grains, and hydraulic barrier properties of the green pelite.

13.4.3.2.3.7 **Progress to Date**

Natural analog investigations at the Oklo and Bangombé sites have focused primarily on the stability and longevity of UO₂, the transport and retardation of radionuclides, the degradation and radiolysis of bitumen, and the production of radiolytic oxidants. Present Commission of European Communities studies have concentrated on Reactors 10, 13, and 16 at Oklo, which

currently experience reducing conditions. Additional emphasis is placed on the spatial distribution of these reactor zones, both geologically and hydrogeologically, in an attempt to explain rock-water interactions via paleo and recent signatures of uranium and fission-product mobilization, within and from the reactor zones at different stratigraphic horizons.

Significant work has already been performed to characterize the Bangombé site. At the 1997 Oklo working group meeting (Louvrat and Davies 1998), results of the first phase of investigations at Bangombé were presented. A comprehensive table in that report presents available data from all Bangombé cores. Bulk and fracture mineralogy studies were conducted on cores from BAX-09 and BAX-13. Petrographic, scanning electron microscope, and chemical analyses have been performed on uraninites and uranium-alteration phases. Microprobe analyses have been performed to determine compositions of uraninites, and a model was developed showing stages of alteration of the deposit. Laboratory studies have been conducted on uraninite dissolution and leachability of other ions. Uranium-series disequilibrium studies have been performed. Other investigations included colloids, microbes, stable isotope and ion groundwater chemistry, uranium sorption and desorption studies, and geochemical modeling.

As an example of natural analog data being used to test models, Gurban et al. (1998) presented results using hydrogeological and geochemical data from Bangombé to compare the outcome of two independent approaches to modeling natural conditions surrounding the reactor. The modeling study was aimed to compare results, using a deterministic, multisolute, reactive coupled code with results using a statistical, performance assessment-oriented code. The authors concluded that, since both codes were able to represent the ongoing processes with similar outcomes (e.g., redox buffer around the reactor, increase in alkalinity because of microbial decomposition of organic material), the two approaches could be used to complement one another and to build tools that can better be used to support performance assessment. At the eighth Natural Analog Working Group meeting in March 1999, results of the second phase of study at Oklo and Bangombé were presented. These results are to be published soon, as the study has concluded.

13.4.3.2.4 Tono Mine, Japan

The Tono region, located approximately 350 km southwest of Tokyo, is the site of Japan's most extensive uranium deposits (Figure 13.4-21). The largest of these deposits the Tsukiyoshi uranium ore body, has been the focus of most of the natural analog studies in the area. This ore body has not been commercially exploited, and only one gallery, at a depth of 150 m below the ground surface, has been constructed. Thus, the ore body can be examined in a relatively undisturbed state. The Tsukiyoshi ore body is approximately 3.4 km long, between 300 to 700 m wide, and is 1 to 3 m thick (Ochiai et al. 1989, p. 127). The primary, unoxidized uranium ore comprises accumulations of coffinite and pitchblende, closely associated with pyrite, altered biotite, or bituminous plant materials, in cleavages in quartz grains, and on mineral grain boundaries in or around the porosity of the sediments (Yoshida 1994). These associations indicate that uranium concentrations and fixation processes have a close relationship with mineralogical phases controlling redox conditions. The secondary, oxidized uranium mineralization is comprised of U-bearing autunite, zippeite, and uranocircite, in association with montmorillonite, limonite, and other minerals in oxidized zones. Rocks with a high uranium

content have a higher permeability and sorption capacity than low uranium zones within the rock mass (Yoshida et al. 1994b, pp. 481, 483).

The ore bodies at Tono lie in paleochannels in the unconformity between Cretaceous granitic basement rocks (the Toki Granite) and overlying Miocene lacustrine sediments, which themselves form the lowest unit in a 200-m-thick sequence of Miocene and Pliocene marine and lacustrine sediments (Mizunami Group) (Figure 13.4-21). The basement granitic rocks contain about 6 ppm of uranium and are considered to be the source of the Tono uranium mineralization. The sandstones and mudstones at the unconformity (the Toki Lignite-bearing Formation) contain significant quantities of carbonaceous material and pyrite in a strongly reducing environment. The uranium mineralization itself occurs in conglomerate, sandstone, and the lignite-bearing formations. The uranium deposit, which is disseminated in the lowermost part of the Mizunami Group, is considered to have formed when uranium in the granite was dissolved into migrating pore fluids and then deposited under more reducing conditions in the lignite-bearing strata (Katayama et al. 1974).

Fission-track dating indicates that the ore deposit is approximately 10 Ma (Ochiai et al. 1989, p. 127). It was split into two sections, about 5 to 10 Ma, by the Tsukiyoshi fault, which has a vertical displacement of 30 m and does not continue upward into the youngest sedimentary rocks in the region, the Seto Group. Consequently, the Tsukiyoshi uranium deposit has been preserved despite fault movement, uplift, subsidence, denudation, deposition, and climatic and sea-level changes since its formation about 10 Ma.

Groundwater in the lowermost Mizunami Group, containing the ore deposit, is of meteoric origin, older than 10 k.y. at a depth of 100 m (Ochiai et al. 1989, pp. 129 to 130), while groundwater in the Seto Group is modern meteoric recharge. Uranium-series nuclides (^{238}U , ^{234}U , and ^{230}Th) in rock samples collected from different locations in the deposit were found to be in nearly equilibrium states (Yusa and Yoshida 1993). This indicates that these nuclides have been maintained in a closed system over a long time. It is considered that movement of uranium and thorium has been confined within a range of a few centimeters (migrated from sediments into the fault gouge) for at least 1 m.y. (Yoshida et al. 1994a). However, it is possible that uranium was transported along the fault by oxidizing groundwater at a sufficiently rapid rate to prevent the development of $^{234}\text{U}/^{238}\text{U}$ disequilibrium. It can be inferred that the uranium ore deposit has been preserved because a deep, chemically reducing geological environment with a minimal flow of groundwater has been maintained for thousands of years (Iwatsuki et al. 1995; Shikazono and Utada 1997).

The natural analog studies at Tono are described by Yusa and Yamakawa (1992), Nohara et al. (1992), and Seo and Yoshida (1994). The objective of current studies is to evaluate U-series radionuclide migration, over about 10 m.y., in both the pristine ore and the ore around the fault.

Preliminary results of U-series disequilibrium studies (Nohara et al. 1992, p. 409) indicate the following:

- Reducing conditions have been maintained for at least the last 1 m.y.
- Although limited uranium migration has occurred along the fault, the greatest uranium migration has occurred in the ore matrix, but this has been limited to less than 1 m over the 1 m.y.
- Radium has been mobilized during the last several thousand years. The relative mobility of radium, as compared to uranium, and the limited migration along faults or fractures are similar to the situation at Nopal I (see Section 13.4.2.3.1.3), although Nopal I is in an oxidizing environment.

13.4.3.2.5 El Berrocal, Madrid, Spain

The El Berrocal study (92 km southeast of Madrid) was conducted from 1991 to 1995. It consisted of teams from 10 institutions in five European Union countries. The primary objective was to understand past and present elemental migration processes to provide field-derived evidence for radionuclide behavior in the geosphere that could be used to constrain transport models for radionuclide release from a geological radioactive waste repository. Results of the study are reported in Rivas et al. (1998). The El Berrocal granite pluton forms the hill upon which the site is located. The granite hosts two uranium ore bodies mined in the 1960s but since abandoned. One of the abandoned mines was the focus of the El Berrocal study. The study generated a large body of geologic, hydrologic, and chemical data from extensive characterization and integrated modeling.

13.4.3.2.6 Palmottu, Finland

The Palmottu natural analog study was based on a small U-Th deposit in southwestern Finland (Figure 13.4-22). The purpose of the study was to improve the scientific basis of performance assessment in fractured, crystalline bedrock under groundwater-saturated conditions. The project was led by the Finnish Geological Survey through the Commission of European Communities and involved participants from Sweden, Spain, France, and the United Kingdom. The project was completed in 1999.

The deposit at Palmottu is hosted by Precambrian gneisses and migmatites whose protoliths were arkoses and greywackes. These high-grade metamorphic rocks are part of the Svecofennian fold belt that extends from southwestern Finland into central Sweden. The ore body was discovered in the late 1970s by airborne geophysical investigations. In the subsequent characterization, 62 boreholes were drilled, with a total length of more than 8 km. Three boreholes, drilled perpendicular to the ore body strike, were investigated as part of the natural analog study (Figure 13.4-23).

The deposit is up to 15 m thick, 400 m long, and 300 m deep, but it is discontinuous in the form of uraniumiferous pegmatites and veins (Figure 13.4-23). The principal ore mineral is disseminated grains of uraninite, thinly coated with coffinite. The average grade of the ore reaches up to 0.1 percent by weight uranium (Ruskeeniemi et al. 1989, p. 602). The uranium is thought to

have been derived during the latest stages of metamorphism, 1,700 to 1,800 Ma from late-stage granitic fluids of the nearby Perniö granite.

The natural analog study has concentrated on processes, such as colloids and matrix diffusion, which may affect radionuclide migration and retardation in fractured crystalline rocks. A major focus has been on understanding the redox control of the system and propagation of the redox front. Other performance assessment applications have included scenario development based on Palmottu, investigation of mobilization within the main uranium mineralization, and interface with the biosphere (Blomqvist et al. 1998). Primary results of the Palmottu natural analog study are given in project reports by Blomqvist et al. (1987, 1991, 1998) and Jaakkola et al. (1989). Summaries of the results from the radionuclide migration investigations are given in papers by Ruskeeniemi et al. (1989), Suutarinen et al. (1991), and Suksi et al. (1991).

The groundwaters, measured in open boreholes, show a distinct layered zonation, with the upper waters being oxidizing, Ca-Na-HCO₃ type, and the lower waters being slightly saline and reducing (Na-Cl-SO₄-CO₃ type) (Ruskeeniemi et al. 1989). The change in water composition and the redox front both occur at about 125-m depth. The pH increases from 7.4 close to the surface to approximately 9.0 at the drillhole bottom (195 m) (Jaakkola et al. 1989, p. 20). Tritium values also decreased with depth to below detectable limits, indicating a lack of meteoric water infiltration at depth.

Uranium is contained in primary uraninite, coffinite, and monazite and is associated with iron-oxides and clay minerals in the more altered areas and as fracture coatings. Coffinite has precipitated along fractures short distances (less than 1 m) from uraninite grains. Significant dissolution of uraninite has occurred at all depths, regardless of the modern, measured oxidation potential. Jaakkola et al. (1989) suggest that the oxidation potential at depth was higher in the past, perhaps because of the infiltration of meteoric waters to greater depths.

Uranium concentration is higher in the oxidizing upper waters than in the lower, more reducing waters, even though the uranium concentration in the rock is greatest at depth (Valkiainen 1989, p. 112). The opposite trend is observed with uranium in particulate matter. Most particulate matter in the upper 100 m contains little or no uranium, whereas uranium at depth is associated predominantly with particulate matter.

Sorption onto fracture coatings, particularly calcite, efficiently retards uranium transport in fractures at Palmottu. Uranium concentrations in calcite up to 1,600 ppm have been measured (Rasilainen et al. 1991 p. 280). The long retention time of uranium in calcite, determined by U-series disequilibrium measurements, has also been recognized. Uranium-234/uranium-238 in the dissolved fraction increases with depth from a value of nearly 1.0, whereas ²³⁴U/²³⁸U in the particulate fraction shows a slight (though less significant) decrease with depth. The ²³⁴U/²³⁸U ratios of extracted phases suggest limited mixing of groundwaters in the study area (Blomqvist et al. 1995, p. 24).

13.4.3.2.7 Summary of Natural Analogs of Saturated Zone Flow and Transport

Sections 13.4.3.2.1 to 13.4.3.2.5 discussed, in some detail, six natural analogs of saturated zone flow and transport. Although these sites are considerably different from Yucca Mountain in their

totality, they were chosen because they had the most relevance to understanding radionuclide migration and sequestration. (To this list, Cigar Lake could have been added; instead, it is considered as a total system analog in Section 13.5.) In addition, these sites have been characterized the most extensively of any natural analogs. The six sites differ significantly in geologic and hydrologic settings and in the nature of U occurrence; nevertheless, a few points of comparison can be made.

The Tono Mine, in a deep crystalline, strongly reducing environment, has the least to offer of the six as an analog to processes that could occur at Yucca Mountain. The Palmottu deposits also occur in a deep crystalline setting, but at Palmottu a redox front occurs at depth, indicating that circulation of oxygenated water has taken place and has caused migration of uranium. At Oklo and Bangombé, uranium occurs at various depths, under reducing and oxidizing conditions, respectively (although reducing groundwaters are thought to be a contributing factor to uranium sequestration at Bangombé). The Bangombé occurrence is somewhat similar to Koongarra and Poços de Caldas in that deposits in the three areas are located in shallow, deeply weathered environments that are subject to monsoonal precipitation and are, at times, unsaturated. However, the host rocks are very different at these three sites (sandstone/shale, quartz-chlorite schist, and carbonatite, respectively), and the chemistry of groundwater-host rock interaction plays a significant role in understanding the migration of uranium and other elements away from their original sites of deposition. Collectively, these three sites may provide a qualitative, overly conservative estimate of radionuclide migration in an unsaturated to saturated environment. At Oklo, U migration on the order of only a few meters has occurred over 2,000 m.y., with evidence that many of the fission products of the critical reactions were retained within the uraninite ore body or a few meters away within the reactor zone.

Overall, the six sites contribute to understanding migration processes at a detailed scale in a variety of different settings. These sites provide a better understanding of the stability of radionuclides over long time frames, allowing the placement of broad bounds on processes such as colloid transport. In addition, they confirm the importance of fracture flow and sorption onto fracture-coating minerals, such as calcite and hematite. As seen in Section 13.4.3.3, although anthropogenic analogs have operated over time periods orders of magnitude shorter than the natural analogs discussed, anthropogenic analogs may also enhance knowledge of radionuclide transport.

13.4.3.3 Anthropogenic Analogs of Saturated Zone Flow and Transport

The purpose of investigating anthropogenic analogs is to obtain a better understanding of the migration of shorter-lived transuranic elements than is amenable to study by natural analogs. Through natural analogs it is possible to observe processes that began thousands to millions of years ago. The disadvantage is that over such long time periods a number of the shorter-lived radioelements of concern at a high-level radioactive waste repository, such as ^{237}Np (half-life 2.14×10^6 years), have decayed to small quantities or are nonexistent. To gain a better understanding of the transport of radionuclides over shorter timeframes and, in many cases, of the distinct migration pathways that are amenable to quantitative modeling, anthropogenic analogs are examined. In this section, in varying degrees of detail, radionuclide transport relative to Chernobyl, the Idaho National Engineering and Environmental Laboratory, Hanford,

and the Nevada Test Site is reviewed, and the applicability of future investigations of selected radionuclide plumes in Russia as anthropogenic analogs is briefly discussed.

13.4.3.3.1 Russian Sites

Hundreds of radionuclide-contaminated sites are found in Russia and the former Soviet republics and in the seas bordering the Russian coastline. The wastes range from low to high levels of radioactivity and resulted from both civilian and military activities. A portion of the readily available literature was surveyed for the purpose of investigating whether information from these sites may be applied usefully as analogs to geologic repository processes. The degree of contamination, source-term composition, and degree of characterization and monitoring that had taken place were considered. Based on the degree of characterization that has already taken place, the most promising future analog investigations would be directed toward assessing the utility of geohydrologic and chemical transport data from the Lake Karachai site and three liquid-waste deep-injection sites at Tomsk, Krasnoyarsk-26, and Dmitrograd.

Lake Karachai, declared to be the most radionuclide-contaminated site in the world (Rumynin et al. 1998, p. 3), plays a unique role in the advancement of knowledge about the subsurface behavior and fate of many hazardous radionuclides. Lake Karachai is located at the southern extent of the Ural Mountains. In the Chelyabinsk region, several surface waste reservoirs between two rivers have been used for more than 45 years to store low- and intermediate-level liquid wastes. Lake Karachai is the largest of the reservoirs. It contains a total of 120 MCi of activity (Rumynin et al. 1998, p. 3). Leakage from the reservoir has resulted in a contamination plume traveling through the underlying fractured, metavolcanic rock aquifer. The liquid wastes have a pH of approximately 7.9 to 9.3 and an inventory consisting of ^{90}Sr , ^{137}Cs , ^{60}Co , and ^{106}Ru , as well as exceedingly high nitrate concentrations (up to 50,000 mg/L in the plume-contaminated brines) (Rumynin et al. 1998, p. 6).

Deep injection of liquid radioactive waste was a preferred disposal methodology in Russia and has been the subject of many papers and a treatise (Rybal'chenko et al. 1998). The concept involved injecting waste into a confined geologic unit within specified boundaries of a permeable geologic medium. Leakage from the confining unit has taken place at the deep injection site of Krasnoyarsk-26. The disposal setting at Krasnoyarsk affords an opportunity to investigate plume dispersion in fractured biotite gneiss. It also affords an opportunity to observe the effects of short-term (decades), radioactivity-caused thermal effects on mineralogy in the injected medium. Additional gathering of background information is planned on the opportunities for building confidence, using data from deep-injection sites.

13.4.3.3.2 Chernobyl, Ukraine, Russia

13.4.3.3.2.1 Introduction

Section 13.4.3.3.2 reviews information from the Chernobyl, Ukraine, accident regarding the distribution of radioactive contaminants and the processes affecting their migration to determine what information can be used to build confidence in conceptual models of unsaturated zone radionuclide transport for Yucca Mountain. Because the Chernobyl Nuclear Power Plant contamination products differed widely from cosmic background and nuclear weapons

radioactive fallout, ejected radionuclides can be used as tracers to better understand coupling of atmospheric, terrestrial, vadose zone, and groundwater transport processes (Belyaev et al. 1997). Although various compilations of Chernobyl data have been prepared, none has focused on information that could be useful to radioactive waste disposal.

The April 1986 Chernobyl accident resulted from explosion of the Unit 4 reactor of the Chernobyl Nuclear Power Plant. Radioactive particles were carried into the atmosphere, spreading to many regions of the globe (Castle 1988; Holloway and Liu 1988; Erlandsson et al. 1987; Eliassen 1990; Rigol et al. 1999; Thiessen et al. 1997). On a regional scale, the accident led to radioactive contamination of fields, rivers, tributaries, canals, drainage ditches, and agricultural lands in the Pripjat and Dnieper river basins of the Ukraine. Of approximately 32.5 million people in the Dnieper basin, about 9 million people who use the Dnieper River as a drinking water source could have potentially been contaminated. No statistics are available on the total number of people who were affected by the accident, in part, because of the difficulty in accounting for all the people who might have been affected, and, in part, because of the difficulty in isolating Chernobyl-induced health effects from effects resulting from other causes.

The total amount of radionuclides released by the accident was estimated to be as much as 150 MCi (Stone 1998, pp. 623 to 625). (A curie is a measure of radionuclide activity: 1 curie (Ci) = 3.7×10^{10} becquerel (Bq); 1 Bq = 1 nuclear transformation per second.) At Chernobyl, the highest single release of radionuclides into the environment resulted from the worst nuclear accident in the world (Shestopalov 1997, p. 224). Research into many environmental and health effects of the Chernobyl accident has become a major international enterprise aimed at understanding long-term transport processes and the effects of exposure to radioactivity (Devarakonda and Hickox 1996; Vasenko 1998; Wendum 1998; Hatano et al. 1998; Moltenbrey 1999).

13.4.3.3.2.2 Hydrogeologic Setting

Ukraine is situated within two large tectonic regions, the East European Platform and the Alpine geosynclinal belt. Figure 13.4-24 shows a map of Europe with an expanded view of the Ukraine and the location of the 30-km-radius Chernobyl Nuclear Power Plant exclusion zone. The term "exclusion zone" refers to an area surrounding the site that was sealed off as an institutional control to prevent further access after the accident. Its total area, except for part of the Kiev reservoir, is 2,044 km² (Shestopalov 1996, p. 3). The Chernobyl region has a humid climate, with mild, short winters having frequent thaws and a warm summer. Average annual precipitation ranges from 500 to 700 mm/yr. (Shestopalov 1997, p. 200).

The Chernobyl Nuclear Power Plant exclusion zone is located in the central part of the Ukrainian Polesiye physiographic province. Its relief consists of slightly elevated denudation plains, with gently waved surfaces, as well as hills, sand ridges, and irregular bogs and kettles. Variations in landscape affect the location and depth of infiltration of surface groundwater. The relatively dense network of Pripjat and Dnieper river tributaries forms valleys of moderate relief. Approximately 40 percent of the land in the exclusion zone is covered by forest, 30 percent by arable farm land, and the remaining 30 percent by urban areas, bogs, and water bodies (Shestopalov 1996, p. 22).

Several aquifers confined by aquitards underlie the exclusion zone (Figure 13.4-25). The Quaternary aquifer extends beneath the entire Chernobyl Nuclear Power Plant exclusion zone. The lower part of this aquifer consists of sands that become coarser with depth; the upper part is composed of loamy sand, loam, and clay. Hydraulic conductivity of the Quaternary sediments ranges from 0.5 to 15 m/day (Shestopalov 1996, p. 20). Infiltration of precipitating water is the main source of the groundwater recharge to the Quaternary aquifer. Groundwater recharge occurs mainly within the Dnieper and Pripjat River drainage basins.

The Eocene aquifer underlies almost the entire territory, except for a small area west of the Chernobyl Nuclear Power Plant exclusion zone. The Eocene aquifer is composed mainly of fine sand, with hydraulic conductivity from 0.1 to 10 m/day (Shestopalov 1996, p. 20). In most of the exclusion zone, the Eocene aquifer is artesian and is separated from the upper Quaternary aquifer by an aquitard composed of Kiev Suite marls. Vertical water exchange between the Quaternary and Eocene aquifers can take place through hydrogeological discontinuities in the aquitard that provide hydraulic connections between aquifers. The Eocene aquifer formerly provided the main water supply of the cities Pripjat and Chernobyl prior to the Chernobyl accident.

The Cenomanian-Callovian (Cretaceous-Jurassic) aquifer underlies the Eocene aquifer and is separated from it by Upper Cretaceous marls and chinks, which generally form a regional aquitard. The Cenomanian-Callovian aquifer sediments consist of sandstone, clay, and flint concretions. Hydraulic conductivity ranges from 1 to 15 m/day. The Cenomanian-Callovian aquifer and the underlying Bajocian (Jurassic) aquifer are hydraulically separated by low-permeability clays and aleurites (metamorphosed clays). These aquifers are the main sources for the water supply to the city of Kiev. Calculations using Darcy's formula showed that within the Chernobyl exclusion zone, lateral flow velocities range from 10 to 200 m/yr. for the Quaternary aquifer and 1 to 15 m/yr. for the Eocene aquifer (Shestopalov 1996, p. 20).

13.4.3.3.2.3 Radionuclide Composition of the Chernobyl-4 Reactor Core and Sources of Contamination

Palmer et al. (1996) listed radionuclides that could be present at Yucca Mountain. Other authors listed radionuclides emitted by the Chernobyl accident, including Loshchilov et al. (1991c), who estimated mass released. These radionuclides are listed in Table 13.4-3, which shows that of the longer-lived radionuclides released at Chernobyl, and detected within the zone affected by the radionuclide fallout, only plutonium (238, 239, 240, 241), U (234, 235, 236, 238), and ²⁴¹Am are also of concern for Yucca Mountain. Among short-lived radioisotopes released at Chernobyl, only ²⁴²Cm is of concern for Yucca Mountain, as it decays to plutonium. Table 13.4-3 also shows that both Chernobyl and Yucca Mountain have numerous common radioelements, but the radioisotopes of concern are different.

During the accident, nuclear fuel in the destroyed reactor was reported to exceed temperatures of about 2,000°C (Shestopalov 1997, p. 206). High temperatures caused evaporation of volatile radioactive elements from the fuel. The fuel was partially released during the explosion in the form of finely dispersed components, which were distributed in the atmosphere. Subsequent fires and fuel heating caused the reactor to continue to expel products of graphite burning, radioactive gases, aerosols, and finely dispersed fuel dust. The size of dust particles ranged from less than 1 µm to hundreds of µm.

The atmospheric oxidation of dispersed nuclear fuel and reactor-containment materials resulted in the formation of fine, highly active, solid particles, called hot particles. A hot particle is defined here as a fuel particle that originated by condensation or adsorption with an activity concentration exceeding 10^5 Bq/g (Shestopalov 1997, p. 235). Hot particles at Chernobyl were formed from:

- Fuel particles containing elements of low volatility
- Condensed matter from the vaporized fuel that formed metallic particles
- Particles of uranium dioxide fuel fused with the metal cladding of the fuel rods
- Fuel mixed with sand or concrete (Loshchilov et al. 1991c; Gudzenko 1992).

Hot particles carried a number of long-lived radionuclides (Kashparov et al. 1996; Shabalev et al. 1997). Tcherkezian et al. (1994, p. 127) determined that hot particles contributed not less than 65 percent of the total activity in the exclusion zone.

13.4.3.3.2.4 Radionuclide Contamination

In this section, some radionuclides of interest (^{137}Cs , ^{90}Sr , ^{234}U , ^{235}U , and ^{241}Pu) released from the Chernobyl explosion are examined. Their sequestration in the atmosphere, geosphere, and hydrosphere are then described. The radionuclides discussed here were chosen on the basis of their concern at Chernobyl, as shown in Table 13.4-3:

13.4.3.3.2.4.1 Radionuclides of Concern

According to data from the Ukrainian State Committee on Geology (Shestopalov 1997, p. 223), an area of about $130,000 \text{ km}^2$ in Ukraine (20 percent of the total territory) was contaminated with ^{137}Cs to a level of at least $1.8 \times 10^{10} \text{ Bq/km}^2$ (10 or more times higher than preaccident conditions). In total, from 1.04×10^{16} to $1.1 \times 10^{16} \text{ Bq}$ of radionuclides were scattered over the Ukraine, with 90 percent being ^{137}Cs . Cesium is strongly retained by clay minerals, humus, and biota. For all soil types, 60 to 95 percent of cesium was strongly bound to soil particles. The area with ^{137}Cs contamination of more than 5 to 15 Ci/km^2 significantly exceeds the area of the exclusion zone. Secondary accumulation of ^{137}Cs in soils is taking place in some areas, where concentrations have increased by a factor of 2 to 3 and locally from 5 to 10. One of the processes affecting the redistribution of contaminants in soils is the resuspension of contaminated soils into the atmosphere (Garger et al. 1997).

Strontium-90 is the radionuclide of greatest concern because it is almost unadsorbed by soils and biota and is only slightly adsorbed by soil humus. Efficient geochemical barriers for this isotope are unknown. Strontium has advanced downward in the unsaturated zone toward the water table and is expected to migrate through groundwater to surface-water reservoirs and then to the Dnieper River. By the spring of 1987, the percentage of water-soluble strontium had not exceeded 1 to 2 percent of the total, whereas by 1992 it had grown to 7 percent in the podzolic soils and to 3 percent in the peat soils.

Lebedev et al. (1992, p. 516) determined that plutonium concentration in soils of the European part of the former USSR varied in different directions from the Chernobyl Nuclear Power Plant, ranging up to tens of mCi/cm^2 . Although plutonium accumulates mostly in soils, its

accumulation in the irrigated lands in the Ukraine to levels that become a health risk may occur only after a long time. This issue with plutonium needs further research, which partly accounts for its high-priority rank in the risk assessment.

In summary, because of their high concentrations, the main radionuclides of concern at Chernobyl are ^{137}Cs and ^{90}Sr . These radionuclides are the focus of attention in the following discussion on contamination and transport.

13.4.3.3.2.4.2 Atmospheric Contamination

The reactor explosion caused radioactive gases and aerosol particles to enter the atmosphere as part of a hot, turbulent jet that reached a height of 1 to 2 km. The jet followed, more or less, the prevailing wind direction and, after some time, became the flow of radioactive-contaminated air (Shestopalov 1996, p. 6). Atmospheric transport affected by weather conditions during burning of the reactor led to radioactive pollution over an area reaching westward to the Atlantic Ocean, southward to the Mediterranean Sea, eastward to eastern regions of the Ukraine, and northward to Arctic regions, eventually reaching China and Japan. About a quarter of the total released radioactivity entered the atmosphere during the first day after the accident. By the fifth day, the release had decreased by approximately six times as a result of mitigation efforts. Over the long term, the wind-borne transport of radionuclides became insignificant in comparison to aqueous migration.

13.4.3.3.2.4.3 Surface Water Contamination

After the Chernobyl Nuclear Power Plant accident, radionuclides that percolated from the land surface through the unsaturated zone were detected in both the unsaturated zone and in groundwater. Radioactive contaminants accumulated in bottom sediments in the Pripyat and Dnieper rivers and in several reservoirs along the Dnieper River. In 1989, the content of ^{137}Cs in the Kiev, Kremenchug, and Kanev reservoirs ranged from 0.2 to 0.5 Bq/L. Cesium and strontium were detected in surface waters in suspended and dissolved forms. From 1989 to 1993, transport by the Pripyat River to the Kiev Reservoir had removed 60 percent of ^{90}Sr from the exclusion zone and 20 percent of ^{137}Cs .

The total amount of ^{137}Cs has been increasing in surface waters by a rate of about 10 to 40 percent per year. Cesium-137 is not hazardous to irrigated agricultural lands away from the exclusion zone because it is not easily removed from contaminated soils within the zone. In contrast, ^{90}Sr in the dissolved state is expected to gradually accumulate in soils and be transferred into agricultural products. One of the important problems is how to retain easily soluble ^{90}Sr in natural deposits, such as the left-bank floodplain of the Pripyat River, where ^{90}Sr content is about 3.7×10^{14} Bq, as well as in about 800 temporary radioactive waste repositories in the exclusion zone (Shestopalov 1997, p. 223). Even though contamination of surface water has not yet posed a public health concern, monitoring is needed to ensure that discharge from the watersheds containing radioactive elements will not contaminate surface waters in the future.

13.4.3.3.2.4.4 Soil Contamination

Deposition and distribution patterns of radioactive material on the ground surface were mainly determined by the pattern of jet and turbulent transport in the atmosphere. Local soil contamination anomalies are present within areas where radionuclides fell with rain. The soils themselves are relatively homogeneous in composition, with mostly podsols and peaty podsols as the topsoil layer in the exclusion zone. However, the overall result was a heterogeneous distribution of radionuclide concentration in soils. Among the areas of highest concentration is the western finger (Shestopalov 1992, p. 7). This plume extends almost in a straight line westward from the Chernobyl Nuclear Power Plant. This finger is 1.5 to 5 km wide; over a distance of less than 70 km, the concentration of ^{137}Cs along its axis decreases from greater than $10,000 \text{ Ci/km}^2$ to 10 Ci/km^2 .

The southern finger splits into five separate tracks and has the highest concentrations of ^{90}Sr and transuranic radionuclides. The widespread northern finger reflects a pattern of rain deposition. In its central part, the ^{137}Cs concentration reaches 500 to $1,500 \text{ Ci/km}^2$. The southwest finger has the most complex shape. The main part of this anomalous zone also has features of rain deposition.

As a result of both radionuclide leaching from the hot particles and their adsorption onto soil, the concentration of mobile forms of radionuclides reaches a maximum and then decreases. It is supposed that the maximum concentration of mobile ^{137}Cs in soils was reached 1.5 to 2.5 yr. after the accident, and a maximum concentration of ^{90}Sr was expected to be reached 6 to 15 yr. after the accident. After May 1986, ^{137}Cs soil contamination had decreased in the exclusion zone by about 25 to 50 percent. The decrease was caused by the following factors: natural radioactive decay of ^{137}Cs (about 20 to 21 percent), partial washout of the surface layer of soil from elevated areas and slopes, soil decontamination, and penetration underground deeper than 20 cm from the soil surface. At the same time, many other areas were affected by the redistribution, causing secondary contamination of ^{137}Cs in local soil depressions, the edges of marshes, and reservoir banks. Absolute concentration of ^{137}Cs in the exclusion zone reached $50,000$ to $150,000 \text{ Ci/km}^2$, which is 5 to 15 times greater than in the so-called "red forest" soils around the Chernobyl Nuclear Power Plant, where intense radioactivity caused leaves to lose chlorophyll and turn red.

The total content of ^{238}U in the soils varies from 0.63 to $2.14 \mu\text{g/g}$ (Sobotovich 1992, p. 44, Table 3.5). Table 13.4-4 illustrates the results of investigations of the vertical migration of U and Pu in soils. This table shows that about 99 percent of the plutonium accumulated within the top 2 cm of the soil layer. This table also shows that the $^{238}\text{U}/^{235}\text{U}$ ratio remained unaffected below a 3-cm depth. The limited migration of plutonium and uranium in soils is explained by these radionuclides being released in the form of radionuclides sorbed to hot metal particles that are relatively stable in the near-surface weathered zone. Silant'-ev et al. (1989) determined that the concentration of radionuclides entering the soil profile decreased exponentially with depth.

13.4.3.3.2.4.5 Cooling Pond

The cooling pond of the Chernobyl Nuclear Power Plant was heavily contaminated as a result of the 1986 reactor accident. From 1989 to 1993, the cooling pond represented one of the major

sources of ^{90}Sr migration from the Chernobyl site to the Dnieper River. Several attempts were made to contain radioactive contamination within the pond. Overestimation of releases via groundwater pathways and design mistakes led to unsuccessful remedial actions in 1986 and later (Bugai et al. 1997). Heterogeneous spatial accumulation of radionuclides occurred not only in the soils and surface waters, but even in the pond (Pinder et al. 1995). A heterogeneous flow and transport pattern from the pond to the groundwater is also likely.

13.4.3.3.2.4.6 Groundwater Contamination

The greatest source of radionuclide contamination to groundwaters is from about 800 radioactive waste disposal sites within the exclusion zone. Soil contamination involved a much larger area than surface water and groundwater contamination (Shestopalov 1992). Cesium-137 and ^{90}Sr contamination was detected in the Cretaceous aquifer at depths of 80 to 120 m (Gudzenko 1992, p. 4). The presence of ^{134}Cs in groundwater (half-life of 2.06 yr.) and the increase of ^{90}Sr concentration by two orders of magnitude (from 4. to 400 mBq/L) confirm that radionuclides of the Chernobyl origin reached groundwater at 50 to 70 m depths within one year after the explosion (Shestopalov 1997, p. 254). Field investigations indicated a lack of correlation between ^{137}Cs soil concentration and its travel time to the water table (Gudzenko et al. 1991, p. 3). Therefore, the soil contamination cannot be used as an indicator of the groundwater contamination.

A hydrogeological study of groundwater contamination in the exclusion zone demonstrated that ^{90}Sr is the most critical radionuclide, because it could locally contaminate water supply sources above acceptable limits. Radioactive contamination of the Eocene aquifer is expected to occur under the entire contaminated area and could locally exceed the maximum permissible concentration in 5 to 10 yr. Maximum concentrations of radionuclides in the deep Cretaceous-Jurassic aquifer used for the water supply of Kiev and other urban areas may be reached by 2010 or 2020. Skurat et al. (1995) estimated that beneath radioactive storage sites in nearby Belarus the groundwater contamination is expected to occur in 10 to 100 yr., with ^{137}Cs concentration not reaching the maximum limit and the ^{90}Sr concentration significantly exceeding it.

13.4.3.3.2.5 Gamma-Spectrometry

For the past 13 yr. field-monitoring data have been collected by more than 40 governmental and private organizations. Monitoring was established over the hydrosphere, geosphere, and biosphere to characterize main processes and pathways for contaminant migration. Radionuclide transport within watersheds of the Pripyat and Dnieper rivers and accumulation and release of radionuclides from bottom sediments have been measured.

The most detailed data have been obtained by gamma-spectrometry surveys on the scales of 1:100,000 (approximately 28 percent of the area) and 1:25,000 (33 percent of the area). In addition, direct gamma-spectrometry measurements of ^{137}Cs were made for the soils of almost all villages and towns. Test soil-sampling was conducted many times along the so-called benchmark network. This is a radial, concentric network of observation points situated on 36 radii (every 10°), with Chernobyl Nuclear Power Plant Unit 4 at the center (Figure 13.4-26). In general, soil contamination of the Chernobyl exclusion zone and adjacent contaminated territories has been characterized using one to four monitoring points per square kilometer. The

monitoring has demonstrated that in order to increase the efficiency of characterization of large areas, soil sampling should be supplemented by borehole gamma measurements (Loshchilov et al. 1991a, pp. 18 and 19).

13.4.3.3.2.6 Radionuclide Transport Processes

Section 13.4.3.3.2.6 discusses the radionuclide transport mechanisms in the exclusion zone and the parameters that affect those processes. Most of the discussion relates to soils. Applications of different models of radionuclide retardation in soils are discussed in papers by Koss and Kim (1990), Mamikhin (1995), Olekhovich et al. (1995), Absalom et al. (1996), and Shestopalov (1997).

13.4.3.3.2.6.1 Biogenic and Colloidal Transport

Biogenic removal of radioactive contamination outside the borders of the Chernobyl Nuclear Power Plant exclusion zone does not exceed several curies per year for ^{137}Cs and ^{90}Sr . Technogenic (remediation-related) migration of radionuclides outside the Chernobyl Nuclear Power Plant exclusion zone is insignificant at less than 1 Ci/yr. Cerium-144 was detected in particles less than 0.02 μm in diameter, which suggests that it could be found in the colloidal state (Ivanov et al. 1991, p. 55). Potential evidence for colloidal transport of other radionuclides has not been demonstrated in the available literature. Only Von Gunten et al. (1988, p. 237) found a very small radioactivity on colloids greater than 0.05 μm in diameter, suggesting the retention of radionuclides by glaciofluvial outwash deposits (pebbles, gravel, sand, clays).

13.4.3.3.2.6.2 Diffusion Coefficients

Laboratory investigations of soil samples from the exclusion zone were conducted to determine the effect of moisture content on the diffusion coefficient of Sr and Cs (Ivanov et al. 1991, p. 54, Table 1). The diffusion coefficients for ^{90}Sr and ^{137}Cs in sand under different saturations are summarized in Table 13.4-5. When the soil saturation increases from 30 to 100 percent, the diffusion coefficient increases by 1.5 to 3 times. These studies confirmed the known significant effect that moisture content has on kinetics in vadose zone soil processes.

13.4.3.3.2.6.3 Retardation of Radionuclides in Soils

Several factors affect retardation of radionuclides in soils, such as the type of pore space and fracture density, drying-wetting cycles, mineralogical composition of sediments and rocks, organic matter content and composition, and chemical composition of pore solution and groundwater, as well as the concentration of radionuclides in dissolved and exchangeable forms. The volume of the exchangeable fraction of strontium and cesium in soils decreased soon after the explosion, but it remained constant in soil samples taken in the 6 yr. thereafter (Rigol et al. 1999). The retardation of ^{137}Cs is enhanced by the presence of organic matter and illitic clay (Hird et al. 1995; Rigol et al. 1999; Smith et al. 1999). Both physical sorption and cation exchange may account for retardation. Table 13.4-6 summarizes the maximum content of dissolved and exchangeable radionuclides in exclusion-zone soils, and presents retardation factors (R) for the total amount of adsorbed radionuclides and distribution coefficients (K_d) characterizing the radionuclide exchange with the soil exchangeable complex.

Gudzenko et al. (1990, p. 123) reported ^{137}Cs retardation factors of 9,200 to 29,000 and the distribution coefficients of 6,550 to 8,550 cm^3/g for two samples of sandy loam, 0 to 5 cm deep. Such high values of K_d and R may be explained by the presence of organic matter in the near-surface zone (Llaurado et al. 1994). For a sand sample from a depth of 30 to 35 cm, these values are smaller: $R = 1,100$ and $K_d = 242 \text{ cm}^3/\text{g}$ (Gudzenko et al. 1990, p. 123).

Konoplev et al. (1988) presented experimental results for ^{90}Sr and ^{137}Cs migration in the main soil types of the exclusion zone and stated that "a significant amount" of nonexchangeable ^{90}Sr and ^{137}Cs is present in the soils. Kononovich et al. (1996) determined that there are fast and slow transport fractions of ^{137}Cs in soil water, with substantially different sorption characteristics. The portion of the fast fraction was about 10^{-3} of the slow one.

Kliashtorin et al. (1994) used field lysimeters to study the migration of radionuclides in different soils. They found that the total concentration of radionuclides— ^{144}Ce , ^{134}Cs , ^{137}Cs , ^{106}Ru , and ^{90}Sr —ranged from 0.5 to 90 MBq/m^2 . Their study determined that 0.01 to 0.6 percent of radionuclides was removed from the 20- to 30-cm layer of soil every year. The mobility of radionuclides in the soil water was highest for ^{90}Sr and was reduced in the following order: ^{106}Ru , ^{134}Cs , ^{137}Cs , and ^{144}Ce .

13.4.3.3.2.6.4 Evidence of Rapid Preferential Flow in the Vadose Zone and Groundwater

Investigations conducted within the area affected by the Chernobyl explosion showed the relatively rapid contamination of the vadose zone and groundwater, which might have occurred because of the phenomenon of fast, preferential flow (Gudzenko et al. 1991; Shestopalov et al. 1995, 2000). Investigation of fast migration in the vadose zone, and its influence on radionuclide contamination within the Chernobyl exclusion zone, involved the evaluation of anomalous morphosculptures, which are small surface depressions (Shestopalov et al. 2000). This investigation involved measuring the concentration of soil-gas radon, CO_2 , and the ratio of $^{222}\text{Rn}/^{219}\text{Rn}$, using ultra-short radio-wave impulses, supplemented by a surface radar survey. Figure 13.4-27 shows the results of field investigations of the $^{222}\text{Rn}/^{219}\text{Rn}$ ratio in soil gases taken in shallow boreholes and the data from the surface radar survey. This figure shows the increased moisture content below the surface depression and corresponding increase in the $^{222}\text{Rn}/^{219}\text{Rn}$ ratio confirming the presence of a near-surface zone of preferential flow. These investigations showed that in the near-surface zones of preferential flow, the flow rate exceeds 2 to 2.5 m/yr . and is higher in depressions by 1 to 1.5 orders of magnitude, in comparison to surrounding areas (Shestopalov et al. 2000).

13.4.3.3.2.7 Chernobyl Summary

Conditions at Chernobyl and Yucca Mountain are different in several major aspects, such as climate, geologic and tectonic setting, and depth to the water table. The Chernobyl catastrophe resulted in steam and fuel vapor explosions and the release of significant quantities of radioactive materials to the environment. Radionuclides that descended from the atmosphere to the land and were distributed through surface water reservoirs then entered the unsaturated zone and percolated downward through zones of preferential flow toward the water table. In contrast, deep disposal of high-level radioactive waste is being planned at Yucca Mountain, where

atmospheric transport will not be a factor and where surface-water transport of radionuclides, if it occurs, would be minor. Furthermore, as shown in Table 13.4-3, the suite of radionuclides of concern at Yucca Mountain is somewhat different from that of Chernobyl.

Even though background conditions and expected modes of contamination for Chernobyl and Yucca Mountain are not directly analogous, what was learned from more than 13 years of investigations of infiltration and contaminant transport within the Chernobyl exclusion zone can provide insight into some of the flow and transport processes at Yucca Mountain. The most important conclusions of this study are the following:

- Spatial and temporal variations of infiltration rates, and fast, preferential flow in the near-surface zone, depend on topography and geomorphological conditions. The near-surface fast infiltration and migration of radionuclides in the unsaturated zone is taking place within land-surface depressions of the exclusion zone. Despite the low level of contamination detected in groundwater, the appearance of Chernobyl radionuclides confirms the presence of localized, preferential, radionuclide transport through the unsaturated zone.
- The rapid groundwater contamination around Chernobyl may not be directly associated with the near-surface zones of preferential flow.

Even though Chernobyl does not provide a good analog for Yucca Mountain, the Chernobyl experience and long-term data sets could be a valuable aid in validating the site characterization methods, monitoring program, and the performance and risk assessment modeling at several other DOE contaminated sites, such as Hanford, Washington, and Oak Ridge, Tennessee. It might be of interest to examine remediation efforts undertaken at Chernobyl (e.g., applying a new foam spray to stop radioactivity leaking from the damaged reactor [Edwards 1997] and phytoremediation [Richman 1996]). Another area of Chernobyl research is the evaluation of flow and transport processes in the vadose zone and groundwater as affected by a number of radioactive waste storage sites located in the Ukraine and Belarus (Serebryanyi et al. 1995). The experience obtained at these sites could be used in evaluating flow and transport processes under leaking tanks and waste disposal areas at a number of DOE sites (e.g., Hanford and the Idaho National Engineering and Environmental Laboratory).

13.4.3.3 Idaho National Engineering and Environmental Laboratory

One of the facilities at the Idaho National Engineering and Environmental Laboratory is the Idaho Chemical Processing Plant. The Idaho Chemical Processing Plant was designed principally to recover highly enriched uranium (greater than or equal to 93 percent ^{235}U) from different fuel types used in naval propulsion, research, and test reactors. From 1952 until 1984, low-level radioactive waste was discharged from the Idaho Chemical Processing Plant directly to the Snake River Plain by means of an injection well and seepage ponds. Over time, a suite of radionuclides has been measured in the aquifer, including ^3H , ^{36}Cl , ^{90}Sr , ^{137}Cs , ^{129}I , and Pu isotopes. Beasley et al. (1998) reported the first measurement of the long-lived radionuclides ^{99}Tc , ^{236}U , and ^{237}Np in the aquifer and their downgradient concentration changes during water transport through fractured basalt. Their study showed that ^{36}Cl and ^{99}Tc behave conservatively during transport, while ^{129}I , ^{236}U , and ^{237}Np were retarded.

The location of the Idaho National Engineering and Environmental Laboratory is shown in Figure 13.4-2. The Idaho Chemical Processing Plant is located east of the Big Lost River, in the south-central part of the Idaho National Engineering and Environmental Laboratory. In Figure 13.4-2, the Idaho Chemical Processing Plant would be located approximately at the first "a" in "Laboratory." Beasley et al. (1998, p. 3875) reported that water in the Snake River Plain aquifer is unconfined, with the highly fractured tops of basalt flows leading to high hydraulic conductivities. Beasley et al. (1998, p. 3876) further stated that the calculated residence time of water in the Snake River Plain is 55 to 82 yr., although water travel times within different parts of the aquifer, from recharge to discharge points, are estimated to range between 12 and 350 yr. Groundwater flow is from the northeast to the southwest, and depth to groundwater varies from approximately 60 m at the northern site boundary to approximately 275 m at the southern site boundary. Beasley et al. (1998, p. 3876) reported that the average hydraulic gradient across the Idaho National Engineering and Environmental Laboratory is approximately 2 m/km, and water travel times between the Idaho Chemical Processing Plant and the southern site boundary have been estimated at 2 m/day.

From 8 to 23 groundwater monitoring wells at the Idaho National Engineering and Environmental Laboratory were sampled for radionuclide measurements in 1991, 1992, and 1994. Activity concentrations were measured for ^{36}Cl , ^{99}Tc , ^{236}U , ^{129}I , and ^{237}Np . To determine the relative mobilities of these radionuclides, individual radionuclide activities in wells near the Idaho Chemical Processing Plant were normalized to those at a distance. Figure 13.4-28 shows a best-fit plot of these normalizations for each radionuclide. The close correspondence in the decrease of ^{36}Cl and ^{99}Tc with distance from the Idaho Chemical Processing Plant suggests that ^{99}Tc , like ^{36}Cl , behaves conservatively in the fractured basalt and that observed concentration decreases occur only as a result of dilution or dispersion (Beasley et al. 1998, p. 3880). Iodine-129 is attenuated and ^{237}Np and ^{236}U are even more attenuated. Because none of the radionuclides discussed was routinely monitored in low-level waste streams discharged from the Idaho Chemical Processing Plant, the possibility cannot be excluded that the relationships shown in Figure 13.4-28 could have arisen from variable discharge rates over time for the radionuclides shown. However, the authors point out that, even though the absolute amounts of radioactivity most likely varied over time, the ratios of radionuclides in the discharges probably were consistent and, therefore, did not affect the composition of radioactivity in the waste streams.

13.4.3.3.4 Hanford Effluent Treatment Facility

13.4.3.3.4.1 Objectives of Hanford Study

The Hanford analog project uses a well-studied saturated zone contaminant plume at Hanford to aid in evaluating the representation and implementation of processes and mechanisms in the Yucca Mountain saturated zone flow and transport model. In particular, focus is on the description of dispersion based on a particle-tracking module and an Eulerian approach in order to provide performance assessment with a more defensible particle-tracking module than presently exists. To date, the new approach has been documented and compared with analytical solutions. The sensitivity of tritium plume migration in dispersion models for site-scale simulations remains to be evaluated. Eventually, the Yucca Mountain saturated zone flow and transport model will be benchmarked against the Hanford tritium plume data and Hanford's previous modeling results. Following this step, a variety of sorbing and nonsorbing

radionuclides will be considered in simulations. Possible candidates include ^{60}Co , ^{137}Cs , ^{129}I , Pu, ^{90}Sr , ^{99}Tc , and U (Cole et al. 1997).

13.4.3.3.4.2 Background

The Hanford Effluent Treatment Facility, also known as the State-Approved Land Disposal Site, is being used as an anthropogenic analog for modeling studies of radionuclide migration in the saturated zone at Yucca Mountain. The Effluent Treatment Facility, located in Area 200 at the Hanford Reservation, is a combined treatment plant and disposal facility. At the Effluent Treatment Facility, waste streams resulting from various cleanup activities are treated and discharged into the unsaturated zone. The treated effluent containing tritium migrates through the soil column to the water table. Tritium was first detected in groundwater monitoring wells in July 1996, roughly 1 yr. after operations began at the site. The plume emanating from the Effluent Treatment Facility site is well characterized and provides a unique opportunity for studying transport of nonreactive and reactive groundwater constituents (Barnett et al. 1997). Migration of the tritium plume has been successfully modeled using the CFEST code (Barnett et al. 1997), enabling a comparison between existing models and the FEHM code (Zyvoloski et al. 1997) used for modeling flow and transport in the saturated zone at Yucca Mountain.

One of the main questions to be addressed in this study is the role of dispersion tensor off-diagonal terms on radionuclide migration. Modeling studies by Pacific Northwest National Laboratory (Wurstner et al. 1995; Barnett et al. 1997) employed a diagonal representation of the dispersion tensor with values for longitudinal and transverse dispersivities of 20 m and 2 m, respectively. However, if flow does not occur along one of the axes, and off-diagonal terms are not incorporated into the model, incorrect behavior of dispersion is obtained. Part of the purpose of this study is to investigate the extent of the discrepancy that can result from neglect of off-diagonal terms. Investigation results are presented in the following section.

13.4.3.3.4.3 Progress to Date

13.4.3.3.4.3.1 Particle-Tracking Methods for Dispersion

As part of the Hanford project, YMP developed a particle-tracking method to handle dispersion in three dimensions in an anisotropic medium. The particle-tracking method used an Eulerian approach. Details of development of the algorithm and theory behind the approach taken await publication. The study showed that incorporation of the off-diagonal terms of the dispersion tensor is important in order to obtain the proper behavior for dispersion that is parallel and perpendicular to the direction of flow, when flow is not parallel to any of the coordinate axes (e.g., in a heterogeneous flow field). In the principal-axes coordinate system, the dispersion tensor is diagonal. As a consequence, a solute plume spreads along the direction of flow according to the longitudinal dispersivity, and occurs perpendicular to the direction of flow according to the transverse dispersivity. Ignoring the off-diagonal terms of the dispersion tensor in the original coordinate system would thus indicate a false behavior of spreading in the direction of the coordinate axes and not in the direction of fluid flow. The off-diagonal terms serve, in effect, to rotate the plume so that it points in the direction of flow.

13.4.3.3.4.3.2 Particle-Tracking Numerical Simulations

Several test cases were executed to confirm the accuracy of the particle-tracking method by comparing them with analytical solutions. All test cases reported were performed on a three-dimensional grid in which flow having an average pore velocity of 34 m/yr. is aligned with the x-axis. The grid dimensions are 10 km × 20 km in the horizontal directions and 500 m in the vertical to represent a domain typical for large-scale flow and transport in an aquifer. In the first test case, the particles were inserted at the inlet within a single cell, and the breakthrough curve at a downstream location (15 km from the inlet) was recorded for the case of longitudinal dispersion with a dispersivity of 100 m. The excellent agreement of the model against an analytical solution in test cases, including a sorbing solute and matrix diffusion combined with the transport solution, showed that these mechanisms are captured by the code.

A similar series of simulations was performed in which the solute was input as a patch on the inlet face of the model. The dimensions of the patch were 3,000 m in the y-direction and 12.5 m in the z-direction, starting at the surface ($z = 0$). A model run, including both longitudinal and transverse dispersion, was carried out with longitudinal dispersivity of 100 m and transverse dispersivity of 0.1 m. As the plume progresses downstream, spreading in the z-direction lowers the maximum concentration of particles and allows the particles to migrate to greater depths. Over long periods of time, at a constant solute injection concentration, the plume approaches a steady-state concentration distribution within the model. The agreement of model and data are fairly good, but the particle-tracking module captures the dispersion process more accurately when larger numbers of particles (e.g., 10^6 as opposed to 10^4) are used.

Preliminary results show the effect of off-diagonal terms of the dispersion tensor for propagation of a plume across the grid at a 45° angle. A simple grid was set up to test the ability of the developed anisotropic particle-tracking module to simulate dispersion. The grid is three-dimensional and has 1,000 nodes. There are 10 equally spaced nodes in the x and y directions, with a spacing of 1,000 m, and 10 equally spaced nodes in the z direction, with a spacing of 450 m. The model has a uniform permeability of 10^{-14} m² and uniform porosity of 10 percent. The simulated flow field has uniform velocity in the x-y plane and 0 velocity in the z direction. The flow velocity in the x-y plane is oriented 45° to the x-axis. This is accomplished by assigning uniform pressure gradients to the boundaries in the x-z and y-z planes and assigning no-flow boundaries at the $z = 0$ and $z = 450$ m planes. The dispersivity tensor is anisotropic.

Two cases were run—one that included off-diagonal components of the dispersion tensor and one that did not. Results for the case that included the off-diagonal components showed that the particles spread out in an ellipsoid, with its major axis oriented along the flow direction. In the case that did not include the off-diagonal elements, the particles again spread out in ellipsoids, but the ellipsoids were oriented with the major axis along the x-direction instead of the flow direction. Results of the simulations demonstrated that the effect of the off-diagonal terms is to rotate the plume along the direction of flow.

13.4.3.3.4.4 Hanford Effluent Treatment Facility Project

Work on the Hanford Effluent Treatment Facility project as an anthropogenic analog for Yucca Mountain has proceeded slowly. The goal of the data transfer was to facilitate construction of a

computational model of flow and transport that could be compared to work already carried out at Hanford. As an initial step, the geometric information for hydrostratigraphy had to be transferred. To date, a preliminary grid has been generated that needs to be checked for consistency with the original grid used with the CFEST software package. After preliminary calculation, if it is decided that different gridding strategies are required (e.g., increased or nonuniform resolution), additional grid refinement will be needed.

The grid consists of uniform, orthogonal grid blocks. Seven materials are represented in the geometric model. The computational grid has eight materials, with the last material identifier indicating the part of the grid that does not overlap and is outside the geometric model. The model extent encompasses the geologic model and forms a parallelepiped with a west-east dimension of 6,775 m, a south-north dimension of 5,225 m, and a depth of 160 m. The parallelepiped is broken into a grid of $39 \times 30 \times 59$ cells of equal size. This grid is superimposed on the geometric model, and material properties of the regular grid are assigned according to the material in which they are contained.

If used, additional testing of the particle-tracking algorithm used in the computer code FEHM would be needed. Calculations using a full dispersion tensor, with off-diagonal terms, would need to be compared with previous modeling work at the Hanford Effluent Treatment Facility site for migration of the tritium plume.

13.4.3.3.5 Nevada Test Site

The 0.75-kiloton underground nuclear test, Cambric, was conducted at the Nevada Test Site in 1965 in tuffaceous alluvium 73 m (220 ft) below the water table (Hoffman and Daniels 1981). Data from a field experiment initiated in 1974 at the Cambric site have provided direct information on the transport rates of radionuclides through alluvium. Tests began after the cavity and chimney were predicted to be filled with groundwater to the preshot static water level. It was assumed that tritium, plutonium, and uranium fission products would be present in the cavity (and in the groundwater within the cavity) and could be used to study possible migration from the cavity (Hoffman and Daniels 1981).

The field study began with the completion of a satellite well 91 m from the Cambric cavity, followed by drilling of a reentry well into the cavity itself. Both solid and liquid samples were taken from the reentry well to determine the radionuclide distribution between the solid material and the groundwater. Water was then pumped from the satellite well to induce an artificial gradient sufficient to draw water from the Cambric cavity through the surrounding rocks.

Approximately two years after pumping began, significant amounts of tritiated water were found in water from the satellite well, signaling the arrival of water from the Cambric cavity region. After almost six years of pumping, the tritium concentration in the pumped water reached a maximum (Hoffman and Daniels 1981). By the end of September 1984, about 60 percent of the initial tritium inventory had been pumped out through the satellite well (Thompson 1986).

Other radionuclides have also been measured in water from the satellite well, including ^{36}Cl , ^{85}Kr , ^{106}Ru , and ^{129}I . During the 10-year experiment ^{90}Sr and ^{137}Cs were not detected in water from the satellite well (Thompson 1986). The ^{36}Cl pulse preceded the tritium pulse in the

satellite well. Krypton was shown to be correlated with tritium but more strongly sorbed onto alluvium than tritium (Thompson 1986). Ruthenium-106 was detected in water from the satellite well and was unretarded in the alluvium. Iodine-129 arrived at the satellite well sooner than tritium.

The Cheshire event took place in 1976 (Buddemeier and Hunt 1988). Detonation occurred at a depth of 1,167 m, approximately 537 m below the water table, in fractured rhyolitic lavas of Pahute Mesa. Water was obtained from two wells, one inside the Cheshire experimental site and the other approximately 300 m away. Tritium, Kr, Sr, Cs, Sb, Co, Ce, and Eu were detected in the pumped water. More than 98 percent of the Co, Ce, and Eu were associated with colloids in samples from both locations. The authors concluded that the presence of colloidal radionuclides outside the cavity indicates radionuclide transport as colloids.

The Benham test was detonated in 1968 at a depth of 1,402 m below the water table. In a recent field test, plutonium was measured in groundwater at the Nevada Test Site ER-20-5 wells at a maximum activity concentration of 0.63 pCi/L (Kersting et al. 1999, p. 57). The ratio of $^{240}\text{Pu}/^{239}\text{Pu}$ indicates that the plutonium originated at the site of the nuclear test, Benham, a distance of 1.3 km from the wells. The minimum distance for plutonium migration at the Nevada Test Site is, therefore, 1.3 km in 28 years. The plutonium detected was associated with colloidal material consisting mainly of clays, zeolites, and silica (Kersting et al. 1999). It is not likely that the plutonium was transported by prompt injection or that its soluble fraction migrated along fast flow paths. Colloidal transport is a possible mechanism for plutonium migration, since colloidal transport of radionuclides was observed at the Cheshire site. However, stability arguments limit the amount of colloids in suspension that are able to migrate. The association of plutonium in colloidal form at the Nevada Test Site indicates the need to incorporate the colloidal transport mechanism into transport process models and performance assessment calculations for radionuclide releases at Yucca Mountain.

INTENTIONALLY LEFT BLANK

13.5 TOTAL SYSTEM ANALOG: CIGAR LAKE

As stated in Section 13.1.5, Cigar Lake is the only total system analog identified for a repository concept. The Cigar Lake deposit, although different from Yucca Mountain in geologic, hydrologic, and chemical conditions, deserves special attention because extensive studies were conducted to match as many features of the ore deposit setting as possible to those of a geologic repository.

The Cigar Lake uranium deposit in northern Saskatchewan, Canada (Figure 13.5-1) was extensively studied as an analog for a radioactive waste disposal vault under water-saturated, reducing conditions located deep below the water table. The Cigar Lake deposit has many similarities to the proposed Canadian spent fuel repository, as well as to the proposed European radioactive waste repositories, as summarized by Goodwin et al. (1989) (Table 13.5-1). Results of the Cigar Lake international natural analog project, involving Canada, Sweden, Spain, and the United States, are documented in progress reports and reviews (Cramer and Sargent 1994; Sargent and Cramer 1986; Cramer et al. 1987; Cramer 1989, 1995a; Cramer and Smellie 1994). The goal of the natural analog project was to investigate the stability of the uraninite as a natural analog for spent nuclear fuel and the mechanisms that caused the retention of the radionuclides in the ore body, particularly the effect of colloids.

The Athabasca Basin in northern Saskatchewan contains several unconformity-type uranium deposits (Figure 13.5-1). These deposits are at the base of the Proterozoic Athabasca Sandstones and are associated with faulting in the basement schists and gneisses of the Archean Canadian shield. The base of the Athabasca Formation constitutes a paleosurface resulting from erosion of the preexisting metamorphic terrain. Located at the southwestern tip of Waterbury Lake, the Cigar Lake ore body lies about 440 m below the surface, where it straddles a ridge in the basement rocks and overlies a fracture zone. The ore is surrounded by a clay-rich halo (5 to 30 m thick), an area substantially depleted in silica and consisting predominantly (more than 80 percent by volume) of kaolinite and illite (Figure 13.5-2). At the contact between the ore and clay halo, a narrow band (1 to 10 m thick) of amorphous iron oxides coats the clays. Above the clay halo, the sandstone is enriched in kaolinite, illite, and other clay minerals and depleted in quartz relative to the surrounding unaltered sandstone. Above this altered zone lies a band of silica-rich sandstone, the quartz cap, in which secondary silica fills fractures in the sandstone. Above the quartz cap, the sandstone is relatively unaltered.

The Cigar Lake ore body, which was discovered in 1981 by airborne geophysical measurements, is the world's richest uranium deposit (Miller et al. 1994, p. 311). The ore body is lens shaped, about 2,000 m long, 20 to 100 m wide, and 1 to 20 m thick. The U ore is uraninite, pitchblende and subordinate coffinite, with an average grade of 8 percent, but reaching 55 percent in some areas. The primary mineralization occurred 1,300 Ma (Cramer and Smellie 1994, p. 2). Although the Cigar Lake deposit is more U-enriched than that at Oklo, spontaneous nuclear fission was not possible in the Cigar Lake deposit because of its younger age. By the time the ore body formed, the natural $^{235}\text{U}/^{238}\text{U}$ ratio had decayed to too low a level to allow a critical mass to be reached. Several major fractures cut the ore body and the clay envelope (Figure 13.5-2). These fractures were originally features of the basement rocks but were reactivated after sandstone deposition and ore formation. The uranium was apparently transported by hydrothermal solutions upward to the base of the unconformity along the fracture

zone and deposited as uraninite at the unconformity when these solutions came into contact with groundwater in the sandstone. These hydrothermal solutions are also responsible for the alteration of the sandstone surrounding the ore body. Perhaps the most outstanding feature of the Cigar Lake deposit is the absence of surface geochemical or radiometric expression of the deposit, despite the fact that the host sandstone is a permeable aquifer cut by fractures (Cramer 1986).

According to Curtis et al. (1999, p. 275), naturally produced plutonium and technetium at the Cigar Lake deposit have migrated short distances but have remained within the deposit. Only one event seems to have disturbed the system since its formation (Cramer 1995b, p. 37). Small, isolated pockets of remobilized uranium have been found in some of the steeply dipping fractures above and in the shield rocks directly beneath the main ore body. The age of this younger event has been estimated at between 320 and 293 m.y., most likely representing the temporary opening of fractures and faults in association with tectonic movement of the North American plate that allowed groundwater to mobilize some of the U (Cramer 1995b, p. 37). Since then, the deposit has been affected only by gradual uplift through erosion of the overlying sandstone. Figure 13.5-2 shows the current setting of the deposit and the extent of sandstone weathering that took place since the last glaciation, 10 ka.

Migration of radionuclides from the deposit into the surrounding rocks has been limited at Cigar Lake by a combination of hydrogeological, mineralogical, and geochemical factors (Cramer 1986). First, the deposit is in a basal sandstone unit, which is the main local aquifer, and this unit has a much higher groundwater flux than the deposit itself. Second, the present fluids are reducing; Eh is estimated at -0.2 to $+0.2$ V (Sunder et al. 1988, p. 470). Consequently, there is little dissolution of the uraninite or of daughter radionuclides contained within. The U concentrations in the groundwater are low (usually much less than 10^{-7} M) (Cramer and Sargent 1994, p. 2240) and are similar to those expected for uraninite equilibrium. Third, the clay-rich zones surrounding the ore have relatively low hydraulic conductivities compared with the sandstone of the overlying aquifer (Cramer and Sargent 1994). This effectively seals the ore zone from bulk groundwater flow and filters out colloids during mass transport from the ore zone. In addition, the clay-rich rocks and hydrothermally altered sandstones are enriched in sulfides, providing effective redox buffering in the undisturbed system (Sunder et al. 1988). Fourth, any radionuclides that dissolve and migrate away from the ore zone encounter a naturally sorptive mineralogical barrier in the form of the clay alteration zone (Cramer 1986, 1995b).

Vilks et al. (1988) studied particulate and colloid matter in groundwater and showed that the concentration of uranium in particles and dissolved uranium are similar. Radiolysis of the groundwater within the ore zone may be the cause of locally oxidizing conditions causing formation of the iron-oxyhydroxides (e.g., goethite) at the top of the ore body, as well as the uranyl minerals (Fayek et al. 1997). Perhaps because of absorption onto amorphous iron-silicon-hydroxides at the ore/clay interface, uranium concentrations in the surrounding sandstone are depleted with respect to the ore body water. Also, the filtration of particulate matter by clay minerals probably plays a role in reducing groundwater uranium concentration (Vilks et al. 1988).

Goodwin et al. (1989) list analog aspects of the Cigar Lake deposit to the planned Canadian radioactive waste disposal concept. These features are also listed in Table 13.5-1. They are

primarily the following: (1) uraninite is a good analog to UO₂ spent nuclear fuel of the Canadian program; (2) the Canadians may use a titanium container, which would alter to have a rutile (TiO₂) coating in an aqueous environment, for which the accessory rutile in the alteration zone of the deposit is a good analog; (3) a planned bentonite and sand buffer is approximated by the illite-rich alteration zone around the ore; and (4) groundwater circulation in the host porous sandstone is much greater than that expected in the planned granitic repository, so the deposit provides a conservative estimate of the effects of circulating groundwater.

INTENTIONALLY LEFT BLANK

13.6 SUMMARY AND CONCLUSIONS

13.6.1 Summary

Carefully selected natural analogs are important tools for understanding flow and transport processes anticipated at a potential nuclear waste repository. In fiscal year 1999, the Yucca Mountain Site Characterization Project (YMP) began to address process model areas that could benefit from improved confidence through natural analog studies. As a first step, Section 13 was prepared to include knowledge gained from previous natural analog studies and new work regarding many relevant natural and engineered barrier system processes. This will help to identify areas of existing analog information that can be used to build confidence in understanding long-term behavior of a waste repository, areas where no appropriate analogs can be identified, and areas where natural analog work could be focused. The key points of each analog or group of analogs that contribute to a process model (e.g., analogs to saturated zone transport), are summarized under their respective sections and are not repeated here.

A number of areas were not covered in this section. These areas included biosphere analogs, microbially-induced corrosion, efficacy of a clay buffer in backfill, the role of organic materials and microbes in enhancing or preventing radionuclide migration, public perception and analogs, and the ways in which other countries, or performance assessment exercises conducted by other agencies in the United States, have used analogs quantitatively in their performance or safety assessments.

Areas identified by performance assessment in which analog studies may contribute to testing and building confidence in models include the seepage threshold and the fraction of waste packages contacted by seeps (including seepage enhanced by thermally-induced drift collapse), alteration of hydrologic properties by mineral precipitation or dissolution, sorption onto fractures, the role of colloid filtration in reducing radionuclide migration, Alloy-22 corrosion, Np solubility, and saturated zone dilution.

Previous YMP Incorporation of Natural Analogs—In the past, most of the YMP's use of natural analogs has been indirect, although a handful of direct uses can be cited. Indirectly, the YMP has acknowledged the role of natural analogs in a repository license application by participation in topical meetings (e.g., various meetings of the Commission of European Communities' Natural Analogue Working Group), in the U.S. Nuclear Regulatory Commission's 1991 workshop on the role of natural analogs in geologic disposal of high-level nuclear waste (Kovach and Murphy 1995), and in a number of studies via the Office of Civilian Radioactive Waste Management's international program. The YMP supported participants in projects at Oklo, Poços de Caldas, Alligator Rivers, and Cigar Lake. The technical reports resulting from these projects contributed to the overall understanding of repository processes. The Office of Civilian Radioactive Waste Management also contributed (along with Sweden, Canada, Switzerland, and the Commission of European Communities) to making a video on natural analogs that has been distributed to repository programs throughout the world for public awareness and educational purposes.

Four examples come to mind of ways in which the YMP has used analogs directly for testing and building confidence in conceptual and numerical process models. First, the concept of viewing

Yucca Mountain as a self analog (i.e., using past thermally-driven hydrochemical processes of secondary mineral formation and mineral alteration zones as a key to future alteration) has been supported by studies at Yellowstone that identify the same mineral alteration assemblages for the same temperature regimes. This increases confidence that the same alteration assemblages could be expected to form under repository conditions. Second, thermochemical data from the Wairakai, New Zealand, geothermal field have been used to increase confidence in thermodynamic parameters for silica minerals in geochemical modeling databases. Third, analog studies such as those reported in Section 13.4.1.2 (e.g., Matyskiela [1997] and others) have been called upon to demonstrate either reduced or enhanced fracture flow caused by thermal-hydrologic-chemical processes. The results of these studies are inconclusive and require additional substantiation (see Section 13.7). Finally, spent nuclear fuel dissolution rates and spent nuclear fuel alteration parageneses (as determined in laboratory experiments) have been compared to those of Nopal I. The results of these studies (summarized in Section 13.3.2.2.1) greatly increase confidence in spent nuclear fuel alteration models.

13.6.2 Conclusions

Conclusions that can be drawn from natural analogs in Section 13 include:

- As noted by others (e.g., Wronkiewicz et al. 1996), the sequence of U alteration paragenesis at Peña Blanca is a very good analog to alteration of uranium oxide spent nuclear fuel. The reaction path of alteration of spent nuclear fuel at Yucca Mountain will be similar to that of geologically young, Pb-free uraninite, with schoepite and becquerelite forming as intermediate products, followed by uranyl silicates. Additional work in the area of spent nuclear fuel analogs is not needed unless it focuses on analogs to alteration under disturbed conditions (e.g., a radical change in groundwater chemistry or erosion) or focuses on alteration of other compositionally-distinct types of fuel that would be disposed.
- Natural glass analog studies, although different in composition in significant ways from borosilicate nuclear waste glass, indicate that glass waste forms will be stable in a repository environment at Yucca Mountain. Higher stability is favored by higher silica and alumina content and by lower alkali content of the glass. Basaltic glass, which is lower in silica and alumina (but simultaneously lower in alkalis) than rhyolitic glass, has been shown to have a hydration rate of 0.001 to 30 μ /ka in the absence of radiation.
- The analogs to common metals (e.g., Fe, Cu, bronze, Ni) presented in Section 13.3.5 serve mainly to demonstrate that under ambient to slightly elevated temperatures, the metals will be stable for thousands of years, even under oxidizing conditions. Because the historical record is unlikely to offer analogs to Ti stability, Ti-bearing minerals (e.g., sphene and rutile) may offer insights.
- A consistent set of parameters was obtained to calibrate the site-wide Box Canyon model to both pneumatic and infiltration tests using the dual permeability approach. Modeling results of the Box Canyon study demonstrated that the dual permeability approach used in large-scale, volume averaged numerical models, such as the

unsaturated zone flow and transport model at Yucca Mountain, can be applied with confidence.

- Preliminary results at Nopal I appear to indicate low actinide mobility in unsaturated siliceous tuffs under semiarid, oxidizing conditions. Uranium-thorium age data indicate that the primary transport of uranium away from the Nopal I deposit along fractures occurred more than 300 ka. The $^{226}\text{Ra}/^{230}\text{Th}$ activity ratios indicate redistribution of radium within the last 5 ka as a result of secondary fluid events. Therefore, the data demonstrate stability over approximately 100 k.y. time scales for U (235, 238), Th, and Pa in fracture-filling materials. In an analogous sense, this stability should extend to transuranics and the rare earth elements. The high mobility of radium can be considered analogous to transport of strontium and cesium. By analogy, the tuffs at Yucca Mountain should have similar retentive properties to impede oxidized uranium mobility.
- Even under criticality conditions at Oklo, less than 10 percent of uranium was estimated to have been mobilized, under far more extreme conditions than those anticipated at Yucca Mountain, where criticality is unlikely.
- At Poços de Caldas, Chapman et al. (1991) showed that plutonium and uranium have reached secular equilibrium in a pitchblende nodule and that the two elements have resided, unfractionated, in a system closed to them, but not closed to groundwater circulation, for the last 100 k.y. within the matrix phonolite. The implication from this observation (i.e., that plutonium and uranium may remain unfractionated in spent nuclear fuel of a repository) needs to be examined more completely.
- Colloidal transport of uranium was shown to be minimal at Koongarra and Poços de Caldas, where filtration of colloids appears to be effective. The observation of rapid transport of colloids at the Nevada Test Site must be tempered by knowledge that the natural system has been disturbed there by both nuclear testing and by pumping. The YMP TSPA-VA assumed no colloid filtration, an assumption that may be unnecessarily conservative.
- Fractures act as both transport pathways and places of retardation at a number of the analog sites. At Nopal I, uranium has been transported short distances, essentially completely along fractures, and is sorbed onto iron oxides and calcites. The same is true at Poços de Caldas. Matrix diffusion appears to have been inconsequential at Nopal I; thus, data from Nopal I is not likely to contribute to improved constraints on matrix diffusion in performance assessment models. Advective transport along fractures has been identified as a more significant transport mechanism than matrix diffusion in all of the analog sites, although matrix diffusion may account for loss of lead in uraninites at Oklo and Cigar Lake (Janeczek and Ewing 1992, p. 157). Even at Palmottu, where migration of uranium has been extensive, sorption onto fracture coatings has been identified as an important retardation mechanism. In the YMP TSPA, transport models are not sensitive to fracture sorption, but analogs suggest that fracture sorption enhances radionuclide retardation significantly.

- Although the study indicated that Chernobyl is generally not applicable as an analog to Yucca Mountain, two relevant points should be reiterated. First, spatial and temporal variations in infiltration rates and fast, preferential flow in the near-surface zone depend on differences in topography and geomorphology; at Chernobyl, these variations are more subtle than at Yucca Mountain. Second, rapid groundwater contamination around Chernobyl may not be directly associated with near-surface zones of preferential flow. The possibility of a similar discrepancy needs to be investigated in Yucca Mountain unsaturated zone flow and transport models in which high infiltration rates at the crest of the mountain may not correlate with data indicative of percolation flux at the potential repository horizon.
- Although the initial conditions and geologic medium are different at the Idaho National Engineering and Environmental Laboratory than at Yucca Mountain, the Beasley et al. (1998) study at the Idaho National Engineering and Environmental Laboratory provides a degree of confirmation of the conservative or retarding nature of a number of the same radionuclides that would be present in a Yucca Mountain repository (e.g., ^{36}Cl , ^{99}Tc , ^{236}U , ^{129}I , and ^{237}Np). This Idaho study provides a good bridge to future anthropogenic analog modeling exercises.

13.7 RECOMMENDATIONS

Given more time, additional potential analogs might have been identified. Some sites might be good potential analogs for certain processes, but the data are not readily available in the published literature (e.g., Mitchell Caverns, East Mojave National Park, California). Work in fiscal year 2000 is focusing on system components for which information appears to be sparse or for which no suitable analogs have been found and on areas that seem promising but for which little data are available.

One of the objectives of Section 13 is to provide a foundation for future direction of natural analog investigations. The following work is recommended:

- The literature search should be updated to include areas that were not covered in this report, such as biosphere processes, the role of microbes in radionuclide immobilization, the efficacy of a clay buffer in backfill, and chemical reactions at a cement-rock or cement-metal interface. The search should include other areas identified by performance assessment and design as their analyses mature. A diligent search for analogs of waste package metals or design enhancements such as backfill might be warranted. Additional radiolysis analogs deserve consideration because it is uncertain whether radiolysis will be a potential problem around waste packages in the Yucca Mountain Site Characterization Project Enhanced Design Alternative II design scenario, in which waste packages are not self-shielded. Furthermore, the role of microbes in the natural system at Yucca Mountain should be reassessed through more focused analog studies, based on observations at Poços de Caldas, where microbes have been cited as being responsible for reprecipitation of uraninite along the redox front and for enhancing the rate of migration of the redox front. The question at Yucca Mountain is whether a sufficient quantity of microbes would be present to affect uranium precipitation, combined with appropriate minerals (e.g., pyrite is absent at Yucca Mountain, but it is key to the microbial sulfur oxidation and uranium fixing at Poços de Caldas).
- Rainier Mesa data should be revisited to evaluate data gaps and determine where additional limited data collection may be necessary. These data could be used in drift seepage models for comparison with seepage under long-term average climate conditions. The data could be used to evaluate episodic pulses, such as those that affect the Paintbrush nonwelded unit, flow patterns and percolation fluxes from geochemical signatures, and sorption in vitric and zeolitic units.
- To understand preferential flow paths and dispersion/dilution in the saturated zone, well-characterized plumes at the Idaho National Engineering and Environmental Laboratory, supported by monitoring and characterization data, appear to be the most suitable and should be applied for testing models of saturated zone flow and transport. Results of the Box Canyon study provide a numerical foundation for future assessment of radionuclide transport at the Idaho National Engineering and Environmental Laboratory.
- Geochemical studies at Nopal I should be extended to the third dimension to ascertain whether preferential flow or drainage has taken place through fractures. This could be accomplished with analyses of rock and mineral samples from a cored borehole.

Samples of groundwater, perched water, and seepage water should be collected to address the extent and spatial dependence of uranium transport from the deposit through groundwater and other issues related to mechanisms controlling uranium concentration and transport, such as colloids, sorption onto fracture coatings, and preferential flow. With the availability of solid and fluid samples, data should be sufficient to model radionuclide transport at Peña Blanca using a natural analog approach based on parent-daughter relationships for the uranium and thorium decay series. The results could be used to understand and predict the mobility (or retardation) of analogous radioactive contaminants at Yucca Mountain.

- Data from vapor-dominated geothermal systems, having high similarity factors to Yucca Mountain (e.g., Larderello, Yellowstone, parts of New Zealand fields) (Table 13.4-1) and having similar thermal-hydrologic-chemical characteristics to those predicted at Yucca Mountain, should be used for building confidence in mineral reactions and rates used in numerical models of thermally coupled processes. Previous thermal-hydrologic-chemical thermodynamic and kinetic modeling studies described in this section should be extended to include the testing of reactive transport codes and models (e.g., TOUGHREACT, FEHM) using natural analog data. Analyses using codes capable of handling reactive transport associated with thermally coupled processes, such as those used in geothermal studies, are needed to represent the potential changes in hydrologic properties caused by mineral precipitation or dissolution. The changes in hydrologic properties and the extent of reaction of host rock to heat will be quite different in dry and saturated systems.
- Portions of the Pahute Ridge intrusive complex should be studied to observe fracture-matrix margins and to provide data for testing and validating porosity-permeability and fracture-matrix interaction models. A detailed petrologic study of devitrified and vitric host rocks as a function of distance from the intrusive contact should allow determination of key mineral reactions and hydrologic effects, including changes in matrix and fracture porosity and permeability. Field observations at the Pahute Ridge complex will also help to estimate kinetically and thermodynamically possible mineral reaction rates and to determine whether mineral reactions increase or decrease matrix or fracture permeability, with the objective of settling the controversy over potential fracture sealing at Yucca Mountain.
- Although most of the thermal-hydrologic-mechanical effects tend to be reversible and of small magnitude (CRWMS M&O 1998a, p. 191), the mechanical influence on the fracture network may require further analysis with respect to large-scale gas-phase flow effects while the repository is at its hottest. An anthropogenic analog, such as Krasnoyarsk-26, Russia, or another heated underground facility with decades of monitoring data, would be useful for building confidence in thermal-hydrologic-mechanical issues, in addition to examining the thermal effects on seepage.
- Some well-constrained analog data sets are available for immediate use. These data sets should be used to test models or make model predictions. The data sets and corresponding process models or total system performance assessment models include:
 - (1) Koongarra dispersion fan data in saturated zone plume dispersion models

(e.g., uranium transport is detected 300 m downstream in dispersion plume over 0.5 to 3 m.y.), (2) Akrotiri trace-element migration in unsaturated zone flow and transport models, (3) Nevada Test Site colloid data in unsaturated zone flow and transport model, (4) Nopal I U-series data in unsaturated zone flow and transport model, and (5) Nopal I uraninite dissolution rates in total system performance assessment models of spent nuclear fuel dissolution.

- The issue of illustrating confidence in operative processes to the public should be addressed, not only through the obvious archaeological materials that have survived for hundreds or thousands of years, but by using the results of some of the more quantitative analogs discussed in this section. In the absence of a total system analog for Yucca Mountain, the approach taken for the Canadian concept (Table 13.5-1), which used a one-to-one matching of repository component to a variety of analogs, would be a good illustration.

For all analog systems or processes studied, a careful review of data and previous modeling studies used is recommended to provide an understanding of the potential analog process or system coupled with comparison of the process or system to site-specific characteristics of the potential Yucca Mountain repository. Where feasible, this analysis should be followed by quantitative use of the analog information to build confidence in conceptual and numerical process models applied to Yucca Mountain.

INTENTIONALLY LEFT BLANK

13.8 REFERENCES

13.8.1 Documents Cited

Ababou, R.; Chowdhury, A.H.; Cragnolino, G.; Dodge, F.T.; Green, R.T.; Gureghian, A.B.; Hsiung, S.M.; Murphy, W.M.; Pabalan, R.T.; Percy, E.C.; Sagar, B.; and Sridhar, N. 1990. *Report on Research Activities for Calendar Year 1990*. Patrick, W.C., ed. NUREG/CR-5817. Washington, D.C.: U.S. Nuclear Regulatory Commission. TIC: 208964.

Absalom, J.P.; Crout, N.M.J.; and Young, S.D. 1996. "Modeling Radiocesium Fixation in Upland Organic Soils of Northwest England." *Environmental Science & Technology*, 30, (9), 2735-2741. Washington, D.C.: American Chemical Society. TIC: 246610.

Ahlers, C.F.; Finsterle, S.; and Bodvarsson, G.S. 1999. "Characterization and Prediction of Subsurface Pneumatic Response at Yucca Mountain, Nevada." *Journal of Contaminant Hydrology*, 38, (1-3), 47-68. New York, [New York]: Elsevier. TIC: 244160.

Airey, P.L. 1986. "Radionuclide Migration Around Uranium Ore Bodies in the Alligator Rivers Region of the Northern Territory of Australia — Analogue of Radioactive Waste Repositories — A Review." *Chemical Geology*, 55, (3/4), 255-268. Amsterdam, The Netherlands: Elsevier Science Publishers B.V. TIC: 246691.

Airey, P.L. 1987. "Application of Natural Analogue Studies to the Long-Term Prediction of Far Field Migration at Repository Sites." *Natural Analogues in Radioactive Waste Disposal, Symposium held in Brussels on 28-30 April 1987*. Côme, B. and Chapman, N.A., eds. Radioactive Waste Management Serial. EUR 11037 EN. Pages 32-41. Norwell, Massachusetts: Graham & Trotman. TIC: 247254.

Airey, P.L.; Duerden, P.; Roman, D.; Golian, C.; Nightingale, T.; Payne, T.; Davey, B.G.; Gray, D.; Snelling, A.; and Lever, D. 1987. "The Prediction of the Long-Term Migration of Radionuclides in the Far Field of High Level Waste Repositories: Results from the Alligator Rivers Natural Analogue Study." *The Geological Disposal of High Level Radioactive Wastes*. Brookins, D.G., ed. Athens, Greece: Theophrastus Publications, S.A. TIC: 243180.

Airey, P.L. and Ivanovich, M. 1985. "Geochemical Analogues of High Level Radioactive Waste Repositories." In Appendix 2 of *Natural Analogue Working Group, First Meeting, Brussels, November 5-7, 1985, Final Meeting Report*. Côme, B. and Chapman, N., eds. EUR 10315. Draft. [Luxembourg, Luxembourg]: Commission of the European Communities. TIC: 248005.

Alba, L.A. and Chavez, R. 1974. "K-Ar Ages of Volcanic Rocks from the Central Sierra Peña Blanca, Chihuahua, Mexico." *Isochron/West*, 10, 21-23. [Socorro, New Mexico: New Mexico Bureau of Mines and Mineral Resources]. TIC: 246110.

Alexander, D.H. and Van Luik, A.E. 1991. "Natural Analogue Studies Useful in Validating Regulatory Compliance Analyses." *Safety Assessment of Radioactive Waste Repositories, GEOVAL-1990, Symposium on Validation of Geosphere Flow and Transport Models, Stockholm*,

[Sweden], 14-17 May 1990. Pages 589-597. Paris, France: Organisation for Economic Co-operation and Development. TIC: 246109.

Allard, T. and Muller, J.P. 1998. "Kaolinite as an In Situ Dosimeter for Past Radionuclide Migration at the Earth's Surface." *Applied Geochemistry*, 13, (6), 751-765. [New York, New York]: Pergamon Press. TIC: 246131.

Arai, T.; Yusa, Y.; Sasaki, N.; Tsunoda, N.; and Takano, H. 1989. "Natural Analogue Study of Volcanic Glass – A Case Study of Basaltic Glasses in Pyroclastic Fall Deposits of Fuji Volcano, Japan." *Scientific Basis for Nuclear Waste Management XII, Symposium held October 10-13, 1988, Berlin, Germany*. Lutze, W. and Ewing, R.C., eds. 127, 73-80. Pittsburgh, Pennsylvania: Materials Research Society. TIC: 203660.

Bandurraga, T.M. and Bodvarsson, G.S. 1999. "Calibrating Hydrogeologic Parameters for the 3-D Site-Scale Unsaturated Zone Model of Yucca Mountain, Nevada." *Journal of Contaminant Hydrology*, 38, (1-3), 25-46. New York, New York: Elsevier. TIC: 244160.

Barnett, D.B.; Bergeron, M.P.; Cole, C.R.; Freshley, M.D.; and Wurstner, S.K. 1997. *Tritium Monitoring in Groundwater and Evaluation of Model Predictions for the Hanford Site 200 Area Effluent Treatment Facility*. PNNL-11665. Richland, Washington: Pacific Northwest National Laboratory. TIC: 246769.

Bath, A.H.; Berner, U.; Cave, M.; McKinley, I.G.; and Neal, C. 1987a. "Testing Geochemical Models in a Hyperalkaline Environment." *Natural Analogues in Radioactive Waste Disposal, Symposium held in Brussels on 28-30 April 1987*. Côme, B. and Chapman, N.A., eds. Radioactive Waste Management Series. EUR 11037 EN. Pages 167-178. Norwell, Massachusetts: Graham & Trotman. TIC: 247254.

Bath, A.H.; Christofi, N.; Neal, C.; Philp, J.C.; Cave, M.R.; McKinley, I.G.; and Berner, U. 1987b. *Trace Element and Microbiological Studies of Alkaline Groundwaters in Oman, Arabian Gulf: A Natural Analogue for Cement Pore-Waters*. Technical Report 87-16. [Wettingen, Switzerland]: Schweiz: Nationale Genossenschaft für die Lagerung Radioaktiver Abfälle. TIC: 244858.

Beasley, T.M.; Dixon, P.R.; and Mann, L.J. 1998. "⁹⁹Tc, ²³⁶U, and ²³⁷Np in the Snake River Plain Aquifer at the Idaho National Engineering and Environmental Laboratory, Idaho Falls, Idaho." *Environmental Science & Technology*, 32, (24), 3875-3881. Easton, Pennsylvania: American Chemical Society. TIC: 243863.

Belyaev, B.N.; Gavrilov, V.N.; Domkin, V.D.; Ivanova, V.P.; Tishkov, V.P.; Tishkova, N.A.; and Tsvetkov, O.S. 1997. "Isotope Composition of Plutonium in Soil and Possibilities of Contamination Source Identification." *Atomnaya Energiya*, 83, (4), 298-304. New York, New York: Consultants Bureau. TIC: 246731.

Benito, P.H.; Cook, P.; Faybishenko, B.; Freifeld, B.; and Doughty, C. 1998. *Analog Site for Fractured Rock Characterization, Box Canyon Pneumatic Connectivity Study, Preliminary Data Analysis*. Draft. Berkeley, California: Lawrence Berkeley National Laboratory. TIC: 247315.

Bish, D.L. and Aronson, J.L. 1993. "Paleogeothermal and Paleohydrologic Conditions in Silicic Tuff from Yucca Mountain, Nevada." *Clays and Clay Minerals*, 41, (2), 148-161. Long Island City, New York: Pergamon Press. TIC: 224613.

Blomqvist, R.; Jaakkola, T.; Niini, H.; and Ahonen, L., eds. 1991. *The Palmottu Analogue Project, Progress Report 1990, The Behaviour of Natural Radionuclides in and Around Uranium Deposits; Nr. 4*. YST-73. Espoo, Finland: Geological Survey of Finland. TIC: 247841.

Blomqvist, R.; Kaija, J.; Lampinen, P.; Paananen, M.; Ruskeeniemi, T.; Korkealaakso, J.; Pitkanen, P.; Ludvigson, J.-E.; Smellie, J.; Koskinen, L.; Floria, E.; Turrero, M.J.; Galarza, G.; Jakobsson, K.; Laaksoharju, M.; Casanova, J.; Grundfelt, B.; and Hernan, P. 1998. *The Palmottu Natural Analogue Project Phase I: Hydrogeological Evaluation of the Site*. EUR 18202 EN. Luxembourg, Luxembourg: Commission of the European Communities. TIC: 247326.

Blomqvist, R.; Lindberg, A.; Raisanen, E.; Suutarinen, R.; Jaakkola, T.; and Sukki, J. 1987. *The Occurrence and Migration of Natural Radionuclides in Groundwater, 1. Preliminary Results of Investigations in the Palmottu U-Th Deposit, Nummi-Pusula, SW Finland*. YST-60. Espoo, Finland: Geological Survey of Finland. TIC: 247696.

Blomqvist, R.; Sukki, J.; Ruskeeniemi, T.; Ahonen, L.; Niini, H.; Vuorinen, U.; and Jakobsson, K. 1995. *The Palmottu Natural Analogue Project, Summary Report 1992—1994, The Behaviour of Natural Radionuclides in and Around Uranium Deposits; Nr. 8*. YST-88. Espoo, Finland: Geological Survey of Finland. TIC: 247142.

Brookins, D.G. 1978. "Retention of Transuranic and Actinide Elements and Bismuth at the Oklo Natural Reactor, Gabon: Application of Eh-pH Diagrams." *Chemical Geology*, 23, 309-323. Amsterdam, The Netherlands: Elsevier Scientific Publishing Company. TIC: 247321.

Brookins, D.G. 1984. *Geochemical Aspects of Radioactive Waste Disposal*. New York, New York: Springer-Verlag. TIC: 206675.

Brookins, D.G. 1986. "Natural Analogues for Radwaste Disposal: Elemental Migration in Igneous Contact Zones." *Chemical Geology*, 55, 337-344. Amsterdam, The Netherlands: Elsevier. TIC: 246170.

Brookins, D.G. 1990. "Radionuclide Behavior at the Oklo Nuclear Reactor, Gabon." *Waste Management*, 10, 285-296. Amsterdam, The Netherlands: Pergamon Press. TIC: 237759.

Bros, R.; Andersson, P.; Roos, P.; Claesson, S.; Holm, E.; and Smellie, J. 1998. "Swedish Investigations on the Bangombé Reactor Zone U-Series Disequilibrium and Time-Scale of Radionuclide Mobilization Processes." *OKLO Working Group, Proceedings of the First Joint EC-CEA Workshop on the OKLO-Natural Analogue Phase II Project held in Sitjes, Spain, from 18 to 20 June 1997*. Louvat, D. and Davies, C., eds. Nuclear Science and Technology Series. EUR 18314 EN. Pages 187-195. Luxembourg, Luxembourg: Commission of the European Communities. TIC: 247320.

Bros, R.; Turpin, L.; Gauthier-Lafaye, F.; Holliger, PH.; and Stille, P. 1993. "Occurrence of Naturally Enriched ²³⁵U: Implications for Plutonium Behaviour in Natural Environments."

Geochimica et Cosmochimica Acta, 57, ([6]), 1351-1356. New York, New York: Pergamon. TIC: 246727.

Bruton, C.J.; Glassley, W.E.; and Bourcier, W.L. 1993. "Testing Geochemical Modeling Codes Using New Zealand Hydrothermal Systems." *Proceedings of the Topical Meeting on Site Characterization and Model Validation, FOCUS '93, September 26-29, 1993, Las Vegas, Nevada*. Pages 240-245. La Grange Park, Illinois: American Nuclear Society. TIC: 102245.

Bruton, C.J.; Glassley, W.E.; and Meike, A. 1995. *Geothermal Areas as Analogues to Chemical Processes in the Near-Field and Altered Zone of the Potential Yucca Mountain, Nevada Repository*. UCRL-ID-119842. Livermore, California: Lawrence Livermore National Laboratory. ACC: MOL.19960408.0126.

Buddemeier, R.W. and Hunt, J.R. 1988. "Transport of Colloidal Contaminants in Groundwater: Radionuclide Migration at the Nevada Test Site." *Applied Geochemistry*, 3, 535-548. Oxford, England: Pergamon Press. TIC: 224116.

Bugai, D.A.; Waters, R.D.; Dzhepo, S.P.; and Skalsk'ij, A.S. 1997. "The Cooling Pond of the Chernobyl Nuclear Power Plant; A Groundwater Remediation Case History." *Water Resources Research*, 33, (4), 677-688. Washington, D.C.: American Geophysical Union. TIC: 245850.

Byers, C.D.; Jercinovic, M.J.; and Ewing, R.C. 1987. *A Study of Natural Glass Analogues as Applied to Alteration of Nuclear Waste Glass*. NUREG/CR-4842. Washington, D.C.: U.S. Nuclear Regulatory Commission. TIC: 231239.

Carey, J.W.; Chipera, S.J.; Vaniman, D.T.; and Bish, D.L. 1997. *Three-Dimensional Mineralogic Model of Yucca Mountain, Nevada*. Milestone SP32B5M4, Rev. 1.1, Draft R0. Los Alamos, New Mexico: Los Alamos National Laboratory. ACC: MOL.19980520.0170.

Carroll, S.; Mroczek, E.; Bourcier, B.; Alai, M.; and Ebert, M. 1995. *Comparison of Field and Laboratory Precipitation Rates of Amorphous Silica from Geothermal Waters at 100 ° C*. Letter Report MOL207. Livermore, California: Lawrence Livermore National Laboratory. ACC: MOL.19960415.0465.

Castle, R.G. 1988. "Radioactivity in Water Supplies." *Journal of the Institution of Water and Environment Management*, 2, (3), 275-284. London, United Kingdom: Institution of Water and Environment Management. TIC: 247561.

Castor, S.B.; Henry, C.D.; and Shevenell, L.A. 1996. *Volcanic Rock-Hosted Uranium Deposits in Northwestern Nevada and Southeastern Oregon - Possible Sites for Studies of Natural Analogues for the Potential High-Level Nuclear Waste Repository at Yucca Mountain, Nevada*. Reno, Nevada: Nevada Bureau of Mines and Geology. ACC: MOL.19960927.0026.

Chapman, N.A.; McKinley, I.G.; Shea, M.E.; and Smellie, J.A.T. 1991. *The Poços de Caldas Project: Summary and Implications for Radioactive Waste Management*. SKB Technical Report 90-24. Stockholm, Sweden: Swedish Nuclear Fuel and Management Company. TIC: 205593.

Chapman, N.A.; McKinley, I.G.; Shea, M.E.; and Smellie, J.A.T., eds. 1992. "The Poços De Caldas Project: Natural Analogues of Processes in a Radioactive Waste Repository, Part I." *Journal of Geochemical Exploration (Special Issue)*, 45, (1-3), 1-603. Amsterdam, The Netherlands: Elsevier. On Order Library Tracking Number-247982

Chapman, N.A.; McKinley, I.G.; and Smellie, J.A.T. 1984. *The Potential of Natural Analogues in Assessing Systems for Deep Disposal of High-Level Radioactive Waste*. KBS Technical Report 84-16. Stockholm, Sweden: Swedish Nuclear Fuel and Waste Management Company. TIC: 205295.

Chapman, N.A. and Smellie, J.A.T. 1986. "Introduction and Summary of the Workshop." *Chemical Geology*, 55, 167-173. Amsterdam, The Netherlands: Elsevier Science. TIC: 246750.

Chapuis, A.M. and Blanc, P.L. 1993. "Oklo - Natural Analogue for Transfer Processes in a Geological Repository: Present Status of the Programme." *Migration of Radionuclides in the Geosphere, Proceedings of a Progress Meeting (Work Period 1991), Brussels, [Belgium], 9 and 10 April 1992*. von Maravic, H., and Moreno, J., eds. EUR 14690 EN. Pages 135-142. Luxembourg, Luxembourg: Commission of the European Communities. TIC: 247139.

Cole, C.R.; Williams, M.D.; Wurstner, S.K.; Thorne, P.D.; and Bergeron, M.P. 1997. *Three-Dimensional Analysis of Future Groundwater Flow Conditions and Transport in the Hanford Site Unconfined Aquifer System: FY 1996 and 1997 Status Report*. PNNL-11801. Richland, Washington: Pacific Northwest National Laboratory. TIC: 246446.

Cowan, G.A. 1976. "A Natural Fission Reactor." *Scientific American*, 235, (1), 36-47. New York, New York: Scientific American. TIC: 233076.

Cowan, R. and Ewing, R.C. 1989. "Freshwater Alteration of Basaltic Glass, Hanauma Bay, Oahu, Hawaii: A Natural Analogue for the Alteration of Borosilicate Glass in Freshwater." *Scientific Basis for Nuclear Waste Management XII, Symposium held October 10-13, 1988, Berlin, Germany*. Lutze, W. and Ewing, R.C., eds. 127, 49-56. Pittsburgh, Pennsylvania: Materials Research Society. TIC: 203660.

Cramer, J. 1995b. "Cigar Lake: A Natural Example of Long-Term Isolation of Uranium." *Radwaste Magazine*, 2, (3), 36-40. La Grange Park, Illinois: American Nuclear Society. TIC: 247698.

Cramer, J.J. 1986. "Sandstone-Hosted Uranium Deposits in Northern Saskatchewan as Natural Analogs to Nuclear Fuel Waste Disposal Vaults." *Chemical Geology*, 55, 269-279. Amsterdam, The Netherlands: Elsevier Science Publishers B.V. TIC: 246760.

Cramer, J.J. 1989. "Natural Analogue Studies on the Cigar Lake Uranium Deposit: An Update." *CEC Natural Analogue Working Group, Third Meeting, Snowbird, Near Salt Lake City, USA, June 15 to 17 1988*. Côme, B. and Chapman, N.A., eds. Nuclear Science and Technology Series. EUR 11725 EN. Pages 50-56. Luxembourg, Luxembourg: Commission of the European Communities. TIC: 7639.

Cramer, J.J. 1995a. *The Cigar Lake Uranium Deposit: Analog Information for Canada's Nuclear Fuel Waste Disposal Concept*. AECL-11204. Pinawa, Manitoba, Canada: Atomic Energy Canada Limited. TIC: 222109.

Cramer, J.J. and Sargent, F.P. 1994. "The Cigar Lake Analog Study: An International R&D Project." *High Level Radioactive Waste Management, Proceedings of the Fifth Annual International Conference, Las Vegas, Nevada, May 22-26, 1994*. 4, 2237-2242. La Grange Park, Illinois: American Nuclear Society. TIC: 210984.

Cramer, J.J. and Smellie, J.A.T. 1994. *Final Report of the AECL/SKB Cigar Lake Analog Study*. AECL-10851. Pinawa, Manitoba, Canada: Atomic Energy of Canada Limited. TIC: 212783.

Cramer, J.J.; Vilks, P.; and Larocque, J.P.A. 1987. "Near-Field Analog Features from the Cigar Lake Uranium Deposit." *Natural Analogues in Radioactive Waste Disposal, Symposium held in Brussels on 28-30 April 1987*. Côme, B. and Chapman, N.A., eds. Radioactive Waste Management Series. EUR 11037 EN. Pages 59-72. Norwell, Massachusetts: Graham & Trotman. TIC: 247254.

Crowe, B.; Self, S.; Vaniman, D.; Amos, R.; and Perry, F. 1983. "Aspects of Potential Magmatic Disruption of a High-Level Radioactive Waste Repository in Southern Nevada." *Journal of Geology*, 91, (3), 259-276. Chicago, Illinois: University of Chicago Press. TIC: 216959.

CRWMS M&O 1998a. "Thermal Hydrology." Chapter 3 of *Total System Performance Assessment-Viability Assessment (TSPA-VA) Analyses Technical Basis Document*. B00000000-01717-4301-00003 REV 01. Las Vegas, Nevada: CRWMS M&O. ACC: MOL.19981008.0003.

CRWMS M&O 1998b. "Near-Field Geochemical Environment." Chapter 4 of *Total System Performance Assessment-Viability Assessment (TSPA-VA) Analyses Technical Basis Document*. B00000000-01717-4301-00004 REV 00. Las Vegas, Nevada: CRWMS M&O. ACC: MOL.19980724.0393.

CRWMS M&O 1998c. "Waste Form Degradation, Radionuclide Mobilization, and Transport Through the Engineered Barrier System." Chapter 6 of *Total System Performance Assessment-Viability Assessment (TSPA-VA) Analyses Technical Basis Document*. B00000000-01717-4301-00006 REV 01. Las Vegas, Nevada: CRWMS M&O. ACC: MOL.19981008.0006.

CRWMS M&O 1998d. "Unsaturated Zone Radionuclide Transport." Chapter 7 of *Total System Performance Assessment-Viability Assessment (TSPA-VA) Analyses Technical Basis Document*. B00000000-01717-4301-00007 REV 00. Las Vegas, Nevada: CRWMS M&O. ACC: MOL.19980724.0396.

CRWMS M&O 1998e. "Saturated Zone Flow and Transport." Chapter 8 of *Total System Performance Assessment-Viability Assessment (TSPA-VA) Analyses Technical Basis Document*. B00000000-01717-4301-00008 REV 00. Las Vegas, Nevada: CRWMS M&O. ACC: MOL.19980724.0397.

CRWMS M&O 1999. *License Application Design Selection Report*. B00000000-01717-4600-00123 REV 01. Las Vegas, Nevada: CRWMS M&O. ACC: MOL.19990528.0303.

CRWMS M&O 2000a. *Seepage Calibration Model and Seepage Testing Data*. MDL-NBS-HS-000004 REV 00. Las Vegas, Nevada: CRWMS M&O. ACC: MOL.19990721.0521.

CRWMS M&O 2000b. *Natural Analogues for the Unsaturated Zone*. ANL-NBS-HS-000007 REV 00. Las Vegas, Nevada: CRWMS M&O. ACC: MOL.19990721.0524.

CRWMS M&O 2000c. *Drift-Scale Coupled Processes (DST and THC Seepage) Models*. MDL-NBS-HS-000001 REV 00. Las Vegas, Nevada: CRWMS M&O. ACC: MOL.19990721.0523.

CRWMS M&O 2000d. *Repository Safety Strategy: Plan to Prepare the Safety Case to Support Yucca Mountain Site Recommendation and Licensing Considerations*. TDR-WIS-RL-000001 REV 04. Las Vegas, Nevada: CRWMS M&O. Submit to RPC URN-0393

Curtis, D.; Benjamin, T.; Gancarz, A.; Loss, R.; Rosman, K.; DeLaeter, J.; Delmore, J.E.; and Maeck, W.J. 1989. "Fission Product Retention in the Oklo Natural Fission Reactors." *Applied Geochemistry*, 4, 49-62. New York, New York: Pergamon Press. TIC: 237970.

Curtis, D.; Fabryka-Martin, J.; Dixon, P.; and Cramer, J. 1999. "Nature's Uncommon Elements: Plutonium and Technetium." *Geochimica et Cosmochimica Acta*, 63, (2), 275-285. [New York, New York]: Pergamon. TIC: 246120.

Curtis, D.B. 1986. "Geochemical Controls on ⁹⁹Tc Transport and Retention." *Chemical Geology*, 55, 227-231. Amsterdam, The Netherlands: Elsevier. TIC: 246745.

Curtis, D.B.; Benjamin, T.M.; and Gancarz, A.J. 1981. "The Oklo Reactors: Natural Analogs to Nuclear Waste Repositories." *The Technology of High-Level Nuclear Waste Disposal*. Hofmann, P.L. and Breslin, J.J., eds. DOE/TIC-4621. Volume 1. Oak Ridge, Tennessee: U.S. Department of Energy, Technical Information Center. TIC: 246763.

Curtis, D.B. and Gancarz, A.J. 1983. *Radiolysis in Nature: Evidence from the Oklo Natural Reactors*. SKB Technical Report 83-10. Stockholm, Sweden: Swedish Nuclear Fuel and Waste Management Company. TIC: 205938.

Dansie, A. 1997. "Early Holocene Burials in Nevada: Overview of Localities, Research and Legal Issues." *Nevada Historical Society Quarterly*, 40, (1), 4-14. Reno, Nevada: Nevada Historical Society. On Order Library Tracking Number-248804

Dayvault, R.D.; Castor, S.B.; and Berry, M.R. 1985. "Uranium Associated with Volcanic Rocks of the McDermitt Caldera, Nevada and Oregon." *Uranium Deposits in Volcanic Rocks, Proceedings of a Technical Committee Meeting, El Paso, Texas, 2 - 5 April 1984*. IAEA-TC-490/30. Pages 379-409. Vienna, Austria: International Atomic Energy Agency. TIC: 247108.

Dearlove, J.P.L.; Green, D.C.; and Ivanovich, M. 1989. "Uranium Transport and the Partitioning of U, Th, and Ra Isotopes Between Solid and Aqueous Phases in the Krunkelbach Mine, Federal Republic of Germany." *Scientific Basis for Nuclear Waste Management XII, Symposium held*

October 10-13, 1988, Berlin, Germany. Lutze, W. and Ewing, R.C., eds. 127, 927-932. Pittsburgh, Pennsylvania: Materials Research Society. TIC: 203660.

De Laeter, J.R.; Rosman, J.K.R.; and Smith, C.L. 1980. "The Oklo Natural Reactor: Cumulative Fission Yields and Retentivity of the Symmetric Mass Region Fission Products." *Earth and Planetary Science Letters*, 50, 238-246. Amsterdam, The Netherlands: Elsevier Scientific Publishing Company. TIC: 237501.

Devarakonda, M.S. and Hickox, J.A. 1996. "Radioactive Wastes." *Water Environment Research*, 68, (4), 608-616. Alexandria, Virginia: Water Environment Federation. TIC: 246746.

DOE (U.S. Department of Energy) 1995. *Applications of Natural Analogue Studies to Yucca Mountain as a Potential High Level Radioactive Waste Repository*. DOE/YMSCO-002. Washington, D.C.: U.S. Department of Energy, Office of Civilian Radioactive Waste Management. ACC: MOL.19980928.0280.

DOE (U.S. Department of Energy) 1998a. *Introduction and Site Characteristics*. Volume 1 of *Viability Assessment of a Repository at Yucca Mountain*. DOE/RW-0508. Washington, D.C.: U.S. Department of Energy, Office of Civilian Radioactive Waste Management. ACC: MOL.19981007.0028.

DOE (U.S. Department of Energy) 1998b. *Total System Performance Assessment*. Volume 3 of *Viability Assessment of a Repository at Yucca Mountain*. DOE/RW-0508. Washington, D.C.: U.S. Department of Energy, Office of Civilian Radioactive Waste Management. ACC: MOL.19981007.0030.

Duerden, P.; Golian, C.; Hardy, C.J.; Nightingale, T.; and Payne, T. 1987. "Alligator Rivers Analogue Project: Review of Research and Its Implications for Model Validation." *Natural Analogues in Radioactive Waste Disposal, Symposium held in Brussels on 28-30 April 1987*. Côme, B. and Chapman, N.A., eds. Radioactive Waste Management Series. EUR 11037 EN. Pages 82-91. Norwell, Massachusetts: Graham & Trotman. TIC: 247254.

Edwards, R. 1997. "Seal for Chernobyl's Cracked Tomb." *New Scientist*, 153, (2067), 18. London, England: IPC Magazines. TIC: 247907.

Eliassen, A. 1990. "Chernobyl: A Summary Case Study with Emphasis on the Transport and Deposition to Scandinavia." Chapter 7 of *The Long-Range Atmospheric Transport of Natural and Contaminant Substances*. Knap, A.H. and Kaiser, M-S., eds. Pages 149-162. Boston, Massachusetts: Kluwer Academic Publishers. TIC: 247562.

Ericson, J.E. 1981. "Durability of Rhyolitic Obsidian Glass Inferred from Hydration Dating Research." *Scientific Basis for Nuclear Waste Management, Proceedings of the Third International Symposium, Boston, Massachusetts, November 17-20, 1980*. Moore, J.G., ed. 3, 283-290. New York, New York: Plenum Press. TIC: 204407.

Erlandsson, B.; Asking, L.; and Swietlicki, E. 1987. "Detailed Early Measurements of the Fallout in Sweden from the Chernobyl Accident." *Water, Air, and Soil Pollution*, 35, (3-4), 335-346. Dordrecht, Holland: D. Reidel Publishing. TIC: 246751.

Faybishenko, B.; Doughty, C.; Steiger, M.; Long, J.C.S.; Wood, T.; Jacobsen, J.; Lore, J.; and Zawislanski, P.T. 1999. *Conceptual Model of the Geometry and Physics of Water Flow in a Fractured Basalt Vadose Zone: Box Canyon Site, Idaho*. LBNL-42925. Berkeley, California: Lawrence Berkeley National Laboratory. TIC: 245840.

Faybishenko, B.; Salve, R.; Zawislanski, P.; Doughty, C.; Lee, K.H.; Cook, P.; Freifeld, B.; Jacobsen, J.; Sisson, B.; Hubbell, J.; and Dooley, K. 1998. *Ponded Infiltration Test at the Box Canyon Site, Data Report and Preliminary Analysis*. LBNL-40183. Berkeley, California: Lawrence Berkeley National Laboratory. ACC: MOL.19981002.0035.

Fayek, M.; Janeczek, J.; and Ewing, R.C. 1997. "Mineral Chemistry and Oxygen Isotopic Analyses of Uraninite, Pitchblende and Uranium Alteration Minerals from the Cigar Lake Deposit, Saskatchewan, Canada." *Applied Geochemistry*, 12, 549-565. Oxford, United Kingdom: Elsevier Science. TIC: 235776.

Finch, R.J. and Ewing, R.C. 1991. "Alteration of Natural UO₂ Under Oxidizing Conditions from Shinkolobwe, Katanga, Zaire: A Natural Analogue for the Corrosion of Spent Fuel." *Radiochimica Acta*, 52/53, 395-401. München, Germany: R. Oldenbourg Verlag. TIC: 237035.

Finch, R.J. and Ewing, R.C. 1992. "Alteration of Natural Uranyl Oxide Hydrates in Si-Rich Groundwaters: Implications for Uranium Solubility." *Scientific Basis for Nuclear Waste Management XV, Symposium held November 4-7, 1991, Strasbourg, France*. Sombret, C.G., ed. 257, 465-472. Pittsburgh, Pennsylvania: Materials Research Society. TIC: 204618.

Flint, L.E. 1998. *Characterization of Hydrogeologic Units Using Matrix Properties, Yucca Mountain, Nevada*. Water-Resources Investigations Report 97-4243. Denver, Colorado: U.S. Geological Survey. ACC: MOL.19980429.0512.

Fridrich, C.J.; Dudley, W.W., Jr.; and Stuckless, J.S. 1994. "Hydrogeologic Analysis of the Saturated-Zone Ground-Water System, Under Yucca Mountain, Nevada." *Journal of Hydrology*, 154, 133-168. Amsterdam, The Netherlands: Elsevier Science B.V. TIC: 224606.

Gancarz, A.; Cowan, G.; Curtis, D.; and Maeck, W. 1980. "⁹⁹Tc, Pb and Ru Migration Around the Oklo Natural Fission Reactors." *Scientific Basis for Nuclear Waste Management, Proceedings of the International Symposium, Boston, Massachusetts, November 27-30, 1979*. Northrup, C.J.M., Jr., ed. 2, 601-608. New York, New York: Plenum Press. TIC: 248272.

Garger, E.K.; Hoffman, F.O.; and Thiessen, K.M. 1997. "Uncertainty of the Long-Term Resuspension Factor." *Atmospheric Environment*, 31, (11), 1647-1656. Oxford, United Kingdom: Elsevier Science. TIC: 246785.

Gauthier-Lafaye, F.; Holliger, P.; and Blanc, P.-L. 1996. "Natural Fission Reactors in the Franceville Basin, Gabon: A Review of the Conditions and Results of a 'Critical Event' in a

Geologic System." *Geochimica et Cosmochimica Acta*, 60, (23), 4831-4852. New York, New York: Elsevier. TIC: 246607.

Gauthier-Lafaye, F. and Weber, F. 1989. "The Francevillian (Lower Proterozoic) Uranium Ore Deposits of Gabon." *Economic Geology*, 84, (8), 2267-2285. El Paso, Texas: Economic Geology Publishing Company. TIC: 246596.

Gauthier-Lafaye, F.; Weber, F.; and Ohmoto, H. 1989. "Natural Fission Reactors of Oklo." *Economic Geology*, 84, (8), 2286-2295. El Paso, Texas: Economic Geology Publishing Company. TIC: 246605.

Glassley, W.E. and Christensen, B.W. 1992. "Water-Rock Interaction in New Zealand Hydrothermal Systems: Comparison of Some Simulated and Observed Geochemical Processes." *High Level Radioactive Waste Management, Proceedings of the Third International Conference, Las Vegas, Nevada, April 12-16, 1992. 1*, 352-356. La Grange Park, Illinois: American Nuclear Society. TIC: 204231.

Golian, C. and Lever, D.A. 1992. "Radionuclide Transport." Volume 14 of *Alligator Rivers Analogue Project*. DOE/HMIP/RR/92/084. Menai, New South Wales, Australia: Australian Nuclear Science and Technology Organisation. TIC: 235988.

Goodell, P. 1985. "Chihuahua City Uranium Province, Chihuahua, Mexico." *Uranium Deposits in Volcanic Rocks, Proceedings of a Technical Committee Meeting, El Paso, Texas, 2 - 5 April, 1984*. IAEA-TC-490/19. Pages 97-124. Vienna, Austria: International Atomic Energy Association. TIC: 247108.

Goodwin, B.W.; Cramer, J.J.; and McConnell, D.B. 1989. "The Cigar Lake Uranium Deposit: An Analogue for Nuclear Fuel Waste Disposal." Appendix B of *Natural Analogues in Performance Assessments for the Disposal of Long Lived Radioactive Wastes*. Technical Reports Series 304. Vienna, Austria: International Atomic Energy Agency. TIC: 7851.

Grambow, B.; Jercinovic, M.J.; Ewing, R.C.; and Byers, C.D. 1986. "Weathered Basalt Glass: A Natural Analogue for the Effects of Reaction Progress on Nuclear Waste Glass Alteration." *Scientific Basis for Nuclear Waste Management IX, Symposium held September 9-11, 1985, Stockholm, Sweden*. Werme, L.O., ed. 50, 263-272. Pittsburgh, Pennsylvania: Materials Research Society. TIC: 206807.

Grossenbacher, K. and Faybishenko, B. 1997. *Spacing of Thermally Induced Columnar Joints in Basalt: Variation with Depth*. Berkeley, California: Lawrence Berkeley National Laboratory, Earth Sciences Division. TIC: 247646.

Gudzenko, V. 1992. "Some Problems of the Radionuclides Migration Research." *Third Research Co-Ordination Meeting on Nuclear Techniques in the Study of Pollutant Transport in the Environment: Interaction of Solutes with Geological Media (Methodological Aspects)*, Vienna, Austria, 22-25 June 1992. Vienna, Austria: International Atomic Energy Agency. TIC: 247334.

Gudzenko, V.V.; Klimchuk, A.B.; Yablokova, N.L.; Gudzenko, G.I.; and Golikova, T.A. 1991. *Osushchestvit' Radiogidrogeologicheskie Obsledovanie Tekhnogennykh Podzemnykh Polosteig. Kieva s Tsel'yu Otsenki Skorosti Proniknoveniya Radionuklidov v Podzemnyu Gidrosferu (To Provide Radiohydrogeological Observations in Underground Adits of the City of Kiev for the Purpose of Evaluating the Velocity of Radionuclide Migration in the Groundwater System)*. Kiev, Ukraine: Institute of Geological Sciences of the Ukrainian National Academy of Sciences. ACC: MOL.20000609.0003.

Gudzenko, V.V.; Shestopalov, V.M.; and Sobotovich, E.V. 1990. "The Isotopic Studies of Subsurface Water Protection from Radioactive Pollution in the Areas of Nuclear Power Plant Siting." *The International Journal of Radiation Applications and Instrumentation. Part E: Nuclear Geophysics*, 4, (1), 119-124. Oxford, England: Pergamon Press. TIC: 247327.

Gurban, I.; Laaksoharju, M.; Ledoux, E.; Made, B.; and Salignac, A.L. 1998. *Indications of Uranium Transport Around the Reactor Zone at Bagombé (Oklo)*. SKB Technical Report 98-06. Stockholm, Sweden: Swedish Nuclear Fuel and Waste Management Company. TIC: 241252.

Hardin, E.L. 1998. *Near-Field/Altered-Zone Models Report*. UCRL-ID-129179 DR. Livermore, California: Lawrence Livermore National Laboratory. ACC: MOL.19980504.0577.

Hardy, C.J. and Duerden, P. 1989. "Progress in the Alligator Rivers Analogue Project." *Nuclear Science and Technology, CEC Natural Analogue Working Group, Third Meeting, Snowbird, Near Salt Lake City, USA, June 15 to 17 1988*. Côme, B. and Chapman, N.A., eds. Nuclear Science and Technology Series. EUR 11725 EN. Pages 43-49. Luxembourg, Luxembourg: Commission of the European Communities. TIC: 7639.

Hatano, Y.; Hatano, N.; Amano, H.; Ueno, T.; Sukhoruchkin, A.K.; and Kazakov, S.V. 1998. "Aerosol Migration Near Chernobyl: Long-Term Data and Modeling." *Atmospheric Environment*, 32, (14-15), 2587-2594. Oxford, England: Pergamon Press. TIC: 247328.

Hevesi, J.A.; Flint, A.L.; and Istok, J.D. 1992. "Precipitation Estimation in Mountainous Terrain Using Multivariate Geostatistics. Part II: Isohyetal Maps." *Journal of Applied Meteorology*, 31, (7), 677-688. Boston, Massachusetts: American Meteorological Society. TIC: 225248.

Hird, A.B.; Rimmer, D.L.; and Livens, F.R. 1995. "Total Caesium-Fixing Potentials of Acid Organic Soils." *Journal of Environmental Radioactivity*, 26, (2), 103-118. New York, New York: Elsevier Science. TIC: 247488.

Hoffman, D.C. and Daniels, W.R. 1981. *Assessment of the Potential for Radionuclide Migration from a Nuclear Explosion Cavity*. LA-UR-81-3181. Los Alamos, New Mexico: Los Alamos National Laboratory. TIC: 204725.

Hofmann, B.A. 1989. "Geochemical Analogue Study in the Krunkelbach Mine, Menzenschwand, Southern Germany: Geology and Water-Rock Interaction." *Scientific Basis for Nuclear Waste Management XII, Symposium held October 10-13, 1988, Berlin, Germany*.

Lutze, W. and Ewing, R.C., eds. 127, 921-926. Pittsburgh, Pennsylvania: Materials Research Society. TIC: 203660.

Holliger, Ph. 1993. "Geochemical and Isotopic Characterization of the Reaction Zones (Uranium, Transuranium, Lead and Fission Products)." [*Oklo Working Group Meeting, Proceedings of the 2nd Joint CEC-CEA Progress Meeting held in Brussels on 6-7 April 1992*]. [von Maravic, H., ed. EUR 14877 EN]. Pages 25-35. [Luxembourg, Luxembourg: Commission of the European Communities]. TIC: 247912.

Holloway, R.W. and Liu, C.K. 1988. "Xenon-133 in California, Nevada, and Utah from the Chernobyl Accident." *Environmental Science and Technology*, 22, (5), 583-586. Washington, D.C.: American Chemical Society. TIC: 247565.

Huang, K.; Tsang, Y.W.; and Bodvarsson, G.S. 1999. "Simultaneous Inversion of Air-Injection Tests in Fractured Unsaturated Tuff at Yucca Mountain." *Water Resources Research*, 35, (8), 2375-2386. Washington, D.C.: American Geophysical Union. TIC: 245633.

IAEA (International Atomic Energy Agency) 1975. *The Oklo Phenomenon, Proceedings of a Symposium, Libreville, Gabon, 23 to 27 June 1975*. Vienna, Austria: International Atomic Energy Agency. TIC: 239176.

IAEA (International Atomic Energy Agency) 1978. *Les Reacteurs de Fission Naturels, Natural Fission Reactors. Proceedings of a Meeting on the Technical Committee on Natural Fission Reactors, Paris, 19 to 21 December 1977*. STI/PUB/475. Vienna, Austria: International Atomic Energy Agency. TIC: 247910.

Isobe, H.; Ewing, R.C.; and Murakami, T. 1994. "Formation of Secondary Uranium Minerals in the Koongarra Deposit, Australia." *Scientific Basis for Nuclear Waste Management XVII, Symposium held November 29-December 3, 1993, Boston, Massachusetts*. Barkatt, A. and Van Konynenburg, R.A., eds. 333, 653-660. Pittsburgh, Pennsylvania: Materials Research Society. TIC: 213541.

Isobe, H.; Murakami, T.; and Ewing, R.C. 1992. "Alteration of Uranium Minerals in the Koongarra Deposit, Australia: Unweathered Zone." *Journal of Nuclear Materials*, 190, 174-187. Amsterdam, The Netherlands: Elsevier Science Publishers. TIC: 246371.

Ivanov, Yu.A.; Kashparov, V.A.; Oreshich, A.A.; and Nechiporenko, O.V. 1991. "Nekotorye Problemy Pochvennoi Khimii Radionuklidov Vybrosa CHAES na Territorii Poles'ya [Some Problems of Soil Chemistry of Radionuclides Ejected from CHNPP on the Poles'ye Area]." *Problemy Sel'skokhozyaistvennoi Radiologii [Problems of Agricultural Radiology]*, 48-61. Kiev, Ukraine: Ukrainian Research Institute of Agricultural Radioecology. ACC: MOL.20000609.0004.

Ivanovich, M.; Duerden, P.; Payne, T.; Nightingale, T.; Longworth, G.; Wilkins, M.A.; Edghill, R.B.; Cockayne, D.J.; and Davey, B.G. 1987. "Natural Analogue Study of the Distribution of Uranium Series Radionuclides Between the Colloid and Solute Phases in the Hydrogeological System of the Koongarra Uranium Deposit N.T., Australia." *Natural Analogues in Radioactive Waste Disposal, Symposium held in Brussels on 28-30 April 1987*. Côme, B. and Chapman,

N.A., eds. Radioactive Waste Management Series. EUR 11037 EN. Pages 300-313. Norwell, Massachusetts: Graham & Trotman. TIC: 247254.

Ivanovich, M. and Harmon, R.S., eds. 1992. *Uranium-Series Disequilibrium: Applications to Earth, Marine, and Environmental Sciences*. New York, New York: Oxford University Press. TIC: 234680.

Iwatsuki, T.; Sato, K.; Seo, T.; and Hama, K. 1995. "Hydrogeochemical Investigation of Groundwater in the Tono Area, Japan." *Scientific Basis for Nuclear Waste Management XVIII, Symposium held October 23-27, 1994, Kyoto, Japan*. Murakami, T. and Ewing, R.C., eds. 353, Part 2, 1251-1257. Pittsburgh, Pennsylvania: Materials Research Society. TIC: 216341.

Jaakkola, T.; Suksi, J.; Suutarinen, R.; Niini, H.; Ruskeeniemi, T.; Söderholm, B.; Vesterinen, M.; Blomqvist, R.; Halonen, S.; and Lindberg, A. 1989. *The Behaviour of Radionuclides in and Around Uranium Deposits. II: Results of Investigations at the Palmottu Analogue Study Site, SW Finland*. YST-64. Espoo, Finland: Geological Survey of Finland. TIC: 247721.

Jakubick, A.T. and Church, W. 1986. *Oklo Natural Reactors: Geological and Geochemical Conditions - A Review*. INFO-0179. Ottawa, Canada: Atomic Energy Board of Canada. TIC: 238711.

Janeczek, J. and Ewing, R.C. 1992. "Dissolution and Alteration of Uraninite Under Reducing Conditions." *Journal of Nuclear Materials*, 190, 157-173. Amsterdam, The Netherlands: Elsevier Science. TIC: 247465.

Jensen, K.A.; Ewing, R.C.; and Gauthier-Lafaye, F. 1997. "Uraninite: A 2 Ga Spent Nuclear Fuel from the Natural Fission Reactor at Bangombé in Gabon, West Africa." *Scientific Basis for Nuclear Waste Management XX, Symposium held December 2-6, 1996, Boston, Massachusetts*. Gray, W.J. and Triay, I.R., eds. 465, 1209-1218. Pittsburgh, Pennsylvania: Materials Research Society. TIC: 238884.

Jercinovic, M.J. and Ewing, R.C. 1987. *Basaltic Glasses from Iceland and the Deep Sea: Natural Analogues to Borosilicate Nuclear Waste-Form Glass*. JSS Project Technical Report 88-01. Stockholm, Sweden: Swedish Nuclear Fuel and Waste Management Company. TIC: 205668.

Jercinovic, M.J.; Ewing, R.C.; and Byers, C.D. 1986. "Alteration Products of Basalt Glass from Frenchman Springs Flow, Wanapum Basalts, Hanford, Washington." *Nuclear Waste Management II, Third Annual Symposium on Ceramics in Nuclear Waste Management, April 28-30, 1986, Chicago, Illinois*. Clark, D.E.; White, W.B.; and Machiels, A.J., eds. *Advances in Ceramics* Volume 20. Pages 671-679. Westerville, Ohio: American Ceramic Society. TIC: 210019.

Johnson, A.B., Jr. and Francis, B. 1980. *Durability of Metals from Archaeological Objects, Metal Meteorites, and Native Metals*. PNL-3198. Richland, Washington: Pacific Northwest Laboratory. TIC: 229619.

Kaplan, M.F. 1980. "Characterization of Weathered Glass by Analyzing Ancient Artifacts." *Scientific Basis for Nuclear Waste Management, Proceedings of the International Symposium, Boston, Massachusetts, November 27-30, 1979*. Northrup, C.J.M., Jr., ed. 2, 85-92. New York, New York: Plenum Press. TIC: 248272.

Kaplan, M.F. and Mendel, J.E. 1982. "Ancient Glass and the Safe Disposal of Nuclear Waste." *Archaeology*, 35, (4), 22-29. New York, New York: Archeological Institute of America. TIC: 247471.

Kashparov, V.A.; Ivanov, Y.A.; Zvarisch, S.I.; Protsak, V.P.; Khomutinin, Y.V.; Kurepin, A.D.; and Pazukhin, E.M. 1996. "Formation of Hot Particles During the Chernobyl Nuclear Power Plant Accident." *Nuclear Technology*, 114, (2), 246-253. La Grange Park, Illinois: American Nuclear Society. TIC: 247464.

Katayama, N.; Kubo, K.; and Hirono, S. 1974. "Genesis of Uranium Deposits of the Tono Mine, Japan." *Formation of Uranium Ore Deposits, Proceedings of a Symposium on the Formation of Uranium Ore Deposits, Athens, Greece, May 6-10, 1974*. IAEA-SM-183/11. Pages 437-452. Vienna, Austria: International Atomic Energy Agency. TIC: 247921.

Kersting, A.B.; Efurud, D.W.; Finnegan, D.L.; Rokop, D.J.; Smith, D.K.; and Thompson, J.L. 1999. "Migration of Plutonium in Ground Water at the Nevada Test Site." *Nature*, 397, 56-59. London, England: Macmillan Publishers. TIC: 243597.

Khoury, H.N.; Salameh, E.; Clark, I.D.; Fritz, P.; Milodowski, A.E.; Cave, M.R.; Bajjali, W.; and Alexander, W.R. 1992. "A Natural Analogue of High pH Cement Pore Waters from the Maqarin Area of Northern Jordan. I: Introduction to the Site." *Journal of Geochemical Exploration*, 46, (1), 117-132. New York, New York: Elsevier Science. TIC: 247469.

Kliashtorin, A.L.; Tikhomirov, F.A.; and Shcheglov, A.I. 1994. "Lysimetrical Study of Radionuclides in the Forests Around the Chernobyl Nuclear Power Plant." *Journal of Environmental Radioactivity*, 24, (1), 81-90. London, England: Elsevier Applied Science Publishers. TIC: 247463.

Knutson, C.F.; Cox, D.O.; Dooley, K.J.; and Sisson, J.B. 1993. "Characterization of Low-Permeability Media Using Outcrop Measurements." *68th Annual Technical Conference and Exhibition of the Society of Petroleum Engineers, Houston, Texas, 3-6 October 1993*. SPE 26487. Richardson, Texas: Society of Petroleum Engineers. TIC: 247011.

Kononovich, A.L.; Kulebakina, L.G.; Kulebakin, O.Y.; Arkhipov, N.P.; and Arkhipov, A.N. 1996. "¹³⁷Cs Migration with Underground Water from the Double Prime Red Forest Double Prime Storage at the Chernobyl NPP." *Atomnaya Energiya*, 81, (6), 455-459. New York, New York: Consultants Bureau. On Order Library Tracking Number-248617

Konoplev, A.V.; Borzilov, V.A.; Bobovnikova, Ts.I.; Virchenko, E.P.; Popov, V.E.; Kutnyakov, I.V.; and Chumichev, V.B. 1988. "Distribution of Radionuclides in the Soil-Water System Due to Fallout After the Chernobyl Disaster." *Soviet Meteorology and Hydrology*, 12, 42-49. New York, New York: Allerton Press. TIC: 247914.

Koss, V. and Kim, J.I. 1990. "Modeling of Strontium Sorption and Speciation in a Natural Sediment-Groundwater System." *Journal of Contaminant Hydrology*, 6, (3), 267-280. Amsterdam, The Netherlands: Elsevier Science. TIC: 247467.

Kovach, L.A. and Murphy, W.M., eds. 1995. *Proceedings of the Workshop on the Role of Natural Analogs in Geologic Disposal of High-Level Nuclear Waste, held in San Antonio, Texas, July 22-25, 1991*. NUREG/CP-0147. Washington, D.C.: U.S. Nuclear Regulatory Commission. TIC: 225202.

Krumhansl, J.L. and Stockman, H.W. 1988. "Site Selection Criteria and Preliminary Results from the Valles Caldera Natural Analog Study." *Proceedings of Workshop IV on Flow and Transport Through Unsaturated Fractured Rock -- Related to High-Level Radioactive Waste Disposal, December 12-15, 1998, Tucson, Arizona*. Pages 249-276. [Tucson, Arizona: University of Arizona]. TIC: 247519.

Lebedev, I.A.; Myasoedov, B.F.; Pavlotskaya, F.I.; and Frenkel', V.Ya. 1992. "Plutonium Content in Soils of the European Part of the Country After the Accident at Chernobyl Nuclear Generating Station." *Atomic Energy, A Translation of Atomnaya Energiya*, 72, (6), 515-520. New York, New York: Consultants Bureau. TIC: 247771.

Leslie, B.W.; Percy, E.C.; and Prikryl, J.D. 1993. "Oxidative Alteration of Uraninite at the Nopal I Deposit, Mexico: Possible Contaminant Transport and Source Term Constraints for the Proposed Repository at Yucca Mountain." *Scientific Basis for Nuclear Waste Management XVI, Symposium held November 30-December 4, 1992, Boston, Massachusetts*. Interrante, C.G. and Pabalan, R.T., eds. 294, 505-512. Pittsburgh, Pennsylvania: Materials Research Society. TIC: 208880.

Leslie, B.W.; Pickett, D.A.; and Percy, E.C. 1999. "Vegetation-Derived Insights on the Mobilization and Potential Transport of Radionuclides from the Nopal I Natural Analog Site, Mexico." *Scientific Basis for Nuclear Waste Management XXII, Symposium held November 30-December 4, 1998, Boston, Massachusetts, U.S.A.* Wronkiewicz, D.J. and Lee, J.H., eds. 556, 833-842. Warrendale, Pennsylvania: Materials Research Society. TIC: 246426.

Lichtner, P.C.; Keating, G.; and Carey, B. 1999. *A Natural Analogue for Thermal-Hydrological-Chemical Coupled Processes at the Proposed Nuclear Waste Repository at Yucca Mountain, Nevada*. LA-13610-MS. Los Alamos, New Mexico: Los Alamos National Laboratory. TIC: 246032.

Lippard, S.J.; Shelton, A.W.; and Gass, I.G. 1986. *The Ophiolite of Northern Oman*. Memoir No. 11. Oxford, England: Blackwell Scientific Publications. TIC: 247675.

Llaurado, M.; Vidal, M.; Rauret, G.; Roca, C.; Fons, J.; and Vallejo, V.R. 1994. "Radiocaesium Behaviour in Mediterranean Conditions." *Journal of Environmental Radioactivity*, 23, (1), 81-100. New York, New York: Elsevier Applied Science Publishers. TIC: 247473.

Loshchilov, N.A.; Bondar, P.F.; and Ivanov, Y.A. 1991a. "Nauchno-Eksperimental'noe Obosnovanie Ekspress-Metodiki Otsenki Zagryazneniya Sel'skokhozyaistvennykh Ugodii Radioaktivnymi Izotopami Tseziya [Scientific-Experimental Substantiation of Express-Method

of Estimation of Contamination of Agricultural Lands by Radioactive Isotopes of Cesium]." *Problemy Sel'skokhozyaistvennoi Radiologii [Problems of Agricultural Radiology]*, Pages 15-36. Kiev, Ukraine: Ukrainian Research Institute of Agricultural Radioecology. ACC: MOL.20000609.0006; MOL.20000629.0595.

Loshchilov, N.A.; Ivanov, Y.A.; Kashparov, V.A.; Levchuk, S.E.; Bondar, P.F.; and Dyrenko, L.V. 1991b. "Vertikal'naya Migratsiya v Pochvakh Poles'ya Radionuklidov Bybrosa ChAES v Razlichnykh Fiziko-Chimicheskikh Formakh [Vertical Migration of Radionuclides of Different Physical-Chemical Forms Ejected from the CHNPP in Soils of Poles'ye]." *Problemy Sel'skokhozyaistvennoi Radiologii [Problems of Agricultural Radiology]*, Pages 36-61. Kiev, Ukraine: Ukrainian Research Institute of Agricultural Radioecology. ACC: MOL.20000609.0005; MOL.20000629.0596.

Loshchilov, N.A.; Kashparov, V.A.; and Polyakov, V.D. 1991c. "Sootnosheniya Transuranovykh Elementov v 'Goryachikh' Chastitsakh, Vypavshikh v Rezultate Avarii v Blizhnei Zone ChAES [Relationships of Transuranium Elements in 'Hot' Particles of the Fallout in the Near-Field Zone of the CHNPP]." *Problemy Sel'skokhozyaistvennoi Radiologii [Problems of Agricultural Radiology]*, Pages 45-48. Kiev, Ukraine: Ukrainian Research Institute of Agricultural Radioecology. ACC: MOL.20000609.0007.

Loss, R.D.; Rosman, K.J.R.; De Laeter, J.R.; Curtis, D.B.; Benjamin, T.M.; Gancarz, A.J.; Maeck, W.J.; and Delmore, J.E. 1989. "Fission-Product Retentivity in Peripheral Rocks at the Oklo Natural Fission Reactors, Gabon." *Chemical Geology*, 76, (1/2), 71-84. Amsterdam, The Netherlands: Elsevier Science. TIC: 247476.

Louvat, D. and Davies, C., eds. 1998. *Oklo Working Group: Proceedings of the First Joint EC-CEA Workshop on the Oklo-Natural Analogue Phase II Project Held in Sitjes, Spain, from 18 to 20 June 1997*. EUR 18314 EN. Luxembourg, Luxembourg: Office for Official Publications of the European Communities. TIC: 247709.

Luckey, R.R.; Tucci, P.; Faunt, C.C.; Ervin, E.M.; Steinkampf, W.C.; D'Agnesse, F.A.; and Patterson, G.L. 1996. *Status of Understanding of the Saturated-Zone Ground-Water Flow System at Yucca Mountain, Nevada, as of 1995*. Water-Resources Investigations Report 96-4077. Denver, Colorado: U.S. Geological Survey. ACC: MOL.19970513.0209.

Lutze, W.; Grambow, B.; Ewing, R.C.; and Jercinovic, M.J. 1987. "The Use of Natural Analogues in the Long-Term Extrapolation of Glass Corrosion Processes." *Natural Analogues in Radioactive Waste Disposal, Symposium held in Brussels on 28-30 April 1987*. Côme, B. and Chapman, N.A., eds. Radioactive Waste Management Series. EUR 11037 EN. Pages 142-152. Norwell, Massachusetts: Graham & Trotman. TIC: 247254.

MacKenzie, A.B.; Scott, R.D.; Linsalata, P.; Miekeley, N.; Osmond, J.K.; and Curtis, D.B. 1991. *Natural Radionuclide and Stable Element Studies of Rock Samples from the Osamu Utsumi Mine and Morro do Ferro Analogue Study Sites, Poços de Caldas, Brazil*. SKB Technical Report 90-16. Stockholm, Sweden: Swedish Nuclear Fuel and Waste Management Company. TIC: 204990.

Malow, G. and Ewing, R.C. 1981. "Nuclear Waste Glasses and Volcanic Glasses: A Comparison of Their Stabilities." *Scientific Basis for Nuclear Waste Management, Proceedings of the Third International Symposium, Boston, Massachusetts, November 17-20, 1980*. Moore, J.G., ed. 3, 315-322. New York, New York: Plenum Press. TIC: 204407.

Mamikhin, S.V. 1995. "Mathematical Model of ^{137}Cs Vertical Migration in a Forest Soil." *Journal of Environmental Radioactivity*, 28, (2), 161-170. New York, New York: Elsevier Science. TIC: 247489.

Maqarin Natural Analogue Site Study Group 1992. *A Natural Analogue Study of the Maqarin Hyperalkaline Groundwaters. I. Source Term Description and Thermodynamic Database Testing*. NAGRA Technical Report 91-10. Wettingen, Switzerland: National Cooperative for the Disposal of Radioactive Waste. TIC: 247316.

Matyskiela, W. 1997. "Silica Redistribution and Hydrologic Changes in Heated Fractured Tuff." *Geology*, 25, (12), 1115-1118. Boulder, Colorado: Geological Society of America. TIC: 236809.

McCright, R.D. 1998. *Corrosion Data and Modeling, Update for Viability Assessment*. Volume 3 of *Engineered Materials Characterization Report*. UCRL-ID-119564, Rev. 1.1. Livermore, California: Lawrence Livermore National Laboratory. ACC: MOL.19980806.0177.

McKinley, I.G.; Bath, A.H.; Berner, U.; Cave, M.; and Neal, C. 1988. "Results of the Oman Analogue Study." *Radiochimica Acta*, 44/45, (II), 311-316. München, Germany: R. Oldenbourg Verlag. TIC: 247492.

McKinley, P.W.; Long, M.P.; and Benson, L.V. 1991. *Chemical Analyses of Water from Selected Wells and Springs in the Yucca Mountain Area, Nevada and Southeastern California*. Open-File Report 90-355. Denver, Colorado: U.S. Geological Survey. ACC: NNA.19901031.0004.

Meijer, A. 1987. *Investigations of Natural Geologic and Geochemical Analogs in Relation to a Potential Nuclear Waste Repository at Yucca Mountain, Nevada*. Milestone R398. Draft. Los Alamos, New Mexico: Los Alamos National Laboratory. ACC: NNA.19900112.0350.

Miekeley, N.; Coutinho de Jesus, H.; Porto da Silveira, C.L.; and Degueudre, C. 1991b. *Chemical and Physical Characterisation of Suspended Particles and Colloids in Waters from the Osamu Utsumi Mine and Morro do Ferro Analogue Study Sites, Poços de Caldas, Brazil*. SKB Technical Report 90-18. Stockholm, Sweden: Swedish Nuclear Fuel and Waste Management Company. TIC: 206355.

Miekeley, N.; Coutinho de Jesus, H.; Porto da Silveira, C.L.; Linsalata, P.; Morse, R.; and Osmond, J.K. 1991a. *Natural Series Radionuclide and Rare-Earth Element Geochemistry of Waters from the Osamu Utsumi Mine and Morro do Ferro Analogue Study Sites, Poços de Caldas, Brazil*. SKB Technical Report 90-17. Stockholm, Sweden: Swedish Nuclear Fuel and Waste Management Company. TIC: 206354.

Miekeley, N.; Jesus, H.C.; Silveira, C.L.P.; and Kuechler, I.L. 1989. "Colloid Investigations in the Poços de Caldas Natural Analogue Project." *Scientific Basis for Nuclear Waste Management XII, Symposium Held October 10-13, 1988, Berlin, Germany*. Lutze, W. and Ewing, R.C., eds. 127, 831-842. Pittsburgh, Pennsylvania: Materials Research Society. TIC: 203660.

Miller, B. and Chapman, N. 1995. "Postcards from the Past: Archaeological and Industrial Analogs for Deep Repository Materials." *Radwaste Magazine*, 2, (1), 32-42. La Grange Park, Illinois: American Nuclear Society. TIC: 247909.

Miller, W.; Alexander, R.; Chapman, N.; McKinley, I.; and Smellie, J. 1994. *Natural Analogue Studies in the Geological Disposal of Radioactive Wastes*. Studies in Environmental Science 57. New York, New York: Elsevier. TIC: 101822.

Moltenbrey, K. 1999. "Extreme Visualization." *Computer Graphics World*, 22, (1), 42-46. Nashua, New Hampshire: PennWell Publishing. TIC: 247567.

Montazer, P. and Wilson, W.E. 1984. *Conceptual Hydrologic Model of Flow in the Unsaturated Zone, Yucca Mountain, Nevada*. Water-Resources Investigations Report 84-4345. Lakewood, Colorado: U.S. Geological Survey. ACC: NNA.19890327.0051.

Murakami, T.; Ohnuki, T.; Isobe, H.; and Sato, T. 1997. "Mobility of Uranium During Weathering." *American Mineralogist*, 82, 888-899. Washington, D.C.: Mineralogical Society of America. TIC: 246053.

Murphy, W.M. 1995. "Natural Analogs for Yucca Mountain." *Radwaste Magazine*, 2, (6), 44-50. La Grange Park, Illinois: American Nuclear Society. TIC: 237929.

Murphy, W.M.; Percy, E.C.; Green, R.T.; Prikryl, J.D.; Mohanty, S.; Leslie, B.W.; and Nedungadi, A. 1998. "A Test of Long-Term, Predictive, Geochemical Transport Modeling at the Akrotiri Archaeological Site." *Journal of Contaminant Hydrology*, 29, 245-279. Amsterdam, The Netherlands: Elsevier Science B.V. TIC: 247211.

Murrell, M.T.; Goldstein, S.J.; and Dixon, P.R. 1997. "Uranium Decay Series Mobility from a Uranium Ore Deposit: Implications for Nuclear Repository Stability." *Eos, Transactions*, 78, (46), F788. Washington, D.C.: American Geophysical Union. TIC: 246604.

National Research Council 1990. *Rethinking High-Level Radioactive Waste Disposal, A Position Statement of the Board on Radioactive Waste Management*. Washington, D.C.: National Academy Press. TIC: 205153.

Naudet, R. 1978. "Etude Parametrique de la Criticite des Reacteurs Naturels." *Les Reacteurs de Fission Naturels, Natural Fission Reactors. Proceedings of a Meeting on the Technical Committee on Natural Fission Reactors, Paris, 19 to 21 December 1977*. Pages 589-599. Vienna, Austria: International Atomic Energy Agency. TIC: 247910.

Neretnieks, I. 1986. "Investigations on Old Bronze Cannons." *CEC Natural Analogue Working Group, Second Meeting, Interlaken, Switzerland, June 17-19, 1986*. Côme, B. and Chapman,

N.A., eds. EUR 10671 EN. Pages 191-197. Luxembourg, Luxembourg: Commission of the European Communities. TIC: 247839.

Nohara, T.; Ochiai, Y.; Seo, T.; and Yoshida, H. 1992. "Uranium-Series Disequilibrium Studies in the Tono Uranium Deposit, Japan." *Radiochimica Acta*, 58/59, ([2]), 409-413. München, Germany: R. Oldenbourg Verlag. TIC: 247568.

Nordstrom, D.K.; Smellie, J.A.T.; and Wolf, M. 1990. *Chemical and Isotopic Composition of Groundwaters and Their Seasonal Variability at the Osamu Utsumi Mine and Morro do Ferro Analogue Study Sites, Poços de Caldas, Brazil*. SKB Technical Report 90-15. Stockholm, Sweden: Swedish Nuclear Fuel and Waste Management Company. TIC: 206353.

NWTRB (Nuclear Waste Technical Review Board) 1990. *Second Report to the U.S. Congress and the U.S. Secretary of Energy*. Washington, D.C.: Nuclear Waste Technical Review Board. ACC: HQX.19901214.0061.

NWTRB (Nuclear Waste Technical Review Board) 2000. *Report to the U.S. Congress and the Secretary of Energy, January to December 1999*. Arlington, Virginia: U.S. Nuclear Waste Technical Review Board. TIC: 247806.

Ochiai, Y.; Yamakawa, M.; Takeda, S.; and Harashima, F. 1989. "Natural Analogue Study on Tono Uranium Deposit in Japan." *Nuclear Science and Technology, CEC Natural Analogue Working Group, Third Meeting, Snowbird, Near Salt Lake City, USA, June 15 to 17 1988*. Côme, B. and Chapman, N.A., eds. Nuclear Science and Technology Series. EUR 11725 EN. Pages 126-138. Luxembourg, Luxembourg: Commission of the European Communities. TIC: 7639.

Ohnuki, T.; Murakami, T.; Sekine, K.; Yanase, N.; Isobe, H.; and Kobayashi, Y. 1990. "Migration Behavior of Uranium Series Nuclides in Altered Quartz-Chlorite Schist." *Scientific Basis for Nuclear Waste Management XIII, Symposium held November 27-30, 1989, Boston, Massachusetts*. Oversby, V.M. and Brown, P.W., eds. 176, 607-614. Pittsburgh, Pennsylvania: Materials Research Society. TIC: 203658.

Olekhovich, N.M.; Makovetskij, G.I.; Galyas, A.I.; Pashkovskij, O.I.; Severin, G.M.; Turtsevich, G.A.; and Yanushkevich, K.I. 1995. "Vertical Transport in Peatbogs of ¹³⁷Cs, Fallen After the Chernobyl NPP Accident." *Inzhenerno-Fizicheskii Zhurnal*, 68, (1), 33-38. Minsk, Republic of Belarus: Akademiia nauk BSSR. ACC: MOL.20000609.0009.

Oliver, T. and Root, T. 1997. *Hydrochemical Database for the Yucca Mountain Area, Nye County, Nevada*. Denver, Colorado: U.S. Geological Survey. ACC: MOL.19980302.0367.

Palmer, C.E.A.; Silva, R.J.; and Bucher, J.J. 1996. *Thermodynamic Data Base Needs for Modeling Studies of the Yucca Mountain Project*. UCRL-ID-125343. Livermore, California: Lawrence Livermore National Laboratory. ACC: MOL.19970123.0014.

Payne, T.E.; Edis, R.; and Seo, T. 1992. "Radionuclide Transport by Groundwater Colloids at the Koongarra Uranium Deposit." *Scientific Basis for Nuclear Waste Management XV*,

Symposium held November 4-7, 1991, Strasbourg, France. Sombret, C.G., ed. 257, 481-488. Pittsburgh, Pennsylvania: Materials Research Society. TIC: 204618.

Pearcy, E.C.; Prikryl, J.D.; and Leslie, B.W. 1995. "Uranium Transport Through Fractured Silicic Tuff and Relative Retention in Areas with Distinct Fracture Characteristics." *Applied Geochemistry*, 10, 685-704. Oxford, United Kingdom: Elsevier Science. TIC: 246848.

Pearcy, E.C.; Prikryl, J.D.; Murphy, W.M.; and Leslie, B.W. 1994. "Alteration of Uraninite from the Nopal I Deposit, Peña Blanca District, Chihuahua, Mexico, Compared to Degradation of Spent Nuclear Fuel in the Proposed U.S. High-Level Nuclear Waste Repository at Yucca Mountain, Nevada." *Applied Geochemistry*, 9, 713-732. New York, New York: Elsevier. TIC: 236934.

Pearcy, E.C.; Prikryl, J.D.; Murphy, W.M.; and Leslie, B.W. 1993. *Uranium Mineralogy of the Nopal I Natural Analog Site, Chihuahua, Mexico.* CNWRA 93-012. San Antonio, Texas: Center for Nuclear Waste Regulatory Analyses. TIC: 246628.

Petit, J.C. 1990. "Migration of Radionuclides in the Geosphere: What Can We Learn from Natural Analogues?." *Radiochimica Acta*, 51, (4), 181-188. München, Germany: R. Oldenbourg Verlag. TIC: 246841.

Petit, J.C.; Della Mea, G.; Dran, J.C.; Magonthier, M.C.; Mando, P.A.; and Paccagnella, A. 1990. "Hydrated-Layer Formation During Dissolution of Complex Silicate Glasses and Minerals." *Geochimica et Cosmochimica Acta*, 54, (7), 1941-1955. New York, New York: Pergamon Press. TIC: 247496.

Pickett, D.A. and Murphy, W.M. 1997. "Isotopic Constraints on Radionuclide Transport at Peña Blanca." *Seventh EC Natural Analogue Working Group Meeting: Proceedings of an International Workshop held in Stein am Rhein, Switzerland from 28 to 30 October 1996.* von Maravic, H. and Smellie, J., eds. EUR 17851 EN. Pages 113-122. Luxembourg, Luxembourg: Office for Official Publications of the European Communities. TIC: 247461.

Pickett, D.A. and Murphy, W.M. 1999. "Unsaturated Zone Waters from the Nopal I Natural Analog, Chihuahua, Mexico - Implications for Radionuclide Mobility at Yucca Mountain." *Scientific Basis for Nuclear Waste Management XXII, Symposium held November 30-December 4, 1998, Boston, Massachusetts, U.S.A.* Wronkiewicz, D.J. and Lee, J.H., eds. 556, 809-816. Warrendale, Pennsylvania: Materials Research Society. TIC: 246426.

Pinder, J.E., III; Bowling, J.W.; Lide, R.F.; and Beatty, L.M. 1995. "The Distribution of ¹³⁷Cs in Sediments of the Littoral Zone of a Former Reactor Cooling Pond." *Journal of Environmental Radioactivity*, 28, (1), 57-71. Amsterdam, The Netherlands: Elsevier Science. TIC: 246842.

Prikryl, J.D.; Pickett, D.A.; Murphy W.M.; and Percy, E.C. 1997. "Migration Behavior of Naturally Occurring Radionuclides at the Nopal I Uranium Deposit, Chihuahua, Mexico." *Journal of Contaminant Hydrology*, 26, 61-69. New York, New York: Elsevier Science B.V. TIC: 242381.

Pruess, K. 1991. *TOUGH2-A General-Purpose Numerical Simulator for Multiphase Fluid and Heat Flow*. LBL-29400. Berkeley, California: Lawrence Berkeley Laboratory. ACC: NNA.19940202.0088.

Rasilainen, K.; Suksi, J.; Blomqvist, R.; Valkiainen, M.; and Ruskeeniemi, T. 1991. "Natural Analogue Studies and Performance Assessments in Finland." *Nuclear Science and Technology, Fourth Natural Analogue Working Group Meeting and Poços de Caldas Project Final Workshop, Pitlochry, 18 to 22 June 1990, Scotland, Final Report*. Côme, B. and Chapman, N.A., eds. EUR 13014 EN. Pages 193-210. Luxembourg, Luxembourg: Commission of the European Communities. TIC: 7819.

Richman, M. 1996. "Terrestrial Plants Tested for Cleanup of Radionuclides, Explosives' Residue." *Water Environment & Technology*, 8, (5), 17-19. Alexandria, Virginia: Water Environment Federation. TIC: 247570.

Rigol, A.; Roig, M.; Vidal, M.; and Rauret, G. 1999. "Sequential Extractions for the Study of Radiocesium and Radiostrontium Dynamics in Mineral and Organic Soils from Western Europe and Chernobyl Areas." *Environmental Science and Technology*, 33, (6), 887-895. Washington, D.C.: American Chemical Society. TIC: 247499.

Rivas, P.; Hernán, P.; Astudillo, J.; Bruno, J.; Carrerra, J.; De la Cruz, B.; Guimerà, J.; Gomez, P.; Ivanovich, M.; Marín, C.; Miller, W.; and Pérez del Villar, L. 1998. *Nuclear Science and Technology, El Berrocal Project*. EUR 17830 EN. Luxembourg, Luxembourg: Commission of European Communities. TIC: 247318.

Rumynin, V.G.; Mironenko, V.A.; Sindalovsky, L.N.; Boronina, A.V.; Konosavsky, P.K.; and Pozdniakov, S.P. 1998. *Evaluation of Conceptual, Mathematical and Physical-and-Chemical Models for Describing Subsurface Radionuclide Transport at the Lake Karachai Waste Disposal Site*. LBNL-41974. Berkeley, California: Lawrence Berkeley National Laboratory. TIC: 246562.

Ruskeeniemi, T.; Niini, H.; Söderholm, B.; Vesterinen, M.; Blomqvist, R.; Halonen, S.; Lindberg, A.; Jaakkola, T.; Suksi, J.; and Suutarinen, R. 1989. "The Palmottu U-Th Deposit in SW Finland as a Natural Analogue to the Behaviour of Spent Nuclear Fuel in Bedrock: A Preliminary Report." *Proceedings of the 6th International Symposium on Water-Rock Interaction, WRI-6, Malvern, August 3-8, 1989*. Miles, D.L., ed. Pages 601-604. Brookfield, Massachusetts: A.A. Balkema. TIC: 247756.

Rybal'chenko, A.I.; Pimenov, M.K.; Kostin, P.P.; Balukova, V.D.; Nosukhin, A.V.; Mikerin, E.I.; Egorov, N.N.; Kaimin, E.P.; Kosareva, I.M.; and Kurochkin, V.M. 1998. *Deep Injection Disposal of Liquid Radioactive Waste in Russia*. Foley, M.G. and Ballou, L.M.G., eds. Columbus, Ohio: Battelle Press. TIC: 247062.

Sargent, F.P. and Cramer, J.J. 1986. "Cigar Lake Project: A U-Deposit Natural Analogue." *CEC Natural Analogue Working Group, Second Meeting, Interlaken, Switzerland, June 17-19, 1986*. Côme, B. and Chapman, N.A., eds. EUR 10671 EN. Pages 93-100. Luxembourg, Luxembourg: Commission of the European Communities. TIC: 247839.

Schorscher, H.D. and Shea, M.E. 1991. *The Regional Geology, Mineralogy and Geochemistry of the Poços de Caldas Alkaline Caldera Complex, Minas Gerais, Brazil*. SKB Technical Report 90-10. Stockholm, Sweden: Swedish Nuclear Fuel and Waste Management Company. TIC: 206335.

Seo, T. and Yoshida, H. 1994. "Natural Analogue Studies of the Tono Uranium Deposit in Japan." *Fifth CEC Natural Analogue Working Group Meeting and Alligator Rivers Analogue Project (ARAP) Final Workshop, Proceedings of an International Workshop, Toledo, Spain, 5 to 9 October 1992*. von Maravic, H. and Smellie, J., eds. EUR 15176 EN. Pages 179-184. Luxembourg, Luxembourg: Commission of the European Communities. TIC: 247317.

Serebryanyi, G.Z.; Rolevich, I.V.; Gvozdev, A.A.; Baklaj, A.A.; Golikova, N.B.; Starobinets, S.E.; and Polivko, L.A. 1995. "The Characteristics of Storage Sites of Radioactive Products of Decontamination Arranged at the Territory of the Republic of Belarus." *Proceedings of the Fifth International Conference on Radioactive Waste Management and Environmental Remediation, ICM '95, Berlin, Germany, September 3-7, 1995*. Slate, S.; Baker, R.; and Benda, G., eds. 2, 1629-1630. New York, New York: American Society of Mechanical Engineers. TIC: 247573.

Shabalev S.I.; Burakov, B.E.; and Anderson, E.B. 1997. "General Classification of 'Hot' Particles from the Nearest Chernobyl Contaminated Areas." *Scientific Basis for Nuclear Waste Management XX, Symposium held December 2-6, 1996, Boston, Massachusetts*. Gray, W.J. and Triay, I.R., eds. 465, 1343-1350. Pittsburgh, Pennsylvania: Materials Research Society. TIC: 238884.

Shestopalov, V.M. 1992. *Research & Development Center of Radiohydrogeological Studies at Field Test Sites, Principal Research Trends*. Kiev, Ukraine: Academy of Sciences of the Ukraine. ACC: MOL.20000629.0592.

Shestopalov, V.M. 1996. *Atlas of Chernobyl Exclusion Zone*. Kiev, Ukraine: [Kartohrafiia]. TIC: 248100.

Shestopalov, V.M., ed. 1997. "Formation of the Radioactive Contamination Field." Chapter 3 of *Chornobyl [Chernobyl] Catastrophe*. Baryakhtar, V.G., ed. Kyiv, Ukraine: Editorial House of Annual Issue. ACC: MOL.20000629.0590.

Shestopalov, V.M.; Bubljas, V.N.; and Kukharenko, D.U. 2000. "Investigation of Fast Migration in the Vadose Zone for Assessment of Groundwater Contamination by Chernobyl Radionuclides." *Abstracts and Selected Chapters from Vadose Zone Science and Technology Solutions*. Looney, B.B. and Falta, R.W., eds. Pages 1-20. Aiken, South Carolina: Westinghouse Savannah River Company. ACC: MOL.20000629.0591.

Shestopalov, V.M.; Bubljas, V.N.; Gudzenko, V.V.; Onishchenko, I.P.; Borodavko, I.V.; and Boguslavsky, A.S. 1995. "Research into Vertical Radionuclide Migration at the R&D Center of Radioenvironmental Studies on Field Test Sites, National Academy of Sciences of Ukraine." *Proceedings of the Fifth International Conference on Radioactive Waste Management and Environmental Remediation, ICM '95, Berlin, Germany, September 3-7, 1995*. Slate, S.; Baker, R.; and Benda, G., eds. 2, 1347-1351. New York, New York: American Society of Mechanical Engineers. TIC: 247578.

Shikazono, N. and Utada, M. 1997. "Stable Isotope Geochemistry and Diagenetic Mineralization Associated with the Tono Sandstone-Type Uranium Deposit in Japan." *Mineralium Deposita*, 32, (6), 596-606. Berlin, Germany: Springer-Verlag. TIC: 247528.

Silant'-ev, A.N.; Shkuratova, I.G.; and Bobovnikova, Ts.I. 1989. "Vertical Soil Migration of Radionuclide Fallout from the Chernobyl Accident." *Soviet Atomic Energy*, 66, (3), 221-225. New York, New York: Consultants Bureau. On Order Library Tracking Number-247772

Skurat, V.V.; Shiryayeva, N.M.; Gvozdev, A.A.; Serebryanyi, G.Z.; Myshkina, N.K.; Starobinets, S.E.; and Kotovich, V.V. 1995. "Operational Conditions of Storages for Products of Decontamination of the Territories of Belarus After the Accident at Chernobyl NPP and Evaluation of Their Radioecological State." *Proceedings of the Fifth International Conference on Radioactive Waste Management and Environmental Remediation: ICM '95, Berlin, Germany, September 3-7, 1995*. Slate, S.; Baker, R.; and Benda, G., eds. 2, 1417-1419. New York, New York: American Society of Mechanical Engineers. TIC: 247579.

Smellie, J. 1995. "The Fossil Nuclear Reactors of Oklo, Gabon." *Radwaste Magazine*, 2, (2), 18-20, 22-27. La Grange Park, Illinois: American Nuclear Society. TIC: 238322.

Smellie, J.A.T., ed. 1998. *MAQARIN Natural Analogue Study: Phase III*. SKB Technical Report 98-04. Two volumes. Stockholm, Sweden: Swedish Nuclear Fuel and Waste Management Company. TIC: 244013.

Smellie, J.; Chapman, N.; McKinley, I.; Penna Franca, E.; and Shea, M. 1989. "Testing Safety Assessment Models Using Natural Analogues in High Natural-Series Groundwaters. The Second Year of the Poços de Caldas Project." *Scientific Basis for Nuclear Waste Management XII, Symposium held October 10-13, 1988, Berlin, Germany*. Lutze, W. and Ewing, R.C., eds. 127, 863-870. Pittsburgh, Pennsylvania: Materials Research Society. TIC: 241379.

Smellie, J.A.T.; Winberg, A.; and Karlsson, F. 1993. "Swedish Activities in the Oklo Natural Analogue Project." [*2nd Joint CEC-CEA Progress Meeting of the Oklo Working Group, Brussels, Belgium, April 6-7, 1992*. von Maravic, H., ed. EUR 14877 EN]. Pages 131-142. [Luxembourg, Luxembourg: Commission of the European Communities]. TIC: 247581.

Smith, J.T.; Fesenko, S.V.; Howard, B.J.; Horrill, A.D.; Sanzharova, N.I.; Alexakhin, R.M.; Elder, D.G.; and Naylor, C. 1999. "Temporal Change in Fallout ¹³⁷Cs in Terrestrial and Aquatic Systems: A Whole Ecosystem Approach." *Environmental Science and Technology*, 33, (1), 49-54. Washington, D.C.: American Chemical Society. TIC: 247525.

Snelling, A.A. 1980. "Uraninite and Its Alteration Products, Koongarra Uranium Deposit." *Proceedings of International Uranium Symposium on the Pine Creek Geosyncline, 1980*. [Ferguson, J. and Goleby, A.B., eds.]. Pages 487-498. [Vienna, Austria: International Atomic Energy Agency]. TIC: 236806.

Snelling, A.A. 1992. "Geologic Setting." Volume 2 of *Alligator Rivers Analogue Project*. SKI TR 92:20-2. Manai, New South Wales, Australia: Australian Nuclear Science and Technology Organisation. TIC: 244675.

Sobotovich, E.V. 1992. *Radiogeokhimiia v Zone Vliianiia Chernobyl'Skoi AES (Radiogeochemistry of the Zone of Influence of Chernobyl NPP)*. Kiev, Naukova Dumka, [Ukraine]: Academy of Sciences of Ukraine. ACC: MOL.20000629.0589.

Stockman, H.; Krumhansl, J.; Ho, C.; and McConnell, V. 1994. *The Valles Natural Analogue Project*. NUREG/CR-6221. Washington, D.C.: U.S. Nuclear Regulatory Commission. TIC: 246123.

Stone, R. 1998. "Ecology: U.S., Ukraine Launch New Chernobyl Lab." *Science*, 281, (5377), 623. Washington, D.C.: American Association for the Advancement of Science. TIC: 247374.

Stout, R.B. and Leider, H.R., eds. 1997. *Waste Form Characteristics Report Revision 1*. UCRL-ID-108314. Version 1.2. Livermore, California: Lawrence Livermore National Laboratory. ACC: MOL.19980512.0133.

Stuckless, J.S. 2000. *Archaeological Analogues for Assessing the Long-Term Performance of a Mined Geologic Repository for High-Level Radioactive Waste*. Open-File Report 00-181. Denver, Colorado: U.S. Geological Survey. On Order Library Tracking Number-248774

Suksi, J.; Ruskeeniemi, T.; Lindberg, A.; and Jaakkola, T. 1991. "The Distribution of Natural Radionuclides on Fracture Surfaces in Palmottu Analogue Study Site in SW Finland." *Radiochimica Acta*, 52/53, (II), 367-372. München, Germany: R. Oldenbourg Verlag. TIC: 247521.

Sunder, S.; Taylor, P.; and Cramer, J.J. 1988. "XPS and XRD Studies of Uranium Rich Minerals from Cigar Lake, Saskatchewan." *Scientific Basis for Nuclear Waste Management XI, Symposium held November 30-December 3, 1987, Boston, Massachusetts*. Apted, M.J. and Westerman, R.E., eds. 112, 465-472. Pittsburgh, Pennsylvania: Materials Research Society. TIC: 203662.

Suutarinen, R.; Blomqvist, R.; Halonen, S.; and Jaakkola, T. 1991. "Uranium in Groundwater in Palmottu Analogue Study Site in Finland." *Radiochimica Acta*, 52/53, (2), 373-380. München, Germany: R. Oldenbourg Verlag. TIC: 247520.

Sverjensky, D.; Bennett, D.G.; and Read, D. 1992. *Geochemical Modelling of Secondary Uranium Ore Formation*. Volume 11 of *Alligator Rivers Analogue Project*. DOE/HMIP/RR/92/081. Menai, Australia: Australian Nuclear Science and Technology Organisation. TIC: 235986.

Tcherkezian, V.; Shkinev, V.; Khitrov, L.; and Kolesov, G. 1994. "Experimental Approach to Chernobyl Hot Particles." *Journal of Environmental Radioactivity*, 22, (2), 127-139. New York, New York: Elsevier Science. TIC: 247526.

Thiessen, K.M.; Hoffman, F.O.; Rantavaara, A.; and Hossain, S. 1997. "Environmental Models Undergo International Test." *Environmental Science and Technology*, 31, (8), 358A-363A. Washington, D.C.: American Chemical Society. TIC: 247527.

Thompson, J.L., ed. 1986. *Laboratory and Field Studies Related to the Radionuclide Migration October 1, 1984-September 30, 1985*. LA-10644-PR. Los Alamos, New Mexico: Los Alamos National Laboratory. TIC: 246828.

Tweed, C.J. and Milodowski, A.E. 1994. "An Overview of the Maqarin Natural Analogue Project – A Natural Analogue Study of a Hyperalkaline Cement Groundwater System." *Fifth CEC Natural Analogue Working Group Meeting and Alligator Rivers Analogue Project (ARAP) Final Workshop, Proceedings of an International Workshop, Toledo, Spain, October 5-9, 1992*. von Maravic, H. and Smellie, J., eds. EUR 15176 EN. Pages 203-209. Luxembourg, Luxembourg: Commission of the European Communities. TIC: 247889.

Tylecote, R.F. 1977. "Durable Materials for Seawater: The Archaeological Evidence." *The International Journal of Nautical Archaeology and Underwater Exploration*, 6, (4), 269-283. New York, New York: Academic Press. TIC: 247572.

Tylecote, R.F. 1979. "The Effect of Soil Conditions on the Long-Term Corrosion of Buried Tin-Bronzes and Copper." *Journal of Archeological Science*, 6, 345-368. New York, New York: Academic Press. TIC: 247517.

Valkiainen, M. 1989. "Finnish Natural Analogue Research." *CEC Natural Analogue Working Group, Third Meeting, Snowbird, Near Salt Lake City, USA, June 15 to 17 1988*. Côme, B. and Chapman, N.A., eds. Nuclear Science and Technology Series. EUR 11725 EN. Pages 110-118. Luxembourg, Luxembourg: Commission of the European Communities. TIC: 7639.

Vaniman, D.T. and Chipera, S.J. 1996. "Paleotransport of Lanthanides and Strontium Recorded in Calcite Compositions from Tuffs at Yucca Mountain, Nevada, USA." *Geochimica et Cosmochimica Acta*, 60, (22), 4417-4433. New York, New York: Pergamon Press. TIC: 231351.

Vasenko, O.G. 1998. "Environmental Situation in the Lower Dnipro River Basin." *Water Quality Research Journal of Canada*, 33, (4), 457-487. Toronto, Ontario: Canadian Association on Water Quality. TIC: 247540.

Vilks, P.; Cramer, J.J.; Shewchuk, T.A.; and Larocque, J.P.A. 1988. "Colloid and Particulate Matter Studies in the Cigar Lake Natural-Analog Program." *Radiochimica Acta*, 44/45, (II), 305-310. München, Germany: R. Oldenbourg Verlag. TIC: 247532.

Von Gunten, H.R.; Waber, U.E.; and Krahenbuhl, U. 1988. "Reactor Accident at Chernobyl: A Possibility to Test Colloid-Controlled Transport of Radionuclides in a Shallow Aquifer." *Journal of Contaminant Hydrology*, 2, (3), 237-247. New York, New York: Elsevier Science. TIC: 247539.

von Maravic, H. and Smellie, J.A.T., eds. 1994. *Fifth CEC Natural Analogue Working Group Meeting and Alligator Rivers Analogue Project (ARAP) Final Workshop, Proceedings of an International Workshop, Toledo, Spain, October 5-9, 1992*. EUR 15176 EN. Luxembourg, Luxembourg: Commission of the European Communities. TIC: 247923.

Waber, N. 1991. *Mineralogy, Petrology and Geochemistry of the Poços de Caldas Analogue Study Sites, Minas Gerais, Brazil II: Morro do Ferro*. SKB Technical Report 90-12. Stockholm, Sweden: Swedish Nuclear Fuel and Waste Management Company. TIC: 206350.

Wallace, A.B. and Roper, M.W. 1981. "Geology and Uranium Deposits Along the Northeastern Margin, McDermitt Caldera Complex, Oregon." *Uranium in Volcanic and Volcaniclastic Rocks, Symposium held in El Paso, Texas, [February 25-27, 1980]*. Goodell, P.C. and Waters, A.C., eds. AAPG Studies in Geology No. 13. Pages 73-80. Tulsa, Oklahoma: American Association of Petroleum Geologists. TIC: 245898.

Wang, J.S.Y. 1991. "Fracture Flow and Matrix Flow in the Unsaturated Zone at Yucca Mountain and at Rainier Mesa." Appendix B of *A Review of Rainier Mesa Tunnel and Borehole Data and Their Possible Implications to Yucca Mountain Site Study Plans*. LBL-32068. Berkeley, California: Lawrence Berkeley Laboratory. ACC: NNA.19920506.0020.

Wang, J.S.Y. 1992. "Variations of Hydrological Parameters of Tuff and Soil." *High Level Radioactive Waste Management, Proceedings of the Third Annual International Conference, Las Vegas, Nevada, April 12-16, 1992*. 1, 727-731. La Grange Park, Illinois: American Nuclear Society. TIC: 204231.

Wang, J.S.Y.; Cook, N.G.W.; Wollenberg, H.A.; Carnahan, C.L.; Javandel, I.; and Tsang, C.F. 1993. "Geohydrologic Data and Models of Rainier Mesa and Their Implications to Yucca Mountain." *High Level Radioactive Waste Management, Proceedings of the Fourth Annual International Conference, Las Vegas, Nevada, April 26-30, 1993*. 1, 675-681. La Grange Park, Illinois: American Nuclear Society. TIC: 208542.

Wendum, D. 1998. "Three Long-Range Transport Models Compared to the ETEX Experiment: A Performance Study." *Atmospheric Environment*, 32, (24), 4297-4305. New York, New York: Pergamon. TIC: 247541.

West, J.M.; McKinley, I.G.; and Vialta, A. 1989. "The Influence of Microbial Activity on the Movement of Uranium at Osamu Utsumi Mine, Poços de Caldas, Brazil." *Scientific Basis for Nuclear Waste Management XII, Symposium held October 10-13, 1988, Berlin, Germany*. Lutze, W. and Ewing, R.C., eds. 127, 771-777. Pittsburgh, Pennsylvania: Materials Research Society. TIC: 203660.

West, J.M.; Vialta, A.; and McKinley, I.G. 1990. *Poços de Caldas Report Number 10 Microbiological Analysis at the Osamu Utsumi and Morro do Ferro Analogue Study Sites, Poços de Caldas, Brazil*. NAGRA NTB 90-28. Baden, Switzerland: Nationale Genossenschaft für die Lagerung Radioaktiver Abfälle. TIC: 206356.

Winograd, I.J. 1986. *Archaeology and Public Perception of a Transscientific Problem – Disposal of Toxic Wastes in the Unsaturated Zone*. Circular 990. Denver, Colorado: U.S. Geological Survey. TIC: 237946.

WoldeGabriel, G.; Keating, G.N.; and Valentine, G.A. 1999. "Effects of Shallow Basaltic Intrusion into Pyroclastic Deposits, Grants Ridge, New Mexico, USA." *Journal of Volcanology*

and *Geothermal Research*, 92, 389-411. Amsterdam, The Netherlands: Elsevier Science. TIC: 246037.

Wolery, T.J. and Daveler, S.A. 1992. *EQ6, A Computer Program for Reaction Path Modeling of Aqueous Geochemical Systems: Theoretical Manual, User's Guide, and Related Documentation (Version 7.0)*. UCRL-MA-110662 PT IV. Livermore, California: Lawrence Livermore National Laboratory. TIC: 205002.

Wollenberg, H.A. and Flexser, S. 1986. "Contact Zones and Hydrothermal Systems as Analogues to Repository Conditions." *Chemical Geology*, 55, 345-359. Amsterdam, The Netherlands: Elsevier Science B.V. TIC: 246171.

Wong, V. 1998. *Gamma-Ray Characterization of Uranium-Series Nuclides and Its Application to the Study of the Peña Blanca Natural Analogue Site, Chihuahua, Mexico*. Ph.D. dissertation. El Paso, Texas: University of Texas at El Paso. TIC: 245933.

Wronkiewicz, D.J.; Bates, J.K.; Wolf, S.F.; and Buck, E.C. 1996. "Ten-Year Results from Unsaturated Drip Tests with UO₂ at 90°C: Implications for the Corrosion of Spent Nuclear Fuel." *Journal of Nuclear Materials*, 238, (1), 78-95. Amsterdam, The Netherlands: North-Holland Publishing Company. TIC: 243361.

Wurstner, S.K.; Thorne, P.D.; Chamness, M.A.; Freshley, M.D.; and Williams, M.D. 1995. *Development of a Three-Dimensional Ground-Water Model of the Hanford Site Unconfined Aquifer System: FY 1995 Status Report*. PNL-10886. Richland, Washington: Pacific Northwest National Laboratory. TIC: 246888.

Yamato, A.; Masuda, S.; and Sakuma, H. 1992. "The High Level Radioactive Waste Management Program in Japan." *High Level Radioactive Waste Management, Proceedings of the Third International Conference, Las Vegas, Nevada, April 12-16, 1992*. 1, 41-48. La Grange Park, Illinois: American Nuclear Society. TIC: 204231.

Yoshida, H. 1994. "Relation Between U-Series Nuclide Migration and Microstructural Properties of Sedimentary Rocks." *Applied Geochemistry*, 9, (5), 479-490. New York, New York: Pergamon. TIC: 247542.

Yoshida, H.; Kodama, K.; and Ota, K. 1994b. "Role of Microscopic Flow-Paths on Nuclide Migration in Sedimentary Rocks: A Case Study from the Tono Uranium Deposit, Central Japan." *Radiochimica Acta*, 66/67, 505-511. München, Germany: R. Oldenbourg Verlag. TIC: 247765.

Yoshida, H.; Yui, M.; and Shibutani, T. 1994a. "Flow Path Structure in Relation to Nuclide Migration in Sedimentary Rocks: An Approach with Field Investigations and Experiments for Uranium Migration at Tono Uranium Deposit, Central Japan." *Journal of Nuclear Science and Technology*, 31, (8), 803-812. Tokyo, Japan: Atomic Energy Society of Japan. TIC: 247763.

Yusa, Y. and Yamakawa, M. 1992. "Tono In-Situ Research Facilities for Studies of the Geological Environment." *Environmental Geology and the Late Quaternary of Japan*. Kato, H.

and Noro, H., eds. 29th IGC Field Trip Guide Book Volume 3. Pages 145-153. Ibaraki, Japan: Geological Survey of Japan. TIC: 247764.

Yusa, Y. and Yoshida, H. 1993. "Migration Behaviour of Natural Radionuclides in Geological Formation, A Case Study of the Tono Uranium Deposits, Japan." *Hoshasen (Japan)*, 20, (1), 29-39. [Tokyo, Japan]: Power Reactor and Nuclear Fuel Development Corporation (PNC), Chubu Works. ACC: MOL.20000609.0008.

Zach, R.; Amiro, B.D.; Bird, G.A.; Macdonald, C.R.; Sheppard, M.I.; Sheppard, S.C.; and Szekely, J.G. 1996. *Biosphere Model*. Volume 4 of *The Disposal of Canada's Nuclear Fuel Waste: A Study of Postclosure Safety of In-Room Emplacement of Used CANDU Fuel in Copper Containers in Permeable Plutonic Rock*. AECL-11494-4. Pinawa, Manitoba, Canada: Atomic Energy of Canada Limited. TIC: 226735.

Zielinski, R.A. 1980. "Stability of Glass in the Geologic Environment: Some Evidence from Studies of Natural Silicate Glasses." *Nuclear Technology*, 51, (2), 197-200. La Grange Park, Illinois: American Nuclear Society. TIC: 247543.

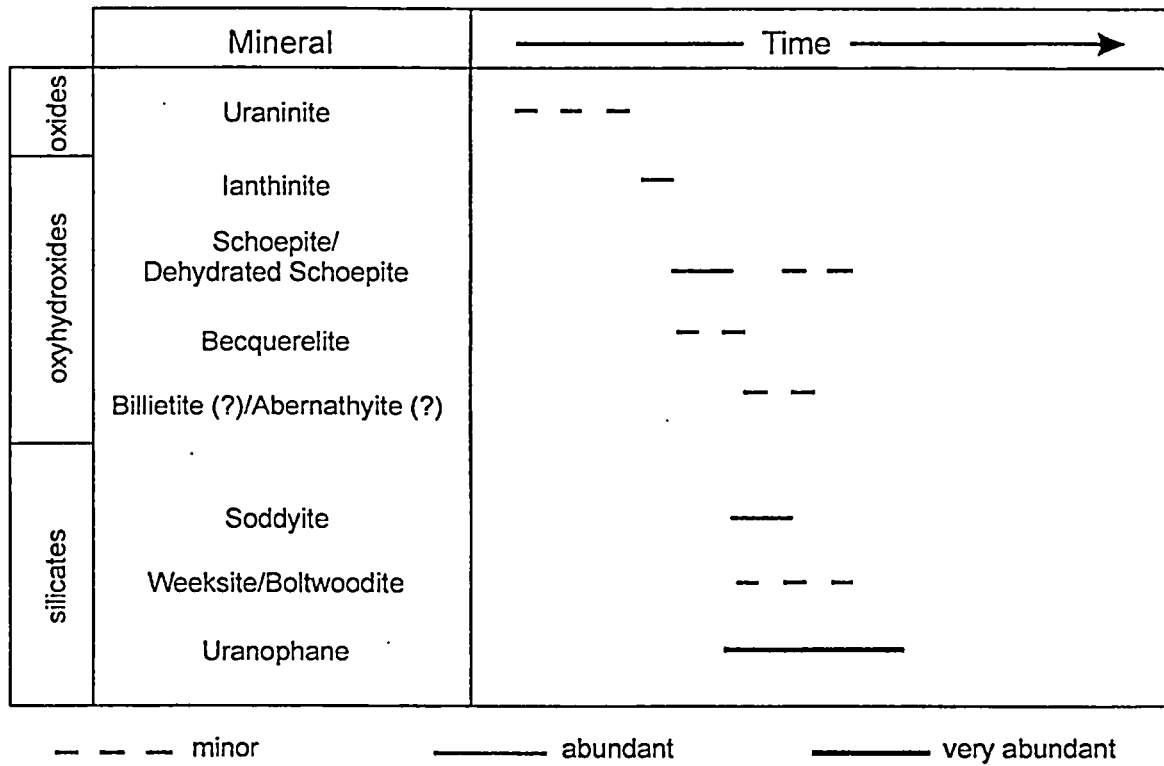
Zyvoloski, G.; Dash, Z.; and Kelkar, S. 1992. *FEHMN 1.0: Finite Element Heat and Mass Transfer Code*. LA-12062-MS, Rev. 1. Los Alamos, New Mexico: Los Alamos National Laboratory. ACC: NNA.19910625.0038.

Zyvoloski, G.A.; Robinson, B.A.; Dash, Z.V.; and Trease, L.L. 1997. *User's Manual for the FEHM Application - A Finite-Element Heat- and Mass-Transfer Code*. LA-13306-M. Los Alamos, New Mexico: Los Alamos National Laboratory. TIC: 235999.

13.8.2 Codes, Standards, Regulations, and Procedures

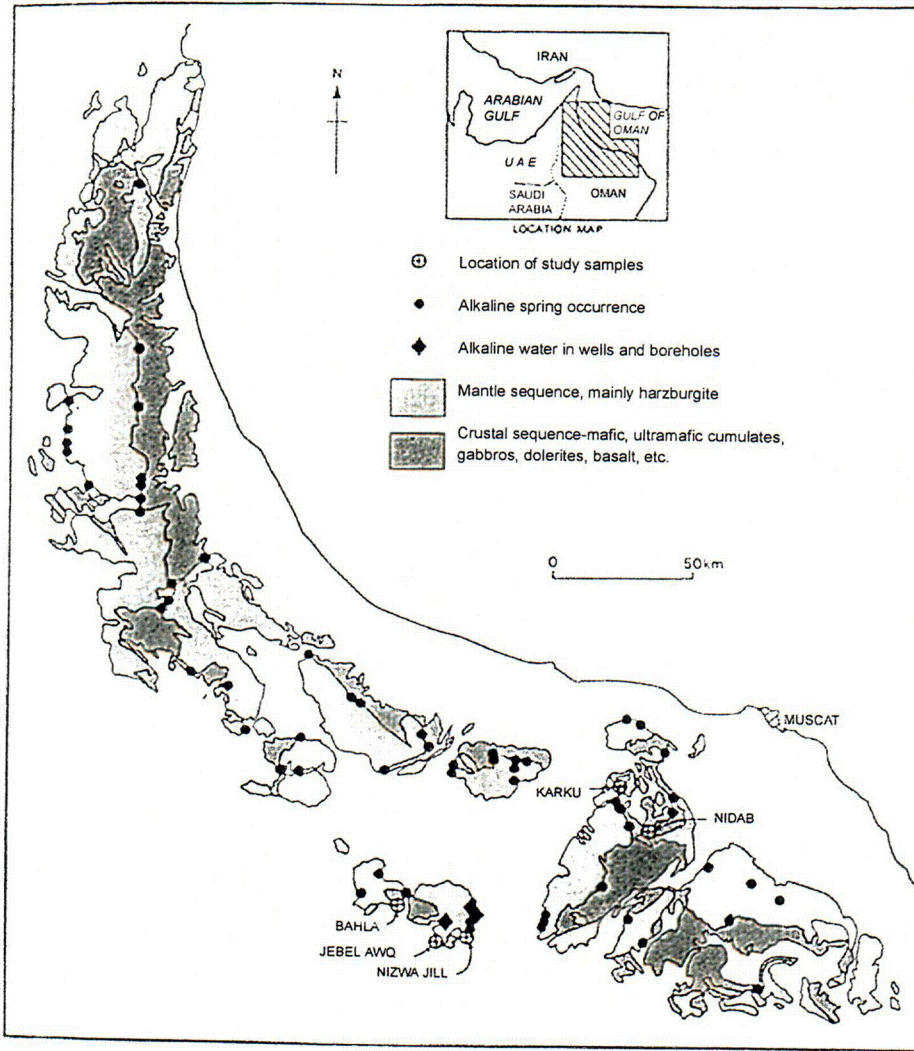
10 CFR 60. Energy: Disposal of High Level Radioactive Wastes in Geologic Repositories. Readily available.

64 FR 8640. Disposal of High-Level Radioactive Wastes in a Proposed Geologic Repository at Yucca Mountain, Nevada. Proposed rule 10 CFR 63. Readily available.



Source: Percy et al. (1993)

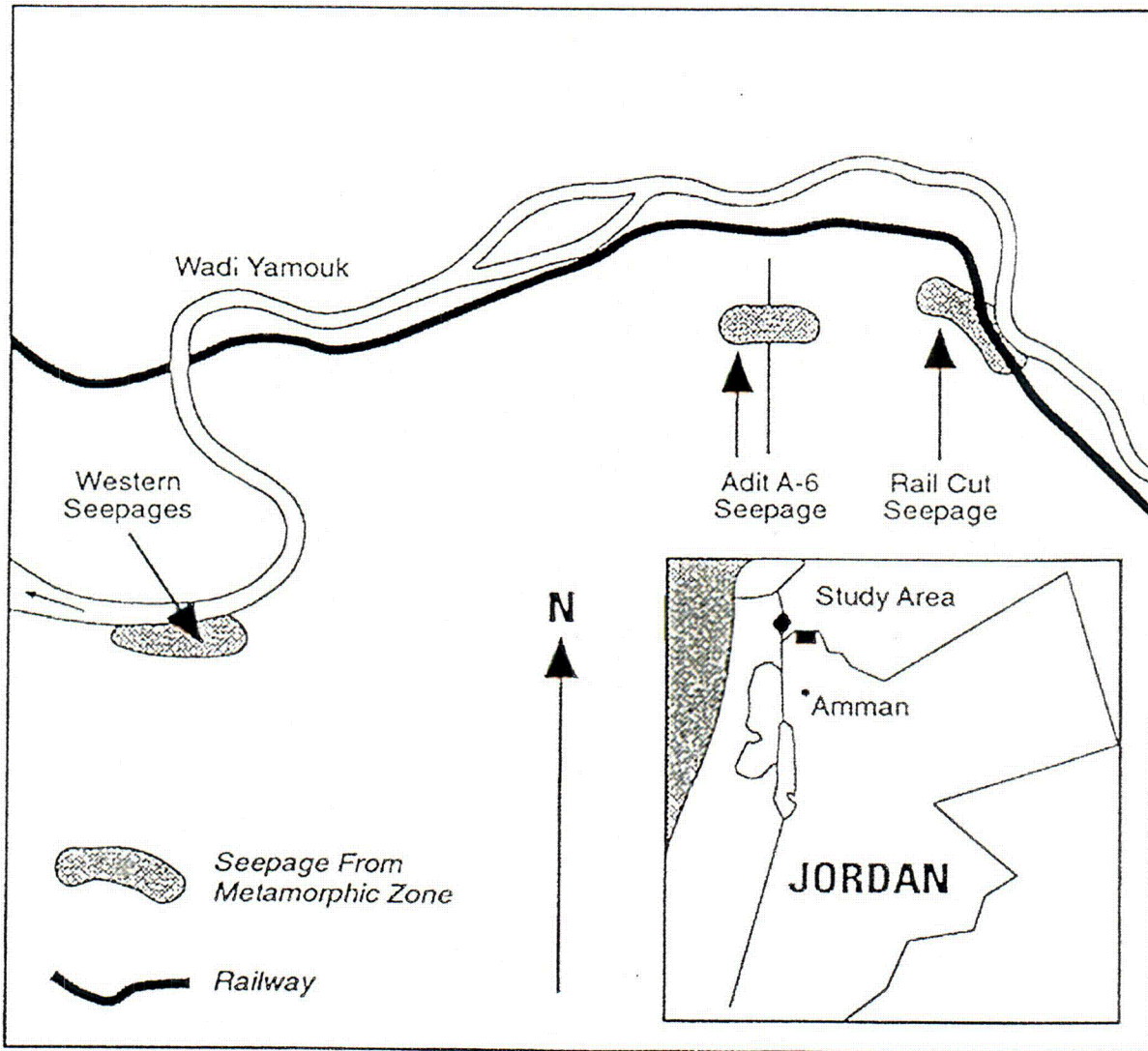
Figure 13.3-1. Relative Sequence of Formation and Abundance of Uranium Minerals at the Nopal I Deposit



Source: Bath et al. (1987b)

NOTE: The locations of springs sampled as part of the Oman natural analog study are shown.

Figure 13.3-2. Distribution of Ophiolites and Hyperalkaline Springs in Northern Oman



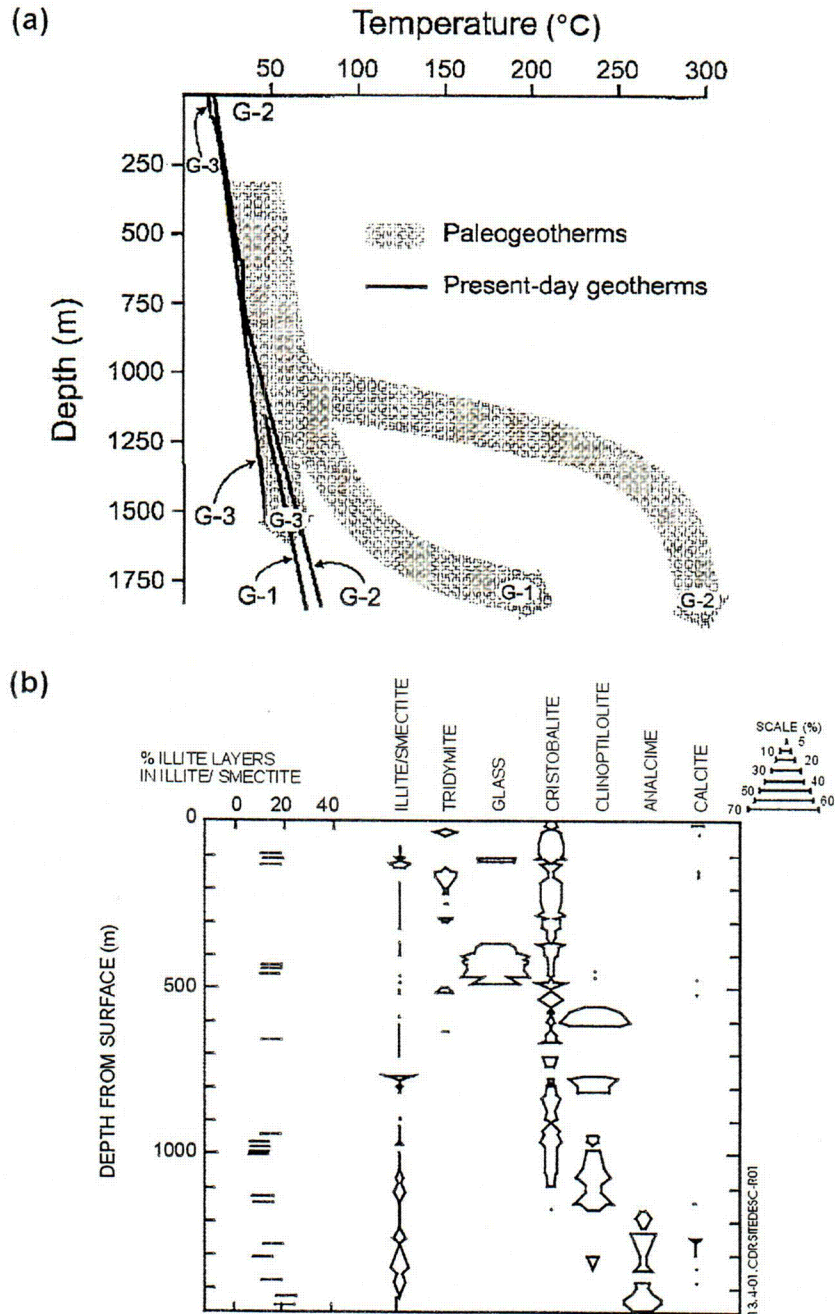
13.3-03.CDR.SITEDESC-R01

Source: Miller et al. (1994)

NOTE: Sites of the hyperalkaline springs are shown.

Figure 13.3-3. Location of the Maqarin Natural Analog Study Site in Northern Jordan

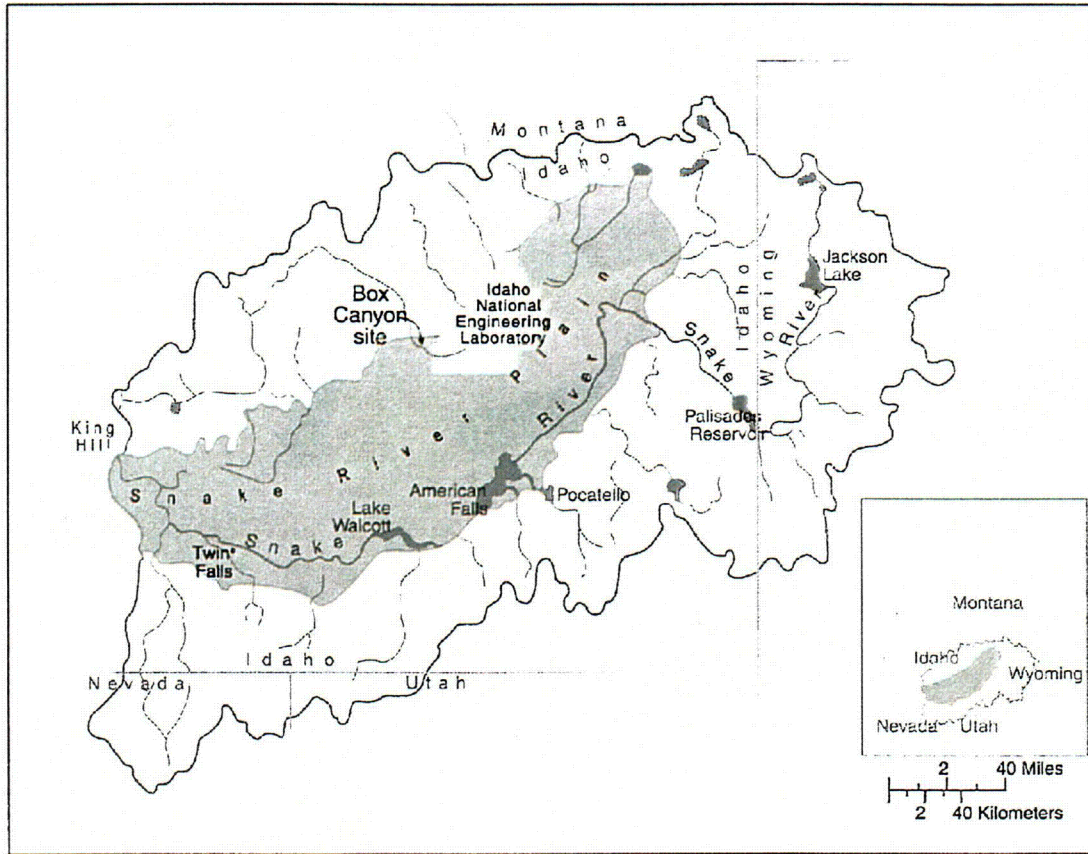
INTENTIONALLY LEFT BLANK



Source: Bish and Aronson (1993)

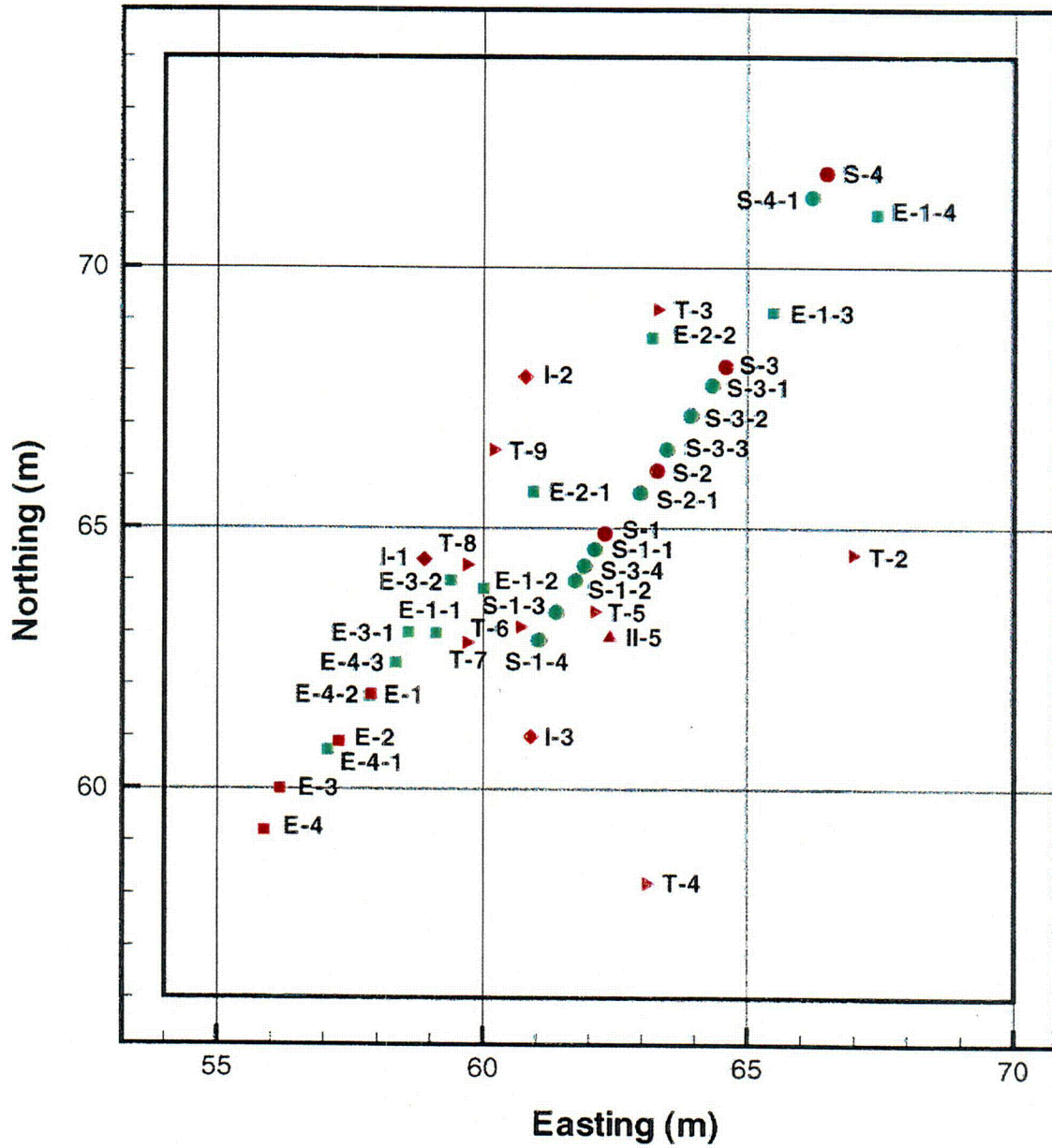
NOTE: Part (a) illustrates paleotemperatures inferred from mineralogical data in drillholes USW G-3, G-2, and G-1, along with present-day temperature profiles. Part (b) compares mineral and glass abundances in drill core USW GU-3/G-3 determined by X-ray powder diffraction.

Figure 13.4-1. Anticipated Mineral Alteration at Yucca Mountain



Source: Faybishenko et al. (1999)

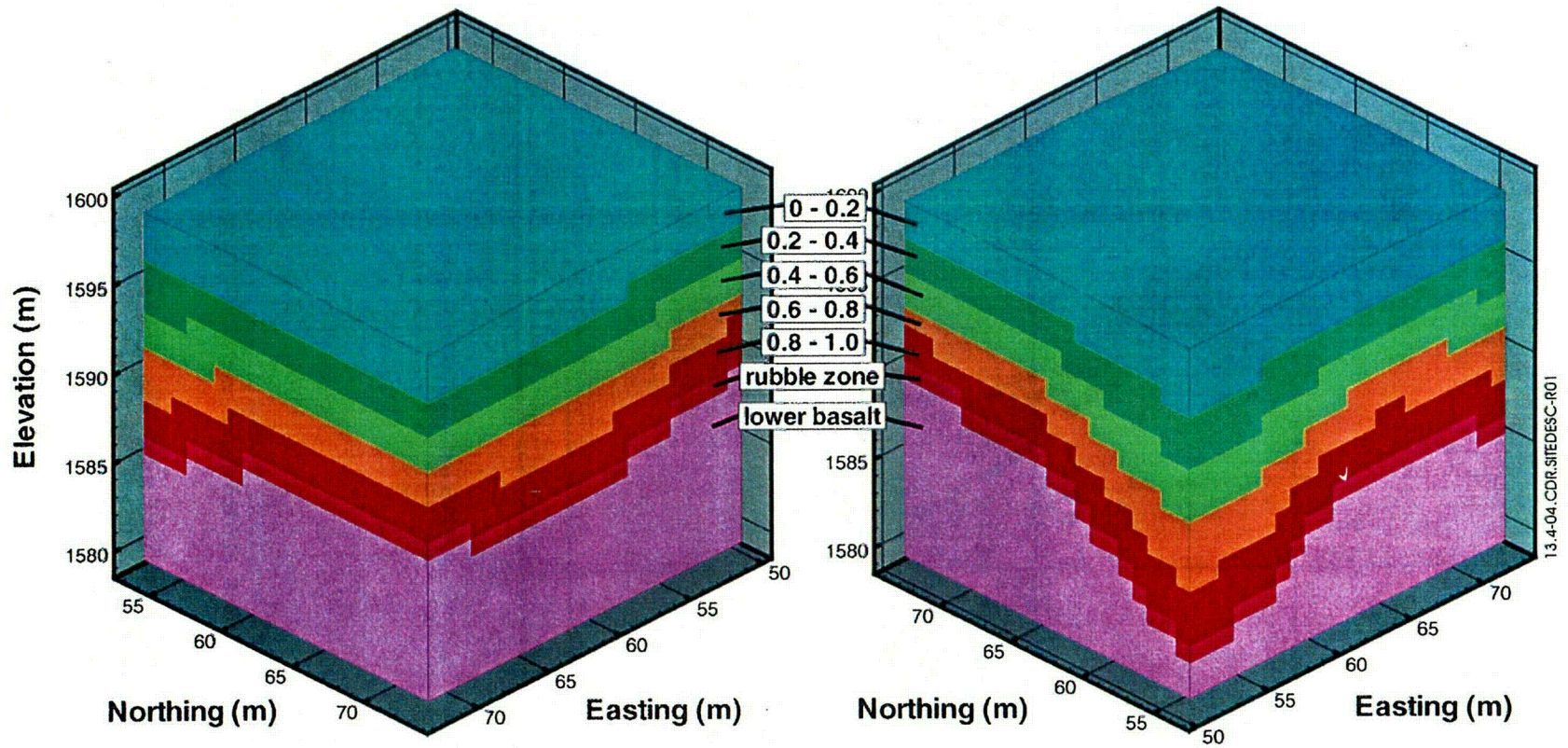
Figure 13.4-2. Map of East Snake River Plain Showing the Location of the Box Canyon Experimental Site



Source: CRWMS M&O (2000b)

NOTE: Labeled symbols represent boreholes. Red symbols: location of borehole top. Green symbols: plan view of observed flow-features in slanted boreholes. Symbol shapes used to identify different borehole groups by name.

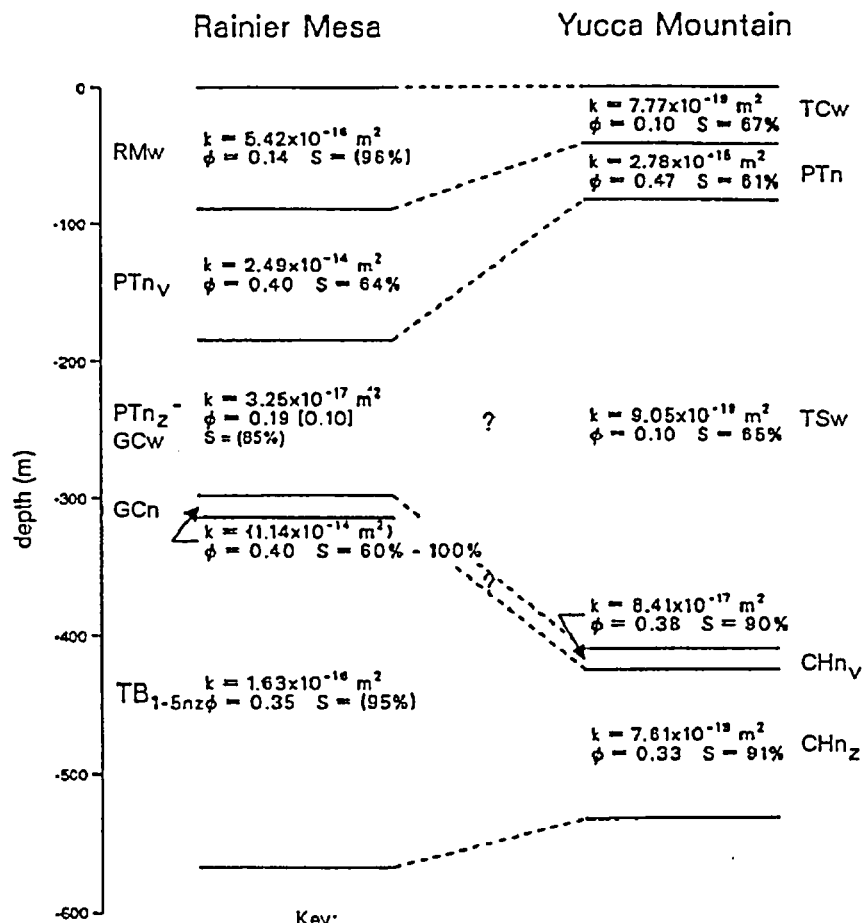
Figure 13.4-3. Plan View of the Locations where Boreholes Intersected Active Water-Conducting Fractures at the Box Canyon Experimental Site



Source: CRWMS M&O (2000b)

NOTE: Zonal information indicated by dimensionless depth (0 to 0.2, etc.)

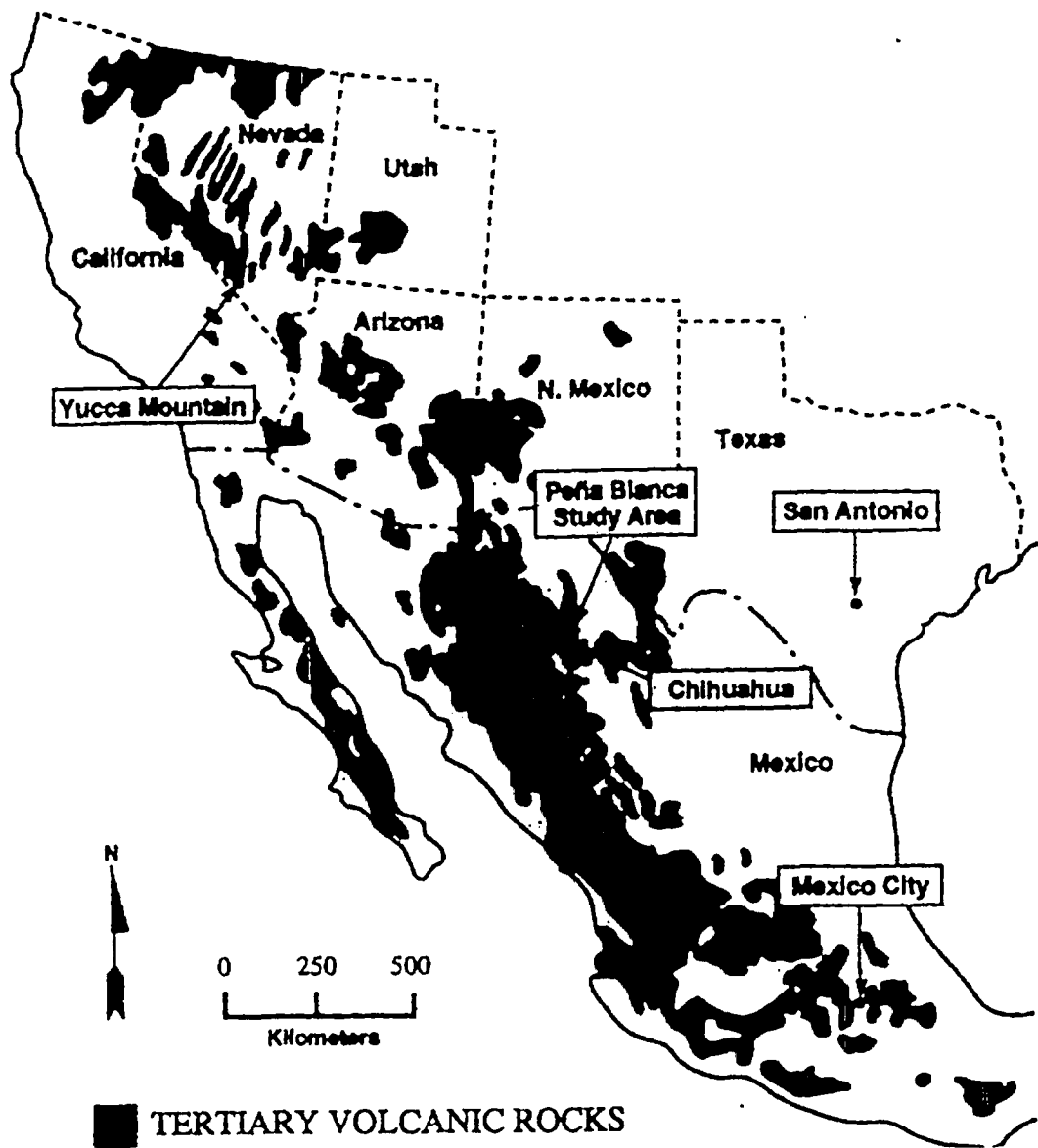
Figure 13.4-4. Two Separate Views of the Box Canyon Numerical Model



13.4-5 CRWSEFDESC.01

Source: Wang et al. (1993, p. 675)

Figure 13.4-5. Comparison between Hydrogeologic Stratigraphic Sections of Rainier Mesa and Yucca Mountain

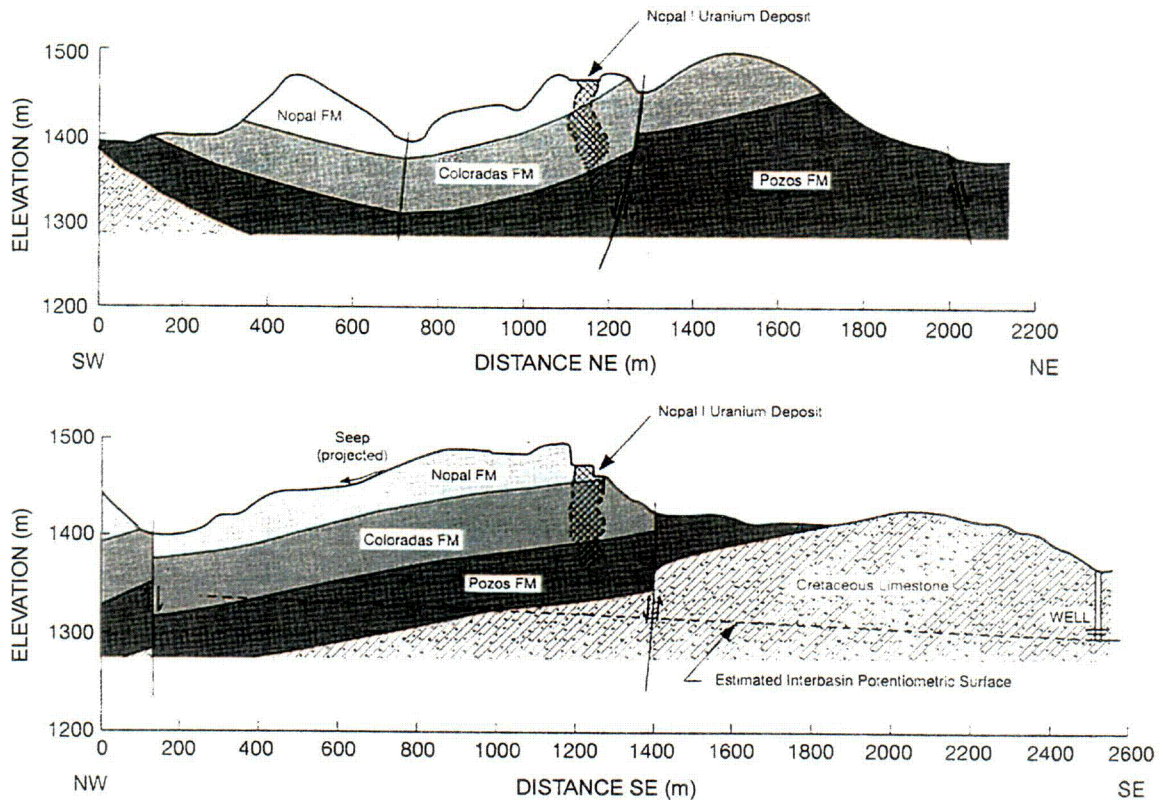


13.4-06.CDR.SITEDESC-R01

Source: Percy et al. (1994, p. 715)

NOTE: The Yucca Mountain potential repository site is located northwest of the Peña Blanca district along a general trend of Tertiary volcanic rocks in the Basin and Range Province.

Figure 13.4-6. Nopal I Uranium Deposit in the Peña Blanca Mining District, Chihuahua, Mexico

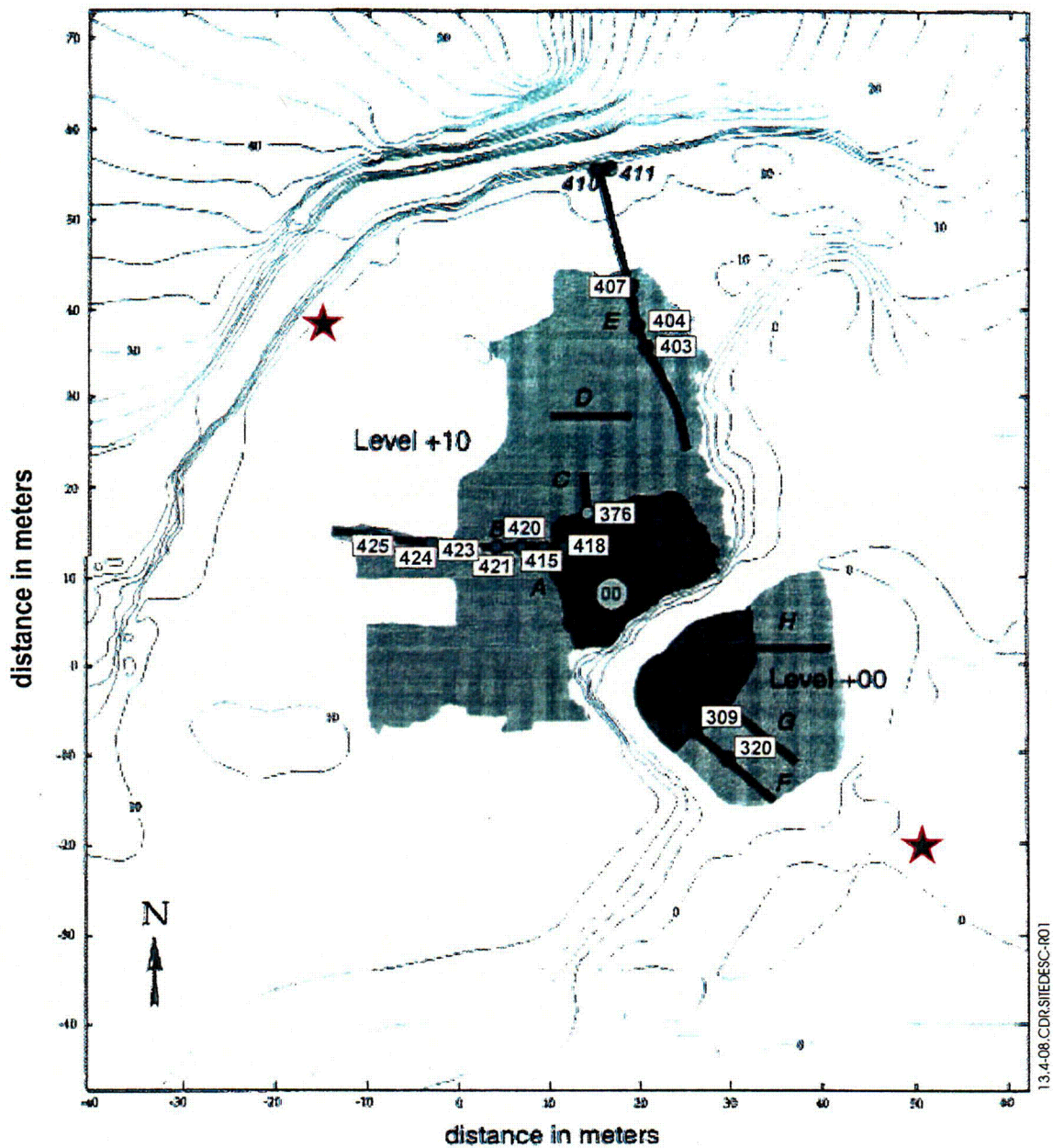


13.4-07.CDR.SITEDESC-R01

Source: Percy et al. (1994, p. 716)

NOTE: Figure illustrates location above the water table and within silicic tuffs of the Nopal and Coloradas formations and the basal conglomerate of the Pozos formation.

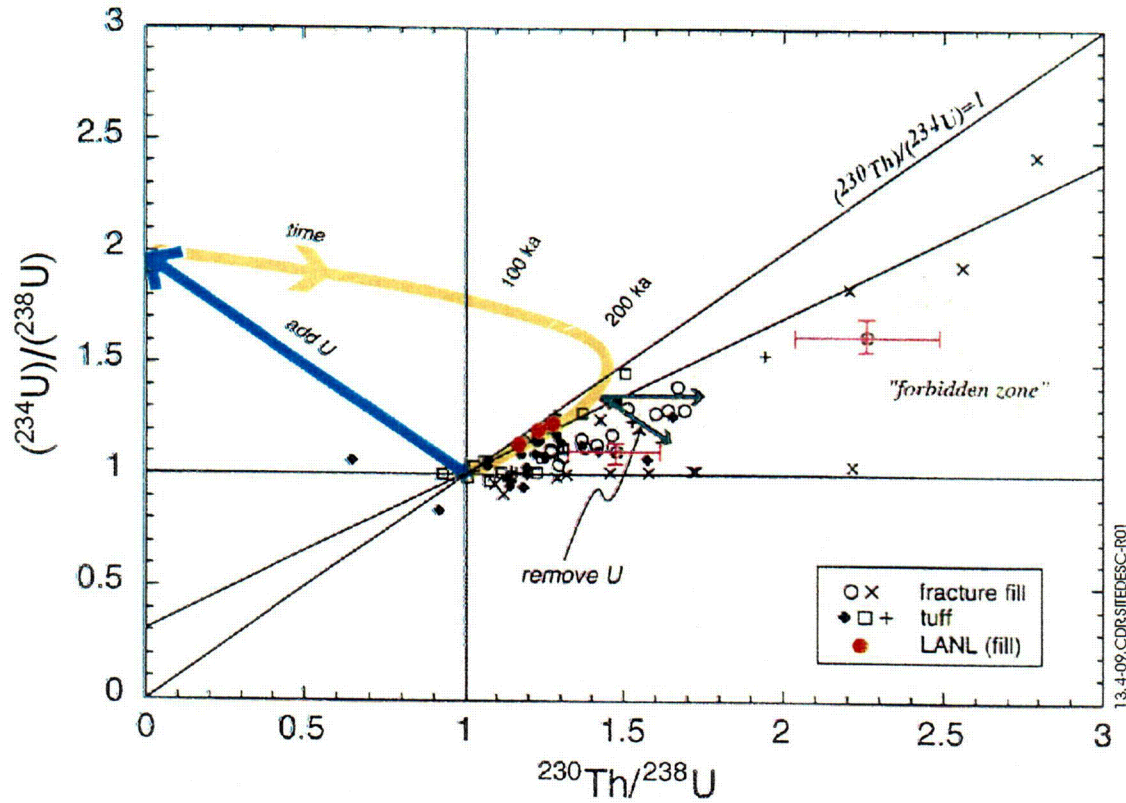
Figure 13.4-7. Orthogonal, Vertical Cross Sections of the Nopal I Deposit



Source: Modified from Pickett and Murphy (1997, Figure 1)

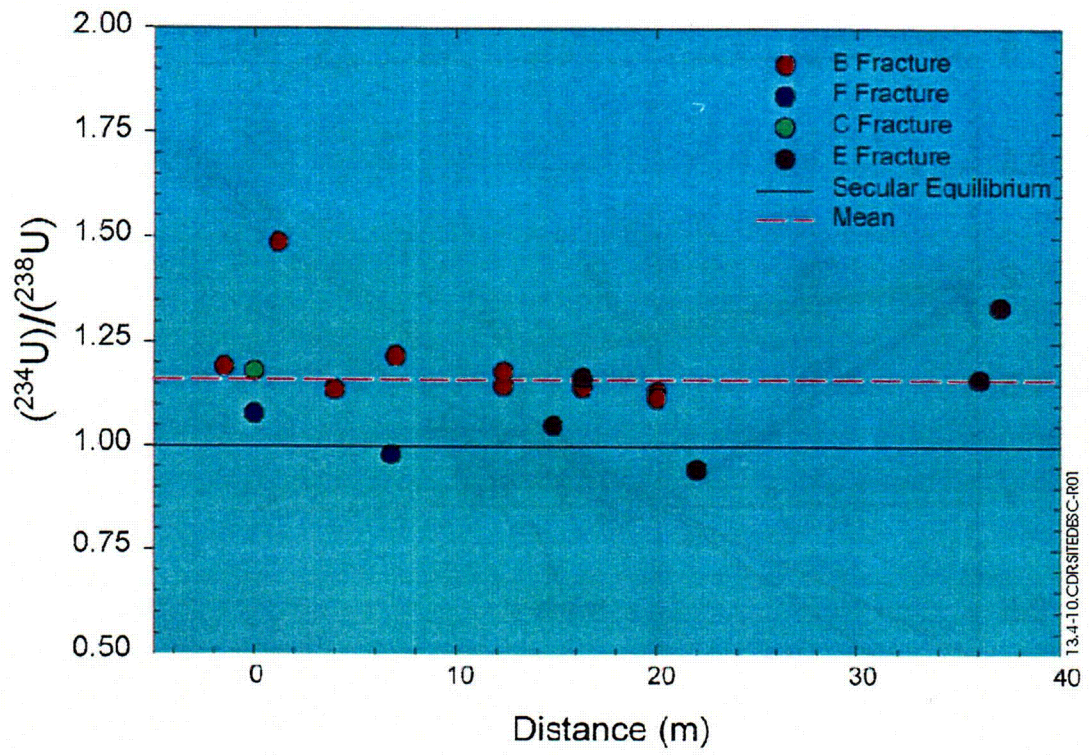
NOTE: The figure illustrates the extent of visible uranium mineralization (black shaded area), major Fractures A to H located near the deposit, numbered sampling locations from CRWMS M&O (2000b), and proposed locations for drilling of near-field groundwater monitoring wells (stars and location marked 00). Most of the samples in the CRWMS M&O (2000b) study were taken along Fracture B. Illegibility of some topographic contour labels does not affect the technical purpose of this figure.

Figure 13.4-8. Topographic Map of Nopal I Area



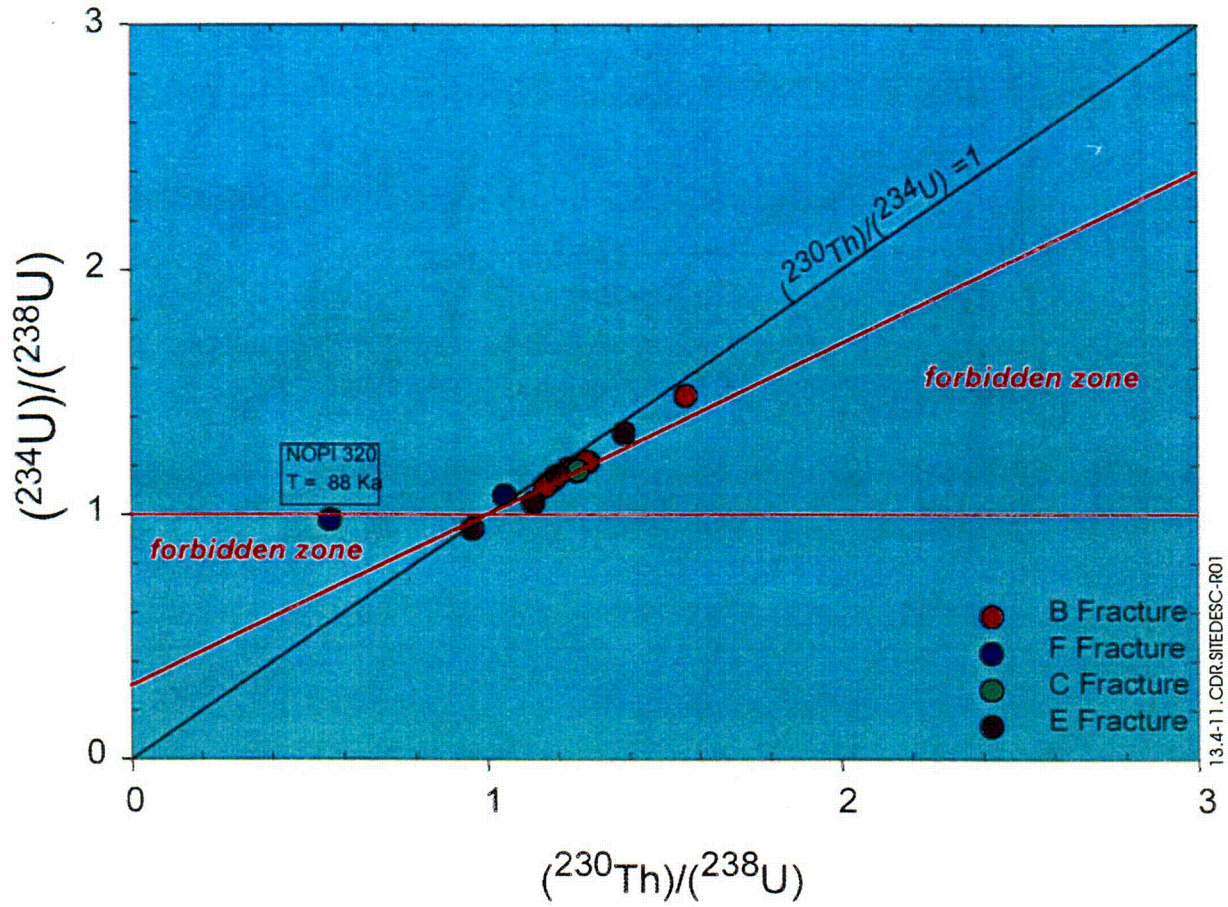
Source: Pickett and Murphy (1997, Figure 4), with added data (identified as LANL) from Murrell et al. (1997)

Figure 13.4-9. Plot of Measurements of Uranium-234/Uranium-238 versus Thorium-230/Uranium-238 for Fracture-Filling Materials Obtained by the Center for Nuclear Waste Regulatory Analyses



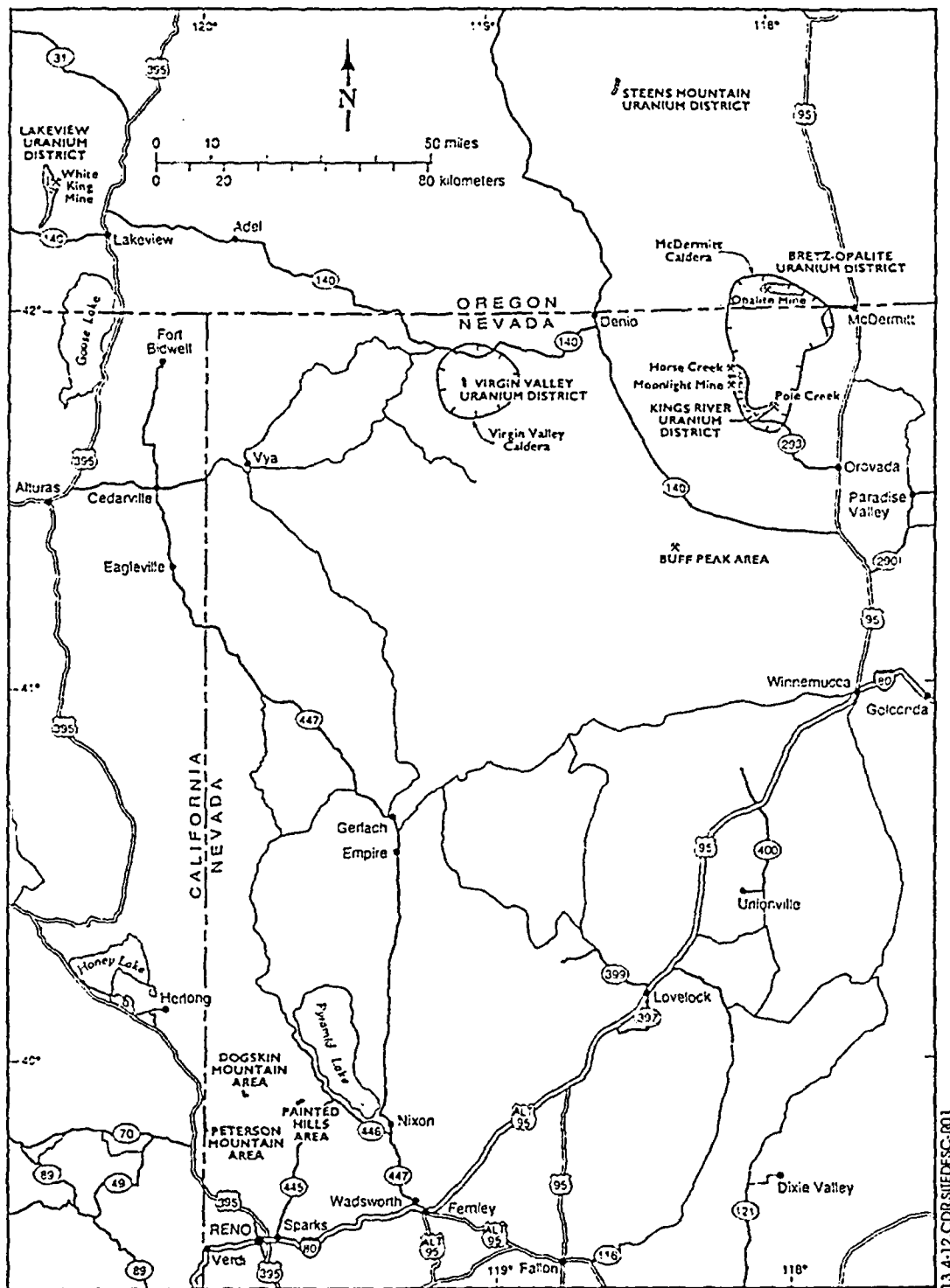
Source: CRWMS M&O (2000b)

Figure 13.4-10. Uranium-234/Uranium-238 Activity Ratios at Distances from the Edge of the Nopal I Deposit for the Fracture Samples



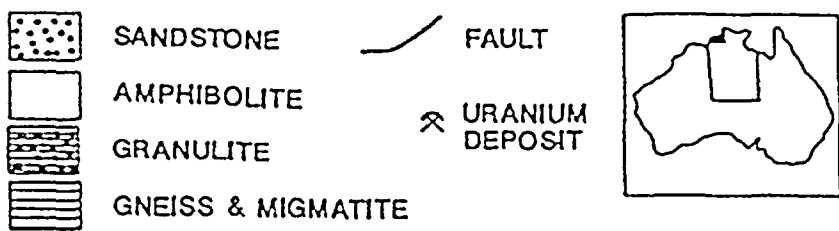
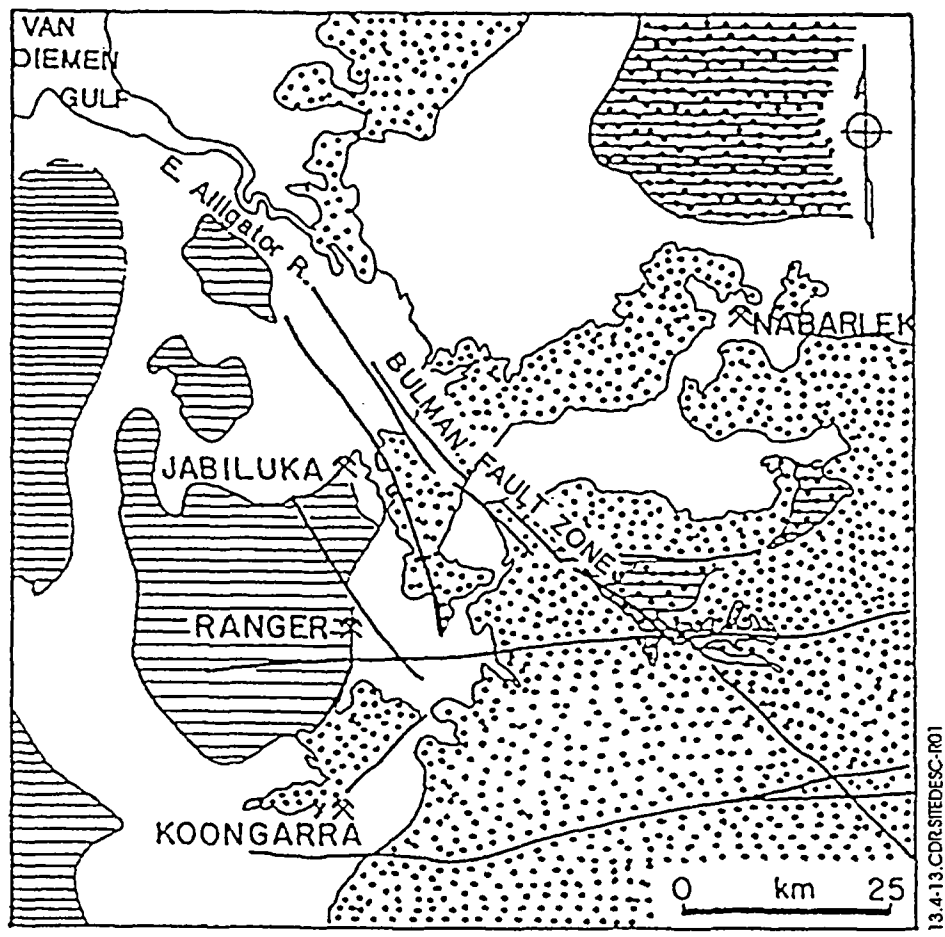
Source: CRWMS M&O (2000b)

Figure 13.4-11. Measurements of Uranium-234/Uranium-238 versus Thorium-230/Uranium-238 for Fracture-Filling Materials at Peña Blanca



Source: Castor et al. (1996, p. 1)

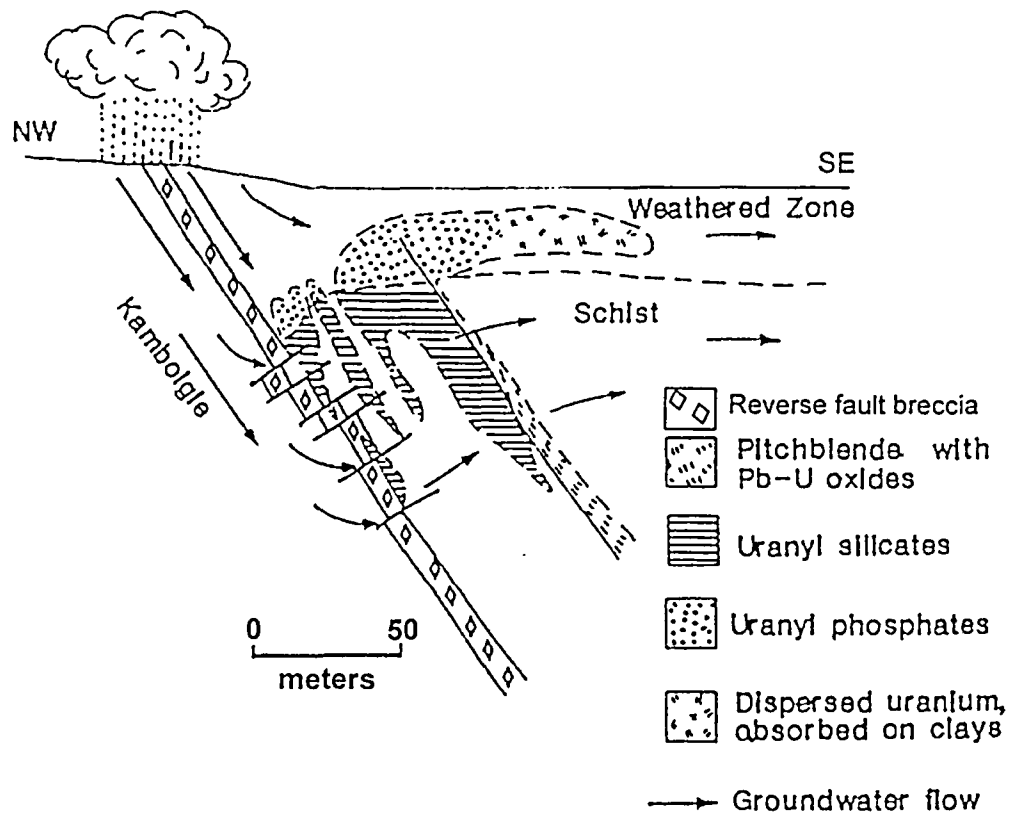
Figure 13.4-12. Location of Uranium Districts in Northwestern Nevada and Southeastern Oregon



Source: Airey (1987)

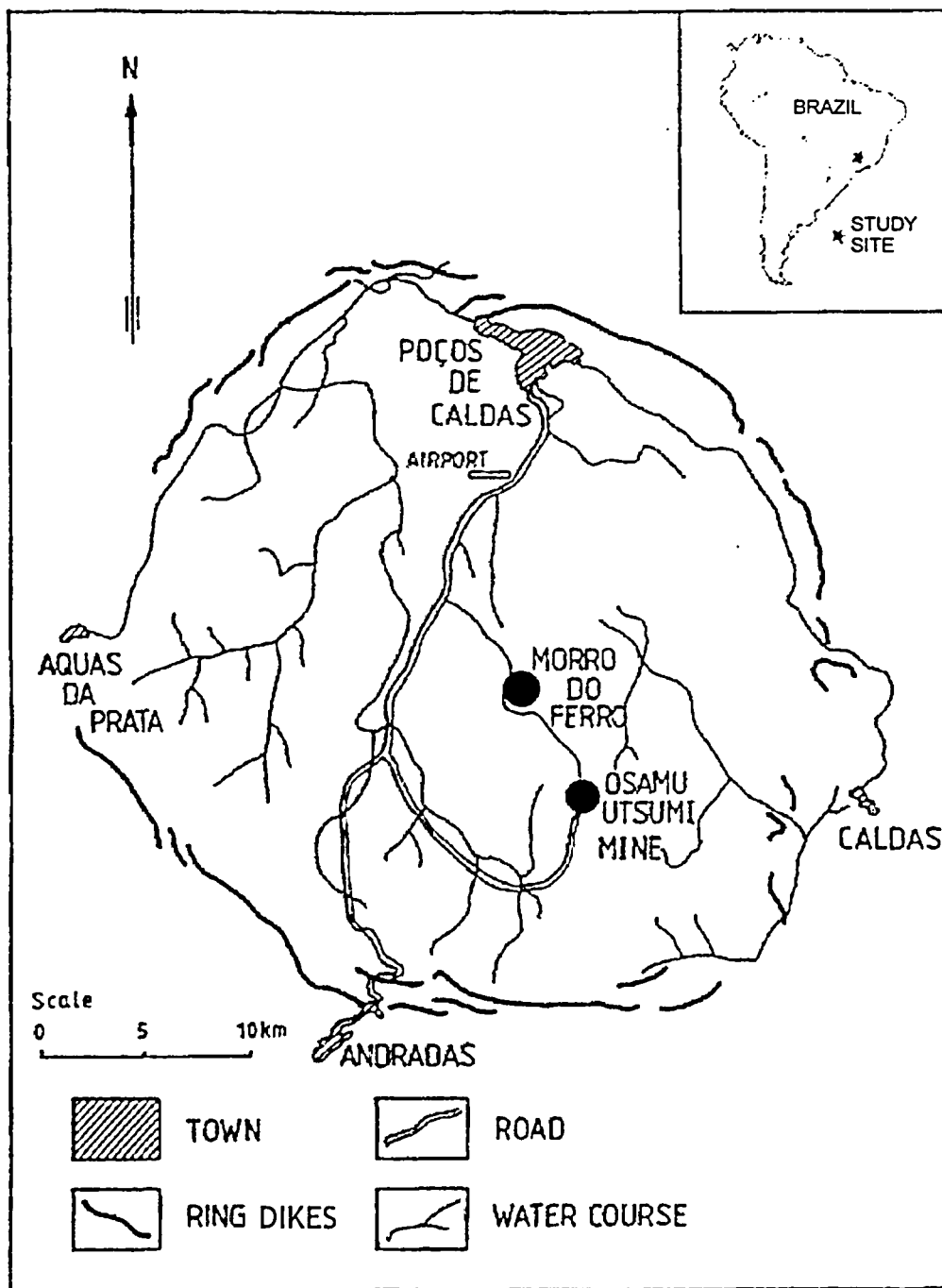
NOTE: The Koongarra deposit was the focus of the Alligator Rivers natural analog study.

Figure 13.4-13. Location of the Uranium Ore Bodies in the Alligator Rivers Region, Northern Territories, Australia



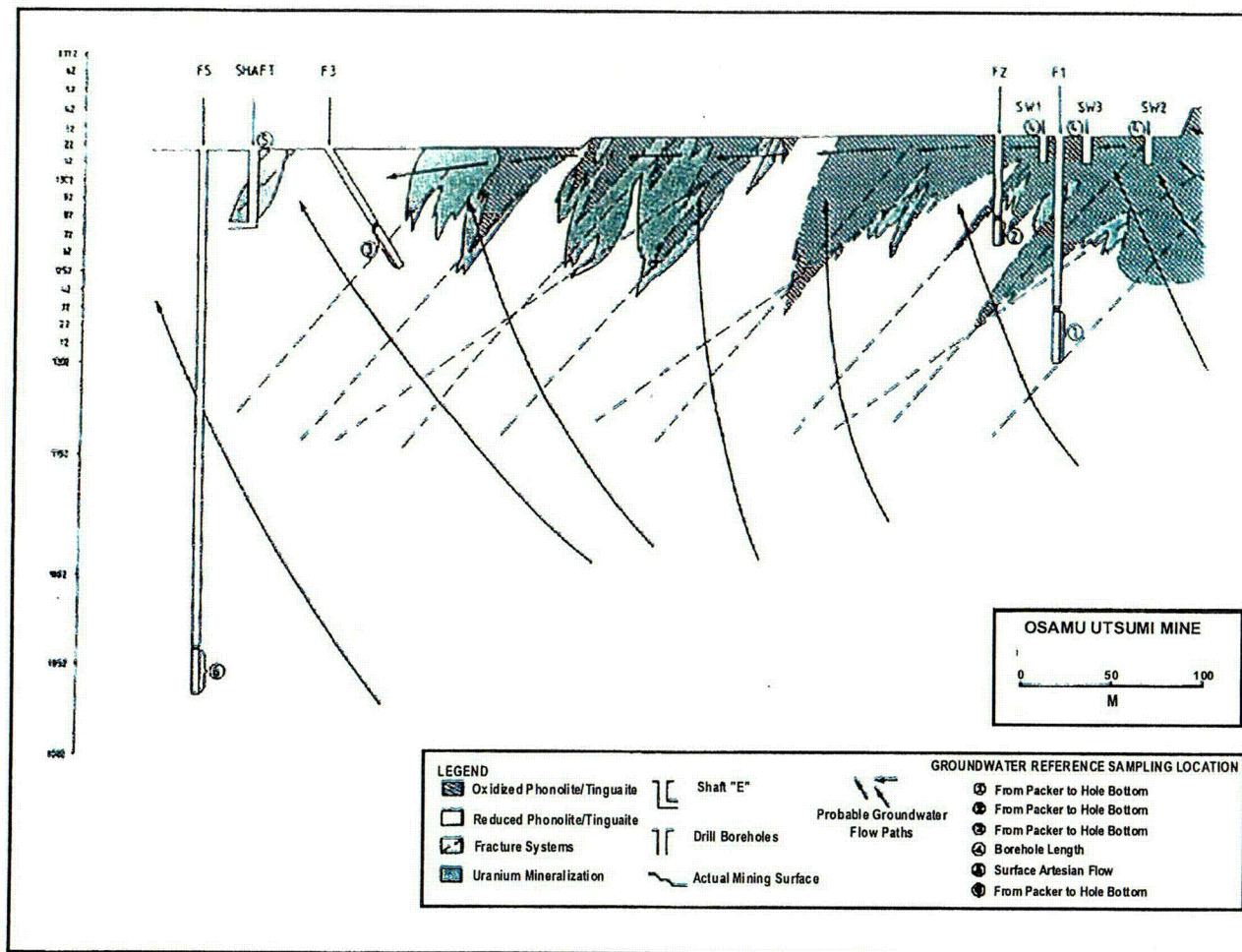
Source: Miller et al. (1994)

Figure 13.4-14. Cross Section through the Koongarra Ore Body Showing the Distribution of the Major Rock Types and Uranium-Bearing Minerals



Source: Chapman et al. (1991)

Figure 13.4-15. Location Map of the Osamu Utsumi Mine and Morro do Ferro Study Sites at Poços de Caldas, Minas Gerais, Brazil

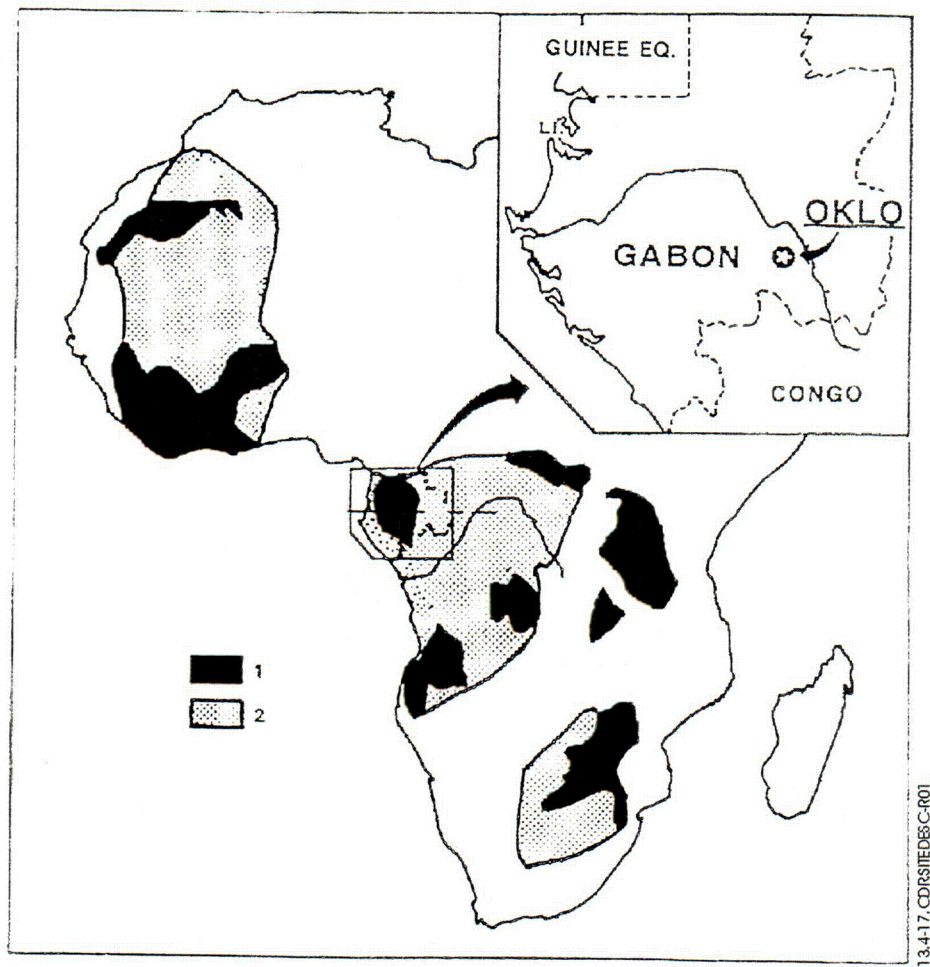


13.4-16.CDR 91EDESC-R01

Source: Chapman et al. (1991, p. 16).

NOTE: Illegibility of vertical axis does not affect the illustrative purpose of this figure.

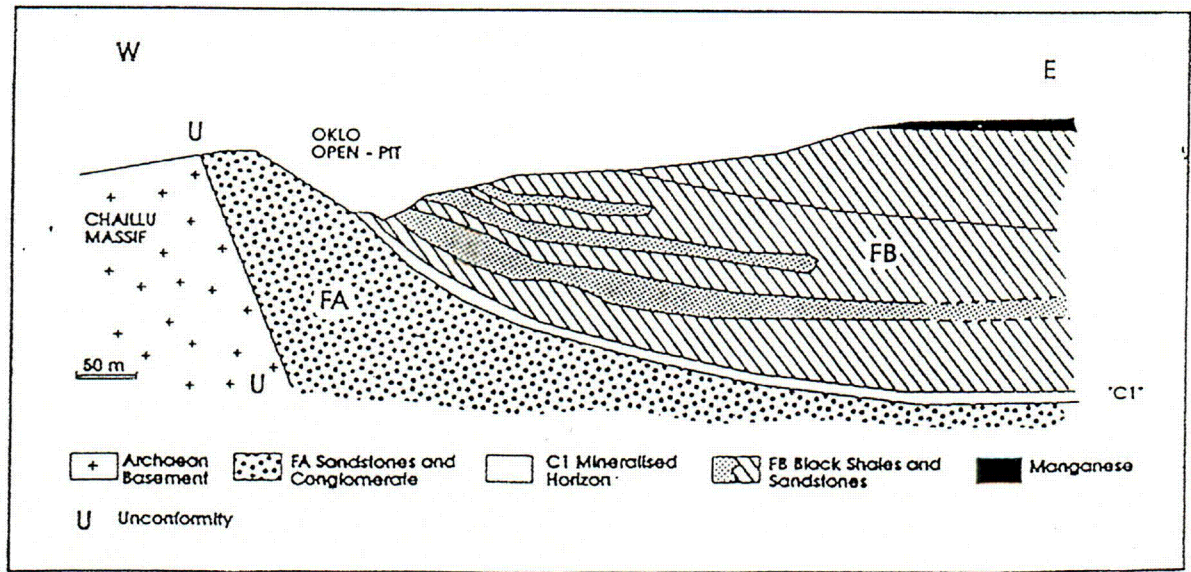
Figure 13.4-16. Cross Section of the Osamu Utsumi Mine Showing the Geology, Hydrology, and Location of the Redox Front



Source: Smellie (1995)

NOTE: Map shows (1) known cratonic areas aged between 1,750 and 2,000 Ma, and (2) probable extensions of those cratonic areas.

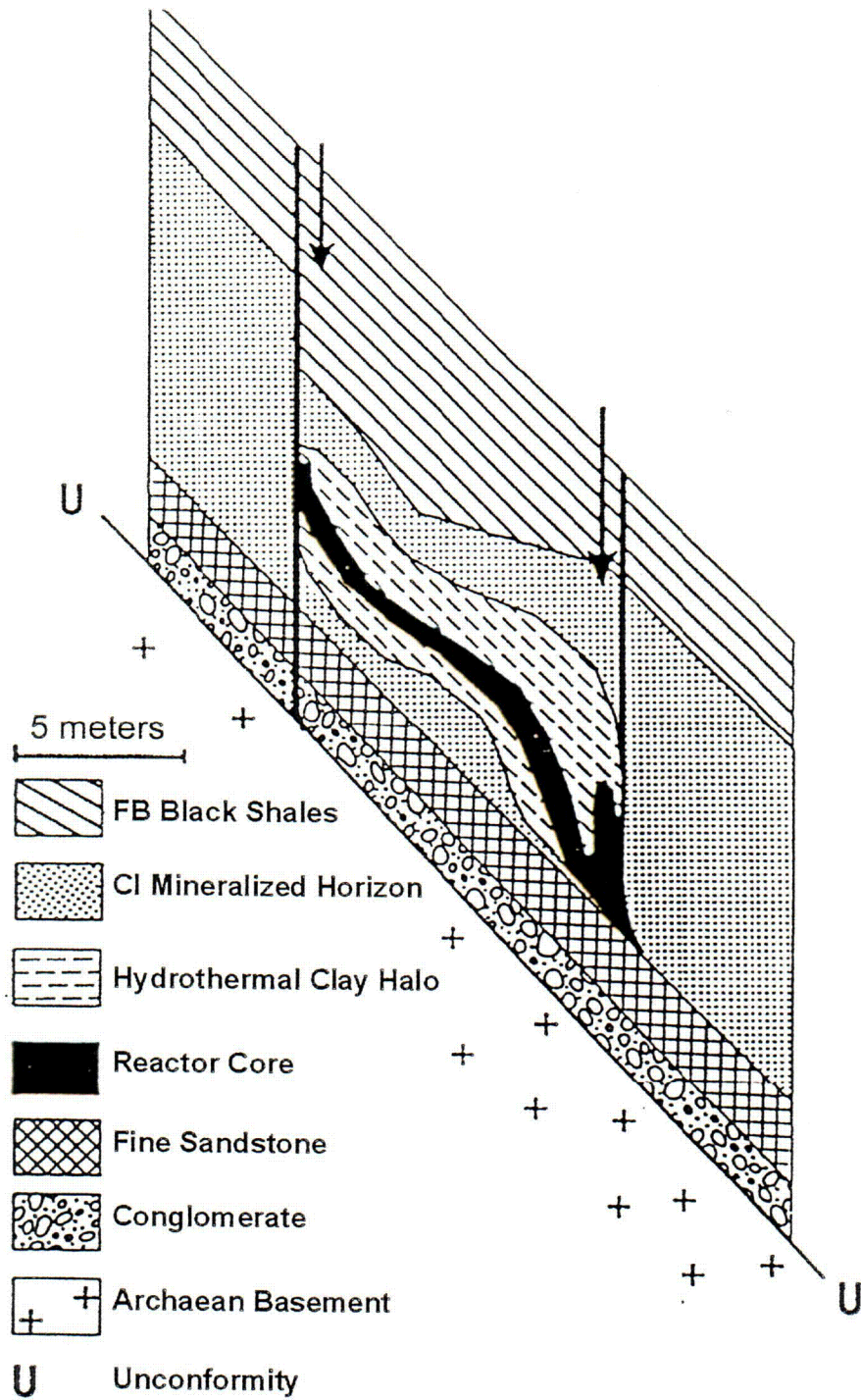
Figure 13.4-17. Location of the Oklo Uranium Deposits, Gabon, Western Africa



Source: Smellie (1995)

NOTE: Indicated is the Oklo open pit showing the position of the C1 layer of pelitic sediments that host the presently mined uranium and the fossil reactor zones.

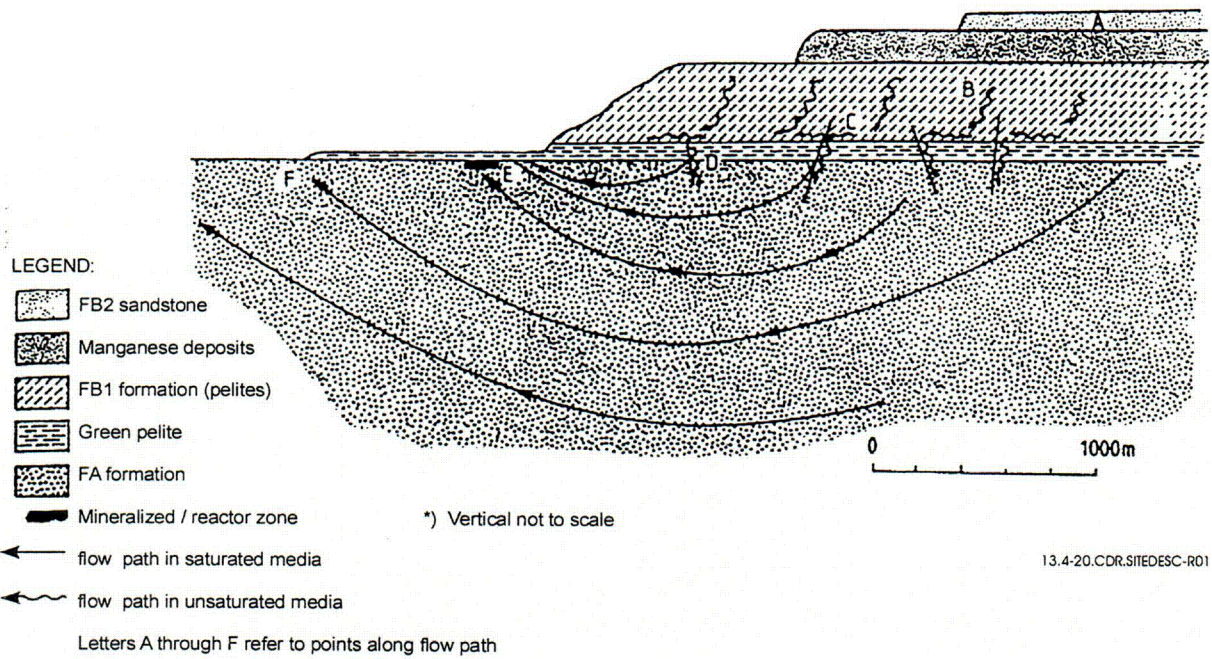
Figure 13.4-18. Schematic Geological Profile across the Western Margin of the Franceville Basin



13.4-19.CDR.SITEDESC-R01

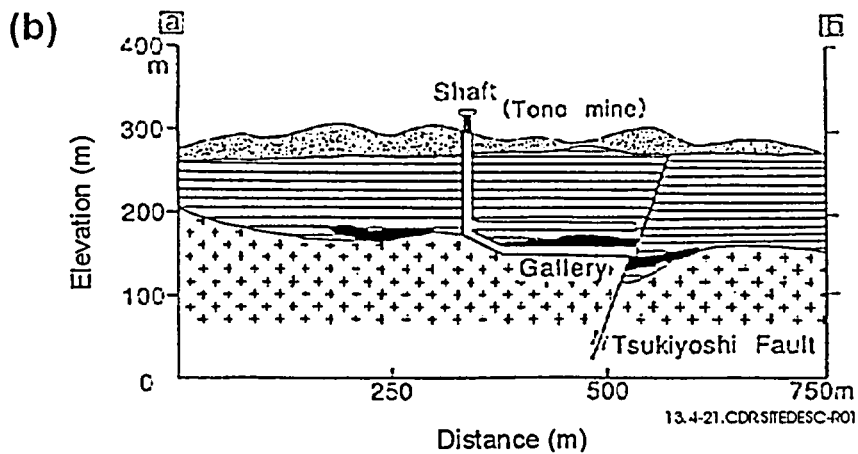
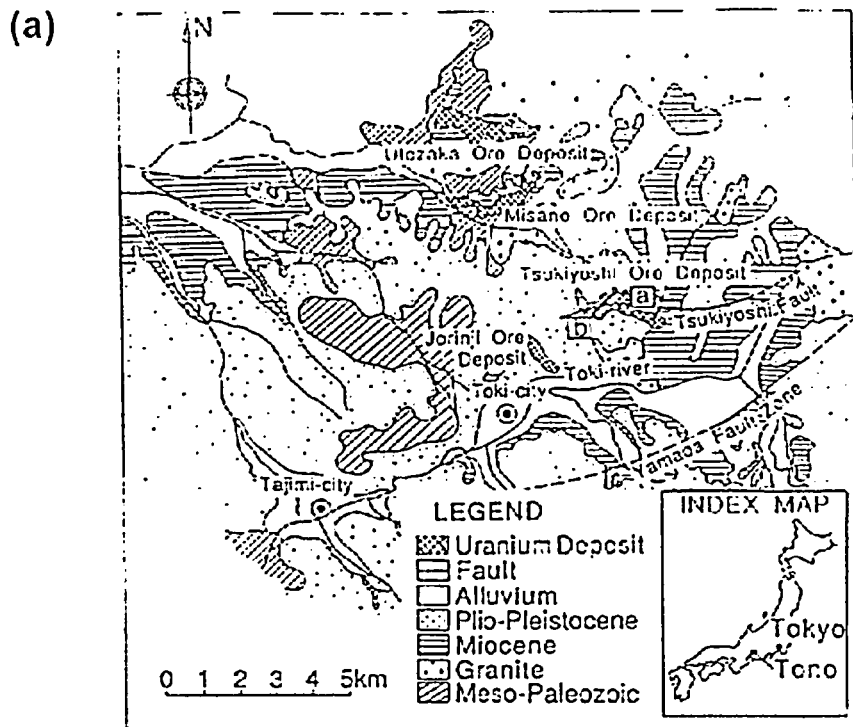
Source: Smellie (1995)

Figure 13.4-19. Idealized Cross Section of a Fossil Reactor Zone at Oklo and Bangombé



Source: Smellie et al. (1993, p. 145)

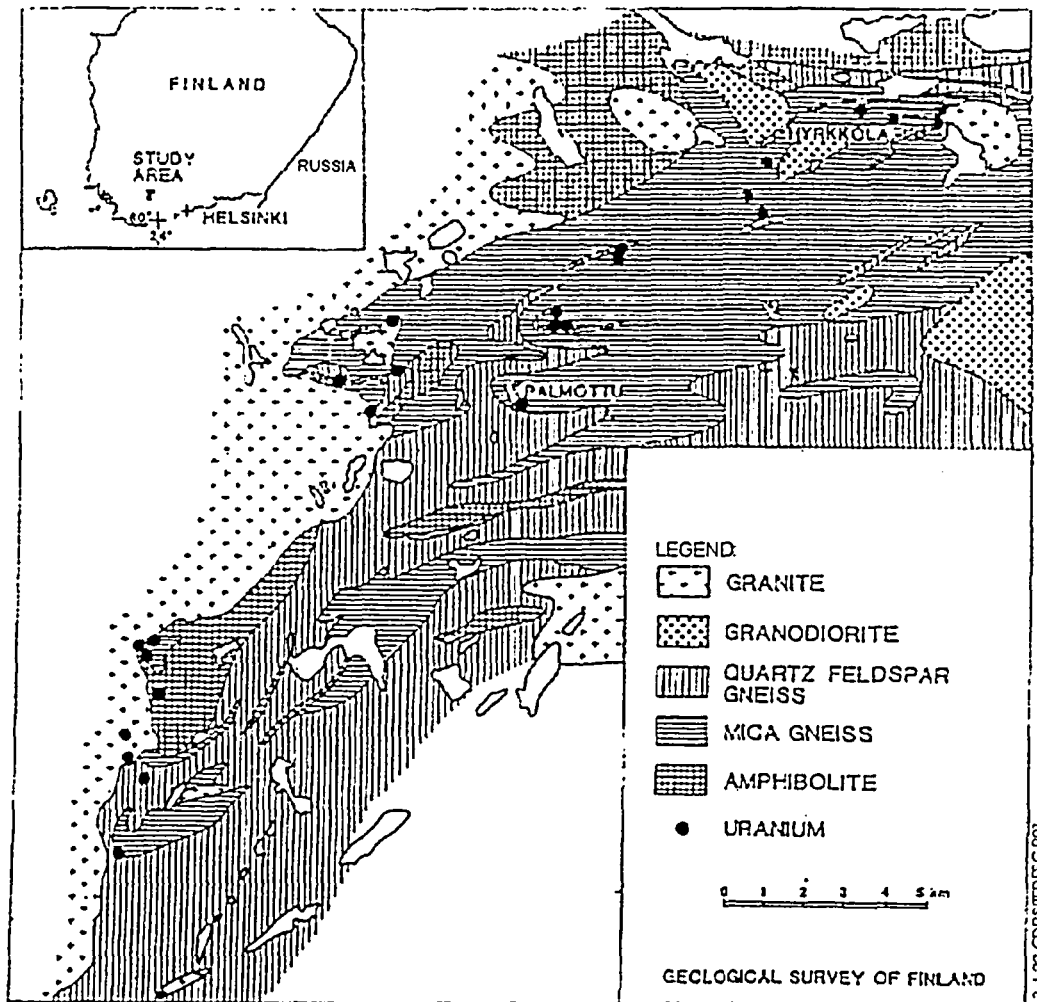
Figure 13.4-20. Schematic Representation of Groundwater Flow Paths in the Bangombé Area



Source: Yusa and Yamakawa (1992)

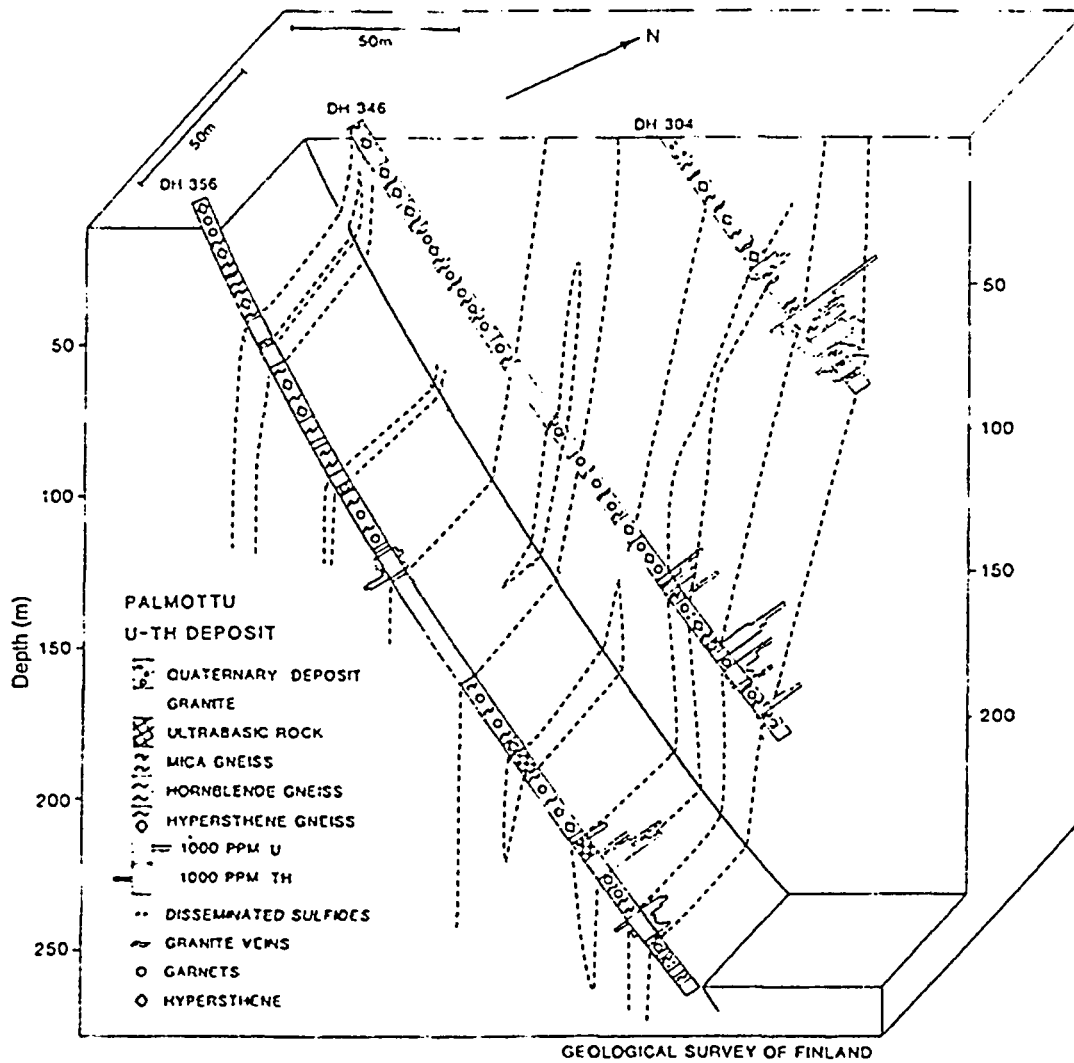
NOTE: Part (a) shows Tono mine site, including regional geology. Part (b) is a cross section through the Tsukiyoshi ore body (black) showing its faulted nature.

Figure 13.4-21. Geology of the Tono Natural Analog Study Site



Source: Blomqvist et al. (1998, p. 11)

Figure 13.4-22. Regional Geologic Map of Palmottu and Location of the Natural Analog Study Site

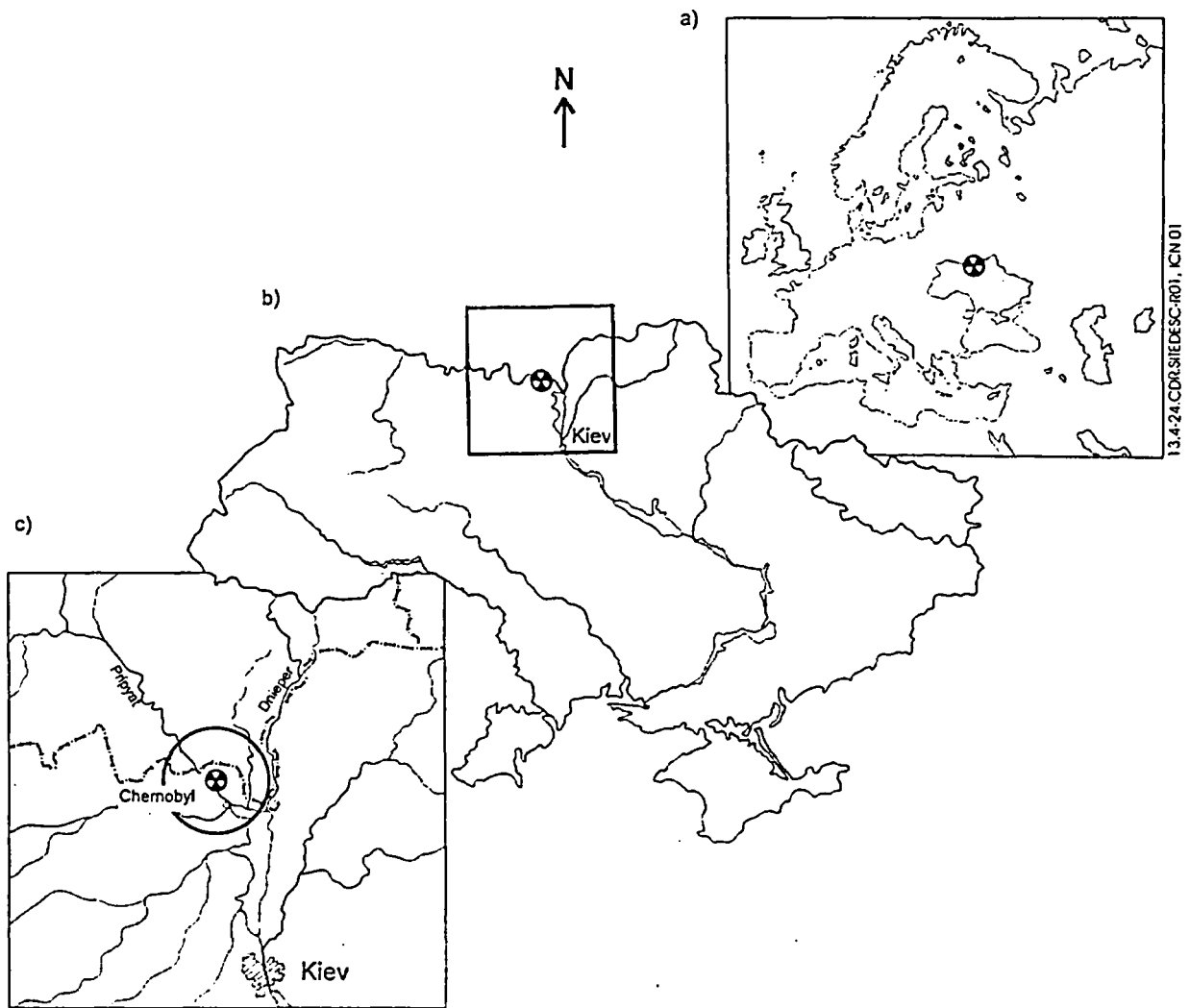


13.4-23.COR.SIIEDESC-R01

Source: Rasilainen et al. (1991)

NOTE: Compiled from drillholes 304, 346, and 356

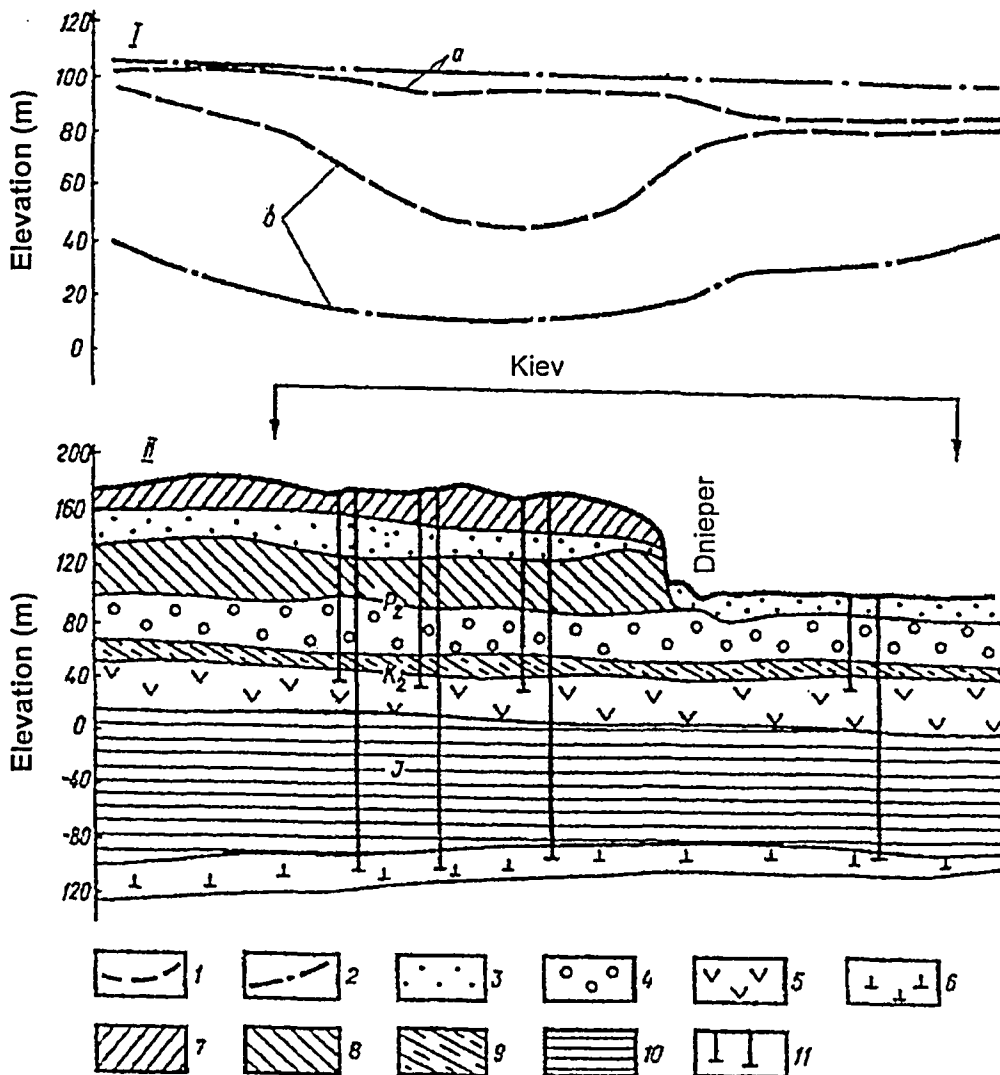
Figure 13.4-23. Lithology at Palmottu with Respective Uranium and Thorium Contents



Source: Shestopalov (1996, p. 1)

NOTE: Part (a) is a map of Europe; part (b), the Ukraine; and part (c), the Chernobyl exclusion zone.

Figure 13.4-24. Location of the 30-km-Radius Chernobyl Nuclear Power Plant Exclusion Zone



13.4-25.CDR.SITEDESC-R01

Source: Shestopalov (1997, p. 257)

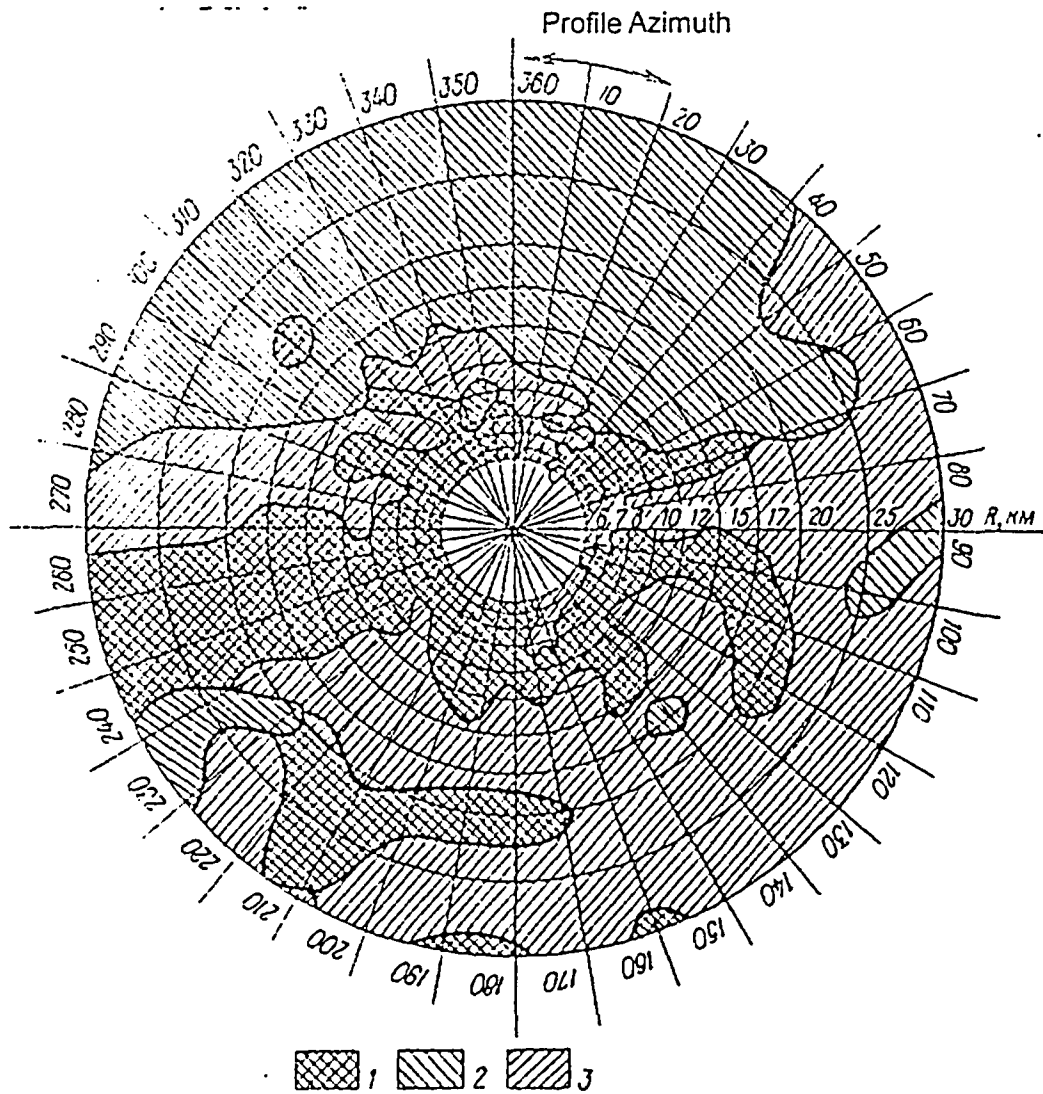
NOTE: I—Water levels:

- 1—Cenomanian-Albian aquifer: (a) prior to water intake, and (b) present conditions
- 2—Bajocian aquifer: (a) prior to water intake, and (b) present conditions

II—Hydrogeological profile:

- 3—Oligocene-Quaternary aquifer (sands, sandy loams)
- 4—Eocene aquifer (sands)
- 5—Cenomanian-Albian aquifer (limestones, chalks, sands, sandstones, gravel)
- 6—Bajocian aquifer (limestones), aquitard deposits
- 7—Quaternary loams and clays
- 8—Kiev (Eocene) marls
- 9—Turonian marls
- 10—Bathonian-Calloviaian clays and clayey limestones
- 11—Boreholes of the Kiev water intake

Figure 13.4-25. Hydrogeological Profile across the Kiev Region

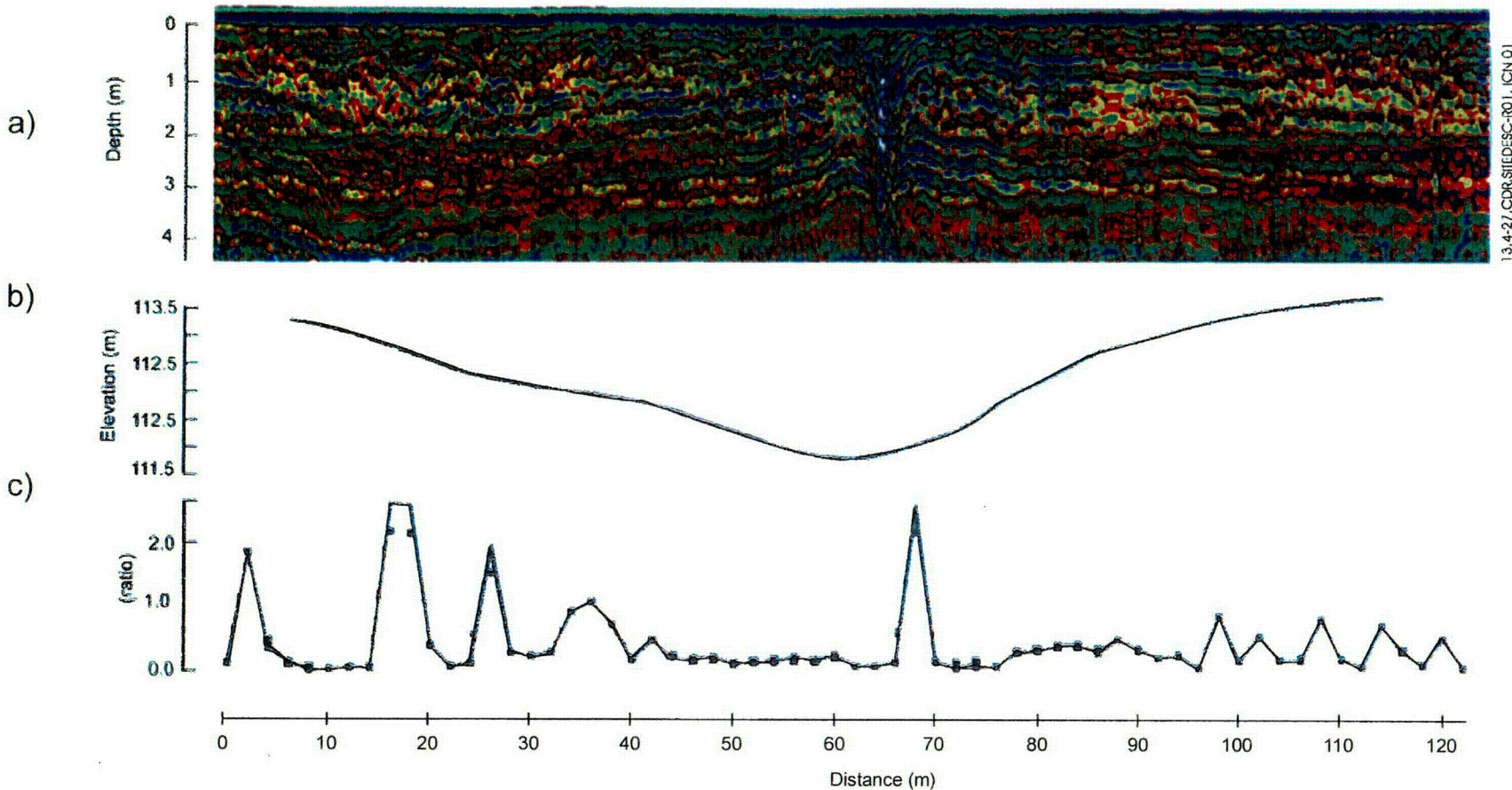


13.4-26.CDR.STEDESC-R01

Source: Sobotovich (1992, p. 82)

NOTE: Part (1) is a zone of contamination primarily by fuel particles; part (2) is a zone of contamination primarily by condensed particles; and part (3) is a zone of contamination by an approximately equal quantity of fuel and condensed particles.

Figure 13.4-26. Soil Sampling Network within the 30-km Chernobyl Exclusion Zone

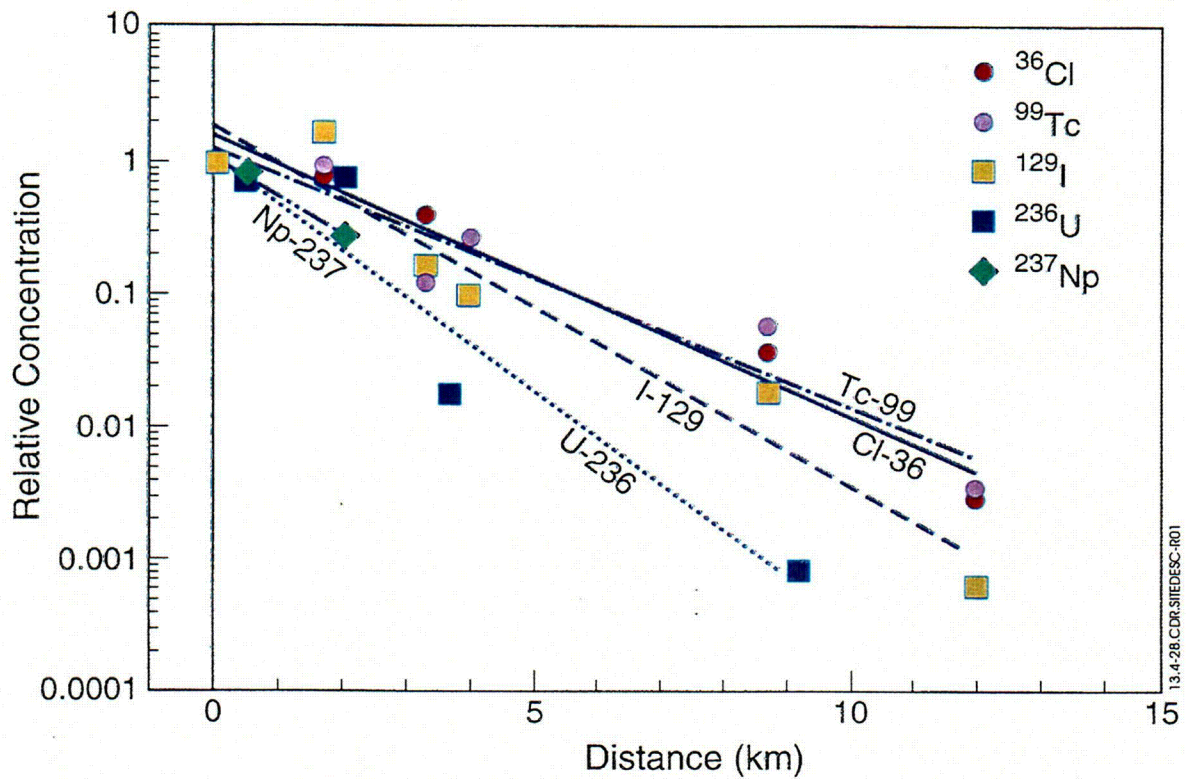


13.4-27/CDR.SHEDESC-RO.1, ICN 01

Source: Modified from Shestopalov et al. (2000)

NOTE: Part (a) shows a radar survey (darker color indicates the increased moisture content in fine sediments), part (b) shows surface elevations, and part (c) shows the radon-222/radon-219 ratio.

Figure 13.4-27. Radon Ratios in Soil at Various Depths and Moisture Content at the Stary Shepelichi Site



Source: Beasley et al. (1998, p. 3,879)

NOTE: For chlorine-36, technetium-99, and iodine-129, the values are normalized to their concentrations in well 57, whereas uranium-236 and neptunium-237 concentrations are normalized to well 123.

Figure 13.4-28. Decrease in Relative Concentrations of Selected Radionuclides in the Snake River Plain Aquifer with Distance from the Idaho Chemical Processing Plant

Table 13.2-1. Process Models and Natural Analogs

Factors Important to Performance (CRWMS M&O 2000d)	Process Model	Analog
Unsaturated Zone Flow and Transport		
Climate	Range of climate conditions	Paleoclimate studies in Great Basin (already in total system performance assessment)
Infiltration	Range of infiltration values	Negev Desert, Mitchell Cavems
Seepage into drifts	Drift seepage model; effect of discrete fractures	Rainier Mesa ^a for wetter conditions; Peña Blanca; Hell's Half Acre
Coupled processes—effects on unsaturated zone flow	Unsaturated zone flow and transport, thermally coupled hydrologic chemical process	Magma intrusion (Papoose Lake Sill)
Coupled processes—effects on seepage	(1) Rockfall and other thermomechanical effects; (2) dryout, permeability changes	(1) Mined openings; (2) magma intrusion (Papoose Lake Sill); geothermal fields
Moisture, temperature, and chemistry on drip shield	Mineral reaction rates	Geothermal fields (e.g., East Mesa, Cerro Prieto), Yucca Mountain as self-analog
Moisture, temperature, and chemistry on waste package	Mineral reaction rates	Geothermal fields, Yucca Mountain as self-analog
Engineered barrier system radionuclide migration—transport through invert	Mineral reaction rates, degradation of invert and other engineered barrier system materials	Geothermal fields, Yucca Mountain as self-analog
Unsaturated zone flow and transport—advective pathways	(1) Unsaturated zone flow; effects of transient flow; (2) effect of water table rise	(1) Peña Blanca; Alligator Rivers; Idaho National Engineering and Environmental Laboratory; Apache Leap; (2) records associated with historical earthquakes in Nevada
Unsaturated zone flow and transport—sorption and matrix diffusion	Unsaturated zone flow and transport	Peña Blanca
Unsaturated zone flow and transport—colloid-facilitated transport	Unsaturated zone flow and transport	Idaho National Engineering and Environmental Laboratory
Coupled processes—effects on unsaturated zone transport	Unsaturated zone flow and transport, thermally coupled hydrologic chemical process	Oman (alkaline plume)
Waste Package Degradation		
Performance of waste package barriers	Degradation of steel alloys and cladding	Meteorites for nickel-base alloy; eskolaite for Cr ₂ O ₃ ; rare-earth phosphates as analog to GdPO ₄ (neutron absorber); Santorini and Asoka pillar (qualitatively)
Microbial-Induced Corrosion		
Moisture, temperature, and chemistry within waste package	Waste package degradation by microbes	(Analysis needed)

Table 13.2-1. Process Models and Natural Analogs (Continued)

Factors Important to Performance	Process Model	Analog
Waste Form Degradation		
Commercial spent nuclear fuel waste form performance	Secondary mineral formation	Hydrothermal uranium deposits, Oklo ^a , Peña Blanca ^a
Defense spent nuclear fuel, Navy fuel, plutonium disposition waste form performance	Secondary mineral formation	None available
High-level radioactive waste glass waste form performance	Stability of glasses	Natural glasses (volcanic), manufactured uranium-bearing glasses
Dissolved radionuclide concentration limits	Solubility of waste form	Hydrothermal uranium deposits
Colloid-associated radionuclide concentrations	Colloids in spent fuel, glass, and plutonium fuel	Peña Blanca
In-package radionuclide transport	Radiolysis, sequestration in secondary minerals	Oklo, Peña Blanca
Saturated Zone Flow and Transport		
Saturated zone flow and transport—advective pathways	Transverse and longitudinal dispersion	Contaminant plumes at U.S. Department of Energy and Environmental Protection Agency sites (e.g., Hanford)
Saturated zone flow and transport—sorption and matrix diffusion	Sorption coefficient in alluvium	Nevada Test Site
Saturated zone flow and transport—colloid-facilitated transport	Colloidal transport in saturated zone	Nevada Test Site, Idaho National Engineering and Environmental Laboratory, El Berrocal, Steenskampskraal ^b
Biosphere		
Biosphere transport and uptake	Plant uptake of radionuclides	Poços de Caldas, Peña Blanca
Disturbed Case Factor		
Volcanism	Volcanism	Nevada-California-Arizona eruptive histories of similar basalt fields
Seismicity	Seismicity	Nevada-California historic earthquakes
Criticality	Criticality	Oklo
Human Intrusion	Human intrusion	None
Engineered Barrier System Design Enhancements		
Performance of backfill	EBS transport	Analog needed
Performance of cements	EBS transport	Maqarin; Krasnoyarsk; New Zealand; Roman concretes
Performance of gettering (sorbptive materials in backfill)	EBS transport	Cigar Lake; Dunarobba Forest; Loch Lomond

Source: this document

NOTE: ^a Strongly recommended by performance assessment

^b Not all analogs listed in Table 13.2-1 are discussed in text.

Table 13.3-1. Comparison of Volcanic Glass and Nuclear Waste Glass Compositions (wt %)

Oxide	Volcanic Glass		Nuclear Waste Glass
	Basaltic	Rhyolitic	
SiO ₂	50.76	74.67	45.48
Al ₂ O ₃	13.62	12.17	4.91
B ₂ O ₃	-	-	14.02
Li ₂ O	-	-	1.98
Na ₂ O	2.48	4.25	9.86
MgO	7.35	0.10	-
K ₂ O	0.18	2.78	-
CaO	10.72	1.68	4.04
TiO ₂	1.66	0.30	-
MnO ₂	0.16	-	0.72
FeO	8.18	3.21	-
Fe ₂ O ₃	4.08	-	2.91
ZnO	-	-	2.50
ZrO ₂	-	-	2.65
Cs ₂ O	-	-	1.42
Other oxides (rare-earth elements, actinides)	-	-	8.00

Source: Modified from Petit et al. (1990, p. 1942)

NOTE -- = not detected

INTENTIONALLY LEFT BLANK

Table 13.4-1. Application of Geothermal Field Information as Analogs to Coupled Processes Anticipated at the Potential Yucca Mountain Repository

Yucca Mountain Issue	Geothermal Analog	Potential Sites	Possible Approach
Multiphase flow (liquid, vapor, gas)	Multiphase flow (liquid, vapor, gas)	All	Numerical modeling, conducting and reviewing geothermal post audits
Hydrologic properties	Hydrologic properties	Kamojang (Indonesia), Tianjin (China), Wairakei (New Zealand), Oguni (Japan), Sumikawa (Japan)	Numerical modeling
Preferential flow	Preferential flow	Wairakei (New Zealand), The Geysers (California), Dixie Valley (Nevada), East Mesa (California), Cerro Prieto (Mexico)	Numerical stochastic modeling, geothermal tracer study results evaluations
Fracture network permeability	Fracture network permeability	All modeled fractured sites (e.g., Cerro Prieto [Mexico], Krafla [Iceland], Matsukawa [Japan], Sumikawa [Japan], Olkaria [Kenya], Krafla [Iceland], Wairakei [New Zealand], The Geysers [California], Kamojang [Indonesia], Larderello [Italy])	Use of reservoir model calibrations
Fracture-matrix interaction	Fracture-matrix interaction	Yellowstone (Wyoming), Long Valley (California), Olkaria (Kenya), Dixie Valley (Nevada)	Field and laboratory experiments, evaluate geothermal tracer study results evaluations
Heat pipes, boiling, and condensation	Heat pipes, boiling, and condensation	The Geysers (California), Kamojang (Indonesia), Matsukawa (Japan), Larderello (Italy)	Numerical modeling to extend measurements
Mineral precipitation and dissolution	Mineral precipitation and dissolution	Larderello (Italy), Fenton Hill (New Mexico), Dixie Valley (Nevada), Wairakei (New Zealand), Broadlands (New Zealand), Long Valley (California)	Laboratory experiments, analog site investigation, numerical modeling
Self-sealing	Caprocks	The Geysers (California), Kamojang (Indonesia), Matsukawa (Japan), Larderello (Italy), Cerro Prieto (Mexico), Reykjanes (Iceland)	Core sample evaluation, water chemistry evaluation, numerical modeling
Mineral alteration	Mineral alteration	Wairakei (New Zealand), Broadlands (New Zealand), Dixie Valley (Nevada), Yellowstone (Wyoming)	Core sample evaluation, numerical modeling
Thermal-hydro-mechanical effects	Subsidence, flow changes	Wairakei (New Zealand), Bulalo (Philippines), Krafla (Iceland)	Numerical modeling

NOTE: The following sites have (a) similar water chemistry to Yucca Mountain, (b) similar geology to Yucca Mountain, and/or (c) similar alteration mineralogy to Yucca Mountain: Larderello (Italy)-b, possibly c; Yellowstone (Wyoming)-a,b,c; Fenton Hill (New Mexico)-b; Dixie Valley (Nevada)-c; Wairakei (New Zealand)-a,b,c; Broadlands (New Zealand)-a,b,c; Long Valley (California)-a,b, possibly c.

Table 13.4-2. Water Chemistry Characteristics of Northwestern Nevada/Southeastern Oregon Uranium Districts

Study Site	Water Type	Temperature (°C)	pH	Total Dissolved Solids (mg/L)	Depth to Water (m)
McDermitt caldera area, Nevada-Oregon	Ca-Na-HCO ₃ -SO ₄	0-28	6.8-9.4	66-724	50
Virgin Valley, nonthermal, Nevada	Na-HCO ₃ -SO ₄	7-24	6.4-9.7	95-184	<60
Virgin Valley, thermal, Nevada	Na-SO ₄ -HCO ₃	26.5-92	7.5-9.05	600-630	<60
Lakeview, Oregon	Ca-Na-HCO ₃	7.8	6.3-8.1	-	0
Steens Mountain, Oregon	-	-	-	-	-
Bottle Creek, Oregon	Ca-Na-HCO ₃ -SO ₄	7-90	6.4-10.1	42-1216	-
Painted Hills, Nevada	-	-	-	-	-
Dogskin Mountain, Nevada	Ca-Na-HCO ₃	-	-	86-121	-
Peterson Mountain, Nevada	-	-	-	-	-
Yucca Mountain, Nevada	Na-HCO ₃ -SO ₄	33.8-44	6.8-8.7	245-530	28-752 ^a

Source: Castor et al. (1996, Table 12)

NOTES: ^a Values greater than 300 m are most representative of the water-level depth beneath Yucca Mountain.
 - = information not available

Table 13.4-3. Comparison of Radionuclides Released from the Chernobyl Unit 4 Reactor to Radionuclides of Concern for Yucca Mountain

Radionuclide	Half-Life	Total Activity of Radionuclides Released at Chernobyl (MCi) ^a	Total Mass of Radionuclides Released at Chernobyl (g) ^a	Present at Chernobyl	Potentially Present at Yucca Mountain ^e
⁶⁵ Zn	243.8 days	—	—	X ^a	—
⁸⁹ Sr	50.5 days	2.2	78.1	X ^{a, b, c}	—
⁹⁰ Sr	29 yr.	0.22	1,496	X ^{a, b, c}	—
⁹³ Mo	3.4 x 10 ³ yr.	—	—	—	X
⁹³ Zr	153 x 10 ⁶ yr.	—	—	—	X
⁹⁵ Nb	34.97 days	—	—	X ^a	—
⁹⁵ Zr	64 days	3.8	177.4	X ^{a, b, c}	—
⁹⁹ Mo	2.75 days	—	—	X ^{b, c}	—
¹⁰³ Ru	39.4 days	3.2	99.8	X ^{a, b, c}	—
¹⁰⁶ Ru	372 days	1.6	496	X ^{a, b, c}	—
¹²⁹ I	1.57 x 10 ⁷ yr.	—	—	—	X
¹³¹ I	8.04 days	7.3	59	X ^{a, b, c}	—
¹³² Te	3.26 days	—	—	X ^{b, c}	—
¹³⁴ Cs	2.06 yr.	0.5	412	X ^{a, b, c}	—
¹³⁵ Cs	2.95 x 10 ⁶ yr.	—	—	—	X
¹³⁷ Cs	30.2 yr.	1	114.9	X ^{a, b, c}	—
¹⁴⁰ Ba	12.75 days	—	—	X ^{b, c}	—
¹⁴⁰ La	1.68 days	—	—	X ^a	—
¹⁴¹ Ce	32.5 days	2.8	98.5	X ^{a, b, c}	—
¹⁴² Ce	5 x 10 ¹⁶ yr.	—	—	—	X
¹⁴⁴ Ce	285 days	2.4	758	X ^{a, b, c}	—
¹⁴⁴ Pm	360 days	—	—	X ^a	—
²³³ U	1.59 x 10 ³ yr.	—	—	—	X
²³⁴ U	2.45 x 10 ⁵ yr.	—	—	X ^c	X
²³⁵ U	7.04 x 10 ⁸ yr.	—	—	X ^c	X
²³⁶ U	2.34 x 10 ⁷ yr.	—	—	X ^c	X
²³⁷ Np	2.14 x 10 ⁶ yr.	—	—	—	X
²³⁸ Pu	87.7 yr.	0.8 X 10 ⁻³	46.7	X ^{a, b, c, d}	X
²³⁸ U	4.47 x 10 ⁹ yr.	—	—	X ^c	X
²³⁹ Np	2.36 days	—	—	X ^{b, c}	—
²³⁹ Pu	24,110 yr.	0.7 X 10 ⁻³	11,410	X ^{a, b, c, d}	X
²⁴⁰ Pu	6,560 yr.	1 X 10 ⁻³	4,390	X ^{a, b, c, d}	X
²⁴¹ Am	433 yr.	—	—	X ^d	X
²⁴¹ Pu	14.4 yr.	0.14	2,072	X ^{a, c, d}	X

Table 13.4-3. Comparison of Radionuclides Released from the Chernobyl Unit 4 Reactor to Radionuclides of Concern for Yucca Mountain (Continued)

Radionuclide	Half-Life	Total Activity of Radionuclides Released at Chernobyl (MCi) ^a	Total Mass of Radionuclides Released at Chernobyl (g) ^a	Present at Chernobyl	Potentially Present at Yucca Mountain ^e
²⁴² Cm	163 days	2.1 X 10 ⁻⁶	3.72 X 10 ⁻⁶	X ^{a, b, c, d}	X
²⁴⁵ Cm	8.5 x 10 ³ yr.	-	-	-	X
²⁴⁶ Cm	4.73 x 10 ³ yr.	-	-	-	X

NOTES: ^a Shestopalov (1997, pp. 260-261)
^b Eliassen (1990, p. 149)
^c Sobotovich (1992, pp. 41-45)
^d Loshchilov et al. (1991c, p. 45)
^e Identified by Palmer et al. (1996) as being of concern at Yucca Mountain
 - = information not available or radionuclide not present;
 X = present at the site

Table 13.4-4. Vertical Distribution of Plutonium and Uranium in Soils in the Vicinity of the Chernobyl Nuclear Power Plant

Depth (cm)	Plutonium-239 and/or 240 (%)	238-Uranium/235-Uranium
0-1	92-96	79.9-103.5
1-2	2.9-7.4	126.7-135.8
2-3	0.3-0.6	129.6-137.3
3-4	0-0.2	137.1-137.8
4-5	0-0.1	137.6-137.8

Source: Modified from Sobotovich (1992, Table 3.6, p. 44)

NOTE: Numbers indicate range of values at six sites.

Table 13.4-5. Diffusion Coefficients for Strontium-90 and Cesium-137 in Low Humus Sand Near the Chernobyl Nuclear Power Plant

Soil Saturation (%)	Strontium-90 (*10 ⁻⁸ cm ² /s)	Cesium-137 (*10 ⁻⁸ cm ² /s)
30	21, 22	0.51, 0.6
60	27, 29	0.6, 0.9
100	48, 53	0.9, 1.8

Source: Modified from Loshchilov et al. (1991b, p. 38)

NOTE: Numbers indicate values obtained by fitting experimental data by two models.

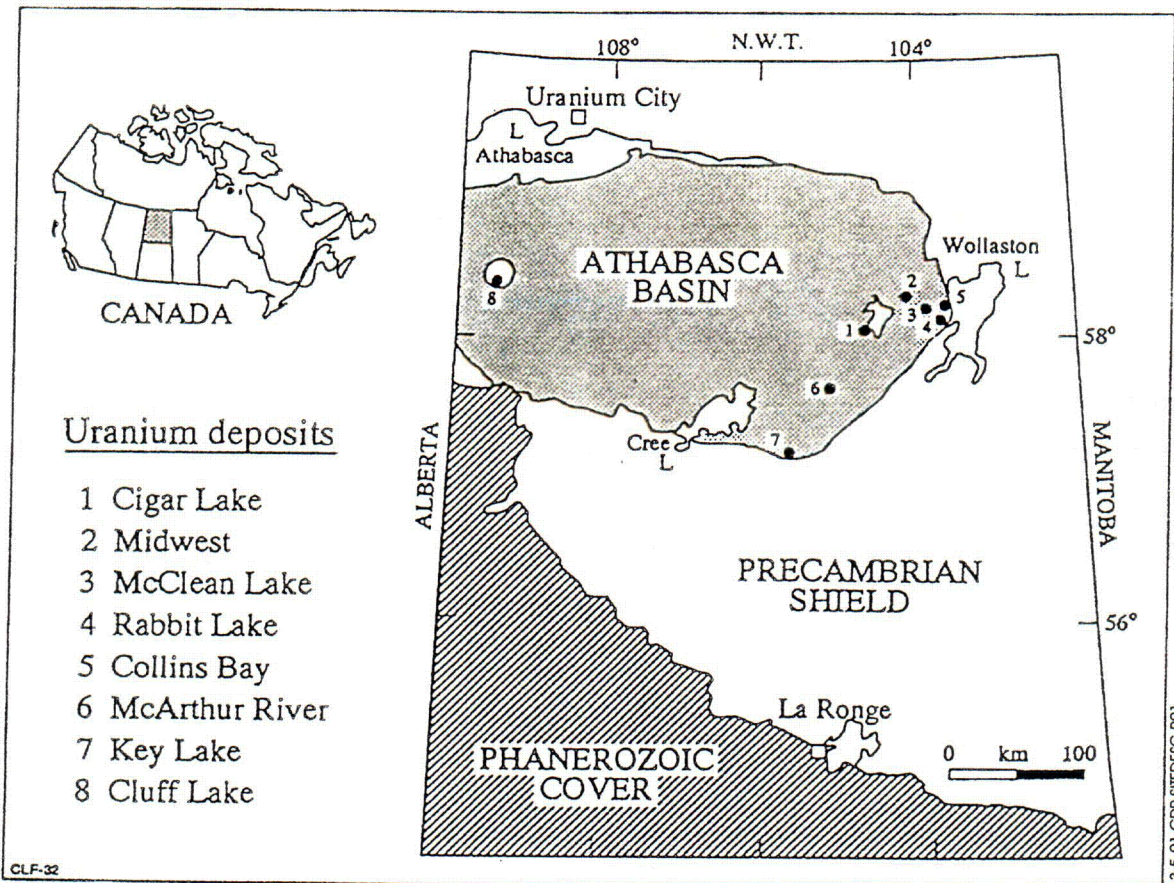
Table 13.4-6. Maximum Content of Dissolved and Exchangeable Radionuclides in Soils of Chernobyl Exclusion Zone and Maximum Values of Retardation Factors and Distribution Coefficients

Radionuclide	Dissolved (%)	Exchangeable (%)	Retardation Factor	Distribution Coefficient (dimensionless)
¹⁴⁴ Ce	3.9	12.7	n.r.	n.r.
¹⁰⁶ Ru	25.8	34	1,420	34
¹³⁴ Cs	18.5	26	n.r.	n.r.
¹³⁷ Cs	12	22.5	5,180	600
⁹⁰ Sr	27	33.5	117	580

Source: Modified from Sobotovich (1992, pp. 83 to 84, Tables 4.16, 4.17, 4.18)

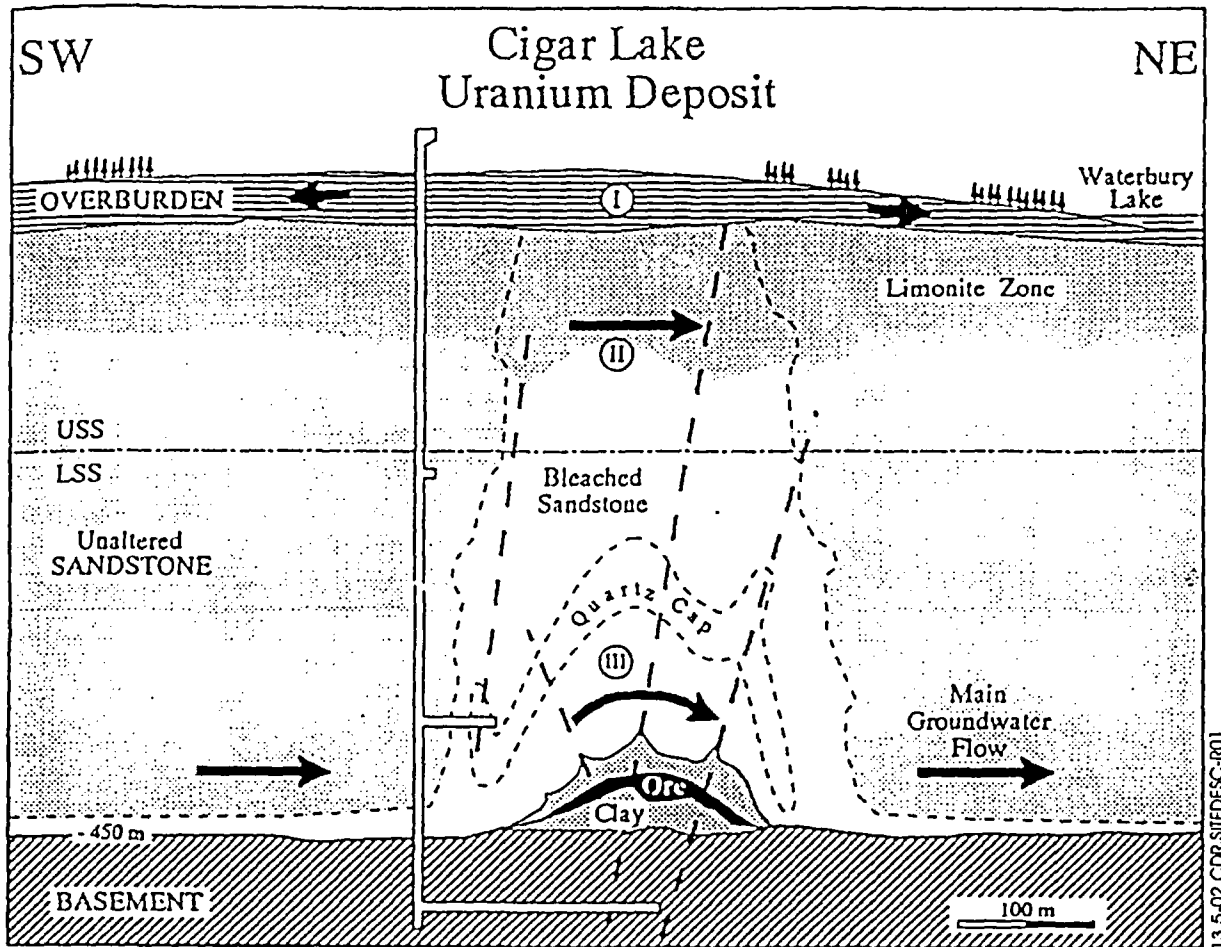
NOTES: Values are maxima measured on 47 samples.
n.r. = not reported

INTENTIONALLY LEFT BLANK



Source: Cramer (1995a, p. 2)

Figure 13.5-1. Location Map Showing Uranium Deposits of the Athabasca Basin in Northern Saskatchewan, Canada



Source: Cramer and Sargent (1994, p. 2,239)

NOTE: This section runs parallel to the direction of regional groundwater flow, and the heavy arrows indicate the general flow directions of groundwater within the three distinct flow regimes (I to III). "USS" refers to the upper sandstone unit; "LSS" refers to the lower sandstone unit.

Figure 13.5-2. Schematic Cross Section through the Cigar Lake Uranium Deposit

Table 13.5-1. Comparison of the Cigar Lake Ore Body with the Canadian Deuterium Uranium Reactor Spent Fuel Repository

Feature		Repository	Ore Body
Waste form	Composition	Used Canadian deuterium uranium reactor fuel—more than 86 wt.% U	Uranium ore—mostly uraninite (UO ₂), grading from 12 to 55 wt.% U
	Stable phase	UO ₂ assumed to be stable	UO ₂ appears to be the stable phase; it has persisted for 1.3 x 10 ⁹ years
	Inventory	1.5 x 10 ⁵ Mg (U) in completed vault	Ore reserve estimated to be 1.5 x 10 ⁵ Mg (U)
	Radioactive isotopes	Fission, activation, and decay products	Spontaneous fission products and decay products
	Dissolution mechanism	Congruent dissolution assumed	Apparently congruent; radiogenic lead from 1.3 x 10 ⁹ years of decay still found in uraninite
	Uranium groundwater concentrations	Solubility limit assumed; the median value is 10 ⁻⁶ M in reducing groundwaters	Observed concentrations in present day reducing groundwaters are less than 10 ⁻⁷ M
Container	Material	Titanium metal ^a	No container analog
Buffer	Material	Mixture of clay and quartz; clay is bentonite	Clay-rich halo in sandstone; mostly illite with quartz
	Hydraulic properties	Bentonite-based buffer; high swelling capacity and very low hydraulic conductivity	Illite-rich clay halo; lower swelling capacity and somewhat higher hydraulic conductivity
	Chemical properties	Assumed to sorb many elements from water, including uranium	Evidence suggests that the clay has retained elements, such as uranium
Geosphere	Thickness of geosphere barrier	Reference depth of the vault is between 500 and 1,000 m	Ore was formed more than 3 km below the surface; its present depth is about 430 m
	Groundwater composition	Groundwaters below about 400 m in the Canadian Shield have salinities in excess of 100 g/L total dissolved solids	Hydrothermal ore-forming solutions had a salinity of 250 to 350 g/L total dissolved solids
	Hydraulic properties	Crystalline host rock, such as granite, is chosen to have a low hydraulic conductivity	Sandstone porosity is 10 to 100 times that of granite; hydraulic conductivities are also higher
	Chemical properties	Assumed to sorb many elements from water; Pb, Ra, and U are strongly sorbed	Sorbs many elements from water; Pb, Ra, and U are strongly sorbed

Table 13.5-1. Comparison of the Cigar Lake Ore Body with the Canadian Deuterium Uranium Reactor Spent Fuel Repository (Continued)

Feature	Repository	Ore Body	
Other	Configuration	Used fuel is isolated by a clay buffer and is located 500 to 1,000 m deep in crystalline rock; entire system is expected to be saturated soon after closure	Uranium ore is isolated by a clay-rich halo and covered by more than 350 m of sandstone; studies suggest that ore has always been saturated
	Colloids	Radionuclide migration due to colloids assumed to be unimportant	Colloids formed in the ore zone are trapped in clay-rich halo
	Timescale	Regulatory criteria require protection for at least 10 k.y.	Uraninite ore has survived more than 1,000 M.y. in water-saturated rock
	Thermal impacts	Peak temperature of less than 100°C for more than 20 k.y.; UO ₂ expected to be stable	Hydrothermal solutions at about 150 to 200°C over 50 M.y.; UO ₂ stable phase at these temperatures
	Environmental impacts	Regulatory criteria place limitations on impacts to man and the environment	No indications (e.g., radiological, thermal, direct geophysical, or geochemical) at the surface that the ore deposit exists

Source: Goodwin et al. (1989)

NOTE: ^aCanada also considered copper containers (Zach et al. 1996).